

ATMS Striping Mitigation Algorithm

Xiaolei Zou
Earth System Science Interdisciplinary Center
University of Maryland

Collaborators:

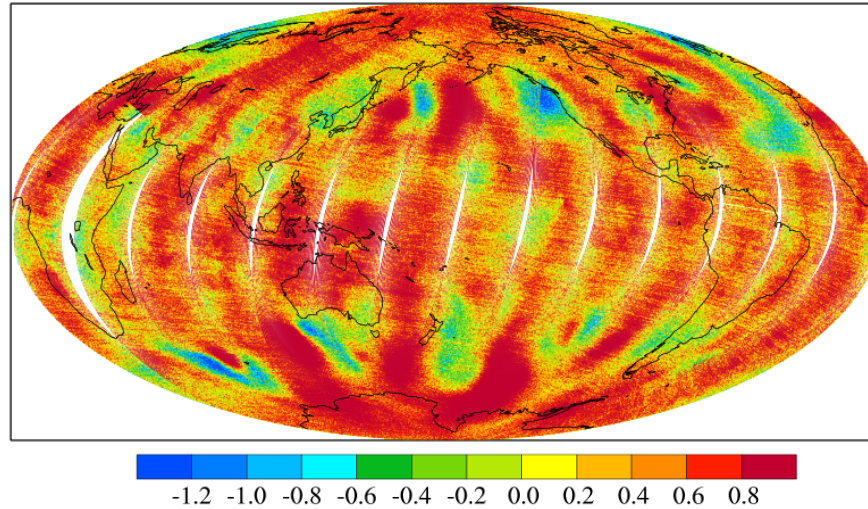
Fuzhong Weng (STAR), Yuan Ma (ESSIC) and Lin Lin (IMSG)

Content

- **Striping Phenomena in Microwave Measurements**
- **Striping Noise Mitigation in ATMS Radiance**
 - Ensemble Mode Decomposition
 - Symmetric Filters
 - Spectral Analysis
 - Striping Index
- **ATMS Noise Characterization Affected by Striping**
 - NEDT
 - Allan Deviation
- **Accomplishments and Future Work**

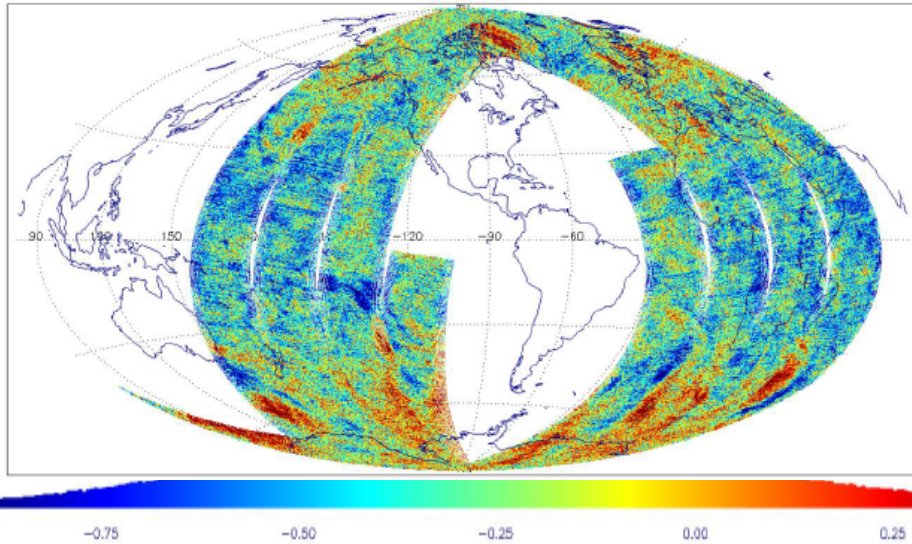
Striping Noise in Global Distributions of ATMS O-B

An along-track
striping noise of
ATMS data in
NWP O-B fields!



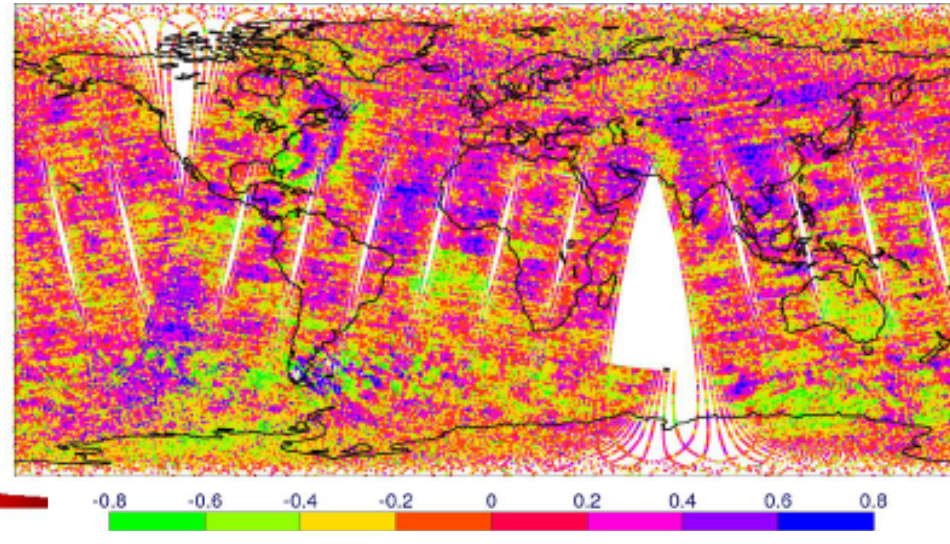
O-B of channel 10
(86 hPa)
Qin, Zou and Weng,
2013, JGR

O-B of channel 8 (250 hPa)



Swadley et al, NRL

O-B of ATMS channel 12 (25 hPa)

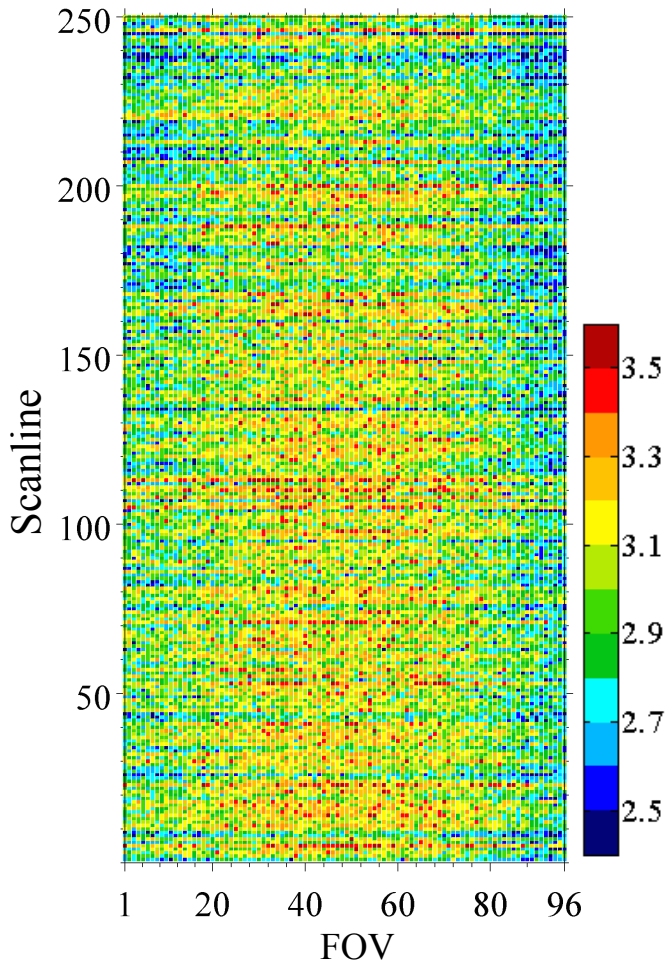


Bormann et al., ECMWF

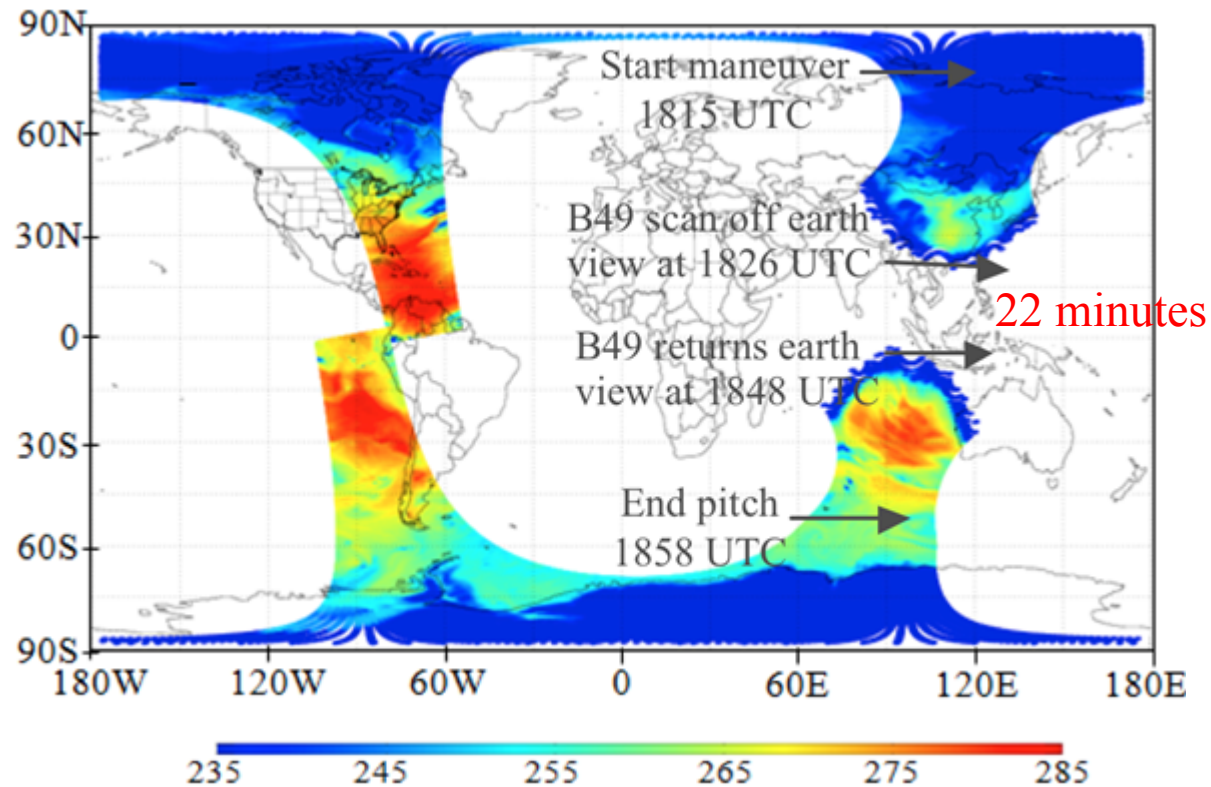
User Complains !

Striping Noise Seen in ATMS On-Orbit Pitch Maneuver Data

Channel 9



ATMS Pitch Maneuver Data Locations and Times



The pitch-over maneuver was performed February 20, 2012.

ATMS Striping Noise and Its Impacts on Users

- SNPP ATMS upper air sounding channels display clear striping noise in NWP model O-B fields, which is disturbing and may degrade ATMS data assimilation impacts on NWP
- At the 19th International TOVS Study Conference (ITSC), NWP users request the ATMS Cal/Val team not only to quantify the striping noise magnitude but also to develop an operational algorithm for elimination of striping noise in ATMS data
- ATMS Cal/Val team was requested to develop 45 days of ATMS de-striping data for EMC, ECMWF and other NWP centers to test the impacts of striping noise on ATMS data assimilation for NWP

Requirements on Striping Noise Mitigation Algorithms

- **Characteristic features of ATMS striping noise**
 - (1) Nearly constant in across-track direction for any single scan
 - (2) Of random magnitude in along-track direction for any swath
- **Challenge**
 - (3) Such striping noise exists in scene counts
- **Requirements on striping mitigation algorithms**
 - (4) Striping noise is removed
 - (5) Small-scale weather features are not altered
 - (6) Feasible for operational implementation

Striping Noise Mitigation Algorithms

- **The PCA/EEMD Algorithm** (good for theoretical analysis of striping noise)

Step I: Compute principal components of ATMS data matrix

Step II: Extract the first few high frequency IMFs from the 1st PC mode to remove striping noise

- **The PCA/SymFilter Algorithm** (good for operational implementation)

Step I: Compute principal components of ATMS data matrix

Step II: Apply a symmetric filter to the 1st PC mode to filter striping noise through an “optimally” weighted averaging

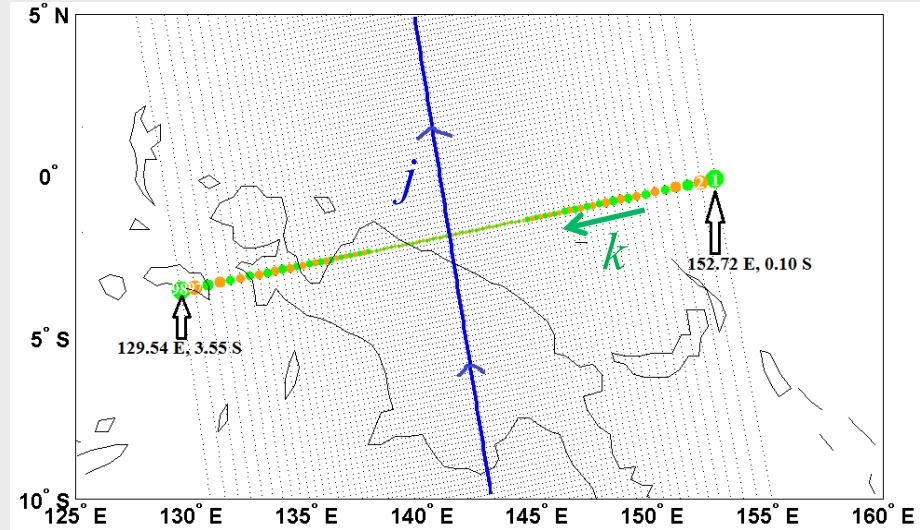
PCA	——	Principal Component Analysis
EEMD	——	Ensemble Empirical Mode Decomposition
SymFilter	——	Symmetric Filter
IMFs	——	Intrinsic Model Functions

Step I: Compute PCs of ATMS Covariance Matrix

1. Form ATMS data matrix

$$\mathbf{A} = \begin{pmatrix} TB_{1,1} & TB_{1,2} & \cdots & TB_{1,j} & \cdots & TB_{1,N} \\ TB_{2,1} & TB_{2,2} & \cdots & TB_{2,j} & \cdots & TB_{2,N} \\ \vdots & & \ddots & & & \\ TB_{k,1} & & & TB_{k,j} & & TB_{k,N} \\ \vdots & & & & \ddots & \\ TB_{96,1} & & & & & TB_{96,N} \end{pmatrix}$$

→ j , along track
 ↓ k , cross track



2. Construct covariance matrix

$$\mathbf{S} = \mathbf{A}\mathbf{A}^T$$

$$\mathbf{S}\vec{e}_i = \lambda_i \vec{e}_i$$

PC modes

3. Mapping ATMS radiance in PC modes

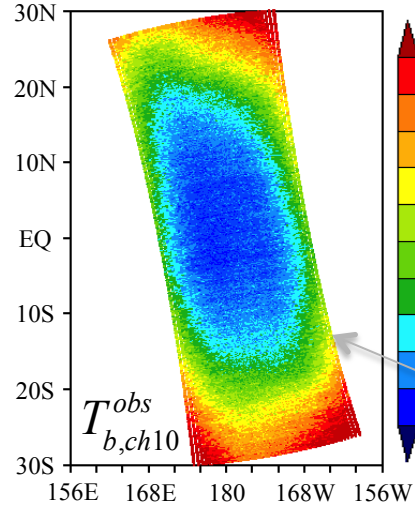
$$\mathbf{A} = \sum_{i=1}^{96} \vec{e}_i \vec{u}_i$$

PC coefficients

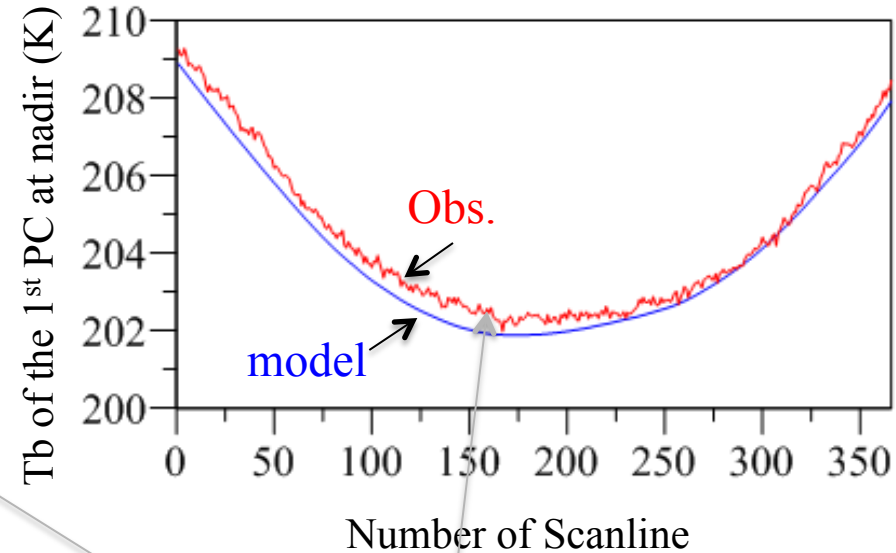
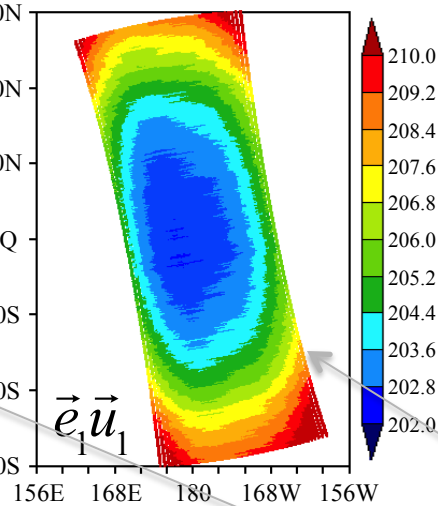
$$\begin{pmatrix} \vec{u}_1 \\ \vdots \\ \vec{u}_{96} \end{pmatrix} = \begin{pmatrix} \vec{e}_1 \\ \vdots \\ \vec{e}_{96} \end{pmatrix} \mathbf{A}$$

PCA Decomposition for ATMS Channel 10

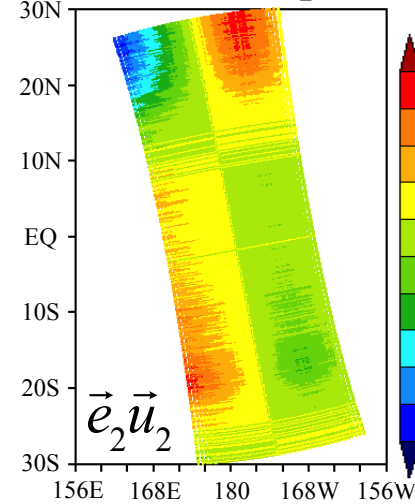
T_b obs.



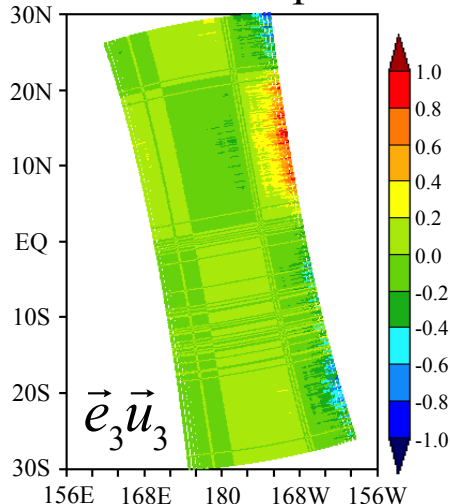
The 1st component



The 2nd component



The 3rd component



An along-track noise oscillations are clearly seen in ATMS radiance measurements of channel 10.

Step II: Extract IMFs from the 1st PC Coefficient

EEMD decomposition:

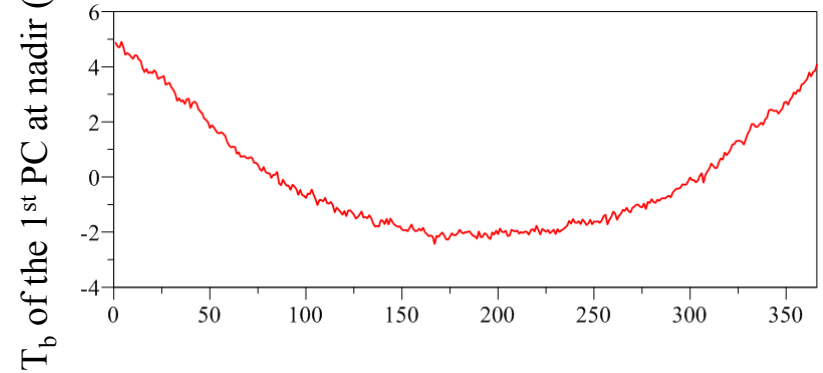
$$T_b^{obs}(t) = \sum_{j=1}^n C_j(t) + R_n(t)$$

$$R_0(t) = T_b(t)$$

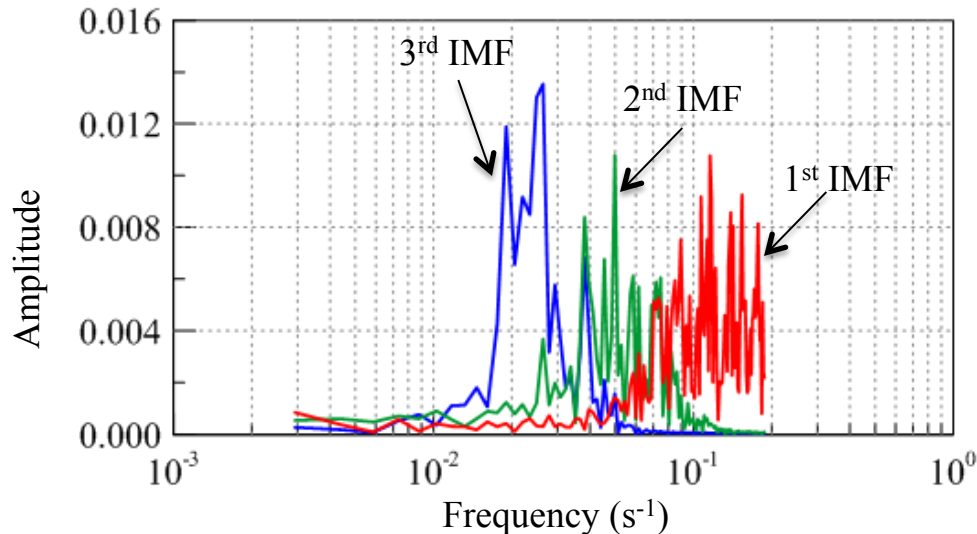
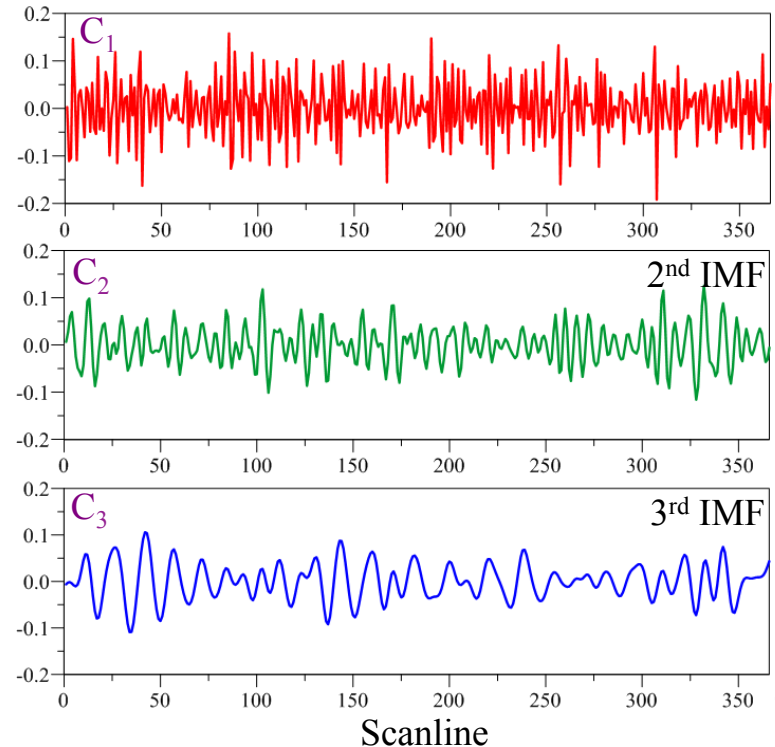
$C_n \leftarrow R_{n-1}$ minus the mean of the envelopes of R_{n-1}

$$R_n(t) = R_{n-1}(t) - C_n$$

The 1st PC coefficient at Nadir

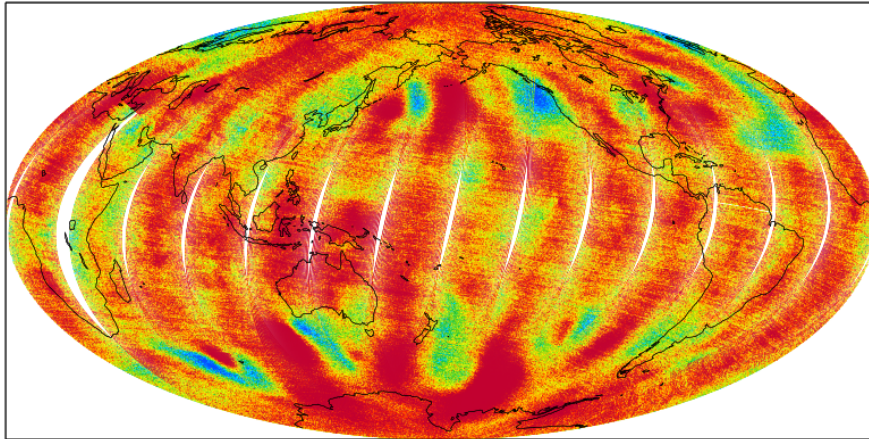


The first three IMFs of the above data series

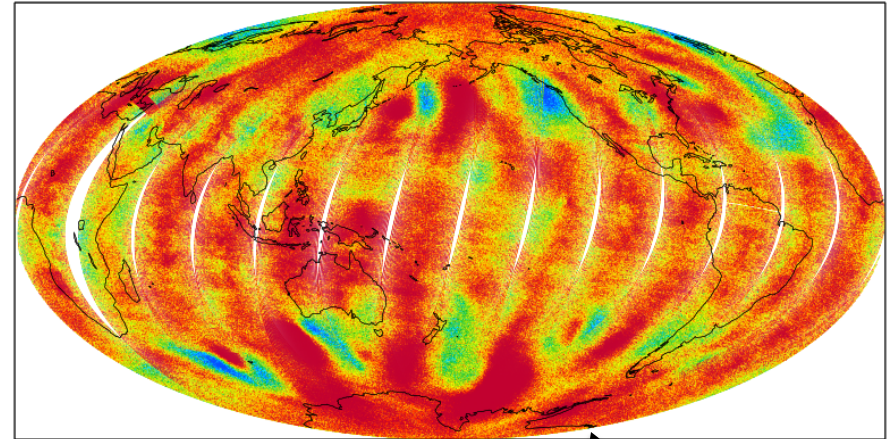


Global O-B Distributions for ATMS Channel 10

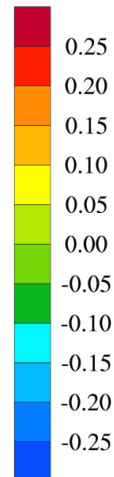
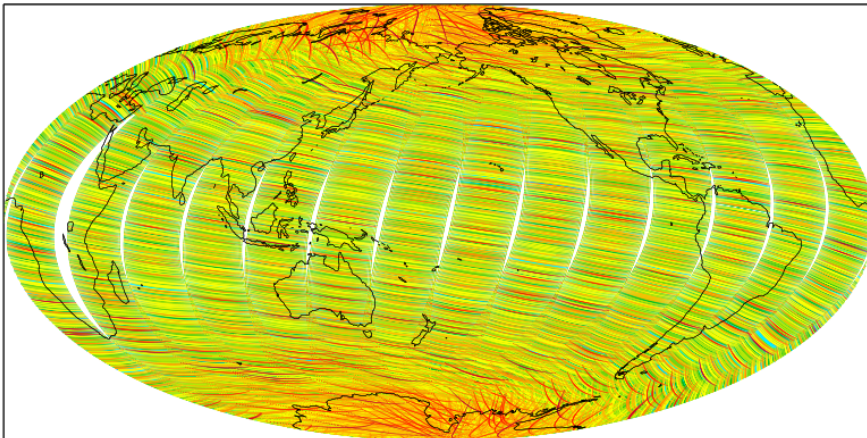
Before de-stripping



After de-stripping



Striping noise mitigated

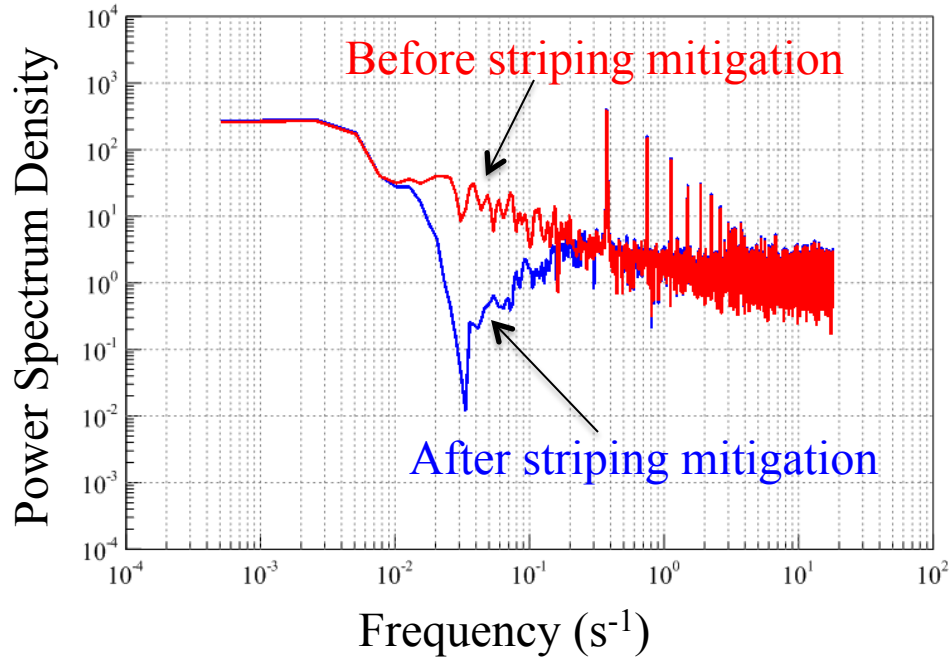


Striping noise is not visibly seen anymore in the global O-B field after de-stripping using the PCA/EEMD algorithm.

Qin, Z., X. Zou and F. Weng (2013)
J. Geophys. Res., **118**, 13214-13229.

Data on 24 February 2012

SNPP ATMS channel 10

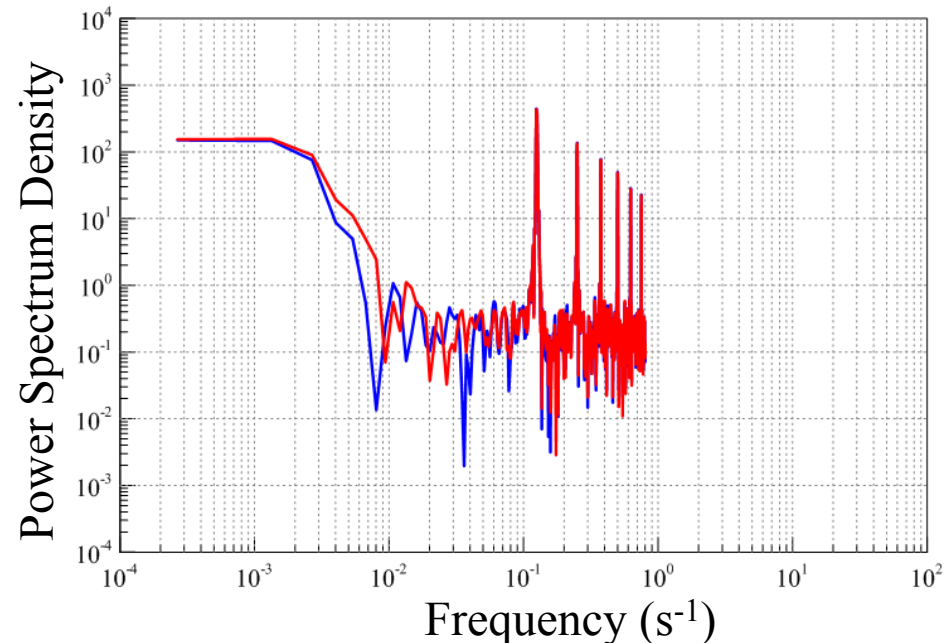


The AMSU-A power spectrum does not have a $1/f$ flicker noise feature within the frequency range (10^{-2} - 10^{-4} s⁻¹). Applying the PCS/EEMD algorithm anyway has negligible effect on AMSU-A spectrum.

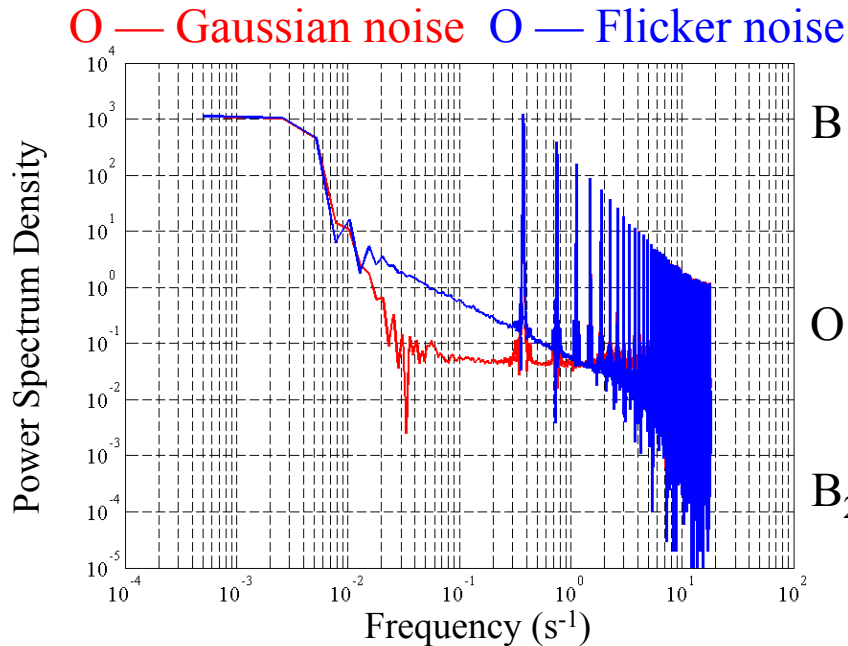
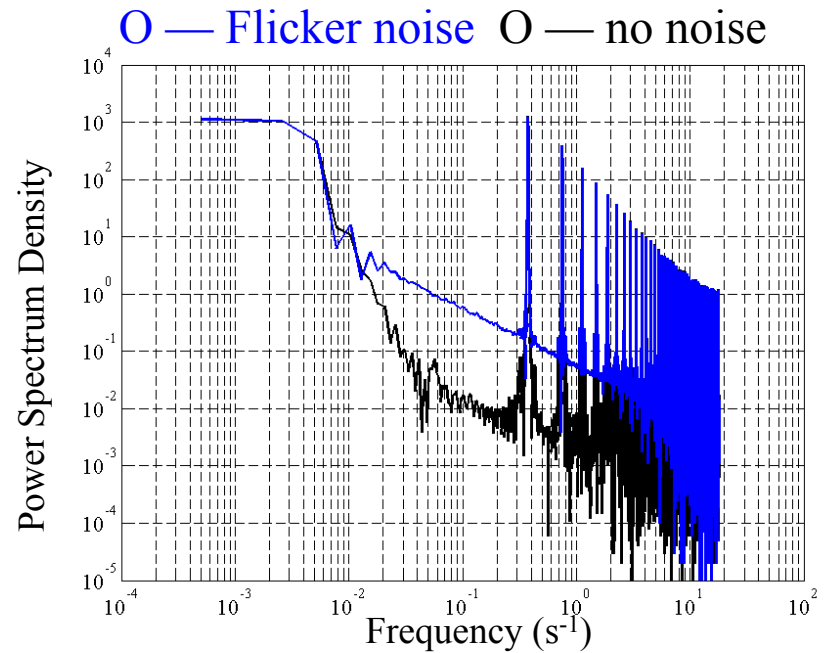
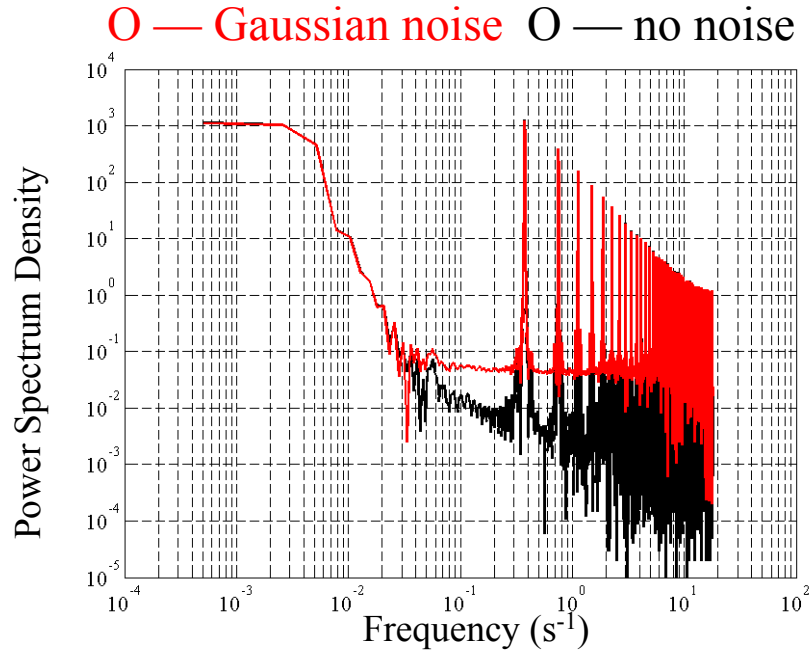
Power Spectral Density Distributions

A $1/f$ flicker noise feature of the ATMS power spectrum within the frequency range (10^{-2} - 10^{-4} s⁻¹) is significantly reduced after striping noise mitigation (SNM).

NOAA-18 AMSU-A channel 9



O-B PSDs When O Is Simulated with Gaussian and Flicker Noise



B — Brightness temperature simulations for ATMS channel 8 with GFS input on May 1, 2014

O — $\begin{cases} B_2 \\ B_2 + \text{Gaussian noise } (\mu = 0, \sigma = 0.283 \text{ K}) \\ B_2 + \text{Flicker noise } (\mu = 0, \sigma = 0.283 \text{ K}) \end{cases}$

B₂ — Brightness temperature simulations for ATMS channel 8 with GFS input on May 5, 2014

Can ATMS striping noise be removed by boxcar or triangular filters by simply increasing the filter span?

Boxcar Filter

$$\bar{T}_{b,i} = \sum_{j=-n}^n \frac{1}{2n+1} T_{b,i+j}$$

$$\mathbf{w}_7^{\text{boxcar}} = \left(\frac{1}{15}, \frac{1}{15}, \dots, \frac{1}{15} \right)$$

$$\mathbf{w}_{17}^{\text{boxcar}} = \left(\frac{1}{35}, \frac{1}{35}, \dots, \frac{1}{35} \right)$$

Constant weighting

Triangular Filter

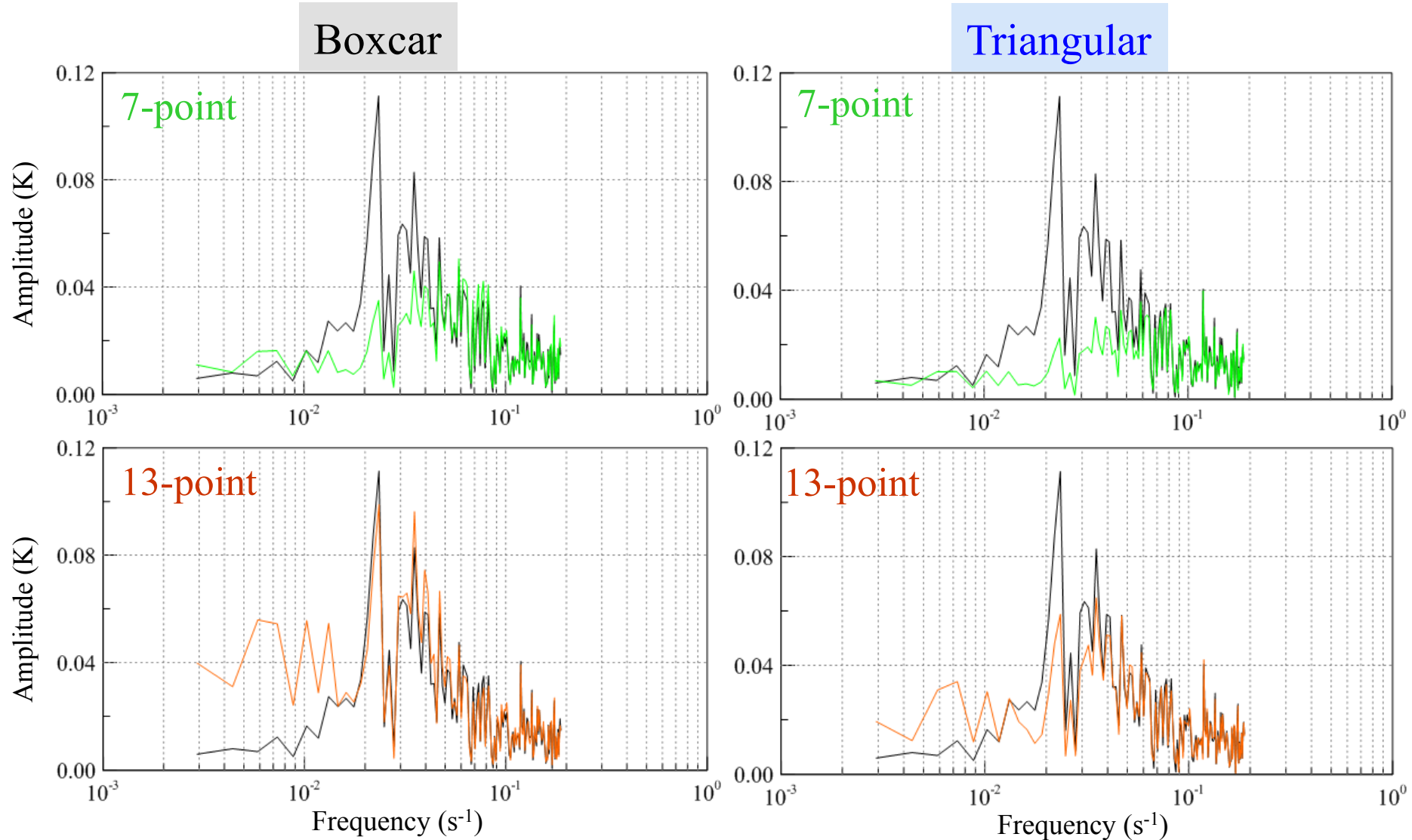
$$\bar{T}_{b,i} = \sum_{j=-n}^n \frac{n+1-|j|}{(n+1)^2} T_{b,i+j}$$

$$\mathbf{w}_7^{\text{triangular}} = \left(\frac{1}{64}, \frac{2}{64}, \dots, \frac{7}{64}, \frac{8}{64}, \frac{7}{64}, \dots, \frac{1}{64} \right)$$

$$\mathbf{w}_{17}^{\text{triangular}} = \left(\frac{1}{324}, \frac{2}{324}, \dots, \frac{17}{324}, \frac{18}{324}, \frac{17}{324}, \dots, \frac{1}{324} \right)$$

Triangular weighting

Noise Spectra Removed by Boxcar and Triangular Filters



Increasing the filter span does make the boxcar and triangular filters to be more effective in removing the striping noise but the larger scales of weather signals could be altered.

Step II: Develop a symmetric filter to remove striping noise

The first PC coefficient

$$\{u_{1,k}\} (k = 1, 2, \dots, K)$$

The filtered first PC coefficient

$$\bar{u}_{1,k} = \sum_{n=-N}^N \alpha_n u_{1,k+n}, \quad \alpha_n = \alpha_{-n}$$

$$u_{1,k} = \sum_{m=0}^{K-1} C_m e^{-i \frac{2\pi mk}{K}} \quad \bar{u}_{1,k} = \sum_{m=0}^{K-1} \bar{C}_m e^{-i \frac{2\pi mk}{K}}$$

$$r_m = \sum_{n=0}^N \alpha_n \cos(2\pi f \Delta t)$$

$$\bar{C}_m = r_m C_m, \quad f = \frac{m}{K \Delta t}, \quad \Delta t = \frac{8}{3} s$$

$$\begin{cases} \min_{\alpha_n} J = \min \sum_{k=1}^K \left(\sum_{n=-N}^N \alpha_n u_{1,k+n} - \bar{u}_{1,k}^{eemd} \right)^2 \\ \sum_{n=-N}^N \alpha_n = 1, \quad \alpha_n = \alpha_{-n} \end{cases}$$

where $\bar{u}_{k,1}^{eemd} = u_{k,1} - \sum_{m=1}^L IMF_m(k)$

$$T_{b,k,i}^{destriping} = e_{1,i} \sum_{n=-N}^N \alpha_n u_{1,k+n} + \sum_{j=2}^{96} e_{j,i} u_{j,k}$$

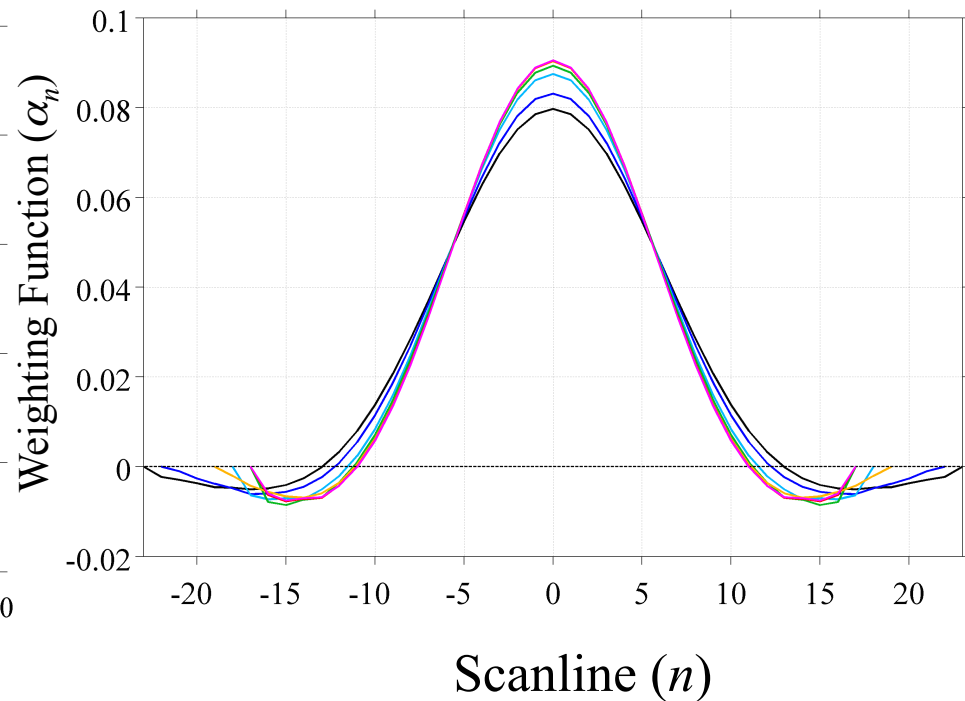
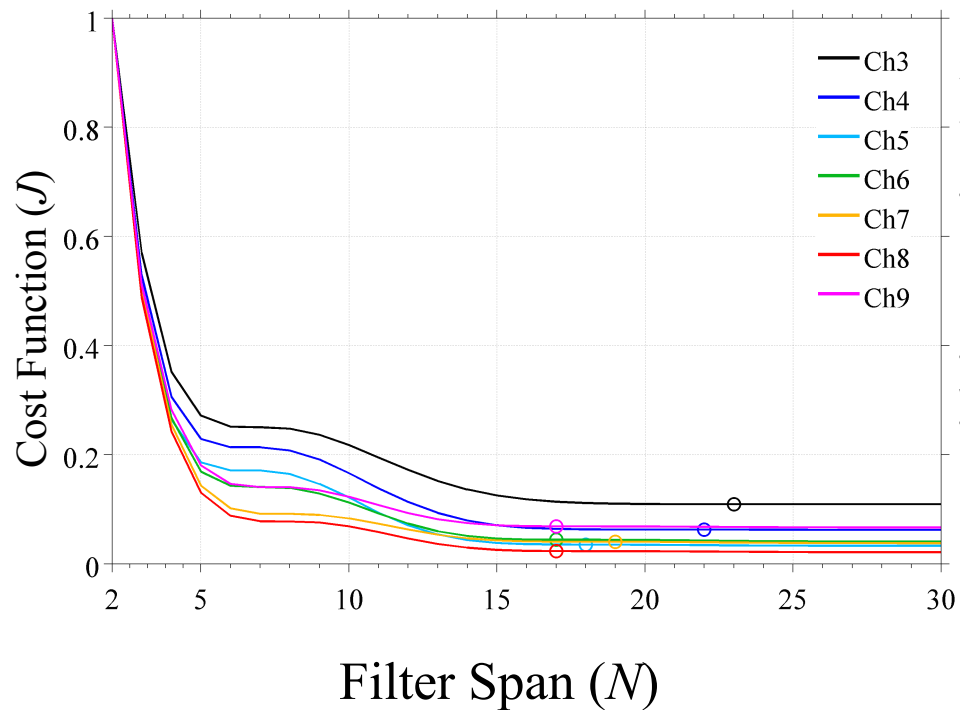
$i = 1, 2, \dots, 96$ represents scan position
 $k = 1, 2, \dots, K$ represents scan line

The Optimal Striping Filters: Numerical Results

$$J = \sum_{k=1}^K \left(\sum_{n=-N}^N \alpha_n u_{1,k+n} - \bar{u}_{1,k}^{eemd} \right)^2$$

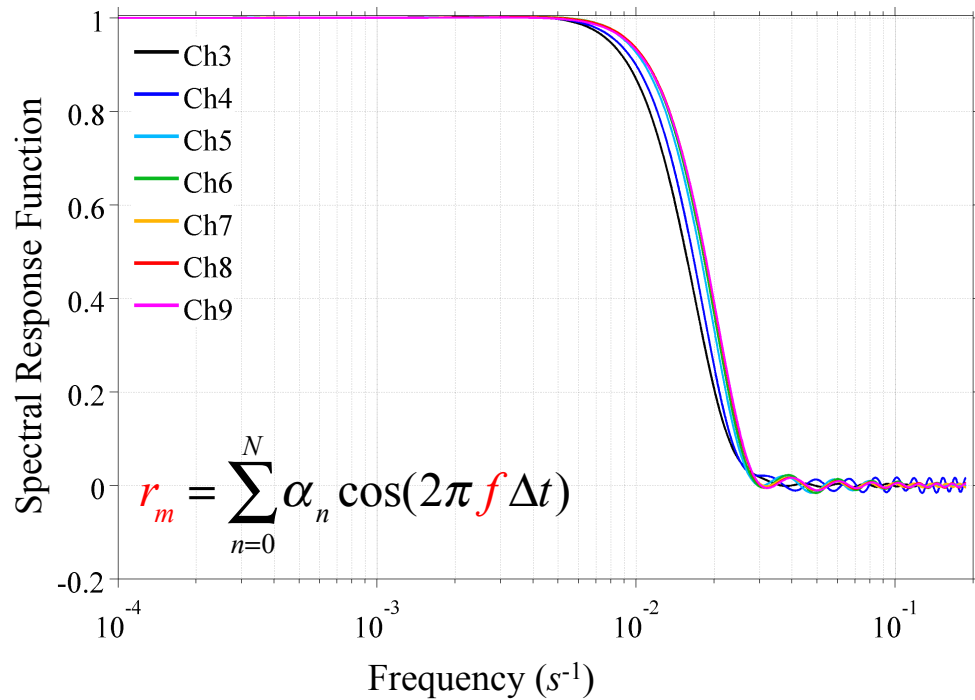
Optimal Weights

$\alpha_{n,ch}$

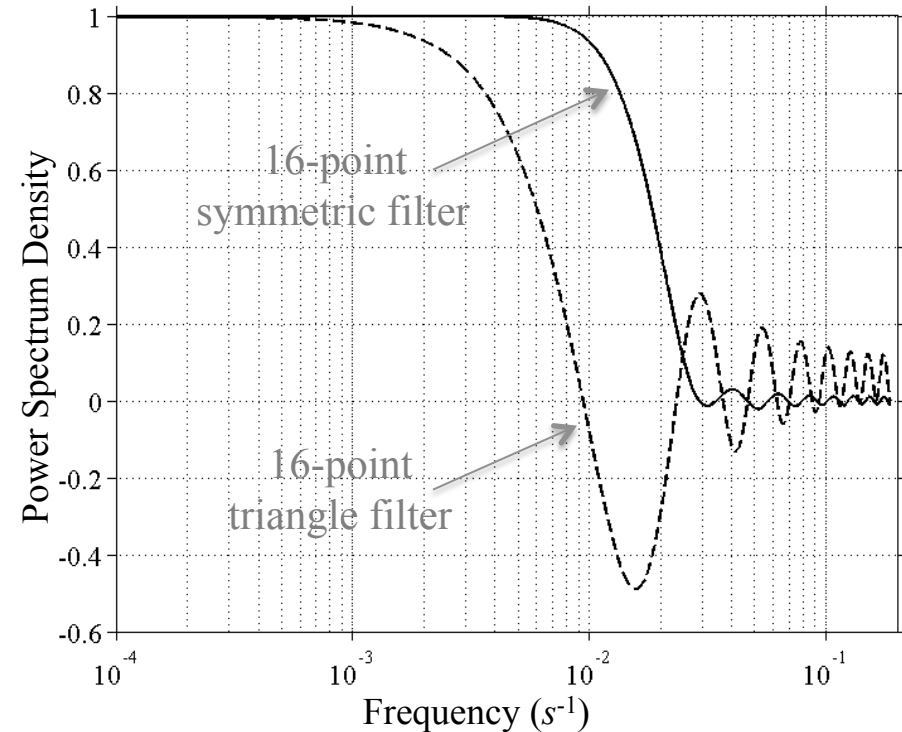


The Spectral Response Function of the PCS/SymFilter

Striping Filters for ATMS Channels 3-9



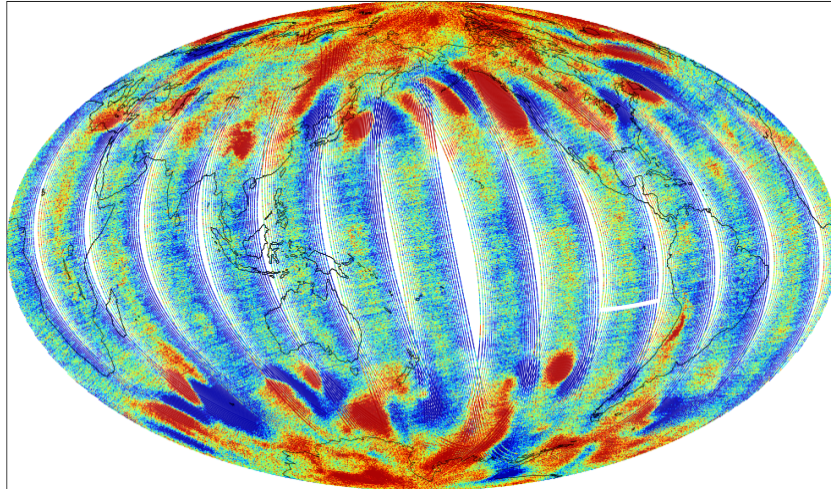
Comparison with a Triangular Filter



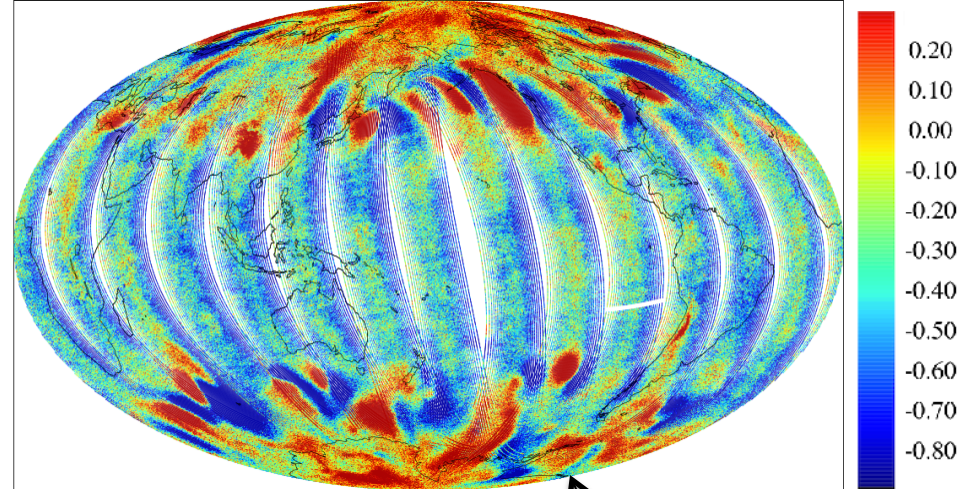
This is a set of optimal filters for ATMS radiances designed to smooth out the striping noise but not to alter lower frequency weather signals.

Global O-B Distributions of ATMS Channel 8

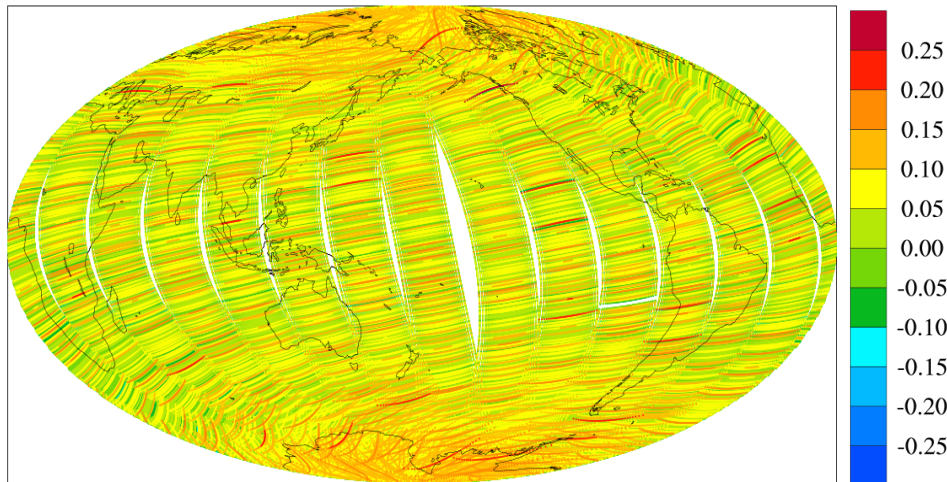
Before de-stripping



After de-stripping



Striping noise filtered



Striping noise is not visibly seen anymore in the global O-B field after de-stripping using the PCA/SymFilter algorithm.

Ma Y. and X. Zou (2015)
J. Geophys. Res., **120**, 6634-6653.

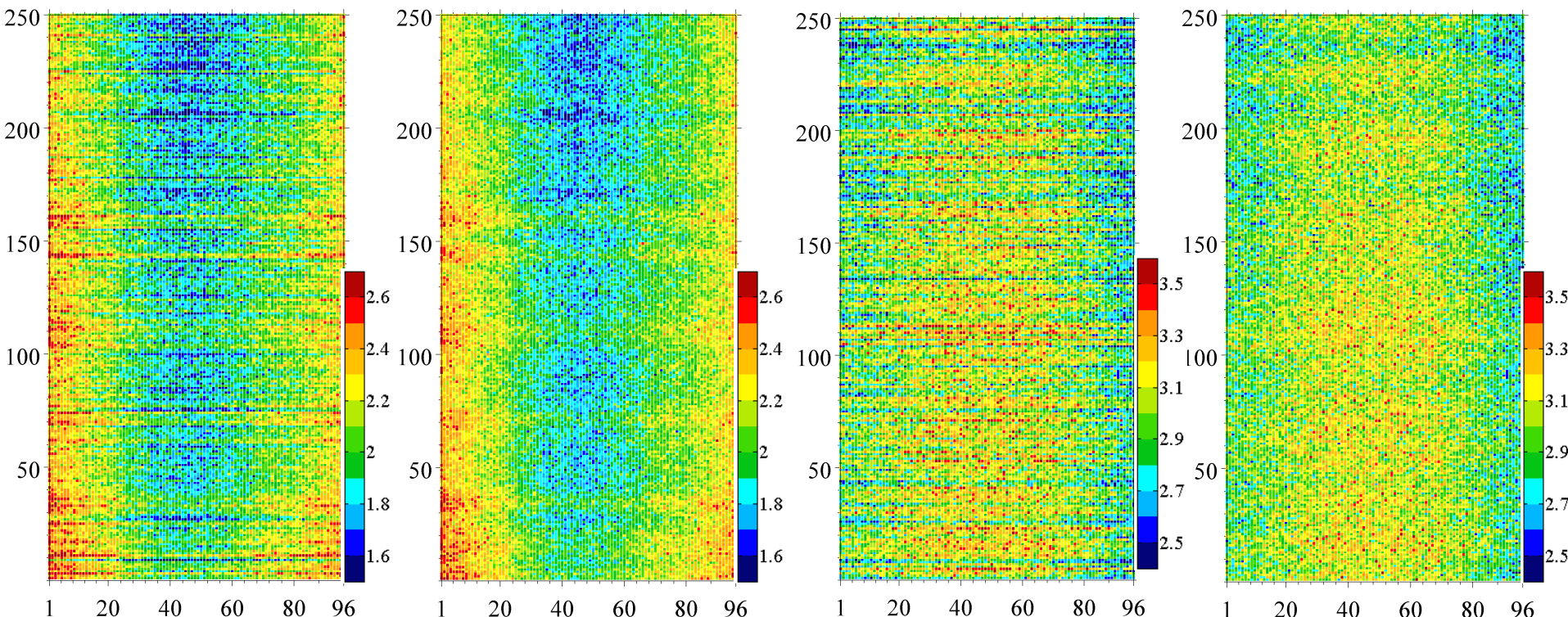
Pitch-Over Maneuver Data before and after Striping Mitigation Using the PCA/SymFilter Algorithm

before de-striping

after de-striping

before de-striping

after de-striping

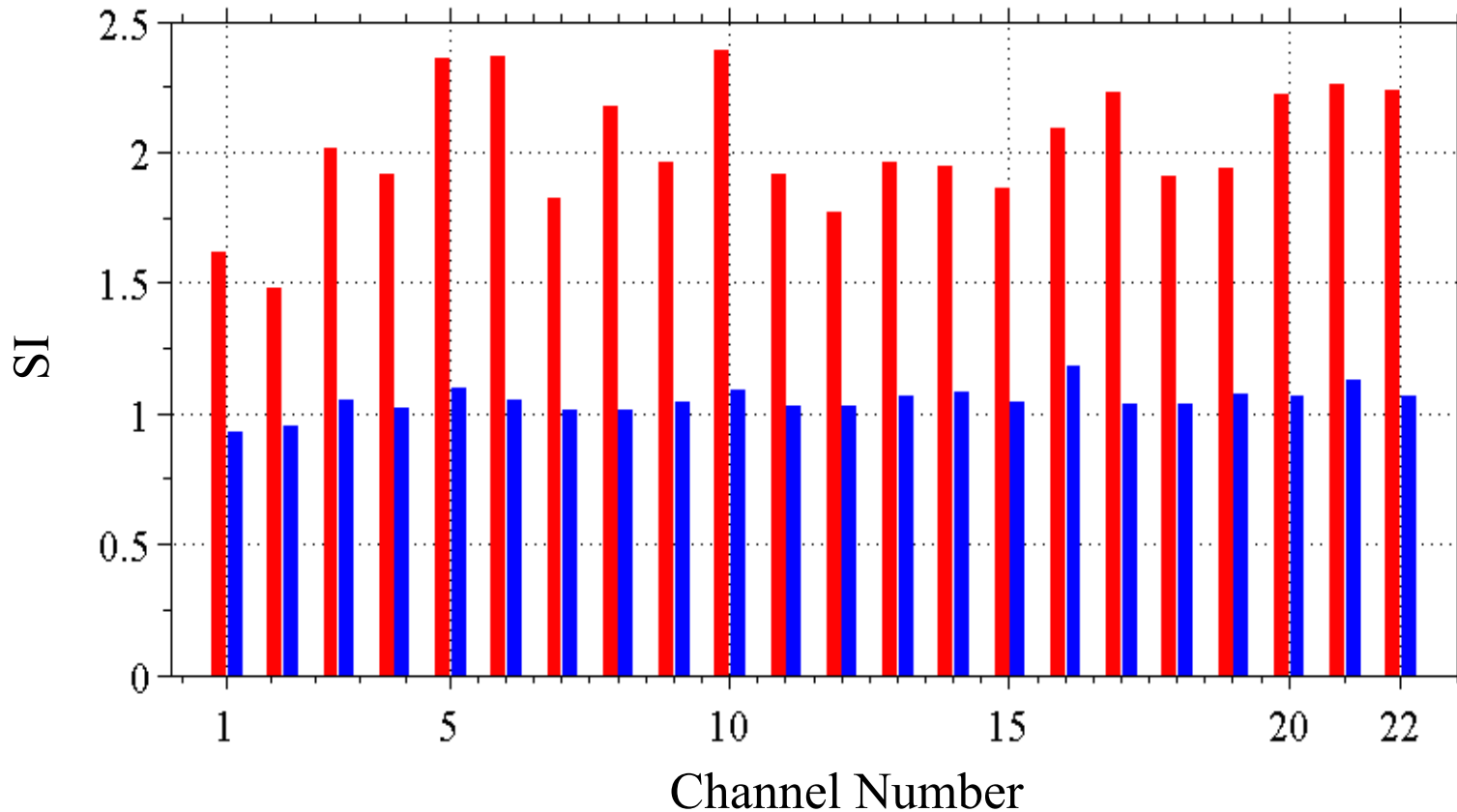


ATMS Channel 1

ATMS Channel 9

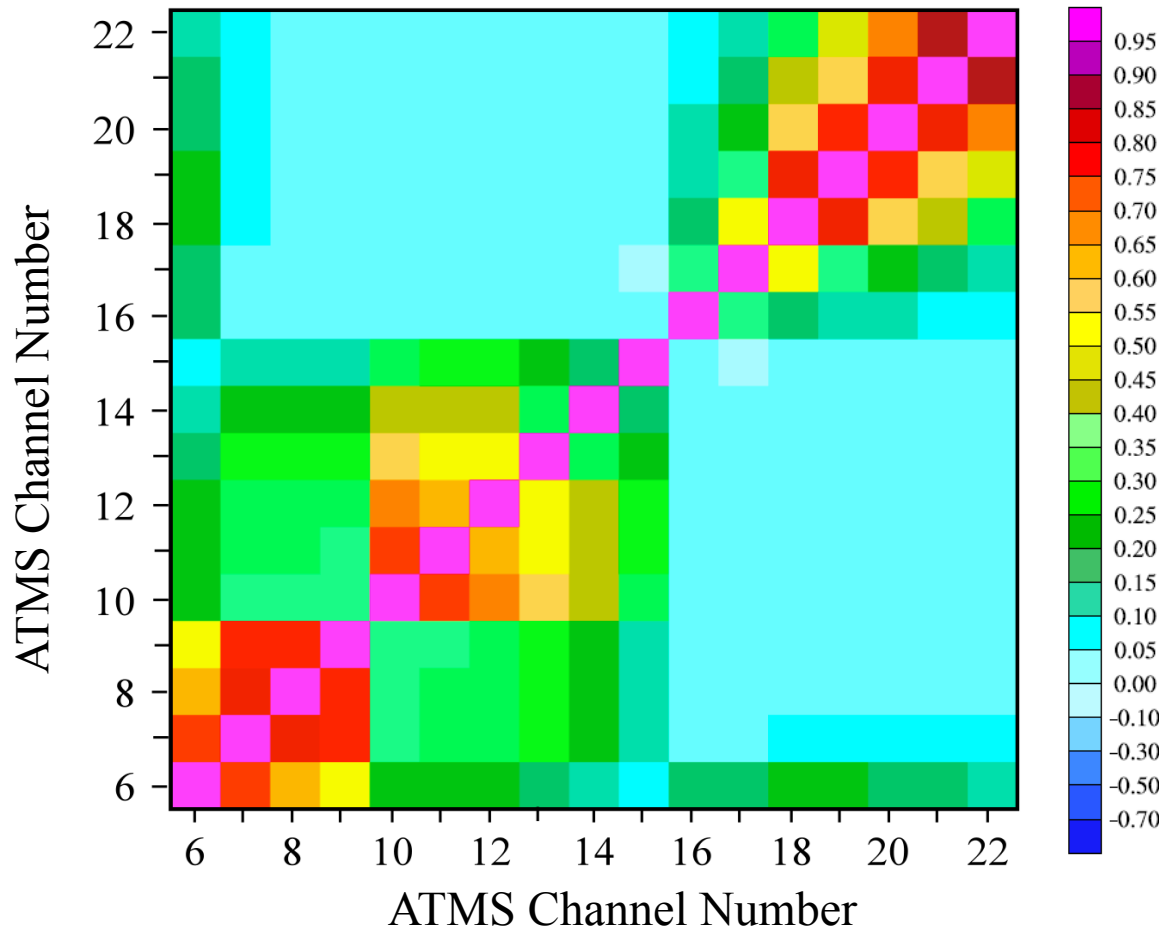
Striping Index (SI)

$$SI = \frac{\sigma_{along-track}^2}{\sigma_{cross-track}^2}$$



SI is significantly reduced to one for ATMS all channels.

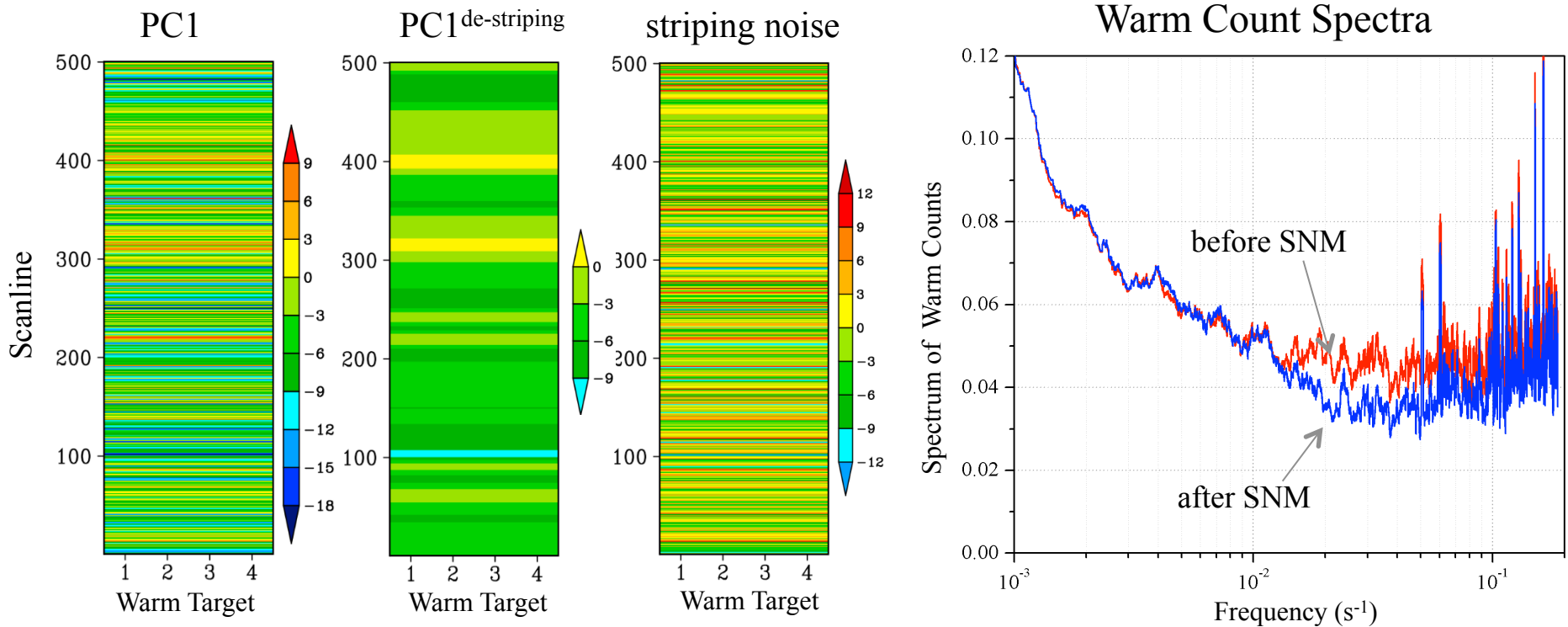
Channel Correlations of Striping Noise



Global data on
February 24, 2012

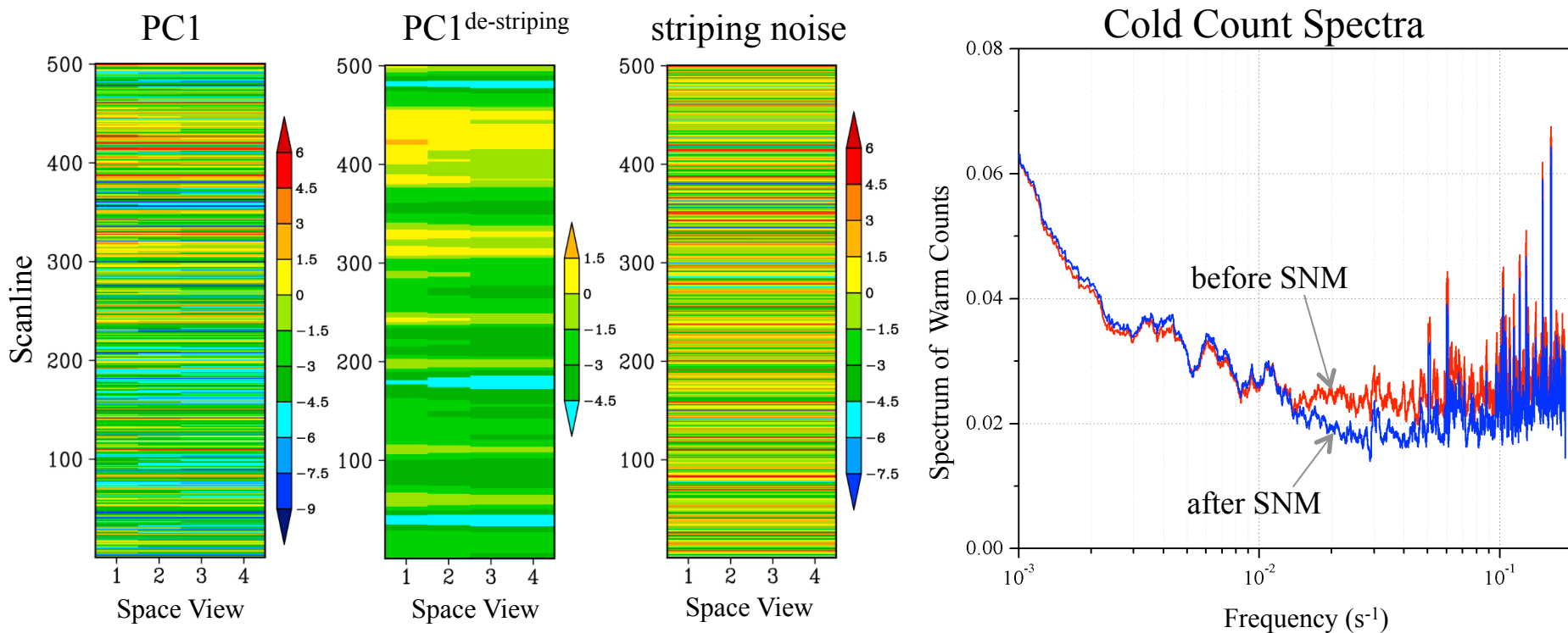
Striping noise is correlated among channels which share the same feed horn: Channel 6-15; Channels 17-22.

Striping Noise in ATMS Calibration Counts of Four Warm Targets



A $1/f$ flicker noise feature within the frequency range (10^{-2} - 10^{-4} s⁻¹) in the warm count spectrum is significantly reduced after de-striping.

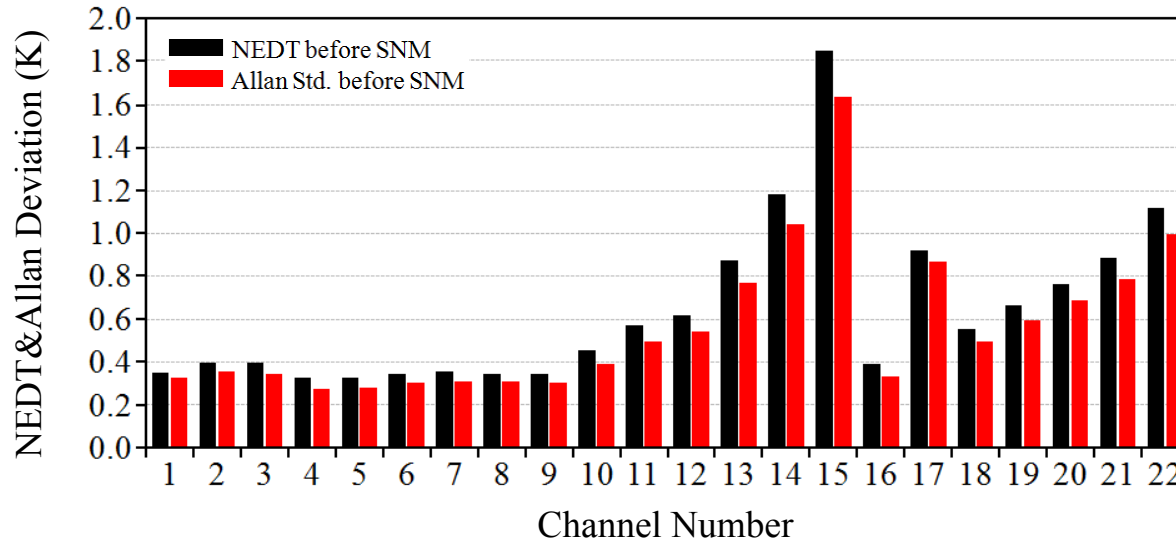
Striping Noise in ATMS Ch 8 Calibration Counts of Four Space Views



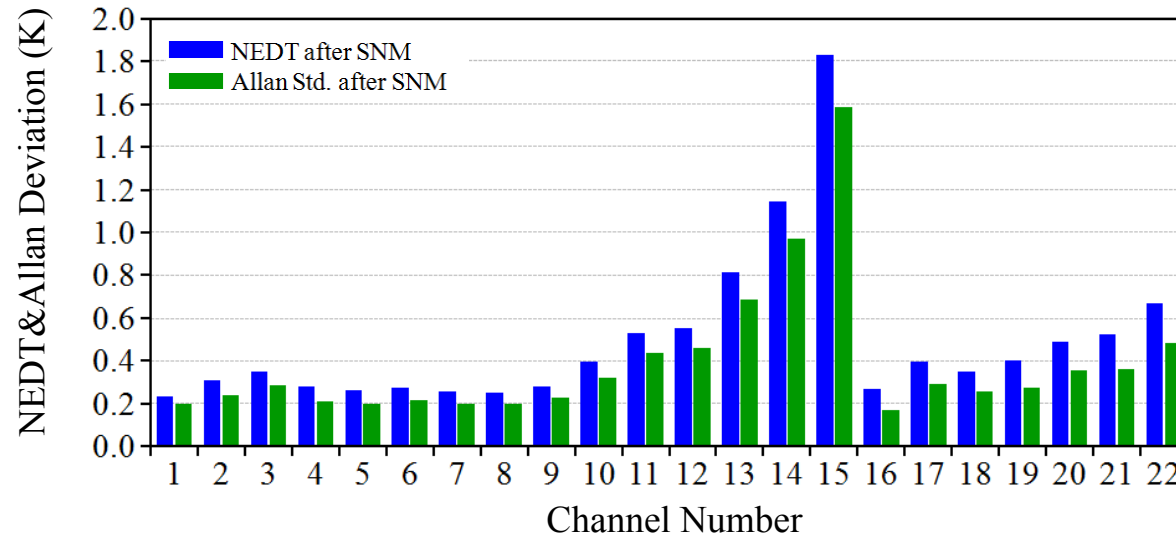
A $1/f$ flicker noise feature within the frequency range (10^{-2} - 10^{-4} s⁻¹) in the cold count spectrum is significantly reduced after de-striping.

The averaged cold count value of 10459.79 over 32364 scan lines for ATMS channel 8 is subtracted.

Impact of Striping Noise on ATMS Noise Characterization

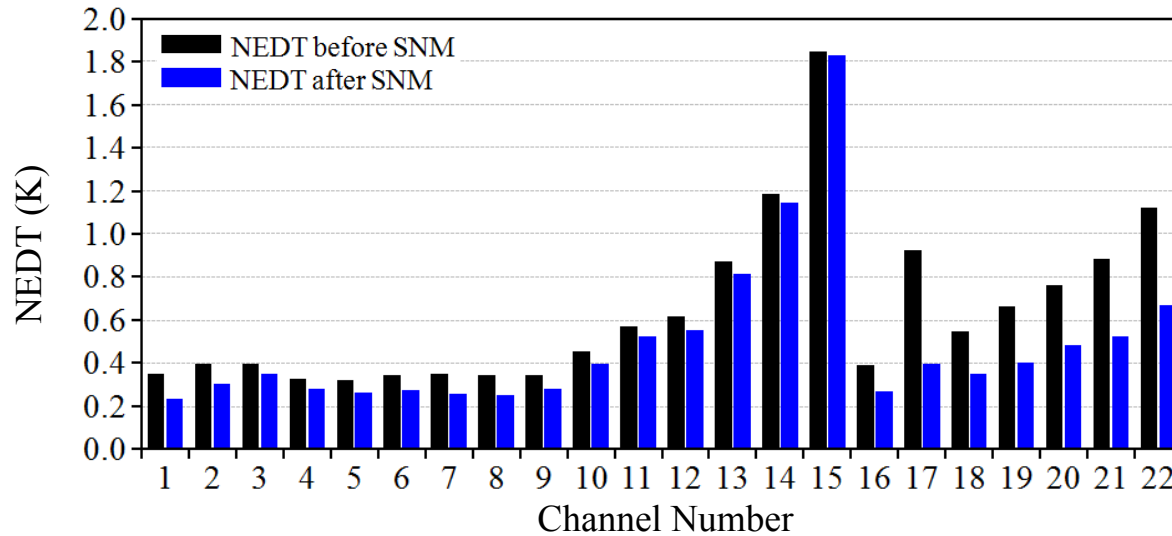


Before striping noise mitigation (SNM)

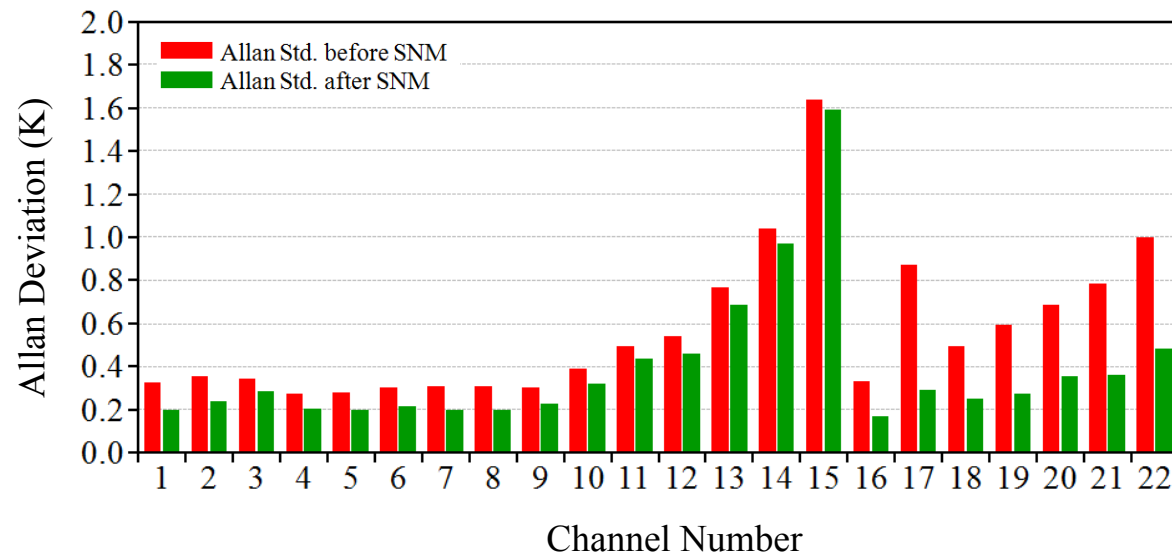


After SNM

Impact of Striping Noise on ATMS Noise Characterization



NEDT



Allan Deviation

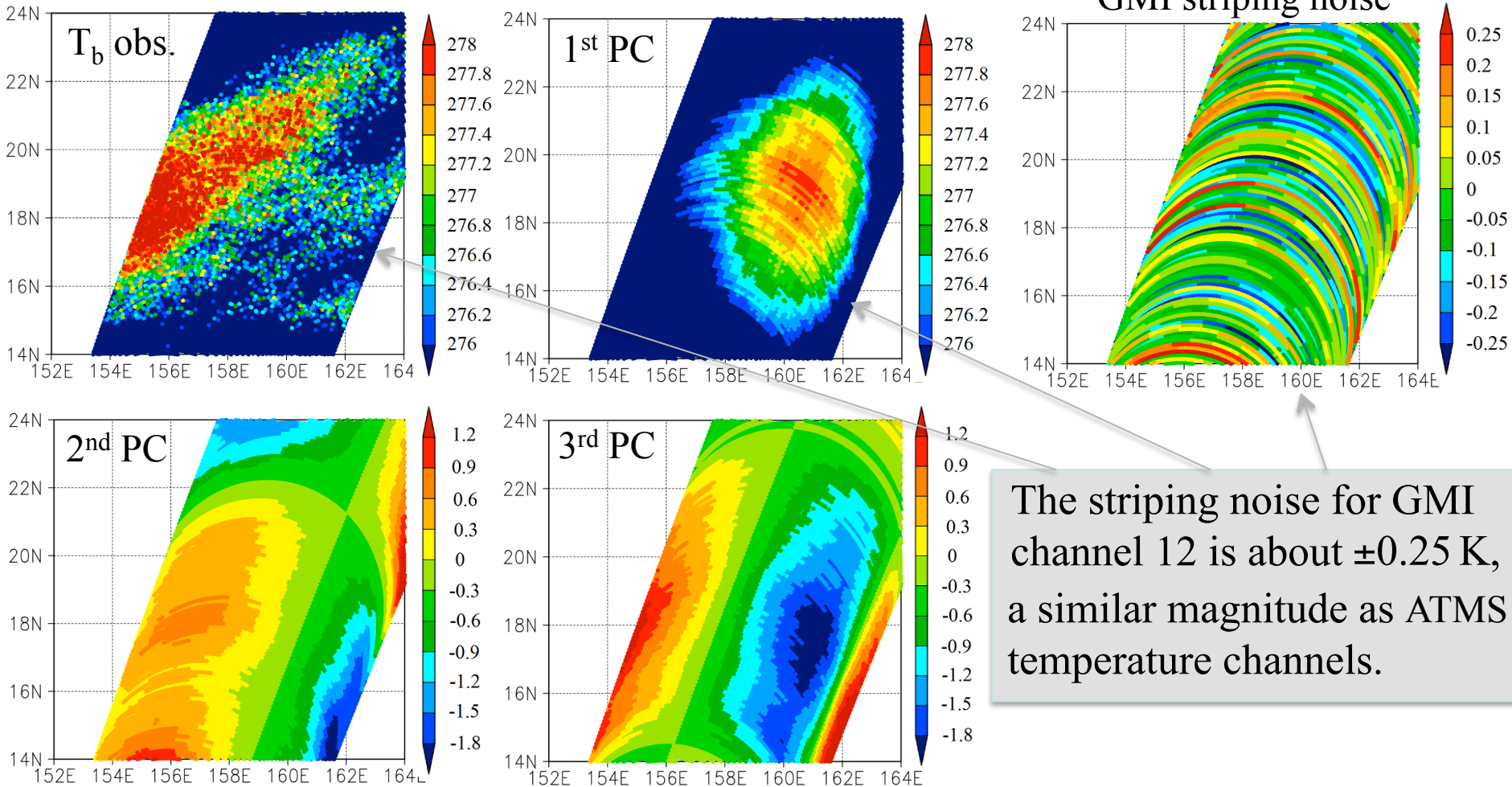
Accomplishments

- ATMS striping noise magnitude in earth scene observations is quantified and verified by pitch maneuver data with consistency
- A striping mitigation algorithm that is feasible for an operational implementation is developed and tested
- 45-day ATMS de-striped radiance data were generated and delivered to several NWP centers (EMC, ECMWF etc.) for testing the striping noise impacts on ATMS data assimilation and subsequent NWP
- The PCA/EEMD algorithm for theoretical analysis of striping noise were published in the JPSS JGR special issue
Qin, Z., X. Zou and F. Weng, 2013: Analysis of ATMS and AMSU striping noise from their earth scene observations. *J. Geophys. Res.*, **118**, 13,214-13,229.
- The PCA/SymFilter algorithm for operational implementation of striping mitigation was published in JGR last month
Ma Y. and X. Zou, 2015: Striping noise mitigation in ATMS brightness temperatures and its impact on cloud LWP retrievals. *J. Geophys. Res.*, **120**, 6634-6653. 27

Planned Future Work

- Prepare for a striping noise evaluation for J1 ATMS channels if needed
- Conduct striping noise analysis and mitigation for other satellite sensors such as CrIS, GMI, AMSR2
- Complete documentation of the impacts of striping noise on ATMS NEDT noise characterization using both the standard deviation and the Allan deviation

A First Look at GPM Microwave Imager (GMI) Data



An along-track noise oscillations seem to also exist in radiance measurements for GMI channel 12 (183.1 ± 3 GHz).

Acknowledgement

This work was supported by NOAA JPSS SDR Program.



NORTHROP GRUMMAN



J1 ATMS Readiness

Edward Kim, *NASA GSFC*

Cheng-Hsuan J. Lyu, *I.M. Systems Group, NASA GSFC*

R. Vincent Leslie, *MIT Lincoln Laboratory*

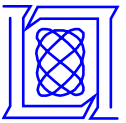
Kent Anderson, *Northrop Grumman Electronic Systems*

JPSS Annual Meeting
August 26, 2015



Outline

NORTHROP GRUMMAN



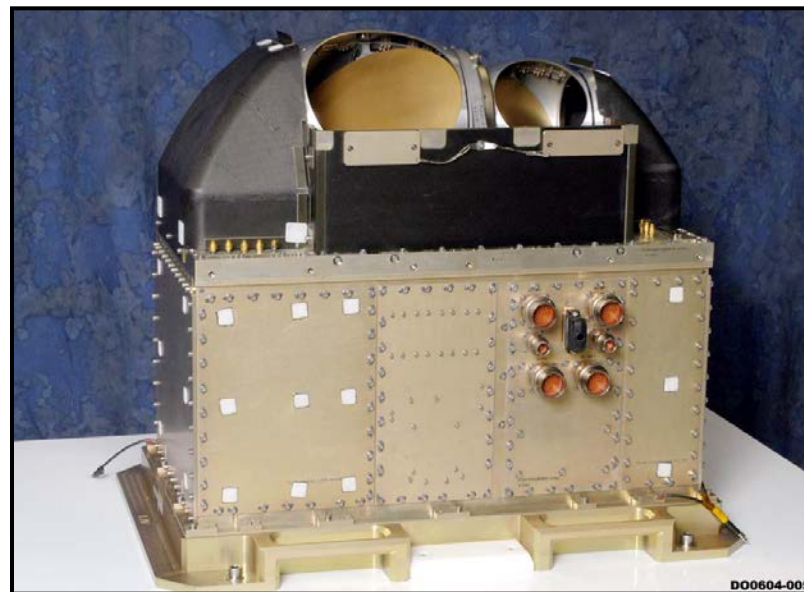
- Differences between S-NPP and JPSS-1 flight units
 - Known issues with S-NPP unit
 - Modifications to J1 unit
- JPSS-1 flight unit status
 - Prelaunch testing
 - Rework & regression testing
 - Notional schedule
- Summary

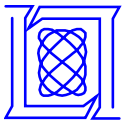


Context



- To provide more context for understanding J1 ATMS readiness, of course the starting point is the S-NPP flight unit
- In particular, the following slides show a sampling of issues discovered on the S-NPP build, and what was modified for the J1 build to try to improve things
- It is not meant to be an exhaustive list
- S-NPP ATMS is working well





1. Scan drive issue

- Non-ideal materials used; accelerated wear → risk of degraded scan, even total stopping of scan
- 2-year investigation of lifetime extension strategies
- “scan reversal” strategy selected
- Scan reversal is currently being tested on orbit
 - Daily
 - Above 75 N latitude to limit NWP impact

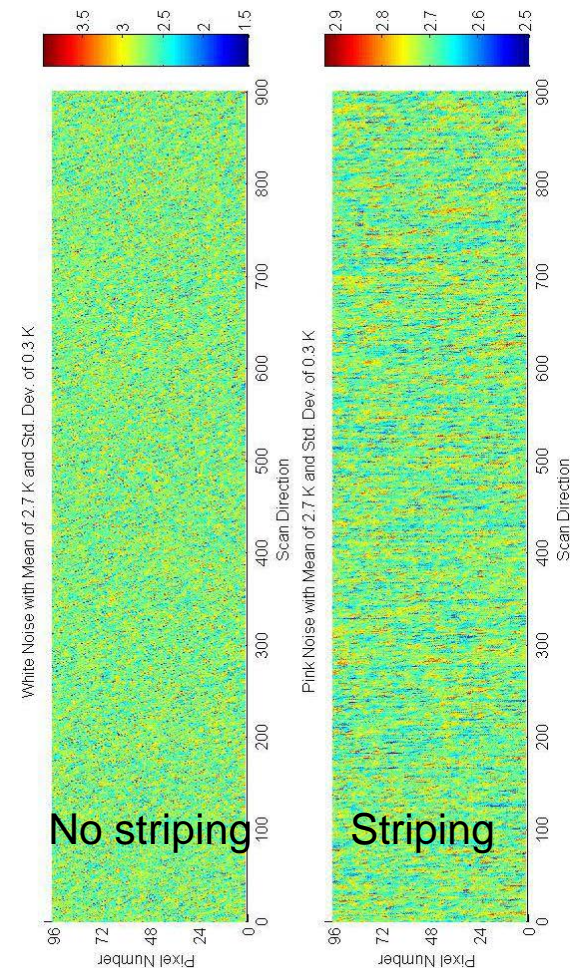
Modifications Made to J1 ATMS

- Bearings re-designed
- Should not be an issue for J1+



2. Increased 1/f noise vs. AMSU (“striping”)

- 1/f noise is present in all electronic measurements; the source is “understood,” and in the hardware
- Studies have since found “striping” in AMSU and MHS data, so it’s not unique to ATMS
- Hardware modifications to the S-NPP flight unit are not an option
- The only option for S-NPP is to adjust averaging of cal parameters to better match noise power spectrum & limit the effects of 1/f on ATMS





Is striping a problem?

NORTHROP GRUMMAN



- ATMS striping is an order 0.1K size issue—i.e., small.
- Note: there is currently no requirement with respect to striping
- ATMS meets its *existing* specs even with striping because *existing* specs do not address striping
- NWP centers say striping is a problem, but have yet to develop a good quantitative metric, so a precise discussion is difficult.
- An NWP striping metric might be an end-to-end metric like:
'X kelvins of striping cause Y % degradation of weather forecast skill.'
- In the absence of a quantitative analysis of striping impact on NWP forecast skill, the flight project is unlikely to be receptive to requests for a new requirement on striping



What can be done about striping?

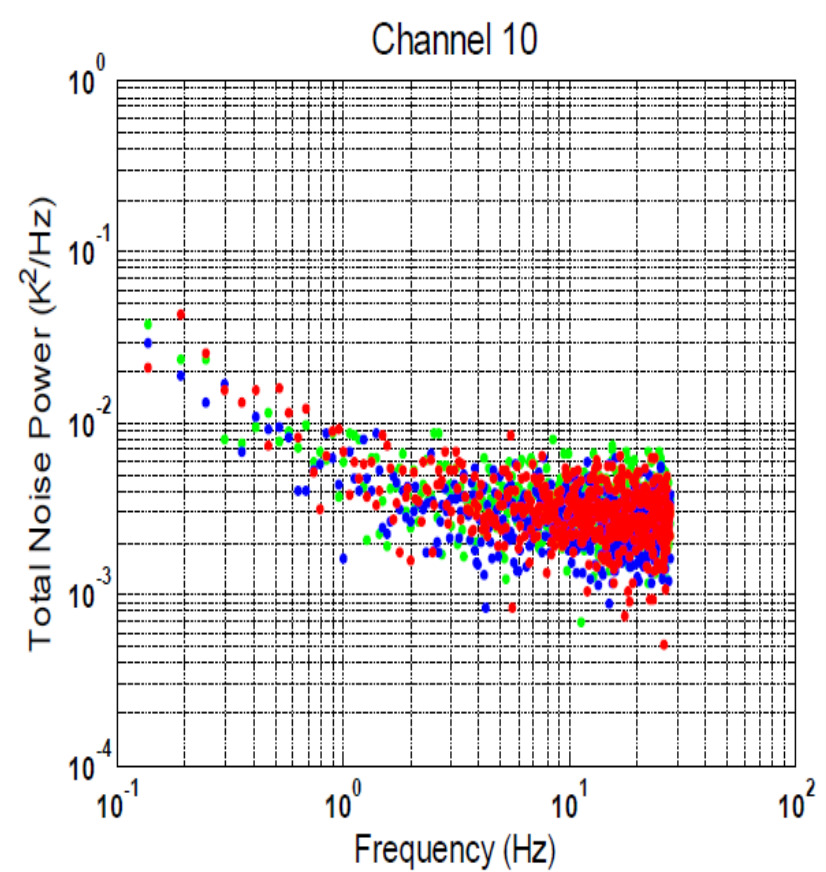
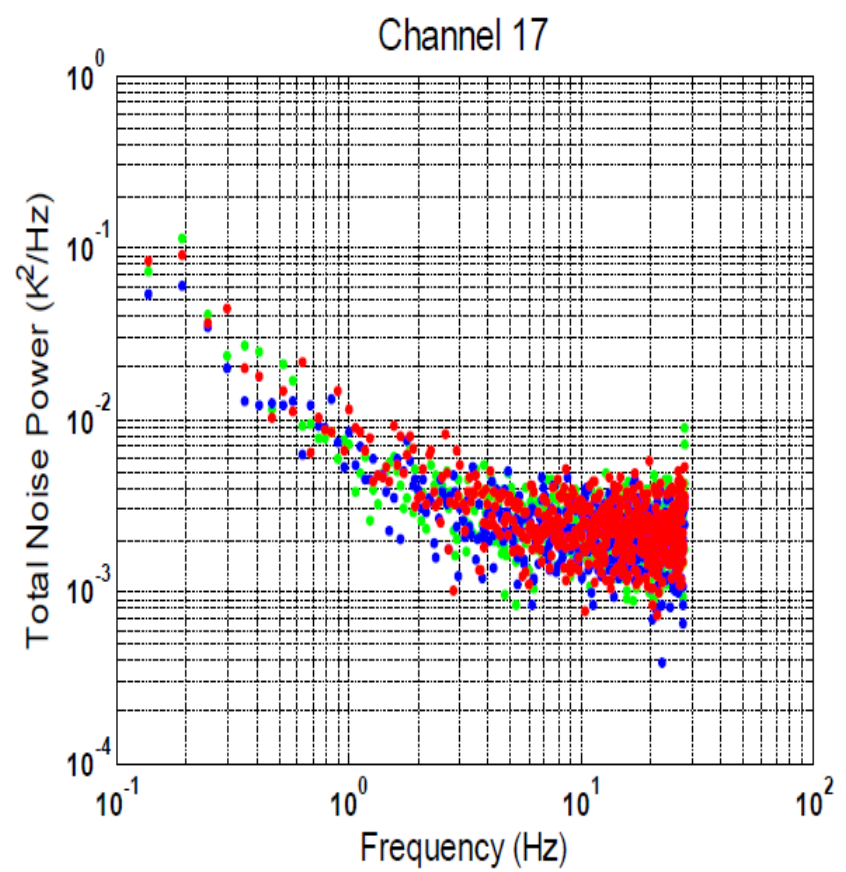
NORTHROP GRUMMAN



- For S-NPP
 - we can't change the hardware, so the only option is modifying the ground algorithm
 - ATMS SDR team has explored adjusting cal parameter averaging
 - Long stares would provide striping-related data
- For J1
 - Too late for hardware changes
 - So main option is to change ground algorithm, like for S-NPP
 - Addn'l ground measurements and on-orbit stares would help
 - The ground measurements (stares) are being done
 - The on-orbit stares have been requested, including deep space
- For J2+
 - Addn'l ground measurements recommended
 - On-orbit stares would be great
 - Beyond that, TBD



Noise Power Spectrum



S-NPP ATMS power spectral densities (green = cold plate temp. of 5.3 C, red is 10.1 C, and blue is 0.7 C). The pink noise (1/f component) is independent of the instrument's temperature. The sensor-level measurements were taken in 9/2005 (green) and the satellite-level testing in 4/2011 (red, blue).



3. Antenna characterizations

- Issues with test facility and methodology used for S-NPP, especially for G-band (183 GHz) channels
- J1 beam efficiency slightly below spec (94% vs. 95%); waiver approved, plus additional tests showed 95% was met



4. Reflector emissivity

- Due to specific construction of reflector (Be-Ni-Au)
- Affects S-NPP and J1 flight units
- Results in scan angle dependent scale factor in TB (“smiles” and “frowns”)
- Physical mechanism verified by special ground test
- Only option for S-NPP is algorithm adjustment

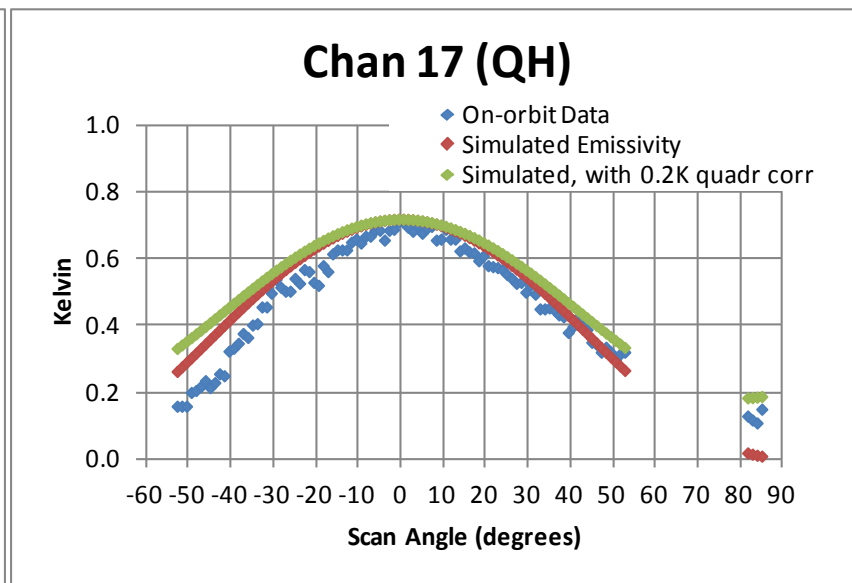
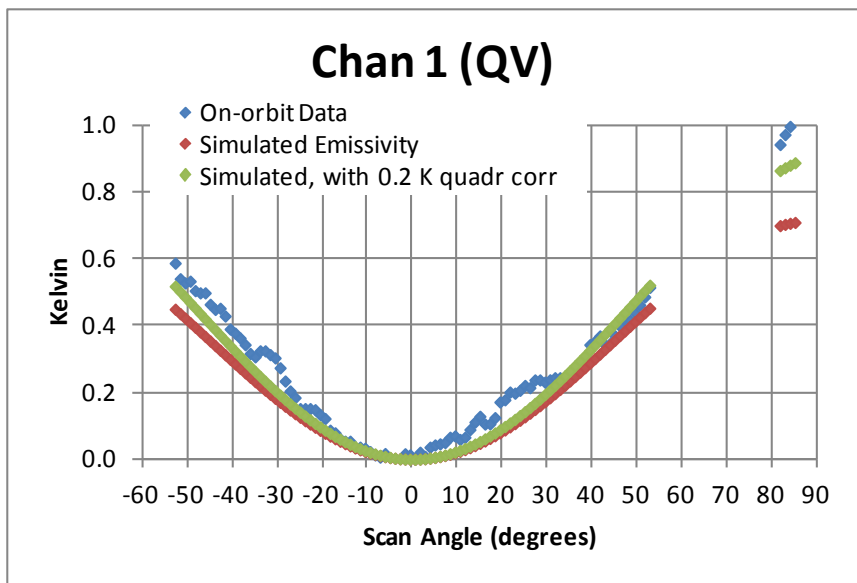
Modifications Made to J1 ATMS

- Discovered too late in J1 build to change J1 hardware
- But same algorithm adjustment as S-NPP will be done
- Not part of J1 re-work, so earliest fix opportunity will be on J2 flight unit



Scan-Dependent Bias from Reflector Emissivity

NORTHROP GRUMMAN



Scan-dependent bias, obtained from S-NPP calibration/validation pitch maneuver, compared to simulated effect of reflector emissivity. Theory confirmed via special ground tests.



5. Spectral Response Functions

- S-NPP SRF data were inconsistently recorded, and not always in digital form
- An extensive data recovery effort yielded digital SRF data for S-NPP; data publicly available

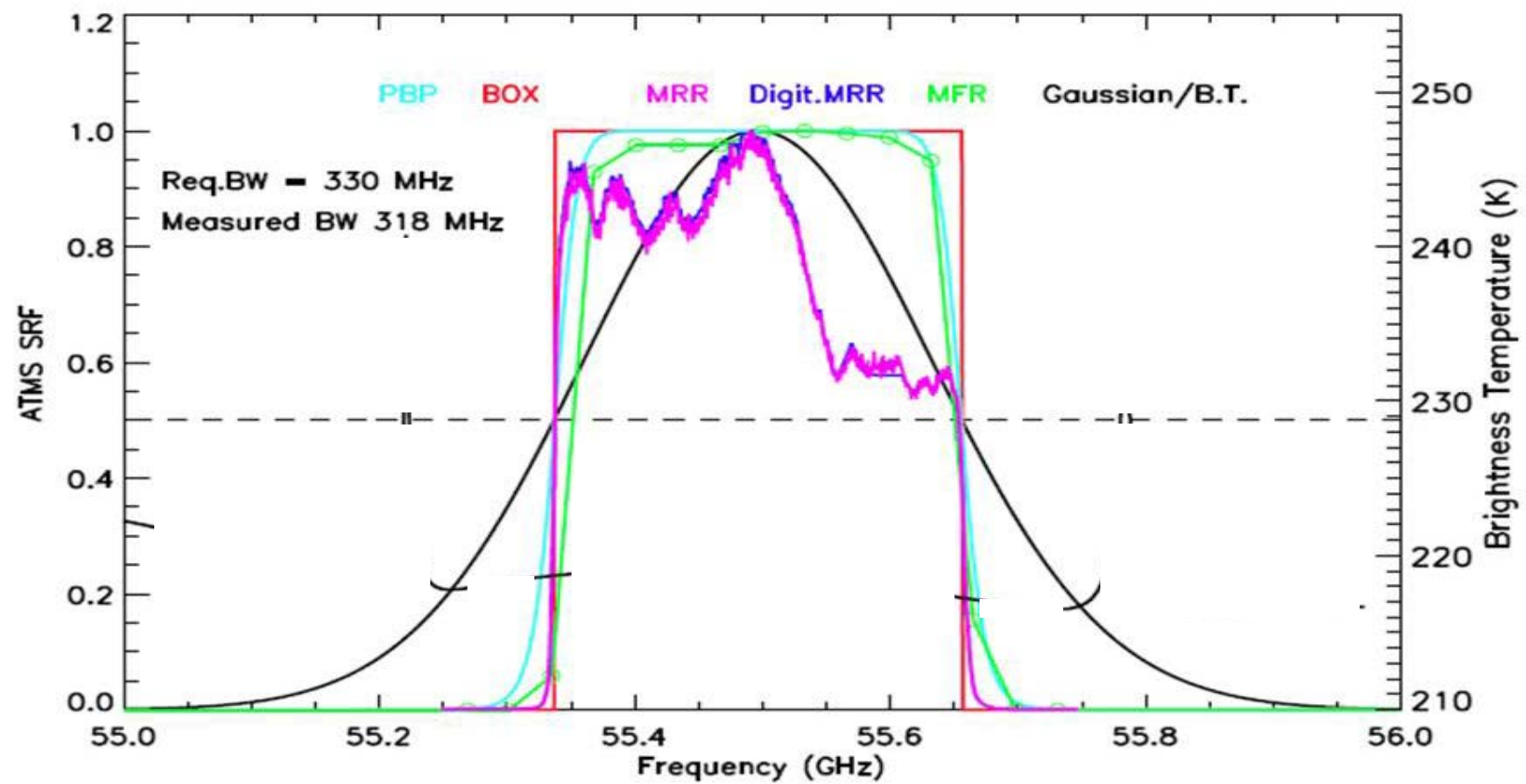
Modifications Made to J1 ATMS

- J1+ deliverables changed to require data in consistent digital form
- J1 SRF data were taken during TVAC 1, and will be available to NWP community



Spectral Response Functions

NORTHROP GRUMMAN



Ideal SRF (BOX) is in red. , The Perfect (electronically achievable) SRF (PBP) is in light blue. S-NPP measured filter response (MFR) and measured receiver-level SRF (MRR) are in green and purple, respectively. A Gaussian filter function with the is in black.



Summary of Example Modifications to J1 ATMS



- Scan drive
 - Bearing design changed to address wear out risk
- Striping
 - Discovered too late to change J1 hardware
 - Use same algorithm adjustment as on S-NPP
 - Additional ground characterization (stares)
 - Also requested on-orbit stares & deep space viewing maneuvers
- Antenna characterization
 - Improved antenna measurement facility & methodology
 - Particularly benefits G-band
- Reflector emissivity
 - Too late to change J1 hardware
 - Use same algorithm adjustment as on S-NPP
- Spectral Response Functions
 - Digital, consistent
 - Otherwise same measurement approach as for S-NPP

Examples only;
Not a complete list



J1 Prelaunch Testing **before today** NORTHROP GRUMMAN



- Prelaunch testing/measurements began Oct 2012
- Environmental tests began May 2013
- TVAC “round 1” began Feb 2014
- Many performance measurements were fine, but
- Significant issues were found
- Decision made Jun 2014 to halt prelaunch testing & perform re-work
- Additional issues were found during re-work
- Eventually 20 of 22 channels were re-worked
- Not all parts of instrument were affected
 - Antenna subsystem not part of re-work
 - Antenna characterization considered complete



J1 ATMS Prelaunch Testing 2015

NORTHROP GRUMMAN



- Pre-Environmental Review (delta-TRR) to perform “regression” testing (repeat TVAC & other environmental tests) was held Aug 19, 2015; **result: go ahead**
- Vibration regression testing successfully **completed**
- EMI/EMC regression testing occurring **this week**
- Regression TVAC (“round 2”) to begin early Sept
- TVAC round 2 should conclude in mid-Oct
- Post-TVAC regression testing through end of Oct
- Pre-ship review in early Nov
- J1 ATMS on J1 spacecraft by Dec



Summary of ATMS Status

NORTHROP GRUMMAN



- S-NPP flight unit status
 - Post-launch validation activities have confirmed S-NPP ATMS is meeting or exceeding its performance specifications (see papers in S-NPP special issue of JGR)
 - On-orbit testing of scan drive mitigation (reversals) is in progress
- J1 flight unit status
 - just completed 1 year of re-work, and begun environmental re-testing
 - If environmentals are problem-free, J1 unit installs on s/c in Nov
 - J1 observatory-level tests partly done using EDU as stand-in
 - J1 observatory-level TVAC probably in early CY2016
 - If those tests stay on schedule, then launch date is looking good
- J2 flight unit status
- procurements have begun

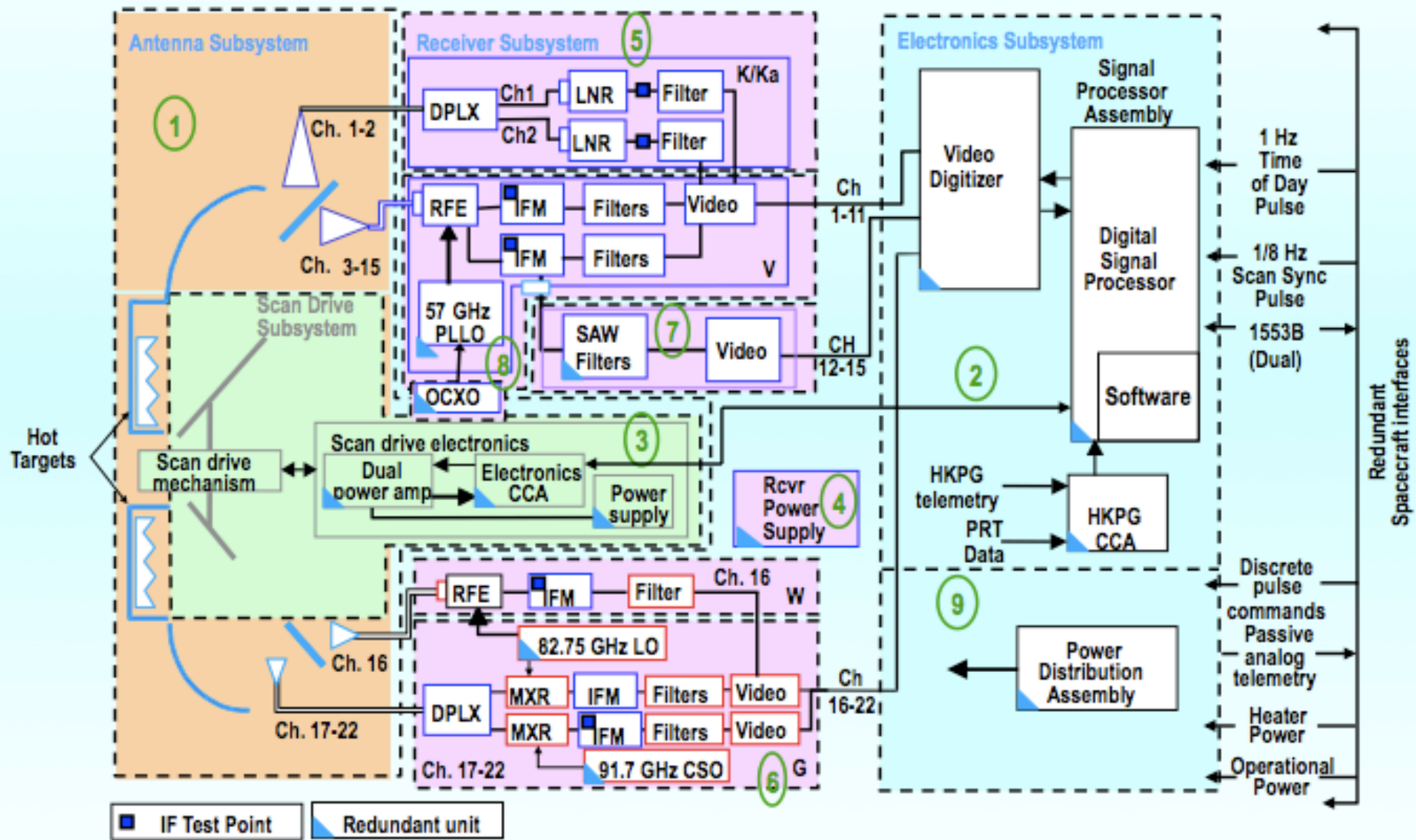


BACKUP



ATMS System Diagram

NORTHROP GRUMMAN





Spectral Differences: ATMS vs. AMSU/MHS

NORTHROP GRUMMAN



Left: AMSU/
MHS

Right: ATMS

AMSU-A

MHS

Ch	GHz	Pol	Ch	GHz	Pol
1	23.8	QV	1	23.8	QV
2	31.399	QV	2	31.4	QV
3	50.299	QV	3	50.3	QH
			4	51.76	QH
4	52.8	QV	5	52.8	QH
5	53.595 ± 0.115	QH	6	53.596 ± 0.115	QH
6	54.4	QH	7	54.4	QH
7	54.94	QV	8	54.94	QH
8	55.5	QH	9	55.5	QH
9	fo = 57.29	QH	10	fo = 57.29	QH
10	fo ± 0.217	QH	11	fo ± 0.3222 ± 0.217	QH
11	fo ± 0.3222 ± 0.048	QH	12	fo ± 0.3222 ± 0.048	QH
12	fo ± 0.3222 ± 0.022	QH	13	fo ± 0.3222 ± 0.022	QH
13	fo ± 0.3222 ± 0.010	QH	14	fo ± 0.3222 ± 0.010	QH
14	fo ± 0.3222 ± 0.0045	QH	15	fo ± 0.3222 ± 0.0045	QH
15	89.0	QV			
16	89.0	QV	16	88.2	QV
17	157.0	QV	17	165.5	QH
18	183.31 ± 1	QH	18	183.31 ± 7	QH
19	183.31 ± 3	QH	19	183.31 ± 4.5	QH
20	191.31	QV	20	183.31 ± 3	QH
			21	183.31 ± 1.8	QH
			22	183.31 ± 1	QH

ATMS has 22 channels and AMSU/MHS have 20, with polarization differences between some channels

- QV = Quasi-vertical; polarization vector is parallel to the scan plane at nadir
- QH = Quasi-horizontal; polarization vector is perpendicular to the scan plane at nadir

■	Exact match to AMSU/MHS
■	Only Polarization different
■	Unique Passband
■	Unique Passband, and Pol. different from closest AMSU/MHS channels

ATMS Full Radiance Calibration (FRC) Implementation and Validation

Hu(Tiger) Yang, Ninghai Sun, Miao Tian, Wanchun Chen, Lin Lin,

Xiaolei Zou, Fuzhong Weng

STAR ATMS SDR Team

August 26, 2015

Outline

- Introduction of ATMS FRC equations
- Implementation of FRC in ADL
- Test of FRC in ADL
- Validation of FRC TDR
- Summary and future work

ATMS Radiance Calibration Equations

The scene radiance is derived as the sum of linear part and nonlinear part:

$$R_b = R_{b,l} + Q_b$$

where the linear term is

$$R_{b,l} = R_w + G_b^{-1}(C_s - C_w)$$

$$G_b = \frac{C_w - C_c}{R_w - R_c}$$

And nonlinear term is

$$Q_b = \mu G_b^{-2}(C_s - C_w)(C_s - C_c) = \mu(R_w - R_c)^2 x(x-1)$$

$$x = \frac{C_s - C_c}{C_w - C_c}$$

Using Taylor expansion for $f(x) = x(x-1)$ at $x_0=0.5$, Nonlinearity term can be expressed as function of the maximum nonlinearity:

$$Q_b = Q^{\max} [4 \cdot (x - 0.5)^2 - 1]$$

$$Q^{\max} = \frac{1}{4} \cdot \mu \cdot (R_w - R_c)^2$$

“ μ ” is a function of instrument temperature and can be determined from TVAC test

$$\mu = aT^2 + bT + c$$

Implementation of Radiance Calibration in ADL

- The spectral radiance of cold end is determined at side lobe corrected cosmic background temperature of 2.73K
- The spectral radiance of warm target radiance is calculated at bias corrected warm load temperature
- Compute calibration gain in radiance, by which the linear part of scene radiance can be derived
- Calculate “mu” parameter from receiver temperature (in °C), from which the maximum nonlinearity Q^{\max} can be derived
- Derive the nonlinear part of scene radiance from Q^{\max} , find the calibrated scene radiance from sum of linear and nonlinear part
- Transfer spectral scene radiance back to brightness temperature by inverse Planck function

ADL Test Environment

Package:

ADL 4.2 with MX 8.8

Version 1: Nonlinearity coefficients derived from temperature

Version 2: Nonlinearity coefficients derived from radiance

Data Ingested:

S-NPP RDR data on April 7, 2015

Output Data:

- TDR/SDR/GEO using full radiance calibration (FRC) algorithm

Validation Provided:

FRC TDR – IDPS TDR

FRC TDR-RTM bias (with ECMWF forecasts as model inputs) by channels

- Global mean
- Global distribution
- Angler dependence

FRC TDR-RTM bias (with GPS-RO as model inputs) for channel 6 to 13

- Global mean

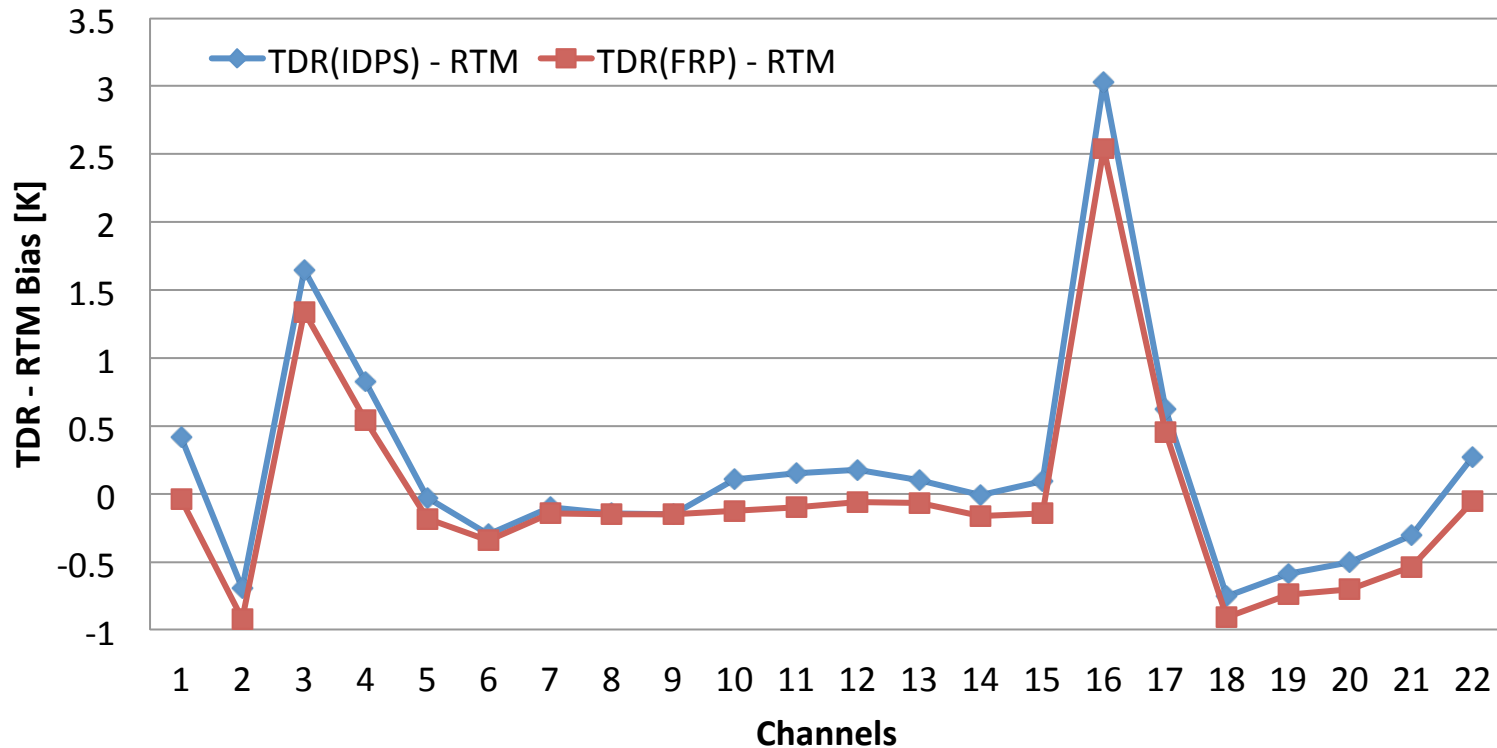
Validation by RTM Simulation- Using ECMWF Forecast Data

- One day ATMS observations are obtained to compare with CRTM simulations using ECMWF analysis forecast data
- Channels 1-6, and 16-22 are over ocean between 55°S to 55°N and cloud liquid water path is less than 0.08 kg/m² to remove water cloud
- Only FOVs 43~58 were used to get global mean

Global Mean TDR-RTM Bias

- Calibrated scene temperature from ADL-Full radiance are consistently lower than IDPS at all ATMS channels
- Major cause of the difference is due to the incorrect application of nonlinearity correction in IDPS

ATMS TDR-RTM Bias using FRP (Red) and using IDPS OPS (Blue)



Global Mean Bias Table

FRC: TDR from ADL with Full Radiance Calibration
RTM: RTM simulation

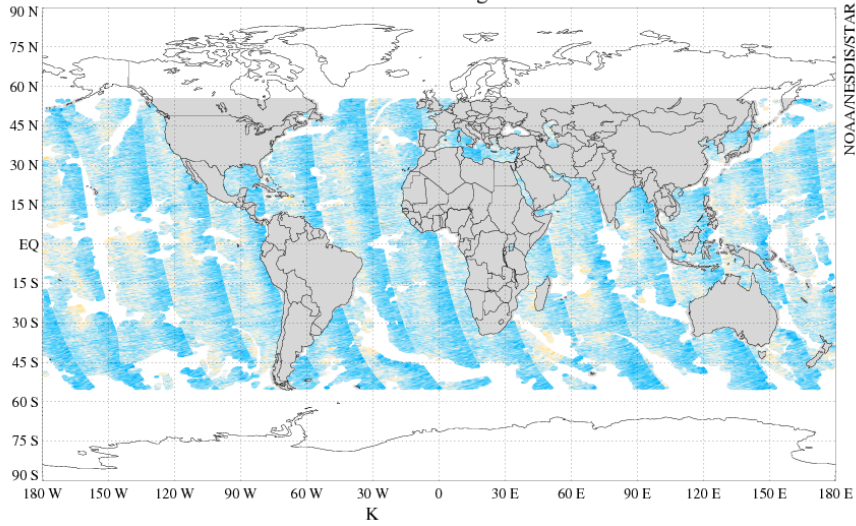
OPS: TDR from IDPS

Ch.	FRC-OPS	FRC-RTM	Ch.	FRC-OPS	FRC-RTM
1	-0.448	-0.039	12	-0.425	-0.057
2	-0.279	-0.923	13	-0.312	-0.069
3	-0.330	1.341	14	-0.243	-0.165
4	-0.352	0.546	15	-0.302	-0.14
5	-0.332	-0.184	16	-0.539	2.543
6	-0.269	-0.339	17	-0.366	0.452
7	-0.274	-0.142	18	-0.330	-0.905
8	-0.462	-0.151	19	-0.357	-0.743
9	-0.166	-0.149	20	-0.393	-0.702
10	-0.464	-0.123	21	-0.391	-0.532
11	-0.495	-0.099	22	-0.486	-0.052

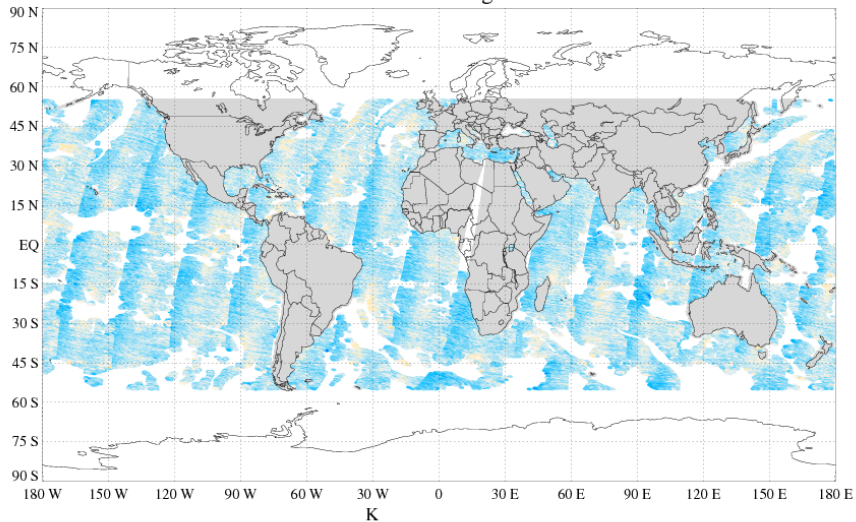
FRC TDR – RTM Global Distribution

Suomi NPP ATMS TDR Global [55°S - 55°N] Bias (FRP TDR - CRTM SIM)
Ch.6 53.596±0.115 GHz QH-POL 2015-04-07

Ascending

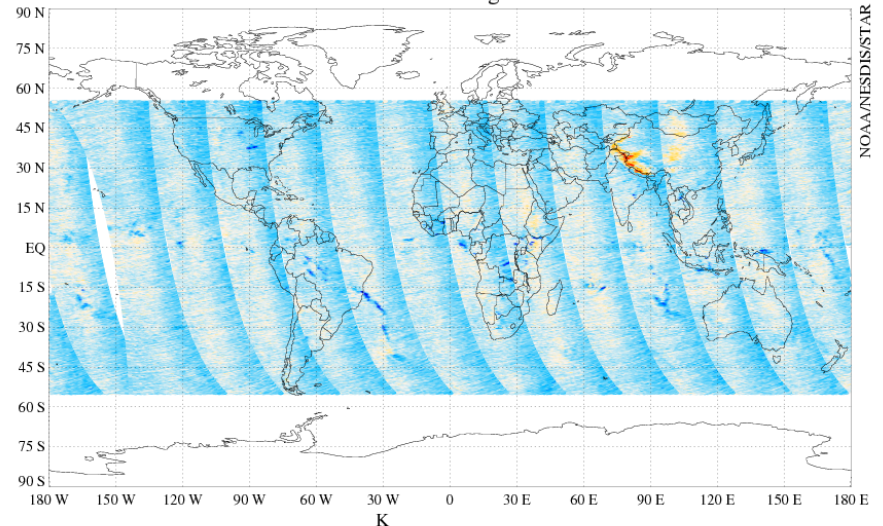


Descending

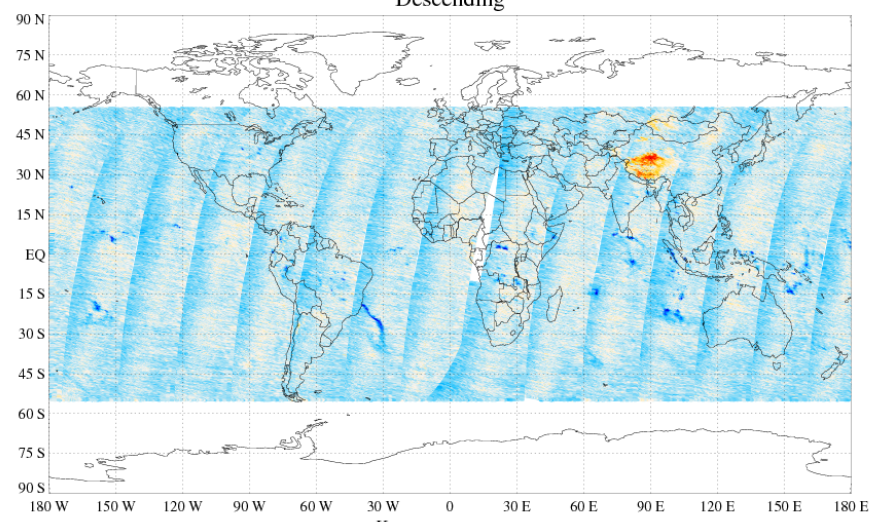


Suomi NPP ATMS TDR Global [55°S - 55°N] Bias (FRP TDR - CRTM SIM)
Ch.7 54.4 GHz QH-POL 2015-04-07

Ascending

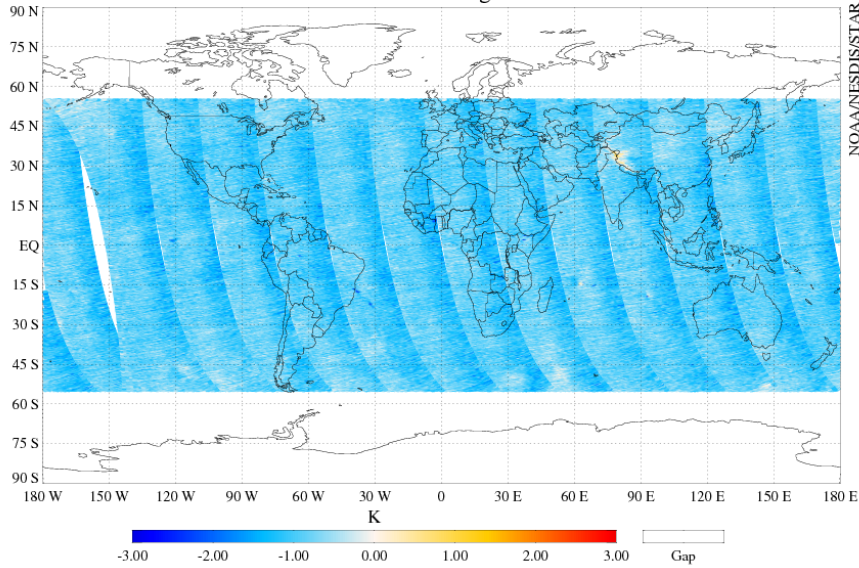


Descending

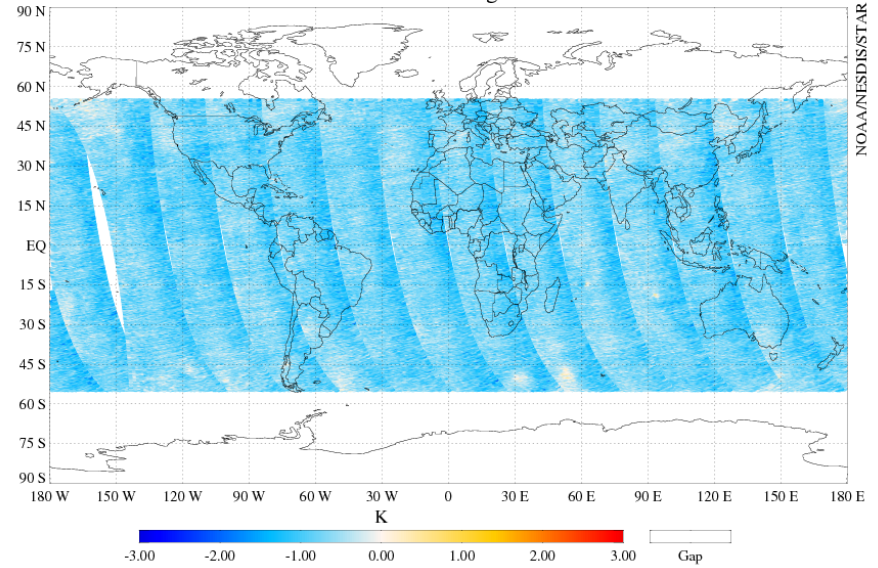


FRC TDR – RTM Global Distribution

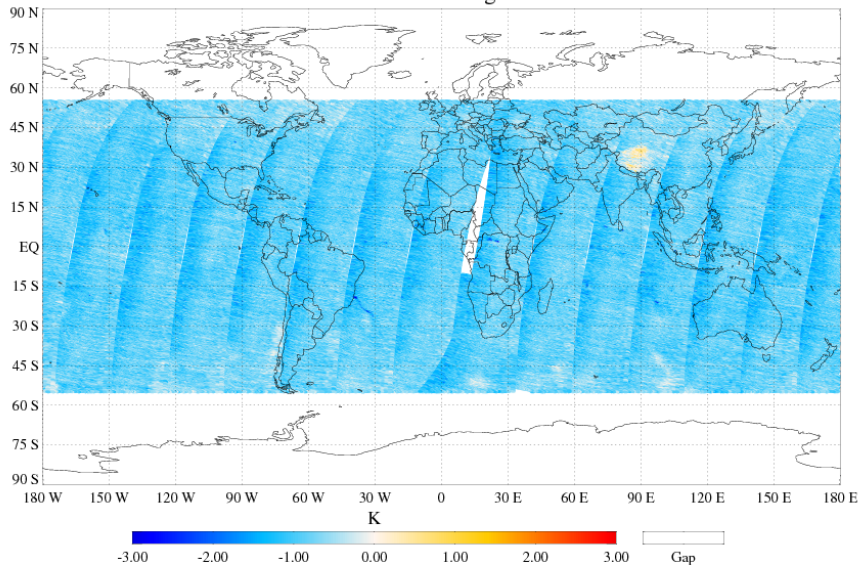
Suomi NPP ATMS TDR Global [55°S - 55°N] Bias (FRP TDR - CRTM SIM)
Ch.8 54.94 GHz QH-POL 2015-04-07
Ascending



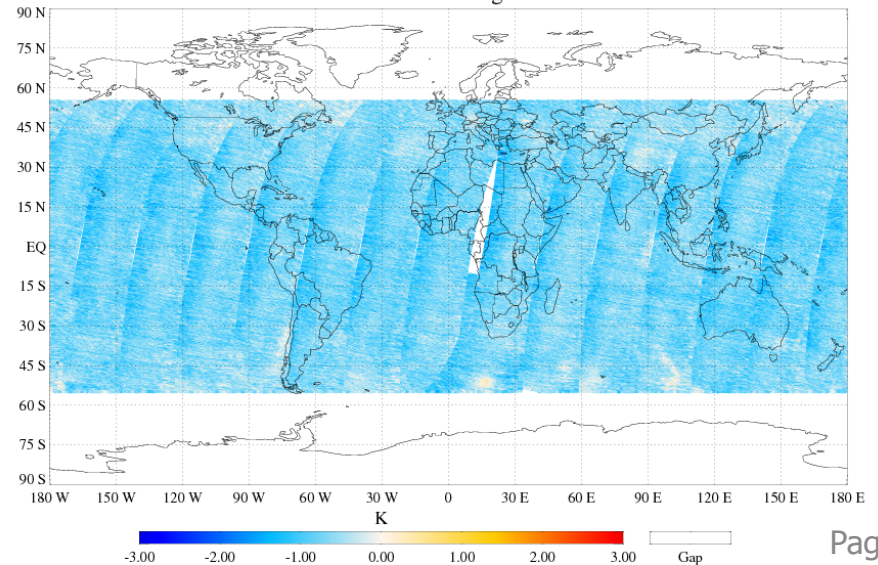
Suomi NPP ATMS TDR Global [55°S - 55°N] Bias (FRP TDR - CRTM SIM)
Ch.9 55.5 GHz QH-POL 2015-04-07
Ascending



Descending



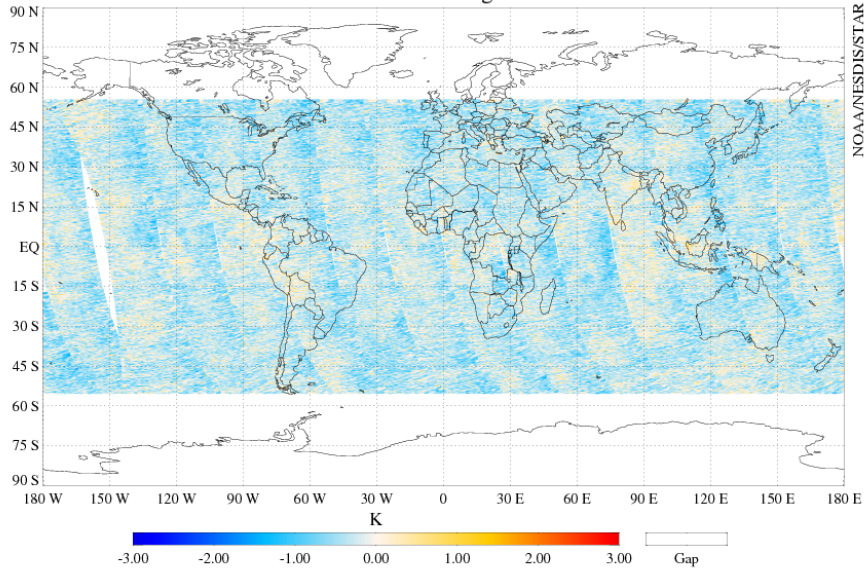
Descending



FRC TDR – RTM Global Distribution

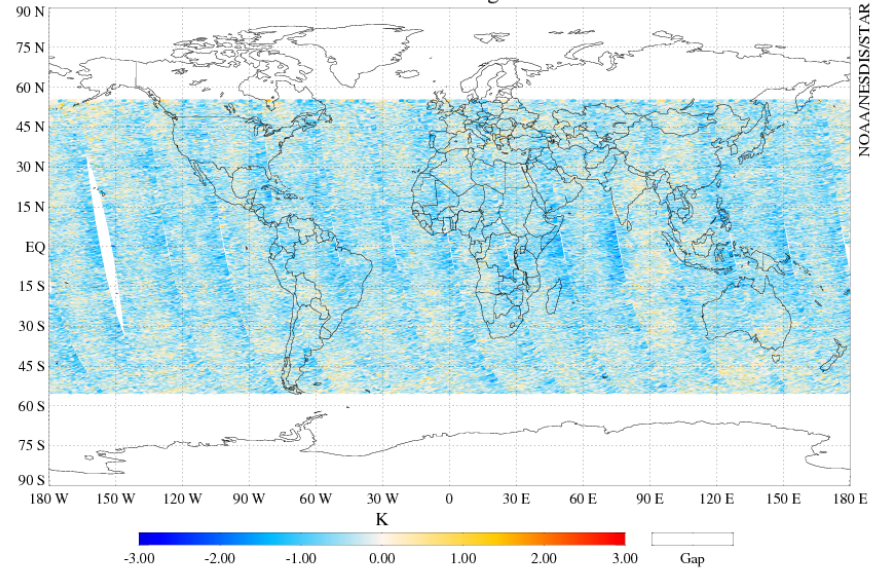
Suomi NPP ATMS TDR Global [55°S - 55°N] Bias (FRP TDR - CRTM SIM)
Ch.10 57.29034 GHz QH-POL 2015-04-07

Ascending

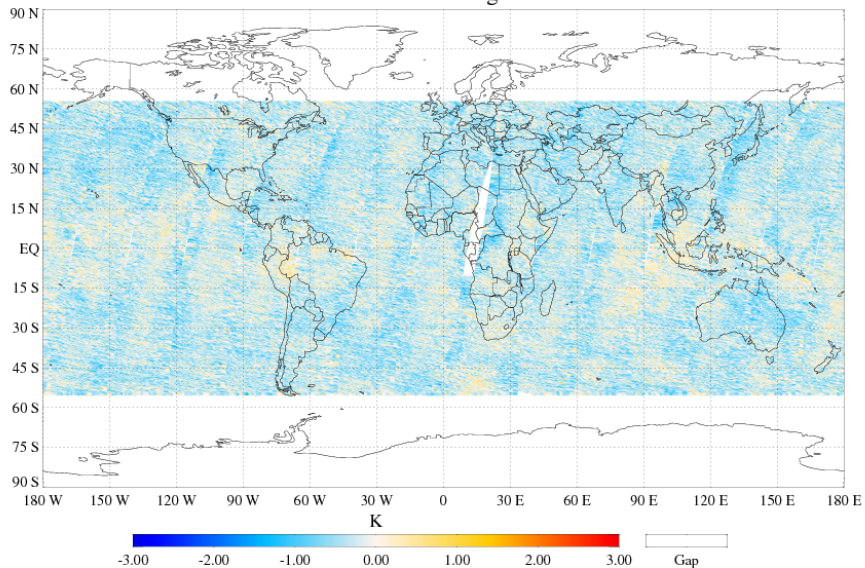


Suomi NPP ATMS TDR Global [55°S - 55°N] Bias (FRP TDR - CRTM SIM)
Ch.11 57.29034±0.217 GHz QH-POL 2015-04-07

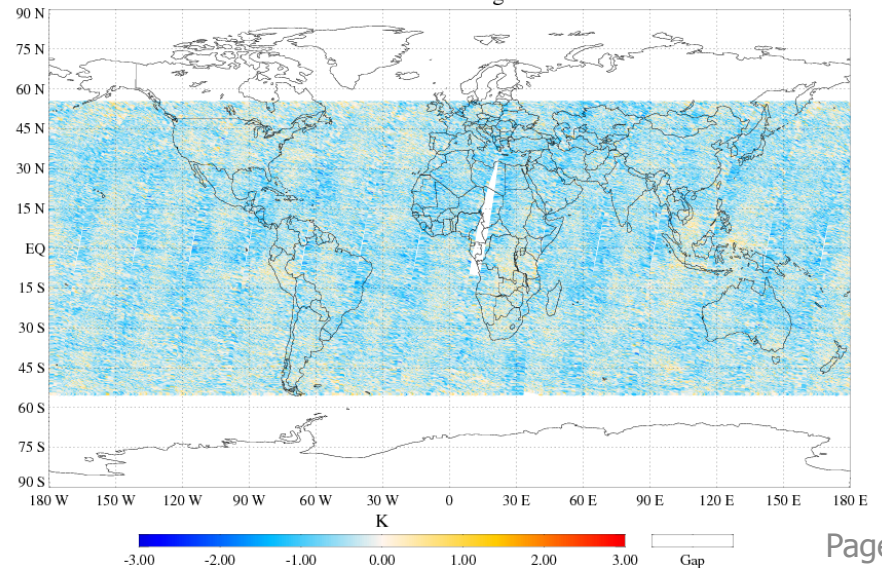
Ascending



Descending



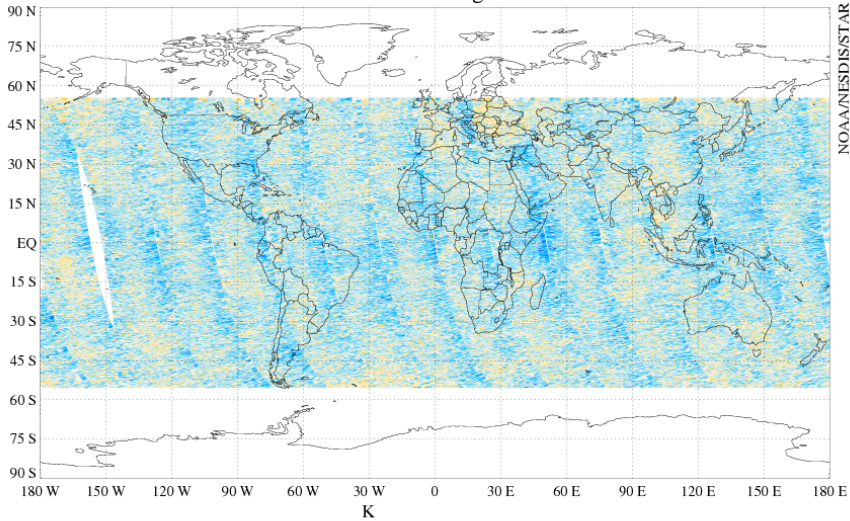
Descending



FRC TDR – RTM Global Distribution

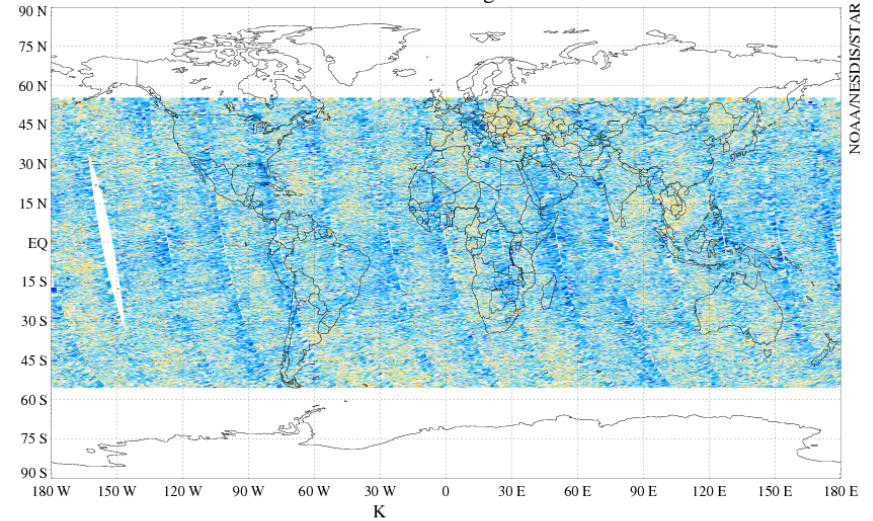
Suomi NPP ATMS TDR Global [55°S - 55°N] Bias (FRP TDR - CRTM SIM)
Ch.12 57.29034±0.3222±0.048 GHz QH-POL 2015-04-07

Ascending

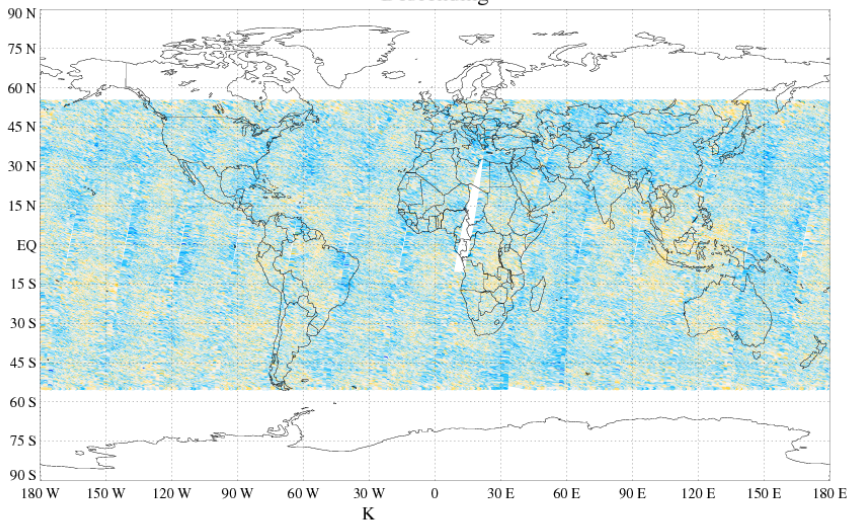


Suomi NPP ATMS TDR Global [55°S - 55°N] Bias (FRP TDR - CRTM SIM)
Ch.13 57.29034±0.3222±0.022 GHz QH-POL 2015-04-07

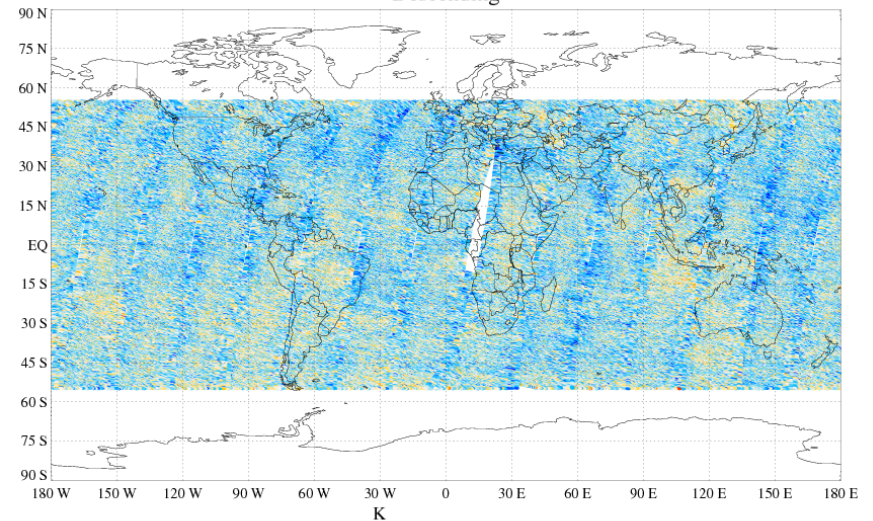
Ascending



Descending

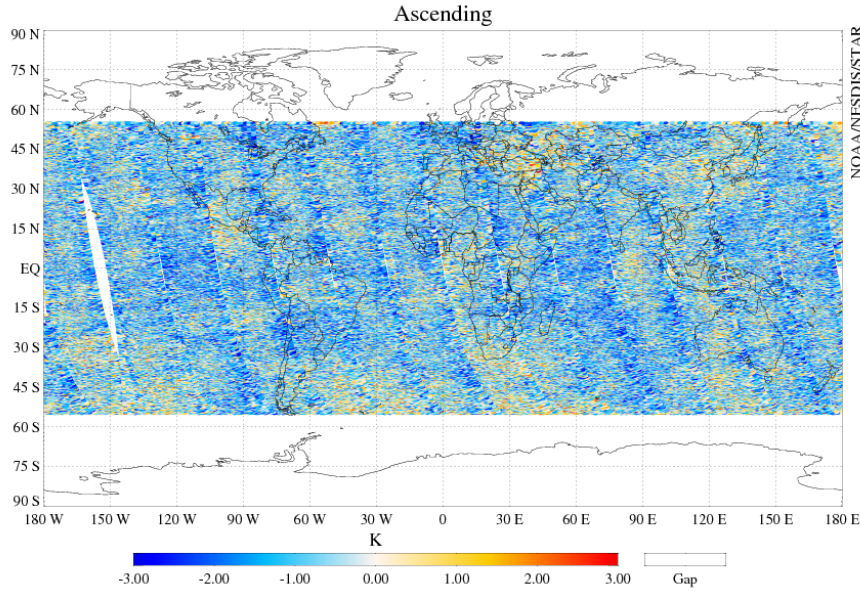


Descending

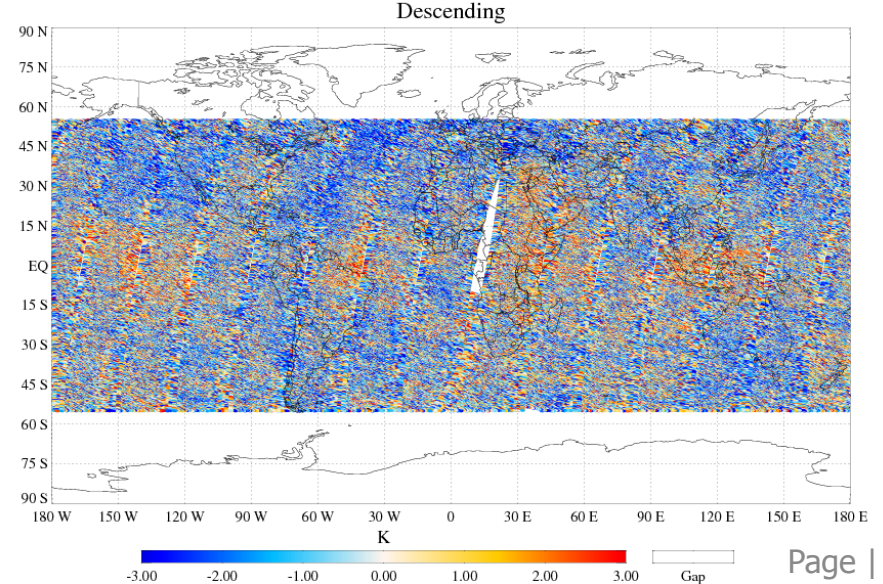
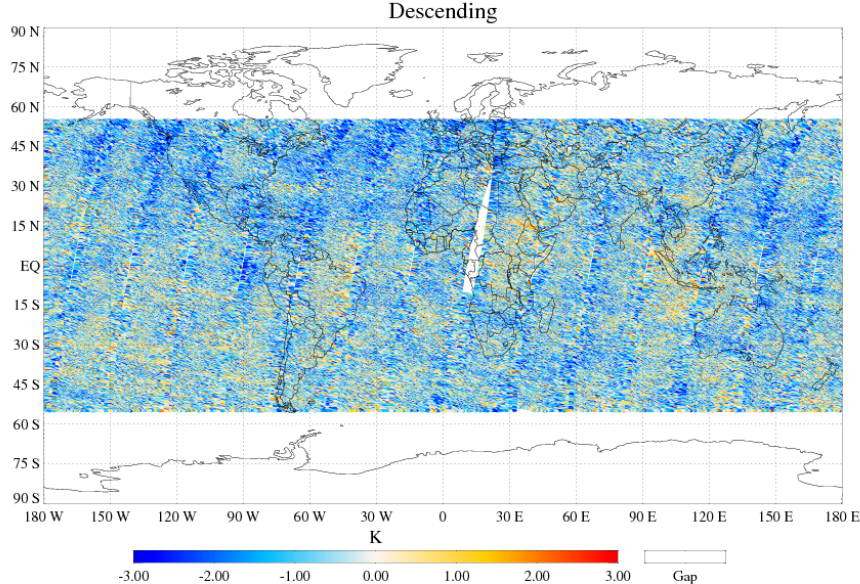
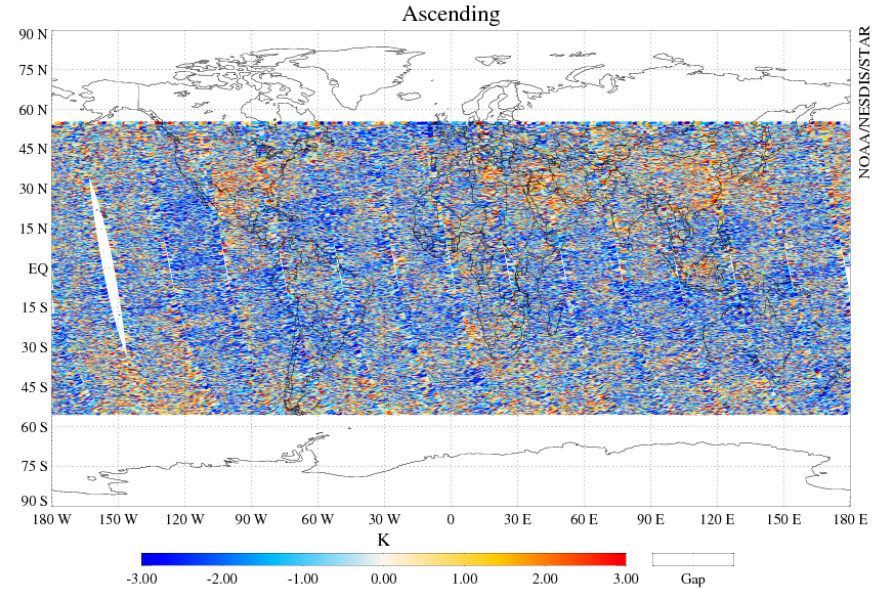


FRC TDR – RTM Global Distribution

Suomi NPP ATMS TDR Global [55°S - 55°N] Bias (FRP TDR - CRTM SIM)
Ch.14 57.29034±0.3222±0.010 GHz QH-POL 2015-04-07



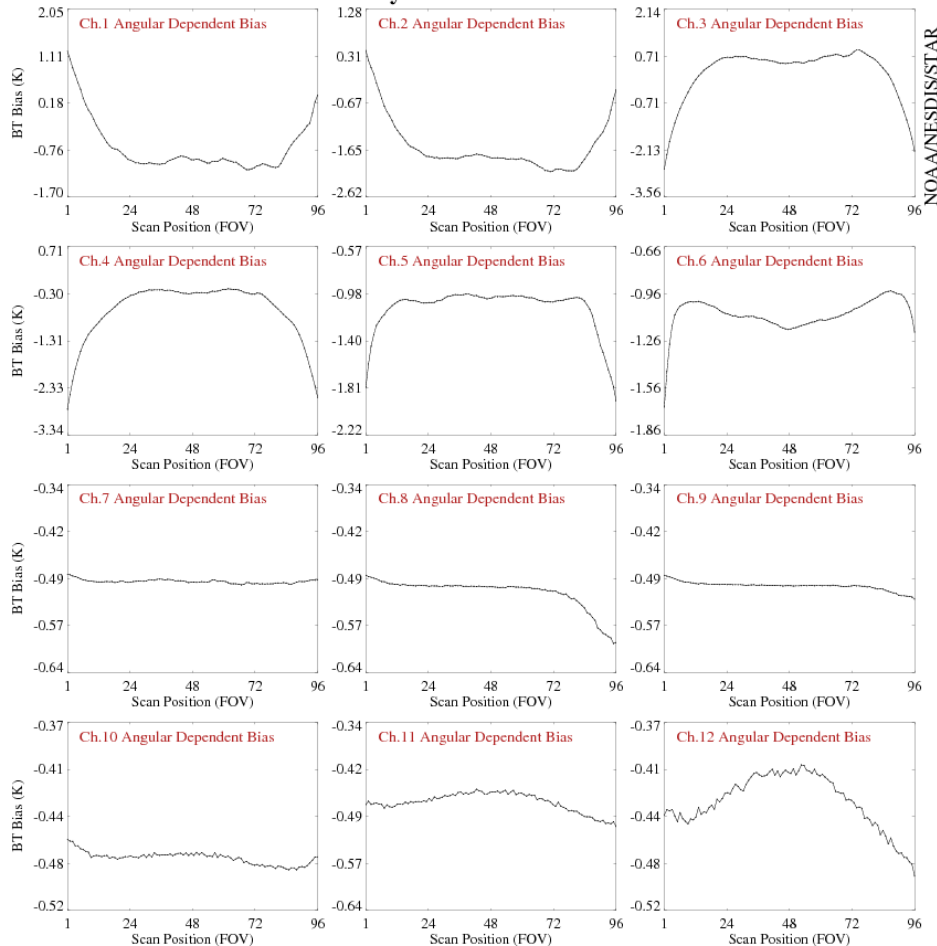
Suomi NPP ATMS TDR Global [55°S - 55°N] Bias (FRP TDR - CRTM SIM)
Ch.15 57.29034±0.3222±0.0045 GHz QH-POL 2015-04-07



FRC TDR – RTM Angular Dependent Bias

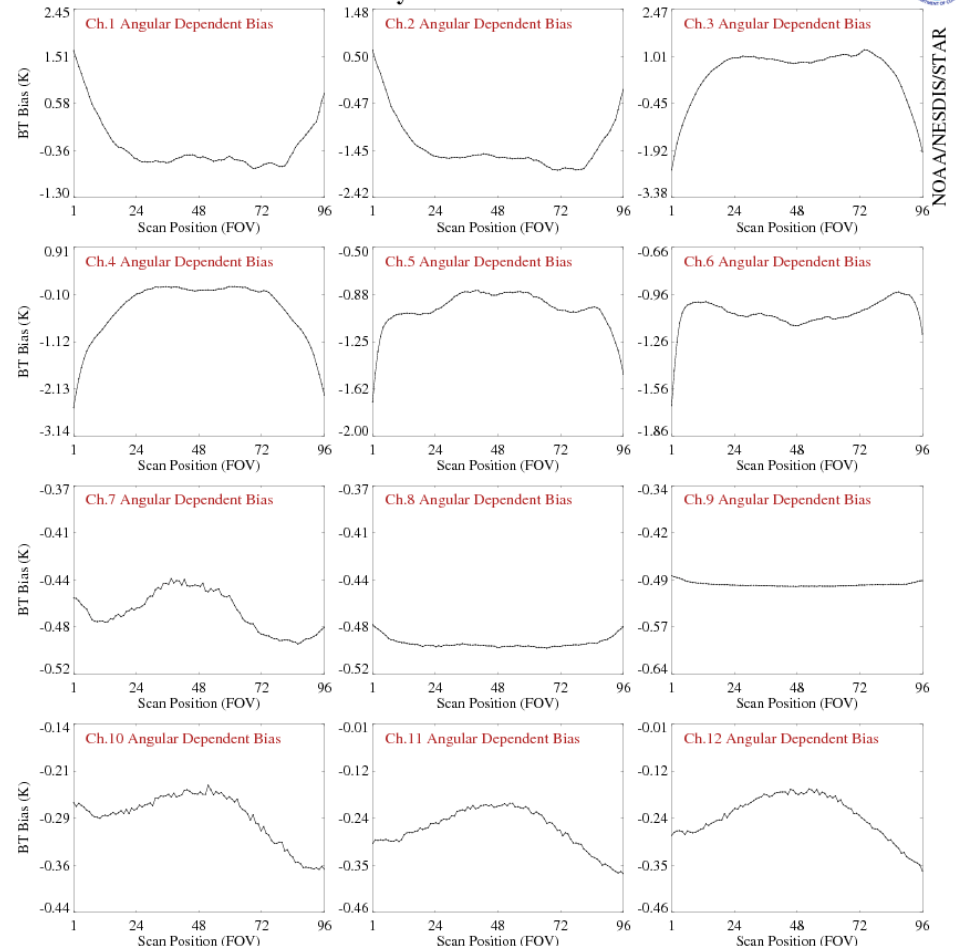
FRC TDR - RTM

Suomi NPP ATMS TDR Scan Angle Dependent Bias (FRP TDR - CRTM SIM)
Daily Mean on 2015-04-07



OPS TDR - RTM

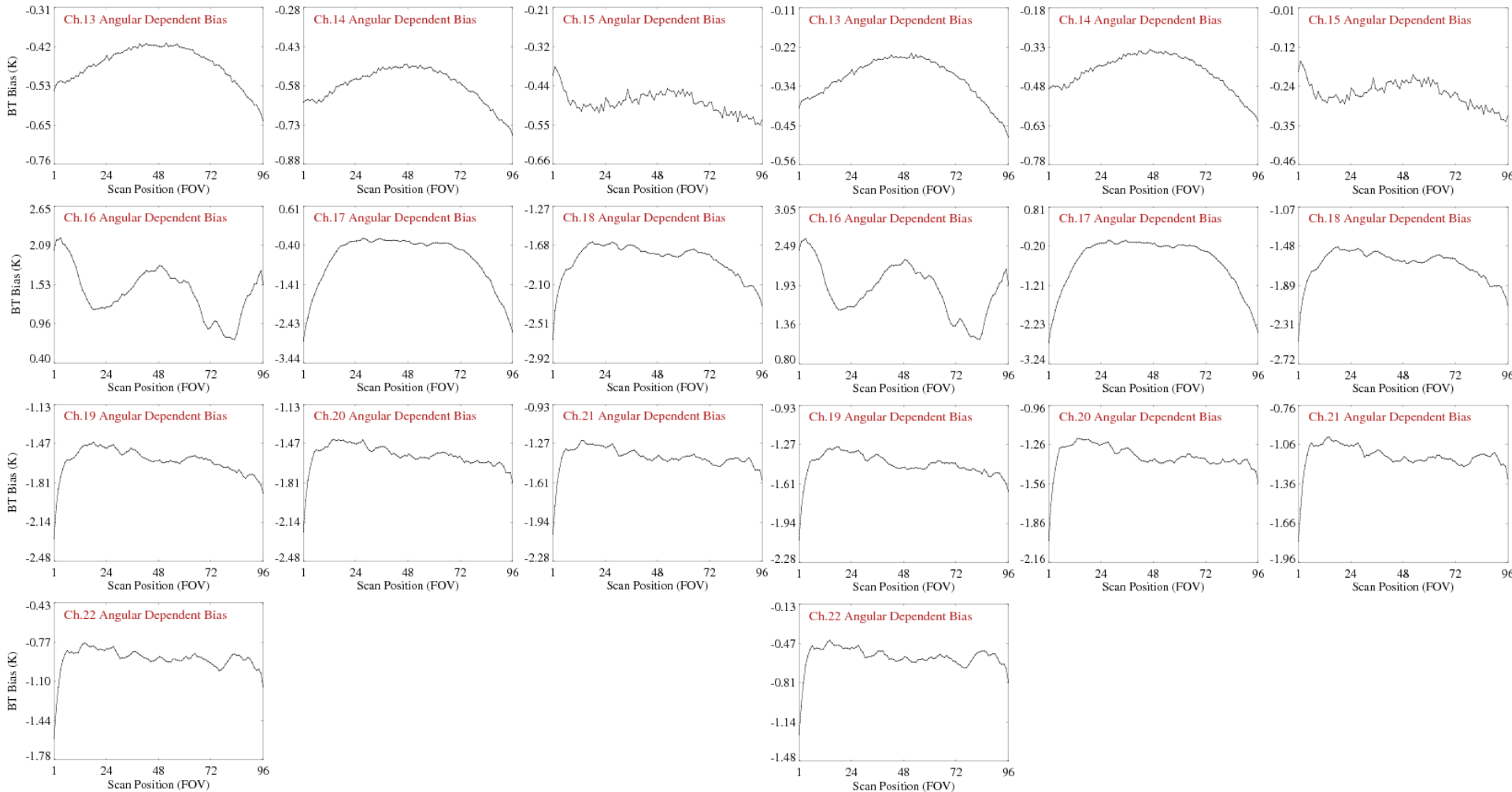
Suomi NPP ATMS TDR Scan Angle Dependent Bias (IDPS TDR - CRTM SIM)
Daily Mean on 2015-04-07



FRC TDR – RTM Angular Dependent Bias

FRC TDR - RTM

OPS TDR - RTM



Validation by RTM Simulation- Using GPS RO Data

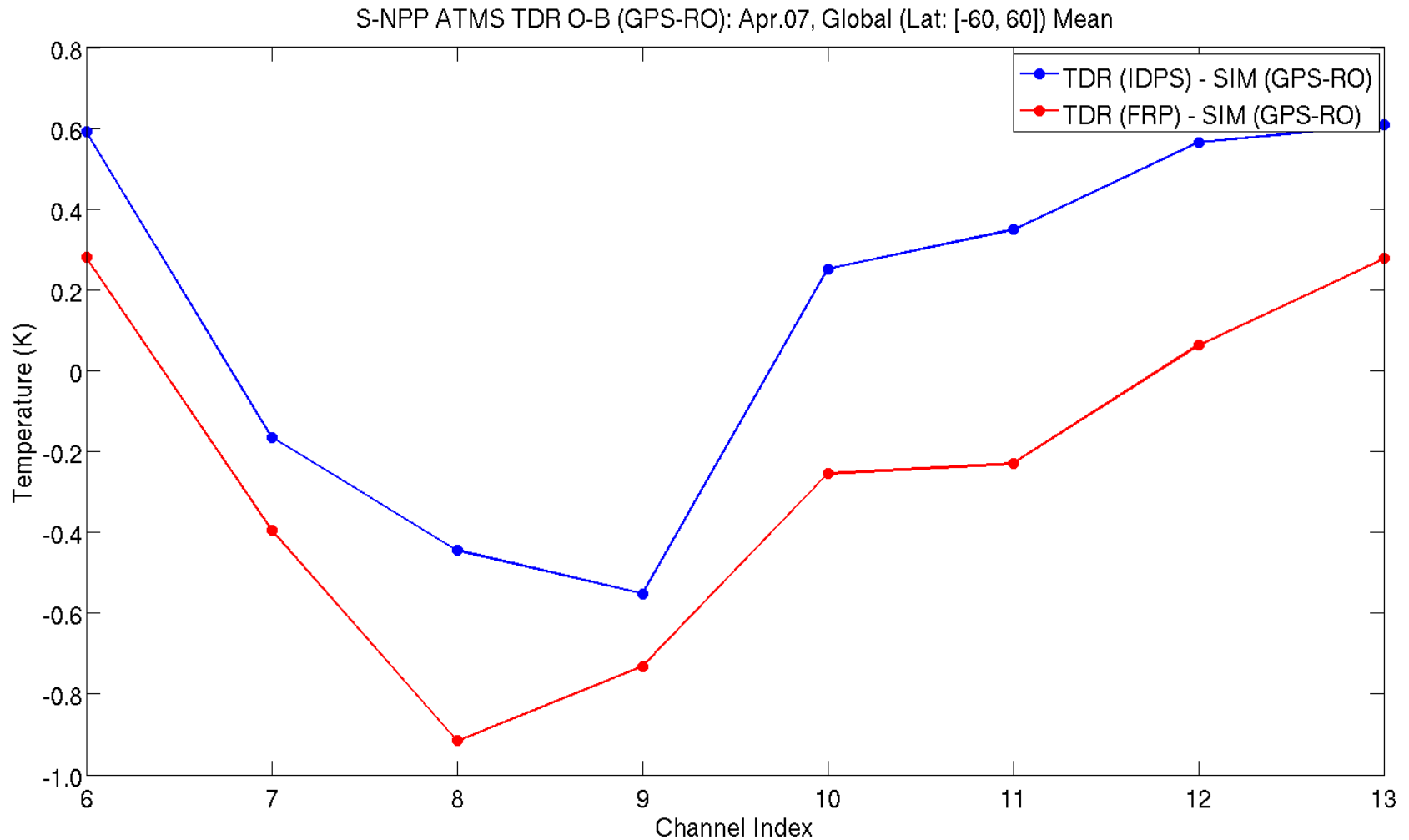
COSMIC (Constellation Observing System for Meteorology, Ionosphere, and Climate): real-time level 2 retrievals; ~1500 ROs daily

Collocation of ATMS and GPS Data:

- Temporal difference $< \pm 3$ hrs
- Spatial distance ≤ 50 km
- Use GPS RO geolocation at the altitude of maximum WF for spatial collocation

Global Mean TDR-RTM Bias

- Bias characteristic is consistent with those from ECMWF simulations
- Calibrated brightness temperature from FRP is lower than IDPS



Summary and Future Work

- Full radiance calibration processing of ATMS has been implemented in ADL software
- There is no interface change made to old ADL version, only some new parameters were added to PCT
- The output TDR products from ADL-Full Radiance are in brightness temperature
- Nonlinearity correction is based on “mu” parameter, which was derived in radiance space from TVAC datasets
- Validation results shows that the overall bias characteristic of TDRs from ADL-FRC is get improved compare with TDRs from IDPS
- Suggest to make ATMS full radiance calibration available in IDPS based on current ADL-Full radiance version
- Future work is to test and implement reflector emission correction algorithm in ADL-FRC for J-1 ATMS TDRs calibration



ATMS Algorithm Verification and Improvements to Reduce Radiometric Biases

**V. Leslie, B. Blackwell, M. DiLiberto, I. Osaretin, J.
Meyer, and M. Tolman (MIT LL)**

Kent Anderson (NGES)

2015 Annual Science Team Meeting

26 August 2015

College Park, MD



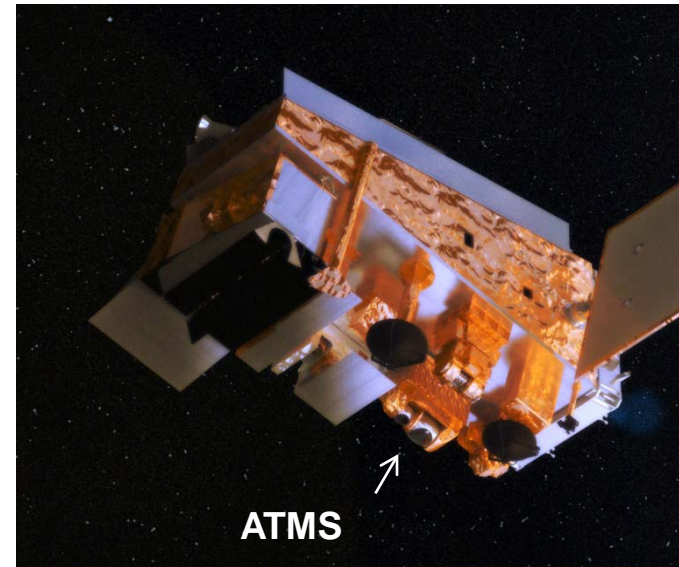
Outline

- **Update on the Flat Reflector Emissivity**
- **Icelandic S-NPP Aircraft Cal/Val Campaign**
- **Radiometric Environment Characterization**
- **On-orbit Single Events Upsets**
- **Future Work**



Pitchover Bias: Potential Explanations

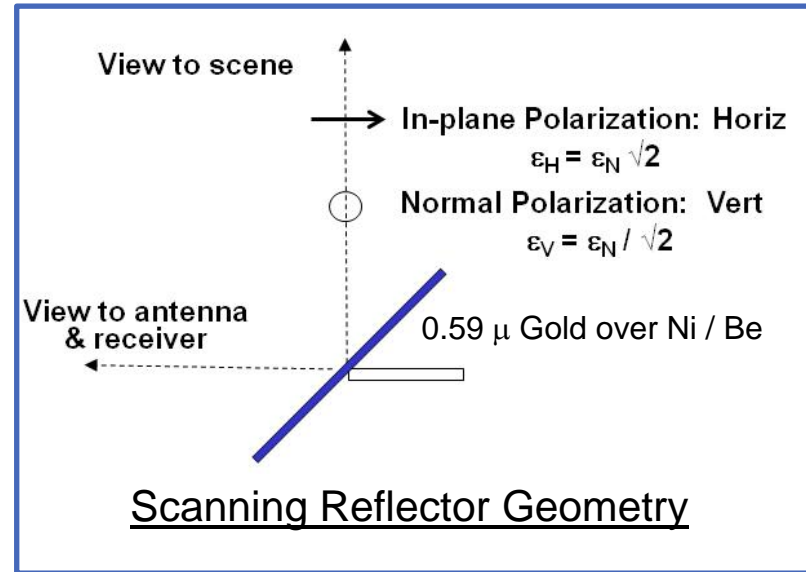
- With the Earthview sector viewing deep space, the radiometric scene is a homogenous and unpolarized source that fills the entire field of view of ATMS
- As an unpolarized scene, the polarization twist or cross-pol. impurity issues are not the primary explanation
- Alignment/pointing errors are unlikely due to strict subsystem quasi-optical alignment requirements that were verified during assembly
- Skimming or spillover is a possibility, but the bias symmetry is difficult to justify
- The bias asymmetry in the response is explained by near-field emission from the satellite, but the ATMS is positioned on the edge of the spacecraft, which doesn't justify the cosine or sine relationship





Potential Explanation: Flat Reflector Emissivity Model

- **ATMS scanning reflector is a gold-plated beryllium flat plate, oriented 45 degrees relative to the wavefront (a nickel layer bonds the two)**
- **Conductive gold surface is a thin layer composed of microcrystalline granules, the emissivity can exceed the theoretical (Hagen-Rubens) emissivity of a perfectly flat bulk material**
- **The layered and rough surface is difficult to accurately model or simulate**
- **Values of the two polarization components can be expressed in terms of the normal emissivity derived from the Fresnel equations for reflections from a plane interface**



Vertical and Horizontal brightness temperatures will be:

$$T_{BV} = \rho_V T_{SV} + \epsilon_V T_R$$

$$T_{BH} = \rho_H T_{SH} + \epsilon_H T_R$$

where : ρ_V = reflectivity of the reflector = $1 - \epsilon_V$,

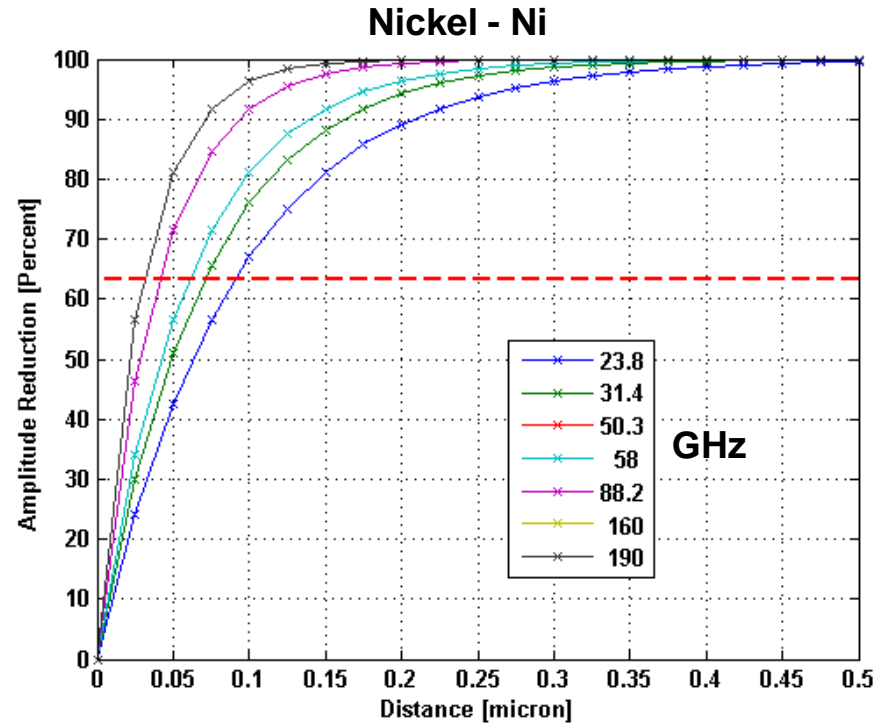
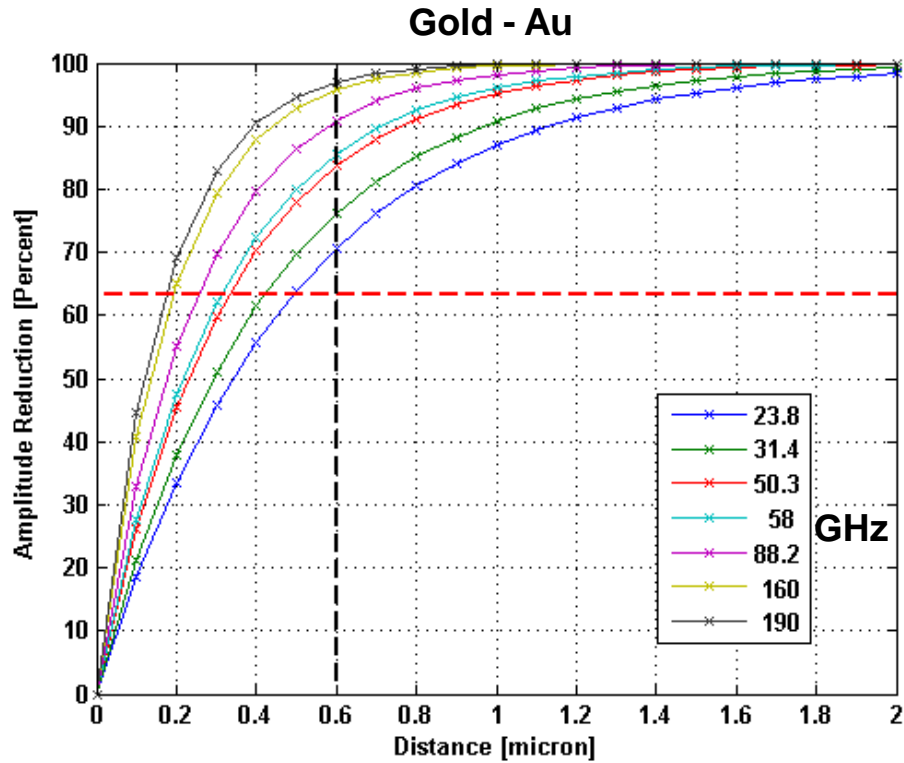
$T_{SV,SH}$ = brightness temperature of the scene, viewed by the reflector

T_R = physical temperature of the reflector

SV = Scene Vertical Pol.
SH = Scene Horiz. Pol.



Penetration Depth in Metal





Adding The Scanning Flat Reflector

When the reflector scans to an angle ϕ , the resulting Quasi-Vertical (QV) and Quasi-Horizontal (QH) outputs:

$$T_{QV} = T_{BV} \cos^2 \phi + T_{BH} \sin^2 \phi \quad \text{Substitute } T_{BV} \text{ and } T_{BH}$$

$$T_{QV} = T_{SV} \cos^2 \phi + T_{SH} \sin^2 \phi + \frac{\epsilon_N}{\sqrt{2}} [T_R + T_{SV} - 2T_{SH}] \sin^2 \phi + \frac{\epsilon_N}{\sqrt{2}} (T_R - T_{SV})$$

$$T_{QH} = T_{BV} \sin^2 \phi + T_{BH} \cos^2 \phi$$

$$T_{QH} = T_{SV} \sin^2 \phi + T_{SH} \cos^2 \phi + \frac{\epsilon_N}{\sqrt{2}} [T_R + T_{SV} - 2T_{SH}] \cos^2 \phi + \frac{\epsilon_N}{\sqrt{2}} (T_R - T_{SV})$$

For the case of an unpolarized ($T_{SH} = T_{SV} = T_{CS}$) scene, at T_{CS} :

$$T_{QV} = T_{CS} + \frac{\epsilon_N}{\sqrt{2}} [T_R - T_{CS}] \sin^2 \phi + \frac{\epsilon_N}{\sqrt{2}} (T_R - T_{CS})$$

$$T_{QH} = T_{CS} + \frac{\epsilon_N}{\sqrt{2}} [T_R - T_{CS}] \cos^2 \phi + \frac{\epsilon_N}{\sqrt{2}} (T_R - T_{CS})$$



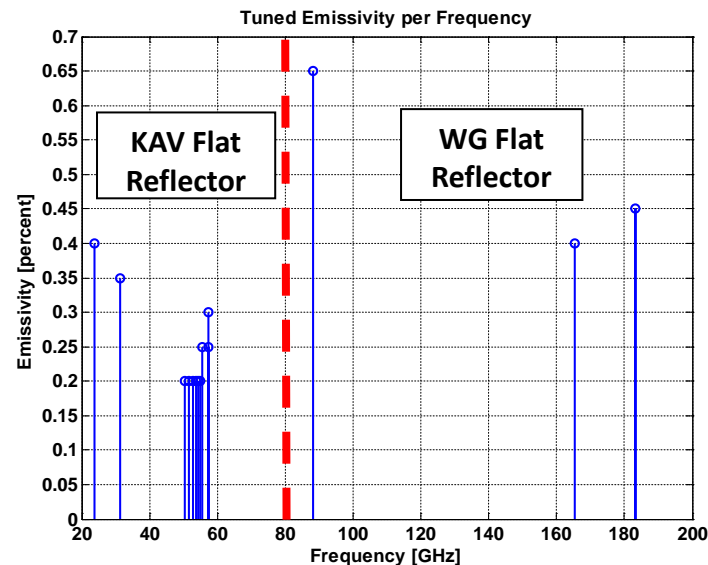
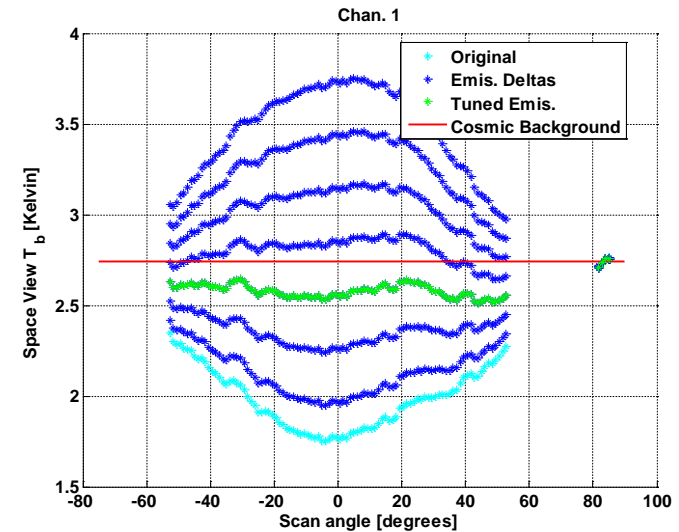
Emissivity Correction Parameters

- **First parameter is the physical temperature of the flat reflector**
 - There is no temperature sensor on the reflector, but there is on the Scan Drive Motor (SDM) and NGES has a thermal model to adjust the SDM temp. to a reflector temp.
 - Calibration algorithm is fairly insensitive to the reflector temperature (i.e., temp. is multiplied by the emissivity), which was confirmed by a rough sensitivity study
- **Second parameter is the normal emissivity for each band (or channel)**
 - Difficult to model or derive a theoretical equation
 - Three empirical methods were used to derive emissivity:
 - Used pitchover maneuver to “fit” a normal emissivity value to each channel
 - Derived from two precision calibration targets at similar temperatures but different angles during TVAC calibration
 - Measured the emissivity of flight-like spares (NGES)



On-orbit Derivation of the Normal Emissivity

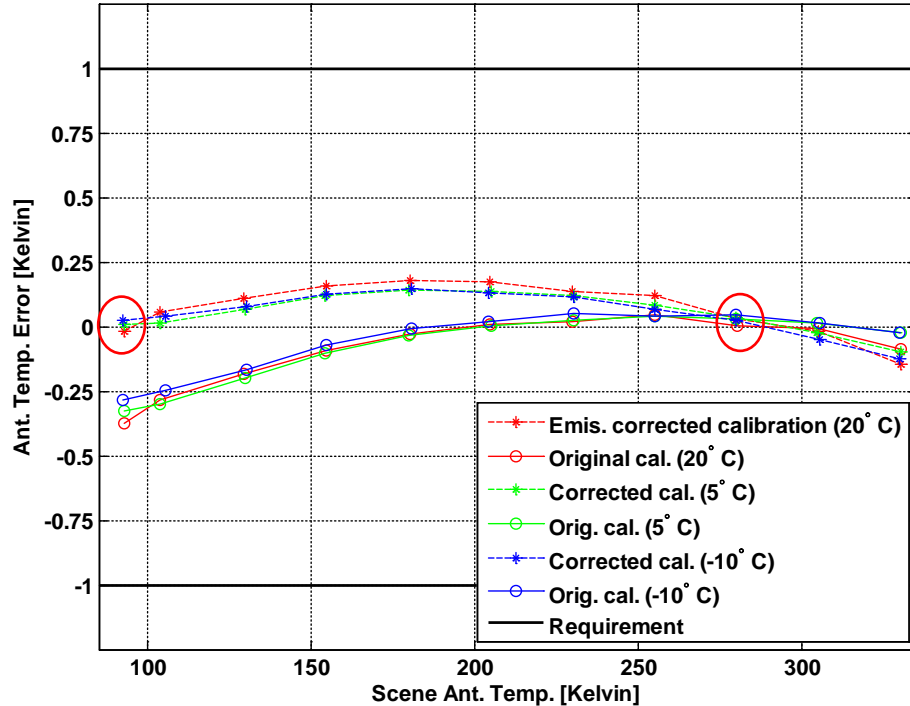
- Swept the normal emissivity in an emissivity-corrected calibration algorithm until the Earth View Sector during the pitchover was flat
- Top figure presents the radiometric EVS results of stepping the emissivity for Channel 1
 - Cyan: original uncorrected result
 - Blue: corrected results at various emissivity steps
 - Green: tuned emissivity that had the lowest EVS standard deviation metric
- Bottom plot gives the derived emissivity for each channel
 - K- and V-band flat reflector is on the left
 - W- and G-band flat reflector is on the right
 - Tuning method was not sensitive to emissivity steps less than 0.05%
- Derived emissivity explained TVAC calibration anomaly



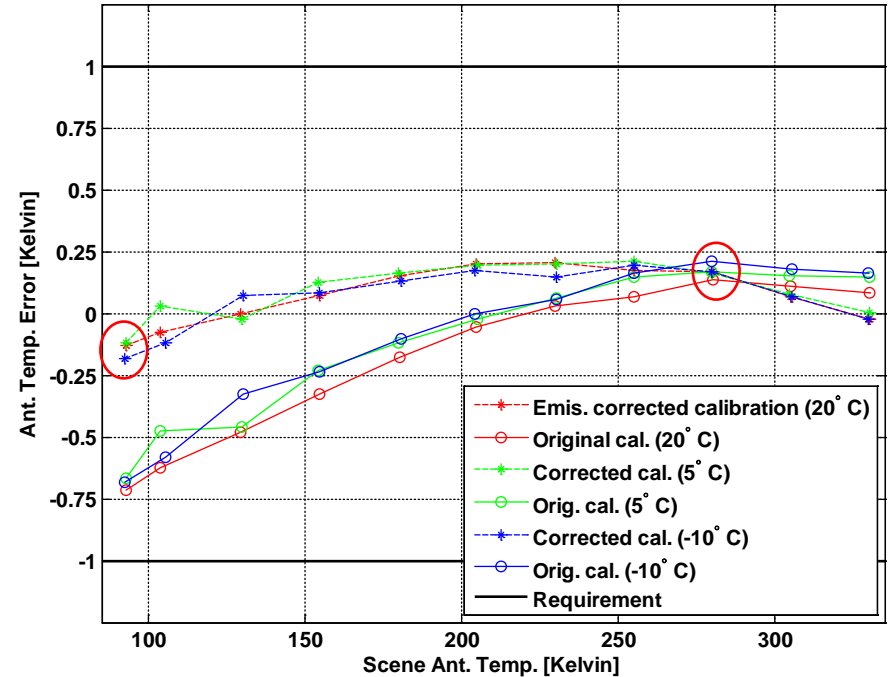


Applying Correction to Calibration Testing

Chan. 1 (23.8 GHz) PFM RC=1 (Side A)



Chan. 16 (87-91.9 GHz) PFM RC=1 (Side A)



- The error of quasi-V channels moved close to zero at the two calibration points
- V-band quasi-H channels also moved closer to zero

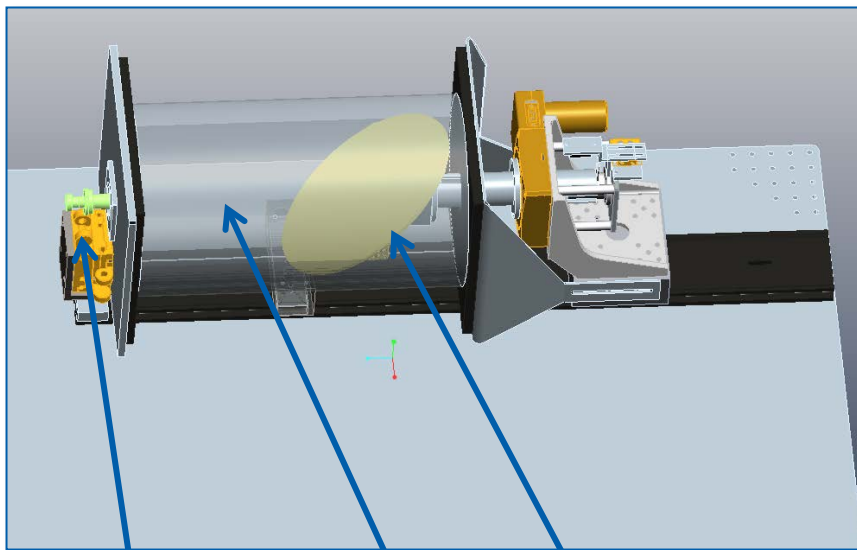


NGES Emissivity Measurement

- **NOAA/NASA asked NGES to measure the emissivity of the flight spare flat reflector to confirm on-orbit measurements**
- **NGES measured the emissivity of three flat reflectors:**
 - Spare flight reflector (Au/Ni/Be)
 - Bulk Aluminum (6061)
 - Stainless Steel (304)
- **Setup and more details coming up:**
 - Flight spare's emissivity trend across bands (i.e., frequency) was verified
 - Absolute values were different than on-orbit measurements
 - Analytical (i.e., Hagen-Rubens) values did not match

Special Test for Reflector Emissivity

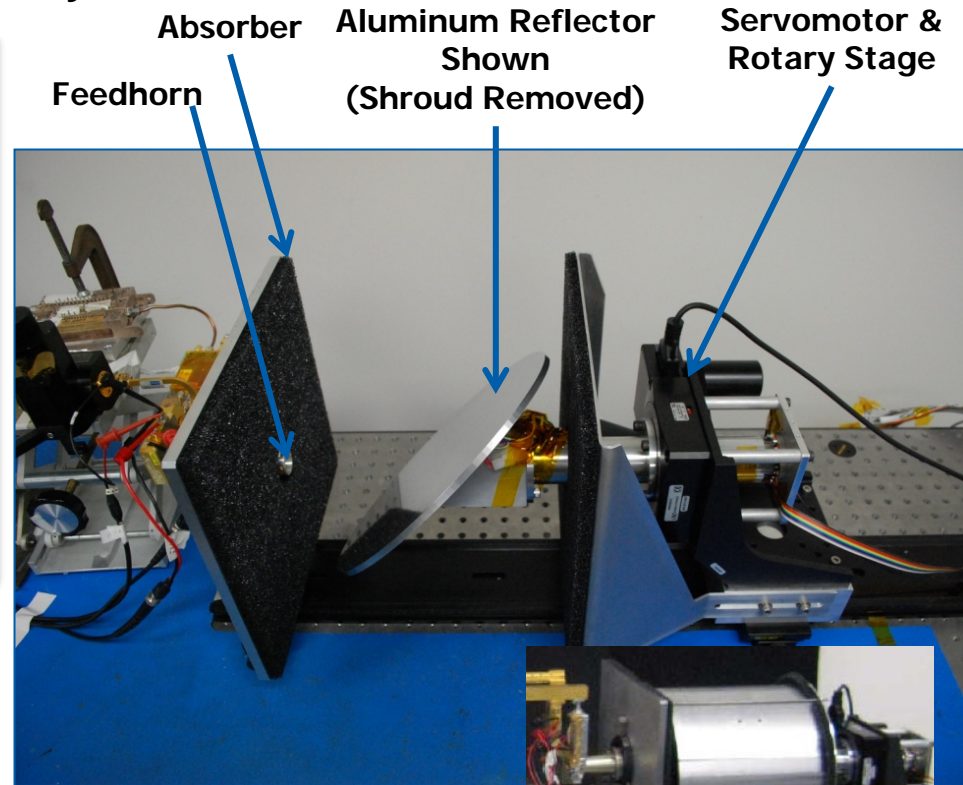
- A special test was performed using a spare flight reflector to make a direct measurement of its polarized emissivity
 - Reflector was heated to produce contrast between reflector emission and energy reflected from a blackbody shroud
 - Reflector rotated at constant rate (1 Hz) and data processing extracted the 2 Hz sinusoidal component due to emissivity



Feedhorn and mm-wave receiver

Shroud (Semi-transparent for illustration)

Beryllium Reflector Oriented 45° to Wavefront

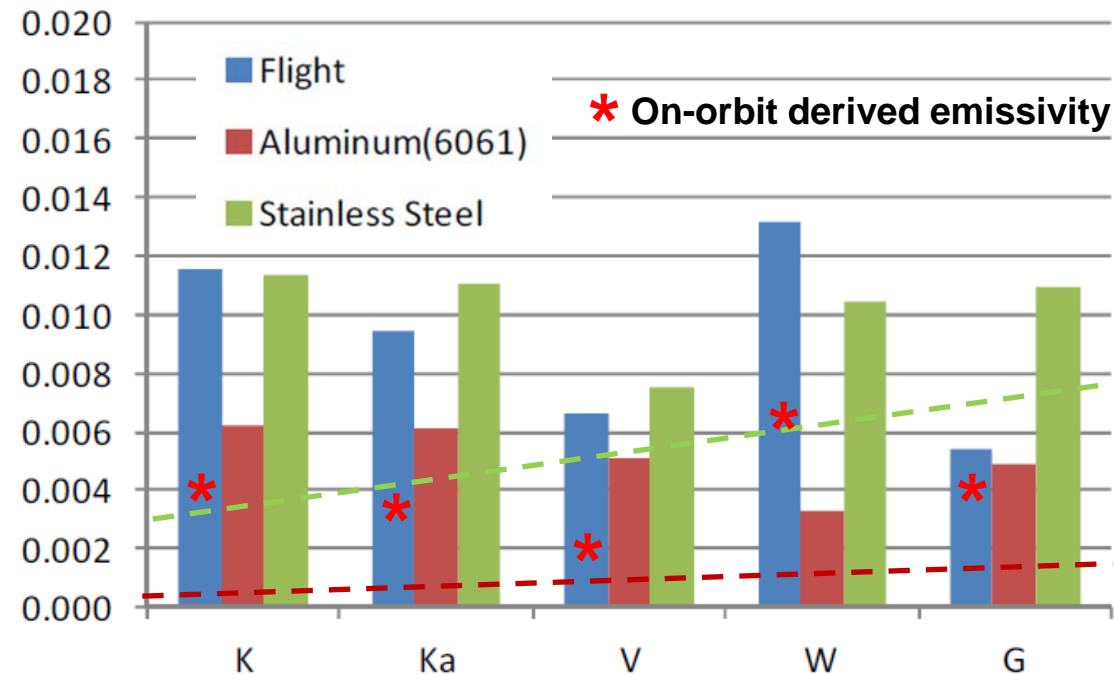


Kent Anderson (NGES)



NGES Test Results

Derived Normal Emissivity



Results:

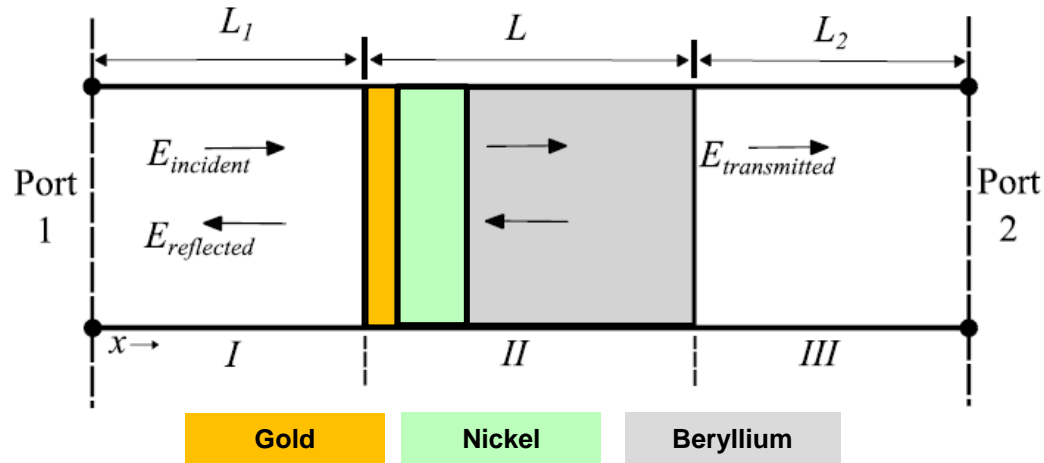
- Flight trend matches on-orbit trend
- No freq. trend with Al or SS
- SS is higher than Al

- Hagen-Rubens expects 2.8 times the emissivity between K and G-band
 - Smooth bulk Al = 0.0005 to 0.0015
 - Smooth bulk SS = 0.0027 to 0.0076
- Hagen-Rubens expects 5 times the emissivity between SS and Al



Simulating the Normal Emissivity

- Non-resonant characterization method using rectangular waveguide



- Numerical computation via HFSS FEA modeling
- Scattering parameters are obtained for waveguide
- Application of Nicolson-Ross-Weir Algorithm is used on computed S-parameters to obtain reflection coefficient
- HFSS Huray roughness model had 10 μm nodule radius and 2.9 Hall-Huray surface ratio



Simulated Emissivity Results for Aluminum and Stainless Steel (WIP)

% emissivity

Channel	Freq. (GHz)	Analytical Emissivity (Al)	Numerical Emissivity (Smooth Al)	Numerical Emissivity (Rough Al)	NGES Measured Al	Analytical Emissivity (SS)	Numerical Emissivity (Smooth SS)	Numerical Emissivity (Rough SS)	NGES Measured SS
1 (QV)	23.8	0.05464	0.054665	0.054666	0.622	0.27046	0.05652	0.05659	1.131
2 (QV)	31.4	0.06276	0.222123	0.222126	0.608	0.31066	0.22458	0.22468	1.102
3 (QH)	50.3	0.07944	0.043947	0.043950	0.514	0.39319	0.18071	0.66068	0.753
6 (QH)	53.59 6	0.08199	0.052666	0.052668		0.40586	0.20756	0.75451	
7 (QH)	54.4	0.08061	0.054264	0.054267		0.40890	0.21316	0.77502	
10 (QH)	57.29	0.08476	0.066365	0.066368		0.41962	0.23857	0.85063	
16 (AV)	88.2	0.10519	0.093227	0.093225		0.52065	0.10177	0.10167	
17 (QH)	165	0.14409			0.325	0.71320		1.041	
18 center (QH)	183.3	0.15164	0.271500	0.271504	0.490	0.75058	0.27663	0.27657	1.092

Still working on modeling surface roughness

Still working on modelling stainless steel

Before analyzing layered flight reflector, simulating Al, SS, and teflon to build confidence



What it means for J1 & J2?

- **For J1, Kent Anderson's (NGES) initial evaluation of the emissivity from the May 2013 TVAC calibration indicated the emissivity was significantly smaller, but a J1 pitchover maneuver is a more reliable measurement because**
 - It's independent of potential Calibration Test Equipment issues
 - Gives multiple angles (i.e., more data) to derive the emissivity
- **For J2, NGES and NASA added these changes:**
 - Specifying 8 micro-inches profile arithmetic mean (R_a) surface roughness for the Be surface prior to nickel plating
 - Polish the nickel-plated surface to < 100 Angstroms surface quality
 - Thicker gold plating (increased from > 0.5 micron to > 1.3 micron)



Review of Calibration Algorithm Changes

- **Correction biases for an observed unpolarized brightness temperature T_B are computed as below:**

$$\Delta T_{QV} = \frac{\varepsilon_N}{\sqrt{2}} [T_R - T_B] \sin^2 \phi + \frac{\varepsilon_N}{\sqrt{2}} (T_R - T_B) \quad \Delta T_{QH} = \frac{\varepsilon_N}{\sqrt{2}} [T_R - T_B] \cos^2 \phi + \frac{\varepsilon_N}{\sqrt{2}} (T_R - T_B)$$

- **Algorithm steps:**
 1. **Add the biases due to reflector emissivity to the cold and warm calibration brightness temperatures**
 - **Scan angles are at 83.3° and 195° respectively**
 - **Use T_R derived from temperature telemetry**
 2. **Add biases to correct for any other error sources**
 3. **Compute gain and offset for the radiometric transfer function**
 4. **Compute uncorrected scene temperatures, based on transfer function gain and offset**
 5. **Add emissivity bias correction for each scene sample (function of scan angle and scene temperature)**



Polarized Scenes

- **Calibration targets and opaque channels use this scene correction term:**

$$\Delta T_{QV} = \frac{\epsilon_N}{\sqrt{2}} [T_R - T_B] \sin^2 \phi + \frac{\epsilon_N}{\sqrt{2}} (T_R - T_B)$$

Use model-adjusted SDM temperature (under T_R)
Use uncorrected T_B (under T_B)
Left out quasi-horiz. (under T_B)

- **Channels sensitive to the surface (i.e., window channels) *should* use this scene correction term (Ch. 1, 2, 3, 4, 16 & 17):**

$$\Delta T_{QV} = \frac{\epsilon_N}{\sqrt{2}} [T_R + T_{SV} - 2T_{SH}] \sin^2 \phi + \frac{\epsilon_N}{\sqrt{2}} (T_R - T_{SV})$$

Need to model relationship between vertical and horizontal polarizations

- **Implementing the surface correction for the window channels requires:**
 - Ability to differentiate between sea and land (e.g., land/sea mask)
 - A model to estimate the brightness temperature difference between the vertical and horizontal polarization, which is a function of scan angle, surface wind speed, and sea surface temperature
 - May not be worth the effort



Status of Implementing Reflector Emissivity in IDPS

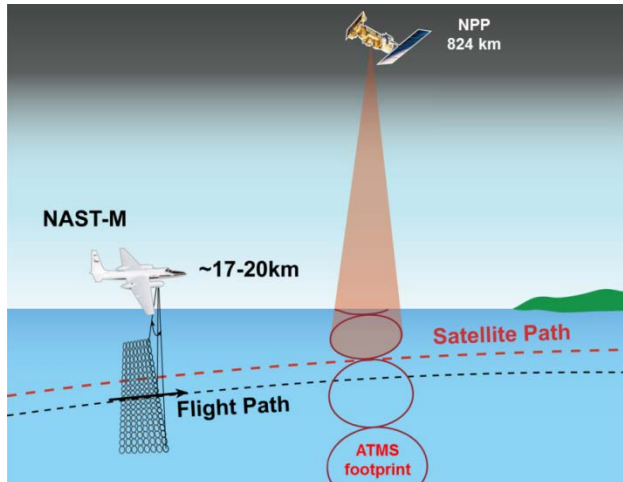
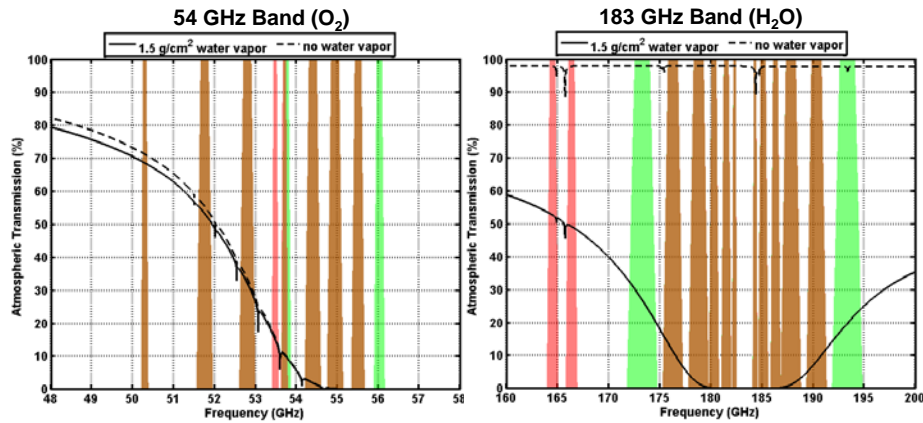
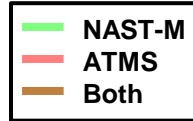
- **Implementing the algorithm in IDPS requires making the Processing Coefficient Table (PCT) larger to hold the additional instrument-specific calibration parameters**
- **Implementation requires a relatively minor code change to the TDR/SDR calibration algorithm**
- **Plan to implement change in ADL, then compare the TDR scan bias against NWP and GPS-RO (Tiger NOAA STAR has implemented it in ARTS and have presentation available)**
- **The TDR-to-SDR conversion, i.e., the scan bias correction from antenna pattern measurements, will have to be reevaluated**



ATMS Calibration Validation Mission March 2015

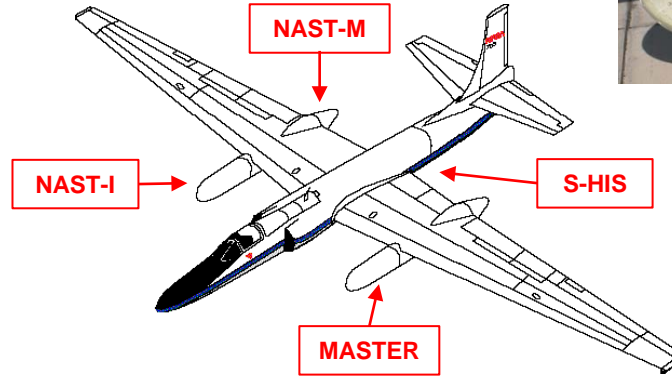
NAST-M

Dual-band, 15-channel microwave sounder similar to ATMS (54, 183) GHz



Mission

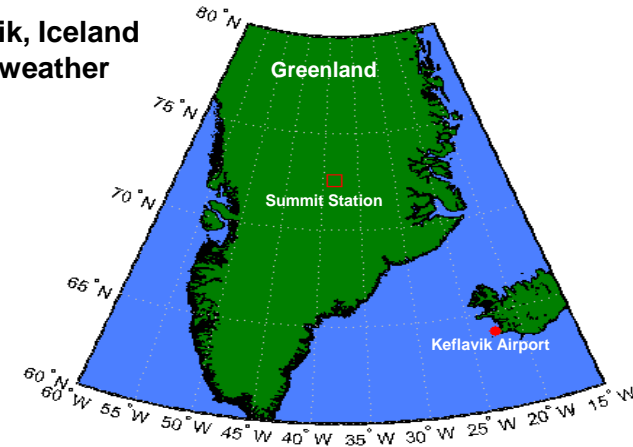
NASA ER-2 Aircraft



<http://www.nasa.gov/>



- Sorties from Keflavik, Iceland
- Greenland Summit weather station





Radiance Versus Modeling Verification

Radiance to Radiance Comparisons

- **Separate sensors measuring nearly the same point at the same time**
- **Examples include Simultaneous Nadir Observations (SNO) or aircraft underflights**
- **Pros: same atmosphere and surface conditions with similar instrumentation**
- **Cons: Different spectral or spatial characteristics and small data sets**

Radiance to Model Comparisons

- **Model the sensor and the atmosphere**
- **Examples include using state-of-the-art NWP, radiative transfer, and surface models**
- **Pros: large amounts of data**
- **Cons: Idealized or measured spectral or spatial characteristics; and modeling errors in the models**



2015 Science Sorties Over Greenland

NAST-M has data from 7 flights ~41 hours

	Full Data Collected
*	Partial Data Collected
	No Data Collected

Data Source	15-Mar	19-Mar	23-Mar	24-Mar	25-Mar	28-Mar	29-Mar
NAST-M		*					
GPS							
Video	*	*					
ER-2 NAV							
SS Ozonesondes							
ECMWF							
Overpass							
NPP	2	1	1	1	1	2	1
Aqua			1		1	1	1
Metop-A			1		1	1	1
Metop-B	1		1		1	1	1
Conditions							
Time Of Day	Day	Day	Day	Day	Day	Day	Day
Surface type	Land	Mixed	Land	Mixed	Land	Land	Land
Weather	Cloudy	Cloudy	Cloudy	Cloudy	Cloudy	Cloudy	Cloudy
Flight Time (H)	5.92	4.58	6.23	4.12	7.45	7.35	6.08

Collected data from 9 S-NPP overflights



2013 Science Sorties Over the Pacific Next to Mexico

NAST-M has data from 12 flights ~81 hours



Data Collected
No Data Collected

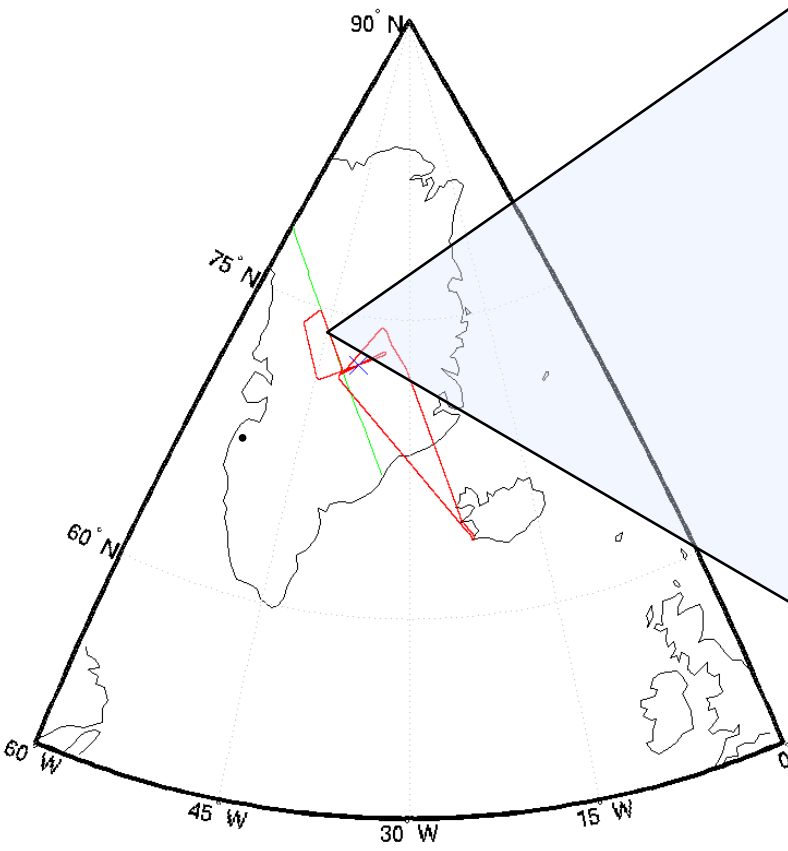
Data Source	May 7th	May 10th	May 15th	May 16th	May 18th	May 20th	May 22nd	May 23rd	May 24th	May 30th	May 31th	June 1st
NAST-M	Green	Green	Green	Green	Green	Green	Green	Green	Green	Green	Green	Pink
GPS	Green	Green	Green	Green	Green	Green	Green	Green	Green	Green	Green	Pink
Video	Green	Green	Green	Green	Green	Green	Green	Green	Green	Green	Green	Pink
ER-2 NAV	Green	Green	Green	Green	Green	Green	Green	Green	Green	Green	Green	Pink
Drop Sonde	Pink	Pink	Green	Green	Pink	Pink	Pink	Pink	Pink	Pink	Pink	Pink
Radioondes	Pink	Pink	Pink	Green	Green	Green	Pink	Green	Green	Pink	Pink	Pink
Salton Sea	Pink	Green	Green	Green	Green	Green	Green	Pink	Pink	Pink	Pink	Pink
NAM	Green	Green	Green	Green	Green	Green	Green	Green	Green	Green	Green	Pink
ECMWF	Green	Green	Green	Green	Green	Green	Green	Green	Green	Green	Green	Pink
Overpass												
NPP	Green	Green	Green	Pink	Green	Green	Pink	Green	Green	Green	Green	Pink
Aqua	Green	Green	Green	Pink	Green	Green	Green	Green	Pink	Pink	Pink	Pink
Metop-A	Pink	Pink	Green	Green	Green	Green	Pink	Pink	Pink	Green	Green	Pink
Metop-B	Pink	Green	Green	Pink	Green	Green	Green	Pink	Green	Pink	Pink	Pink
Conditions												
Time Of Day	Day	Day	Day	Day	Day	Day	Day	Day	Day	Night	Night	Pink
Surface type	Ocean	Mixed	Mixed	Mixed	Land	Land	Land	Ocean	Land	Ocean	Mixed	Pink
Weather	Cloudy	Clear	Clear	Scattered	Thin Cirrus	Scattered	Clear	Cloudy	Scattered	Scattered	Clear	Pink
Flight Time (H)	6.35	5.98	7.63	8.13	6.25	8.47	9.2	6.58	8.03	6.22	8.18	0

Collected data from 9 S-NPP overflights

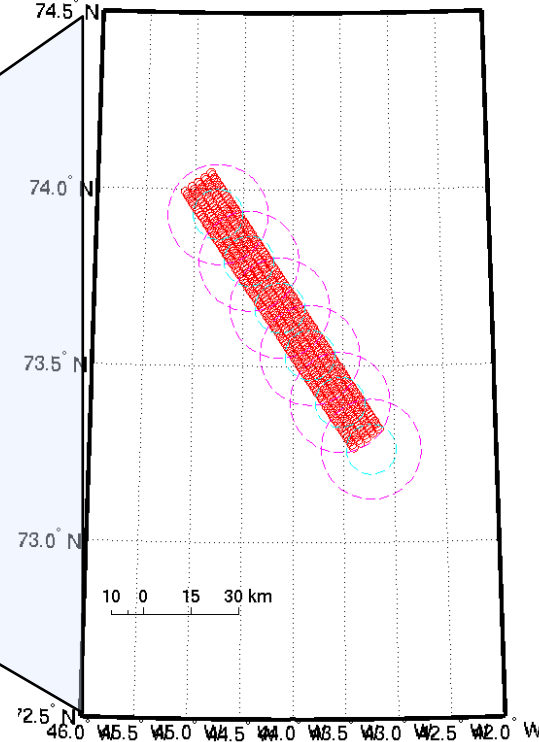


23 March ER-2 Flight Path and NPP Track

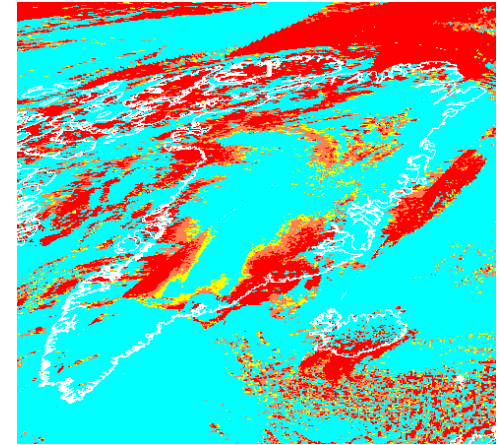
— ER-2 flight path
— NPP track



NAST-M and ATMS Coincident Measurements
23-Mar-2015 14:23:26 to 23-Mar-2015 14:23:39



— NAST-M 7.5°
— "pseudo nadir" ATMS 54 GHz 2.2°
— "pseudo nadir" ATMS 18.3 GHz 1.1°



VIIRS Cloud Mask
(blue is cloudy)

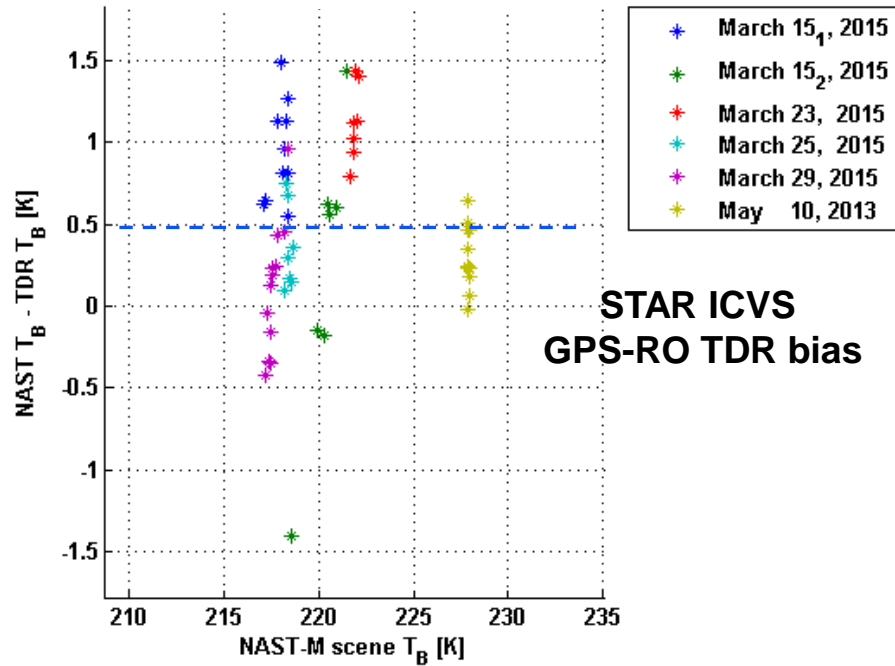


NAST-M Camera image
from underpass

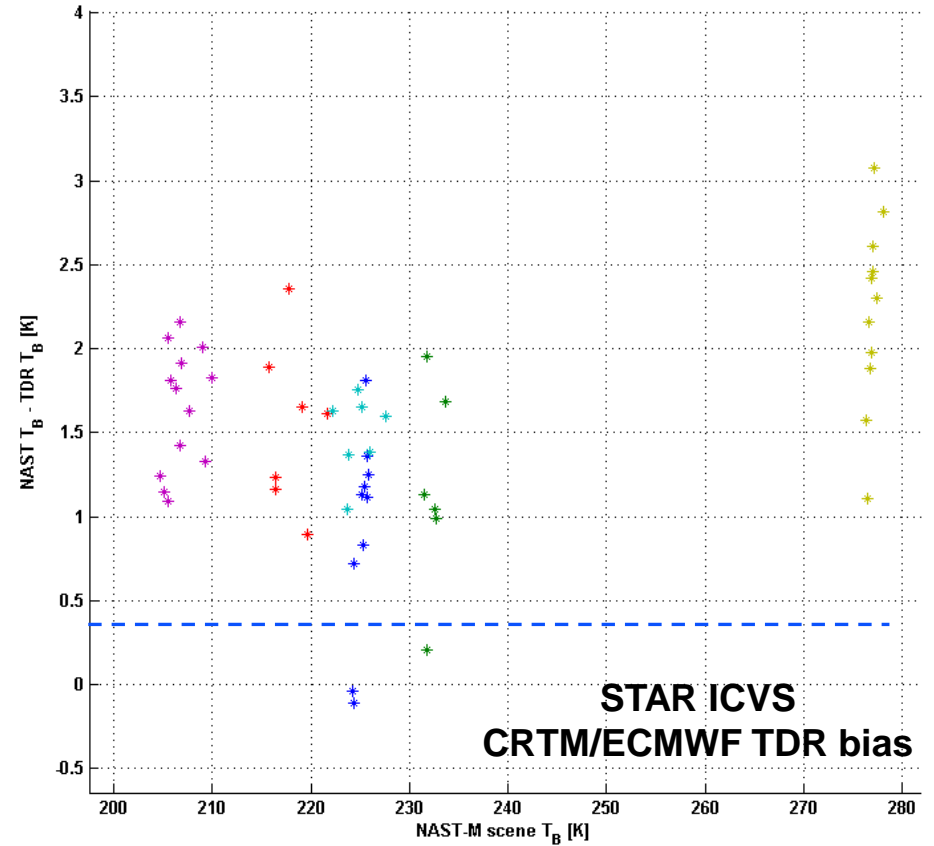


Examples of NAST-M TDR Bias

Ch. 8: 54.94 GHz



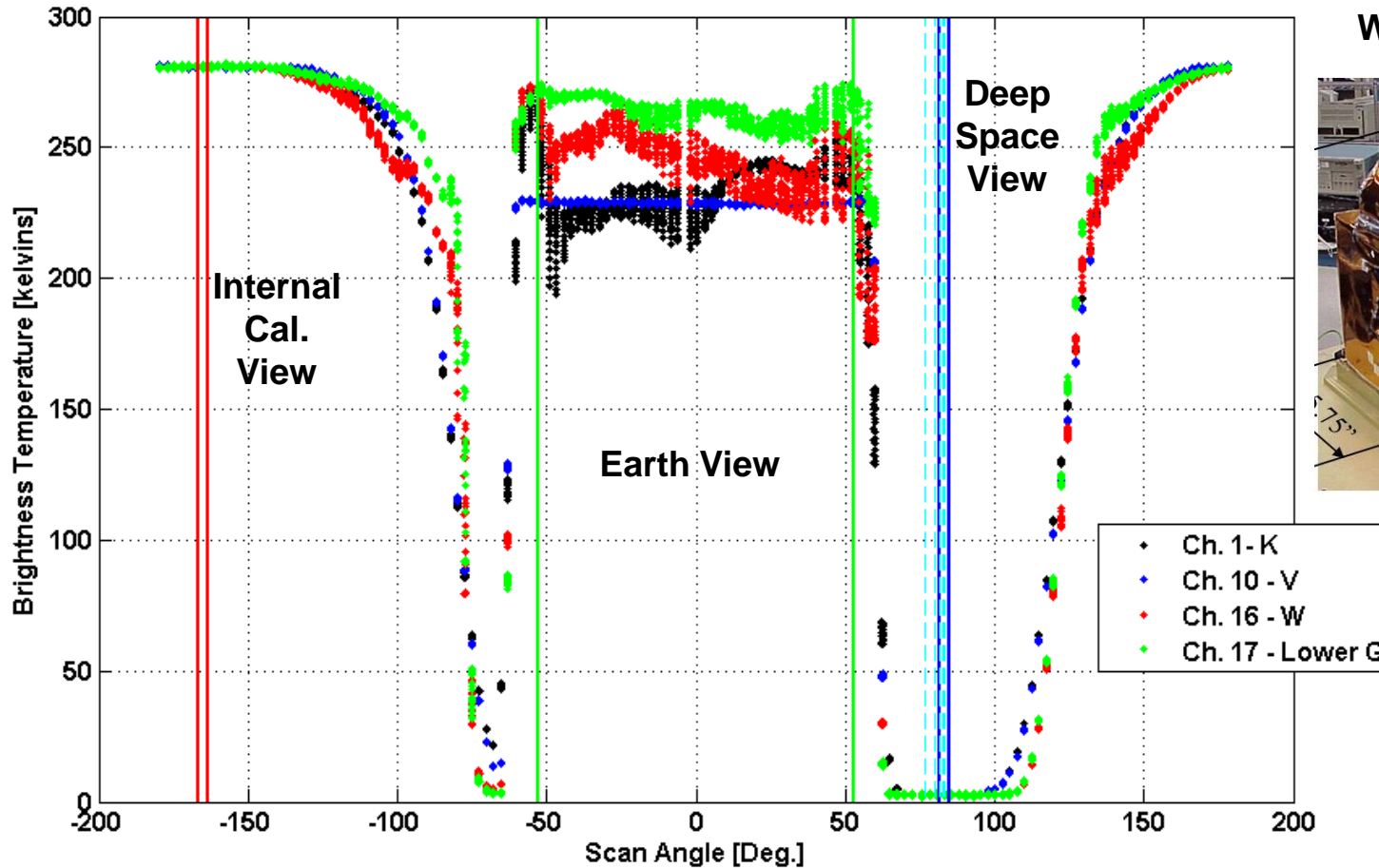
Ch. 19: 183 +/- 4.5 GHz





S-NPP Radiometric Environmental Characterization

Resulted from S-NPP ATMS Scan Reversal, which has contiguous sampling



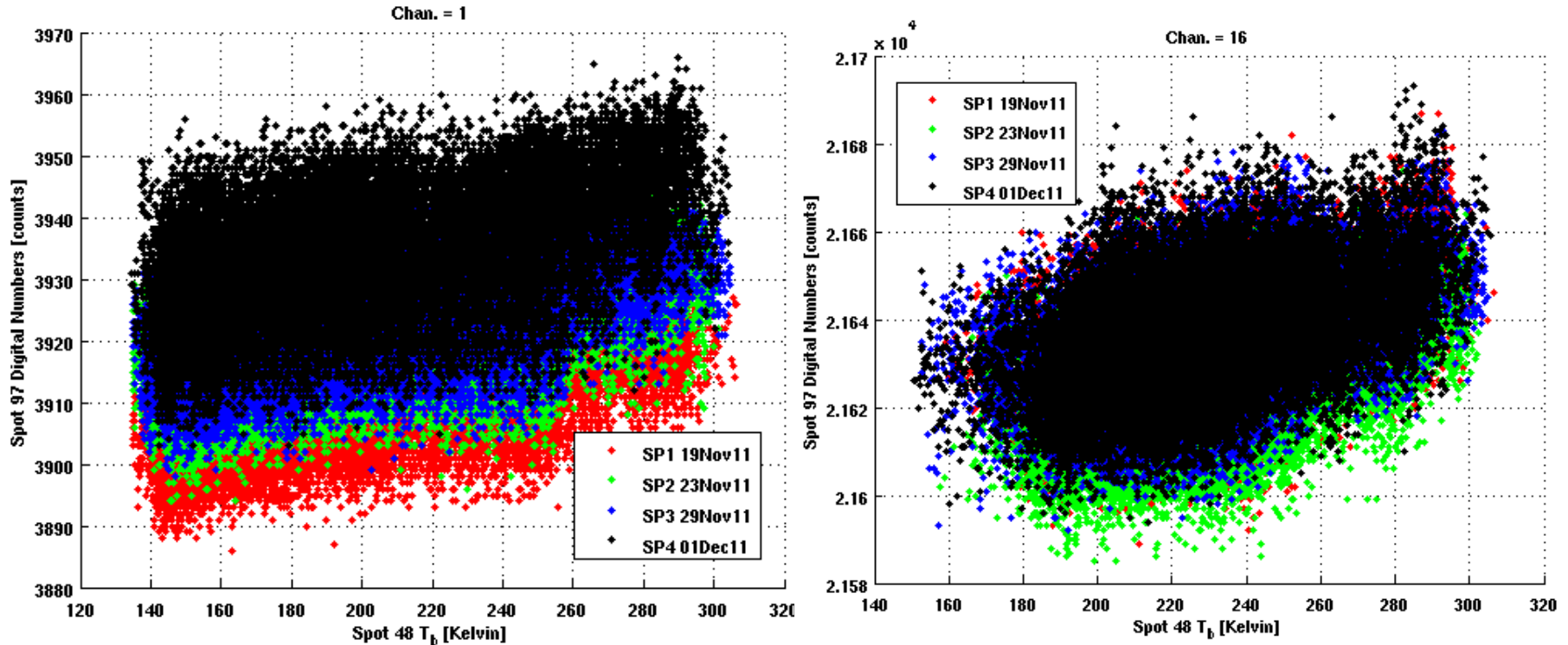
Anti-sun side

K/Ka 5.2° BW
 V 2.2°
 W 2.2°
 G 1.1°

Diagnostic mode in continuous sampling gives 2.43° spacing (360/148)



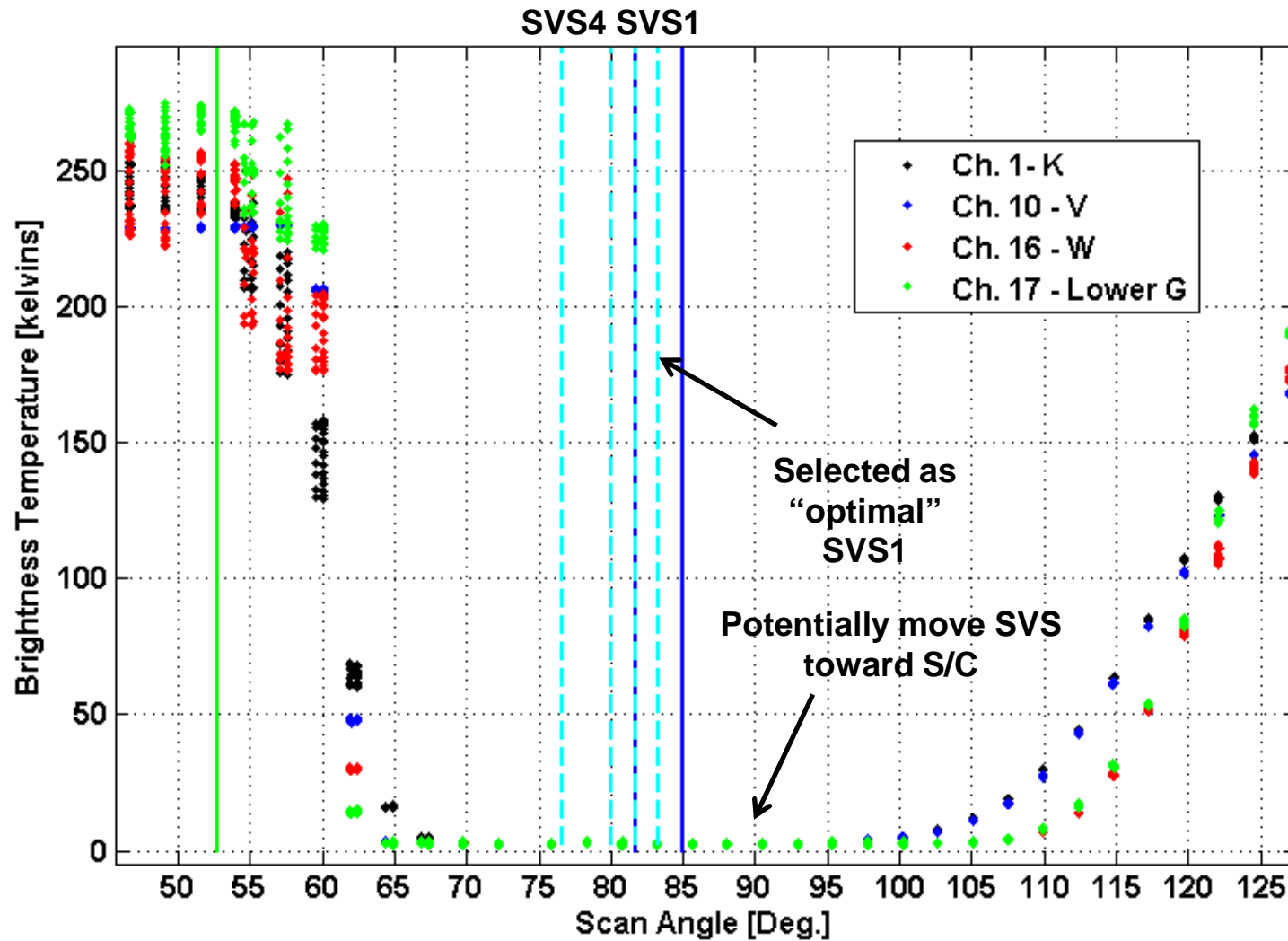
Scatter Plots: SV Spot 97 Cnts vs EV 48 Tb



- Plots above indicate a correlation between EV T_b and SV counts
- Disclosure: T_b calibrated using all 8 calibration measurement (4 SV & 4 HC)
- Channels affected seem to be the quasi-V polarized channels (Ch. 1, 2, & 16)
- May be some correlation in V-band window channel (Ch. 3).
- Spot 100 of the SVS had similar response
- Correlation coefficient about the same for all SVS spot 97 (between 0.4 to 0.55)



Potential to Move Space View Sector





Review of ATMS Single Event Upsets

- **Two types of SEU have been identified**
- **One type of event impacts the radiometric counts**
- **Another type of event impacts the Scan Drive Motor & resolver**
- **All events found are either in or near the South Atlantic Anomaly or near the polar regions**
- **ATMS recovers very quickly with minimum number of pixels impacted, but TDR/SDR Quality Flags (QFs) were not tripped**
- **Team should investigate altering QF to inform user of these events**

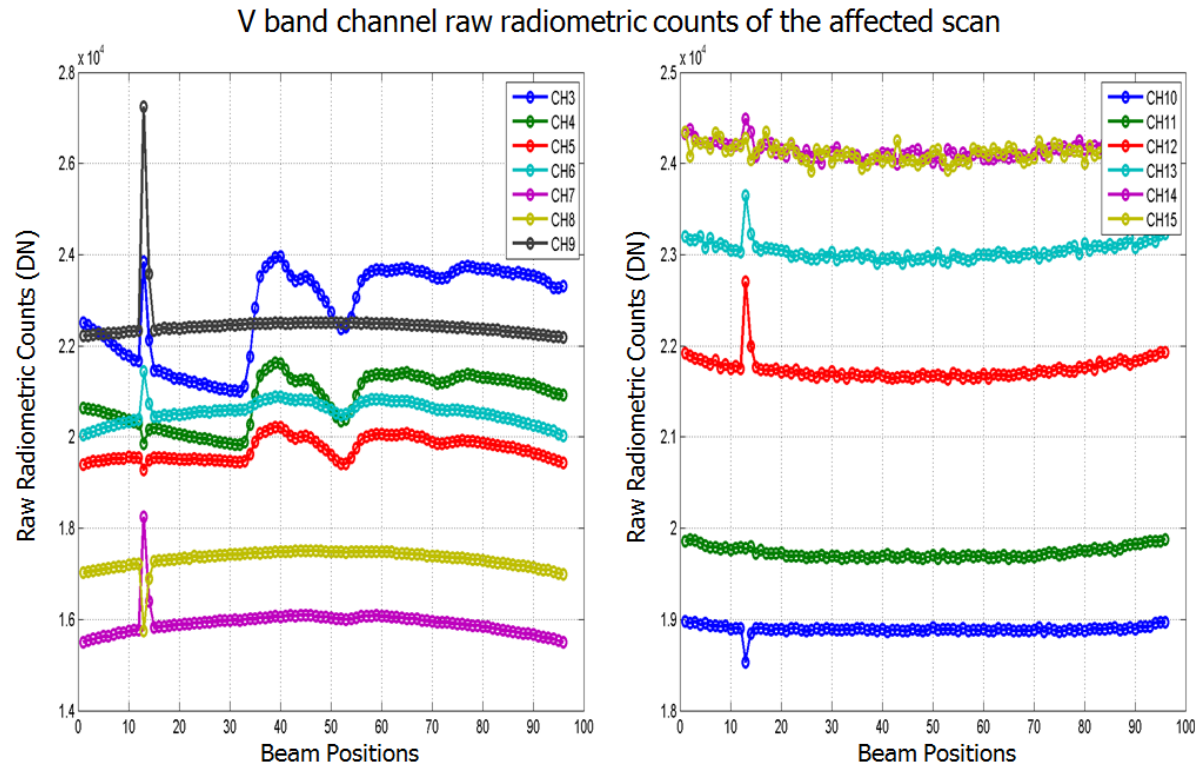


Radiometric SEU

- **NGAS Sept. 8, 2014 investigation showed “random” positive and negative spike pattern per V-band Channels**

Only V Band Channels Are Affected and the Anomaly can be both Positive and Negative

NORTHROP GRUMMAN



5
Degui Gu & Alex Foo (NGAS)

**Positive Spikes:
Channels 3, 6, 7, 9, 12,
13, 14, 15**

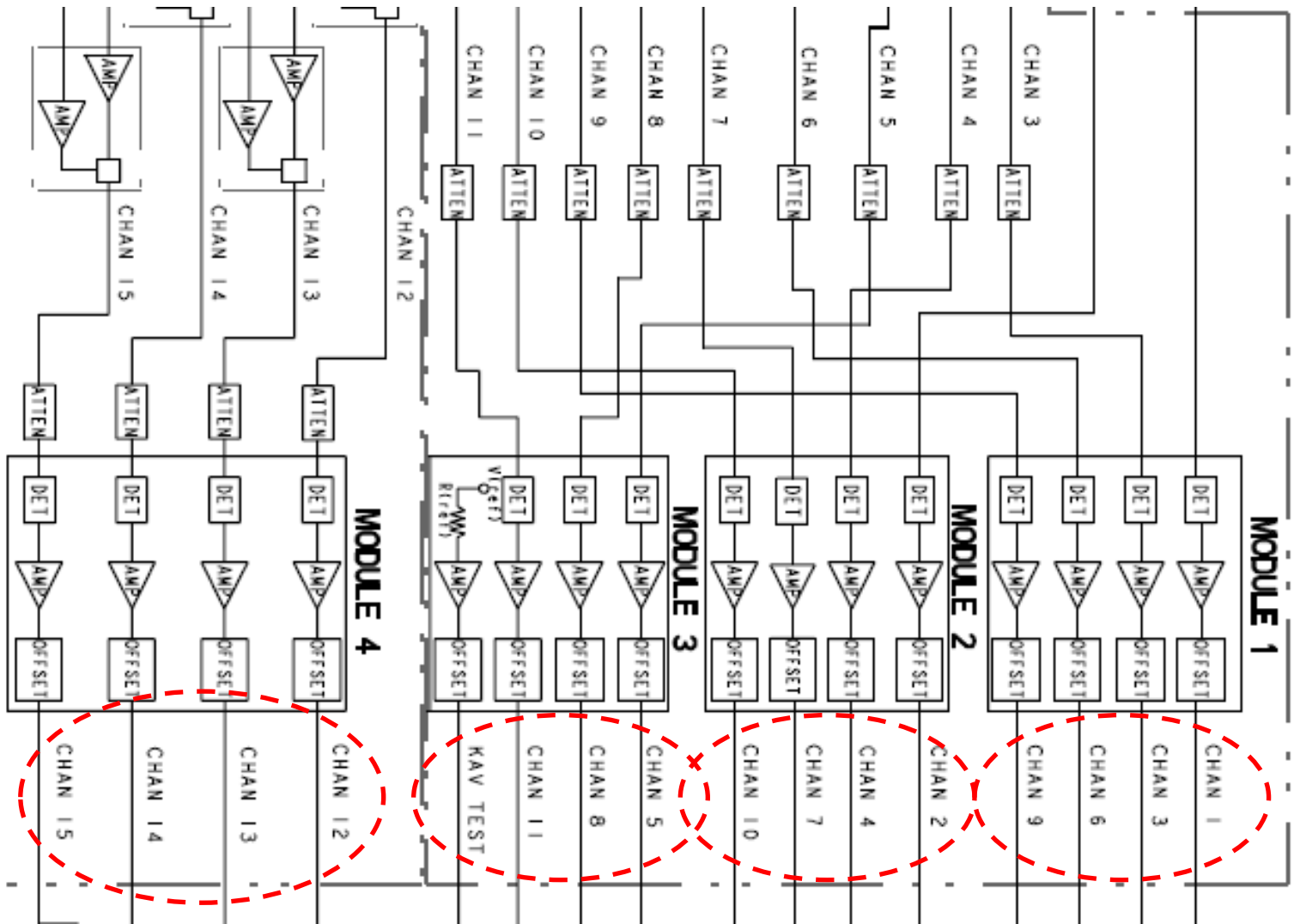
**Negative Spikes:
Channels 4, 5, 8, 10**

Undetermined: Channel 11

**Initially characterized
by Sung-Yung Lee
(NASA JPL)**



Section of ATMS Flow Diagram



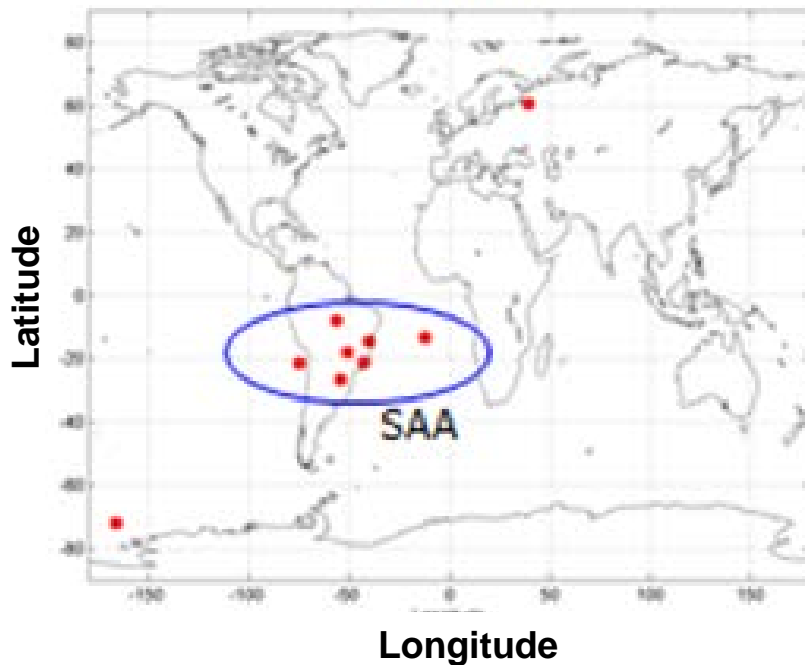


NGAS SEU Characterization of Radiometric Event

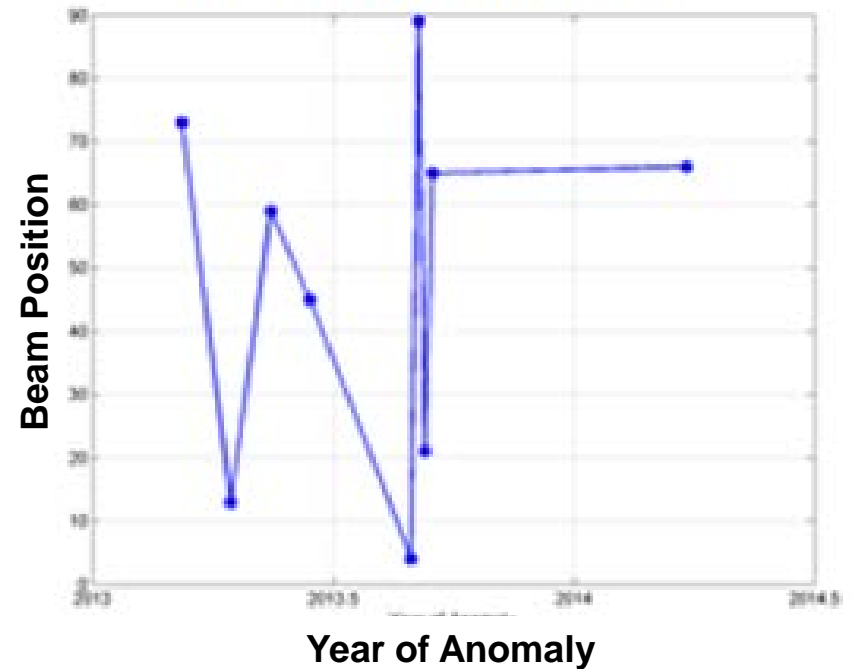


Spatial Characteristics

Location

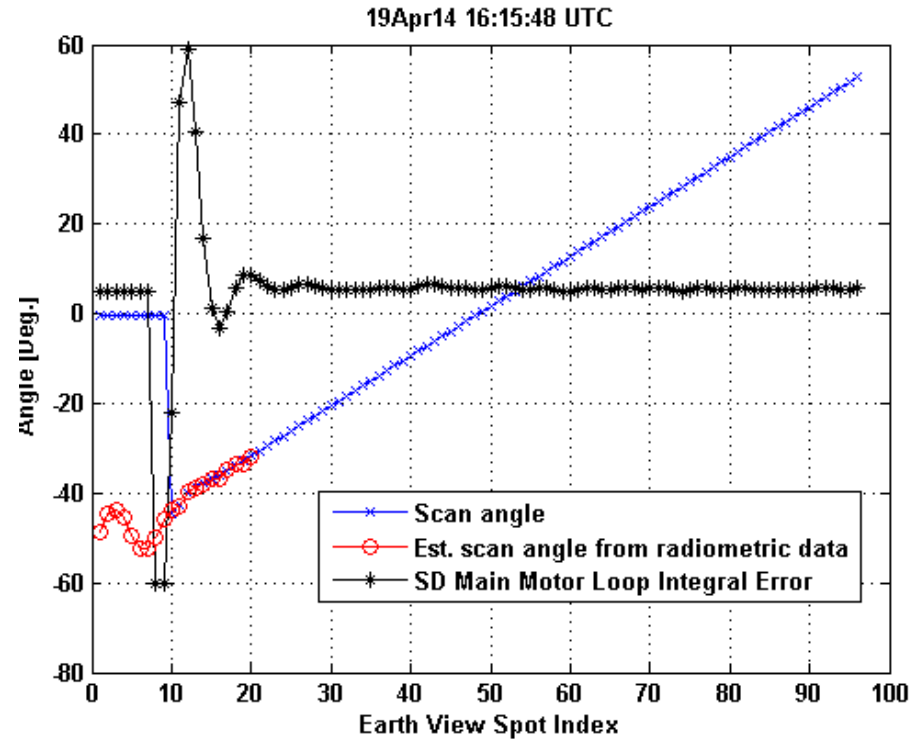
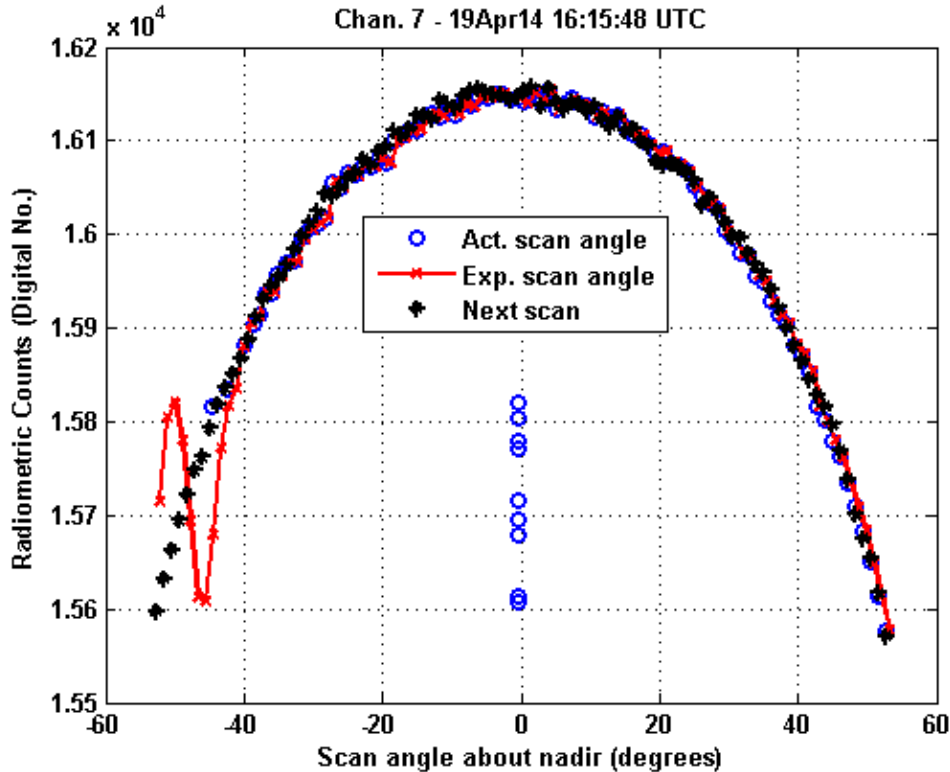


Time and Beam Position





Scan Drive Motor SEU

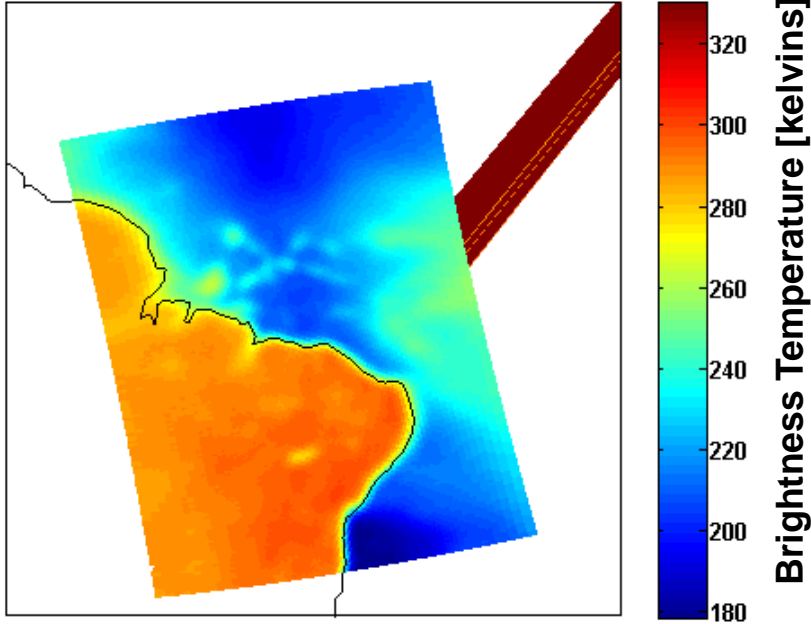


Reconstructed scan angles during event does seem to indicate that the SDM continues toward nadir, but starts to react to the zero resolver values (i.e., goes in reverse) before correcting itself.

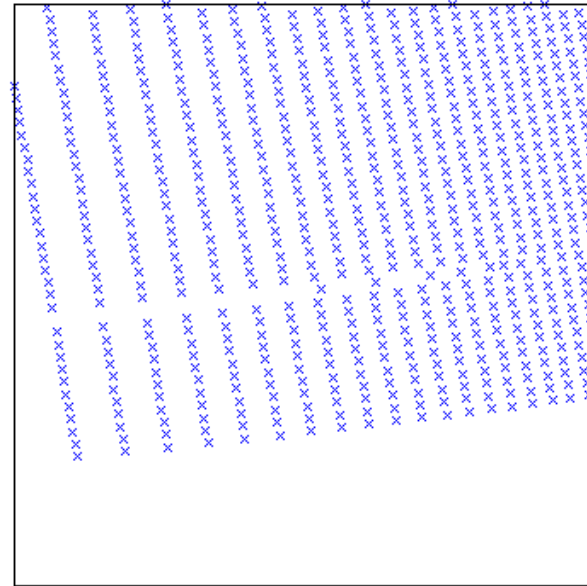


Radiance & Geolocation (SDR) Data Products

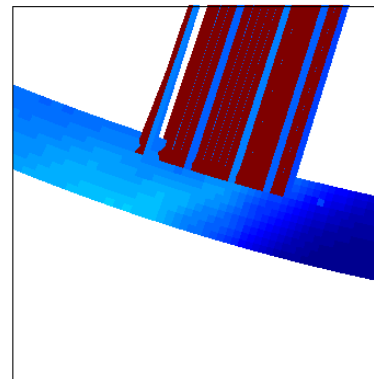
19 April 2014



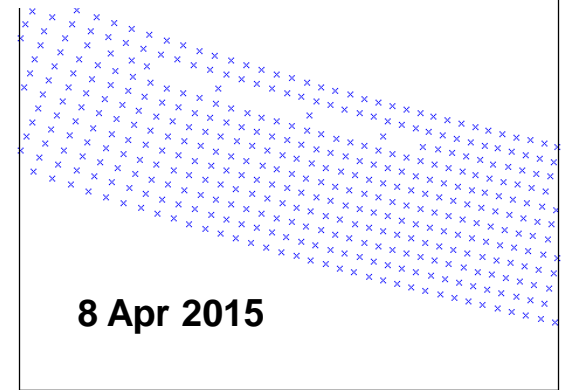
19 April 2014



Radiance "fill" values also had latitude and longitude fill values (-999.5)

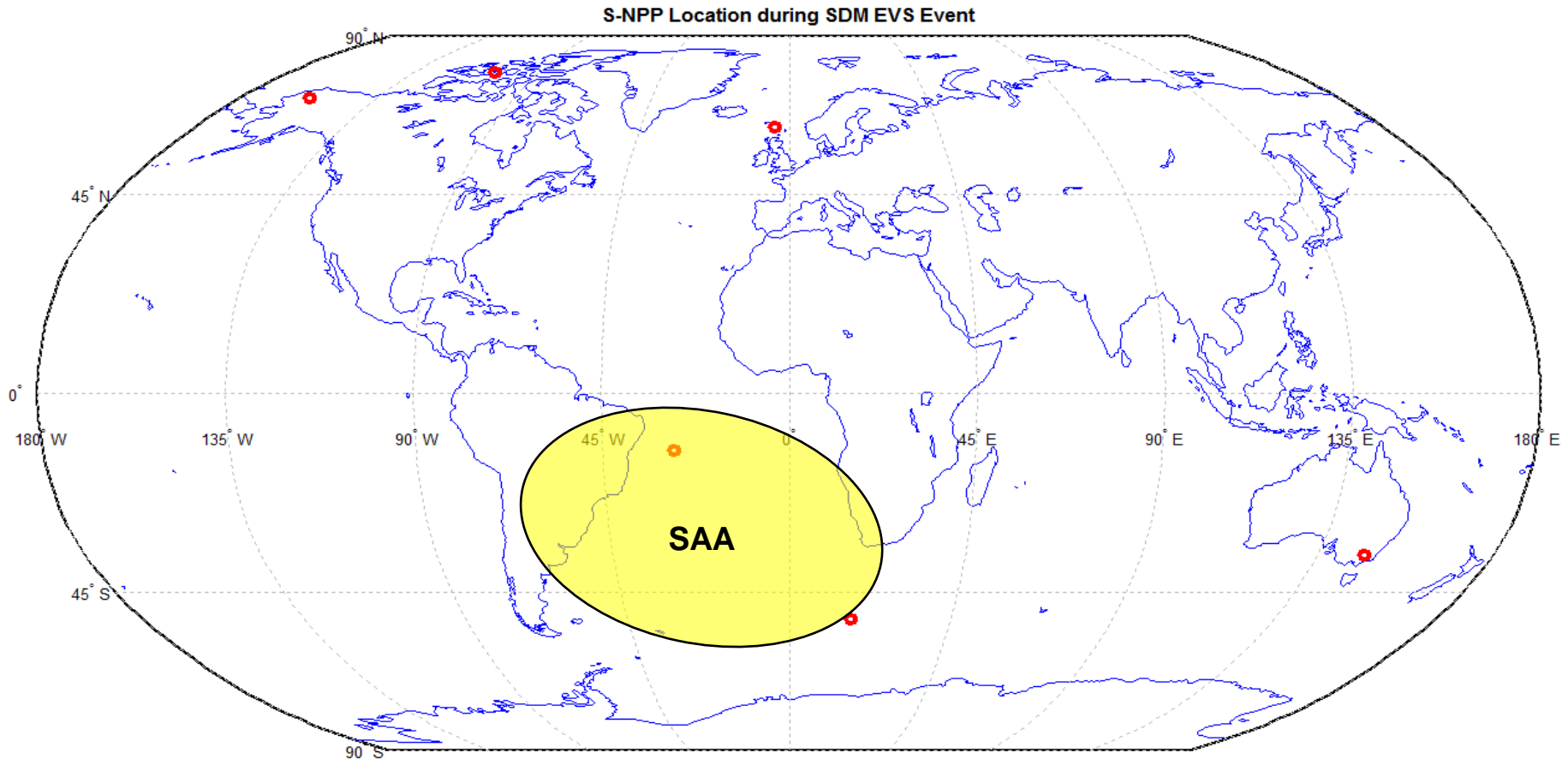


8 Apr 2015





S-NPP Location at Start of SDM Event



About one or two SDM SEUs occur per month



Future Work

- **Flat reflector emissivity**
 - Continue to investigate emissivity with modeling
 - Implement the emissivity correction in IDPS and add coefficients to the ATMS SDR PCT
 - Get user and science community sign off
- **NAST-M**
 - Return to 2013 campaign to increase the data set
 - Continue with NAST-M upgrade that will add K & Ka channels
- **Advocate for J1 spacecraft maneuvers and radiometric environment characterization in the PLT**
- **Investigate developing data product quality flags for ATMS Single Event Upsets**



Backup Slides



Comparison to Previous ATMS Emissivity Study Results

Channel	Frequency	Analytical Emissivity (Bulk Ni Layer)	Numerical Emissivity	Analytical Emissivity (Bulk Au Layer)	PFM Pitch-Over Derived Emissivity LL	PFM Ground Calibration Derived Emissivity (NGES)
1 (QV)	23.8 GHz	0.0008545	0.0007060	0.0005083	0.004	0.0038
2 (QV)	31.4 GHz	0.0009815	0.0024944	0.0005838	0.0035	0.00363
3 (QH)	50.3 GHz	0.0012422	0.0004398	0.0007389	0.002	0.0025
6 (QH)	53.596 GHz	0.0012830	0.0004143	0.0007627		
7 (QH)	54.4 GHz	0.0012919	0.0004438	0.0007684		
10 (QH)	57.29 GHz	0.0013257	0.0005008	0.0007885		
16 (AV)	88.2 GHz	0.0016450	0.0014246	0.0009784	0.0065	0.00662
17 (QH)	165 GHz	0.0022533	0.0008428	0.0013403	0.004	0.00354
18 min (QH)	176.3 GHz	0.0023257	0.0008060	0.0013833	0.0045	0.0043
18 center (QH)	183.3 GHz	0.0023714	0.0006445	0.0014105		
18 max (QH)	190.3 GHz	0.0024163	0.0011150	0.0014372		



Calibration Algorithm Correction

Correction impacts three parts of the calibration equation:

$$T_{measured} = g \times (C_{scene} - C_{sv}) + T_{sv} \quad (\text{Eq. 3}) \quad \text{SV = Space View}$$

1. The deep space radiometric counts are corrupted by the reflector's physical temperature and must be corrected in the deep space brightness temperature:

T_{DS} = Deep Space T_b

$$T_{sv} = \rho \times T_{DS} + \varepsilon_{sv} \times T_{refl} = T_{DS} + \frac{\varepsilon_n}{\sqrt{2}} \times \sin^2(\phi_{sv}) \times (T_{refl} - T_{DS}) \quad (\text{Eq. 4})$$

2. Since the hot and cold calibration views are at different angles, the gain must be corrected for the reflector emissivity contribution:

$$g = \frac{T_{HC} + \varepsilon_{HC} \times (T_{refl} - T_{HC}) - T_{DS} - \varepsilon_{sv} \times (T_{refl} - T_{DS})}{C_{HC} - C_{sv}} \quad (\text{Eq. 5})$$

HC = Hot Cal (i.e., ambient)

3. Finally, the scene brightness temperature is corrupted and this correction must be applied:

$$T_{scene} = \frac{T_{measured} - \varepsilon_x \times T_{refl}}{1 - \varepsilon_x} \quad (\text{Eq. 6})$$

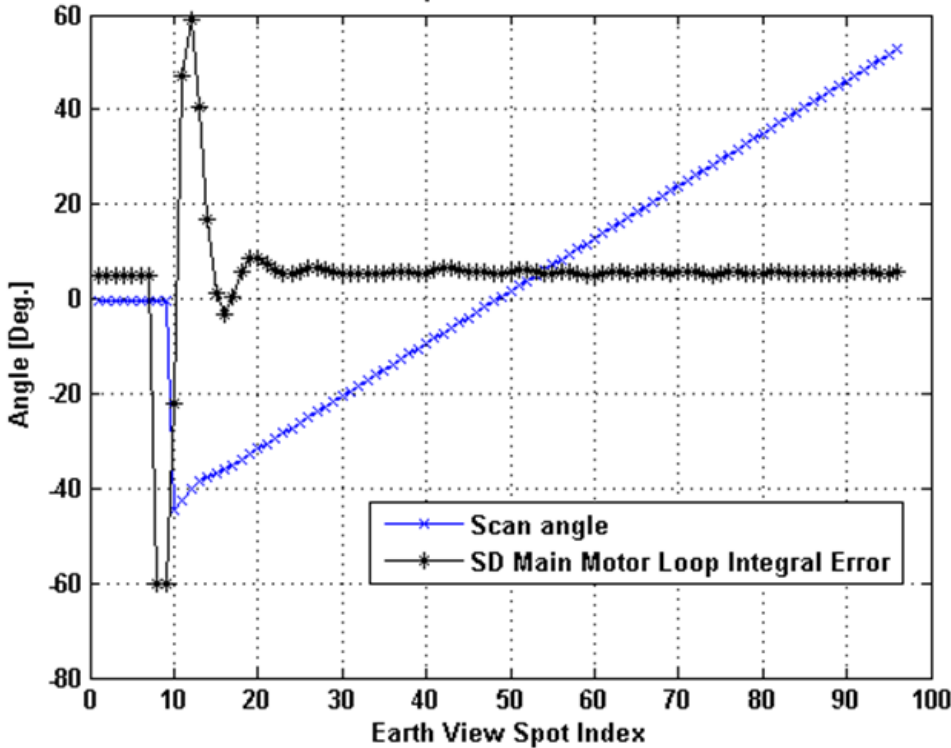
ε_x is the quasi-V (QV) or quasi-H (QH) emissivity



Loop Integral Error & Main Motor Current During an Event

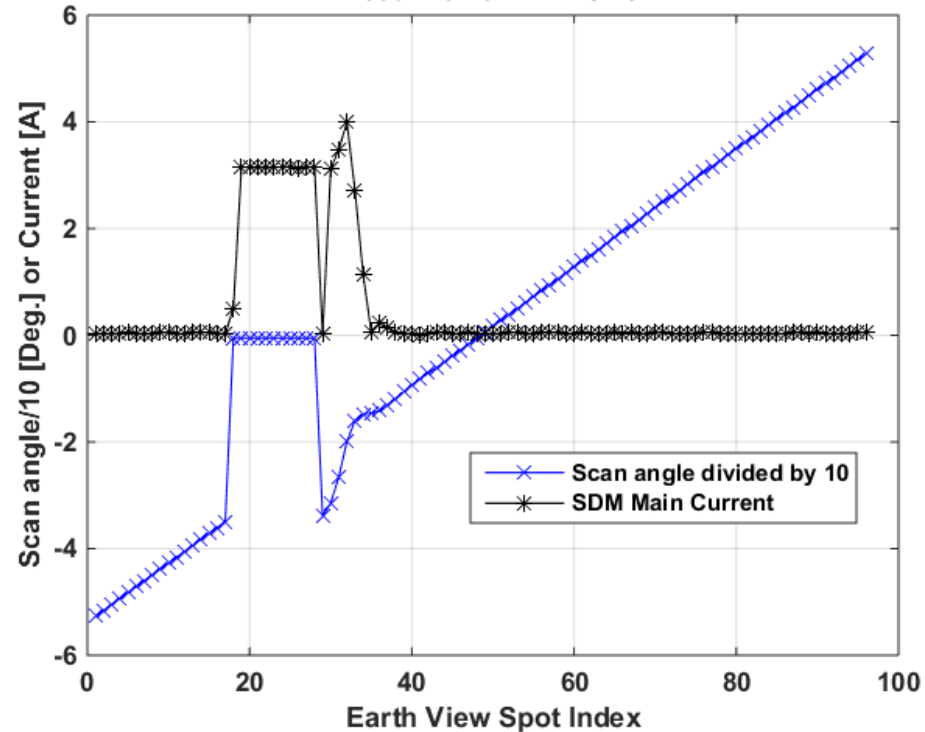
19Apr2014

19Apr14 16:15:48 UTC



15Jan2015

15Jan15 13:44:12 UTC

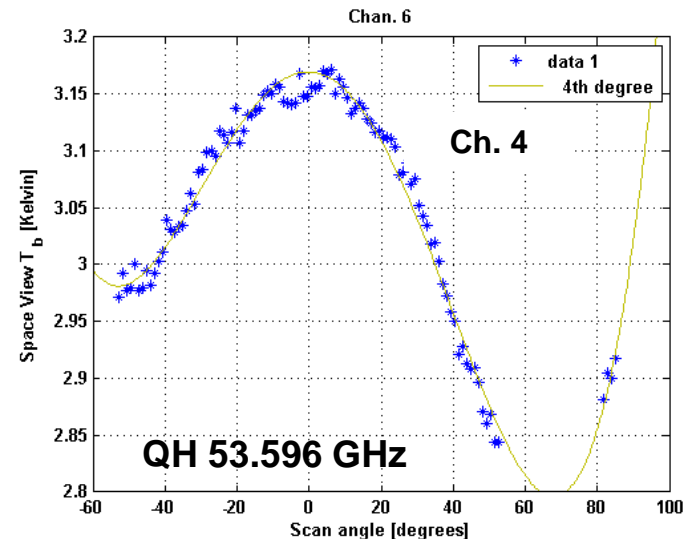
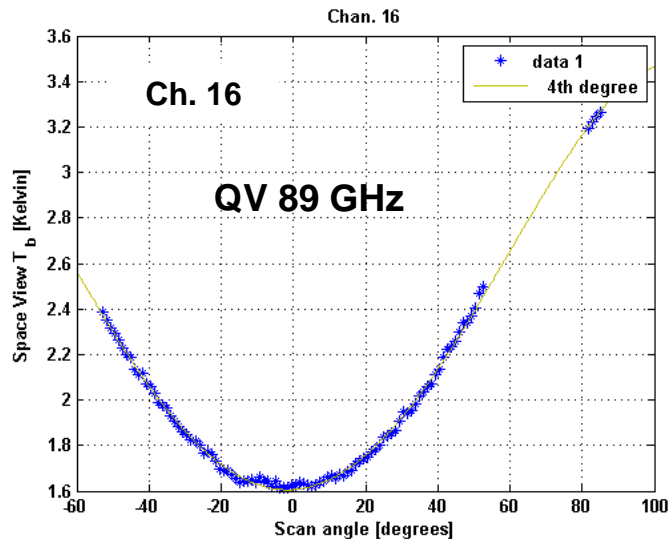
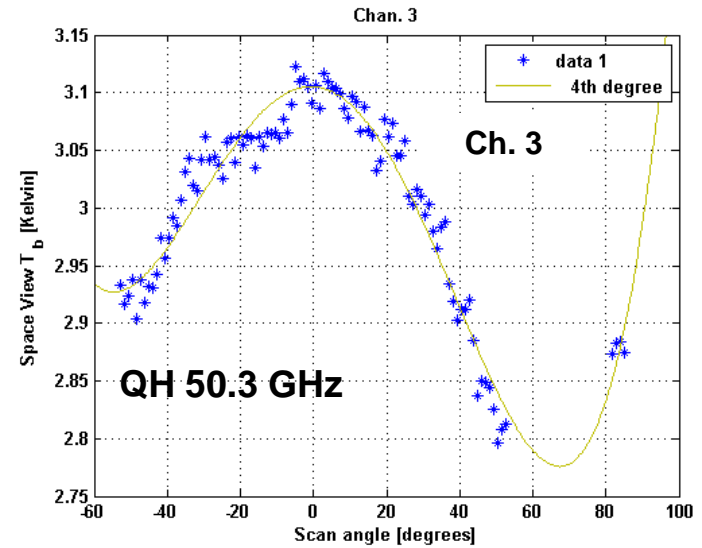
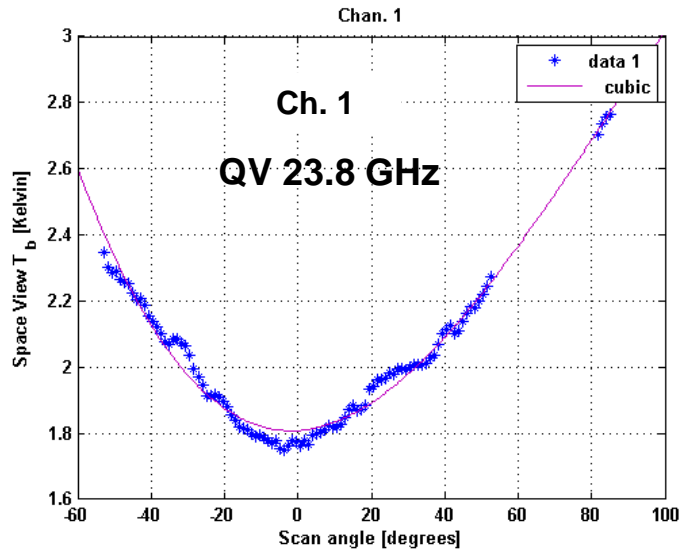


Once the scan angle returns (see left), the scan angle value is in approximately the same location as it left off.

The Loop Integral Error changes before the resolver (i.e., scan angle) returns to correct values



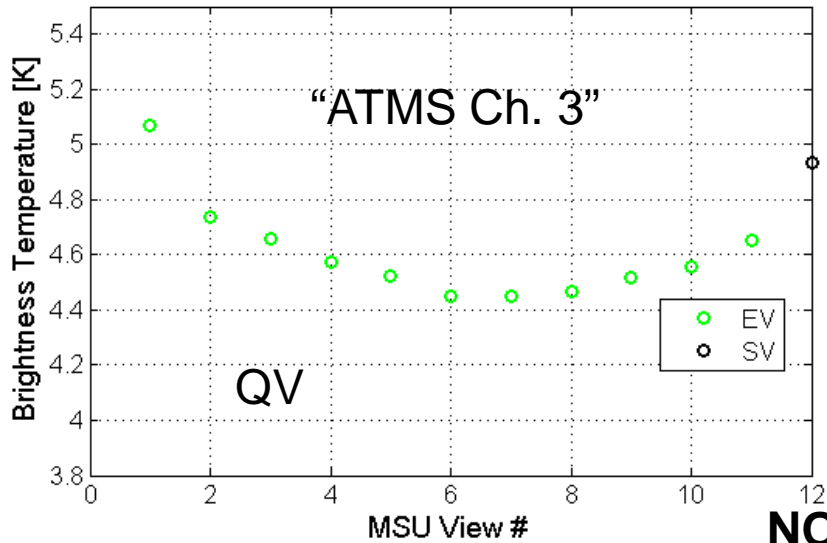
S-NPP Pitchover ATMS Scan Angle Bias



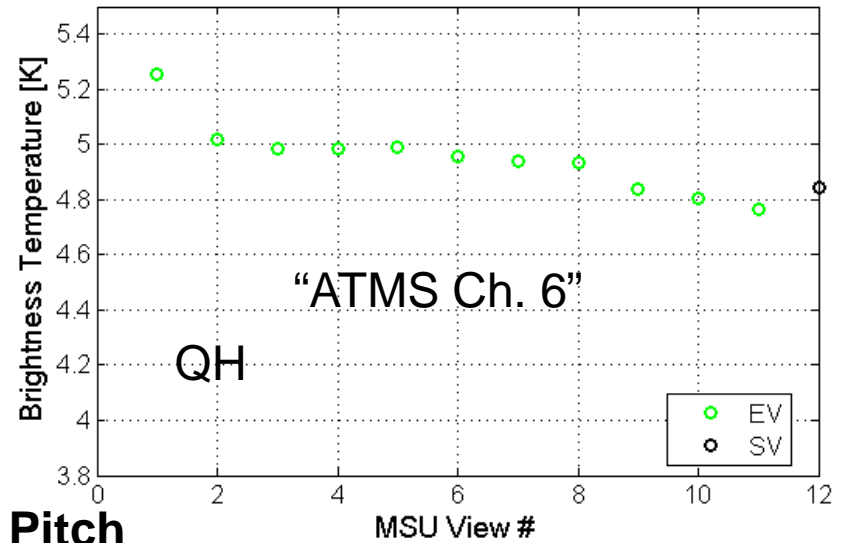


NOAA-14 MSU Deep Space Scan Bias

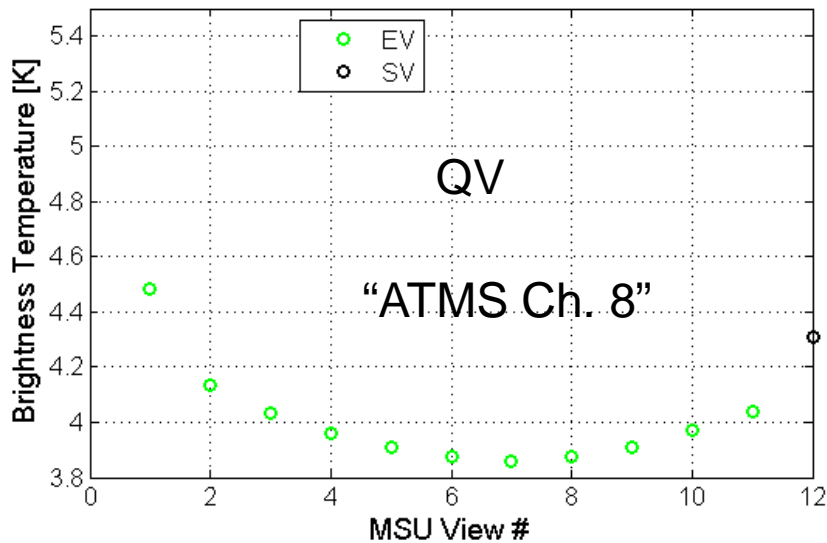
MSU Ch. 1 50.36 GHz



MSU Ch. 2 53.74GHz

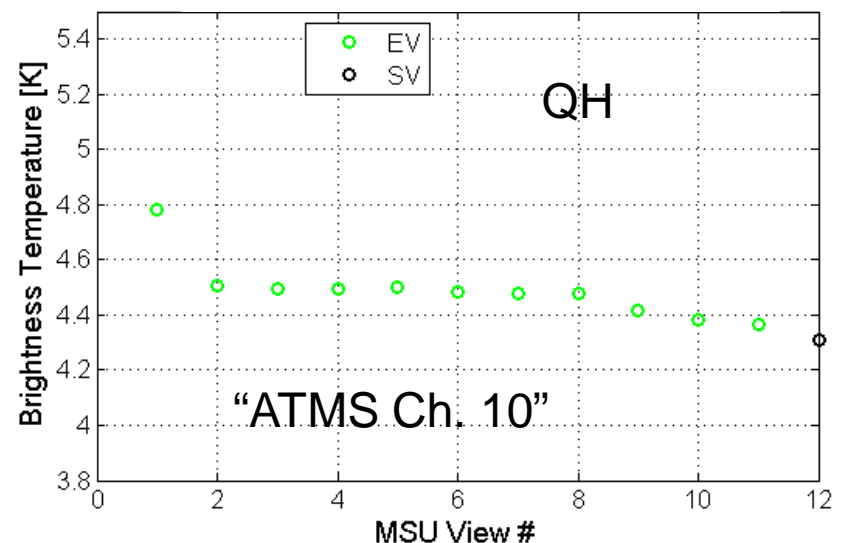


MSU Ch. 3 54.96 GHz



**NOAA-14 Pitch
Over Maneuver**

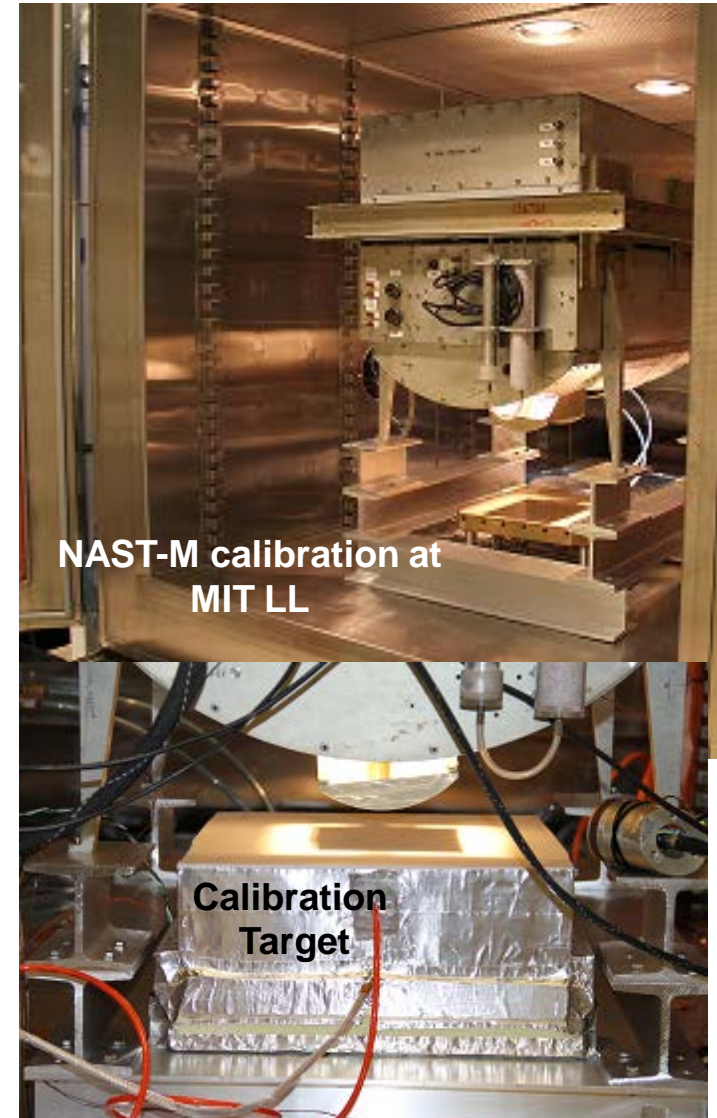
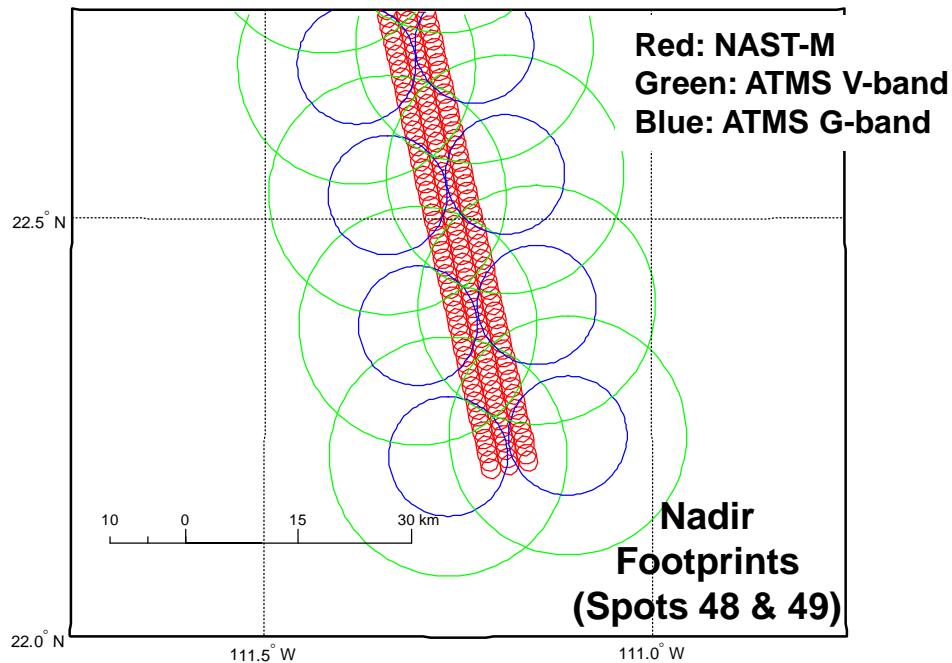
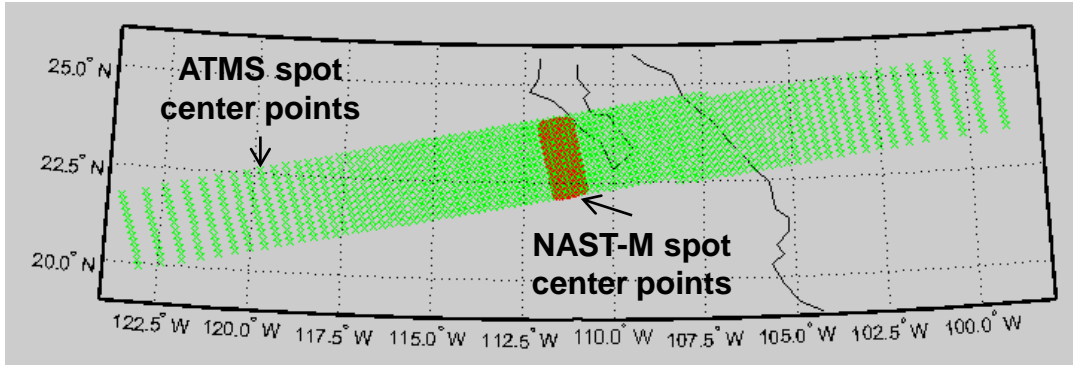
MSU Ch. 4 57.95 GHz





S-NPP Mission Cal/Val Campaign

10 May 2013 Sortie over Gulf of CA





ATMS Geolocation Validation and Trending

Yang Han¹, Fuzhong Weng¹, Xiaolei Zou², Hu Yang², Kris Robinson³, and Ninghai Sun¹

1. NOAA Center for Satellite Applications and Research, College Park, MD
2. ESSIC, University of Maryland, College Park, MD
3. Space Dynamic Laboratory, Utah State University



Outline



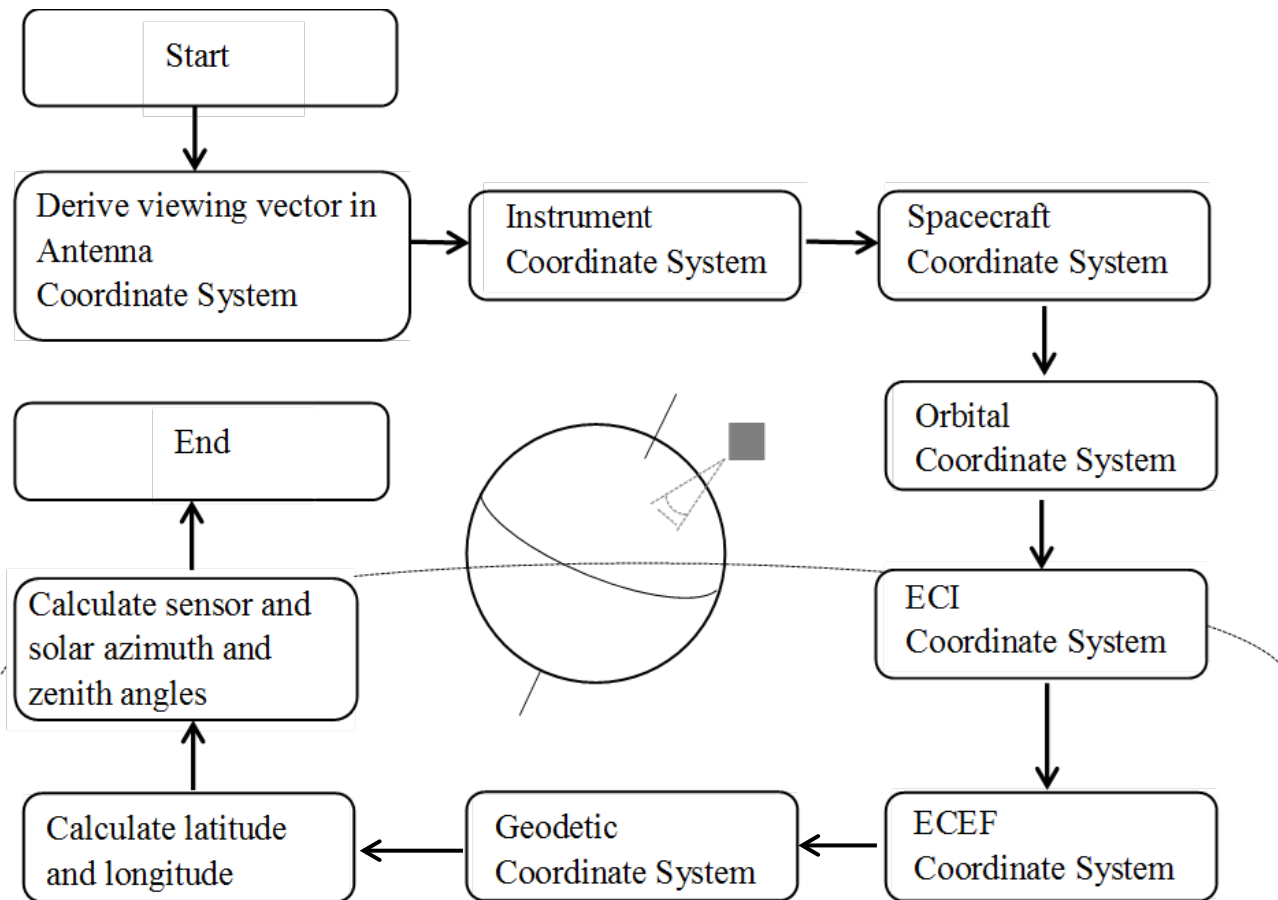
- **S-NPP ATMS Geolocation Accuracy Requirement**
- **S-NPP ATMS Geolocation Calculation Flow Chart**
- **S-NPP ATMS Geolocation Accuracy Validation Methods**
 - Coastline Detection Method (CDM)
 - Land-sea Fraction Method (LFM)
- **S-NPP ATMS Geolocation Accuracy Validation Results**
- **Summary**
- **Path Forward**



ATMS Geolocation Accuracy Requirement



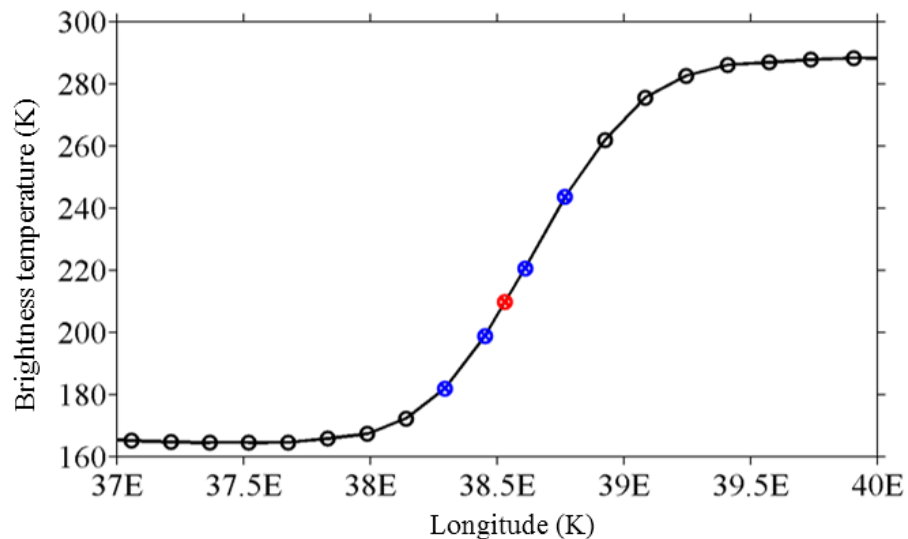
- **Pointing Accuracy Definition**
 - At each beam position, in both the scan (crosstrack) and the spacecraft velocity (downtrack) directions, the beam pointing accuracy is defined as the difference between the intended and actual beam electrical boresight directions
- **Pointing Accuracy Requirement (S-NPP, AE-28100)**
 - +/-0.10 degrees for the 1.1 degrees beamwidth channels (G-band)
 - +/-0.15 degrees for the 2.2 degrees beamwidth channels (V/W-band)
 - +/-0.30 degrees for the 5.2 degrees beamwidth channels (K/Ka-band)
- **Pointing Accuracy Requirement (JPSS, AE-28300)**
 - For each position, the pre-launch static beam-pointing error shall be no greater than 0.50 degrees, 3 sigma, per axis for all channels



Coordinate system transformation from antenna coordinate to geodetic coordinate

Coastline Detection Method (CDM)

- a. Fit a cubic polynomial to brightness temperatures at four consecutive FOVs that cross a coastline
- b. Find the coastline by calculating inflection point when preset conditions are satisfied
- c. Obtain geolocation errors in latitude and longitude by computing the perpendicular distance between the inflection point and GSHHS database

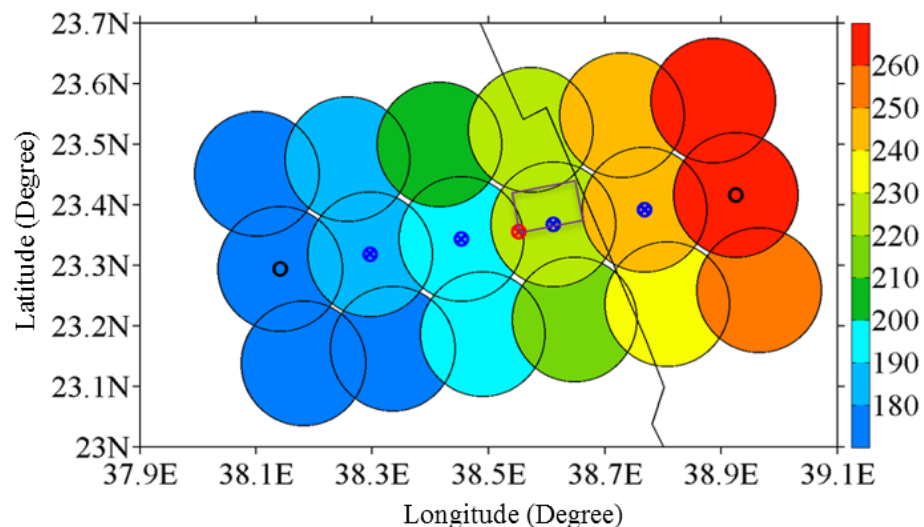


Recommendation on scene selection,

1. High thermal contrast between land and water
2. Infrequent cloud cover
3. No unusual terrain features

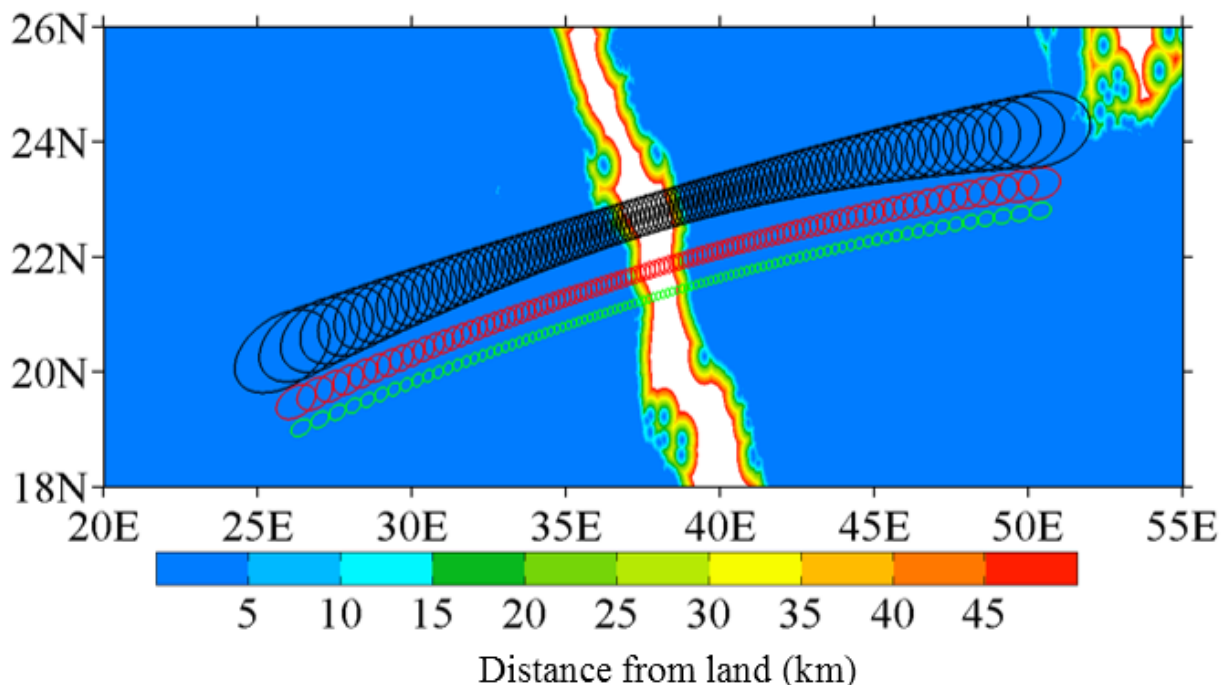
Selected coasts for validation,

- a) North Africa western coast
- b) Caspian Sea coast
- c) Red Sea coast



Land-sea Fraction Method (LFM)

- Collocate land sea mask within ATMS FOVs
- Simulate brightness temperature with land sea mask datasets
- Define cost functions by shifting the land sea mask in the along-track and cross-track directions
- Detect geolocation accuracy by minimizing cost functions

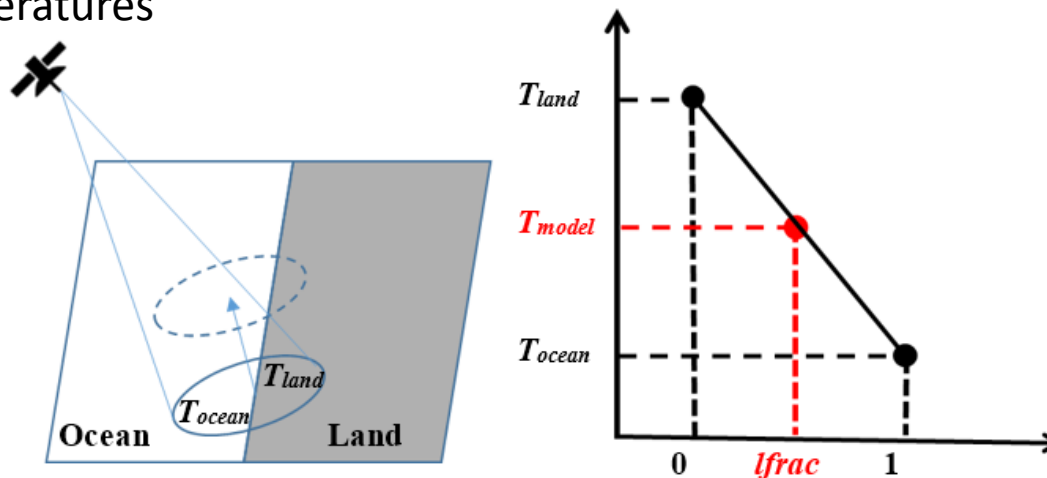


Collocating land sea mask datasets with ATMS FOVs at beam width of 5.2 (black), 2.2 (red), and 1.1 (green) degree

Construct brightness temperature simulation model according to statistical analysis of the scene measurements

$$T_{Model} = T_{sea} + lfrac \cdot (T_{land} - T_{sea})$$

T_{land} and T_{ocean} is the average brightness temperature in land and ocean, respectively. $lfrac$ is the land-sea fraction in a satellite footprint, and T_{model} is the corresponding brightness temperatures



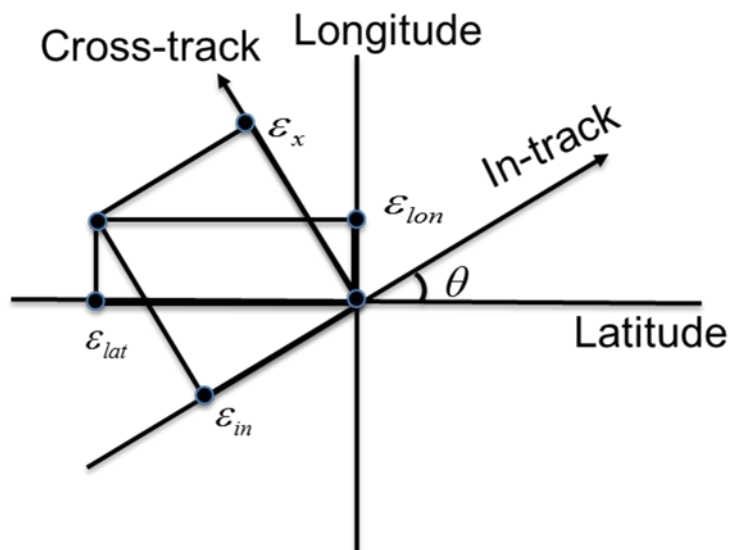
Minimize Chi-square function by shifting the land sea mask datasets in north-south and east-west directions to find the best matched land sea mask fractions

$$\chi^2 = \sum_{FOVs} (T_{OBS} - T_{Model})^2$$

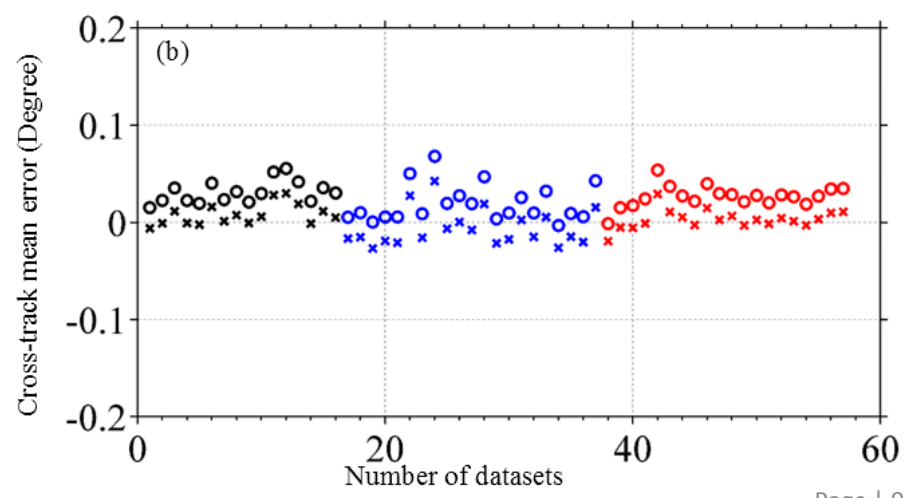
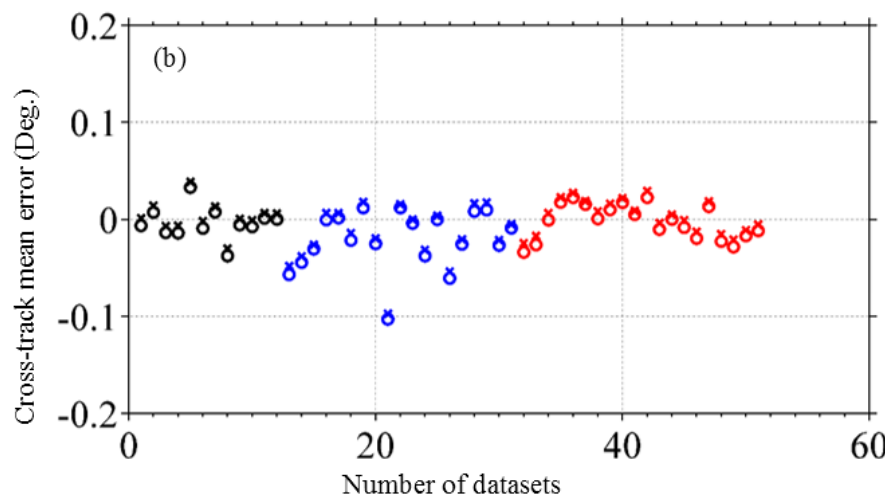
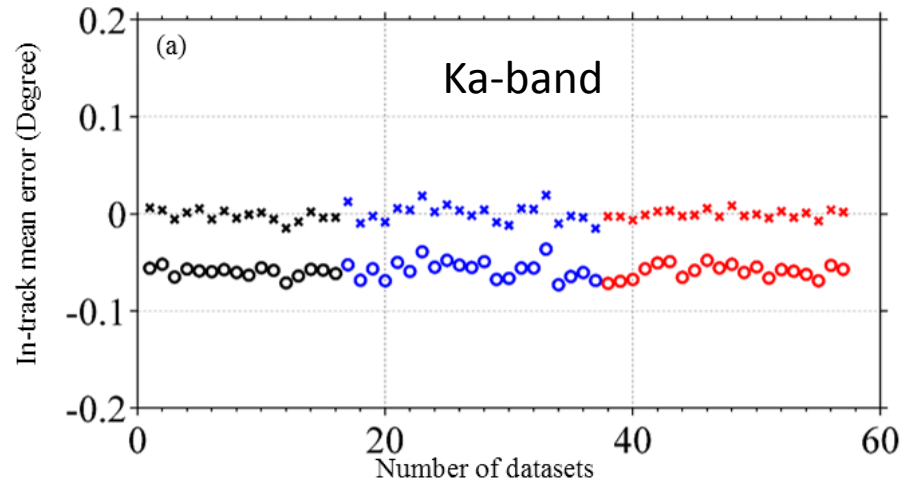
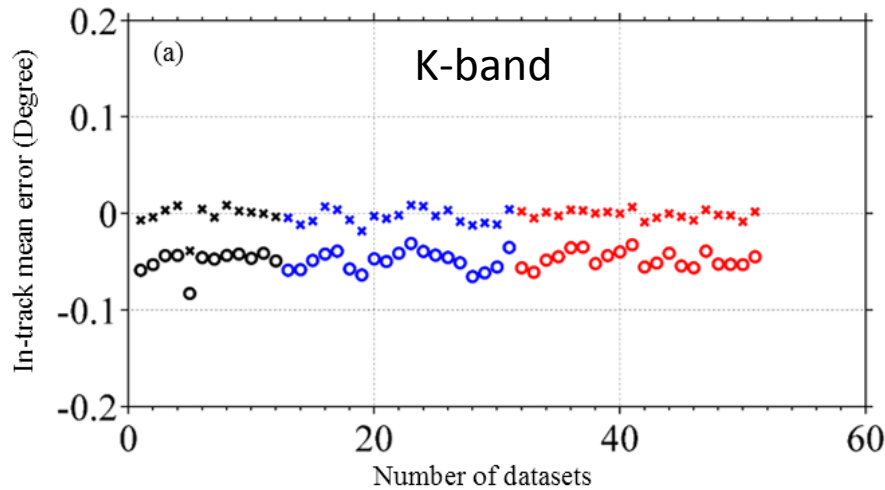
Geolocation errors in latitude (ϵ_{lat}) and longitude (ϵ_{lon}) can be mapped to in-track (ϵ_{in}) and cross-track (ϵ_x) errors by the following equation, where θ is the spacecraft heading angle

$$\begin{bmatrix} \epsilon_x \\ \epsilon_{in} \end{bmatrix} = \begin{bmatrix} \sin \theta & \cos \theta \\ \cos \theta & -\sin \theta \end{bmatrix} \begin{bmatrix} \epsilon_{lat} \\ \epsilon_{lon} \end{bmatrix}$$

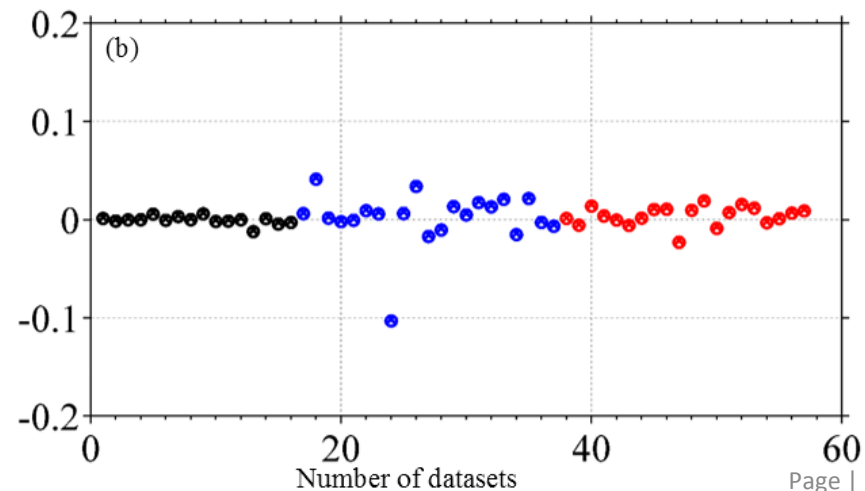
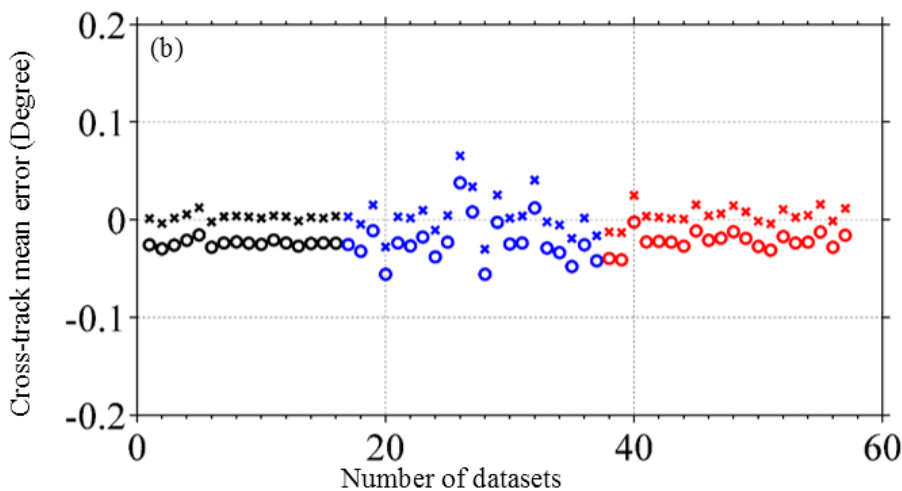
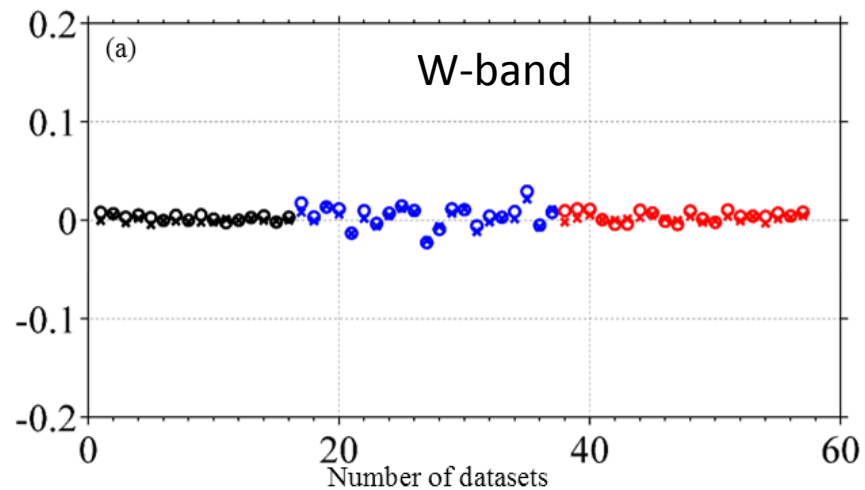
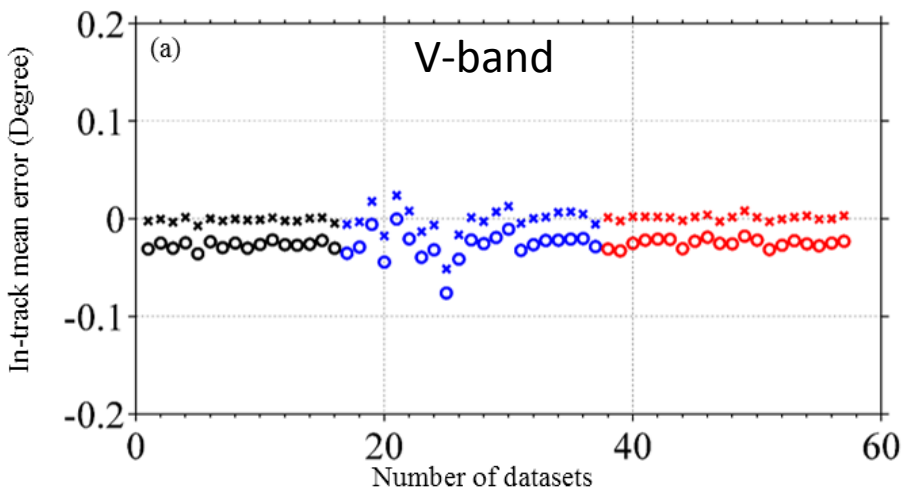
Transformation from latitude and longitude to in-track and cross-track coordinate



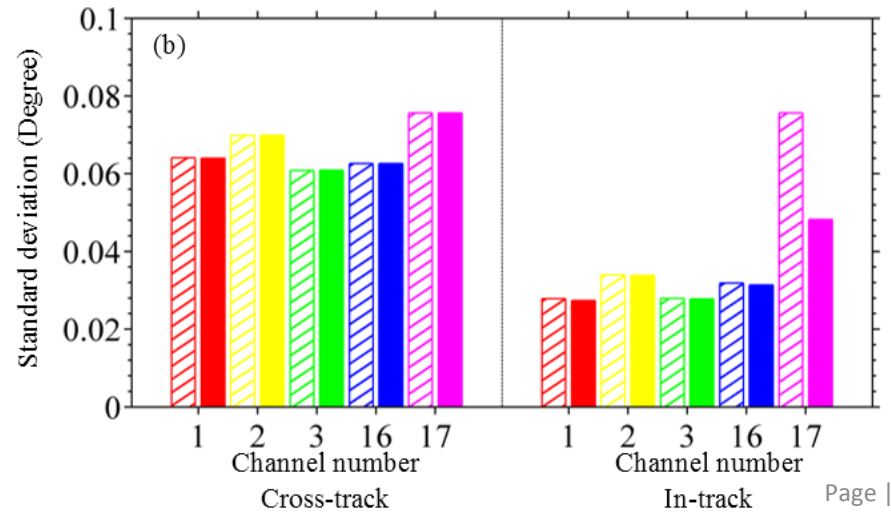
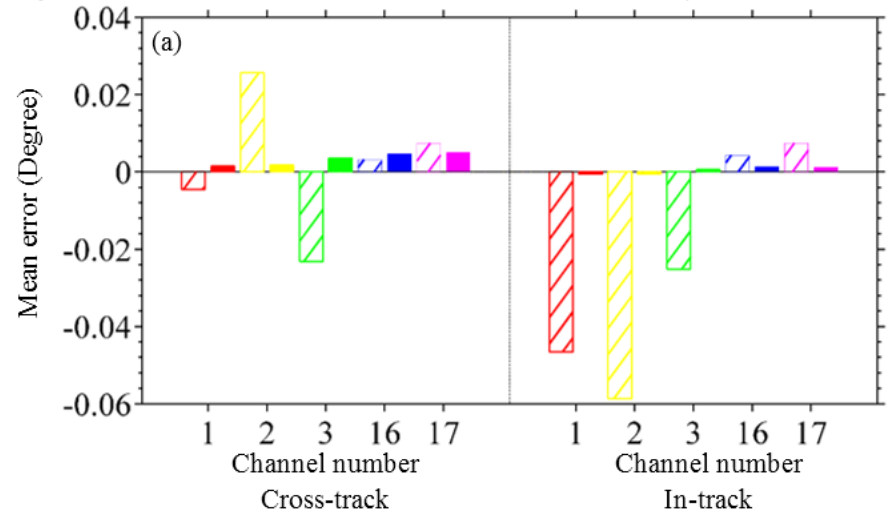
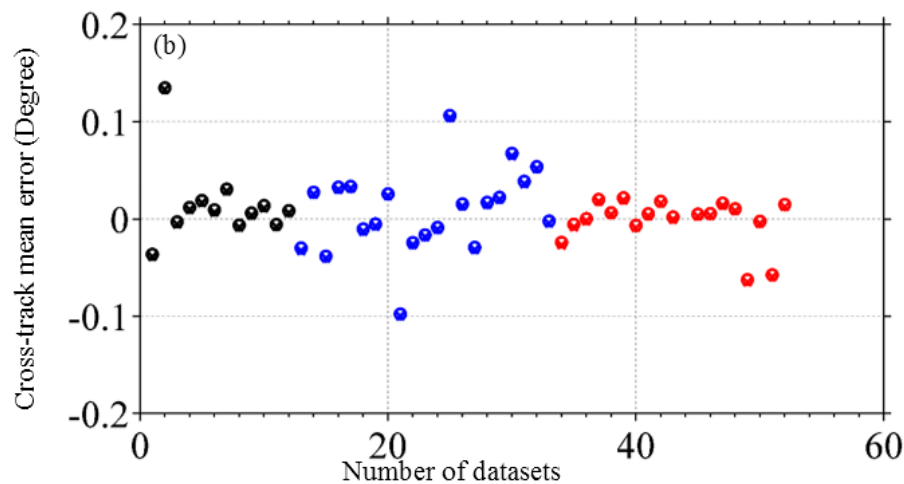
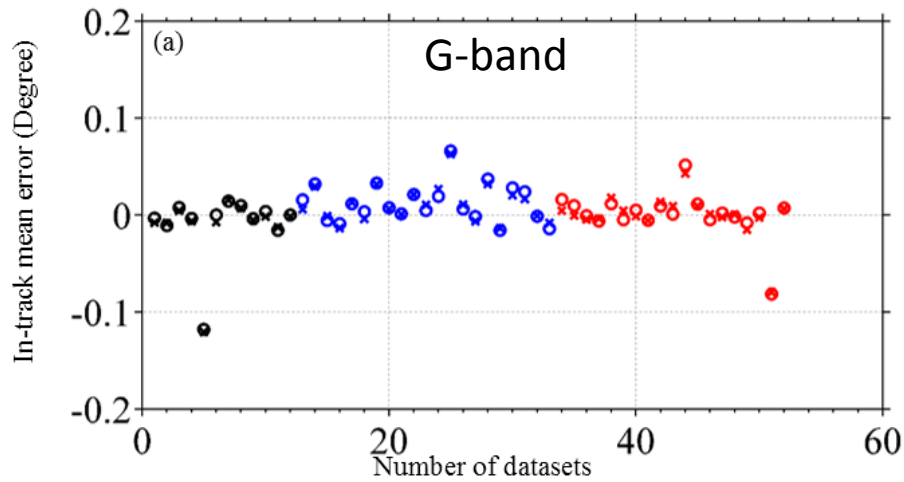
In-track and cross-track mean errors over North Africa western coast (black), Caspian Sea (blue), and Red Sea (red) before (circle) and after (cross) geolocation error correction.



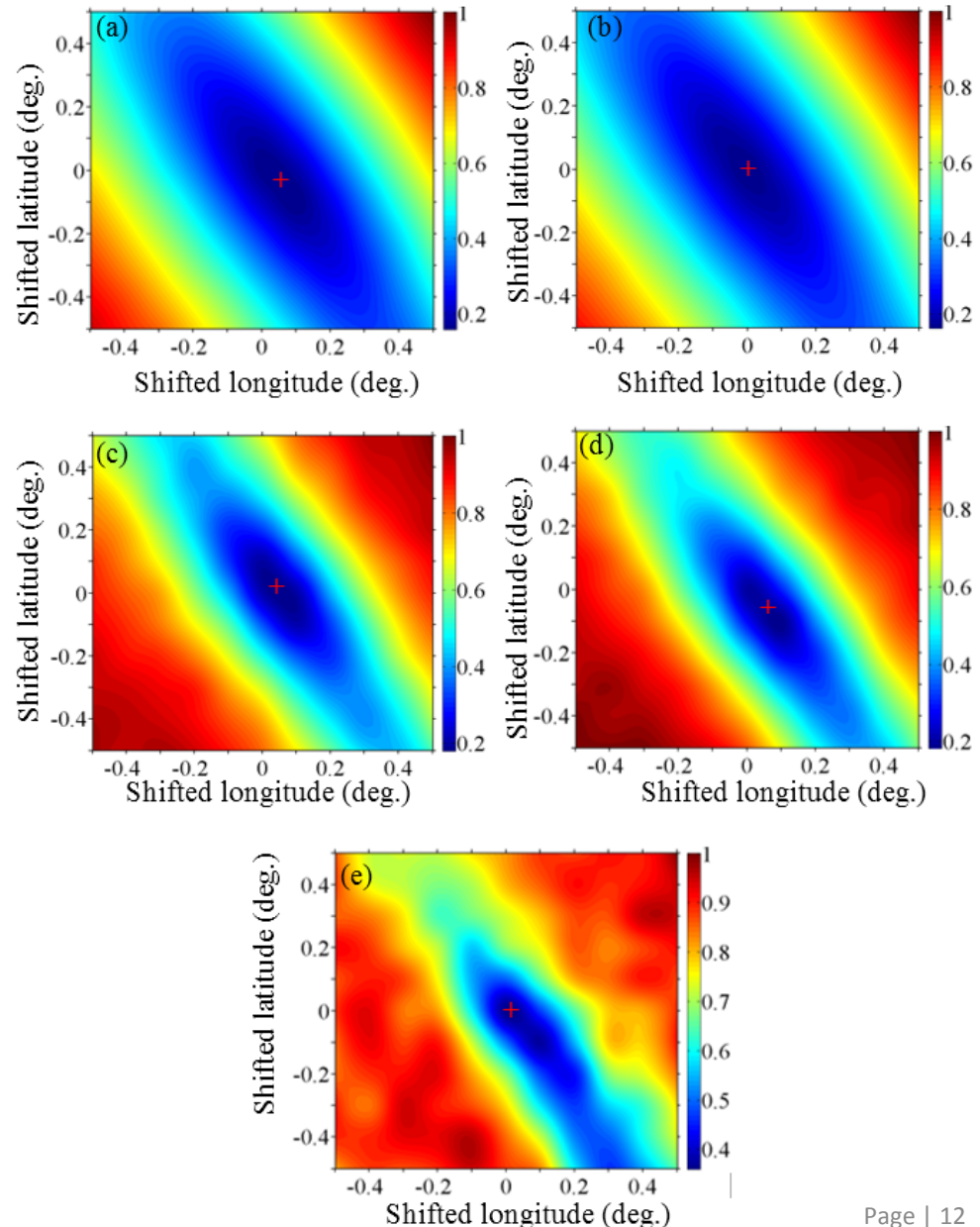
ATMS Geolocation Accuracy Validation Results (CDM)



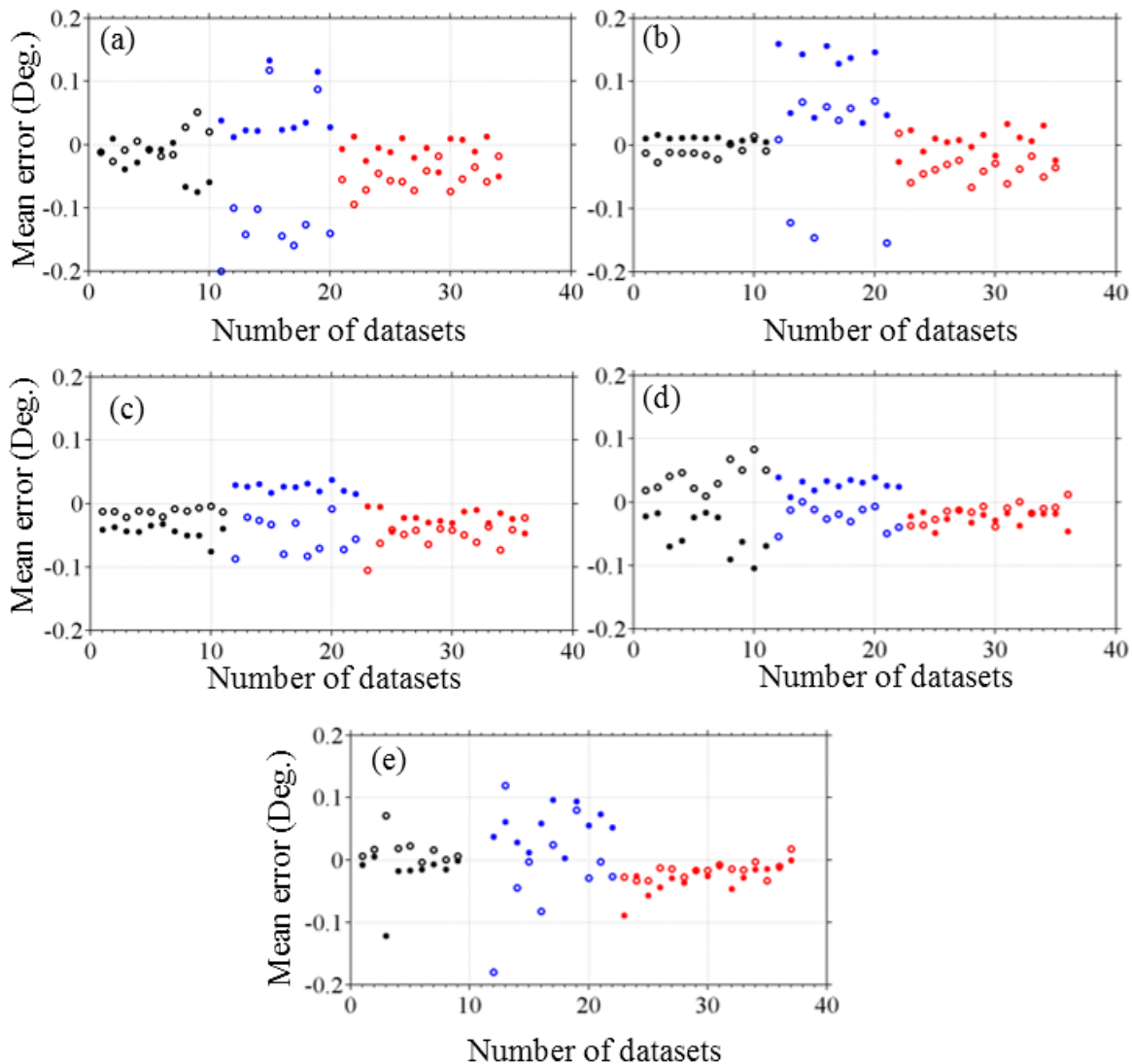
In-track and cross-track mean errors and standard deviation before and after geolocation error correction by bands



Cost functions for ATMS
K/Ka/V/W/G-band. The
minimized coast functions is at (-
0.074, 0.082), (-0.001, -0.002),
(0.001, 0.0510), (-0.1010, 0.0880)
and (-0.0010, 0.0110)



In-track (solid circle) and cross-track (open circle) mean errors ATMS K/Ka/V/W/G-band over North Africa western coast (black), Caspian Sea (blue), and Red Sea (red)



Latitude and longitude errors are recommended to be corrected in instrument alignment by pitch, roll and yaw angle adjustments

First transformation is from geodetic coordinate (ENU) to Earth spherical coordinate (IJK)

$$T_{IJK/ENU}^{loc} = \begin{bmatrix} -\sin \theta_{loc} & -\sin \varphi_{loc} \cos \theta_{loc} & \cos \varphi_{loc} \cos \theta_{loc} \\ \cos \theta_{loc} & -\sin \varphi_{loc} \sin \theta_{loc} & \cos \varphi_{loc} \sin \theta_{loc} \\ 0 & \cos \varphi_{loc} & \sin \varphi_{loc} \end{bmatrix}$$

Second transformation is from Earth spherical coordinate (IJK) to instrument coordinate (XYZ)

$$T_{XYZ/IJK}^{sat} = (T_{IJK/XYZ}^{sat})^T = \begin{bmatrix} \vec{x} & \vec{y} & \vec{z} \end{bmatrix}^T$$

The beam vector in instrument coordinate (XYZ) can be obtained from observed beam vectors in geodetic coordinate (ENU) by,

$$\vec{b}_{XYZ} = T_{XYZ/IJK}^{sat} T_{IJK/ENU}^{loc} \vec{b}_{ENU}$$

	K	Ka	V	W	G
Roll	-0.0525	0.1645	-0.1967	-0.0103	0.0186
Pitch	0.3538	0.4388	0.1992	-0.0219	-0.0132
Yaw	-0.0938	-0.0594	-0.0524	0.0682	-0.0954



Summary



- S-NPP ATMS in-track and cross-track geolocation errors meet the requirement
- According to this study, ATMS in-track and cross-track geolocation error is,
 - $(-0.0466, -0.0046)$ for K-band
 - $(-0.0587, 0.0257)$ for Ka-band
 - $(-0.0251, -0.0232)$ for V-band
 - $(0.0043, 0.0032)$ for W-band
 - $(0.0023, 0.0075)$ for G-band
- A rotation correction matrix is derived based on the analysis to improve the geolocation accuracy



Path Forward



- STAR ICVS will add S-NPP ATMS geolocation accuracy long term trending parameters
- Attempt to implement geolocation correction in OPS
- Validate JPSS-1 ATMS mounting matrix



J1 CrIS SDR Algorithm and Software

Yong Han and Yong Chen

Acknowledgement: CrIS SDR science team for the development and improvement of J1 CrIS SDR algorithm

STAR JPSS Science Team Annual Meeting, August 24-28, 2015



Outline



- J1 CrIS SDR baseline algorithm/software
- Proposed J1 CrIS SDR algorithm/software updates
- Summary and future work



Baseline J1 CrIS SDR Algorithm/Software



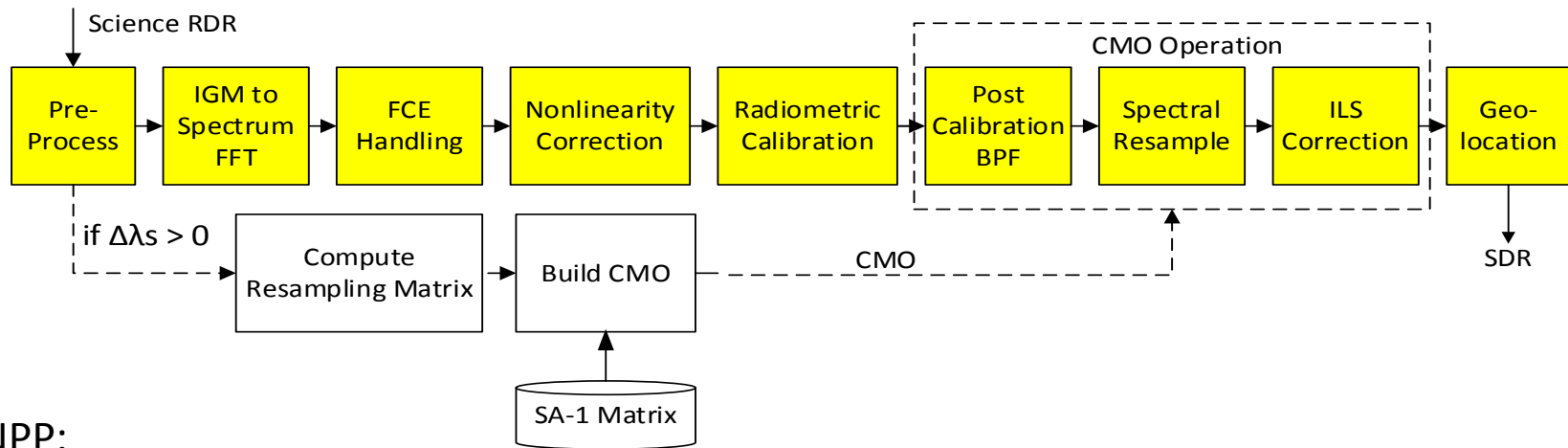
J1 Baseline Algorithm/Software



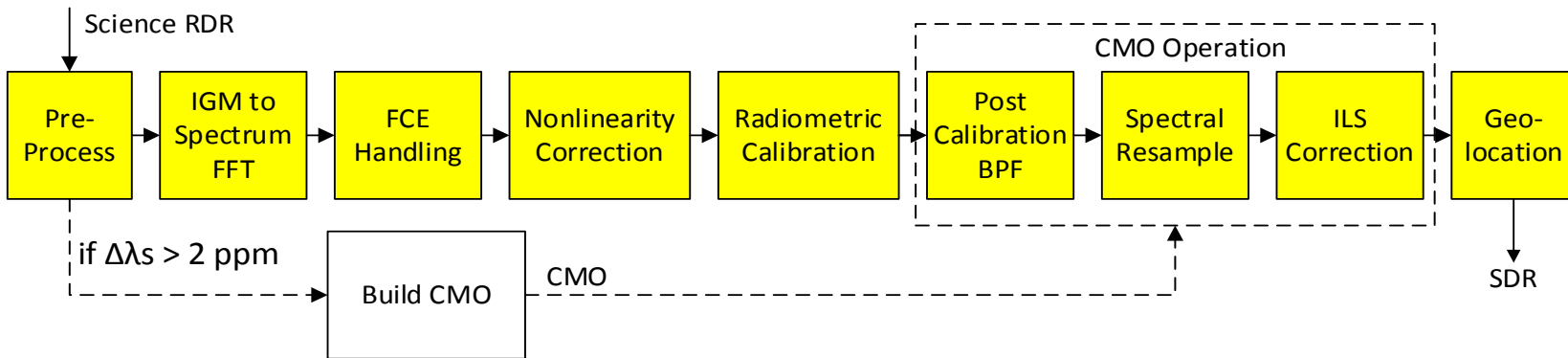
- Delivered on January 30, 2015
- New FCE module delivered on May 30, 2015
- Software/software changes
 - Capable to process both normal and full spectral resolution SDRs
 - Backward compatibility (multiple calibration algorithms implemented)
 - CMO file separated into two files: 1) SA-1 matrix; 2) backup of Engineering packet
 - Resampling matrix calculation following neon calibration
 - Resampling and self-apodization matrix algorithms are modified to reduce spectral ringing artifacts
 - Spectral calibration (CMO) applied to radiance noise (NEdN) calculation
 - New FCE detection/correction module

SDR Processing Flow

JPSS-1:



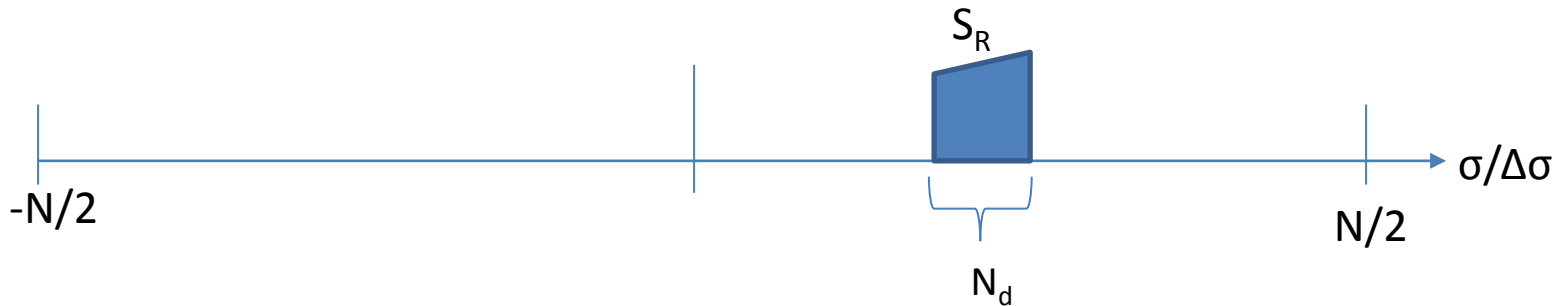
S-NPP:



JPSS-1: resampling is performed on un-decimated spectral domain (large N) and the matrix calculation is updated with Mooney's equation:

$$F[k, k'] = \frac{\Delta\sigma_s}{\Delta\sigma_u} \frac{\text{Sin}\left(\pi \frac{\sigma_{s,k'} - \sigma_{u,k}}{\Delta\sigma_u}\right)}{N \text{Sin}\left(\pi \frac{\sigma_{s,k'} - \sigma_{u,k}}{N\Delta\sigma_u}\right)}$$

Mooney, 2014



S-NPP: small N and the Eq has a minor error:

$$F[k, k'] = \frac{\text{Sin}\left(\pi \frac{\sigma_{s,k'} - \sigma_{u,k}}{\Delta\sigma_u}\right)}{N_d \text{Sin}\left(\pi \frac{\sigma_{s,k'} - \sigma_{u,k}}{N_d \Delta\sigma_s}\right)}$$

- Big N is used in the J1 delivery; the J1 resampling algorithm is consistent with the Double-FFT method (see backup slides)

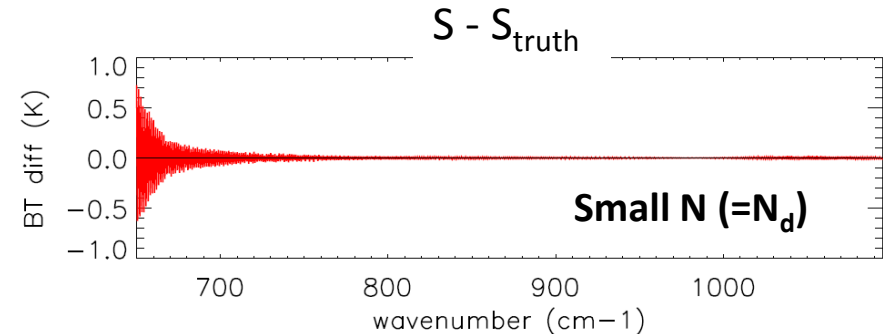
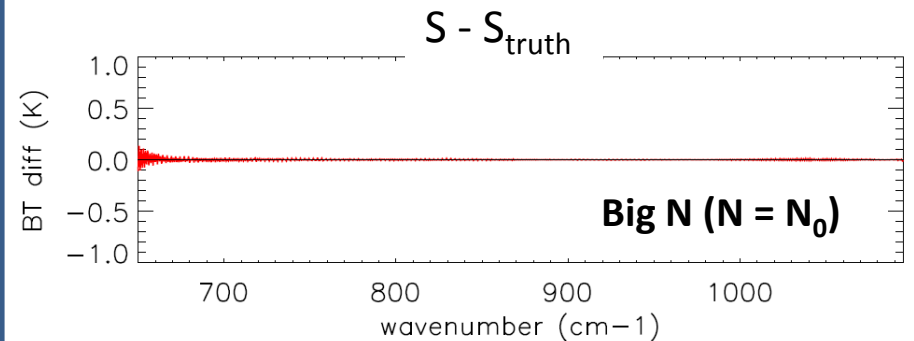
JPSS-1:

$$S_{k'} = \frac{\Delta\sigma_s}{\Delta\sigma_u} \sum_{k=0}^{N_d-1} S_k \frac{\text{Sin}\left(\pi \frac{\sigma_{s,k'} - \sigma_{u,k}}{\Delta\sigma_u}\right)}{N \text{Sin}\left(\pi \frac{\sigma_{s,k'} - \sigma_{u,k}}{N\Delta\sigma_u}\right)}$$

S-NPP:

$$S_{k'} = \sum_{k=0}^{N_d-1} S_k \frac{1}{N_d} \frac{\text{Sin}\left(\pi \frac{\sigma_{s,k'} - \sigma_{u,k}}{\Delta\sigma_u}\right)}{\text{Sin}\left(\pi \frac{\sigma_{s,k'} - \sigma_{u,k}}{N_d \Delta\sigma_s}\right)}$$

Comparison of using big N and small N
(simulated results)



$N_d = 866$ (LW), 1052 (MW), 799 (SW)

$N = 20784$ (LW), 21040 (MW), 20744 (SW)

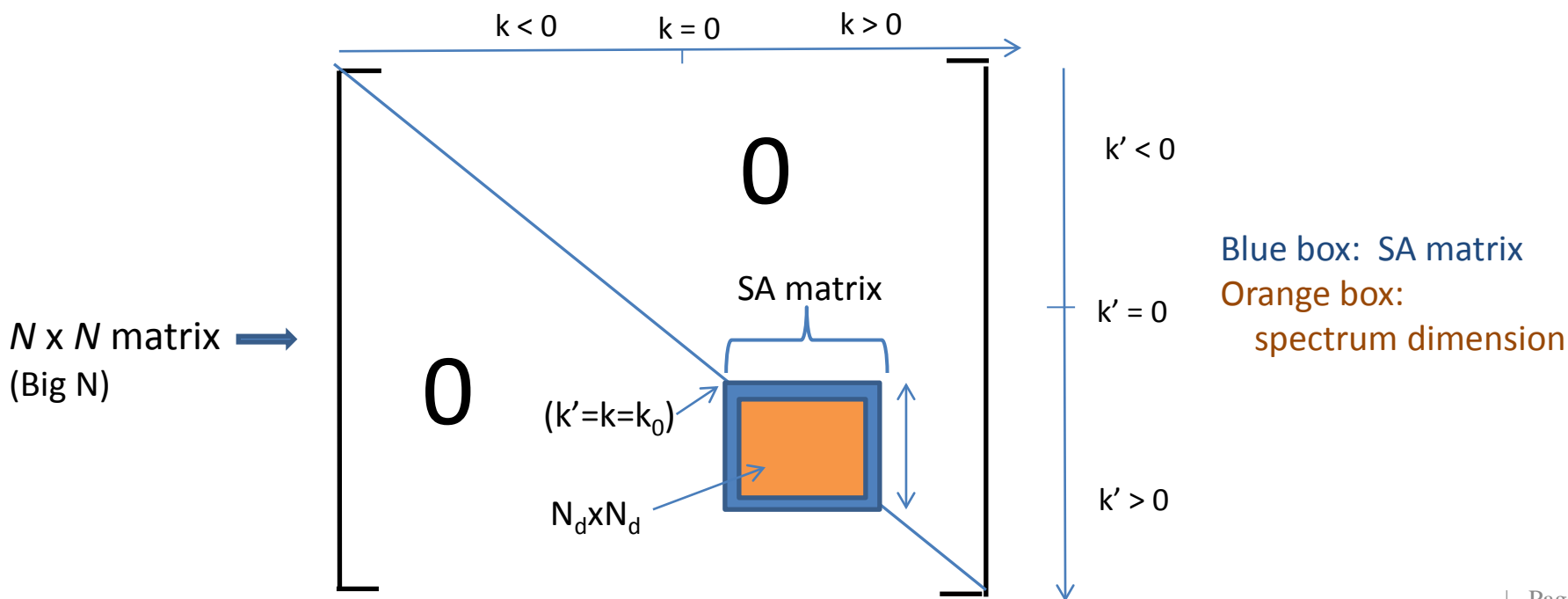
Expansion factor β :

- JPSS-1: 1.4 (LW), 2 (MW), 2 (SW)
- SNPP: 1.1, (LW, MW, SW)

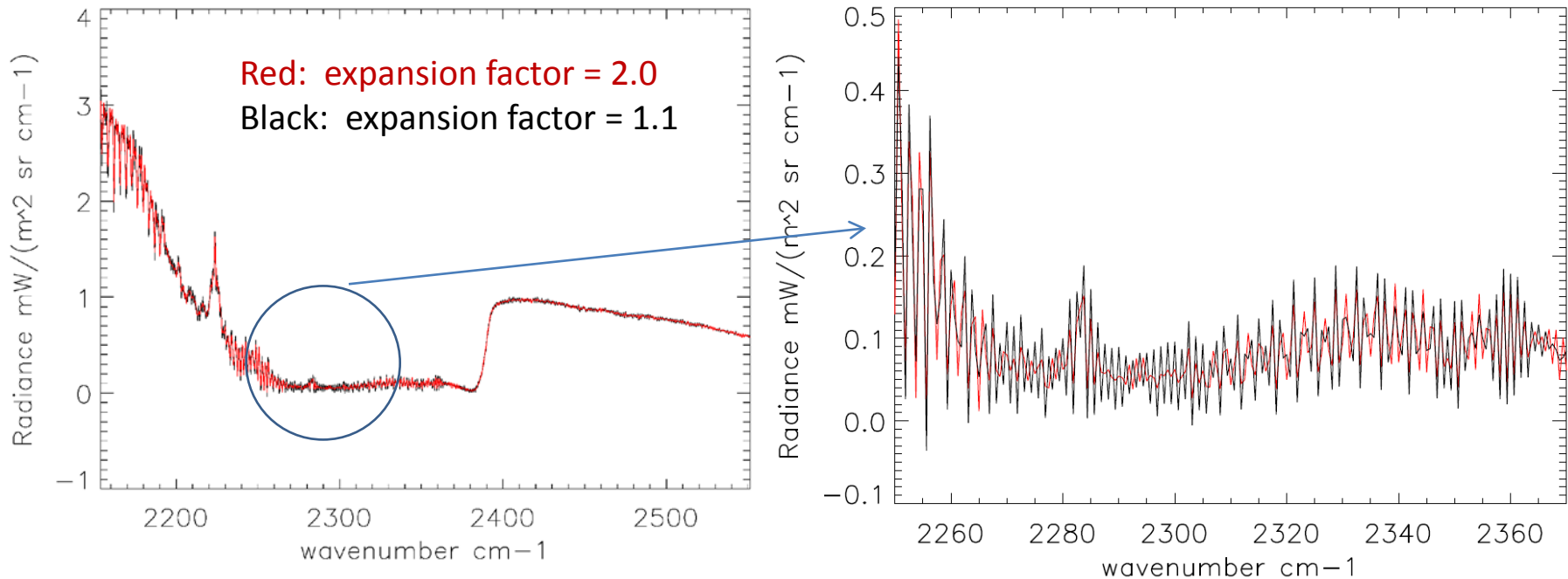
- Big N is used, consistent with the resampling algorithm
- Results of using big N and small N differ little

$$SA[k', k] = \int_{\alpha_{\min}}^{\alpha_{\max}} \text{psinc}((k_0 + k') - \alpha(k_0 + k), N) ILS(\alpha) d\alpha$$

$$\sum_{k'=k_0}^{k_0 + \beta N_d - 1} SA[k', k] \approx 1$$



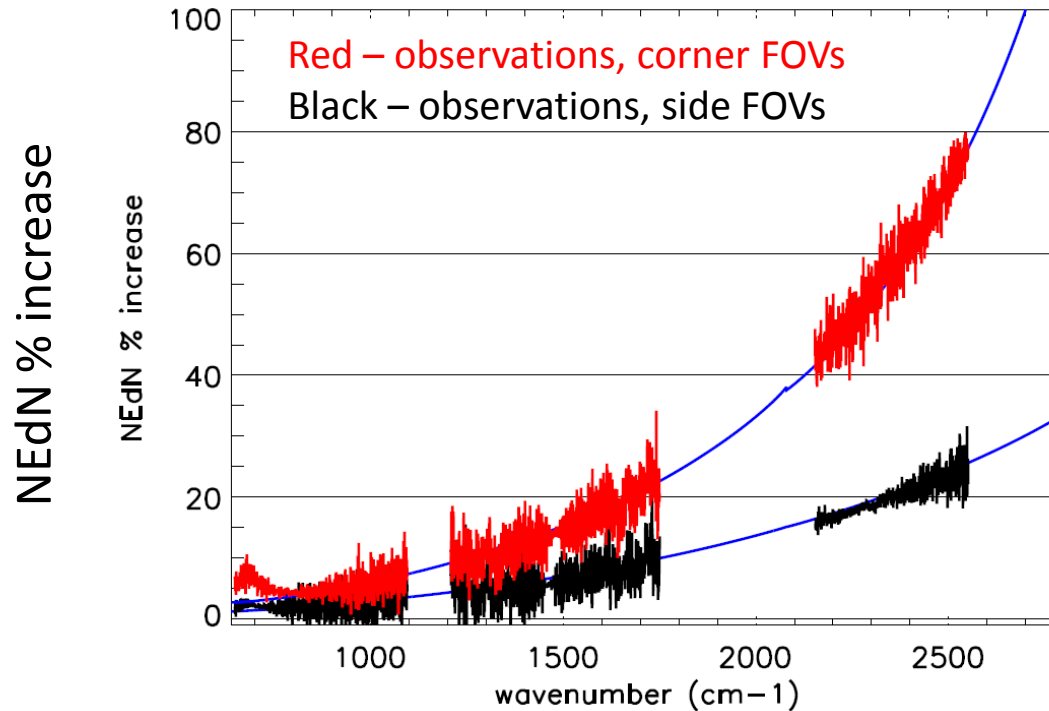
The self-apodization (SA) matrix expansion factor is increased from 1.1 to 2.0 for the SW bands to reduce ringing artifacts



NEdN Algorithm

JPSS-1: CMO applied to NEdN calculation

S-NPP: no CMO applied to NEdN calculation



For FSR SDR processing, NEdNs in MW and SW bands are significantly increased by self-apodization (SA) correction



Proposed J1 CrIS SDR Algorithm/Software Updates



Summary of Proposed Updates



- All the updates described in the following slides have already been implemented in the ADL code
- Software/algorithm updates
 - Use of full interferogram data points (reducing ringing artifacts)
 - Raised-cosine post-filter and adjustable filter parameters (reducing ringing artifacts)
 - Algorithm 4 and UMBC CCAST calibration (reducing ringing artifacts)
 - Band-dependent lunar intrusion thresholds added to the PCT file (improving lunar intrusion detection)
 - Sign change for the cross-track offset angles to remove the reordering of the FOV positions in geolocation calculation (?)

- Non-circular FIR filtering is an issue which was first brought out by Dan Mooney
- UW demonstrated that it is a root-cause of the ringing artifacts
- UW proposed the following solution to reduce the ringing artifacts (presented on 12 March 2014 team telecon):

(1) Divide out the ideal filter:
 $\text{FFT}(\text{NF} * \text{DM}) / \text{FFT}(\text{NF})$

(2) Transform back to the time domain by zero-padding to reconstruct a good approximation to the original DM IFG

(3) Truncate the reconstructed IFG by an amount equivalent to about 5 decimated points

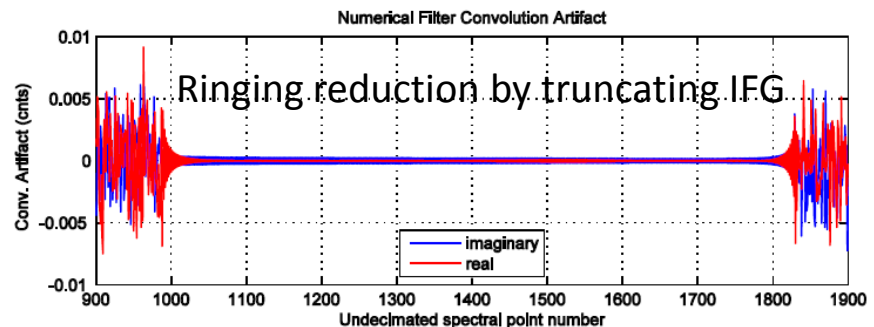
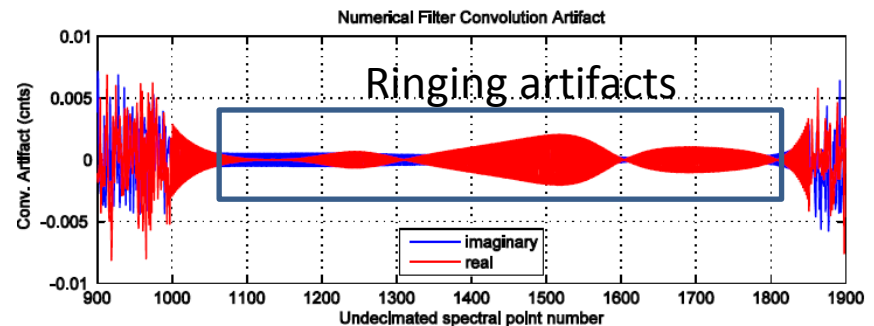
(4) FFT the truncated reconstructed IFG to the spectrum

DM – diagnostic mode interferogram (IFG)

NF – FIR filter

NF*DM – non-circular convolution

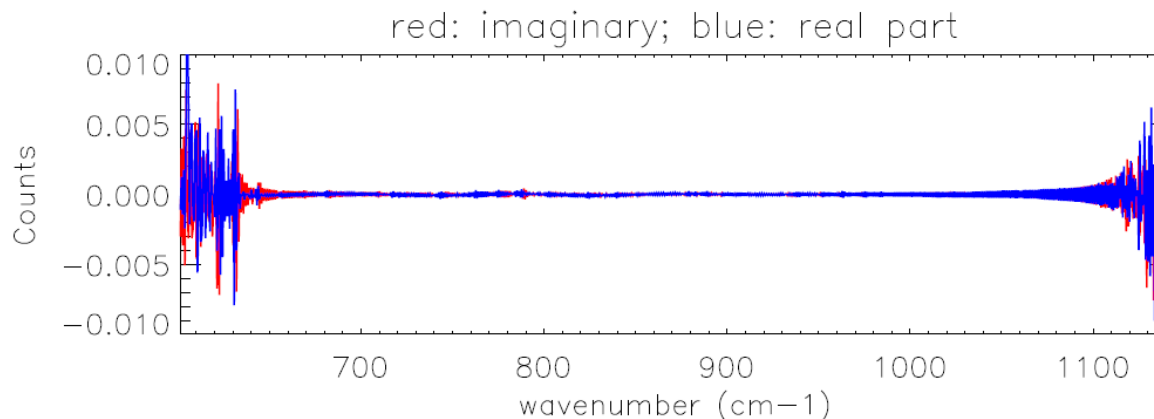
Raw spectrum difference from truth



- STAR demonstrated that the UW method can be implemented in the spectral domain with the big N resampling matrix F (see backup slides):

$$S = F \cdot (S_{raw} / FIR) \quad F[k', k] = \frac{\Delta\sigma_s}{\Delta\sigma_u} \frac{\text{Sin}(\pi \frac{\sigma_{s,k'} - \sigma_{u,k}}{\Delta\sigma_u})}{N_{big} \text{Sin}(\pi \frac{\sigma_{s,k'} - \sigma_{u,k}}{N_{big} \Delta\sigma_u})}$$

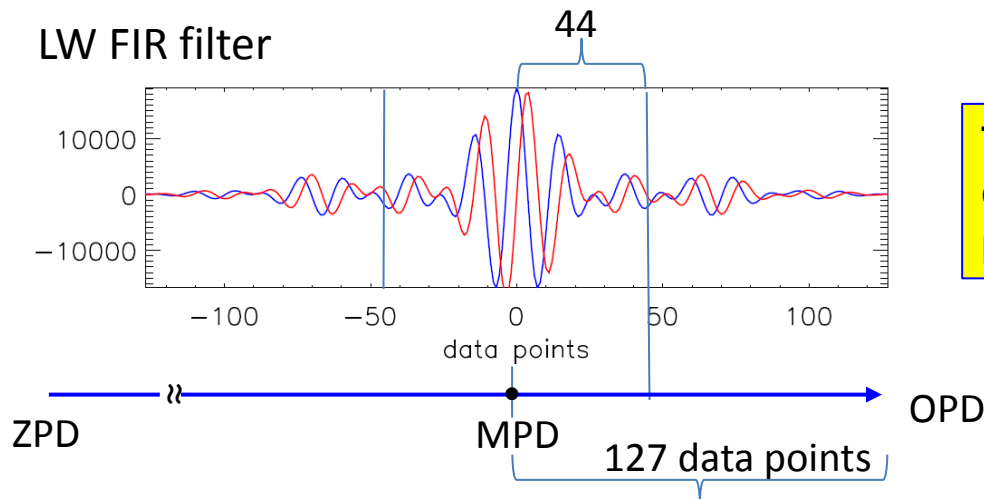
Performed in spectral domain:



Extending Interferogram (3/4)

- We need 5 or more additional decimated data points beyond MPD for ringing reduction
- In the following we demonstrate even using the two data points currently dropped off by the SDR algorithm can significantly reduce the ringing artifacts:

	LW	MW	SW
Data points used in J1 baseline codes	864	1050	797
Available data points N_d	866	1052	799
$N_d * DF$	20784	21040	20774
Un-decimated points beyond MPD ($\lambda = 1546.23D-7$ cm)	88	344	78

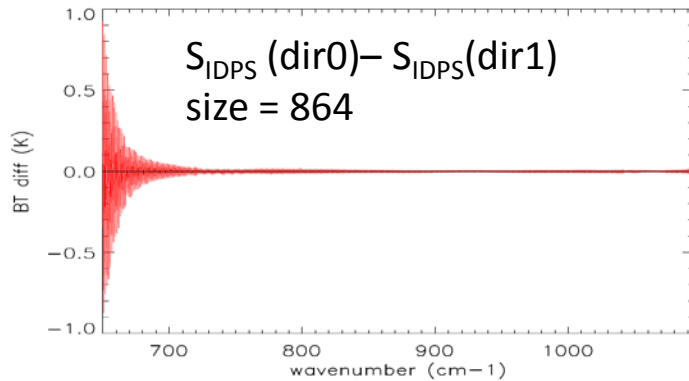


The extended 44 undecimated data points comprise the core of the needed 127 data points beyond the MPD

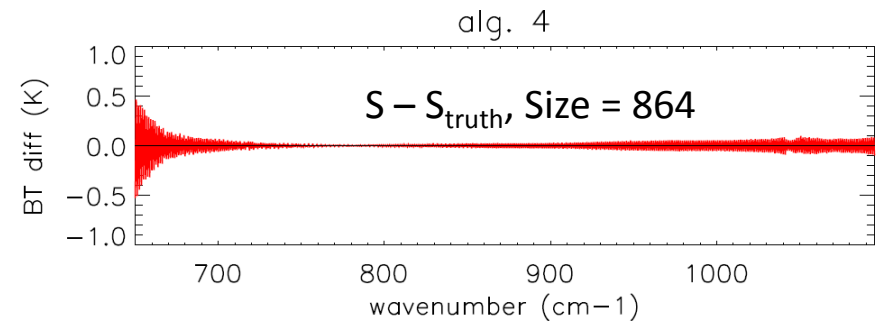
- Use of the two extra data points significantly reduces the ringing artifacts caused by the non-circular FIR filtering

Sweep direction difference (FOV-5)

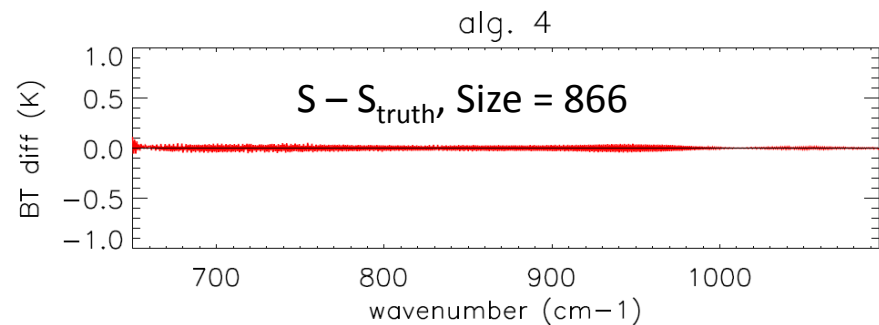
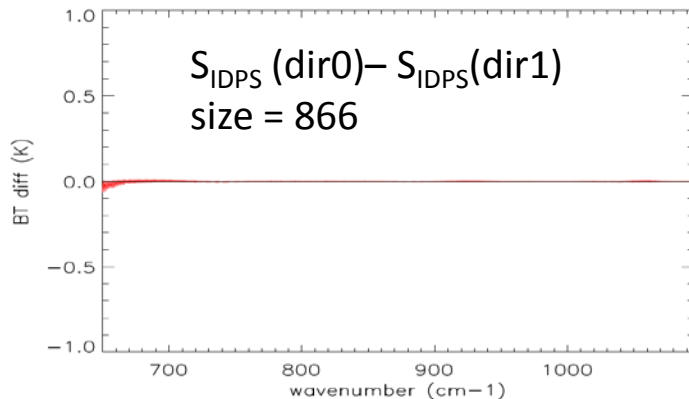
$N_d = 864$



Difference from truth (FOV-1)



$N_d = 866$



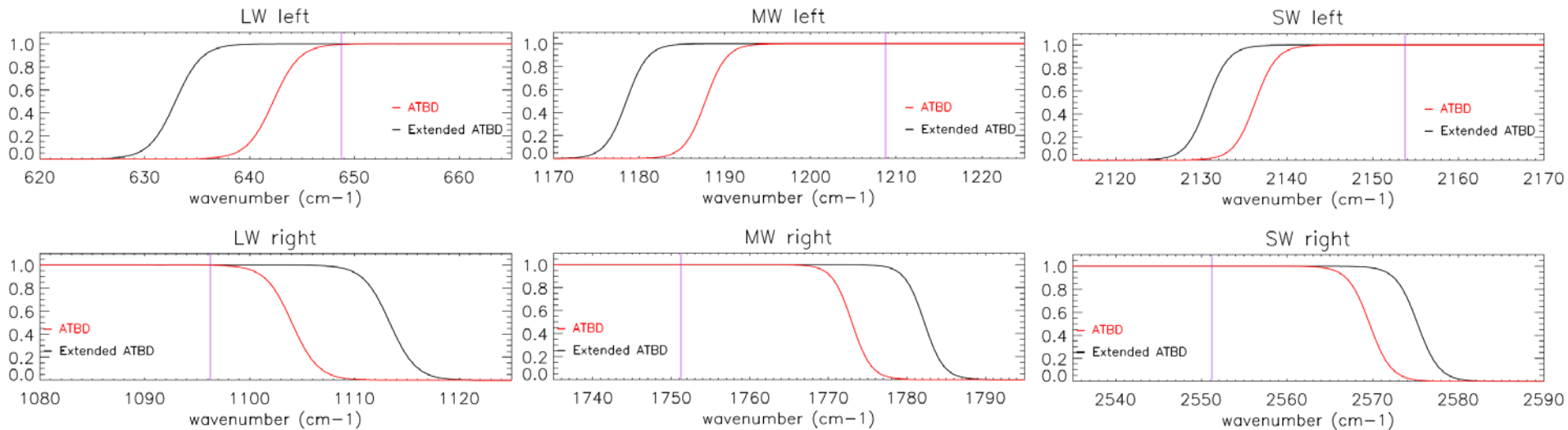
Simulated results

Extending BPF Width (1/2)

Post-filter parameters:

Black – proposed improvement Red – baseline J1 code

	k0	k1	a1	a2	a3	a4
LW	78	790	30 (15)	0.5	30 (15)	0.5
MW	95	959	59 (44)	0.5	59 (44)	0.5
SW	84	716	41 (32)	0.5	41 (32)	0.5



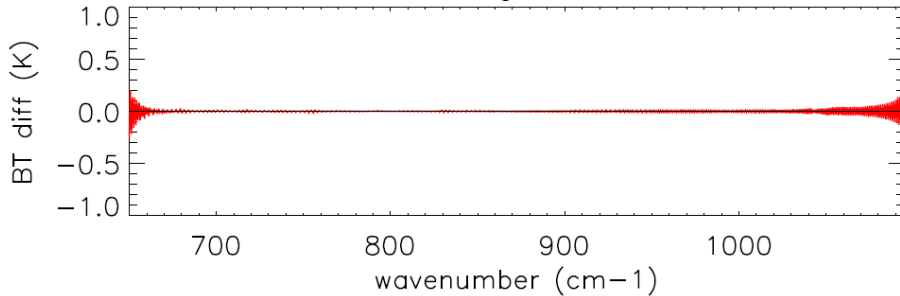
Use of a wider PF preserves useful information for edge channels

Extending BPF Width (2/2)

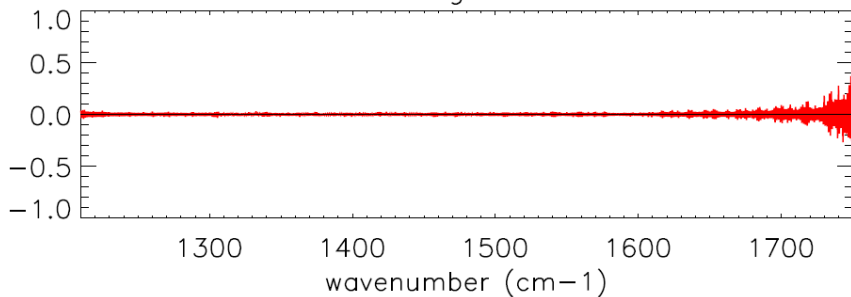
- Use of a wider PF preserves useful information for edge channels

Narrow Post-filter (FOV-5)

alg. 4

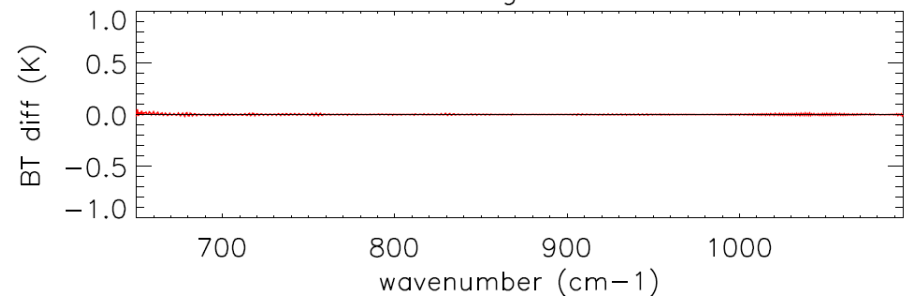


alg. 4

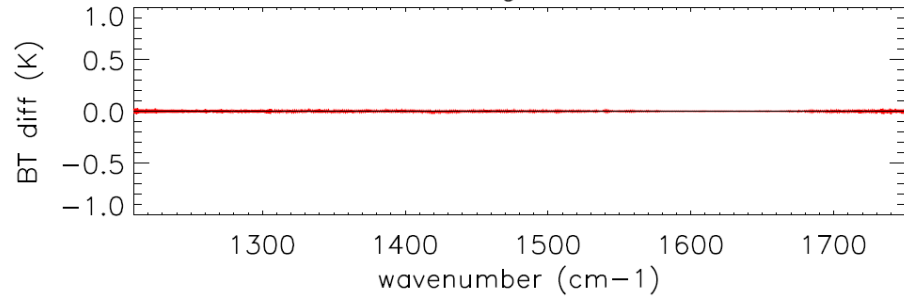


Wide Post-filter (FOV-5)

alg. 4



alg. 4





Improving Calibration Equation (1/2)



- Equations differ mainly in how the ratio $\Delta S_1 / \Delta S_2$ is filtered before spectral calibration
- The order of spectral calibration components does not have a significant impact
- Algorithm 4 allows the use of a wider PBF f (if no aliasing, f is not needed)

J1 baseline (algorithm 1):

$$S_{Cal} = SA^{-1} \cdot F \cdot \left\{ f \cdot \frac{\Delta S_1}{\Delta S_2} \right\} ICT$$

Algorithm 4:

$$S_{Cal} = ICT \cdot \frac{F \cdot SA^{-1} \cdot \left\{ f \cdot \frac{\Delta S_1}{\Delta S_2} \right\} |\Delta S_2|}{F \cdot SA^{-1} \cdot \left\{ f \cdot |\Delta S_2| \right\}}$$

Responsivity as a filter

$$\Delta S_1 = FIR^{-1}(S_e - \langle S_{DS} \rangle)$$

$$\Delta S_2 = FIR^{-1}(\langle S_{ICT} \rangle - \langle S_{DS} \rangle)$$

Responsivity removed after spectral calibration

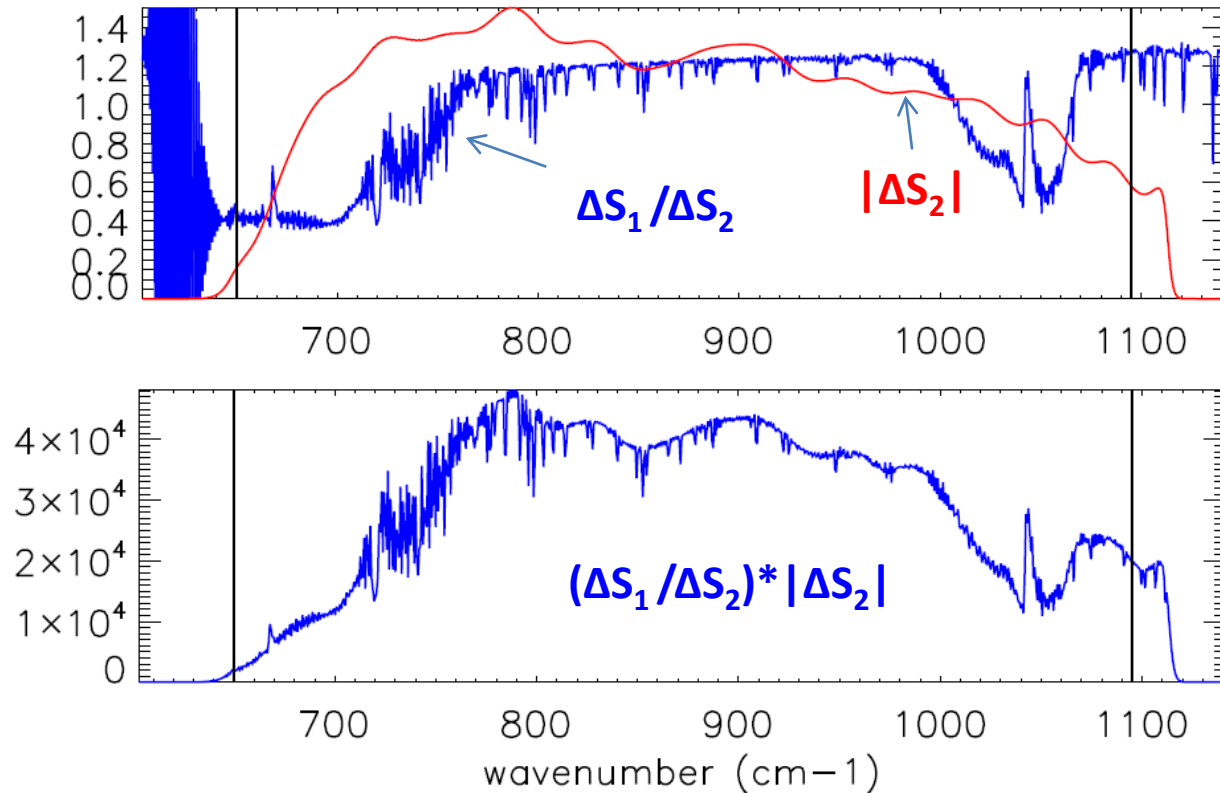
$$= ICT \cdot \frac{F \cdot SA^{-1} \cdot f \cdot \left\{ \frac{\Delta S_1}{Phase(\Delta S_2)} \right\}}{F \cdot SA^{-1} \cdot f \cdot \left\{ \frac{\Delta S_2}{Phase(\Delta S_2)} \right\}}$$

Predina's original form

UMBC CCAST:

$$S_{Cal} = ICT \cdot F \cdot SA^{-1} \cdot \left\{ f \cdot \frac{\Delta S_1}{\Delta S_2} \right\}$$

- The A4 calibration equation performs spectral calibration on radiometric ratio $\Delta S_1 / \Delta S_2$ filtered with $|\Delta S_2|$ (related to responsivity)



- The following slides show results of obs-cal, sweep direction difference and FOV-to-FOV difference for the LW band (results for MW & SW bands are included in the backup slides)

J1 baseline:
$$S_{Cal} = SA^{-1} \cdot F \cdot f \cdot \left\{ \frac{\Delta S_1}{\Delta S_2} ICT \right\}$$

$$N_d = 864 \text{ (LW)}, 1050 \text{ (MW)}, 797 \text{ (SW)}$$

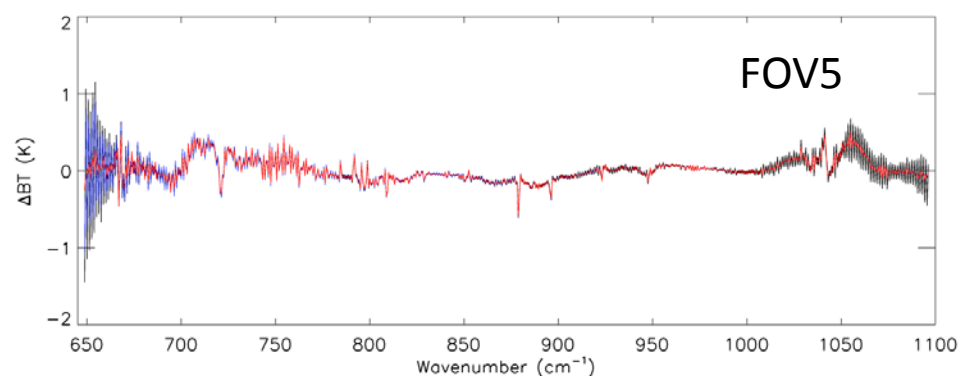
Algorithm 4:
$$S_{Cal} = ICT \cdot \frac{F \cdot SA^{-1} \cdot f \cdot \left\{ \frac{\Delta S_1}{\Delta S_2} |\Delta S_2| \right\}}{F \cdot SA^{-1} \cdot f \cdot |\Delta S_2|}$$

$$N_d = 866 \text{ (LW)}, 1052 \text{ (MW)}, 799 \text{ (SW)}$$

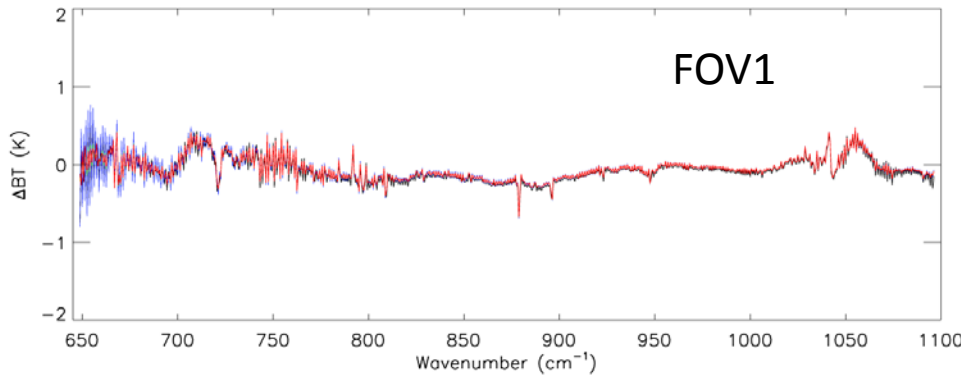
Wider f

$$BT_{obs} - BT_{lbl}$$

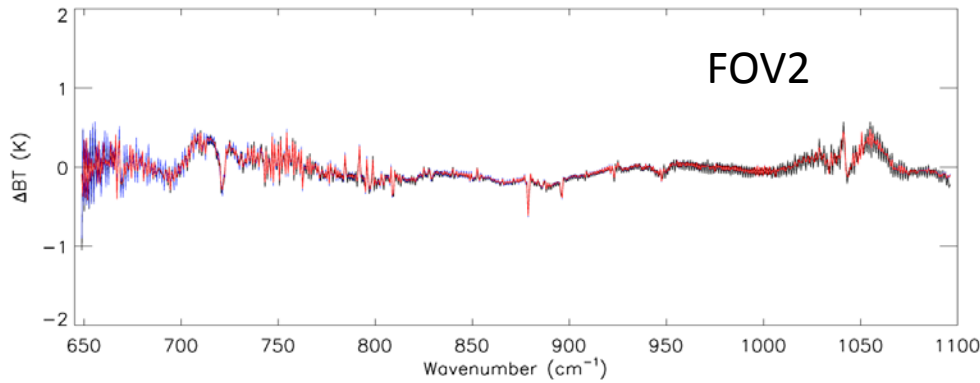
Responsivity is used
in BT_{lbl} calculation



— J1 baseline

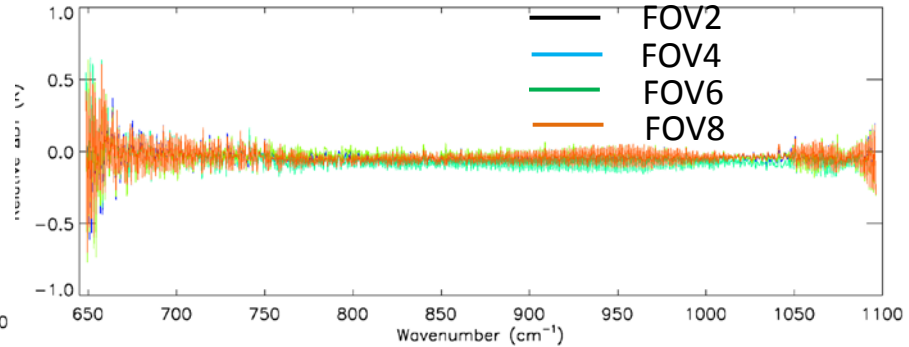
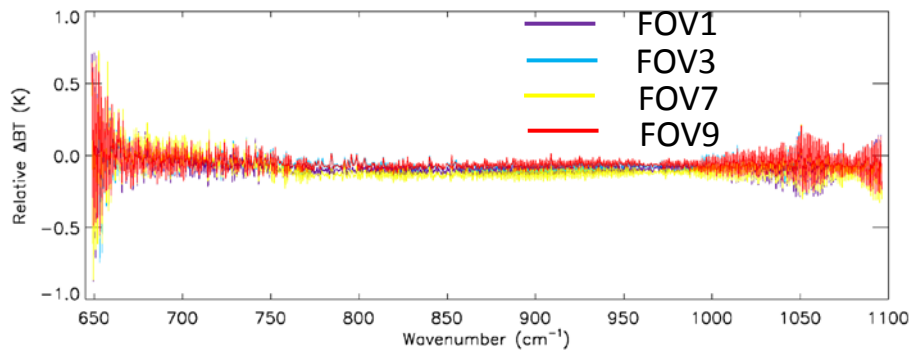


— A4

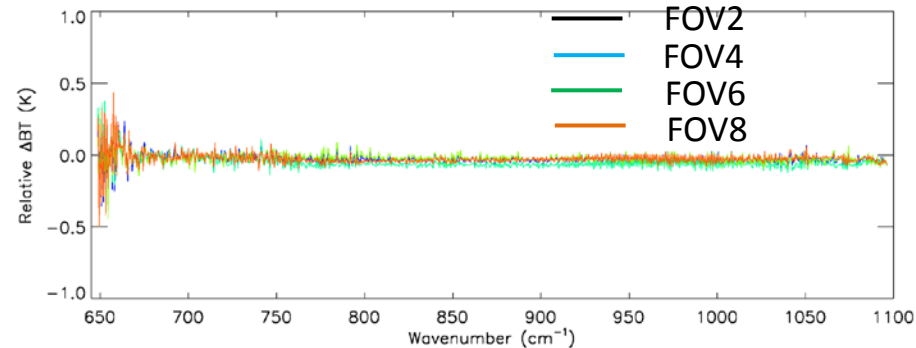
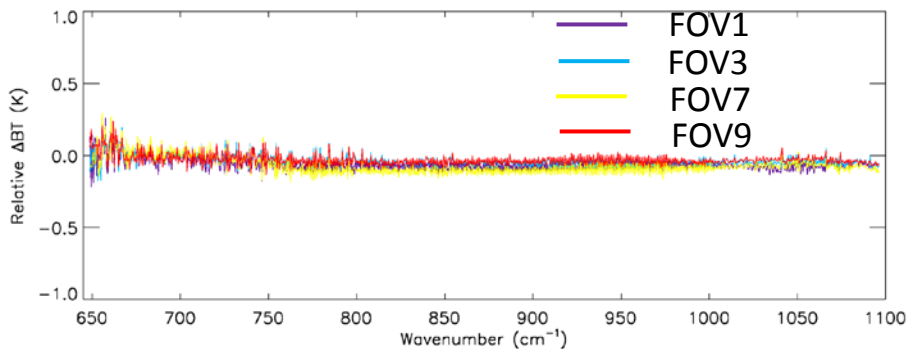


FOV-2-FOV Comparison

J1 baseline



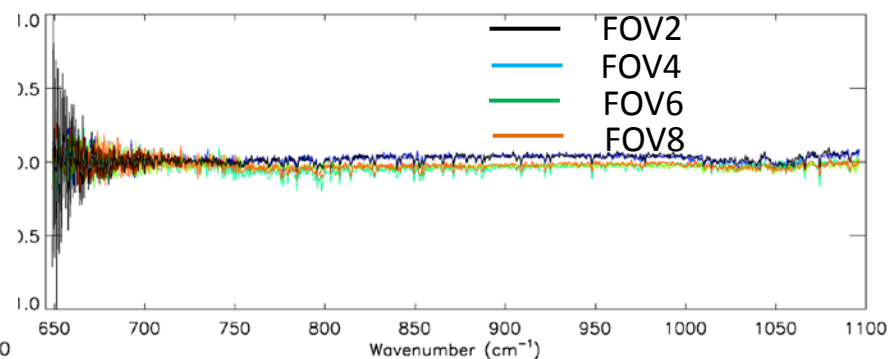
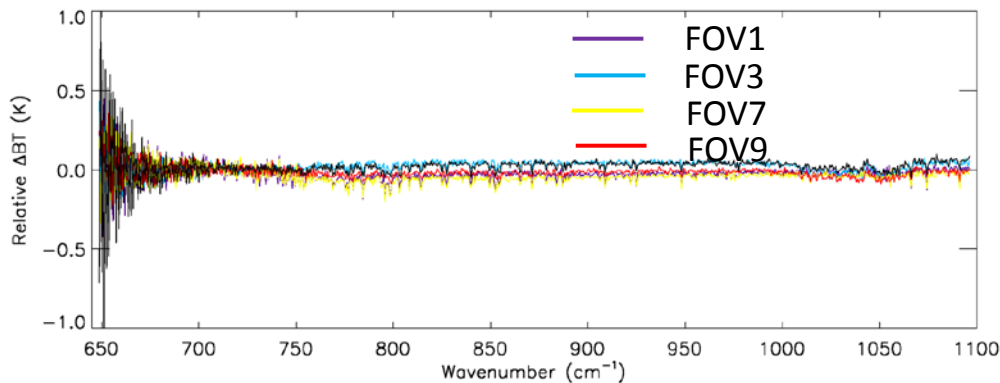
Algorithm 4



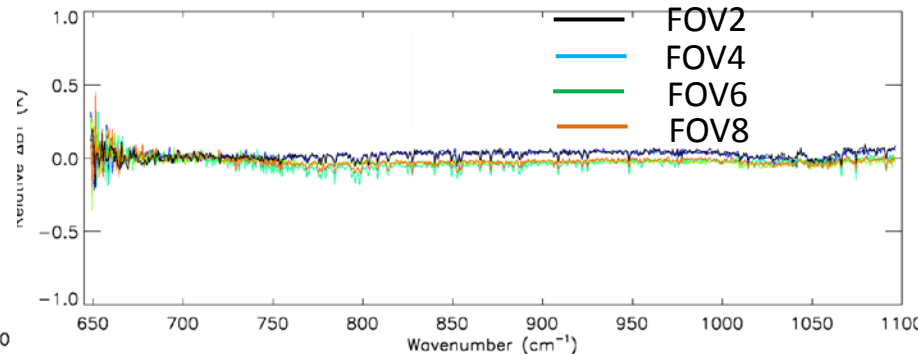
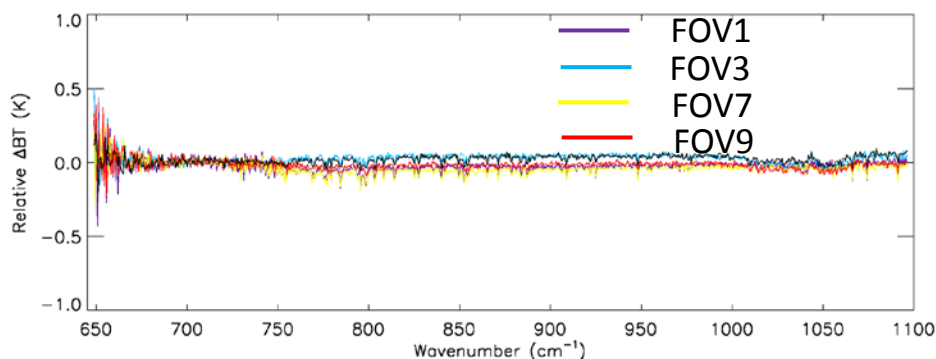
$$(BT_{obs} - BT_{lbl})_{fov_i} - (BT_{obs} - BT_{lbl})_{fov_5}$$

Sweep Direction Differences

J1 baseline



Algorithm 4



$$(BT_{obs} - BT_{lbl})_{fwd} - (BT_{obs} - BT_{lbl})_{rev}$$



Schedule for Delivery



- The updates described in this presentation will be delivered before the end of 2015 through the DR system
- The updates will also include UMBC calibration equation with flexible parameters to adjust the filter width and position
- The updates will also include the use of band-dependent lunar intrusion thresholds
- The updates can also include the geolocation algorithm correction (need team consensus)



Summary & Future Work



- The baseline J1 CrIS SDR software was delivered with the capability to process FSR SDRs and the backward compatibility for old data
- The proposed updates will significantly reduce radiance ringing artifacts
- The proposed updates will be delivered in December 2015
- Future work:
 - Algorithm evaluation for extended interferograms expected to be available before the end of 2015
 - Post-filter optimization
 - Continuation of evaluations of calibration algorithms
 - Lunar intrusion algorithm improvement
 - Impulse noise spike handling



Backup Slides

Double FFTs vs. Resampling

- Shown here is the equivalence between the double-difference and resampling methods

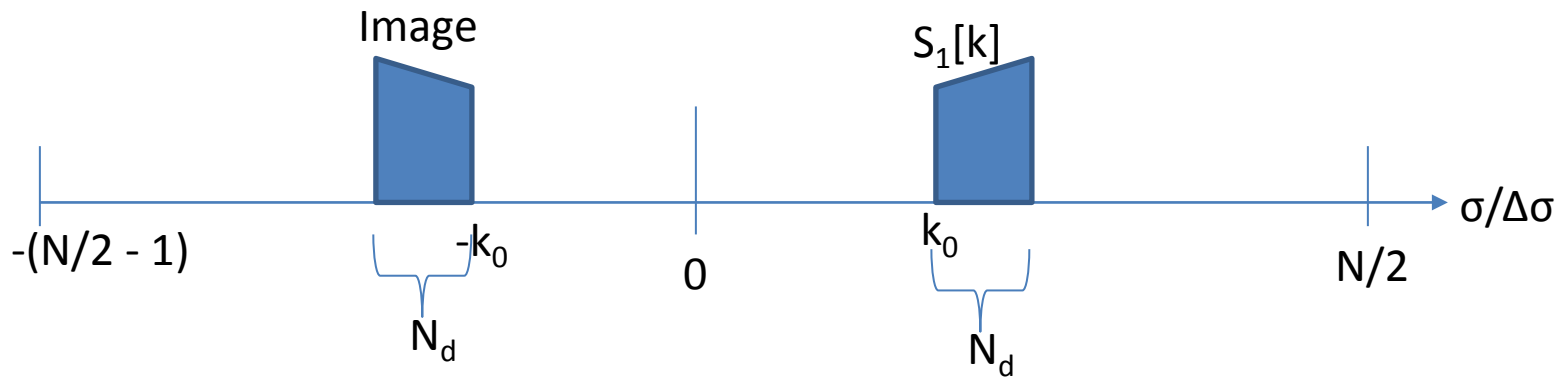
Start with the raw decimated complex spectrum $\{S_0[k], k = 1, N_d\}$

Double-FFT step 1: divide the raw spectrum by the FIR spectrum as

$$S_1[k] = S_0[k] / \text{FIR}[k]$$


Double-FFT step 2: pad zeros to form the spectrum shown below,

$$S_2[k] = \begin{cases} S_1[k - k_0] & k = [k_0, k_0 + N_d - 1] \\ S_1[-k - k_0] & k = [-(k_0 + N_d - 1), -k_0] \\ 0 & \text{otherwise} \end{cases}$$



Double-FFT step 3: Perform discrete Fourier Transform

$$I_2[n] = \sum_{k=-(N/2-1)}^{N/2} S_2[k] e^{i2\pi nk/N} \Delta\sigma_s \quad \Delta\sigma_s = \frac{1}{\lambda_s \cdot N_d \cdot DF}$$

 Sampling wavelength

Double-FFT step 4: truncate $I_2[n]$ at N_t so that $N_t \lambda_s \approx 1.6 \text{ cm}$ and then transform it back to spectrum, which is on the user grid $\Delta\sigma_u = \frac{1}{N_t \Delta x}$:

$$S_3[k] = \sum_{n=-(N_t/2-1)}^{N_t/2} I_2[n] e^{i2\pi nk/N_t} \Delta x \quad \Delta x = \frac{1}{N \cdot \Delta\sigma_s}$$

Double-FFT step 5: take the in-band channels from $S_3[k]$ to get the final spectrum:

$$S = \{S_3[k], k = k_a \dots k_b\} \text{ with a spectral resolution}$$

where $k_a \Delta\sigma_u = \sigma_{k_a}$ and $k_b \Delta\sigma_u = \sigma_{k_b}$ are the starting and ending wavenumbers of the in-band spectrum

Double FFTs vs. Resampling

- Derivation of resampling matrix

Insert the I_2 expression in Double-FFT step 3 into the S_3 expression in Double-FFT step 4:

$$\begin{aligned}
 S_3[k] &= \sum_{n=-(N_t/2-1)}^{N_t/2} \left\{ \sum_{k'=-N/2}^{N/2} S_2[k'] e^{i2\pi k' n / N} \Delta\sigma_s \right\} e^{-i2\pi k n / N_t} \Delta x \\
 &= \Delta\sigma_s \Delta x \sum_{k'=-N/2}^{N/2} S_2[k'] \sum_{n=-(N_t/2-1)}^{N_t/2} e^{-i2\pi n (k/N_t - k'/N)} \\
 &= \frac{N_t}{N} \sum_{k'=-N/2}^{N/2} S_2[k'] \frac{1}{N_t} \sum_{n=-(N_t/2-1)}^{N_t/2} e^{-i2\pi n (k - k' \frac{N_t}{N}) / N_t} \\
 &= \frac{N_t}{N} \sum_{k'=-N/2}^{N/2} S_2[k'] \text{Psinc}\left(k - k' \frac{N_t}{N}, N_t\right) \\
 &= \frac{\Delta\sigma_s}{\Delta\sigma_u} \sum_{k'=-N/2}^{N/2} S_2[k'] \text{Psinc}\left(\frac{k\Delta\sigma_u - k'\Delta\sigma_s}{\Delta\sigma_u}, N_t\right)
 \end{aligned}$$

where the relationship $\frac{N_t}{N} = \frac{\Delta\sigma_s}{\Delta\sigma_u}$ is derived from $\Delta\sigma_u = \frac{1}{N_t \Delta x}$ and $\Delta x = \frac{1}{N \cdot \Delta\sigma_s}$

- Derivation of resampling matrix

Copy the last equation from previous slide to here:

$$S_3[k] = \frac{\Delta\sigma_s}{\Delta\sigma_u} \sum_{k'=-N/2}^{N/2} S_2[k'] \text{Psinc}\left(\frac{k\Delta\sigma_u - k'\Delta\sigma_s}{\Delta\sigma_u}\right)$$

If we only keep the non-zero terms in the above equation (remember $S_2[k]$ is made of $S_1[k]$ by padding zeros:

$$S_3[k] = \frac{\Delta\sigma_s}{\Delta\sigma_u} \left\{ \sum_{k'=-k_0}^{-k_0+N_d-1} S_2[k'] \text{Psinc}\left(\frac{k\Delta\sigma_u - k'\Delta\sigma_s}{\Delta\sigma_u}\right) + \sum_{k'=k_0}^{k_0+N_d-1} S_2[k'] \text{Psinc}\left(\frac{k\Delta\sigma_u - k'\Delta\sigma_s}{\Delta\sigma_u}\right) \right\}$$

- Derivation of resampling matrix

Only the spectrum in the positive frequency domain is what we need; the contribution from the image spectrum (spectrum in the negative frequency domain) is negligible. Thus, the above resampling equation becomes

$$\begin{aligned}
 S_3[k] &= \frac{\Delta\sigma_s}{\Delta\sigma_u} \sum_{k'=k_0}^{k_0+N_d-1} S_2[k'] \text{Psinc}\left(\frac{k\Delta\sigma_u - k'\Delta\sigma_s}{\Delta\sigma_u}, N_t\right) \\
 &= \frac{\Delta\sigma_s}{\Delta\sigma_u} \sum_{k'=0}^{N_d-1} S_1[k'] \text{Psinc}\left(\frac{\sigma_{u,k} - \sigma_{s,k'}}{\Delta\sigma_u}, N_t\right)
 \end{aligned}$$

where $\sigma_{u,k} = k\Delta\sigma_u$ and $\sigma_{s,k'} = k'\Delta\sigma_s$ are the wavenumbers on the user and sensor grids

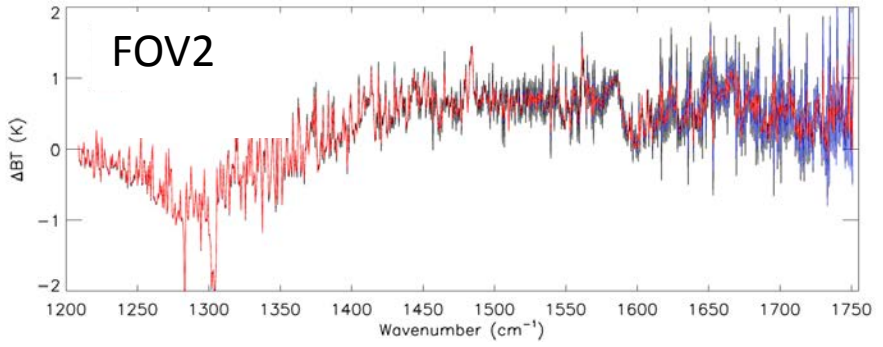
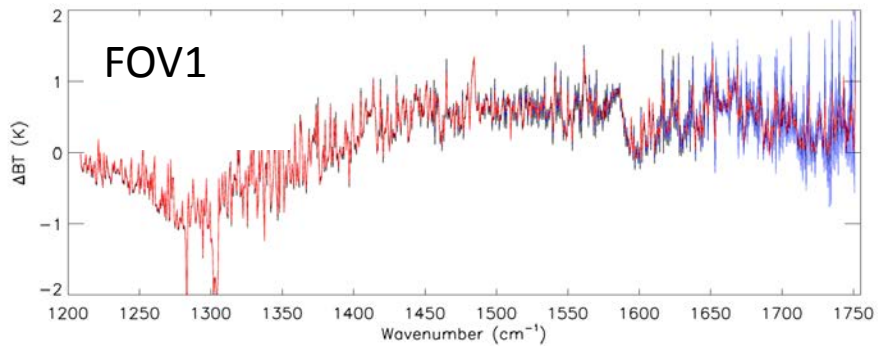
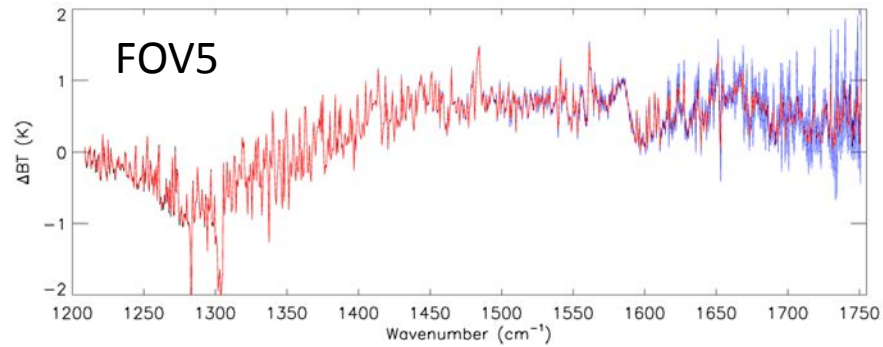
Since N_t is a large number, replace it with N_0 of the undecimated data points will not affect the result of the above equation; thus we have the following final resampling equation matrix:

$$F[k, k'] = \frac{\Delta\sigma_s}{\Delta\sigma_u} \text{Psinc}\left(\frac{\sigma_{u,k} - \sigma_{s,k'}}{\Delta\sigma_u}, N_0\right)$$

Observation Compared to LBL Simulation (MWIR Band)

$$BT_{obs} - BT_{lbl}$$

Responsivity is used
in BT_{lbl} calculation



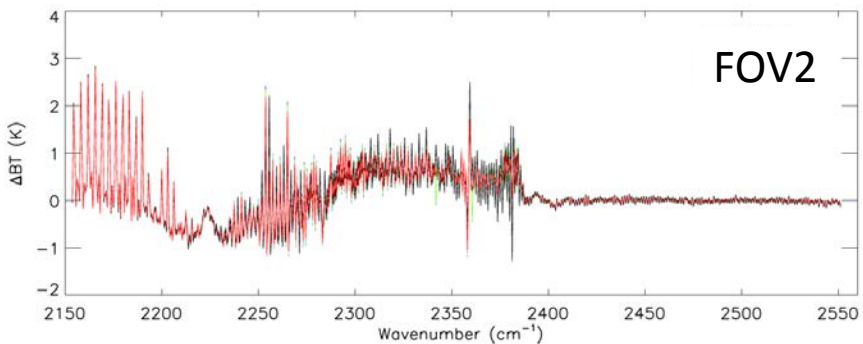
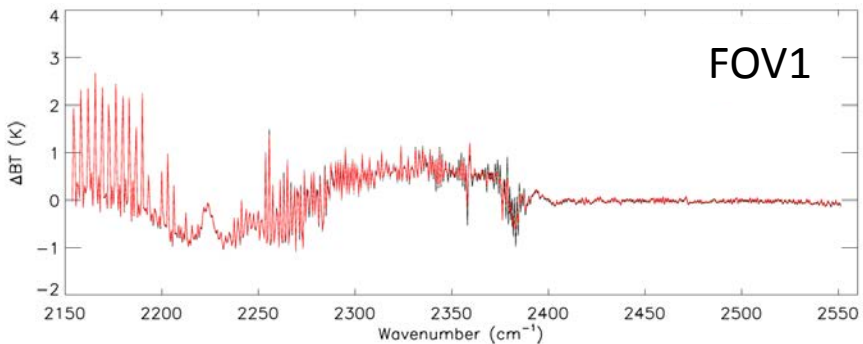
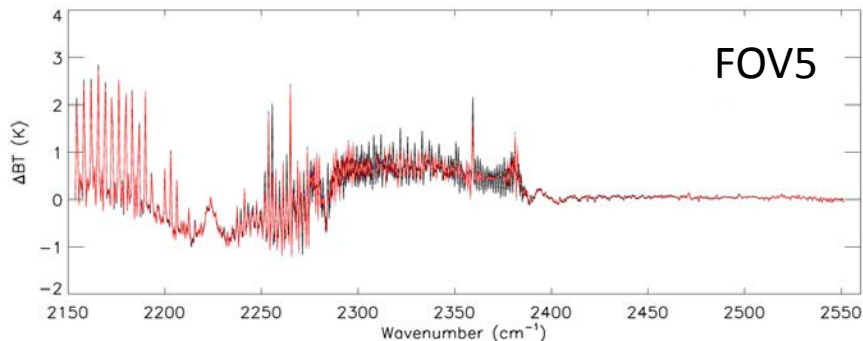
— J1 baseline

— Proposed updates

Observation Compared to LBL Simulation (SWIR Band)

$$BT_{obs} - BT_{lbl}$$

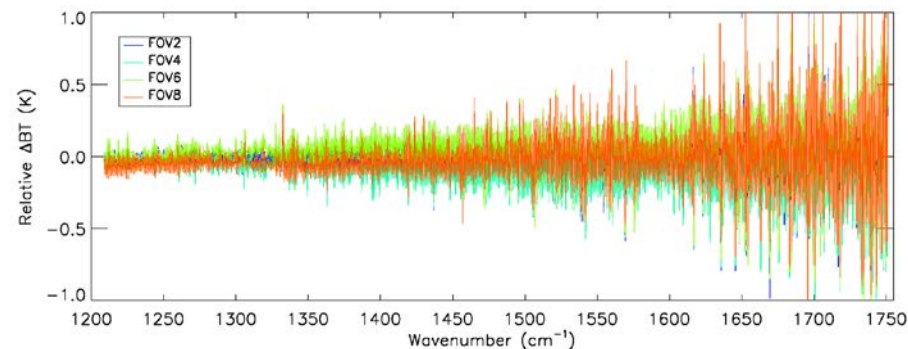
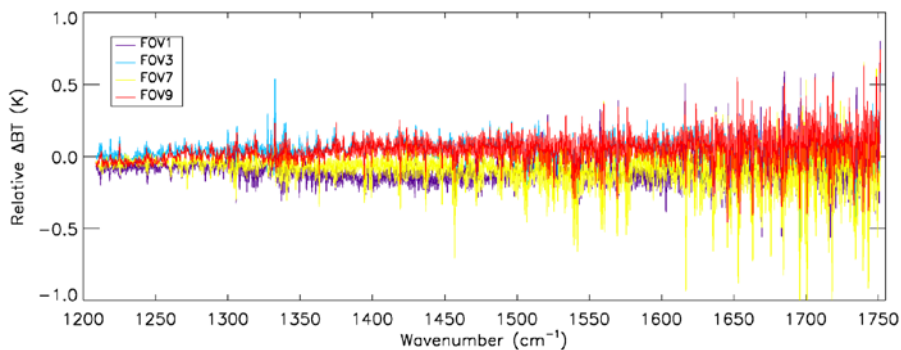
Responsivity is used
in BT_{lbl} calculation



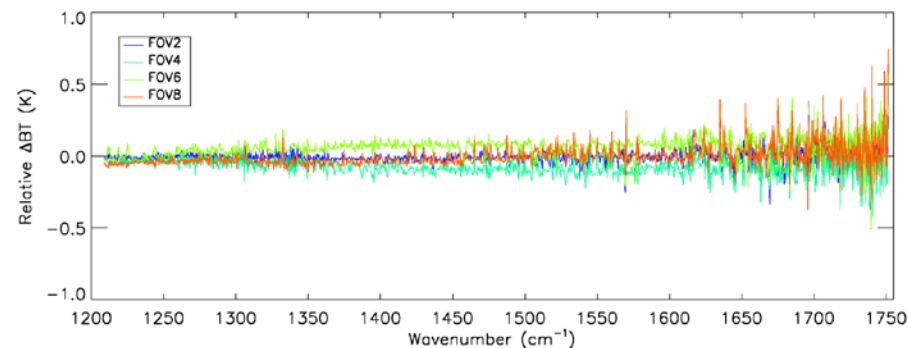
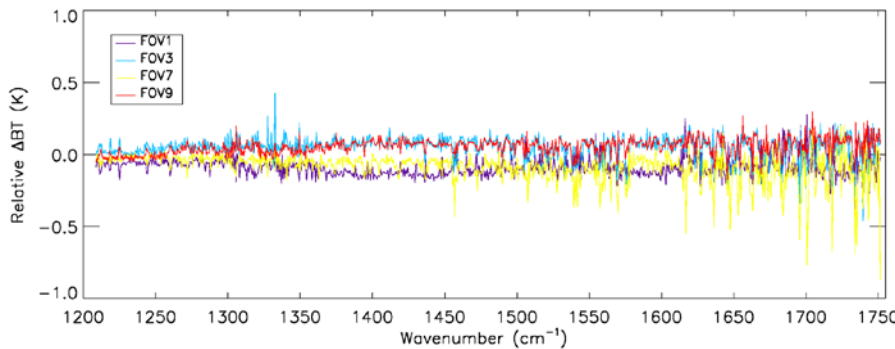
— J1 baseline
— Proposed updates

FOV-2-FOV Comparison (MWIR Band)

J1 baseline



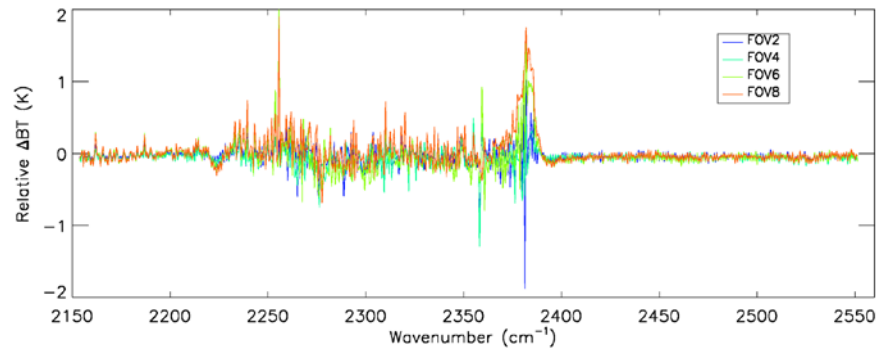
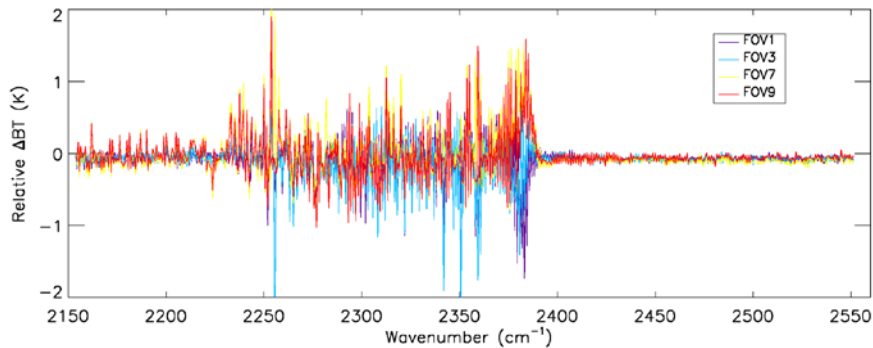
Proposed updates



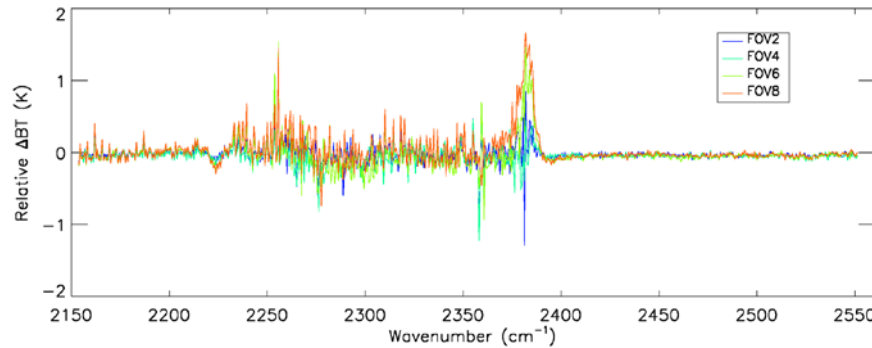
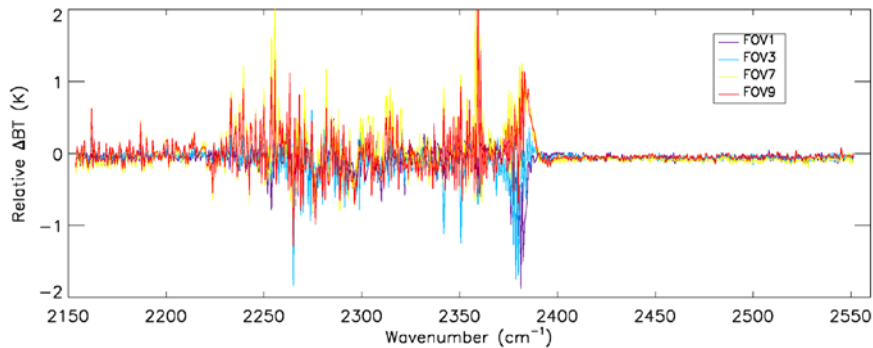
$$(BT_{obs} - BT_{lbl})_{fov_i} - (BT_{obs} - BT_{lbl})_{fov_5}$$

FOV-2-FOV Comparison (SWIR Band)

J1 baseline



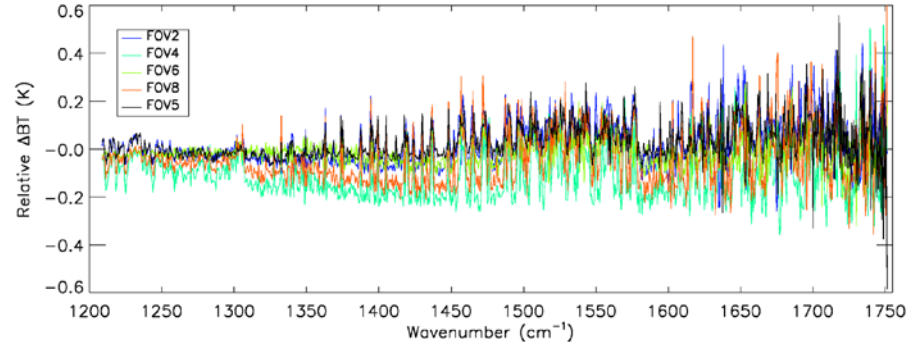
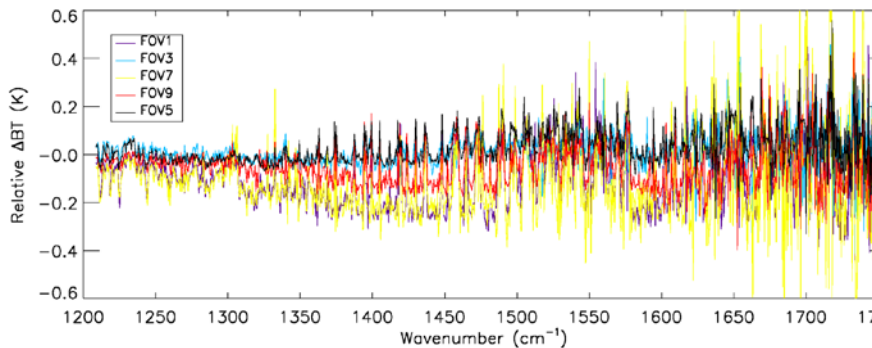
Proposed updates



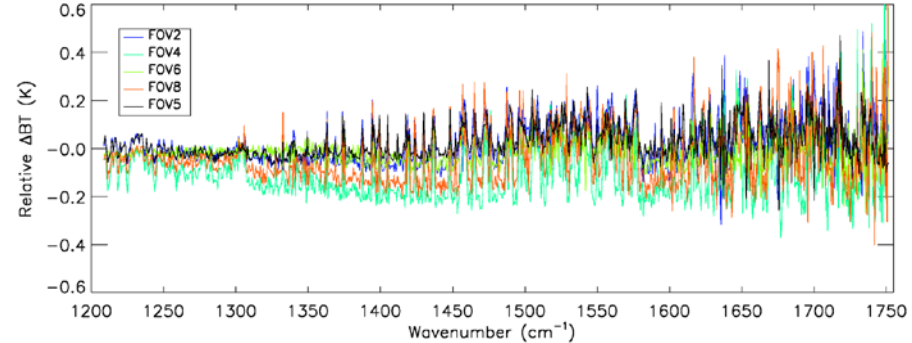
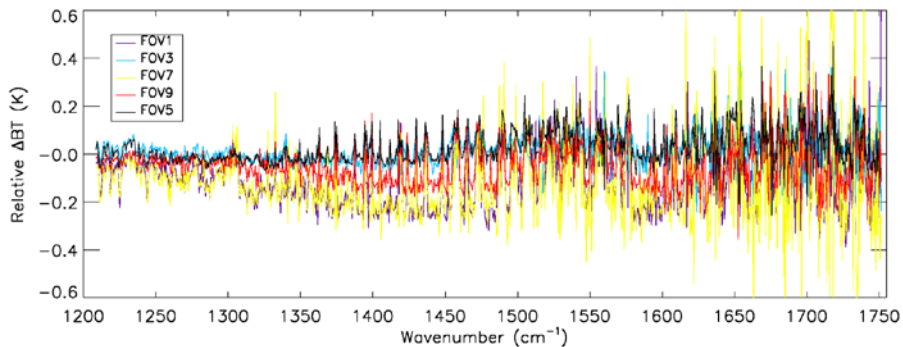
$$(BT_{obs} - BT_{lbl})_{fov_i} - (BT_{obs} - BT_{lbl})_{fov_5}$$

Sweep Direction Differences (MWIR Band)

J1 baseline



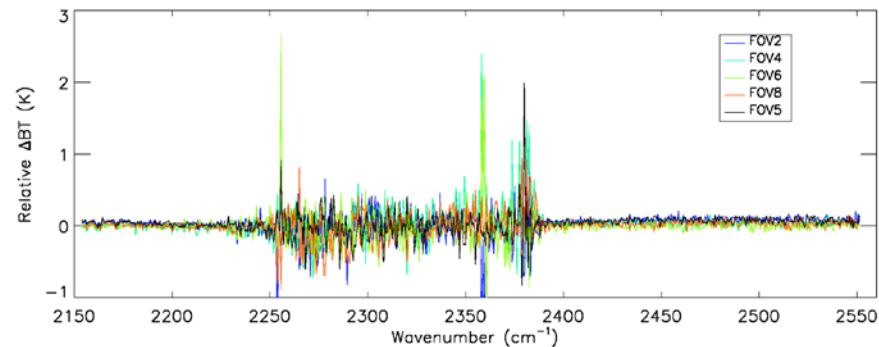
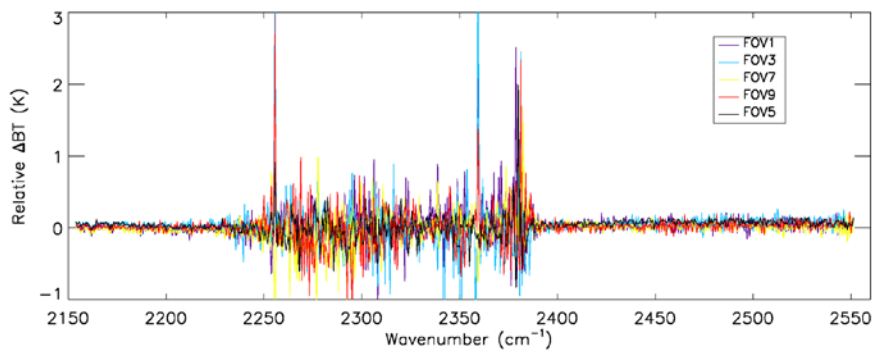
Proposed updates



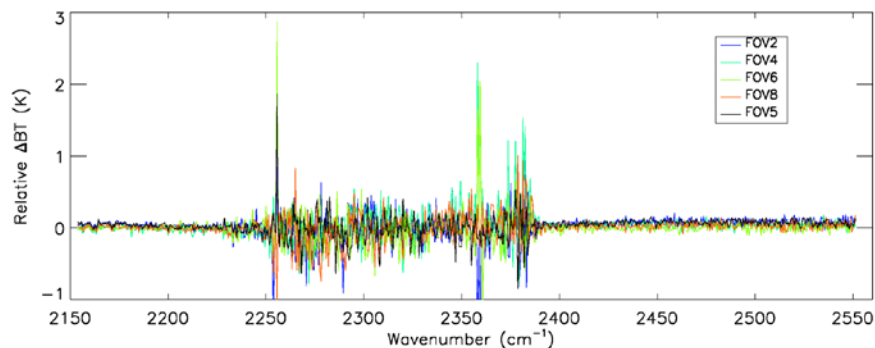
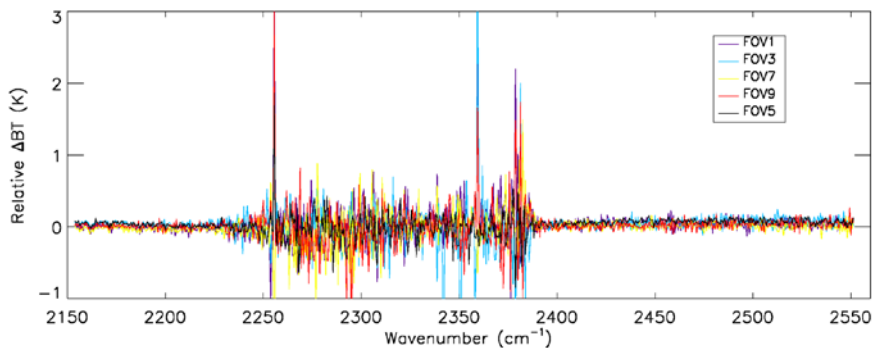
$$(BT_{obs} - BT_{ibl})_{fwd} - (BT_{obs} - BT_{ibl})_{rev}$$

Sweep Direction Differences (SWIR Band)

J1 baseline



Proposed updates



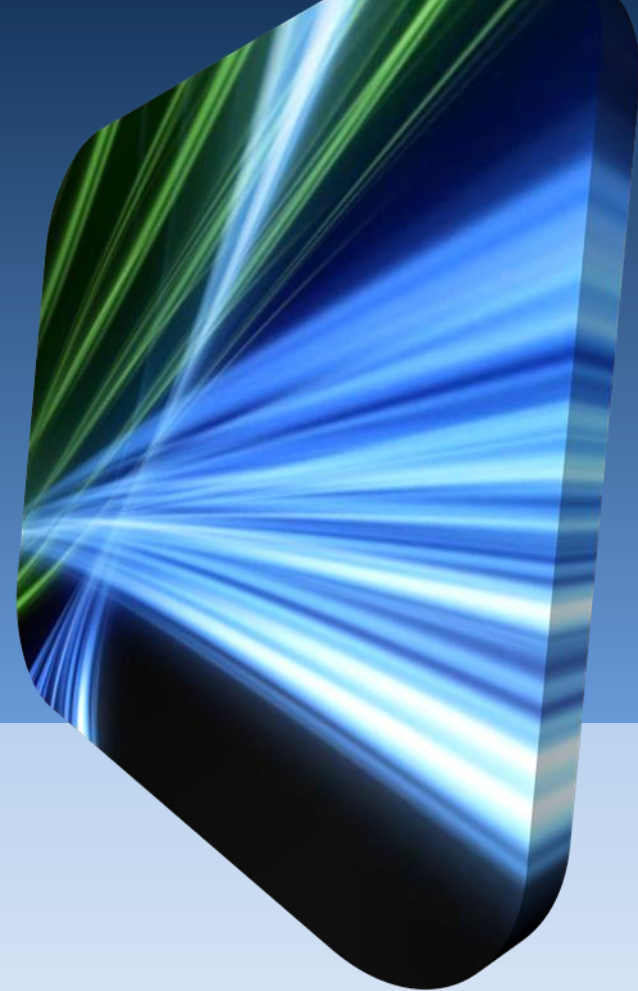
$$(BT_{obs} - BT_{lbl})_{fwd} - (BT_{obs} - BT_{lbl})_{rev}$$

CrIS Calibration Reference Uncertainty (ICT vs. ECT)

Joe Predina
Richard Hertel

Logistikos Engineering LLC, Fort Wayne, IN

STAR JPSS Science Team Annual Meeting
Session 6c: ATMS/CrIS Breakout
August 24-28, 2015
College Park, MD

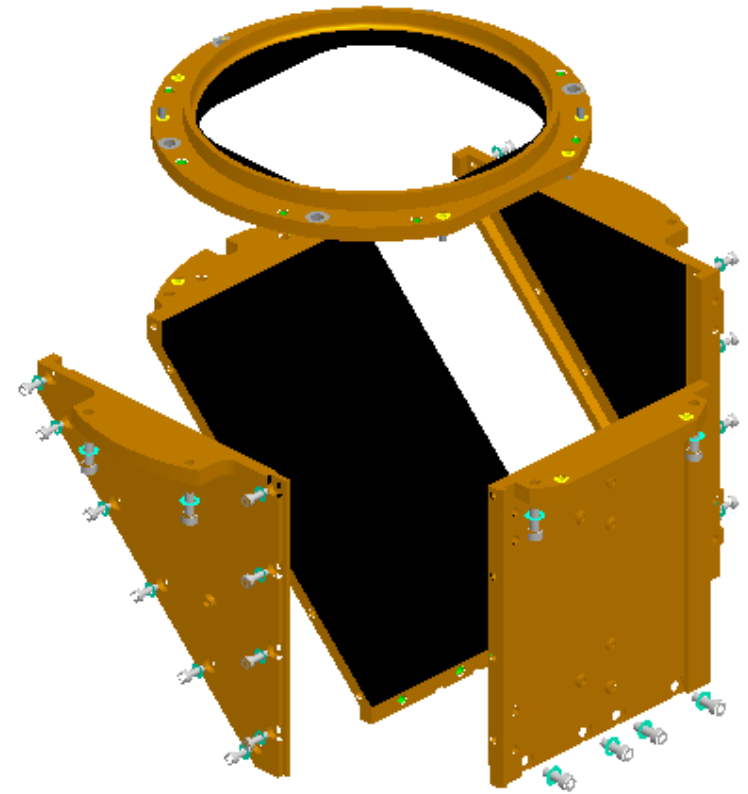
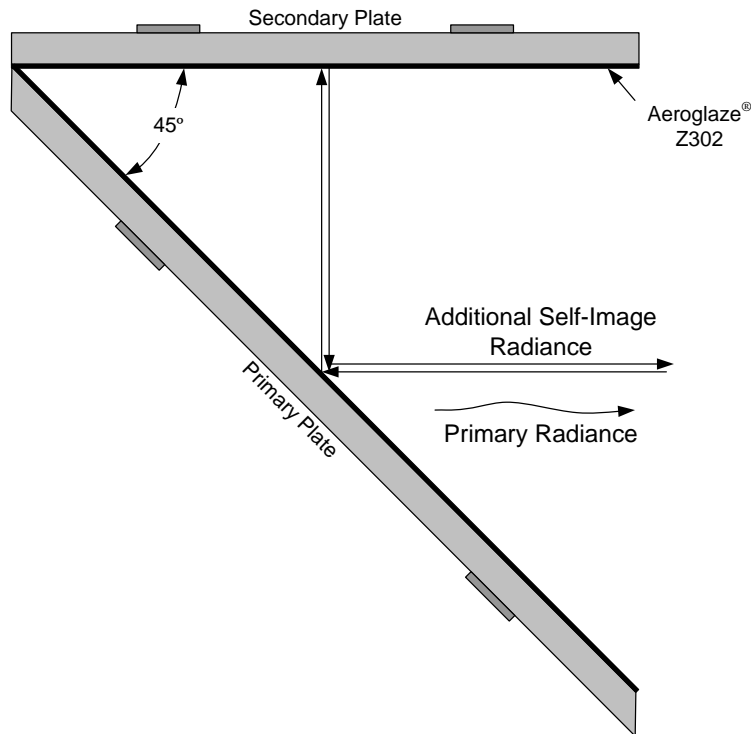


Acknowledgements

- The authors would like to acknowledge the following Harris Engineers for their contribution in TVAC data analysis and CrIS selloff documentation related to the topic of this presentation
 - Steven Wells
 - Jeff Garr
 - Rebecca Malloy (Frain)
 - Lawrence Suwinski

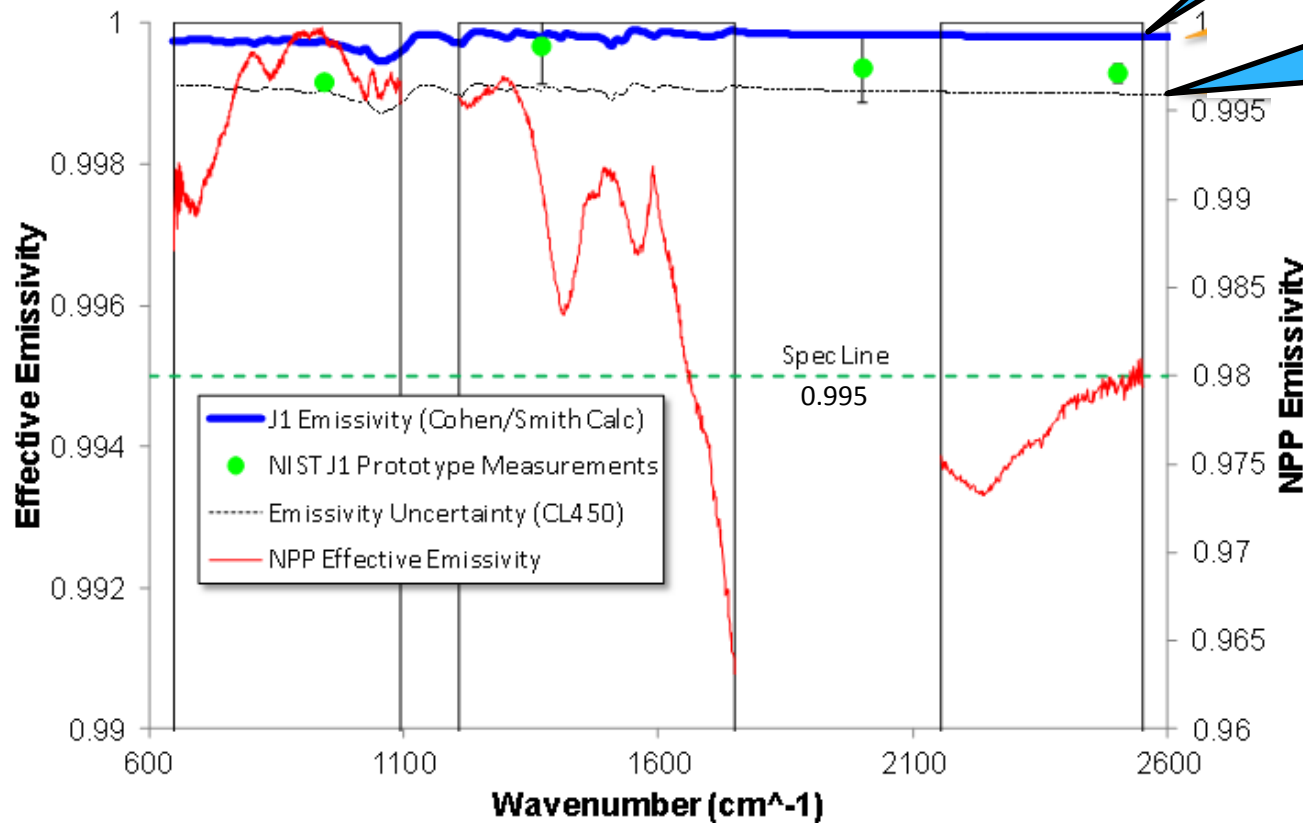
Improved Internal Calibration Target (ICT) Is Deployed on CrIS J1 Instrument

- Specular 3-bounce trap blackbody design
- Largely immune to stray light from surrounding environment
- Instrument sees radiance from ICT plus a very dim reflected image ($<0.5\%$) of itself which is accounted for in SDR radiance modeling
- ICT temperature uncertainty much lower



J1 Instrument ICT Emissivity Significantly Improved Over NPP Instrument

NPP Effective ICT Emissivity vs. J1 Predicted Effective Emissivity Based on Coupon Measurements and Modeling. NIST Testing of Prototype J1 ICT Effective Emissivity Also Shown



Beginning of life performance in TVAC (CL300)

With Worst Case Post launch contamination (CL450)

- J1 Emissivity (Cohen/Smith Calc)
- NIST J1 Prototype Measurements
- Emissivity Uncertainty (CL450)
- NPP Effective Emissivity

Spec Line
0.995

Better ICT Stray Light Rejection

Results in Elimination of Numerous Reflected Error Sources

• Benefits

- 45° ICT cavity angle causes off-axis stray light entering ICT to leave ICT off-axis
- More accurate calibration performance because many sources of radiance uncertainty have been eliminated
- Simplified SDR processing

View From	To	Fractional View to Environment (NPP)	Fractional View to Environment (J1 and up)
ICT Base	ICT Walls	0.000	0.000
ICT Base	ICT Base	0.000	0.000
ICT Base	ICT Baffle	0.175	0.000
ICT Base	Scan Baffle	0.508	0.000
ICT Base	Scan Mirror		
ICT Base	Frame	0.214	0.000
ICT Base	Opto-Mechanical Assembly (OMA)		
ICT Base	Warm Beamsplitter	0.086	0.000
ICT Base	Cold Beamsplitter	0.008	1.000
ICT Base	Space	0.009	0.000

Radiance Error Sources That No Longer Need to Be Modeled for JPSS

Only Remaining Term to Model

Four Error Categories Contribute to CrIS J1 ICT Radiometric Error

39 mK ICT Temperature Uncertainty Dominates (WC EOL)

% Uncertainty
Relative to a 287 K
Black Body Radiance

ICT Radiance Uncertainty		
Band	EOL	BOL
LWIR	0.121%	0.083%
MWIR	0.158%	0.121%
SWIR	0.217%	0.177%

**39 mK (1 sigma)
RSS Temperature Error
Dominates ICT
Radiometric Uncertainty**

RSS

Radiance Uncertainty Due to Diffuse ICT Reflections		
Band	EOL	BOL
LWIR	0.01%	0.01%
MWIR	0.03%	0.03%
SWIR	0.04%	0.04%

Radiance Uncertainty due to Emissivity Knowledge		
Band	EOL	BOL
LWIR	0.05%	0.03%
MWIR	0.04%	0.02%
SWIR	0.05%	0.03%

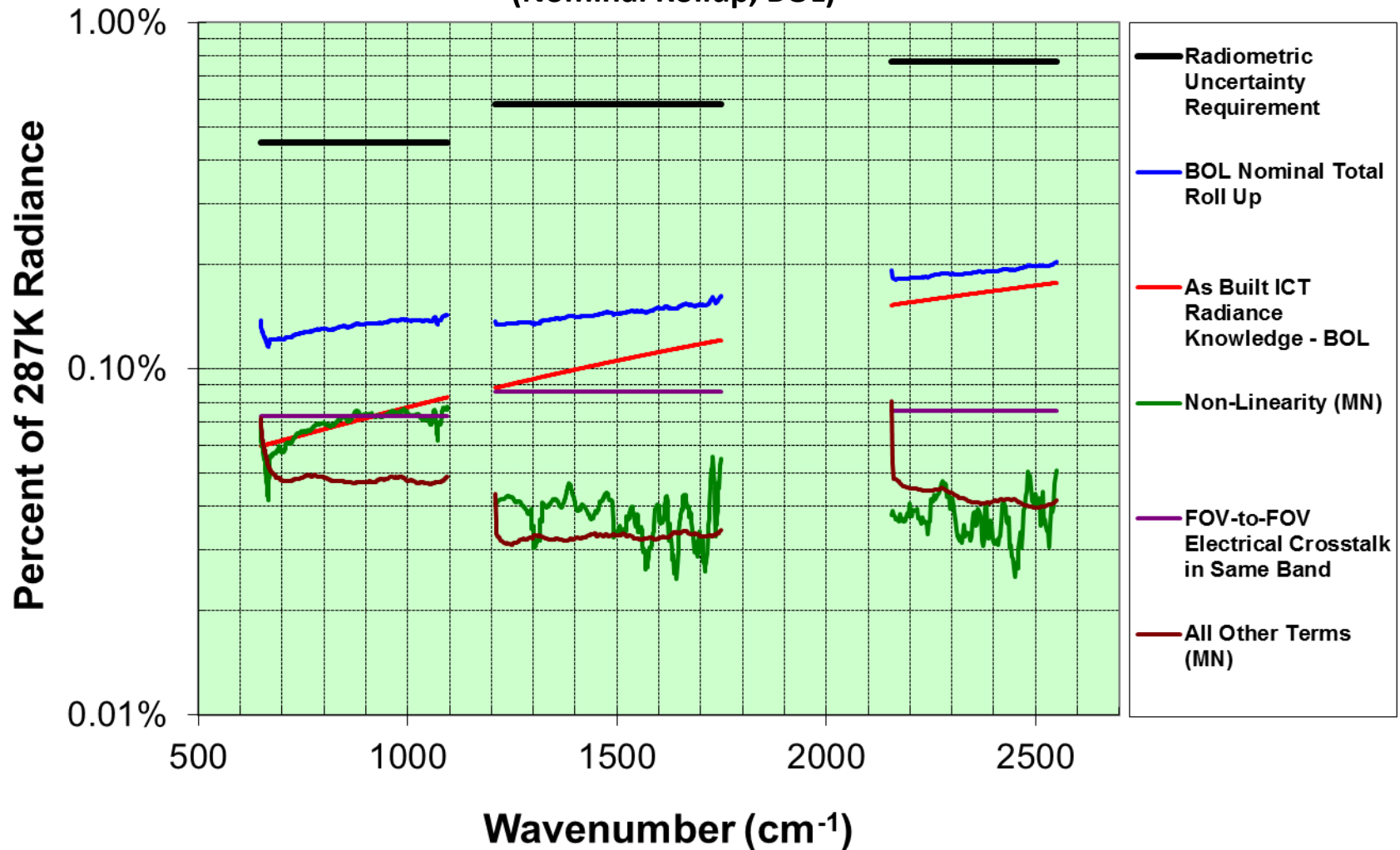
Radiance Uncertainty Due to ICT Temperature Error		
Band	EOL	BOL
LWIR	0.07%	0.07%
MWIR	0.12%	0.12%
SWIR	0.17%	0.17%

Radiance Uncertainty Due to Unmodeled ICT External Environment		
Band	EOL	BOL
LWIR	0.08%	0.02%
MWIR	0.09%	0.01%
SWIR	0.11%	0.01%

- EOL contamination (CL 450)
- ICT external environment temperature difference (4.5 K)
- Includes effect of SDR environmental model correction
- Specular emissivity uncertainty
 - NIST coupon characterization
 - Emissivity uniformity (FOV)
 - Target vignetting
 - EOL contamination (CL 450)
 - EOL paint aging
- PRT calibration **17.5 mK**
- Electronic readout **12.5 mK**
- PRT electrical bias error **11 mK**
- Temperature gradients
 - Lateral FOV to FOV) **12 mK**
 - Axial (paint worst case) **28 mK**
- Other **3 mK**
- Unmodeled reflection from CrIS instrument
 - Beamsplitter emission
 - Aft optics emission
 - FTS mirror emission
- EOL contamination (CL 450)

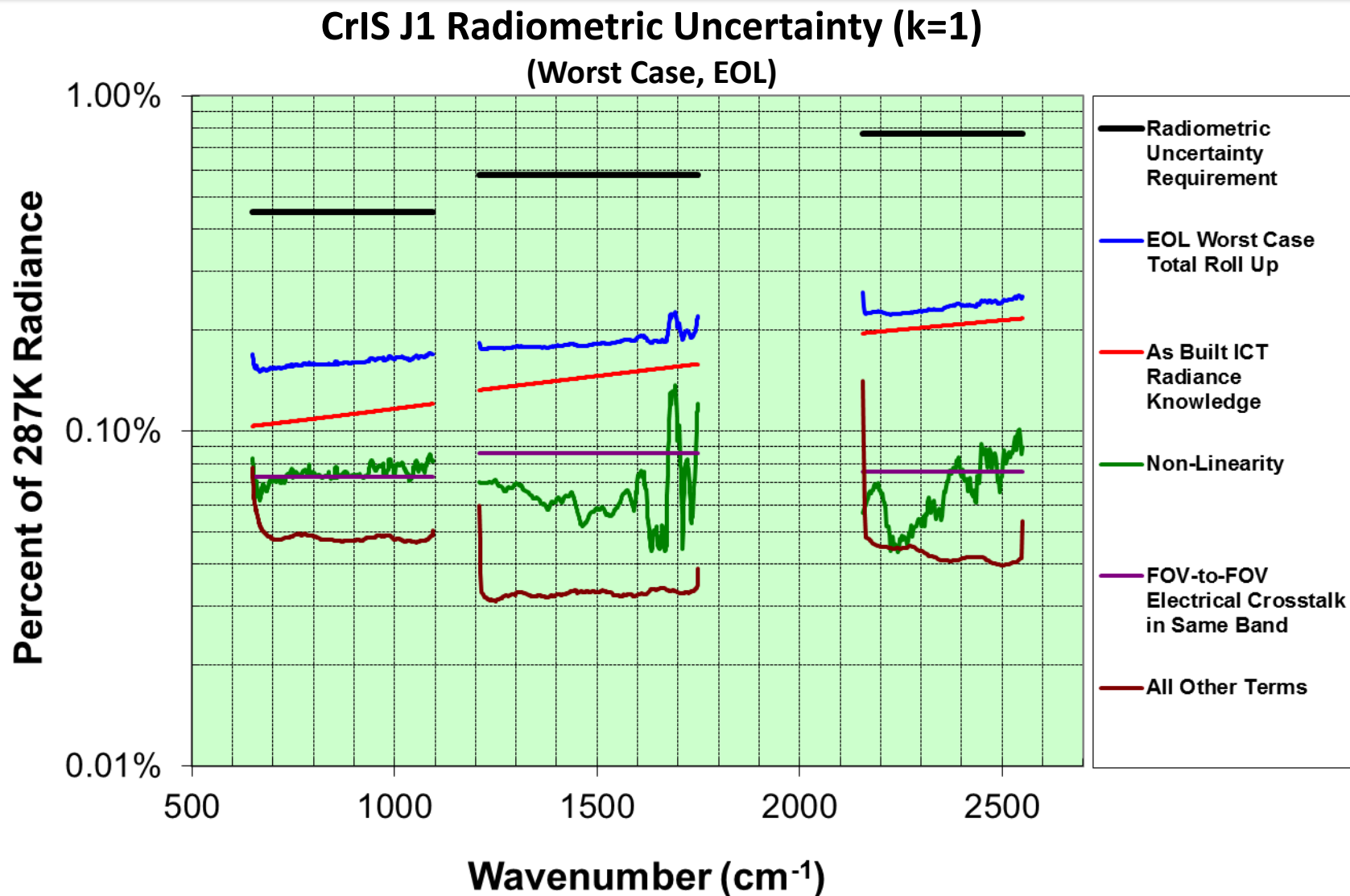
CrIS Internal Calibration Target (ICT) Remains the Dominant Source of Radiometric Uncertainty

CrIS J1 Radiometric Uncertainty (k=1) (Nominal Rollup, BOL)



Same Holds True for Mission Worst Case End-of-Life (EOL)

(Only a modest Degradation estimated from BOL to EOL)

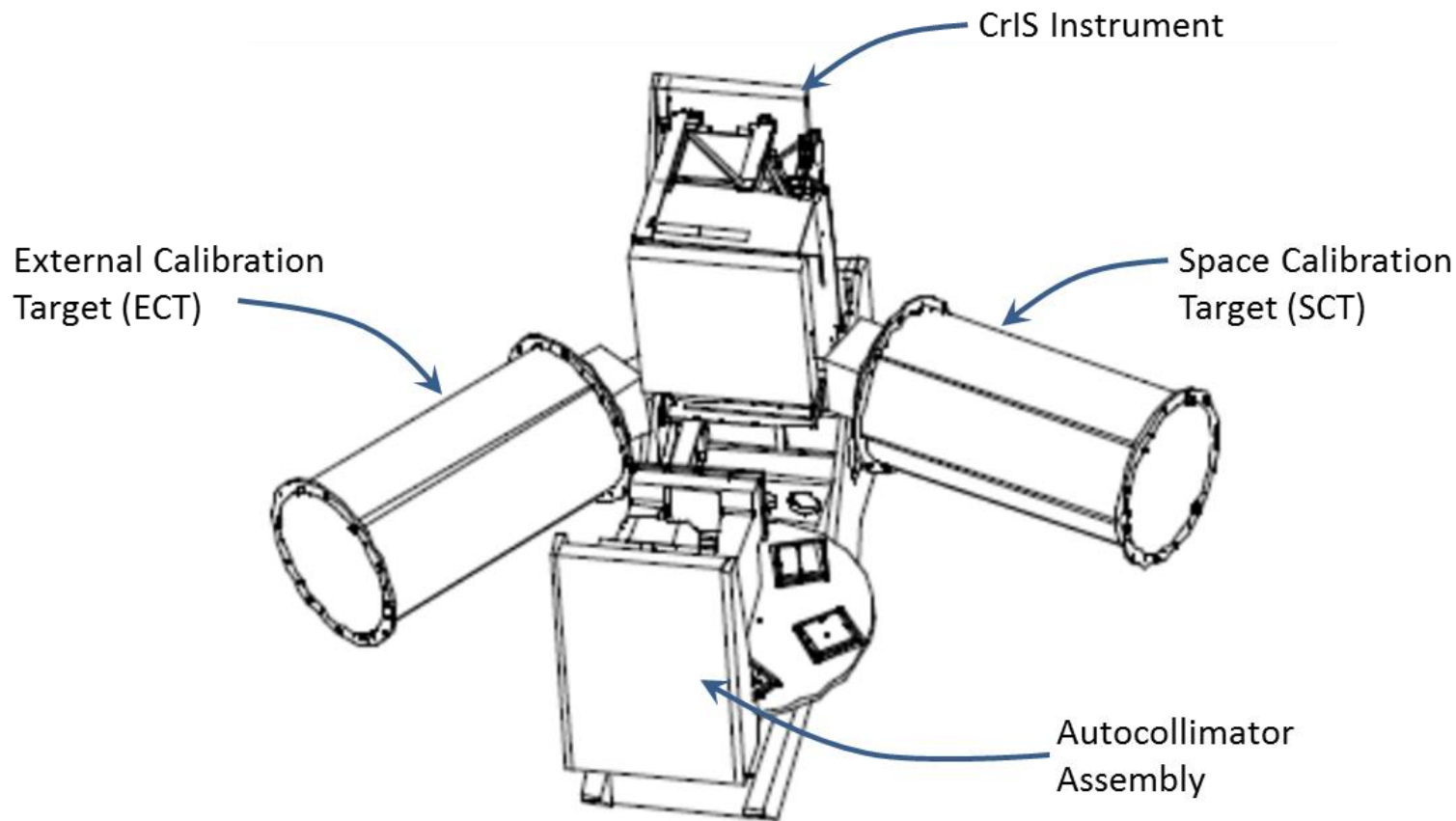


CrIS J1 ICT Radiometric Performance Is Climate Trending Class. How Can This Be Validated During TVAC?

- **CrIS ICT Radiometric Performance Expected**
 - **>0.9995 emissivity (specular)**
 - **39 mK (1 sigma) temperature uncertainty predicted (worst season on-orbit)**
 - **24 mK (1 sigma) temperature uncertainty predicted (during TVAC)**

External Calibration Target (ECT) & Space Calibration Target (SCT) Used to Verify Radiometric Performance During TVAC

Test Configuration Inside TVAC Chamber



External Calibration Target (ECT) Role in CrIS Testing

- **ECT Is Essential in Four Instrument Tests**
 - NEdN characterization
 - **Validation** of radiometric responsivity vs. wave number
 - **Validation** of long term (30 day) radiometric stability
 - Radiance source for radiometric linearity characterization
- **ECT NOT Used to “Calibrate” CrIS.....ECT used only for validation**
 - CrIS radiometric calibration is derived only from ICT
 - NIST traceable temperature calibration is via...
 - ICT PRTs with NIST-traceable temperature calibration
 - Two precision NIST traceable resistors used to compare with each PRT’s temperature dependent resistance
 - Algorithm using PRT-specific coefficients & pre-launch precision resistor values
 - Long term PRT & precision resistor stability built into CrIS

ECT Is a Full Aperture 5 Bounce Specular Target (non-uniform temperature is primary limitation)

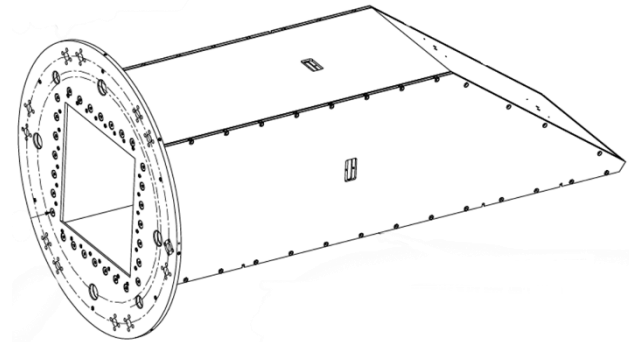
- ECT Characteristics TVAC Testing (as originally designed)

- >0.9995 emissivity (specular)
- Temperature uncertainty
 - 100 mK (1 sigma) (design requirement)
 - 70 mK (1 sigma) analysis

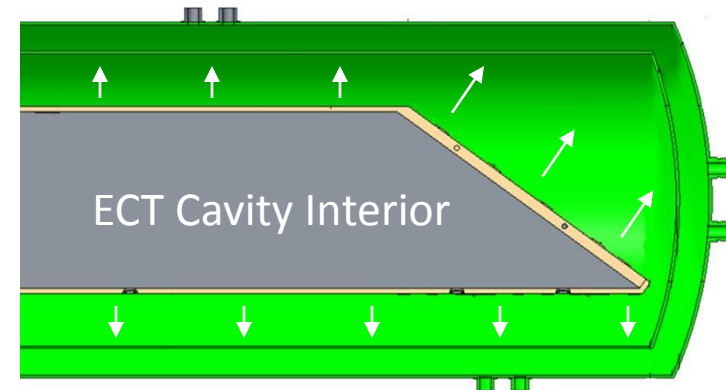
- Issues During TVAC

- Temperature readout error high as 150 mK at start of TVAC due to electronic instrumentation issues
- ECT was 12 years old.....so were most of the PRT calibrations
- Large thermal gradients present within ECT
 - Caused by LN₂ cooled heat sink combined with high power heaters used for thermal set point control
 - **Up to 500 mK temperature gradient** through thickness of ECT primary target plate
 - **Up to 400 mK temperature gradient** along length of ECT primary target plate

ECT 3D View



Cross Section of ECT
Inside LN₂ Dewar



Purpose of ECT Calibration Enhancement Is to Reduce ECT Radiometric Uncertainty

- **Objective**

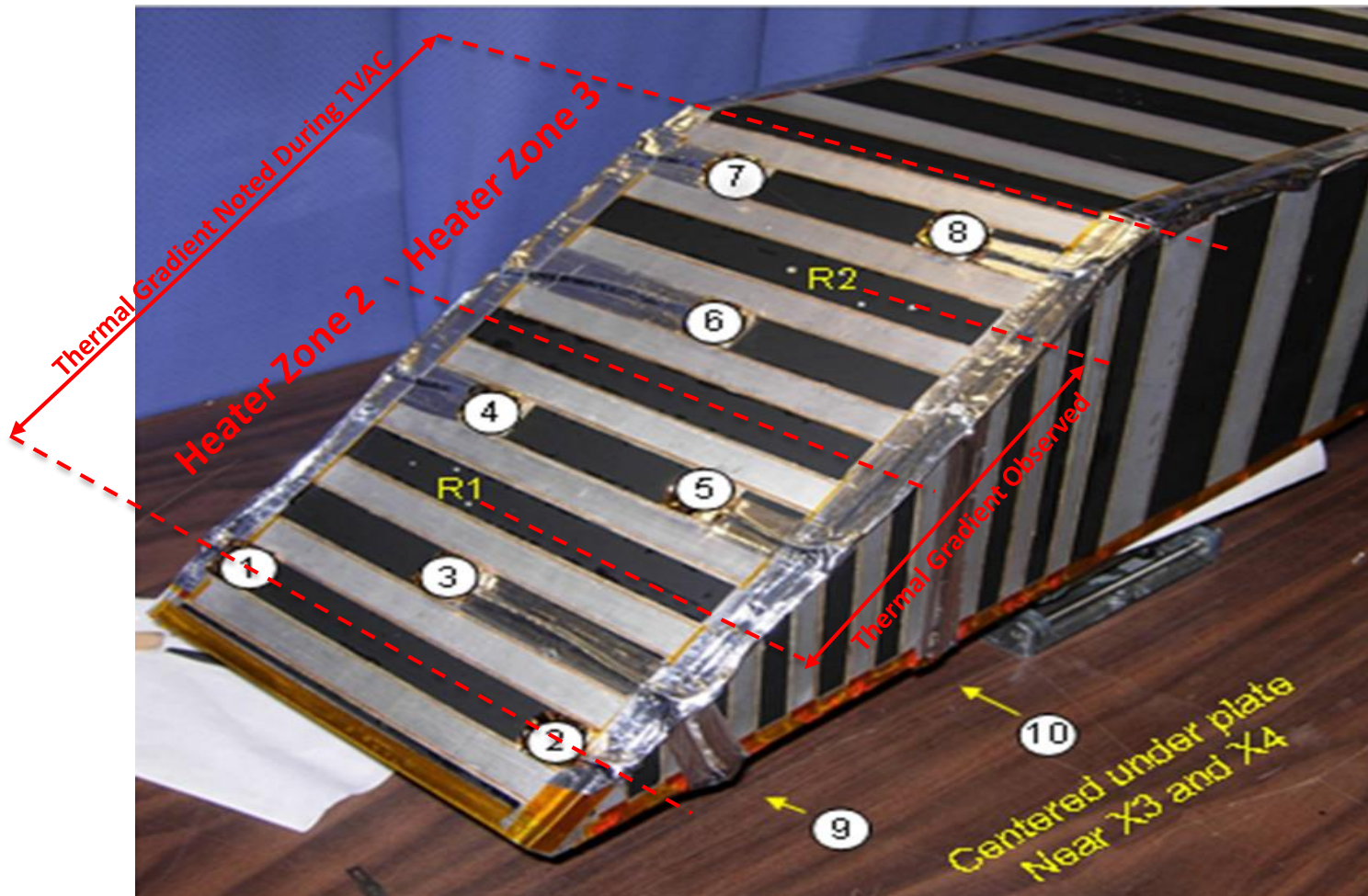
- Determine the temperature bias of all ECT PRTs relative to the R2 PRT primary temperature reference
- Anchor all ECT PRT temperature calibrations to the 8 monitor PRTs mounted on the ECT primary wedge plate surface that were calibrated against multiple NIST references in 2012
- Characterize and remove electronic readout error of ECT PRTs
- Use results to calculate a more accurate ECT radiance for TVAC acceptance testing

- **Method**

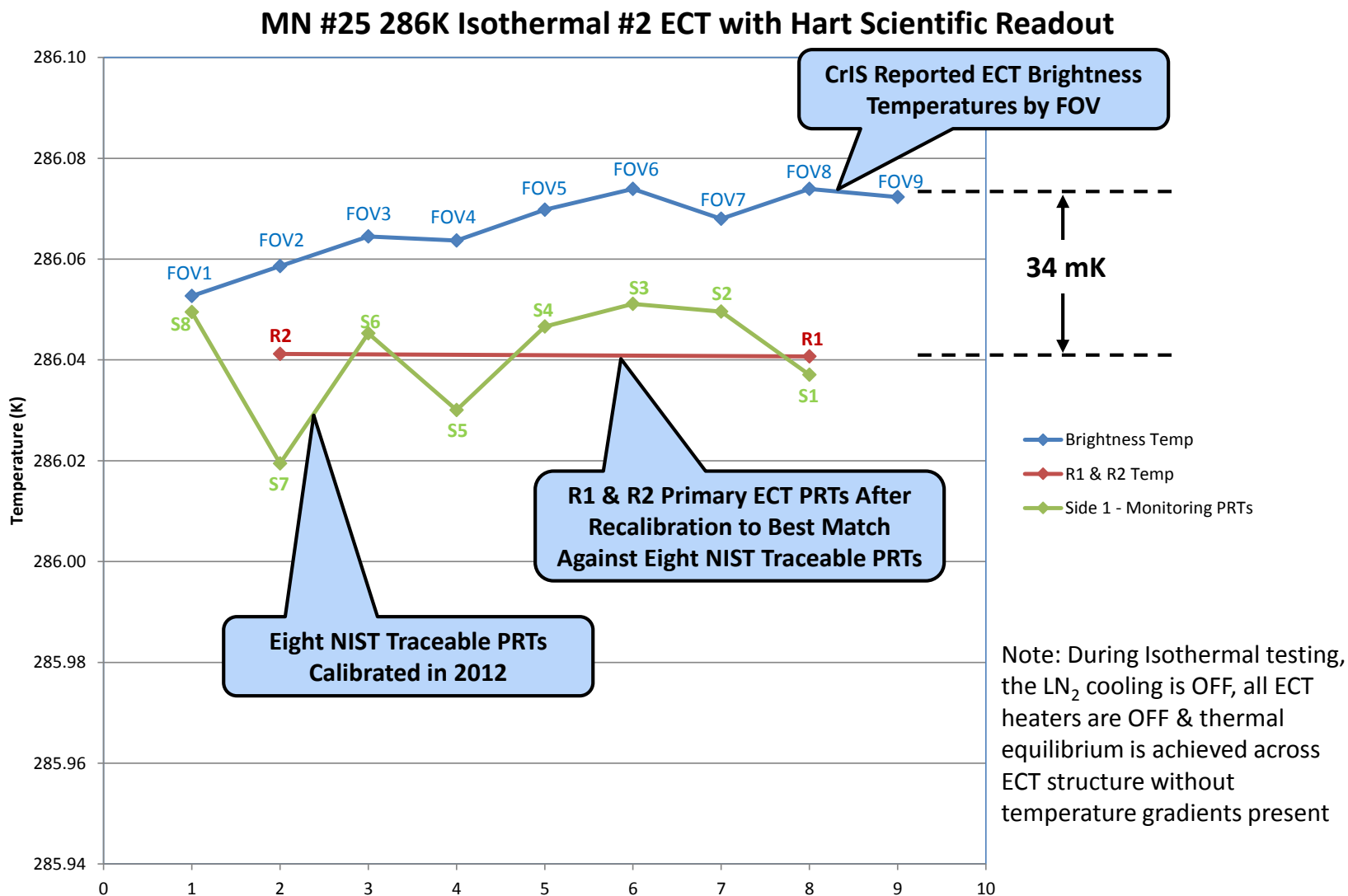
- Perform multiple isothermal ECT tests that can be used to determine relative PRT temperature offsets under a uniform temperature condition
- Use a high precision readout meter for at least one of the isothermal tests so that relative bias errors can be fully attributed to aged PRT calibration coefficients
- Use isothermal test with high precision electronic readout to anchor PRT R1 & R2 reported temperatures to the family of 8 monitor PRTs mounted on ECT wedge plate
- Use 10 ohm, 25 ohm and 100 ohm precision NIST traceable resistor references to calibrate meters used during TVAC testing

Eight Externally Mounted PRTs with 9 mK NIST Traceable Uncertainty Were Used to Re-establish Temperature Calibration

- R1 & R2 PRT are primary temperature sensors
- S1 through S8 PRTs used for calibration enhancement under isothermal conditions



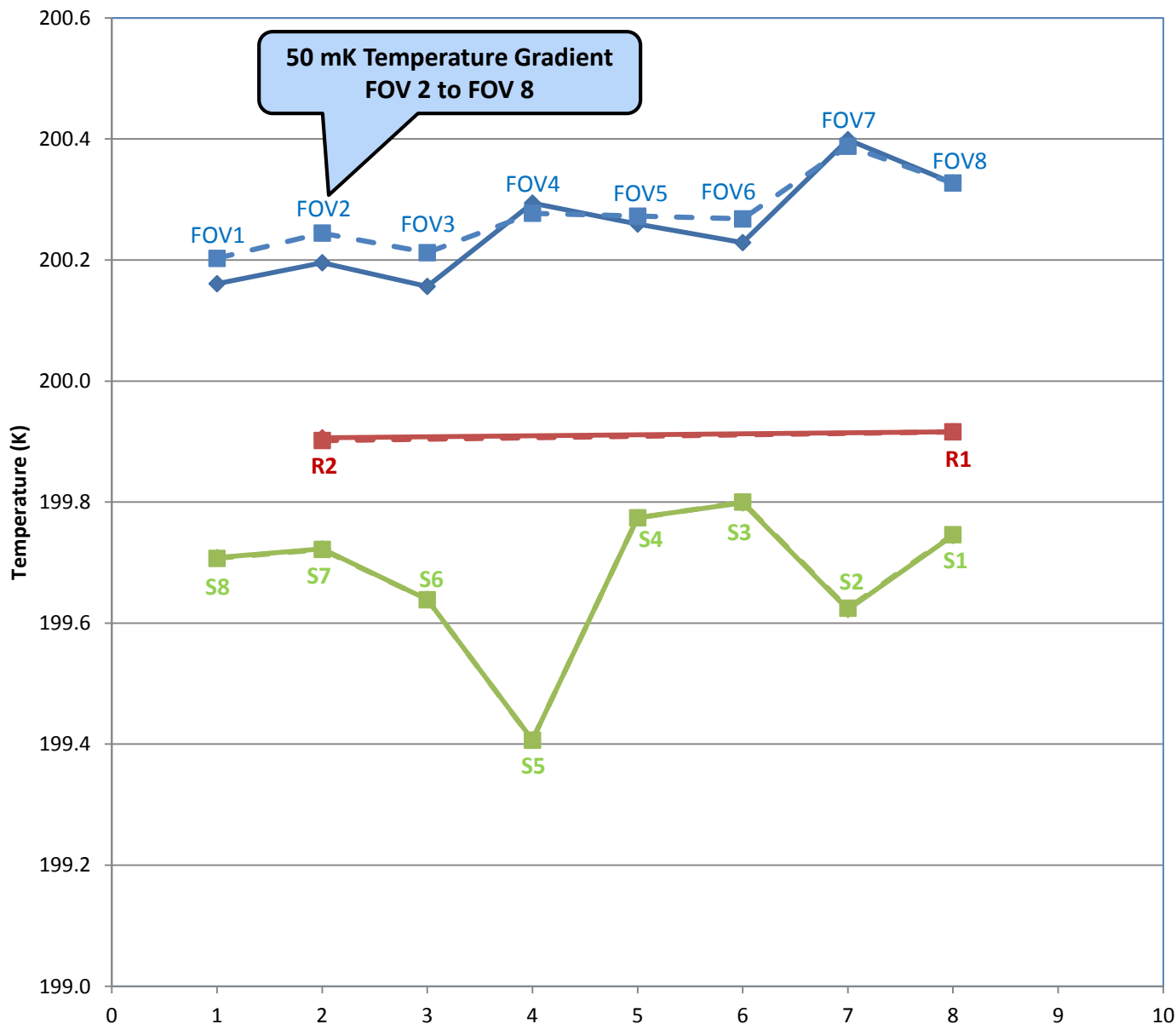
ICT & ECT Temperatures Matched within 34 mK During TVAC Isothermal ECT Test Conducted at Mission Nominal



Thermal Gradients Were Still Present on ECT During Normal TVAC Testing

MN 200K ECT Plateau

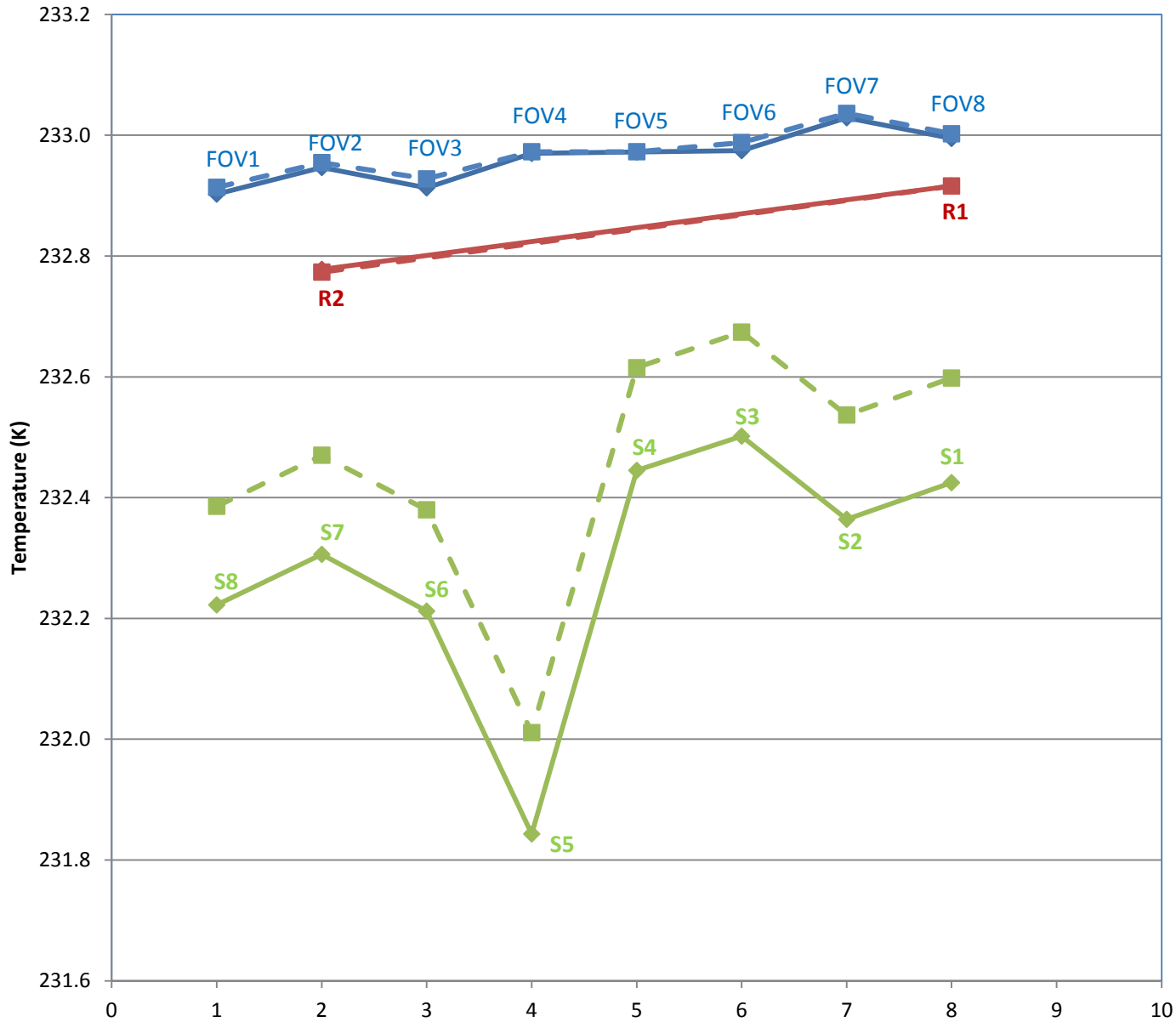
MW Brightness temperatures are used for the 200K plateau. Due to the use of the MW band FOV 9 is excluded.



- Side 1 - Brightness Temp
- Side 2 - Brightness Temp
- Side 1 - R1 & R2 Temp
- Side 2 - R1 & R2 Temp
- Side 1 - Monitoring PRTs
- Side 2 - Monitoring PRTs

MN 233K ECT Plateau

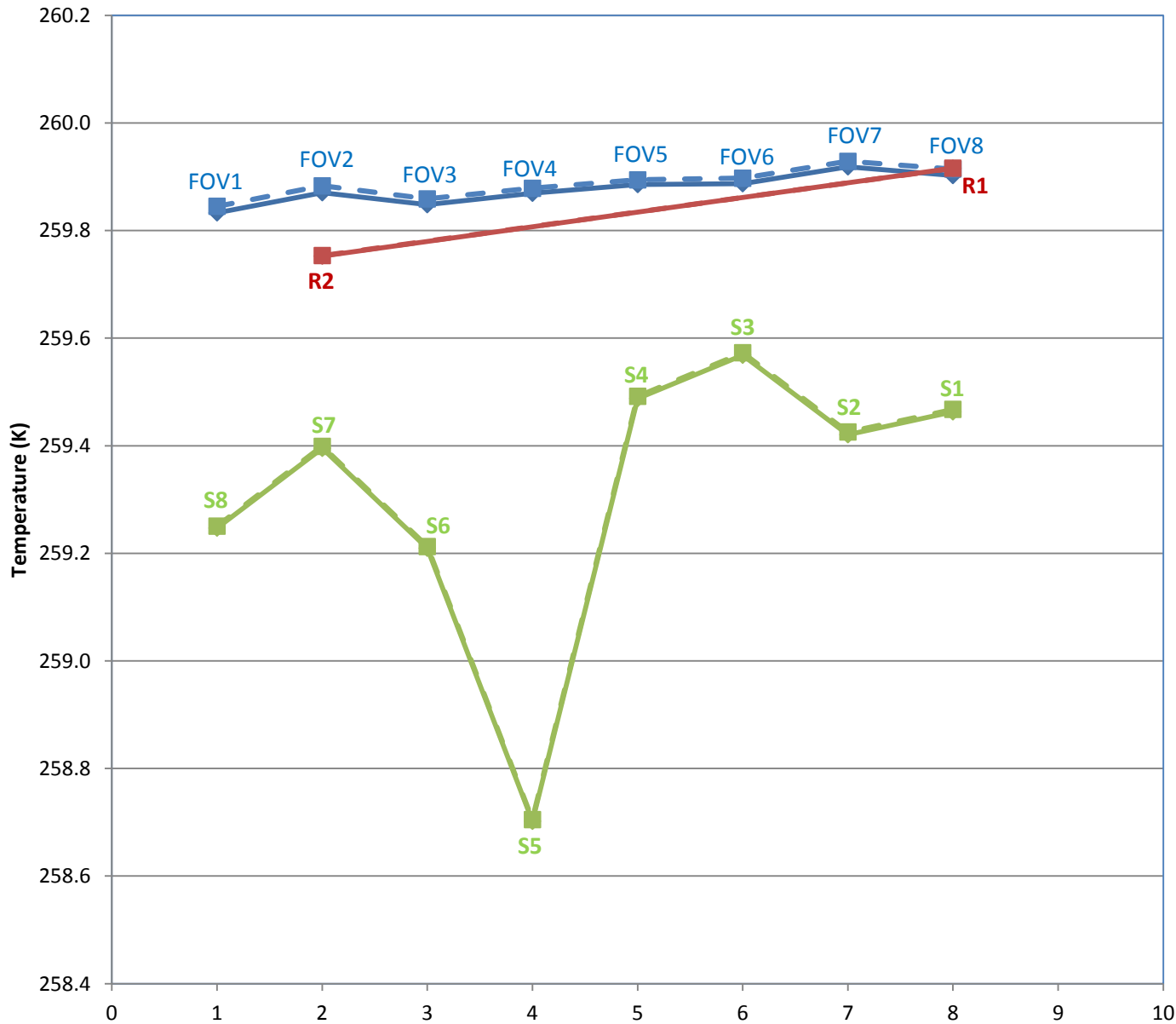
MW Brightness temperatures are used for the 233K plateau. Due to the use of the MW band FOV 9 is excluded.



- Side 1 - Brightness Temp
- Side 2 - Brightness Temp
- Side 1 - R1 & R2 Temp
- Side 2 - R1 & R2 Temp
- Side 1 - Monitoring PRTs
- Side 2 - Monitoring PRTs

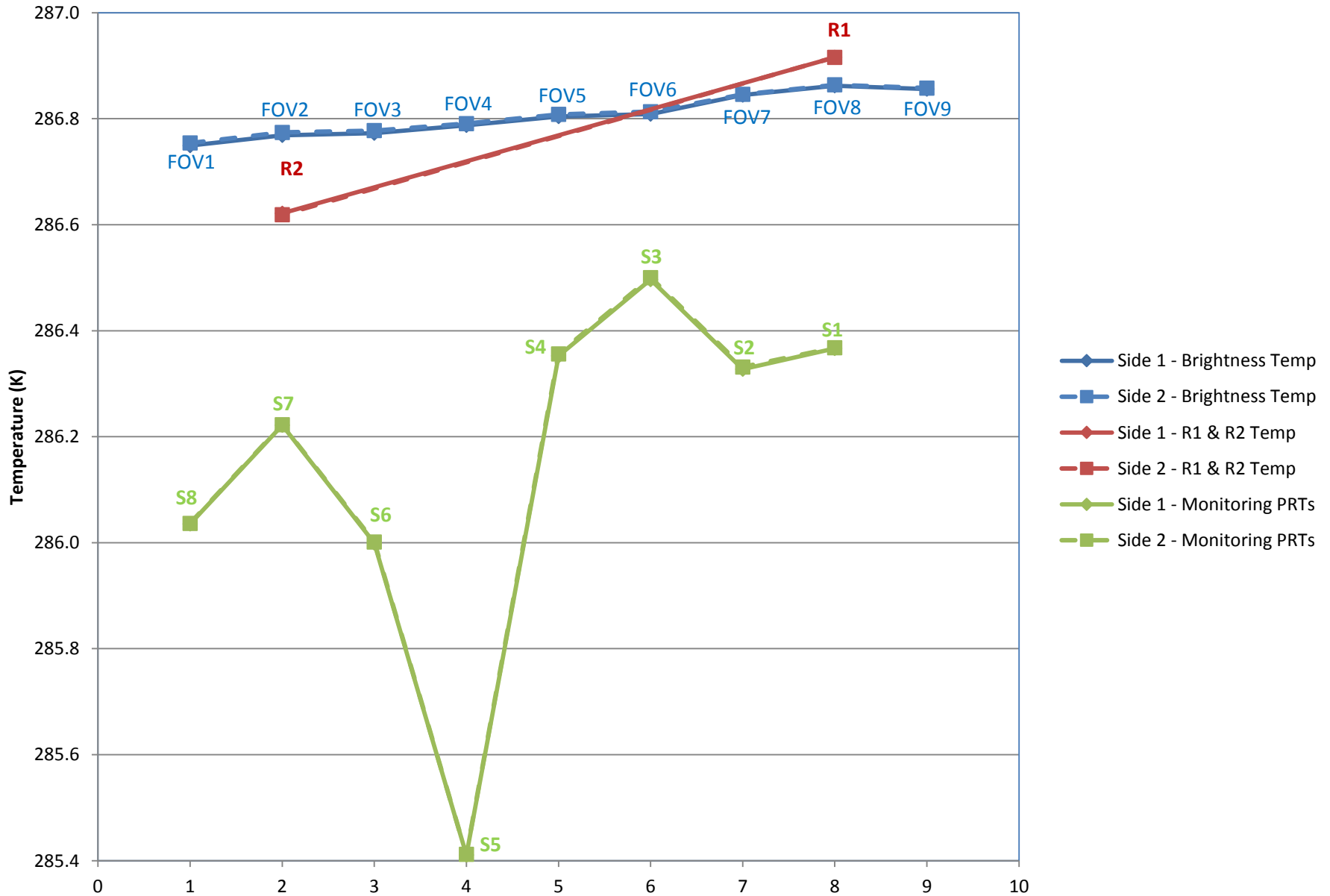
MN 260K ECT Plateau

MW Brightness temperatures are used for the 260K plateau. Due to the use of the MW band FOV 9 is excluded.



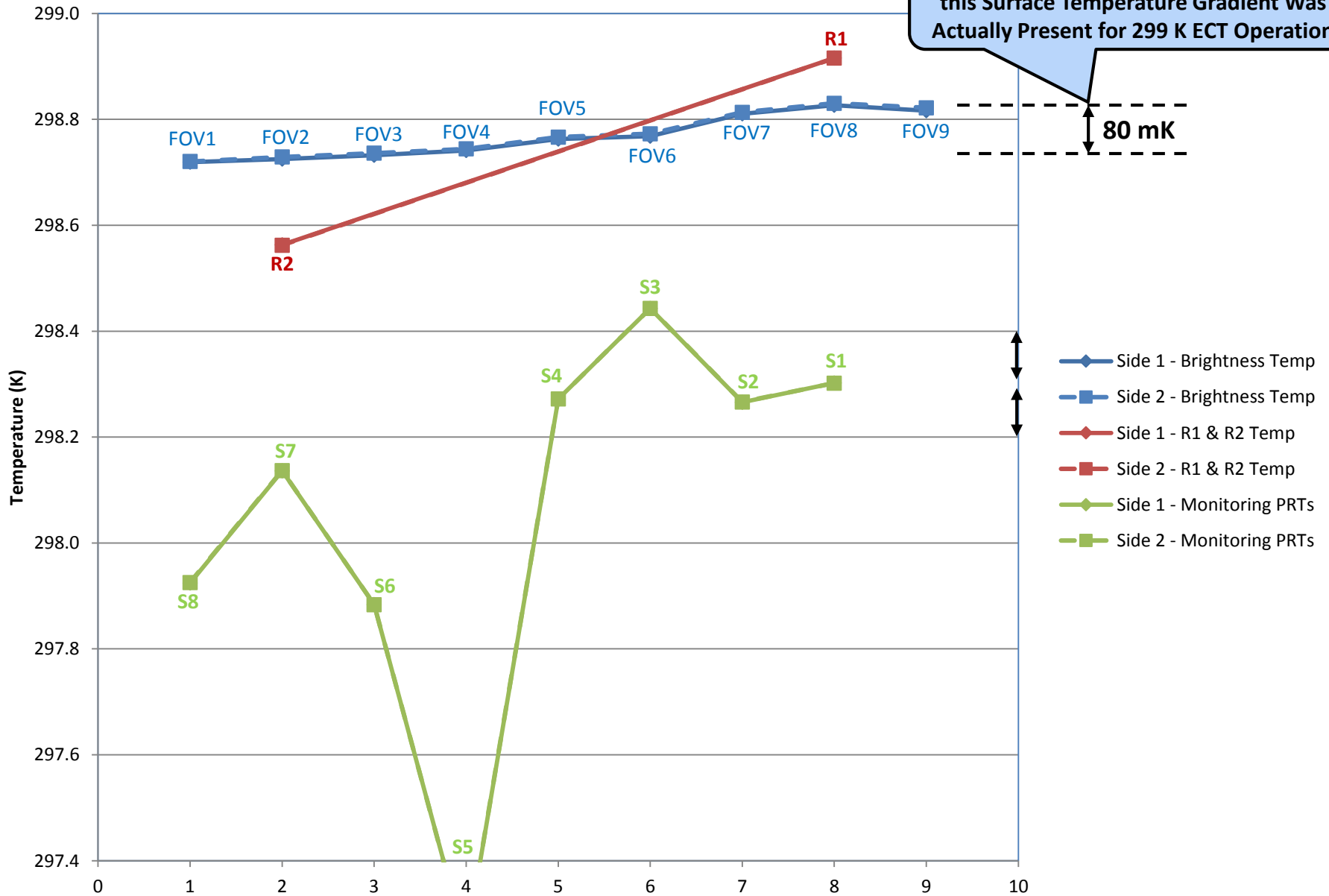
- Side 1 - Brightness Temp
- Side 2 - Brightness Temp
- Side 1 - R1 & R2 Temp
- Side 2 - R1 & R2 Temp
- Side 1 - Monitoring PRTs
- Side 2 - Monitoring PRTs

MN 287K ECT Plateau



MN 299K ECT Plateau

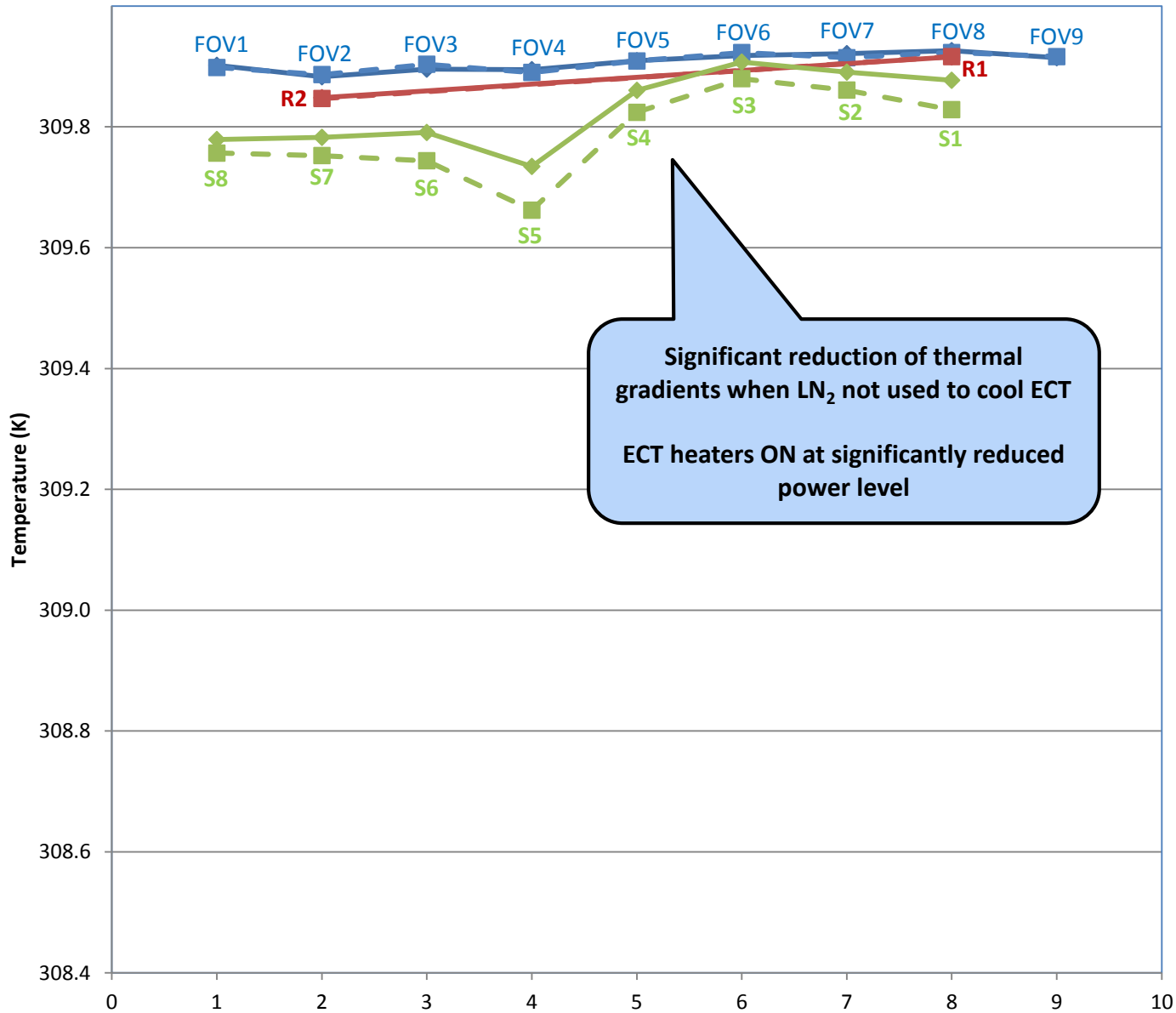
Subsequent NIST TXR Testing Verified this Surface Temperature Gradient Was Actually Present for 299 K ECT Operation



- Side 1 - Brightness Temp
- Side 2 - Brightness Temp
- Side 1 - R1 & R2 Temp
- Side 2 - R1 & R2 Temp
- Side 1 - Monitoring PRTs
- Side 2 - Monitoring PRTs

80 mK

MN 310K ECT Plateau



Note: LN₂ not used for this test condition

Significant reduction of thermal gradients when LN₂ not used to cool ECT
ECT heaters ON at significantly reduced power level

- Side 1 - Brightness Temp
- Side 2 - Brightness Temp
- Side 1 - R1 & R2 Temp
- Side 2 - R1 & R2 Temp
- Side 1 - Monitoring PRTs
- Side 2 - Monitoring PRTs

Substantially Improved ECT Design for Future J2 TVAC Testing Believed Possible & Would Be Beneficial

(1 of 3)

- **Desired Objectives**

- **Temperature uncertainty knowledge..... 30 mK (1 sigma)....NIST traceable**
 - **ECT portion of budget.....28 mK**
 - **Electronic readout portion of budget.....10 mK**
- **Maximum temperature gradient (primary plate) 45 mK**

- **Promising Concept Under Investigation at Harris for J2 TVAC**

- **LN₂ cooling replaced by variable temperature circulator**
- **ECT cavity is directly liquid cooled near ECT input aperture.....does not rely on radiative cooling**
- **Regulate temperature slightly above liquid cooled heat sink temperature using low power heaters**

TVAC ECT Instrumentation Was Augmented By Analysis to Provide Meaningful Validation of CrIS Radiometric Calibration

(2 of 3)

- **ECT Performance Enhancements for Radiometric Calibration**

- PRT electronic readout errors eliminated using NIST traceable calibration resistor references
- Primary ECT temperature sensor (R1 & R2) calibration re-establish using eight NIST traceable PRT references (9 mK uncertainty) during an ECT isothermal test
- Three ECT isothermal tests spanning CrIS J1 TVAC performed to demonstrate ECT temperature knowledge stability (R1 & R2) with only a 26 mK discrepancy noted



- **ECT & ICT temperature calibration match to within 34 mK**

TVAC ECT Instrumentation Is Augmented By Analysis to Provide Meaningful Validation of CrIS Radiometric Calibration

(3 of 3)

- **ECT Thermal Gradients Removed Analytically in TVAC Data Analysis**
 - NIST Transfer Radiometer (TXR) verified ECT thermal gradients match brightness temperatures reported by CrIS in all FOVs (299 K test result)
 - CrIS SWIR & MWIR linear detectors used to map ECT surface temperature gradients when collecting data at each ECT set point temperature (200 K, 233 K, 265 K, 287 K, 299 K & 310 K)
 - Correct ECT reported temperature by FOV for radiometric analysis

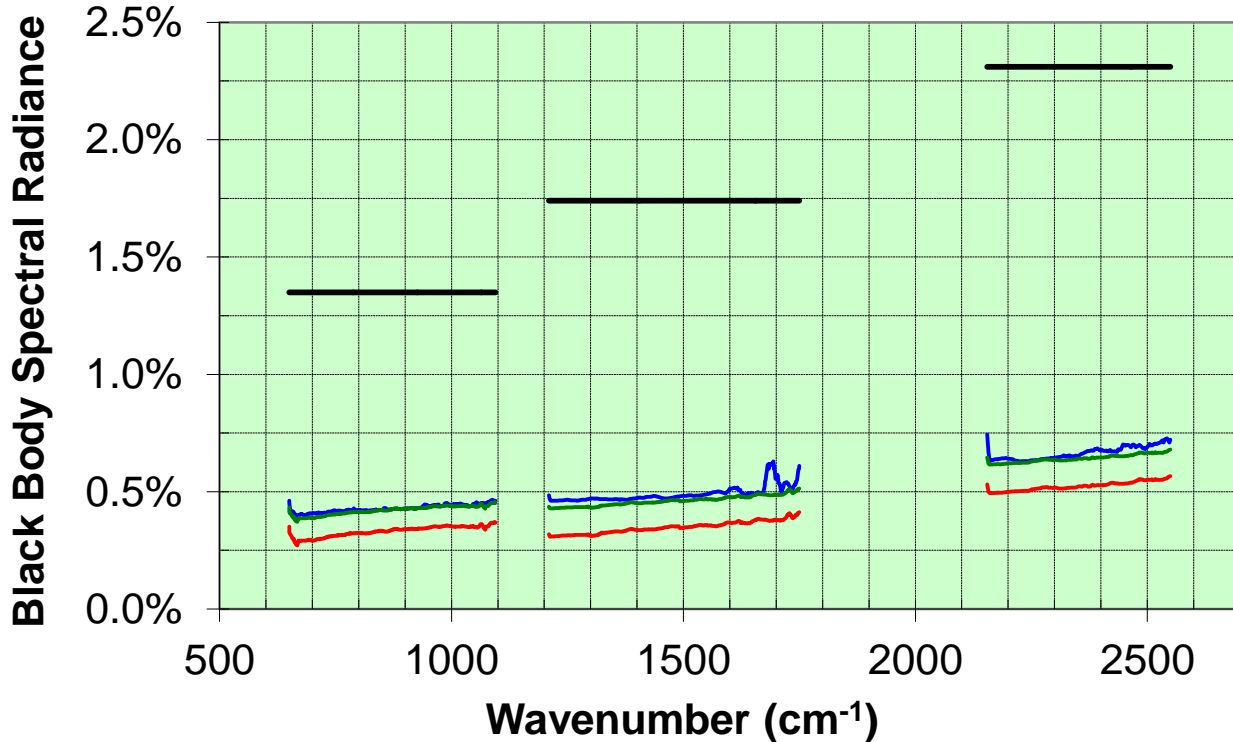


- **LWIR & MWIR linearity testing can use ECT source with enhanced surface temperature knowledge that accurately accounts for thermal gradients**

Radiometric Uncertainty Relative to NEdT Performance

CrIS J1 Radiometric Uncertainty (k = 3) for 287 K Scene

CrIS J1 Radiometric Uncertainty with Respect to a Black Body Spectrum



Radiometric Uncertainty Gain Factors

- Detector Temperature Changes Over 4 Minutes
- Changes in DA Bias Tilt Over 4 Minutes
- Changes in Optical Flatness Over 4 Minutes
- Polarization Change ICT to Scene
- As Built ICT Radiance Knowledge
- As Built ICT Radiance Knowledge - BOL
- Non-Linearity
- Non-Linearity (MN)
- Electronic Delay Drift Over 4 Minutes
- Electronic Gain Drift Over 4 Minutes
- Changes in Channel Spectra Over 4 Minutes
- OPD Sampling Rate Drift Over 4 Minutes
- Other Small Effects

Radiometric Uncertainty Offset Factors

- Polarization Effects (Offset)
- Optics Temperature Changes Over 4 Minutes
- FOV-to-FOV Electrical Crosstalk in Same Band
- FOV-to-FOV Crosstalk Between Bands
- FOV-to-FOV Crosstalk Between Bands (MN)
- Solar Scattering JPSS Orbit

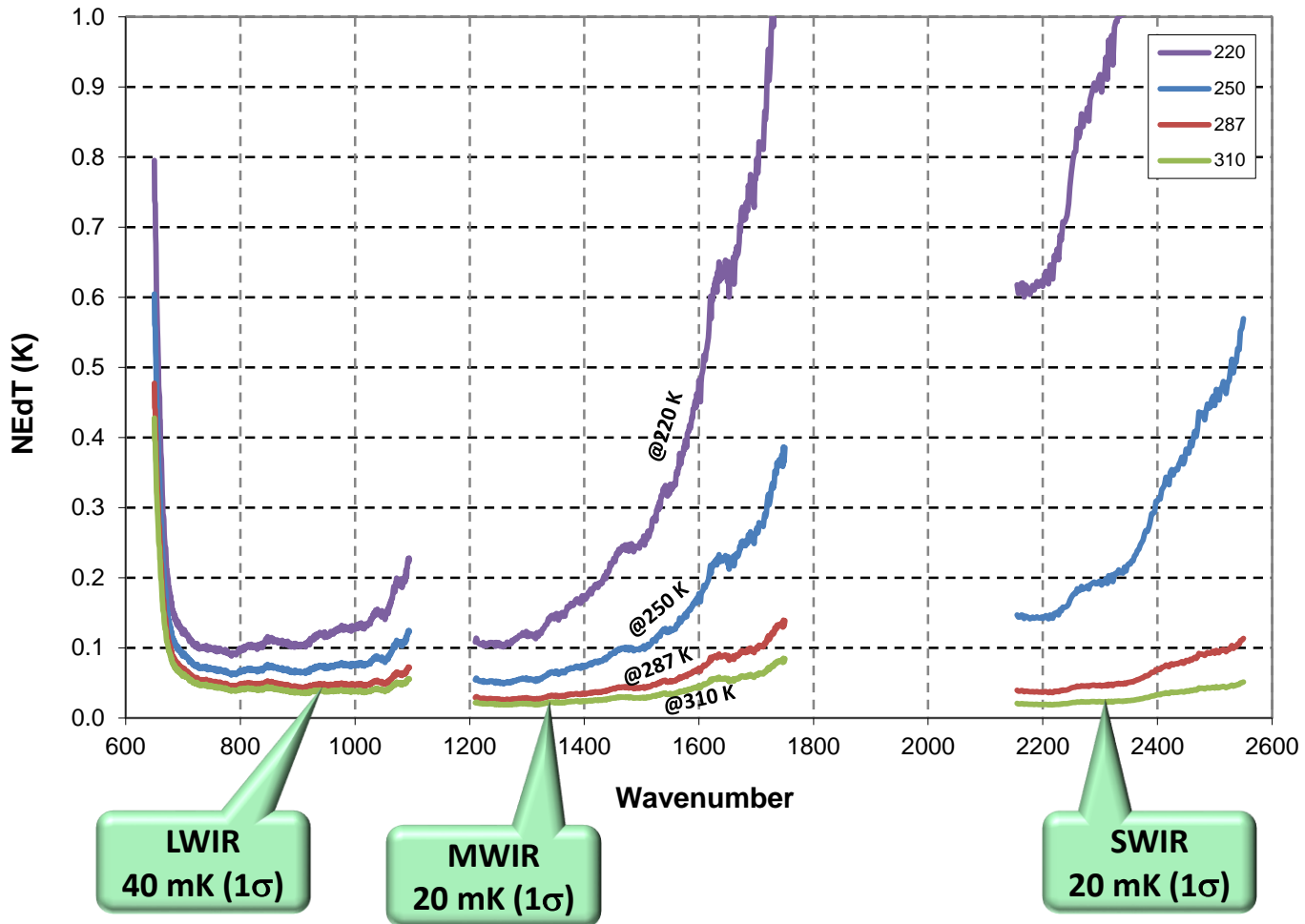
- EOL Worst Case k = 3, T = 287 K
- EOL Nominal k = 3, T = 287 K
- BOL Nominal k = 3, T = 287 K
- Specification k = 3, T = 287 K

Modified (1) CrIS J1 Radiometric Unc & Long Term Stability Roll-Ups (EOL & BOL) - 081715 rjh v12.xlsx

Typical CrIS Noise Temperature Plots

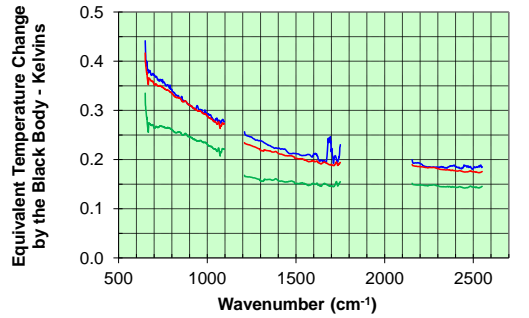
(from Suomi NPP J1 CrIS Is Similar)

Equivalent Noise Temperature at Four Scene Temperatures

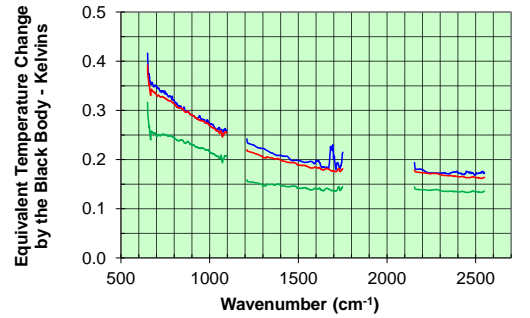


CrIS J1 Radiometric Temperature Uncertainty Estimates (k = 3) for Various ECT Black Body Scene Temperatures

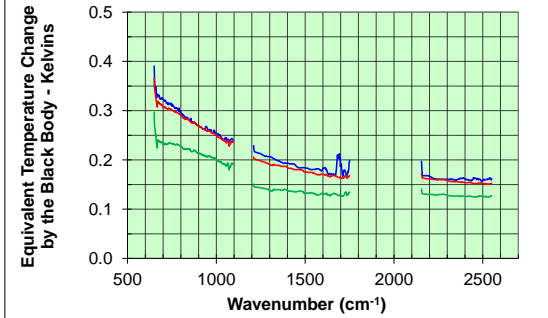
T = 310 K



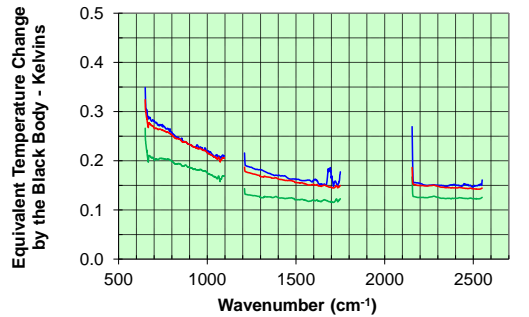
T = 299 K



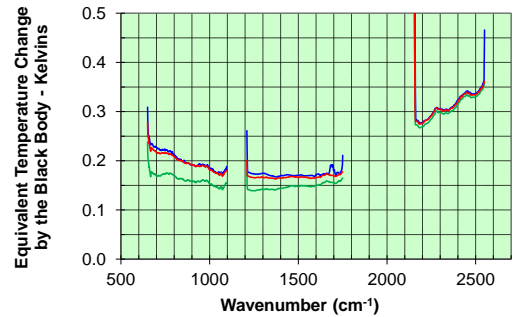
T = 287 K



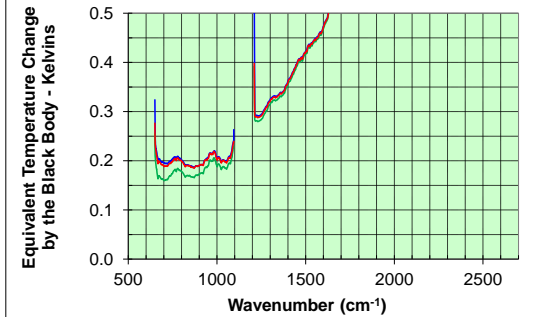
T = 265 K



T = 233 K



T = 200 K



CrIS Noise Performance (NEdT, k=1) Is Small
Compared to the Radiometric Uncertainty Equivalent Temperature Error (k=3)

Modified (1) CrIS J1 Radiometric Unc & Long Term Stability Roll-Ups (EOL & BOL) - 081715 rjh v12.xlsx

J1 CrIS Radiometric Calibration

Dave Tobin, Hank Revercomb, Joe Taylor, Bob Knuteson, Dan DeSlover, Lori Borg, Graeme Martin
Space Science and Engineering Center, University of Wisconsin-Madison

2015 JPSS Science Teams Annual Meeting

Session 6c: ATMS/CrIS Breakout

NOAA Center for Weather and Climate Prediction, College Park, MD

26 August 2015

Outline

- Radiometric Calibration Equations
 - In-orbit and TVAC
- Diagnostic Mode data analysis
 - Out-of-band signal analysis, including nonlinearity
- ECT view data analysis
 - Linear calibrations
 - ECT view temperature analysis
 - Nonlinearity determinations
- Radiometric Uncertainty (RU) estimates
 - ICT parameter uncertainties
 - Nonlinearity uncertainty
 - RU for TVAC ECT view data
 - Example RU for In-orbit sky view
- Polarization Effects
 - Theory and impact on Calibration
 - S-NPP CrIS/VIIRS comparison examples
- Summary and Future Work

Acknowledgements

- Lawrence Suwinski, Rebecca Malloy, Steve Wells ... of Exelis/Harris
- Joe Predina, Logistikos
- Mark Esplin, SDL
- Dave Johnson, NASA
- Yong Han, NOAA

Radiometric Calibration Equations*

TVAC:
$$N_{ECT} = Re\{(C'_{ECT} - C'_{ST}) / (C'_{ICT} - C'_{ST})\} (R_{ICT} - R_{ST}) + R_{ST}$$

On-Orbit:
$$N_{Earth} = Re\{(C'_{Earth} - C'_{SP}) / (C'_{ICT} - C'_{SP})\} R_{ICT}$$

with:

ECT: External Calibration Target

ST: Space Target

ICT: Internal Calibration Target

SP: Deep Space view

Complex spectra: $C = FFT(\text{Interferogram})$

Nonlinearity Corrections: $C' = C \cdot (1 + 2 a_2 V_{DC})$

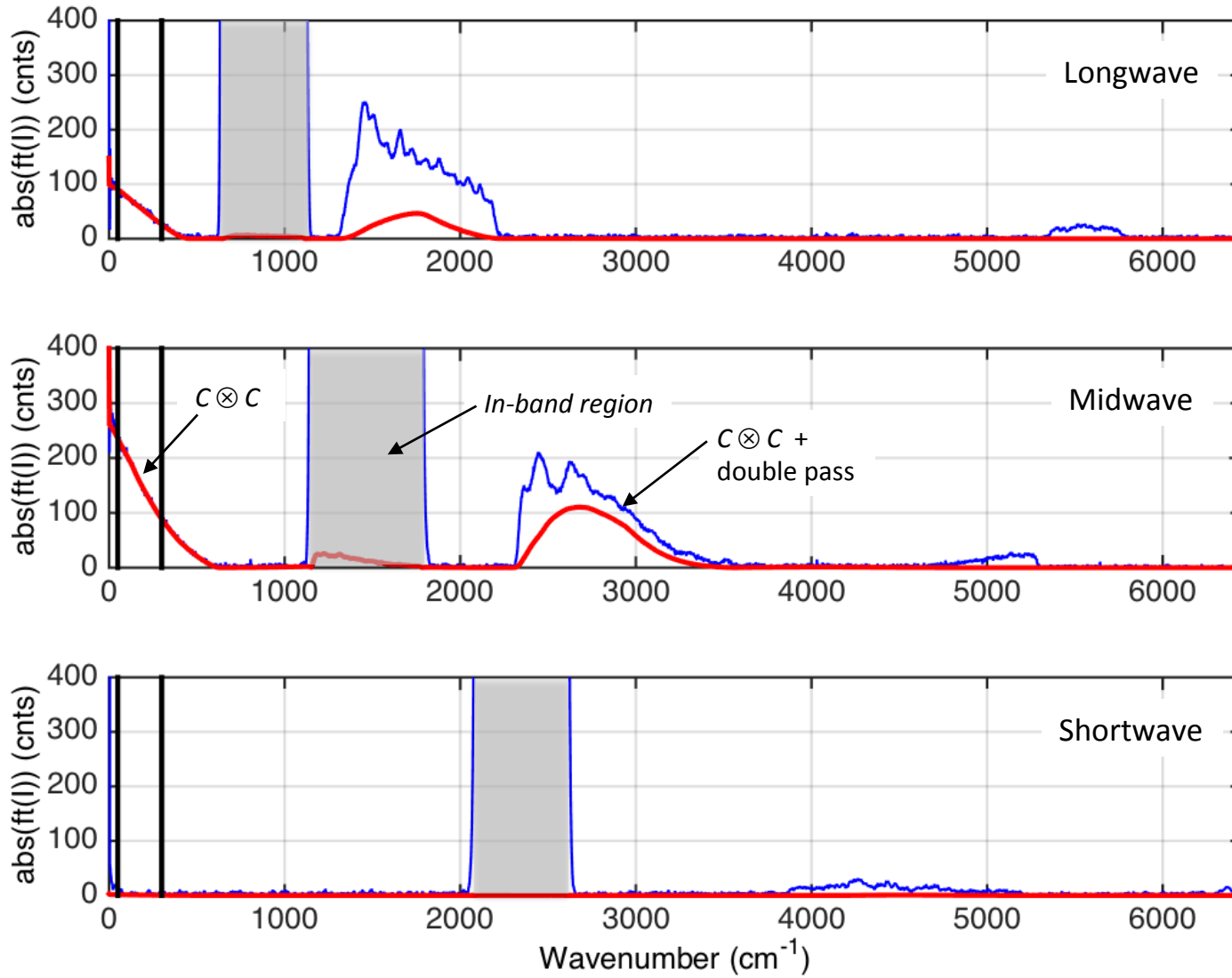
Predicted ICT view Radiances: $R_{ICT} = B(T_{ICT}) - r_{spec} [R_{specBG} - B(T_{ICT})] - r_{diff} [R_{diffBG} - B(T_{ICT})]$

Predicted ST view Radiances: $R_{ST} = \epsilon_{ST} B(T_{ST}) + (1 - \epsilon_{ST}) B(T_{ICT})$

* Not addressing spectral calibration and/or spectral ringing impacts on calibration in this presentation.

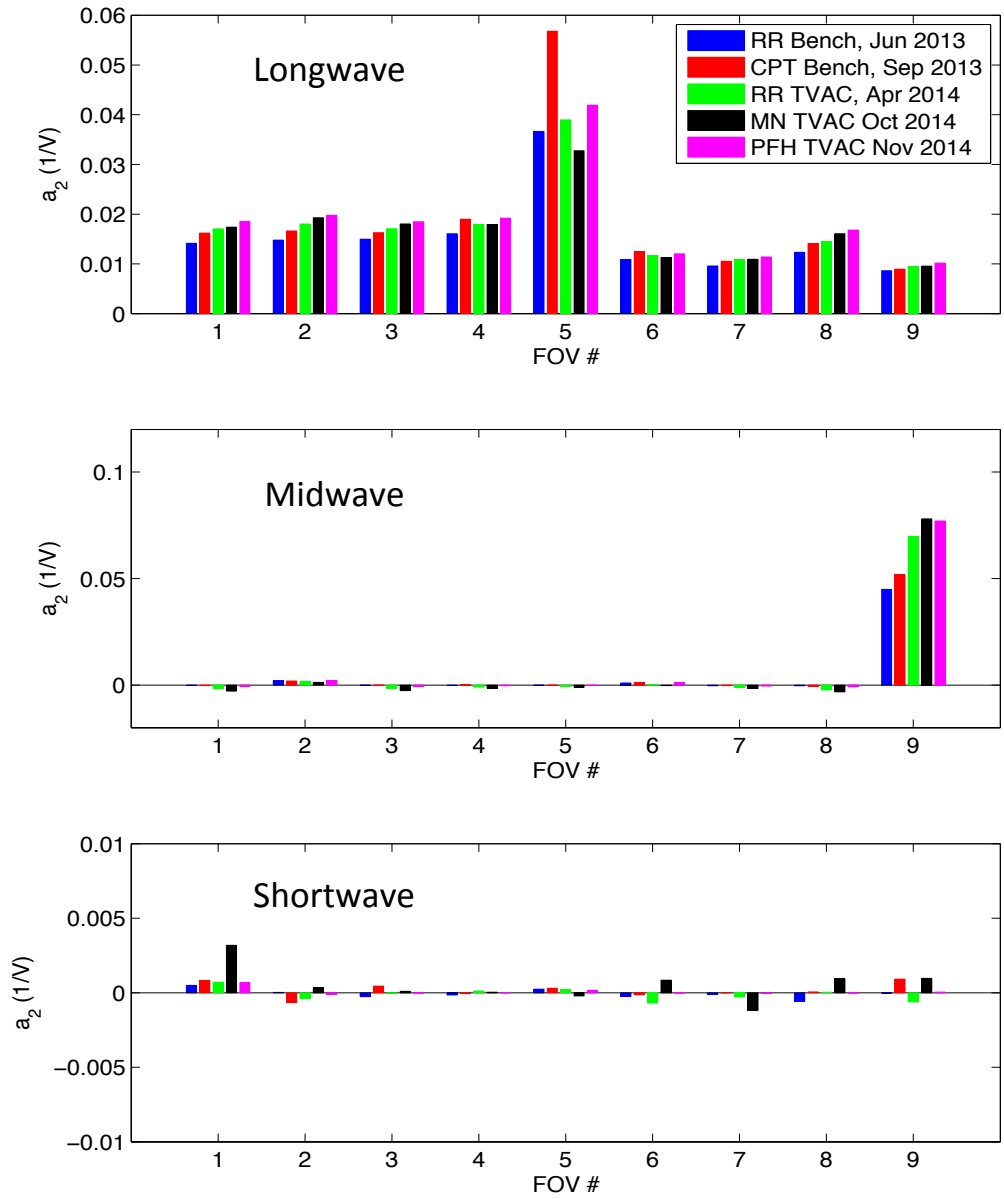
Diagnostic Mode Data

Example FOV9 ICT view spectra, Mission Nominal TVAC



Diagnostic Mode Data

quadratic nonlinearity coefficients, a_2 , from various DM datasets



$$a_2 = -Re\{ C/C \otimes C \}$$

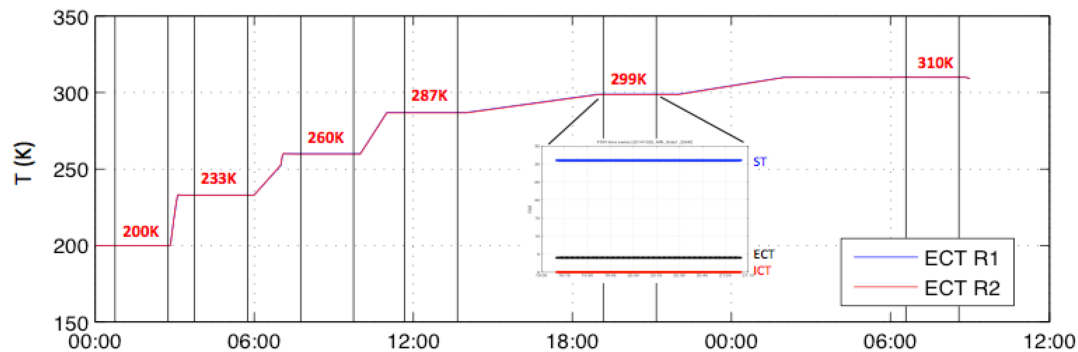
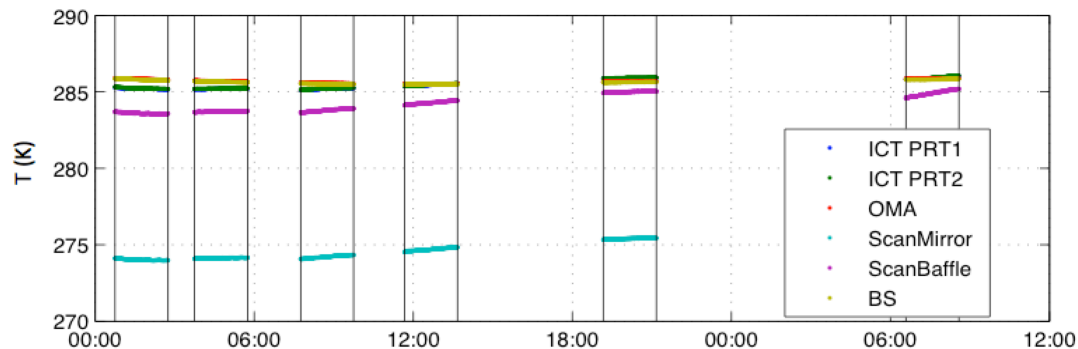
for 50-300 cm^{-1}

Diagnostic Mode Data, Key Findings:

- Out-of-band signals in the DM data show quadratic nonlinearity behavior. There are no obvious signs of higher order nonlinearities.
- These values are in good agreement with similar analyses performed by Exelis.
- All FOVs in the longwave band show significant levels of nonlinearity. With the exception of FOV5, all longwave FOVs have roughly the same level of quadratic nonlinearity (of roughly the same level of magnitude as S-NPP longwave FOVs). FOV5 is roughly twice as nonlinear as the other longwave FOVs.
- With the exception of FOV9, the midwave FOVs show very low levels of nonlinearity. The FOV9 a_2 value is roughly half that of the most non-linear midwave FOV (FOV7) on S-NPP.
- While small, all five of the a_2 values for midwave FOV2 are positive, suggesting there may be a small amount of nonlinearity. This requires further investigation.
- All shortwave FOVs show very small a_2 values. Further work is required to assess if there is a very low level of nonlinearity indicated in these results.
- Some larger differences are noted between the different tests. Further analysis is needed to determine if these are indicative of real changes in nonlinearity or due to other uncertainties in the results.

ECT view data analysis, Radiometric Nonlinearity Determination:

- Normal Mode ECT view data collected for six set-point temperatures
- FOV dependent ECT temperatures derived from linear SW and linear MW CrIS observations
- Quadratic Nonlinearity coefficients, a_2 , determined by minimizing ECT view residuals



Timeline of Mission Nominal Side 1 ECT view data collected on 25-26 October 2014

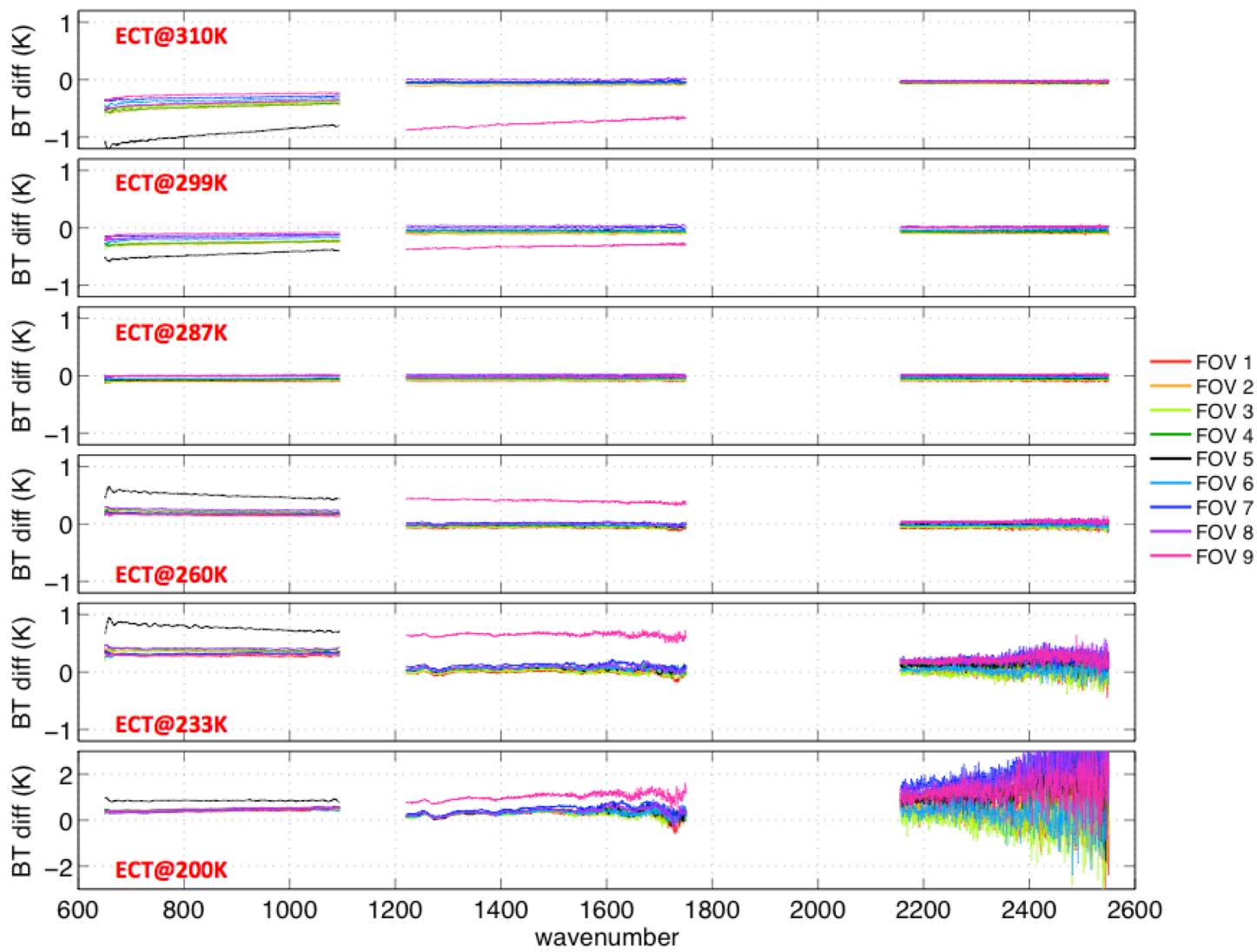
ECT view data analysis, ECT view residuals for linear calibrations

ECT view residuals,
 $N_{ECT} - R_{ECT}$ with

$$R_{ECT} = \varepsilon_{ECT} \cdot B(T_{ECT}) + \dots \\ (1 - \varepsilon_{ECT}) \cdot B(T_{ICT})$$

$$R_{ST} = e_{ST} \cdot B(T_{ST}) + \dots \\ (1 - e_{ST}) \cdot B(T_{ICT})$$

T_{ECT} = mean of backplate
R1, R2 measurements



ECT view residuals for linear calibrations.

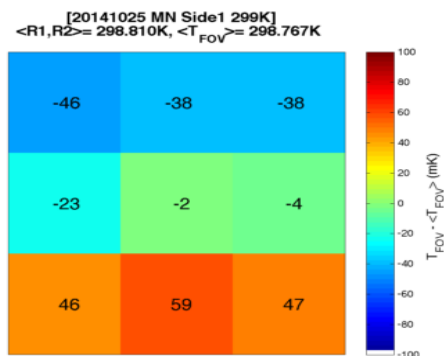
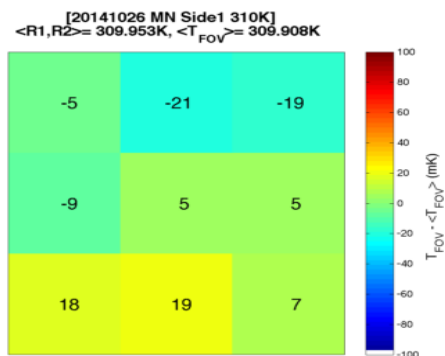
Key observations:

- 1) The shortwave band spectra show negligible nonlinearity signals, with the residuals largely independent of ECT temperature,
- 2) Shortwave band residuals display a FOV pattern consistent with a vertical temperature gradient on the backplate of the ECT,
- 3) Residuals for the 287K set-point, where $TECT \sim TICT$, do not show spectral features correlated with the ICT emissivity, providing confidence in the knowledge of the ICT predicted radiances.
- 4) The longwave and midwave band residuals display noticeable nonlinear behavior for midwave FOV9 and all of the longwave FOVs, with negative residuals for the 310K and 299K setpoints above the ICT calibration temperature and positive residuals for the 260K, 233K, and 200K setpoints below the ICT calibration temperature,
- 5) The size of the nonlinearity signals are generally consistent with nonlinearity information from Diagnostic Mode data analysis, with midwave FOVs 1-8 displaying negligible nonlinearity, midwave FOV9 displaying large nonlinearity, and all longwave band FOVs displaying similar levels of nonlinearity but with FOV5 larger by about a factor of 2.
- 6) ECT residuals in the shortwave band for 233 and 200K show non-Plankian behavior consistent with uncertainties in the reflected component of the ECT and ST predicted radiances and also higher scatter in brightness temperature due to noise.

ECT view data analysis, example ECT temperatures from linear SW FOV spectra

310 K

$\langle R1, R2 \rangle - \langle T_{FOV} \rangle = 45 \text{ mK}$
 $\max(T_{FOV}) - \min(T_{FOV}) = 38 \text{ mK}$

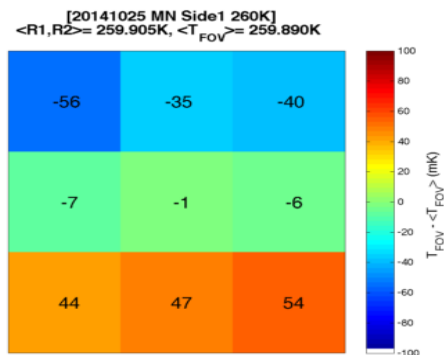
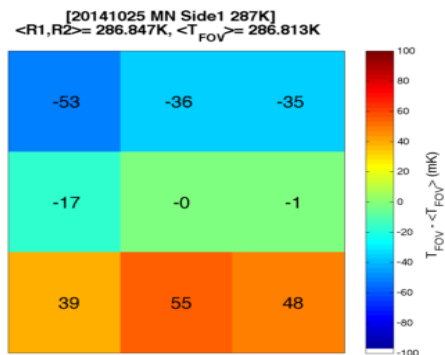


299 K

$\langle R1, R2 \rangle - \langle T_{FOV} \rangle = 43 \text{ mK}$
 $\max(T_{FOV}) - \min(T_{FOV}) = 105 \text{ mK}$

287 K

$\langle R1, R2 \rangle - \langle T_{FOV} \rangle = 34 \text{ mK}$
 $\max(T_{FOV}) - \min(T_{FOV}) = 108 \text{ mK}$

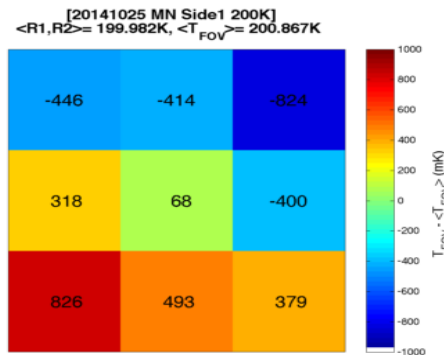
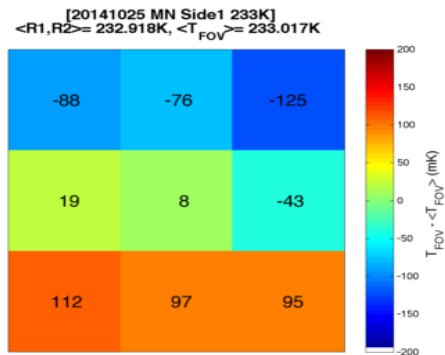


260 K

$\langle R1, R2 \rangle - \langle T_{FOV} \rangle = 15 \text{ mK}$
 $\max(T_{FOV}) - \min(T_{FOV}) = 110 \text{ mK}$

233 K

$\langle R1, R2 \rangle - \langle T_{FOV} \rangle = -99 \text{ mK}$
 $\max(T_{FOV}) - \min(T_{FOV}) = 237 \text{ mK}$



200 K

$\langle R1, R2 \rangle - \langle T_{FOV} \rangle = 0.8 \text{ K}$
 $\max(T_{FOV}) - \min(T_{FOV}) = 1.6 \text{ K}$

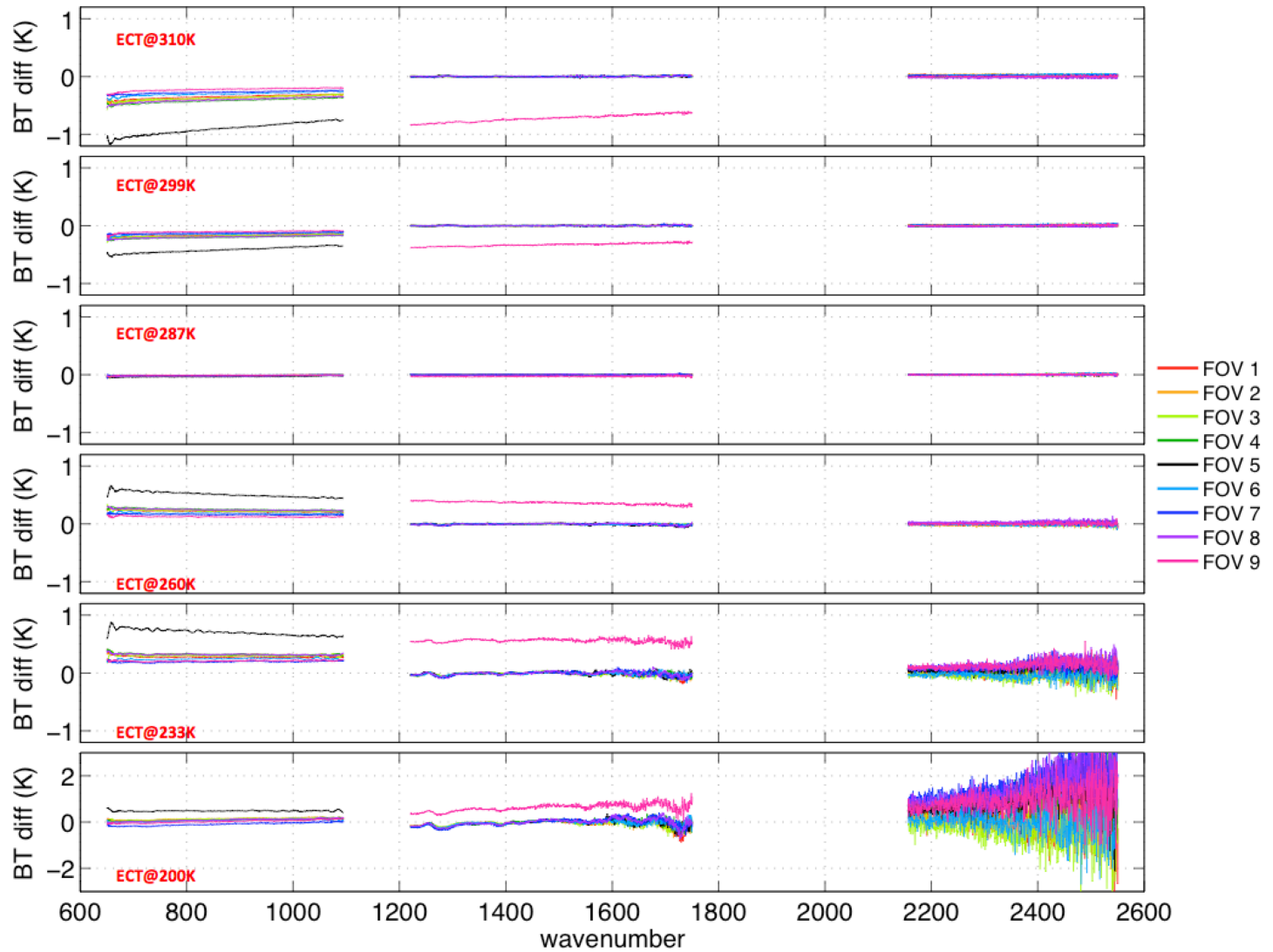
ECT view data analysis, ECT view residuals for linear calibrations

ECT view residuals,
 $N_{ECT} - R_{ECT}$ with

$$R_{ECT} = \varepsilon_{ECT} \cdot B(T_{ECT}) + \dots \\ (1 - \varepsilon_{ECT}) \cdot B(T_{ICT})$$

$$R_{ST} = e_{ST} \cdot B(T_{ST}) + \dots \\ (1 - e_{ST}) \cdot B(T_{ICT})$$

T_{ECT} = FOV dependent
values determined from
calibrated spectra for
linear SW and MW FOVs



ECT view data analysis, ECT view residuals, with optimized a_2 values

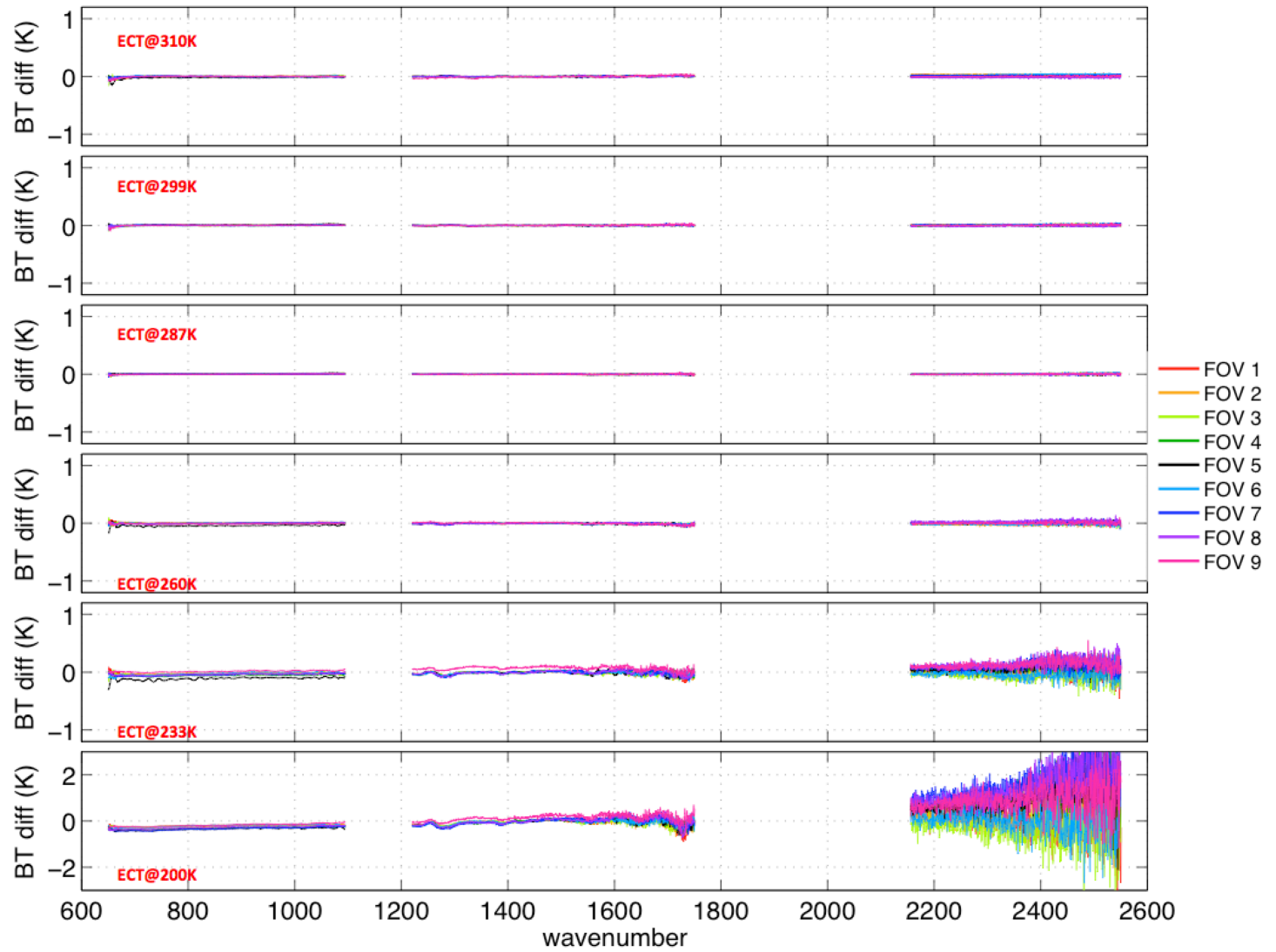
ECT view residuals,
 $N_{ECT} - R_{ECT}$ with

$$R_{ECT} = \varepsilon_{ECT} \cdot B(T_{ECT}) + \dots \\ (1 - \varepsilon_{ECT}) \cdot B(T_{ICT})$$

$$R_{ST} = e_{ST} \cdot B(T_{ST}) + \dots \\ (1 - e_{ST}) \cdot B(T_{ICT})$$

T_{ECT} = FOV dependent
values determined from
calibrated spectra for
linear SW and MW FOVs

a_2 values determined to
minimize the 310K, 299K,
and 260K residuals.



ECT view data analysis, ECT view residuals, with optimized a_2 values

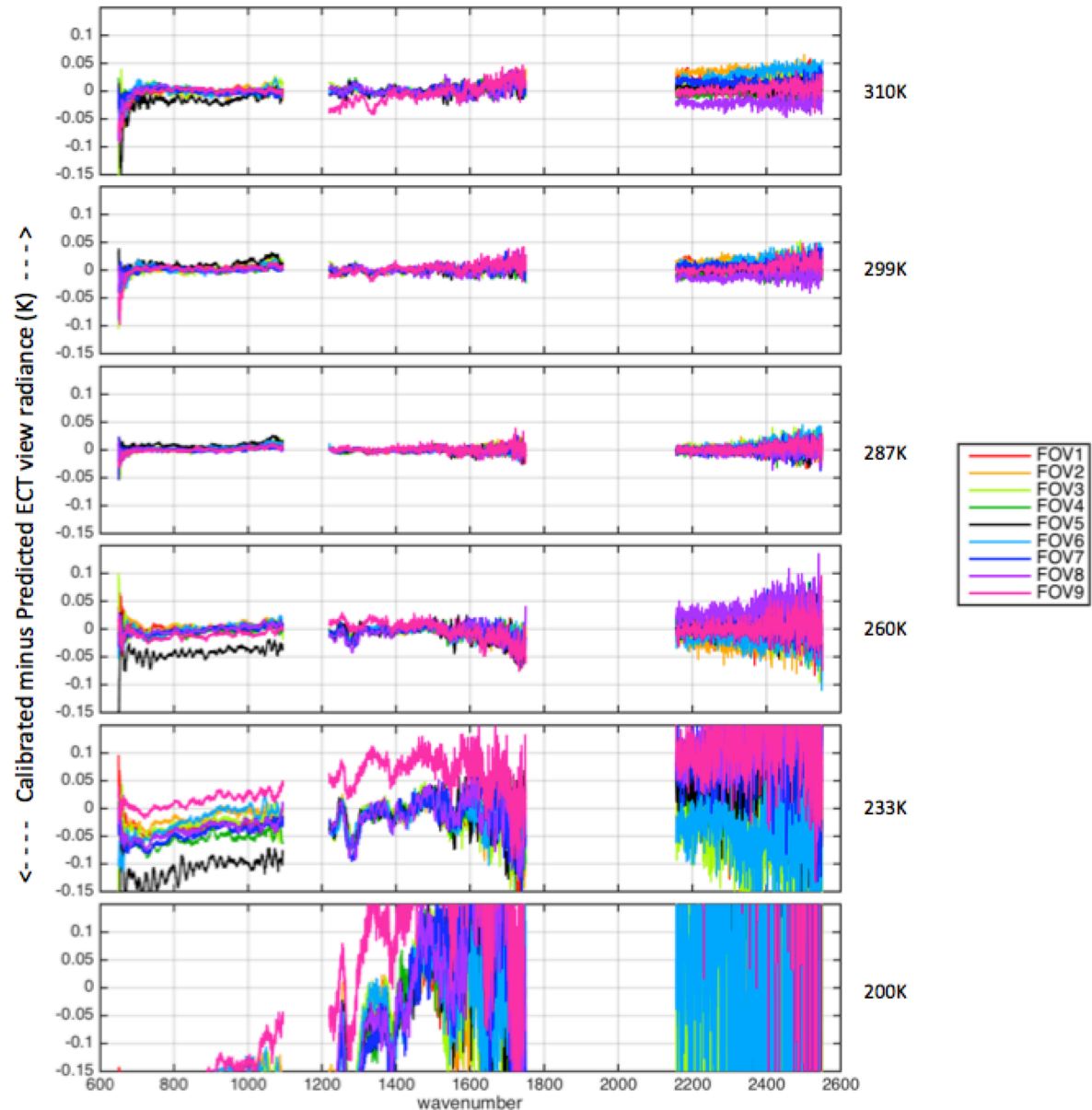
ECT view residuals,
 $N_{ECT} - R_{ECT}$ with

$$R_{ECT} = \varepsilon_{ECT} \cdot B(T_{ECT}) + \dots \\ (1 - \varepsilon_{ECT}) \cdot B(T_{ICT})$$

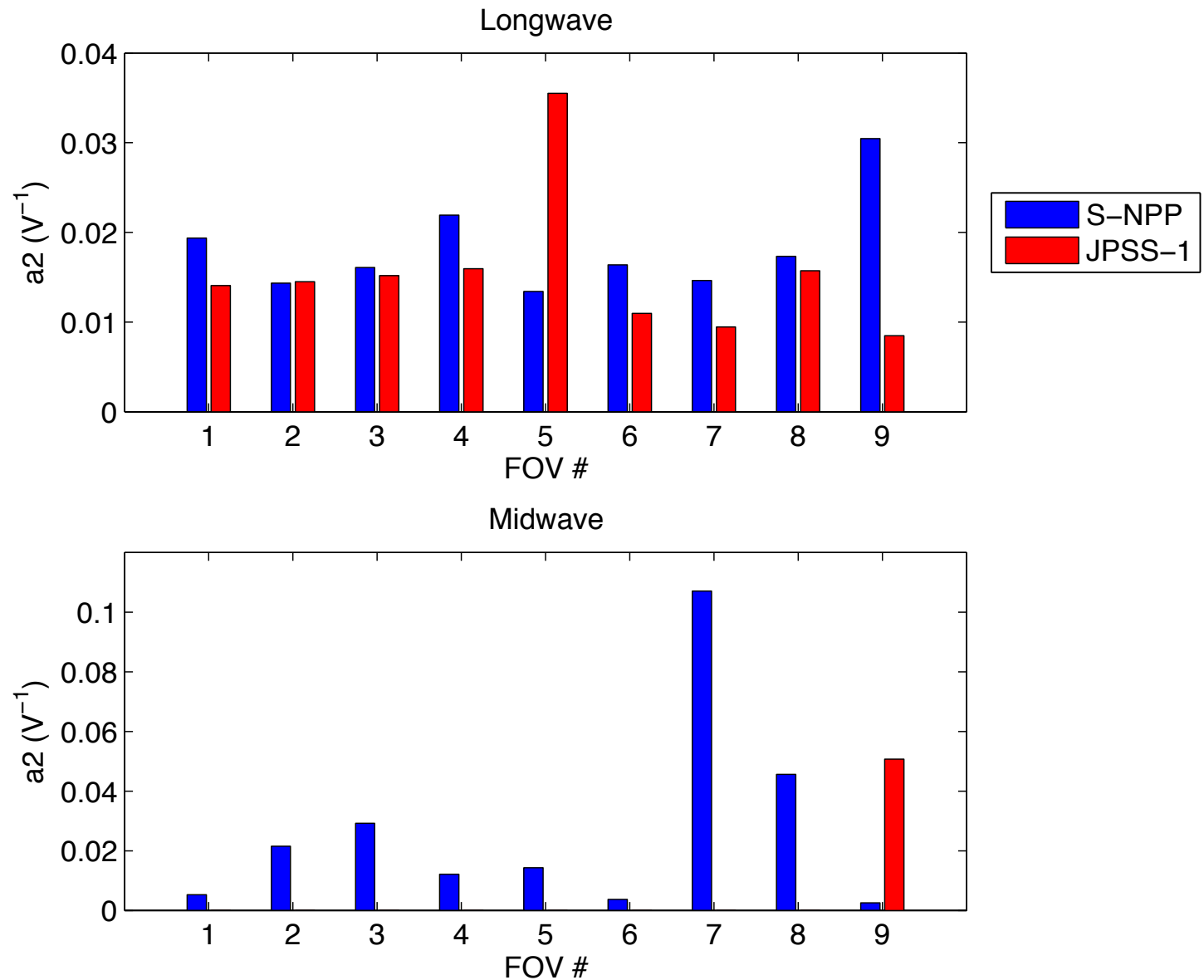
$$R_{ST} = e_{ST} \cdot B(T_{ST}) + \dots \\ (1 - e_{ST}) \cdot B(T_{ICT})$$

T_{ECT} = FOV dependent
values determined from
calibrated spectra for
linear SW and MW FOVs

a_2 values determined to
minimize the 310K, 299K,
and 260K residuals.



J1 Quadratic Nonlinearity coefficients from stepped ECT data, and comparison to S-NPP



ECT view residuals and Nonlinearity Determination.

Summary:

- 1) Temperature gradients of $\sim 0.1\text{K}$ exist on the backplate of the ECT, and there are significant uncertainties in the absolute calibration of the ECT backplate R1 and R2 temperature sensors.
- 2) Using calibrated CrIS spectra for linear FOVs, this analysis relies on the absolute calibration of the CrIS ICT to determine the FOV dependent ECT temperatures for the various ECT set-points. Pending results of NIST TXR measurements of the ECT, we may re-do this analysis using new ECT temperatures. We endorse the efforts for a new ECT.
- 3) Quadratic nonlinearity coefficients are optimized/determined to reduce ECT residuals at 310K, 299K, and 260K, and resulting residuals are 50 mK or less. Residuals for 233K and 200K are larger and not used in the optimization due to larger uncertainties at these temperatures associated with the ECT and ST emissivities and temperatures.
- 4) J1 nonlinearity is qualitatively similar to S-NPP nonlinearity, with all LW FOVs showing appreciable nonlinearity and some very linear MW FOVs.
- 5) These J1 a2 values are included in the current Engineering Packet for initial on-orbit calibrations, and during the early Cal/Val phase the a2 values will be fine tuned to create optimal consistency of the radiometric calibration of LW and MW Earth view spectra (same approach as was used for S-NPP).

J1 Pre-Launch ECT view Radiometric Uncertainty (RU) Estimates

Perturbation of the TVAC Calibration Equation:

$$N_{ECT} = Re\{(C'_{ECT} - C'_{ST}) / (C'_{ICT} - C'_{ST})\} (R_{ICT} - R_{ST}) + R_{ST}$$

Nonlinearity Corrections: $C' = C \cdot (1 + 2 a_2 V_{DC})$

Predicted ICT view Radiances: $R_{ICT} = B(T_{ICT})$ (ignoring small reflected contributions)

Predicted ST view Radiances: $R_{ST} = \epsilon_{ST} B(T_{ST}) + (1 - \epsilon_{ST}) B(T_{ICT})$

Predicted ECT view Radiances:

$$R_{ECT} = \epsilon_{ECT} B(T_{ECT}) + (1 - \epsilon_{ECT}) B(T_{ICT})$$

Parameter Uncertainties:

N_{ECT} parameter	Nominal Value	3-sigma Unc.
LW a_2	0.01 – 0.03 V ⁻¹	25%
MW a_2	0, 0.05 V ⁻¹	25%
T_{ICT}	287 K	0.114 K
ϵ_{ST}	0.9995	0.0009
T_{ST}	104 K	6 K
$T_{ST, Refl}$	287 K	9 K

R_{ECT} parameter	Nominal Value	3-sigma Unc.
ϵ_{ECT}	0.9995	0.0009
T_{ECT}	200 – 310K	0.2 K
$T_{ECT, Refl}$	287 K	15 K

J1 Radiometric Uncertainty (RU) Estimates: Predicted ICT radiance.

Predicted ICT view radiance for the specular 3-bounce trap design includes an emissive term and reflected terms due to the specular and diffuse reflections of the ICT:

$$R_{ICT} = B(T_{ICT}) - r_{spec} [R_{specBG} - B(T_{ICT})] - r_{diff} [R_{diffBG} - B(T_{ICT})]$$

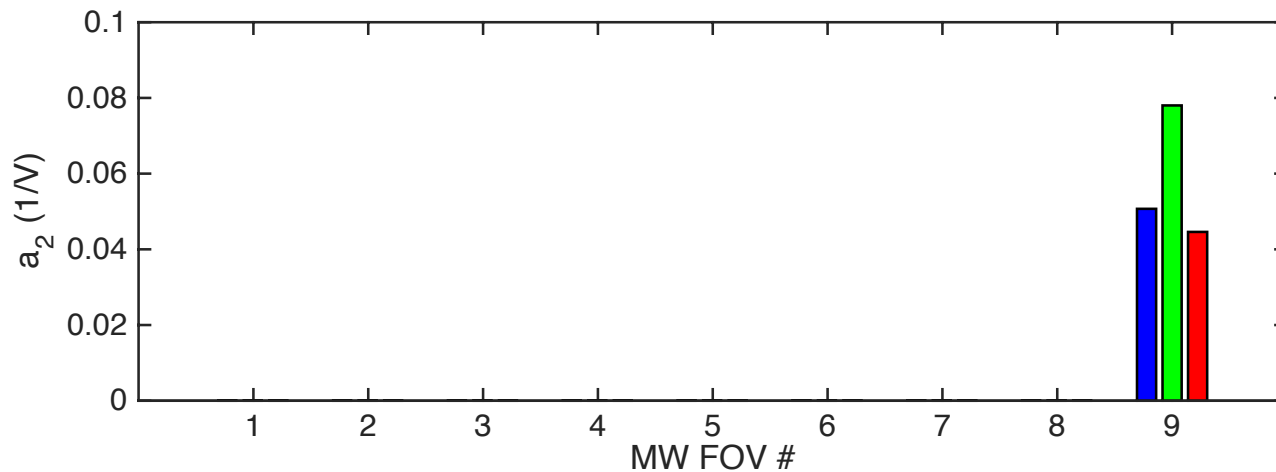
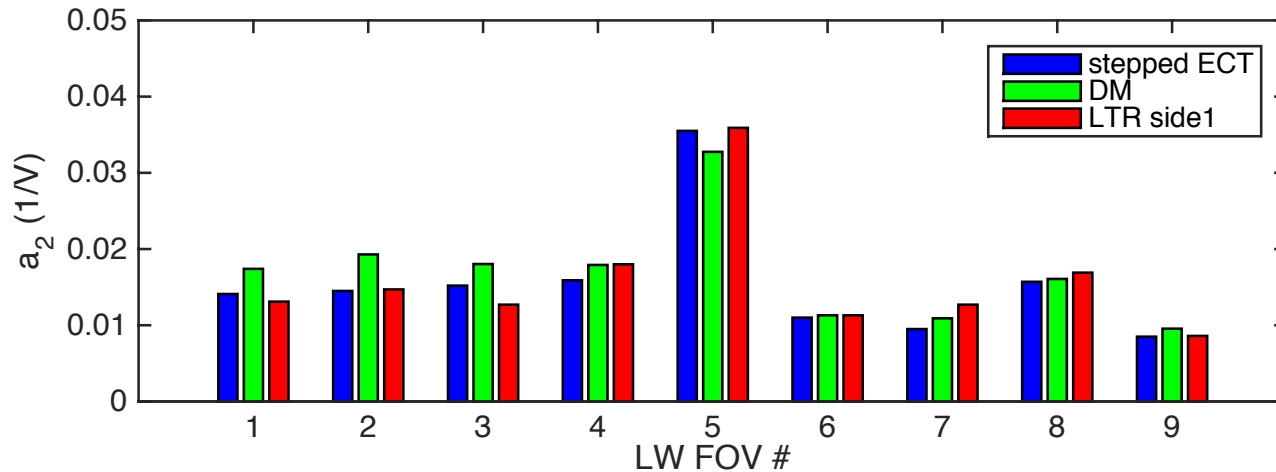
The specular reflection term is computed as reflection from the beamsplitter and is estimated as $\frac{1}{2} r_{spec} B(T_{ICT})$. r_{spec} is $\sim 0.03\%$ and the specular reflection term is approximately 10 mK in BT with an uncertainty of 5 to 10 mK.

For the diffuse term, r_{diff} is very small and the diffuse emitting surfaces have temperature very close to T_{ICT} . This results in this diffuse reflection term being very small, on the order ~ 5 mK with uncertainty of 5 to 10 mK.

For the emissive term $B(T_{ICT})$, T_{ICT} has an uncertainty of 114 mK, significantly larger than the reflected term contributions and uncertainties. (A large fraction of the TICT uncertainty is due to the thermal gradient from the PRT sensor location to the ICT emitting surfaces).

For the following RU estimates, uncertainties in predicted ICT radiances include T_{ICT} contributions only and uncertainties in the reflected terms are ignored.

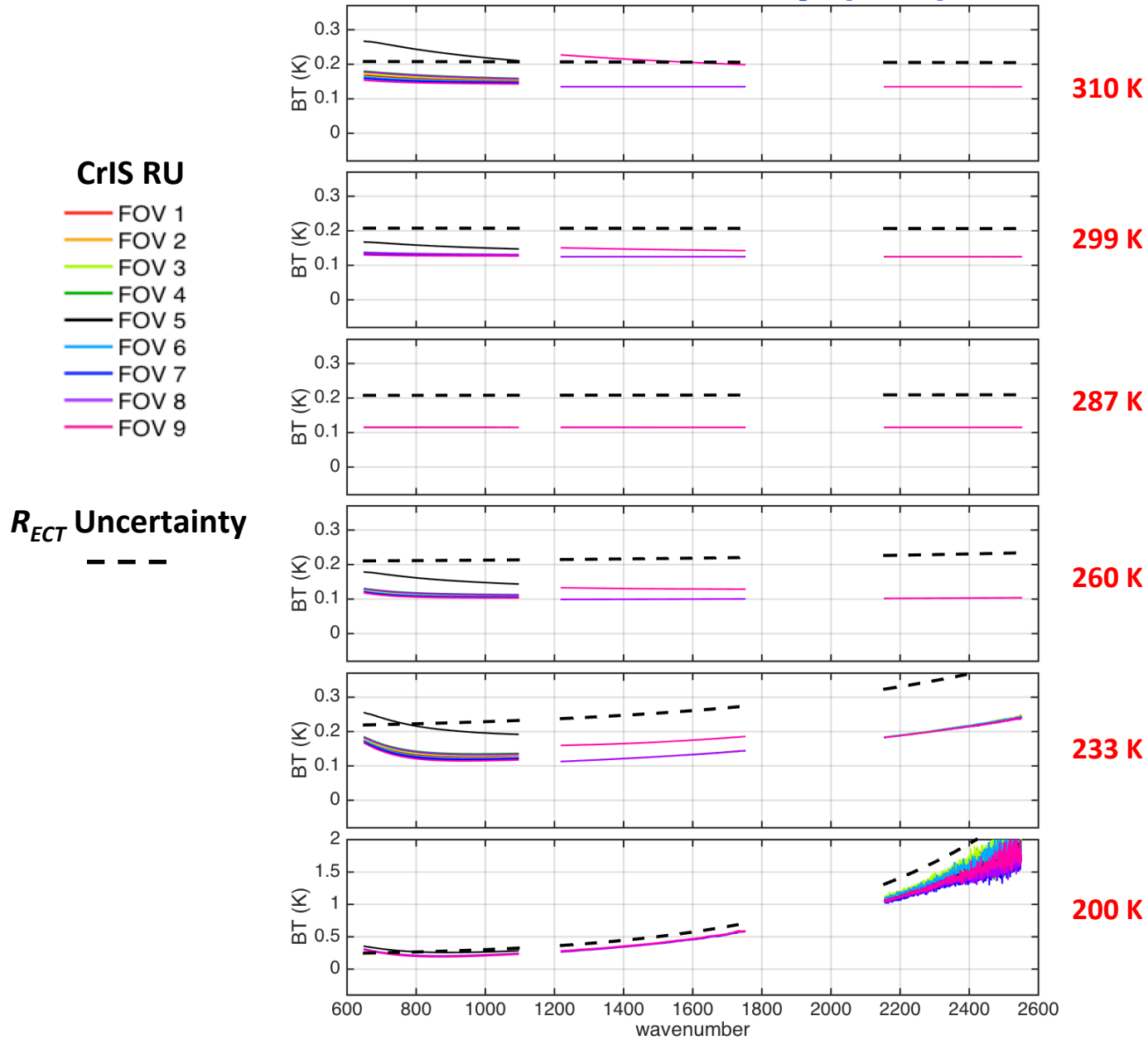
J1 Pre-Launch Nonlinearity Uncertainty



Comparison of quadratic nonlinearity coefficients from three pre-launch test data analysis methods: Stepped ECT view NM data, Diagnostic Mode harmonics, Long term repeatability c/o Mark Esplin.

J1 Pre-Launch ECT view

Radiometric Uncertainty (RU) Estimates



J1 Pre-Launch Earth view Radiometric Uncertainty (RU) Estimates

Perturbation of the in-orbit Calibration Equation using S-NPP Earth view data

$$N_{Earth} = Re \{ (C'_{Earth} - C'_{SP}) / (C'_{ICT} - C'_{SP}) \} R_{ICT}$$

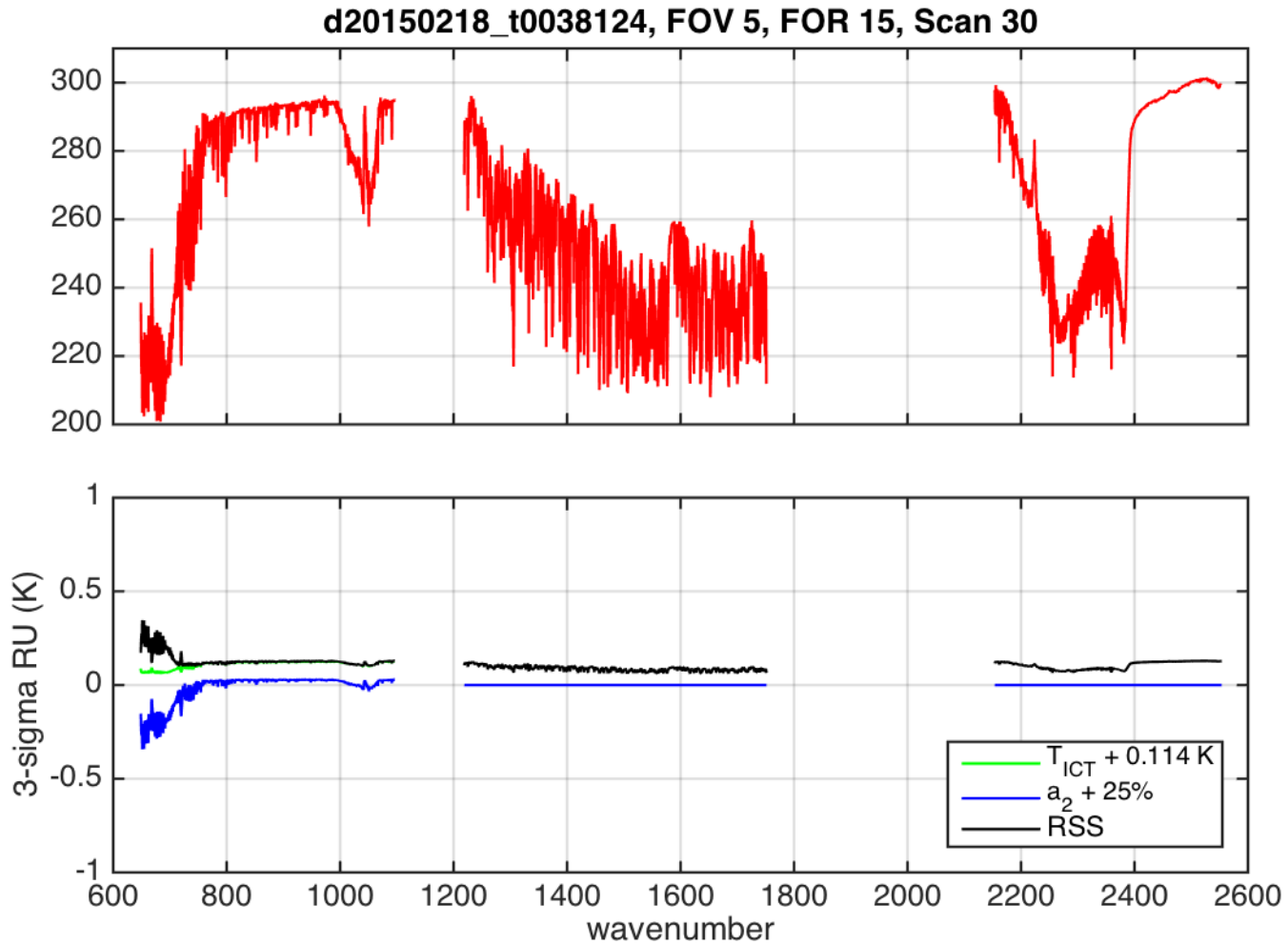
Nonlinearity Corrections: $C' = C \cdot (1 + 2 a_2 V_{DC})$

Predicted ICT view Radiances: $R_{ICT} = B(T_{ICT})$ (ignoring small reflected contributions)

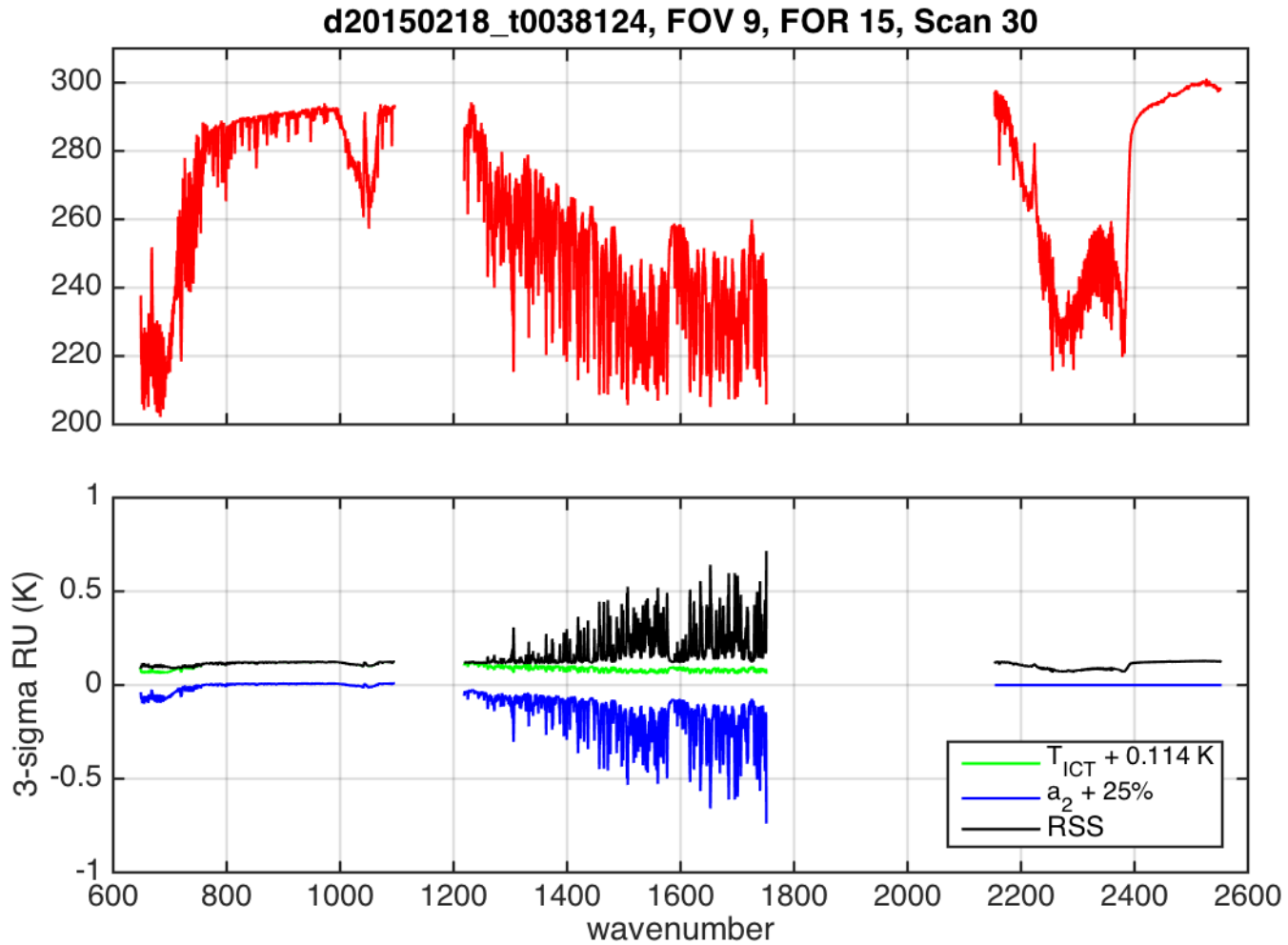
Parameter Uncertainties:

N_{Earth} parameter	Nominal Value	3-sigma Unc.
LW a_2	0.01 – 0.03 V ⁻¹	25%
MW a_2	0, 0.05 V ⁻¹	25%
T_{ICT}	287 K	0.114 K

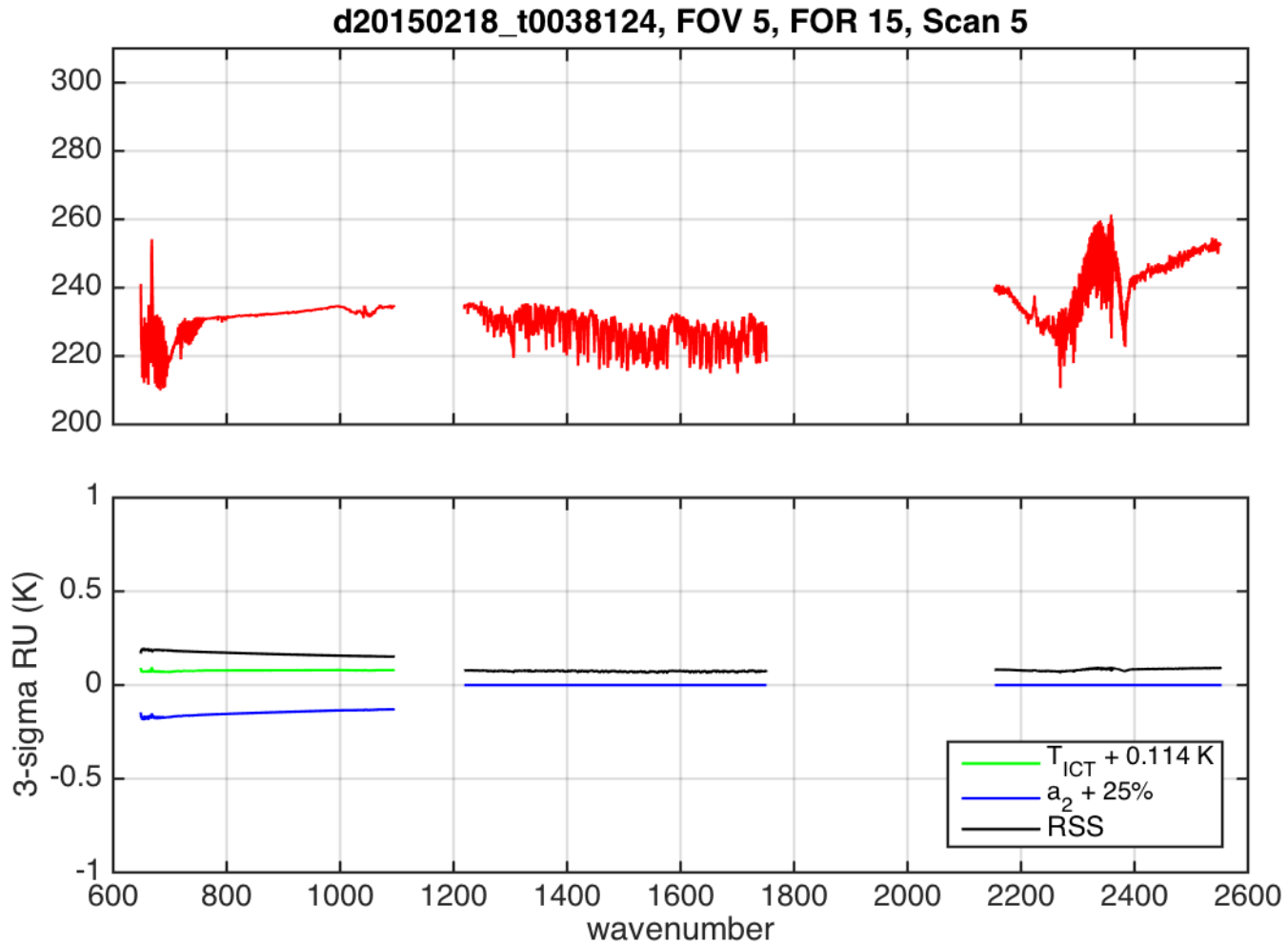
J1 Pre-Launch Earth view RU Estimates



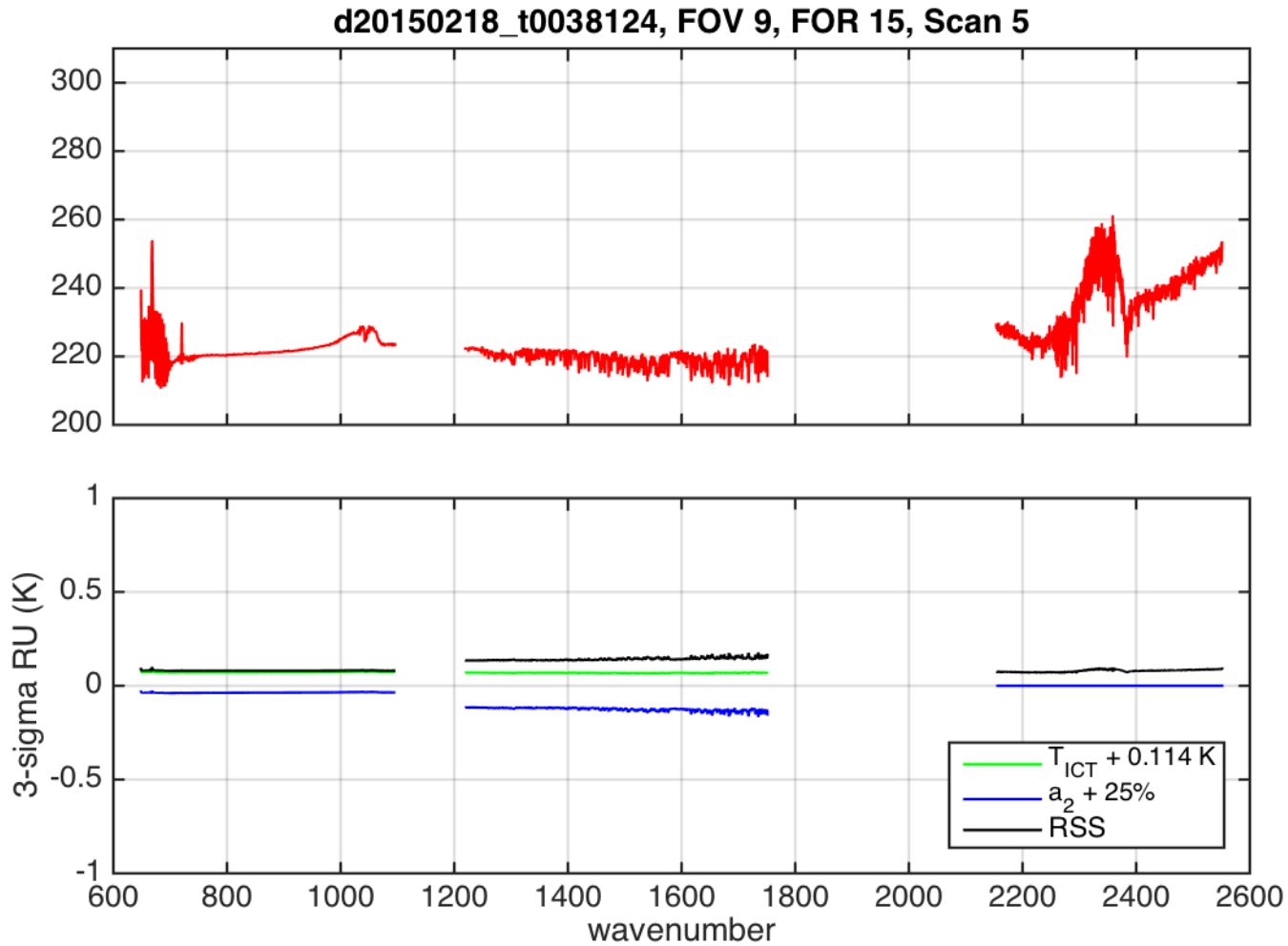
J1 Pre-Launch Earth view RU Estimates



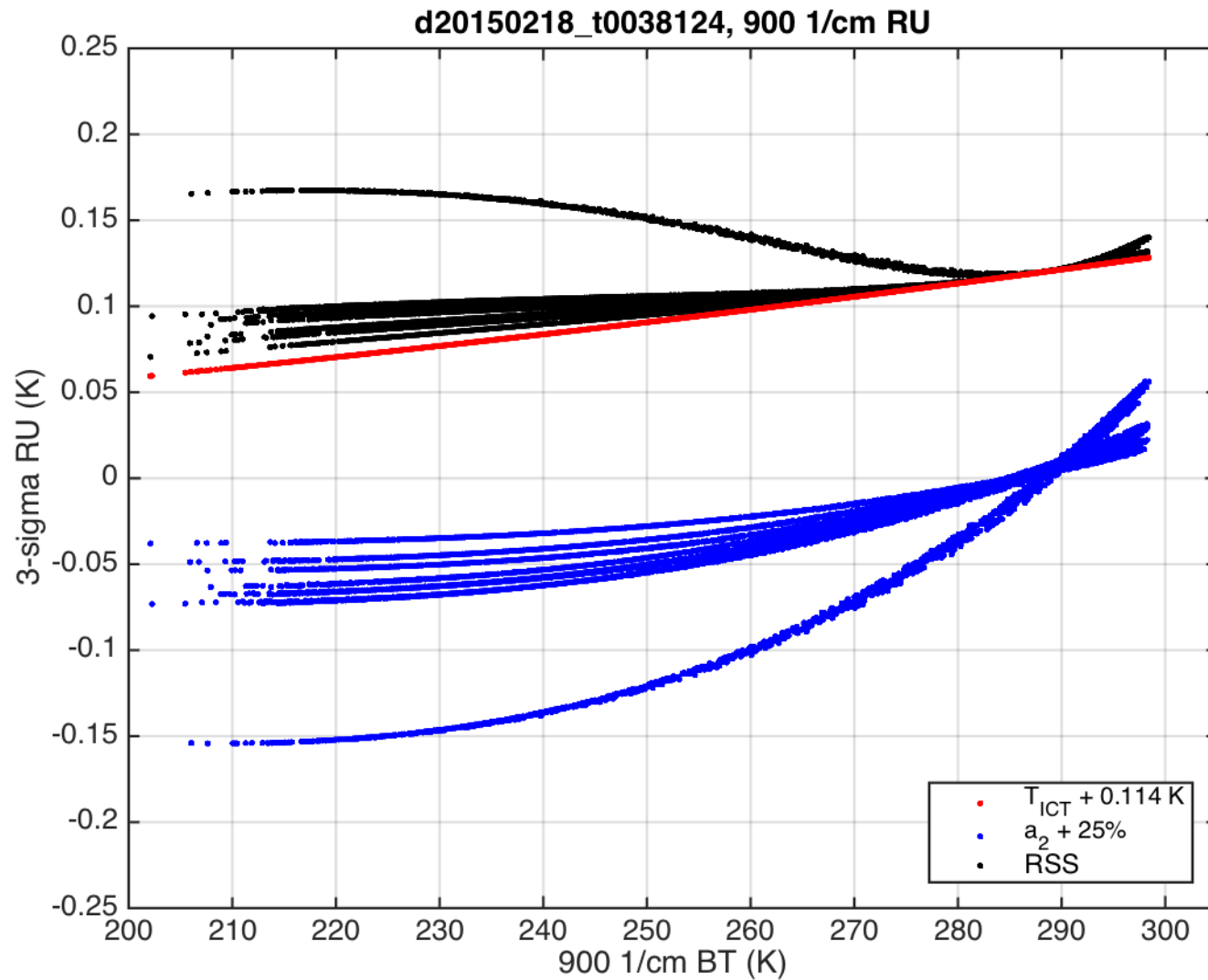
J1 Pre-Launch Earth view RU Estimates



J1 Pre-Launch Earth view RU Estimates



J1 Pre-Launch Earth view RU Estimates



J1 Pre-launch RU summary

- **Pre-launch RU estimates for J1 CrIS are very similar to S-NPP estimates, and are dominated by ICT temperature and nonlinearity contributions.**
 - **ICT temperature uncertainty for J1 is very similar to S-NPP.**
 - **J1 CrIS has negligible contributions from ICT reflected terms due to the improved ICT design and implementation.**
 - **8 of the 9 MW FOVs are very linear on J1, whereas only MW FOVs 6 and 9 are linear on S-NPP. LW nonlinearity magnitude on J1 is very similar to S-NPP.**
 - **Pre-launch J1 nonlinearity coefficient uncertainty is approximately a factor of 2 lower than that of S-NPP.**
- **Nonlinearity coefficient tuning using Earth view data will reduce the MW FOV9 uncertainty to very small levels (using linear MW FOVs as reference), and LW nonlinearity consistency among FOVs will be optimized.**
- **Opposed to Exelis/Harris RU estimates, these RU estimates do not yet include contributions due to polarization, cross-talk, or other smaller contributions.**

CrIS Calibration Bias due to Polarization.

Introduction:

- Incident radiance is partially polarized by reflection from the scene select mirror (SSM); there is a small degree of polarization in the IR for uncoated gold mirrors
- The orientation of the polarization axis of the scene select mirror changes with scene mirror rotation.
- When coupled with the polarization sensitivity of the sensor, this produces a radiometric modulation of the detected signal that is dependent on the rotation angle of the scene select mirror and creates a calibration error.

CrIS Calibration Bias due to Polarization.

Current Model:

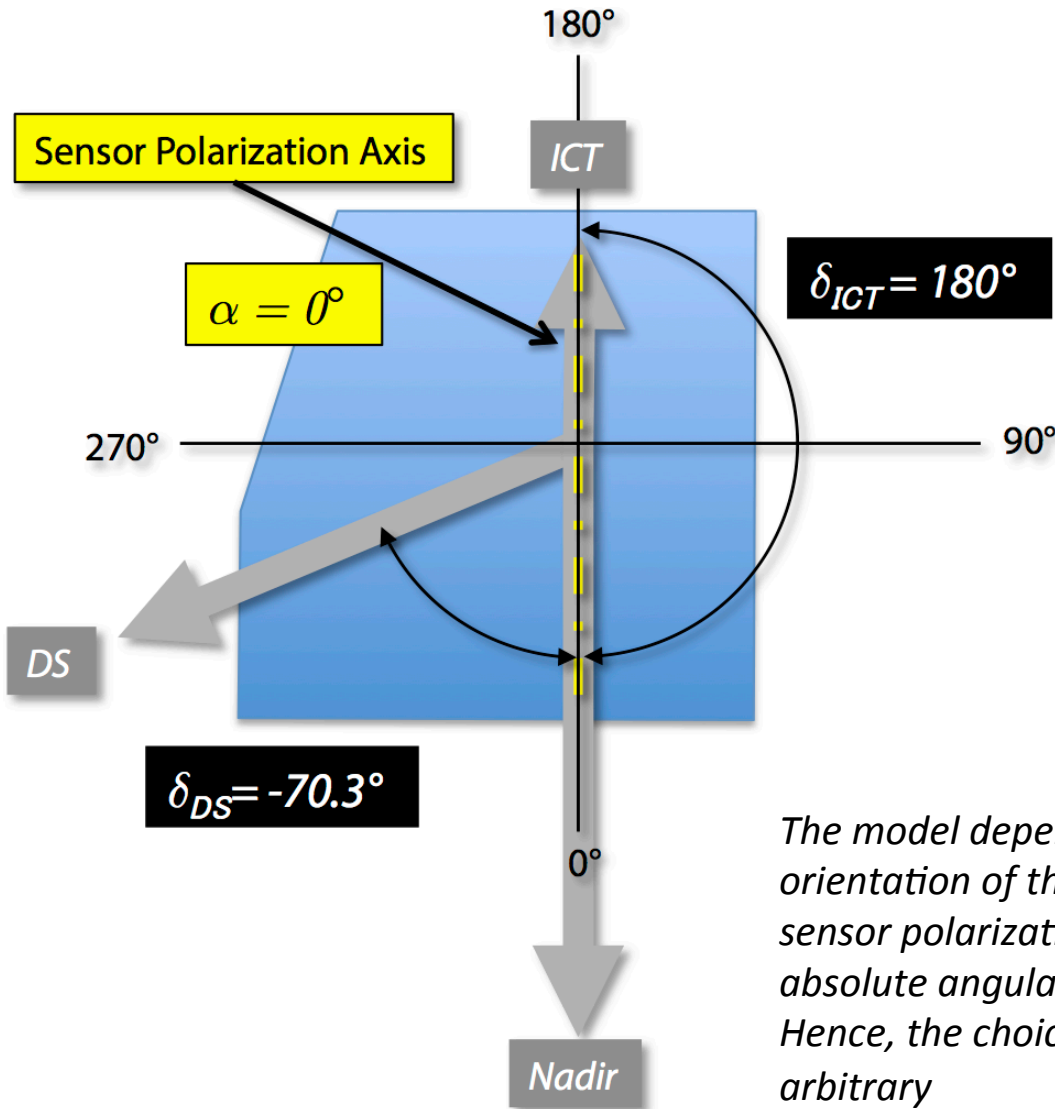
- For CrIS the bias due to ignoring polarization can be approximated as:

$$E_p \cong p_r p_t \left\{ (L_s - B_{SSM}) [\cos 2(\delta_s - \alpha) + \cos 2\alpha] \right\}$$

where p_r and p_t are the SSM and sensor polarizations, L_s is the scene radiance, B_{SSM} is $B(T_{SSM})$, δ_s is the scene mirror angle, and α is the sensor axis orientation angle.

- Currently using spectrally independent values for scene mirror polarization and sensor polarization: $p_r = 0.0055$, $p_t = 0.08$ (average values provided by Joe Predina)
- Selected nadir view as 0° for α and δ
- Have assumed that sensor polarization orientation is dominated by the beamsplitter ($\alpha = 0^\circ$). The impact of other optical elements need to be evaluated (dichroics in particular).
- Will revise model as better information becomes available, but these preliminary values allow us to demonstrate the nature and potential calibration bias due to uncorrected polarization.

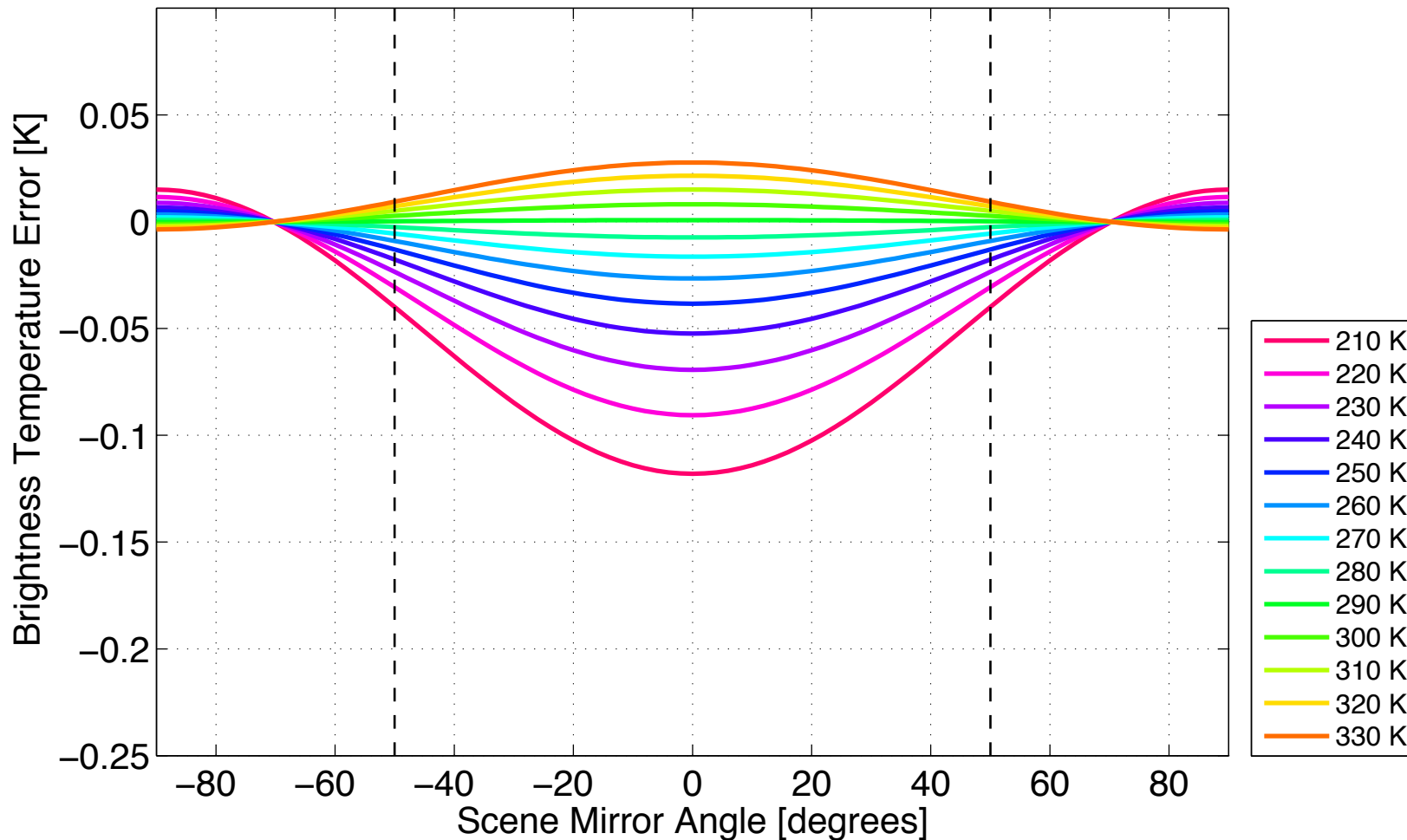
CrIS Calibration Bias due to Polarization. Current Model:



The model depends on the relative orientation of the scene mirror and sensor polarization axes, not the absolute angular position of either. Hence, the choice of the 0° position is arbitrary

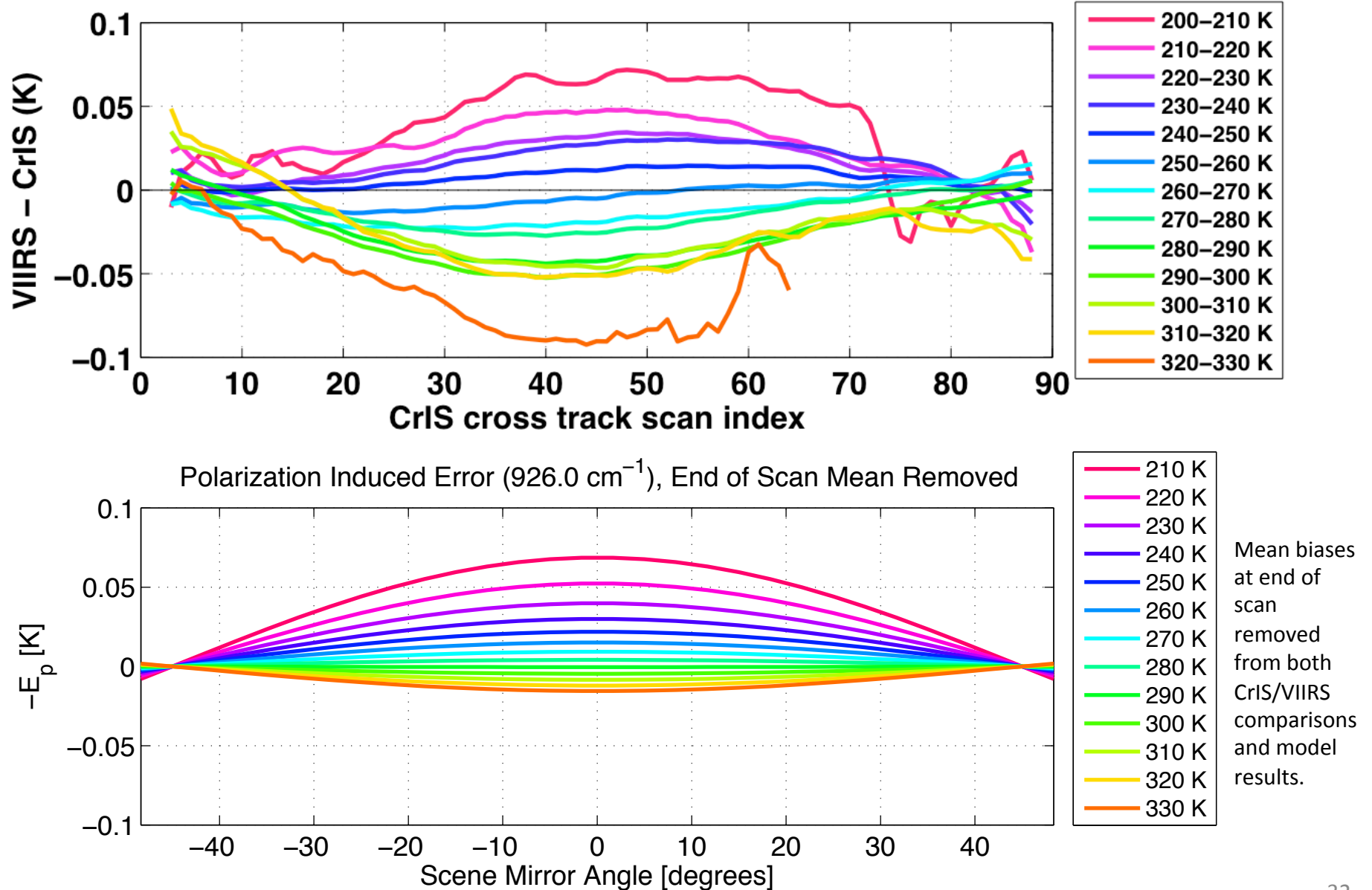
CrIS Calibration Bias due to Polarization. Model Results at 900 cm⁻¹

Polarization Induced Error (900.0 cm⁻¹), Brightness Temperature
 $\delta_H = 180.00$, $\delta_C = -70.30$, $\alpha = 0.00$



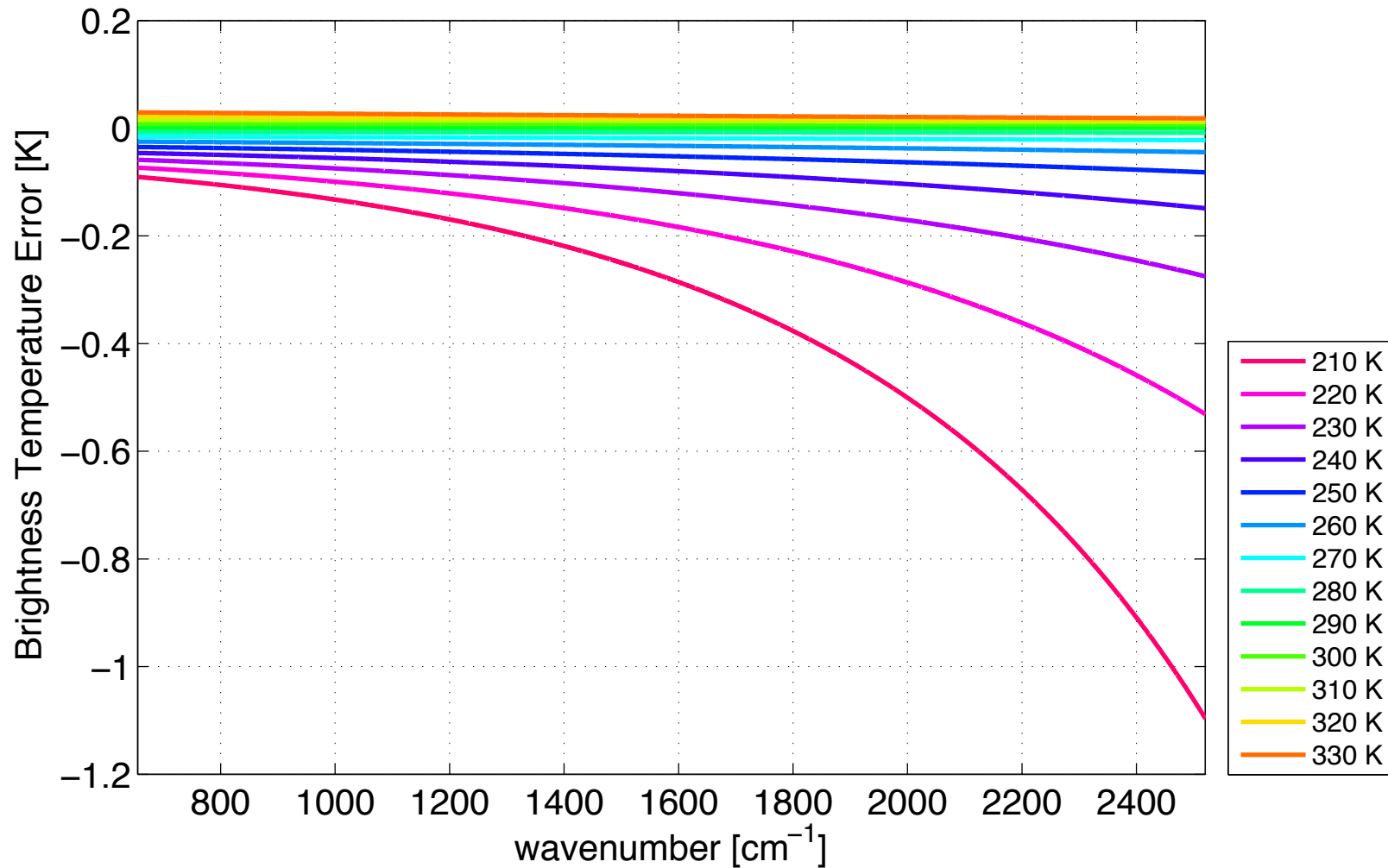
CrIS Calibration Bias due to Polarization.

Band 15 CrIS/VIIRS comparisons and 11 μm Model Results



CrIS Calibration Bias due to Polarization. Model Results at nadir (FOR15)

Polarization Induced Error (SSM angle = -1.67°), Brightness Temperature
 $\delta_{hbb} = 180.00$, $\delta_{cbb} = -70.30$, $\alpha = 0.00$



CrIS Calibration Bias due to Polarization. Summary

- **Current CrIS Calibration does not account for polarization effects.**
- **However, we should expect systematic effects due to the design of the sensor and there is evidence of the effects in observed spectra.**
- **A correction module suitable for use in the SDR algorithm is being developed.**
- **Additional measurements of key optical components should be performed to ensure accurate corrections.**

J1 CrIS Radiometric Calibration: Overall Summary

- **J1 CrIS pre-launch calibration uncertainty is dominated by ICT temperature knowledge (114 mK) and quadratic nonlinearity coefficient uncertainty (~25%).**
- **Radiometric Uncertainty estimates for TVAC ECT views are less than ~0.3 K. After nonlinearity tuning, differences between CrIS calibrated spectra and predicted ECT view spectra are less than ~0.1 K for scene temperatures of 233K-310K.**
- **Using pre-launch parameters and uncertainties, RU for example Earth view spectra has been estimated. With the exception of FOVs with largest nonlinearity (LW5 and MW9), RU is less than a few tenths K.**
- **CrIS has systematic biases due to Polarization which varies with scan angle, scene temperature, and wavelength, and associated correction modules are being developed for consideration in the SDR algorithm.**

J1 CrIS Radiometric Calibration: Future Work

- **The ICT temperature knowledge uncertainty (114 mK) includes a large contribution (~75 mK) due to the estimated gradient from the PRTs to the emitting surface; We plan to investigate this further and possibly account for part of the gradient in the effective ICT temperature and reduce its uncertainty.**
- **Pending results of NIST TXR measurements of the ECT, we may revisit our nonlinearity analysis.**
- **After launch, nonlinearity coefficients will be fine-tuned to create optimal consistency among MW FOVs and LW FOVs for Earth view data, using the most linear FOVs/detectors as reference. This should reduce the uncertainty for FOVs with largest nonlinearity including LW5 and MW9.**
- **Pursue additional polarization measurements and study the impact of polarization corrections on Earth view spectra, including near-nadir comparisons with other sensors via SNOs, and the impact on cold scene SW band calibration.**

Summary Continued: J1 CrIS is as good or better than S-NPP CrIS

- **J1 ICT emissivity is higher and well characterized**
- **ICT temperature uncertainties similar**
- **Nonlinearity:**
 - **LW: overall a2 magnitudes are similar but J1 and S-NPP have different FOV dependence.**
 - **MW: 8 of 9 detectors on J1 are very linear.**
- **Both expected to have similar polarization effects**

Other Work

- **S-NPP LW FOV5 cold scene anomaly**
- **S-NPP SW cold scene biases**
- **Correction for on-board non-circular FIR filtering (spectral ringing, extended interferograms)**
- **Choice of Calibration Equation (spectral ringing)**

CrIS Spectral Calibration

L. Larrabee Strow, Howard Motteler, Sergio De Souza-Machado, and Steven Buczowski

UMBC

Department of Physics *and*
Joint Center for Earth Systems Technology

August 25, 2015



Overview

- JPSS-1 CrIS thermal vacuum (TVAC) spectral testing
- SNPP CrIS in-orbit spectral calibration performance
- SNPP CrIS Stability: three-year trends in CrIS radiances
- Mid-Wave Non-linearity in High Resolution Mode

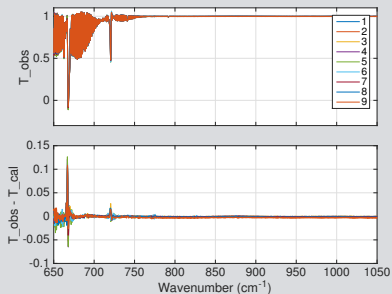
JPSS-1 CrIS Spectral Calibration in TVAC

- Spectral calibration has two components:
 - Absolute spectral calibration, provided by Neon lamp, which is calibrated in TVAC.
 - Apodization smearing of ILS due to off-axis detectors. Need accurate effective detector positions to correct, as determined in TVAC.
- Both Neon and focal plane geometry derived from analysis of gas cell spectra.
- 1 ppm accuracy requires modeling to ~ 0.001 in transmittance!

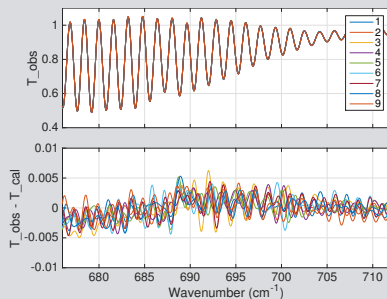
1 ppm accuracy keeps NWP bias correction standard deviation small enough (if using multiple FOVs).

LW CO₂ Spectra (MN, Side 1)

Full CO₂ Spectrum



Region Fitted

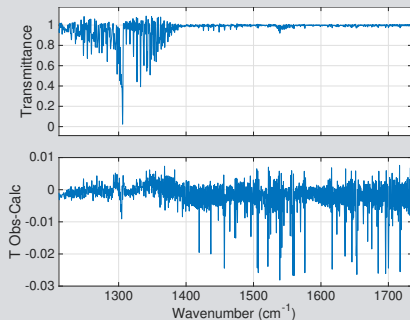


Observations

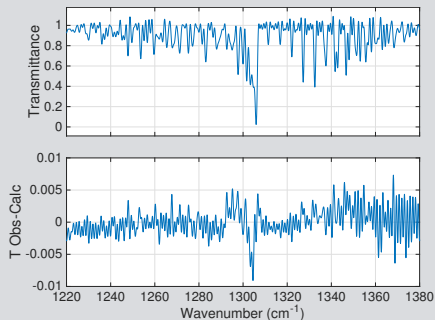
- Avoid CO₂ Q-branch region, spectroscopy limitation (in RTA too!). LBLRTM (AER) and kCARTA (UMBC) give similar results.
- Slight baseline shift near 687 cm^{-1} ?

CH₄ Spectra

Full Spectrum (H₂O contamination)



Region Fitted

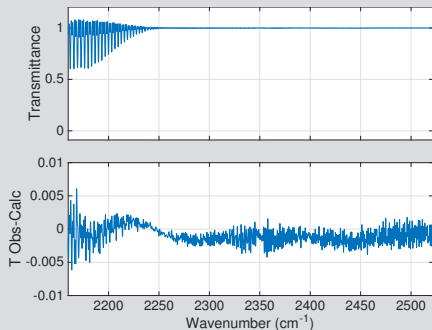


Observations

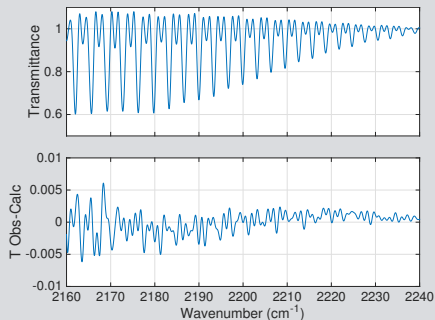
- Avoid water vapor contamination
- Small amount of Q-branch line-mixing evident near 1300 cm⁻¹ (can be ignored in fit).

CO Spectra

Full Spectrum



Region Fitted



Observations

- Minor baseline oscillation, should average out.
- Spectroscopy better here than in long-wave or short-wave



Test Summary

Δ Neon (from FM-1) = 2.8 ± 0.2 ppm or 703.45036

Test ID	T	Side	Neon (ppm)	P_log (torr)	P_fit (torr)	fit-log (torr)	Lien
11-20_CO2	PQL	1	-1.8	41	22	-19	Bad P
11-25_CO2	PQL	2	0.5	40	27	-13	Bad P, 775 cm-1?, Fringes
10-16_CO2	MN	1	3.1	40	40	0	
10-18_CO2	MN	2	3.9	40	40	0	Fringes
11-09_CO2s1	PQH	1	4.6	40	40	0	NH3, Fringes
11-09_CO2s2	PQH	2	2.6	41	37	-4	NH3, Fringes
11-20_NH3	PQL	1	6.0	20	18	-1	FOV9 way off
11-19_NH3	PQL	2	3.9	21	18	-3	
10-16_NH3	MN	1	3.6	39	37	-2	
10-27_NH3	MN	1	12.1	21	40	19	Bad P
10-18_NH3	MN	2	11.9	40	6	-34	Bad P
11-09_NH3	PQH	1	12.6	20	34	14	Bad P
09-27_NH3	PQH	2	10.8	39	7	-32	Bad P
11-20_CH4	PQL	1	2.1	41	30	-12	Bad P
10-16_CH4	MN	1	2.8	40	40	0	
10-18_CH4	MN	2	2.6	42	42	-0	
11-05_CH4	PQH	1	2.8	41	41	0	
11-19_CO	PQL	1	2.6	45	45	0	
10-15_CO	MN	1	3.1	42	42	0	
10-18_CO	MN	2	2.6	41	41	0	
10-02_CO	PQH	1	3.1	40	26	-14	Bad P

PPM Errors (ShortWave Example)

Uncorrected ν Offsets

520	370	520
370	0	370
520	370	520

x,y offset Correction

-17	-12	-17
-12	0	-12
-17	-12	-17

Error after x,y Adjustment (SW)

-1.2	-0.7	-2.3
-1.0	0	0.2
-1.6	-0.8	-1.7

Error after δr Adjustment (SW)

0.2	0.3	-0.9
0.0	0	1.2
-0.2	0.1	-0.3

Only 3 numbers needed to nearly reach 1 ppm!

For all three focal planes max error = 2.8 ppm, only 6 detectors needed adjustments to keep errors below 1 ppm.

All detector placements relative to interferometer axis driven to zero in Engineering Packet data.

JPSS-1 TVAC Conclusions: Spectral

- Focal plane detector positions determined to 1 ppm
- Neon calibration determined to 1 ppm, only 2.8 ppm difference from SNPP (probably alignment)
- Excellent fits to gas cell data

Recommendations

- Delete NH_3 tests: not successful and not needed!
- Substitute with longwave test with gas cell filled with CO_2 broadened by air. These are fabulously accurate spectra, this will help NWP assimilation via an improved RTA in region not easy to bias correct.



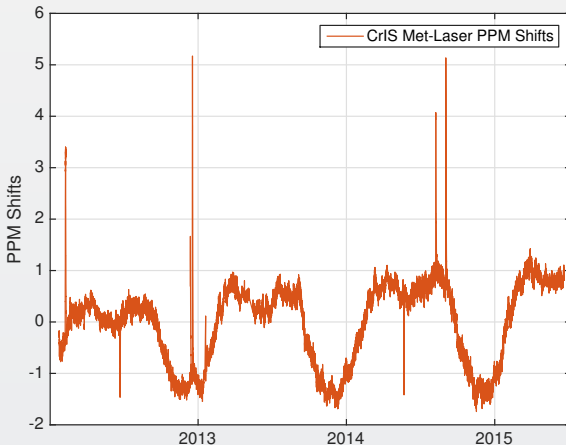
SNPP In-Orbit Spectral Calibration

- Concentrate on stability
- Post-launch modifications:
 - Focal plane x,y offsets adjusted
 - Slight change to radius (gravity release of telescope)
 - Neon unchanged
- Neon lamp drifts (emission geometry) main possible source of spectral calibration drifts.

Approach

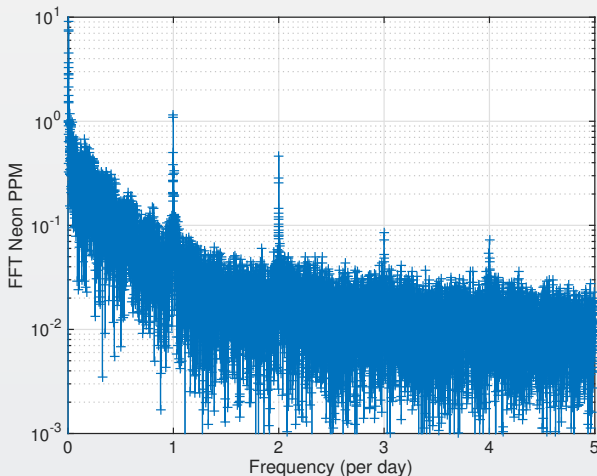
- Neon calibration determined from clear tropical up-welling spectra vs simulations using cross-correlation.
- CrIS SDR produced by IDPS only tracks Neon to 2 ppm.
- Consequently, cannot use IDPS SDRs to track Neon calibration.
- This Work: re-processes full mission SDRs with UW/UMBC CCAST SDR testbed, follow the Neon at all times.
- CCAST algorithm used is one of two approaches under consideration for JPSS-1.

Metrology Laser Shifts a/c to Neon Lamp



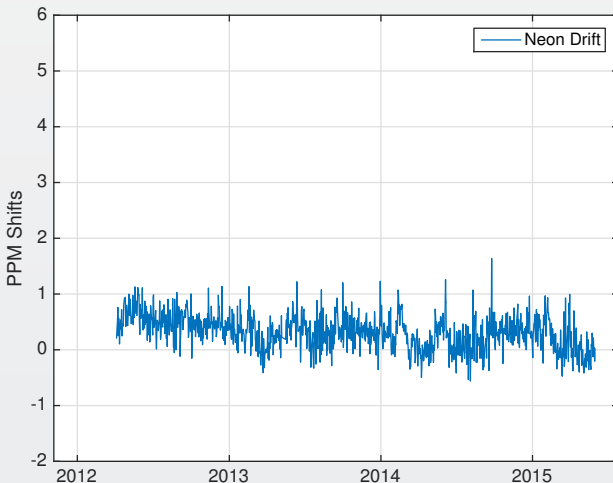
This is possibly due to the thermal control of the metrology laser being impacted by the external IR radiation environment.

Fourier Analysis of Neon Time Series



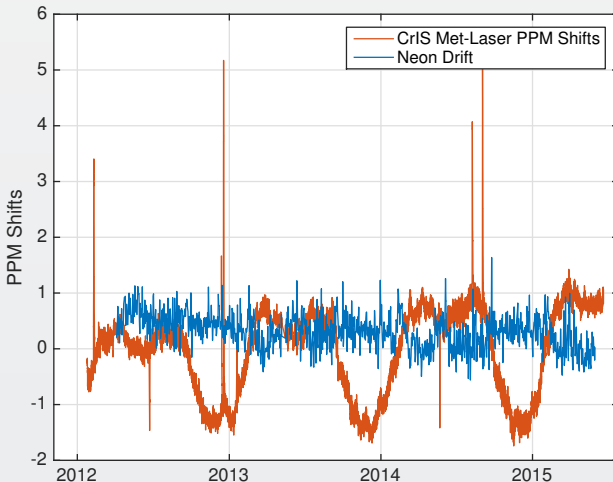
Hash on previous slide is the 1-day cycle seen here. Albedo effect on metrology laser wavelength?

Neon Drifts from Upwelling Radiances



This is a once/day measurement from clear tropical ocean scenes.

Neon Drifts from Upwelling Radiances

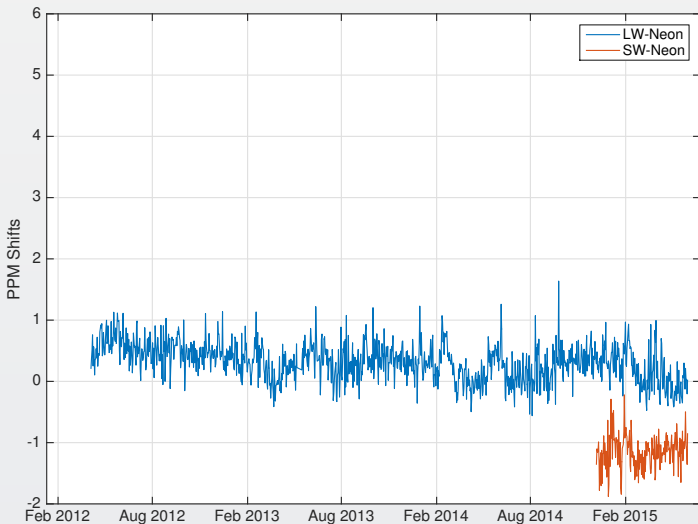


This is a once/day measurement from clear tropical ocean scenes.

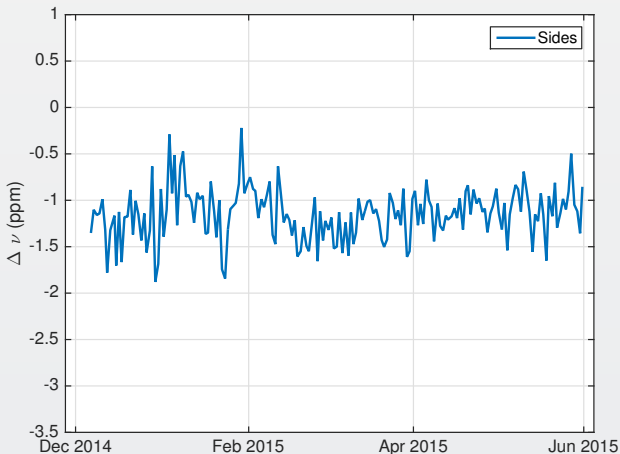
Conclusions: SNPP CrIS Neon Stability

- Most of variability in the metrology laser wavelength is real.
- There may be a slight drift in the Neon wavelength.
- A linear fit to the derived Neon wavelength gives -0.13 ± 0.12 ppm/year. Possibly a 0.5 ppm change since early 2012.
- For NWP assimilation, these drifts may be removed with dynamic bias correction.
- They are identical for all 9 FOVs.

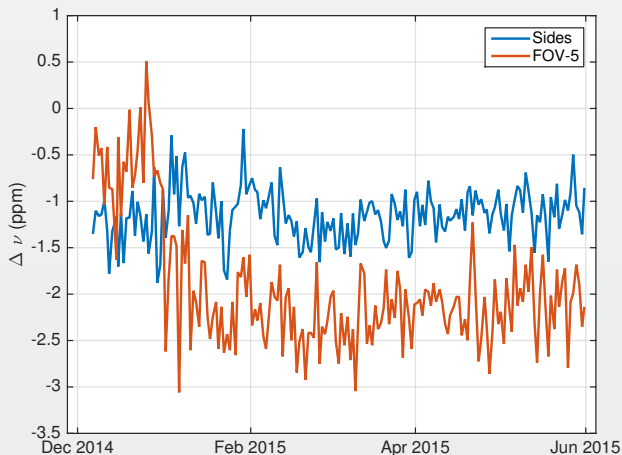
Neon Calibration using High-Res CrIS Radiances



Neon Calibration using High-Res CrIS Radiances



Neon Calibration using High-Res CrIS Radiances

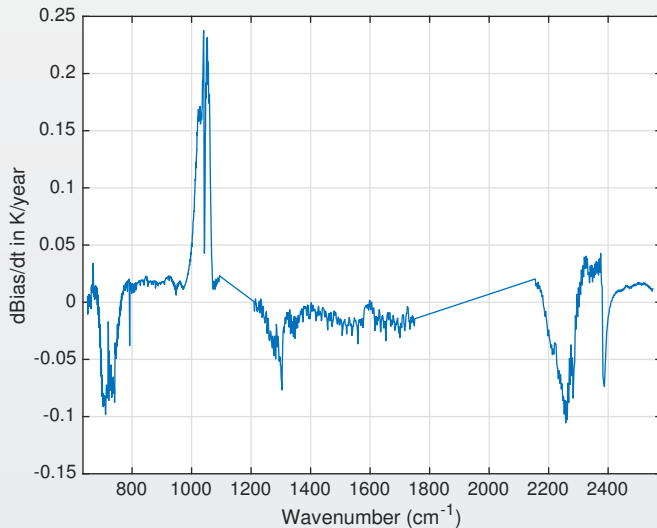


2.5 ppm shift in FOV-5 at end of December??

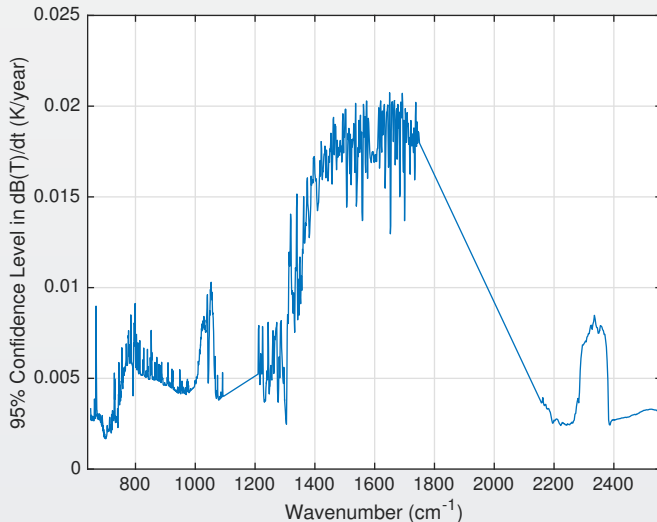
Estimation of CrIS In-Orbit Stability: Approach

- Start with CCAST processed SDRs (stable algorithm)
- CCAST converts to normal-resolution post Dec. 2015
- Subset for clear, ocean tropical scenes (uniformity filter)
- Match each scene of ERA Interim re-analysis and compute simulated radiance
- Create daily average of observed and simulated radiances (365 x 3) long time series.
- Fit time series bias (Obs-Simulated) for linear rate (and seasonal terms).
- Perform an Optimal Estimation retrieval on bias time series ($d(\text{bias})/dt$) spectrum to determine geophysical time derivatives. (O_3 is only column offset.)

CrIS Linear B(T) Bias Rate over Three Years



2- σ Uncertainty in CrIS Linear B(T) Bias Rate



OE Fit Results

Units are all per year

CO2 (ppm)	2.35 +- 0.008	Full rate
O3 (%)	-1.22 +- 0.006	Relative to ERA
N2O (ppb)	0.82 +- 0.014	Full rate
CH4 (ppb)	7.79 +- 0.182	Full rate
CFC11 (ppt)	0.10 +- 0.016	Full rate
SST (K)	0.016 +- 0.000	Relative to ERA

Comparison to In-Situ for CO₂

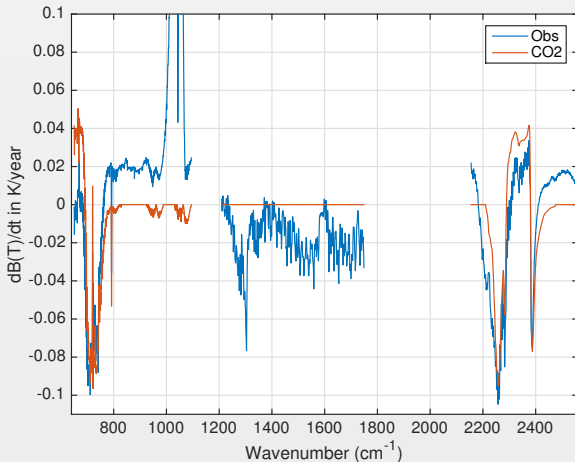
- NOAA/ESRL Global Mean CO₂ Rate for 2012-2014: 2.25 ppm/year
- CrIS - ESRL = 0.1 ppm/year implies CrIS stability of 0.005K/year.

Comparison to In-Situ for SST

- ERA SST is a measurement: GHRSSST
- CrIS - ERA = 0.016K/year

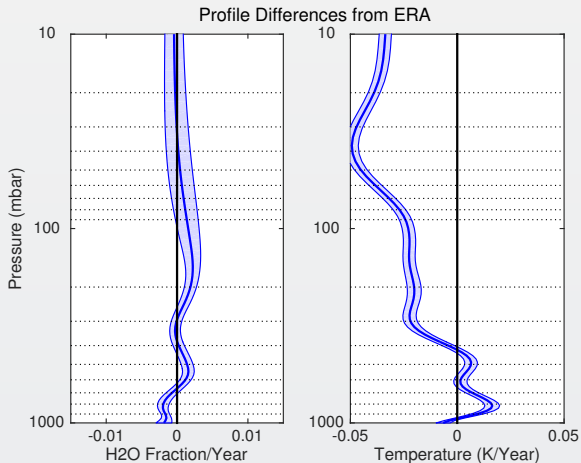
NOAA/ESRL CH₄ from 2012-2015 varies from 5-10 ppb/year

CO₂ Contribution to Spectral Bias



Issue in stratospheric sounding channels, we should differ from ERA by 0.04K/year! Could ERA not be able to bias correct for CO₂ in the upper strat?

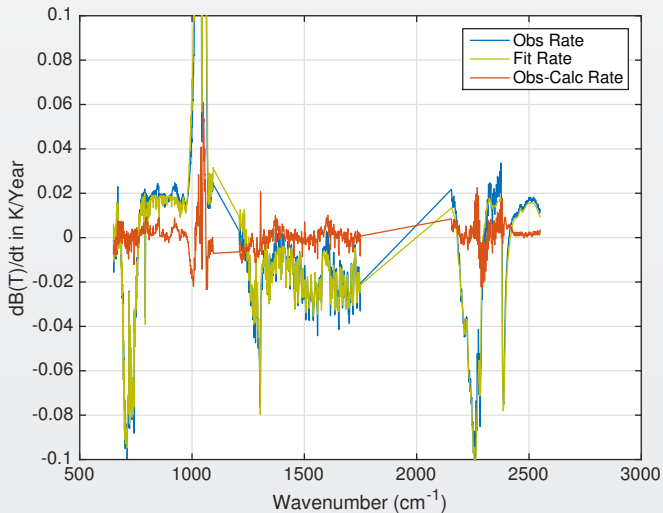
OE Profile Differences from ERA



For these altitude it is difficult to find a standard for temperature bias correction? Or is the CO_2 rate not constant with altitude?

Fit Residuals

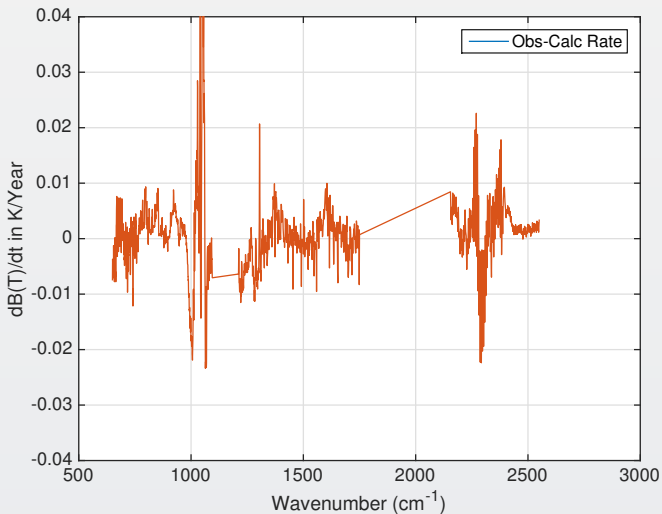
Requirements for Inter-Instrument Agreement



How well can we fit CrIS radiance time derivatives?

Fit Residuals

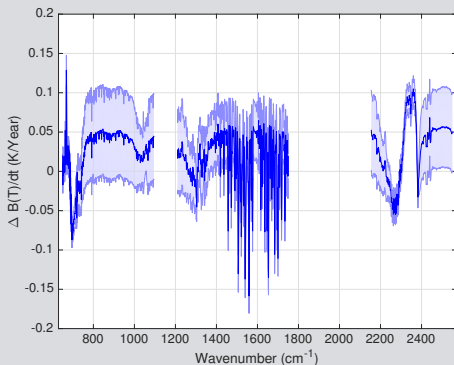
Requirements for Inter-Instrument Agreement



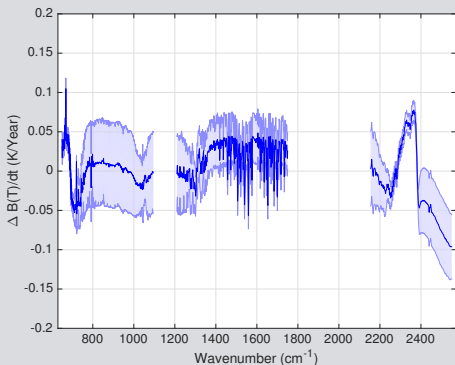
How well can we fit CrIS radiance time derivatives?

Globally Averaged Changes in CrIS B(T)

dBT/dt Night with 95% Uncertainty



dBT/dt Day with 95% Uncertainty

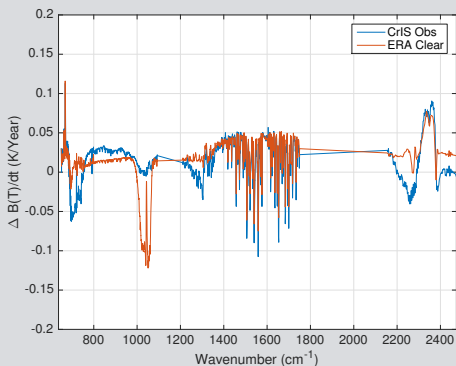


CO_2 forcing well defined (low uncertainty). Cloud and surface temperature response highly variable, need longer time span to lower uncertainty.

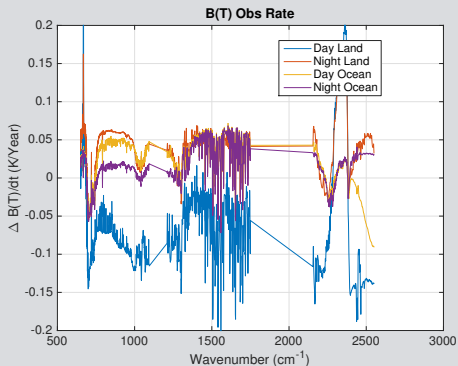
CrIS Global $\Delta B(T)$

Versus ERA-Clear and Binned by Day/Night/Land/Ocean

Day + Night dBT/dt: Obs, ERA-Clear



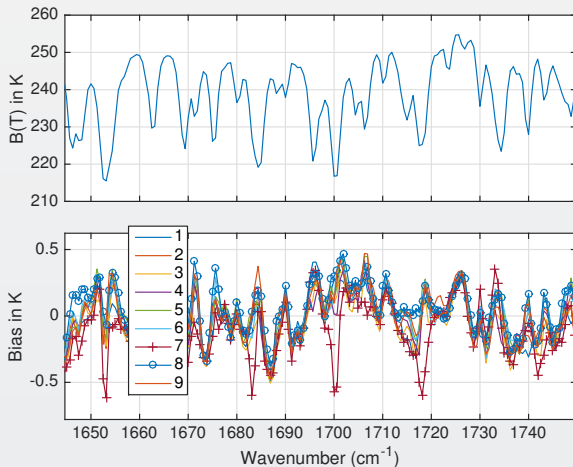
dBT/dt: Day/Night/Land/Ocean



ERA global (day + night) clear sky linear rate very close to CrIS observations (except for minor gas forcings).

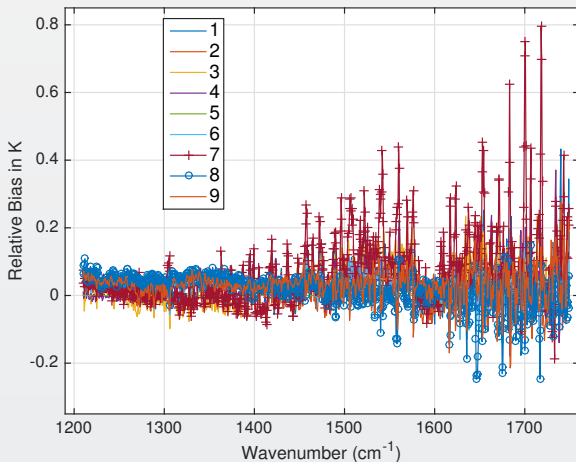
Day, Land rates very different from others. Day ocean suggests increasing clouds.

Mid-Wave Non-Linearity in High-Resolution Mode



Tropical clear bias vs ECMWF, Hamming apodized high-spectral resolution radiances from CCAST.

Mid-Wave Non-Linearity in High-Resolution Mode



Same as previous slide, but now subtracting all biases from FOV-5 bias.



Space Dynamics

LABORATORY

Utah State University Research Foundation

J1 CrIS Noise Performance & Impulse-Noise/Bit-Trim Mask Optimization

Mark Esplin, Deron Scott, Bryce Walker, and Ben Esplin



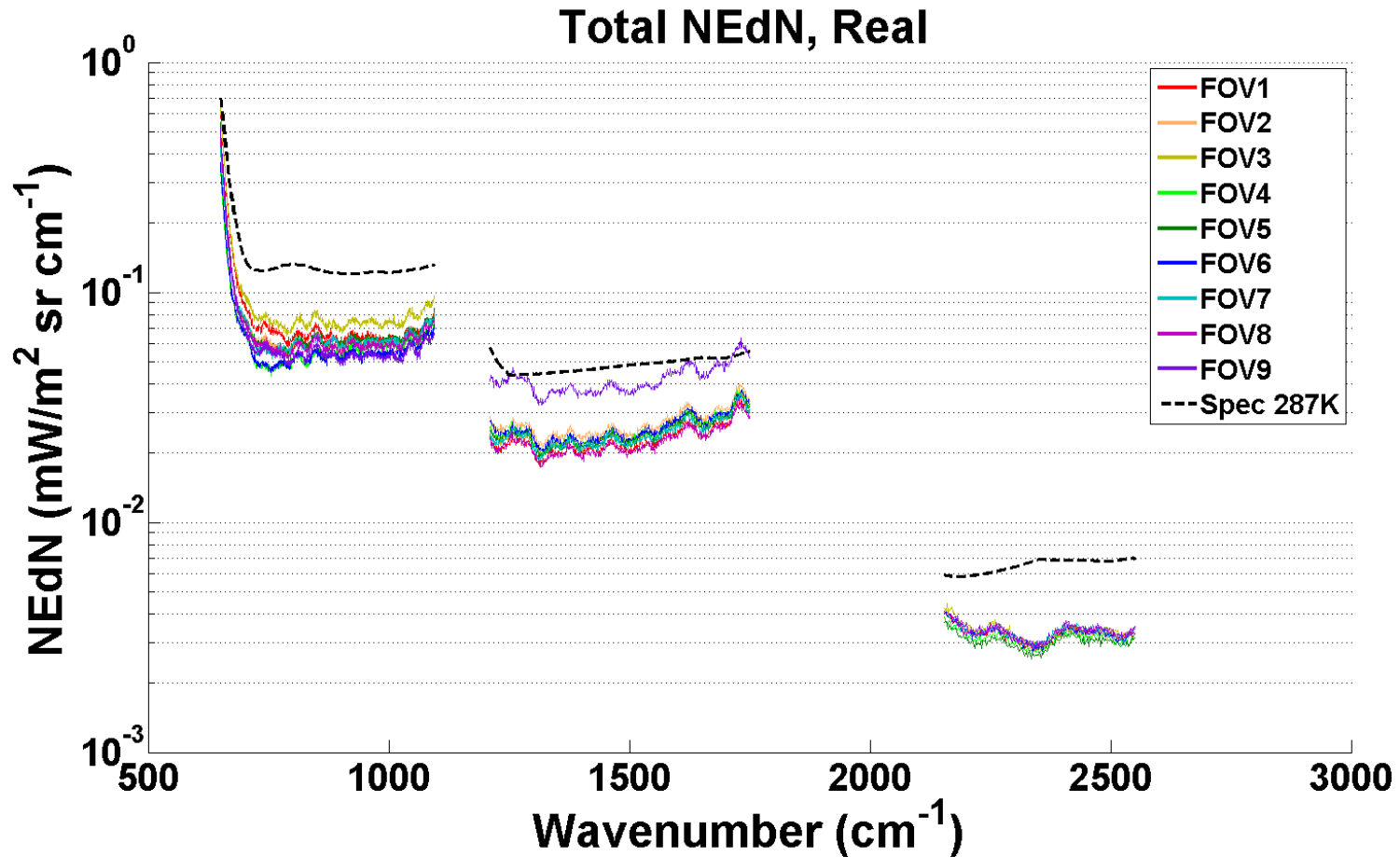
Outline

- ▶ Excellent CrIS NEdN performance
- ▶ NEdN subtle issues
 - NEdN dependency on photon flux sometimes not as expected
 - Differences in electrical side1 to side 2
- ▶ Optimizing bit-trim mask
- ▶ Impulse mask considerations
 - Radiation causes spikes in interferograms
 - Detecting/correcting spikes in FIR filtered interferograms

Extensive J1 NEdN Measurements During TVAC

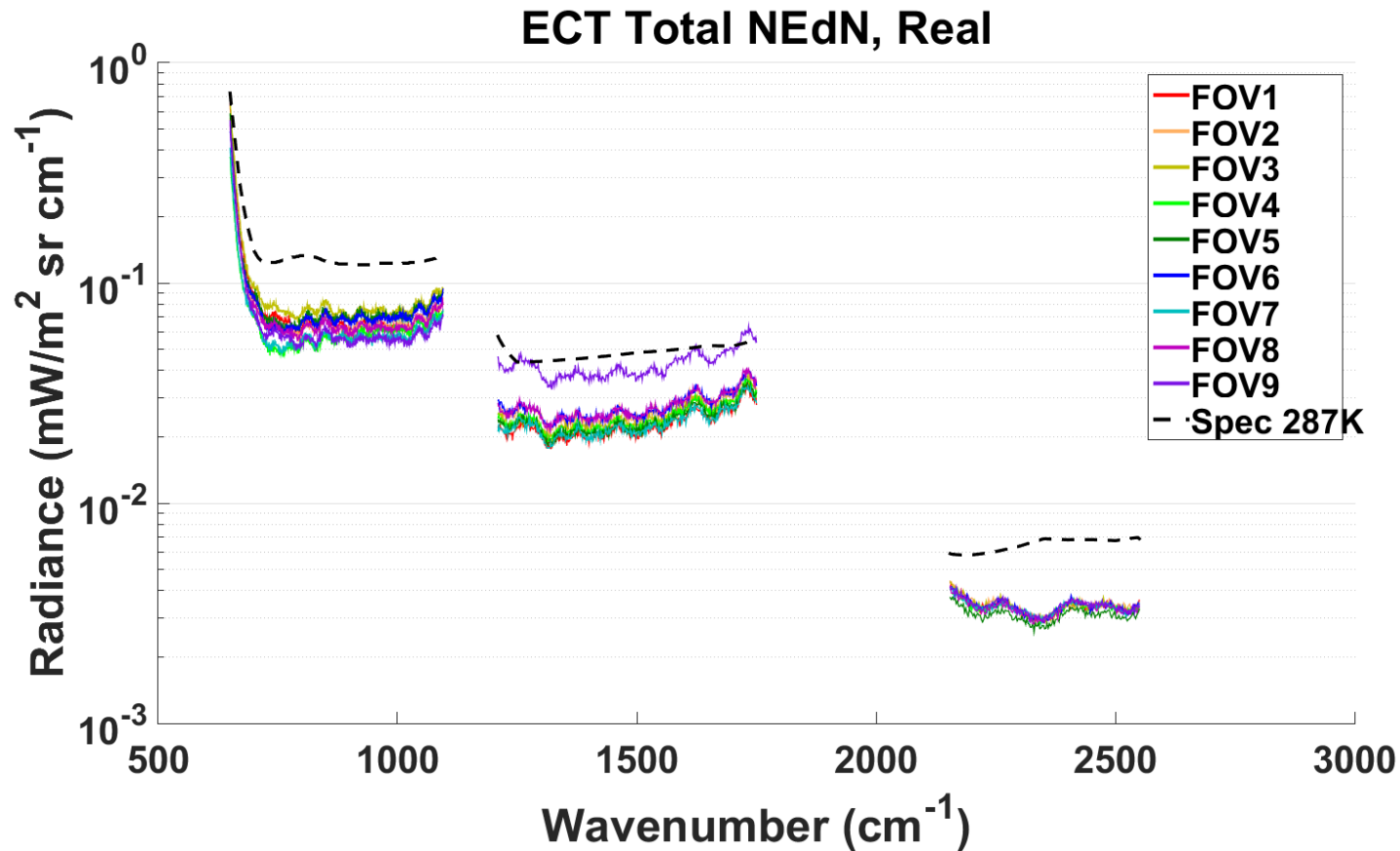
- ▶ NEdN from both operational and staring mode
- ▶ Three sensor plateaus
 - (PFL) Proto Flight Low (ICT at about 262 K)
 - (MN) Mission Nominal (ICT at about 278 K)
 - (PFH) Proto Flight high (ICT at about 314 K)
- ▶ Both electronic sides
- ▶ Different power supply voltages
- ▶ With induced vibration

Example Staring MN NEdN



- ▶ MW FOV9 out of family with other FOVs
- ▶ MW FOV9 slightly above spec value
- ▶ MN (Mission Nominal) plateau staring mode

Operational Mode MN NEdN

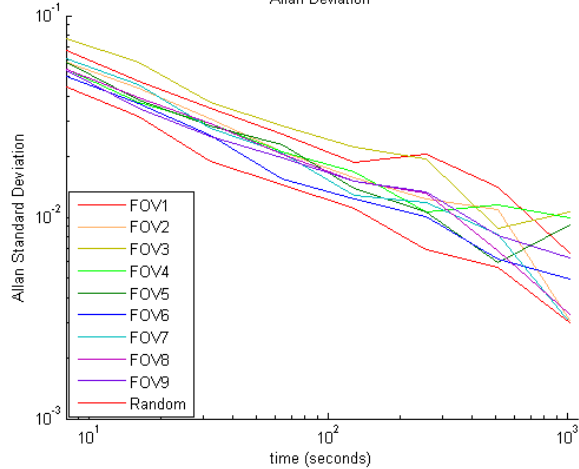


- ▶ Staring and operational mode NEdN nearly identical
- ▶ MN 287 K ECT, side 1

Allan Deviation

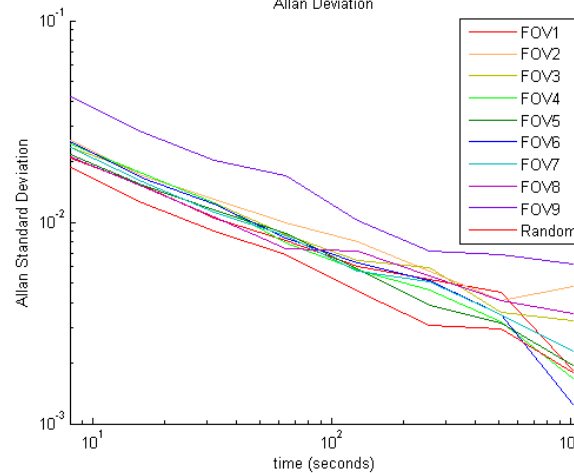
LWIR

Allan Deviation



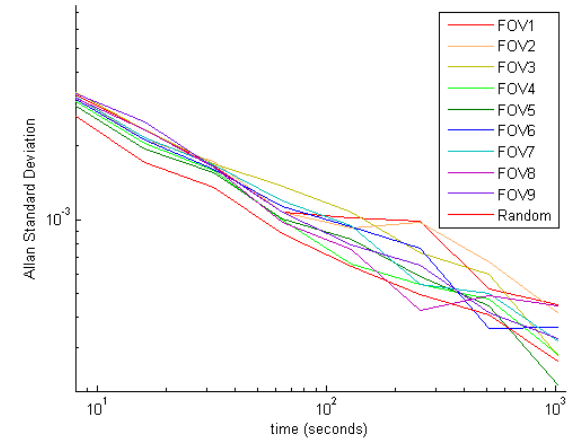
MWIR

Allan Deviation



SWIR

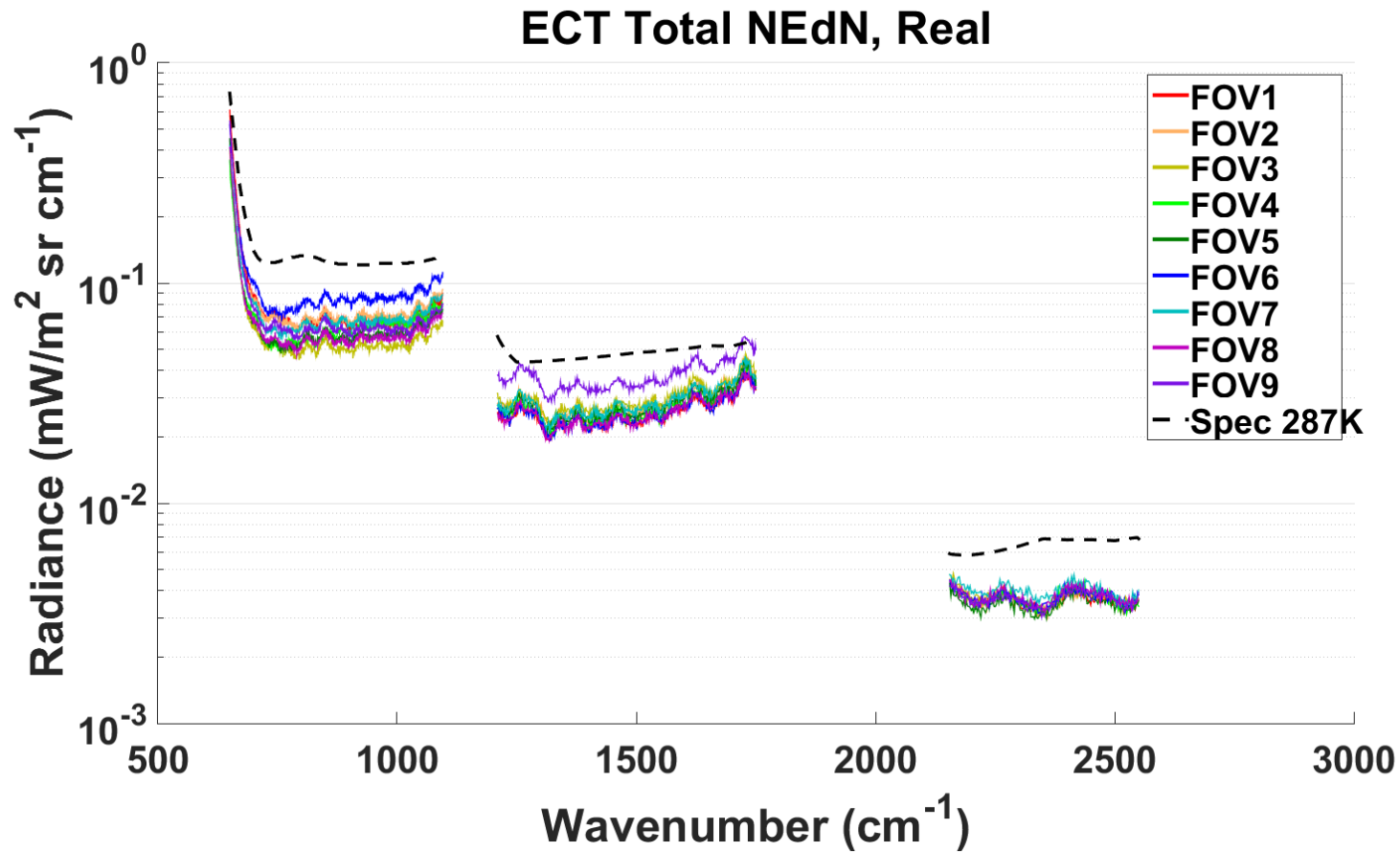
Allan Deviation



- ▶ Alternative way to characterize noise behavior
- ▶ Standard deviation of sets with increased averaging
- ▶ Single spectral channel per band (868, 1234, 2528 cm^{-1})
- ▶ MN, 287 K ECT, operational mode, side 1
- ▶ Bottom trace is Matlab random noise

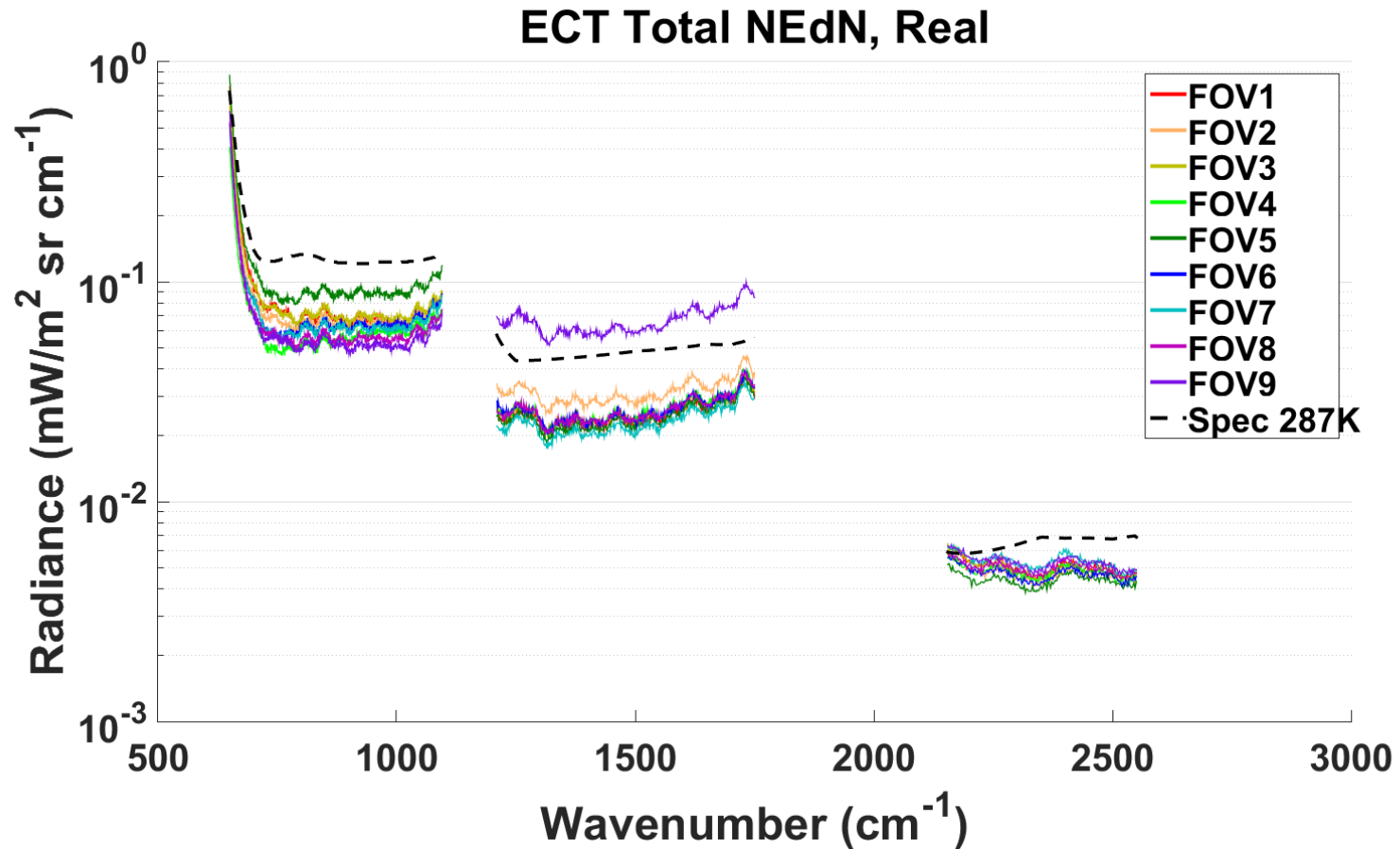
<http://www.allanstime.com/AllanVariance/>

PFL NEdN



- ▶ PFL (Proto Flight High) temperature plateau
- ▶ Operational mode, 287 K ECT, side 1

NEdN Slightly Higher for PFH



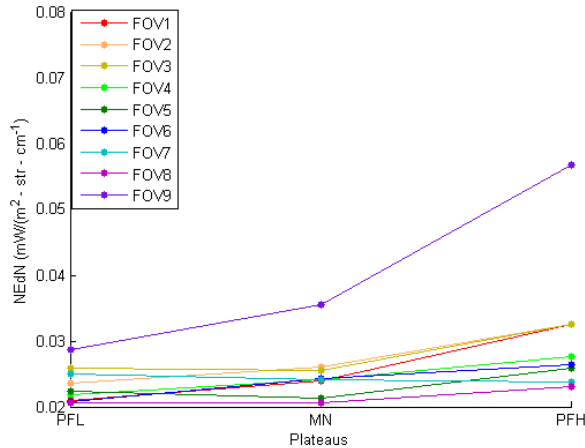
- ▶ PFH (Proto Flight High) temperature plateau
- ▶ Slightly higher NEdN
- ▶ Operational mode, 287 K ECT, side 1

NEdN Verses Photon Flux

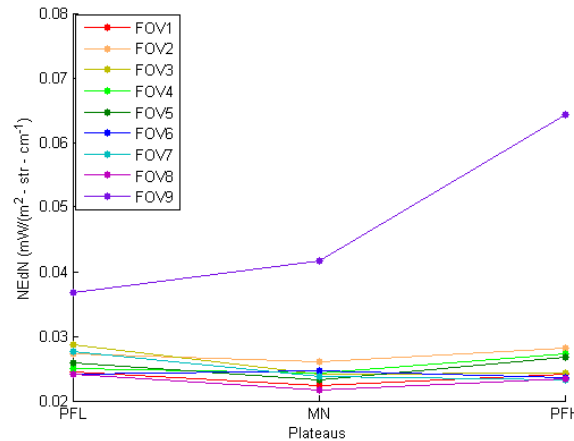
- ▶ NEdN expected to increase with photon flux
- ▶ Band averaged NEdN of operational mode data
 - LWIR 680-1020 cm^{-1} , MWIR 1220-1600 cm^{-1} , SWIR 2160 – 2400 cm^{-1}
- ▶ In general NEdN increases with photon flux as expected
- ▶ Exception for large contrast between ECT and CrIS sensor
- ▶ Excess noise seen in PFL and PFH
- ▶ Behavior may be due to ground testing vibration issue
- ▶ Vibration issues also seen during SNPP CrIS TVAC

MWIR Operational NEdN

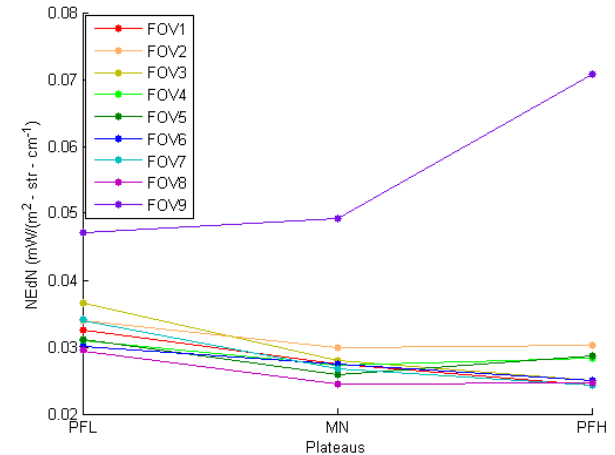
200 K



287 K



310 K



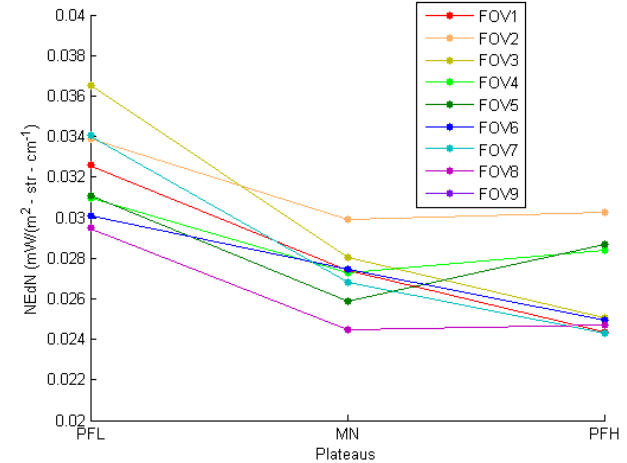
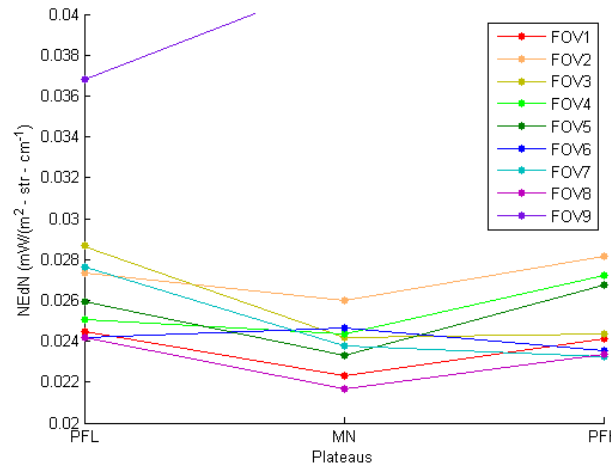
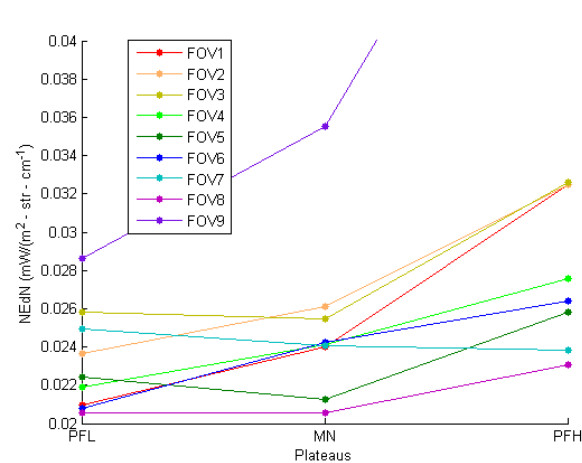
- ▶ Average NEdN goes up with photon flux
- ▶ MW FOV9 NEdN consistently increases with photon flux
- ▶ Component of NEdN difference between sensor and ECT

MWIR Expanded Scale

200 K

287 K

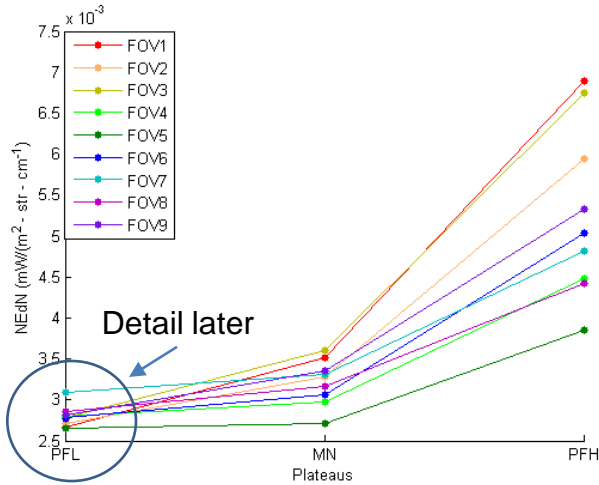
310 K



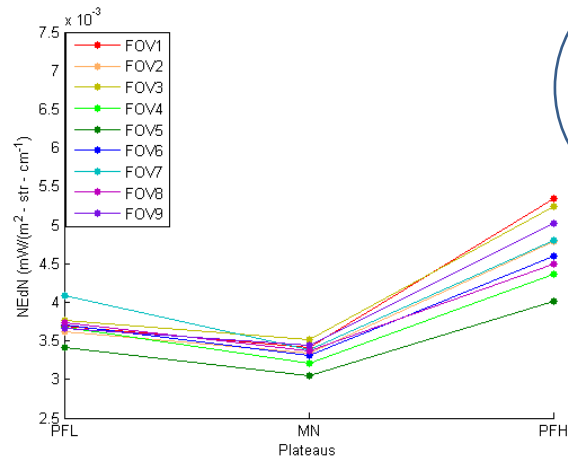
- ▶ Average NEdN goes up with photon flux
- ▶ Component of NEdN difference between sensor and ECT

SWIR Operational Mode

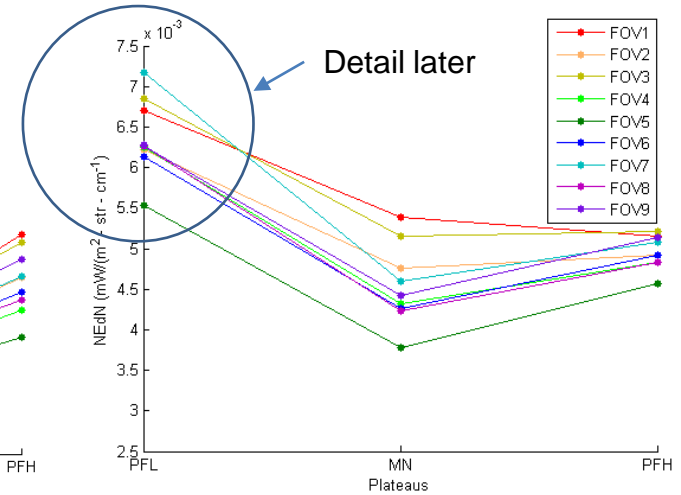
200 K



287 K

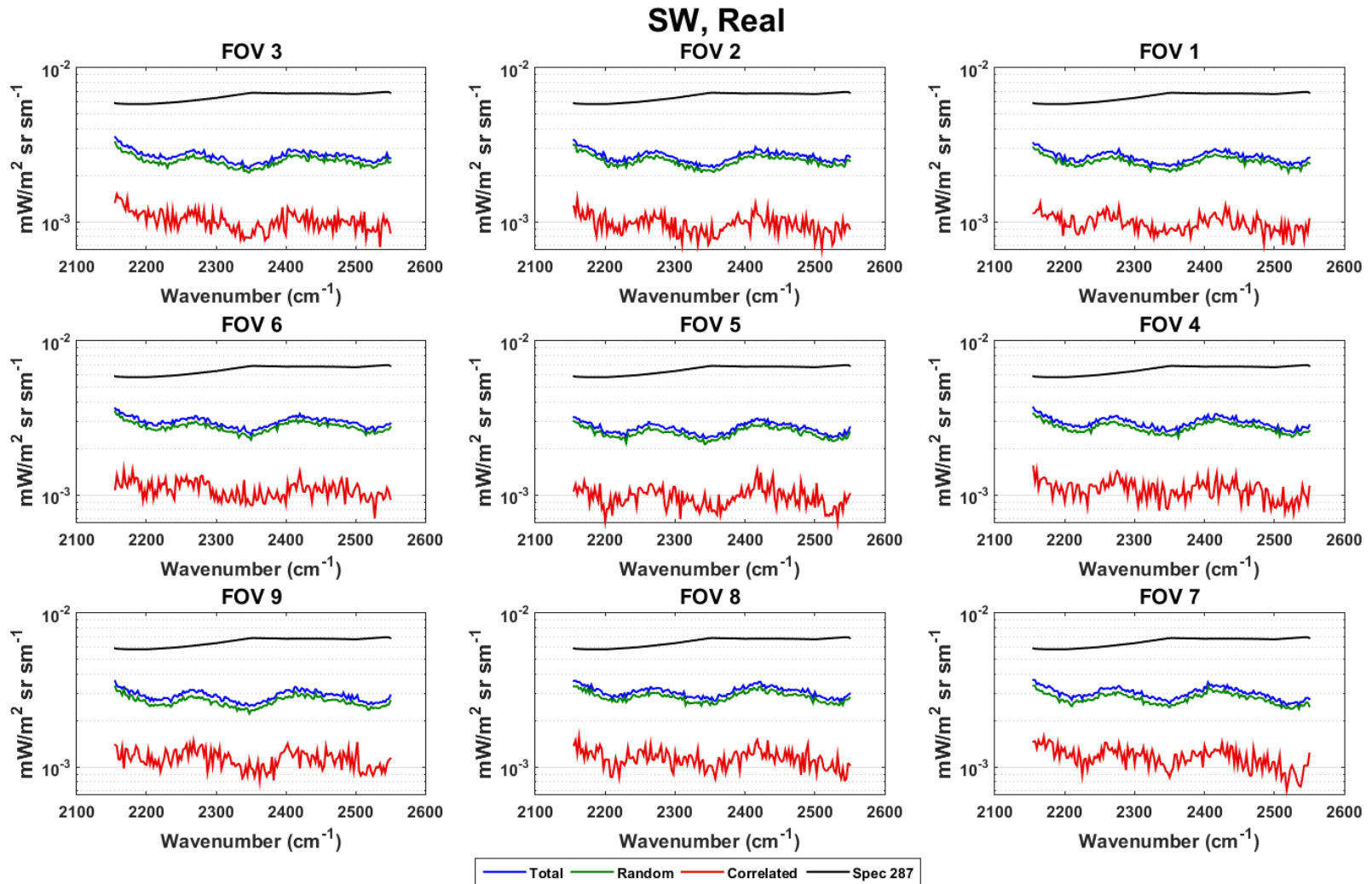


310 K



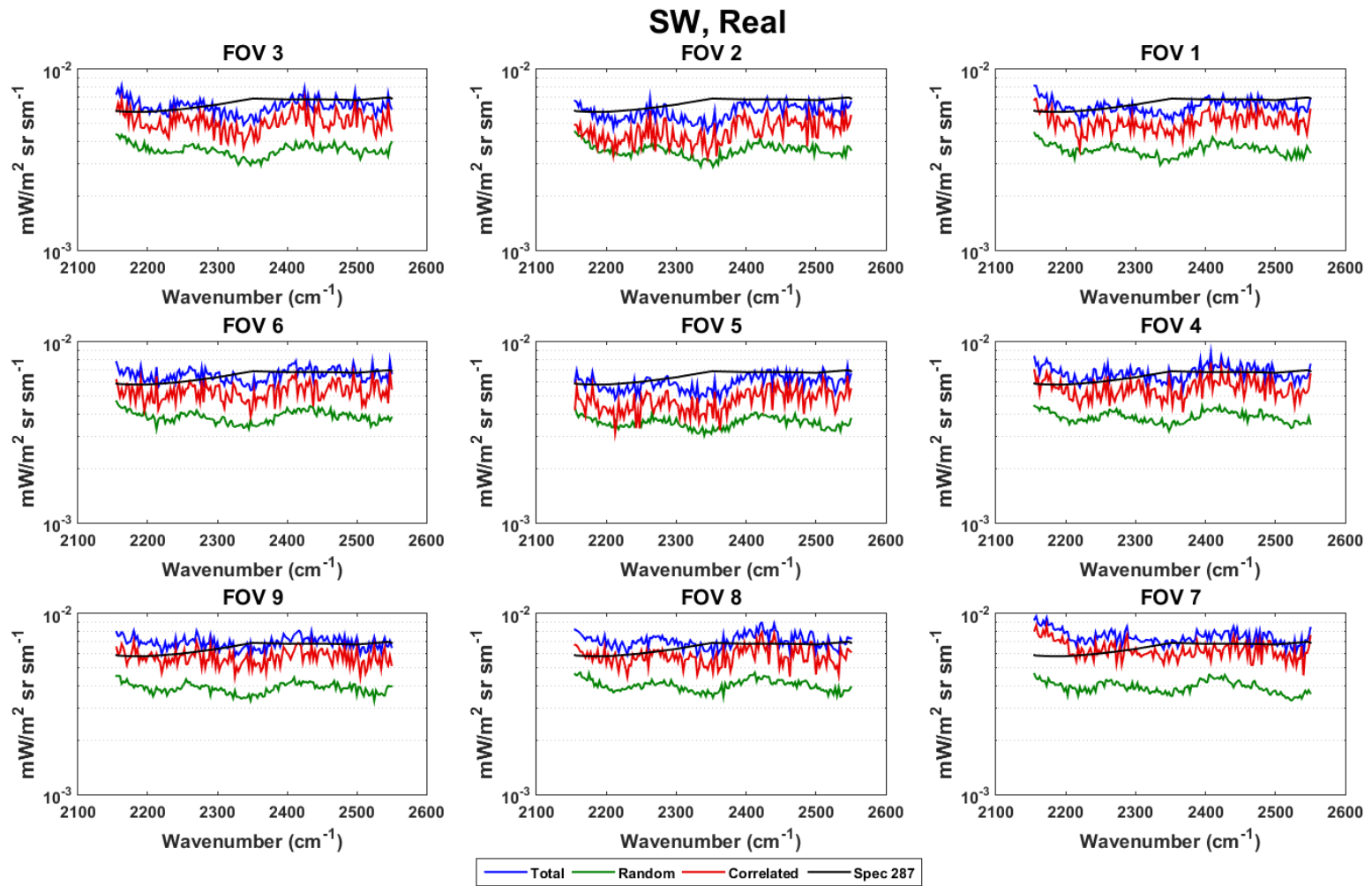
- ▶ Average NEdN goes up with temperature
- ▶ Component of NEdN difference between sensor and ECT
- ▶ Possible indication of vibration effects
- ▶ Staring mode data didn't show as large effect

PFL 200 K ECT



► Spectrally correlated noise is insignificant

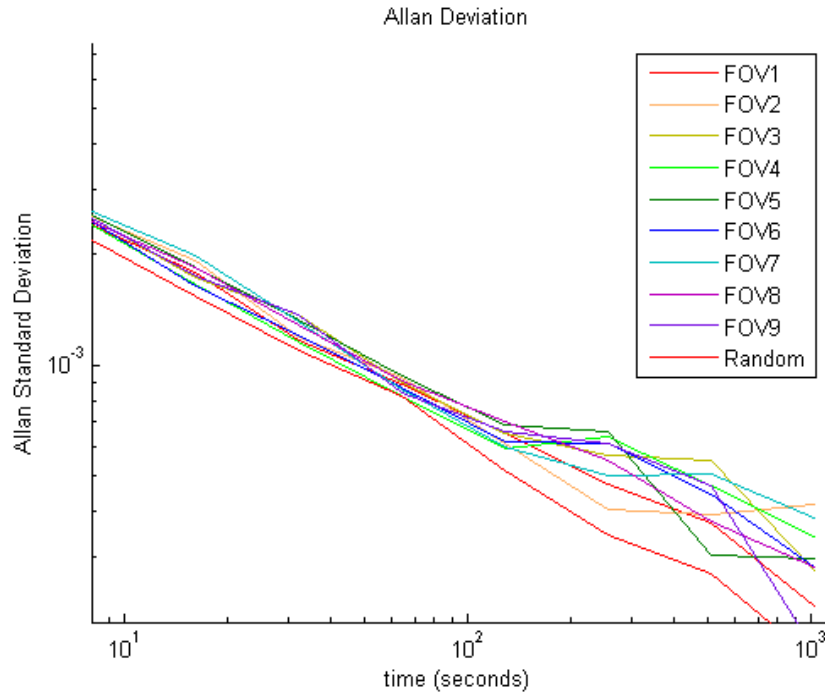
PFL 310 K ECT



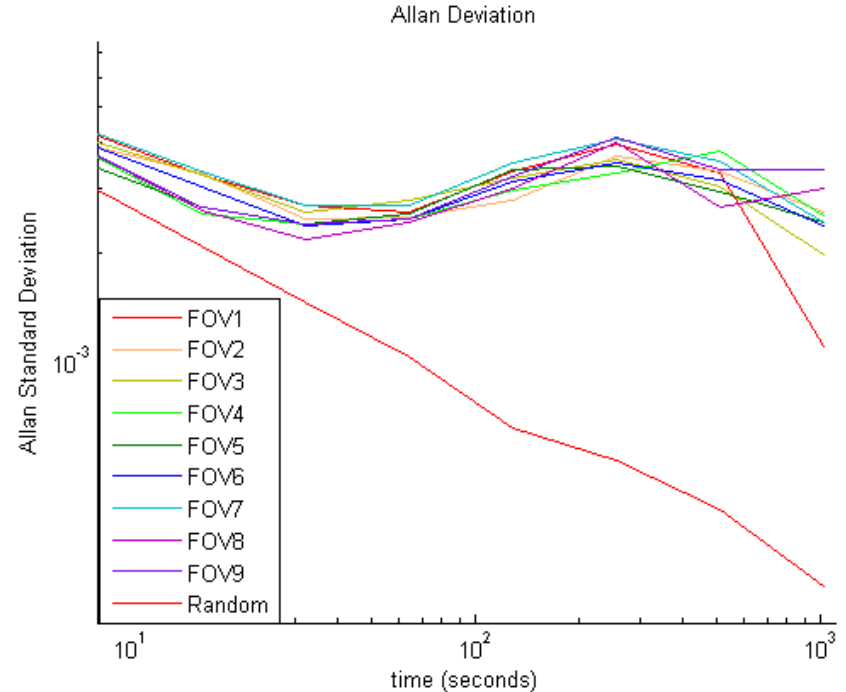
► Spectrally correlated noise dominates random noise

Allan Deviation Also Show Non-Ideal Behavior

PFL 200 K ECT



PFL 310 K ECT

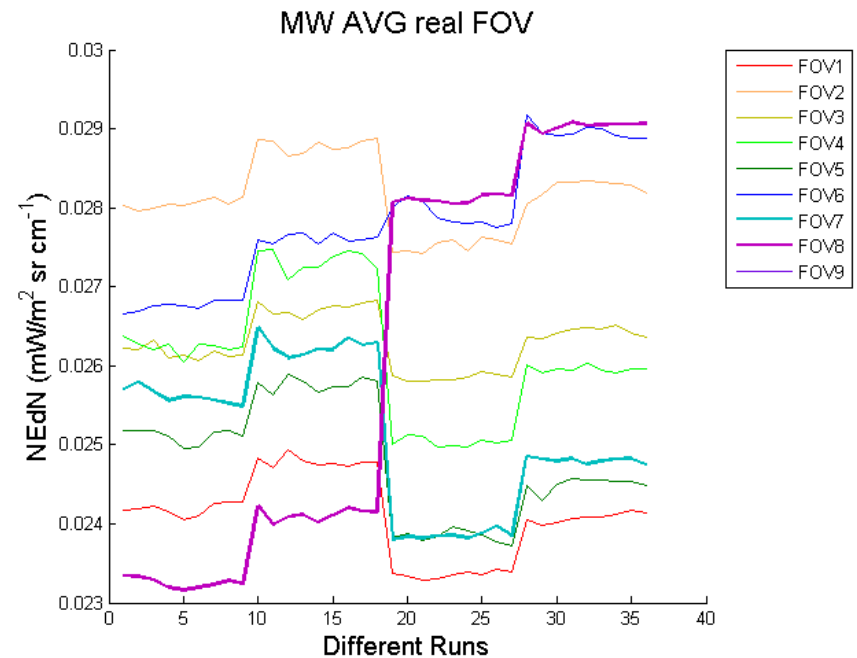
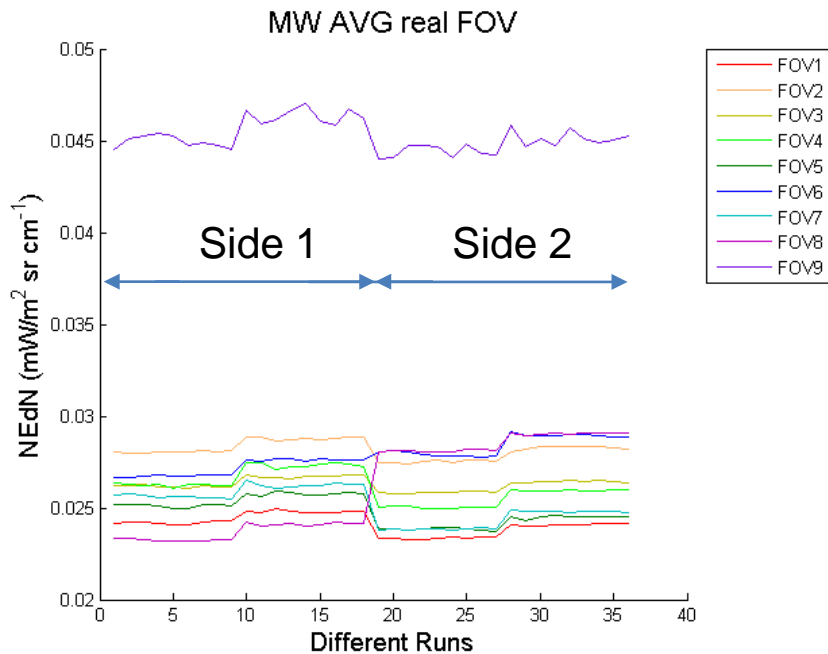


- ▶ Same cases as previous two slides
- ▶ In 310 K case noise increased and character changed
- ▶ Bottom plot Matlab random number generator

Electronic Side 1 Side 2 NEdN Differences

- ▶ Differences in NEdN between side 1 and side 2 have been observed
- ▶ Actual differences or random measurement error?
- ▶ Operational data more representative of on-orbit operation
- ▶ LTR (Long Term Repeatability) data set
 - Consists of 36 collections 2 hours each
- ▶ Averaged over spectral band to produce one NEdN point for each FOV per 2 hour measurement
 - Removed LWIR NEdN tail (band averaged over $750 - 1050 \text{ cm}^{-1}$)
 - Only real data shown, imaginary results are similar
- ▶ Concatenated measurements into one time series
- ▶ First half side 1, second half side 2

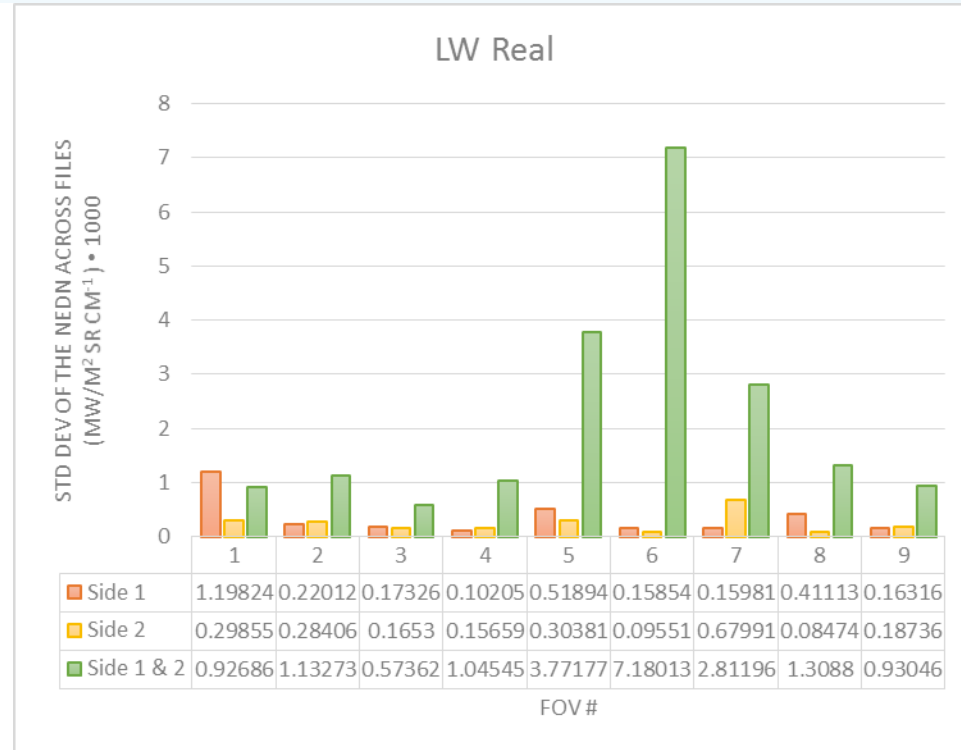
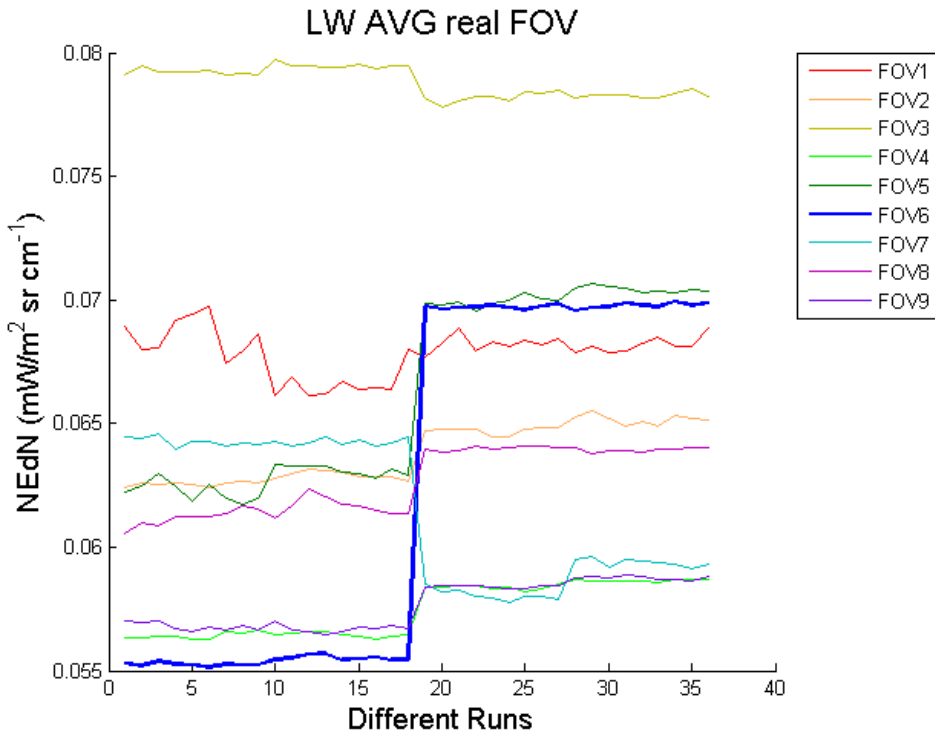
NEdN Trend for MWIR LTR



With FOV9 Removed

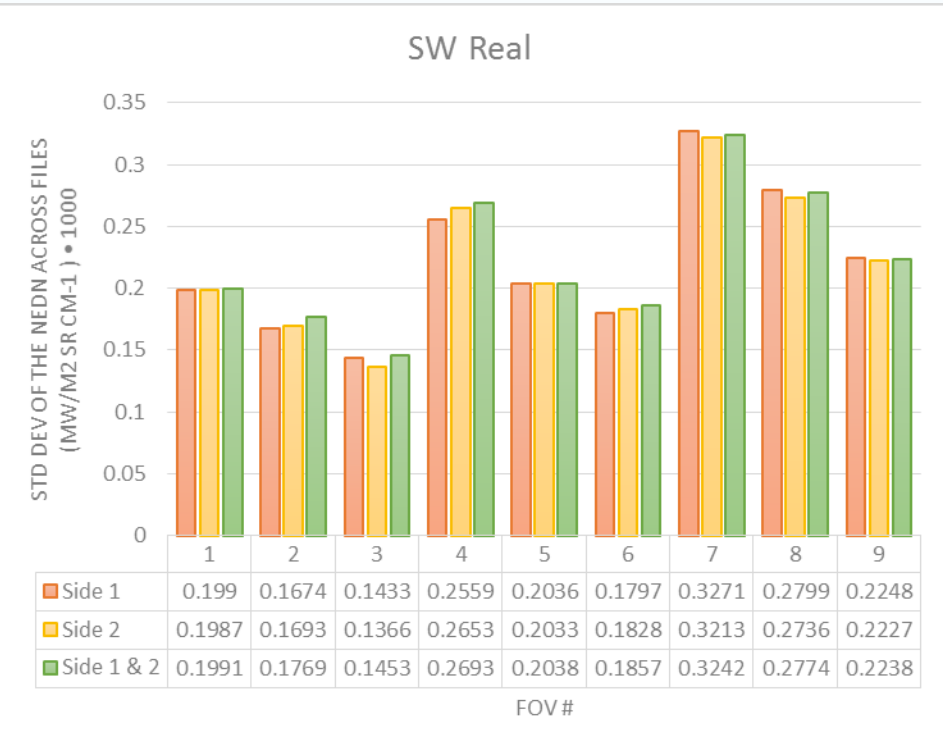
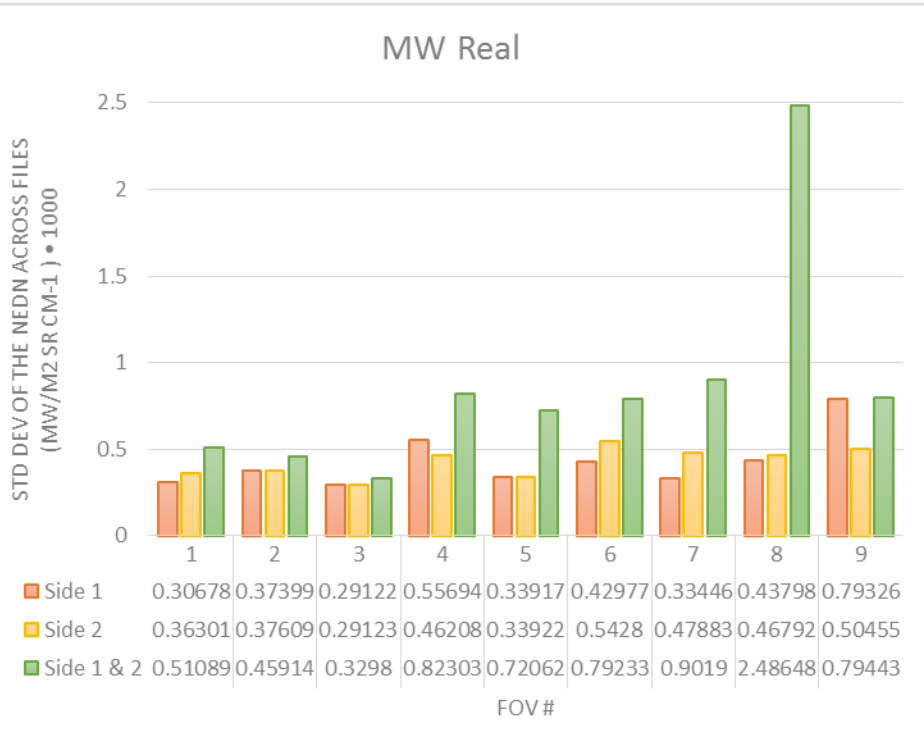
- ▶ FOV9 is out of family
- ▶ FOV 8 has positive side 1 to side 2 jump
- ▶ FOV7 has negative jump

LWIR LTR



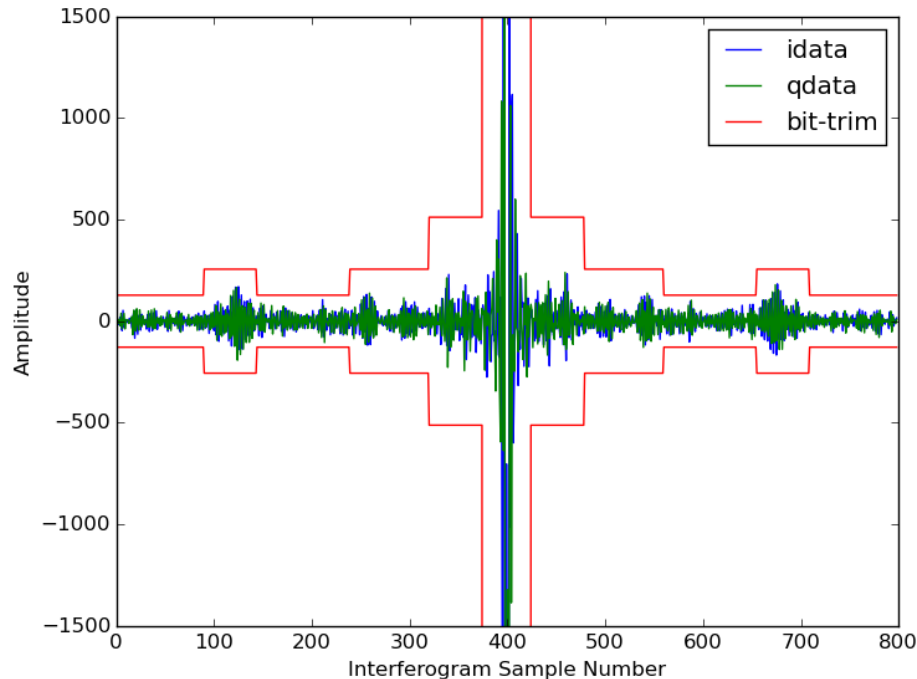
- ▶ Bar chart gives alternative view of data
- ▶ Bars are the standard deviation of data for side 1, side 2, and combined side 1 and side 2
- ▶ Shows if differences are statically significant

MWIR and SWIR LTR



- ▶ MW FOV8 shows large side 1 side 2 difference
- ▶ SW side 1 to 2 differences are not statistically significant

Bit-Trim Mask Optimization

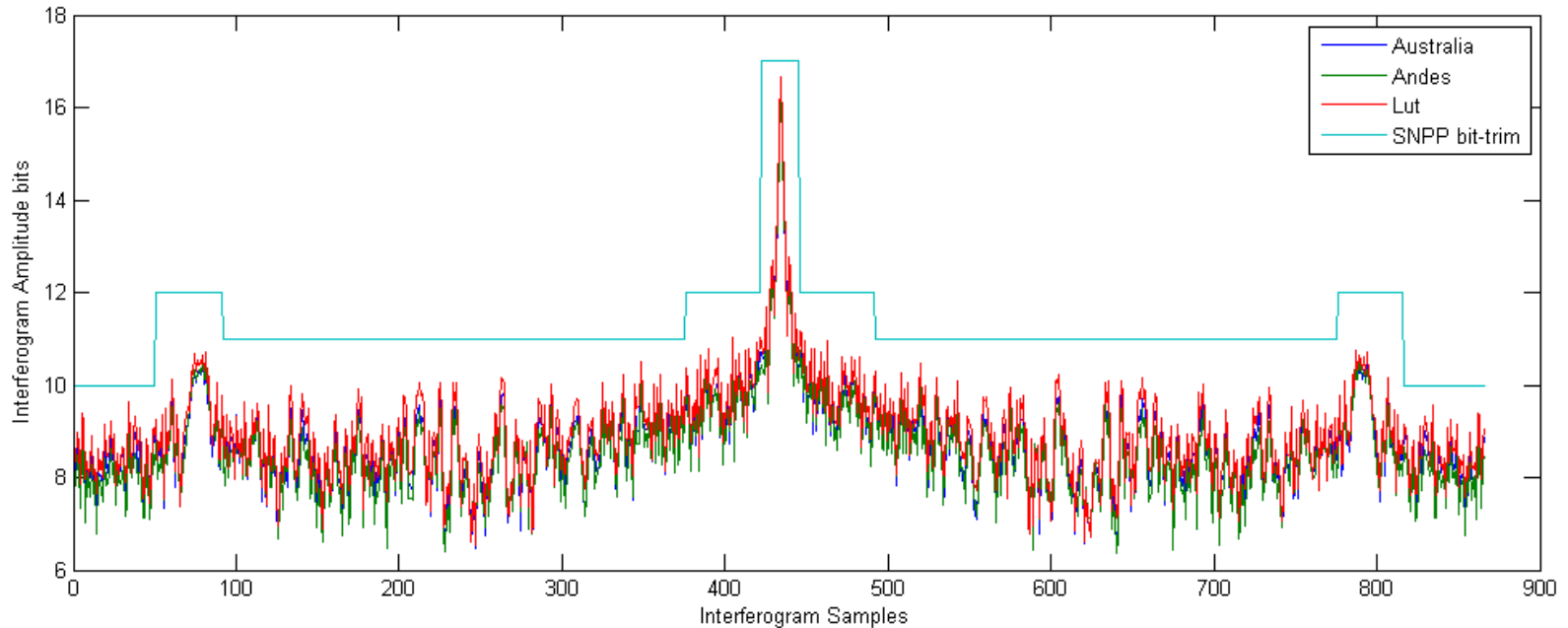


- ▶ Number of bits needed to define an interferogram depends on interferogram position
- ▶ Larger number of bits needed near center, less in wings
- ▶ Lut Desert Iran, 6/21/2015

Bit-Trim Mask Optimization

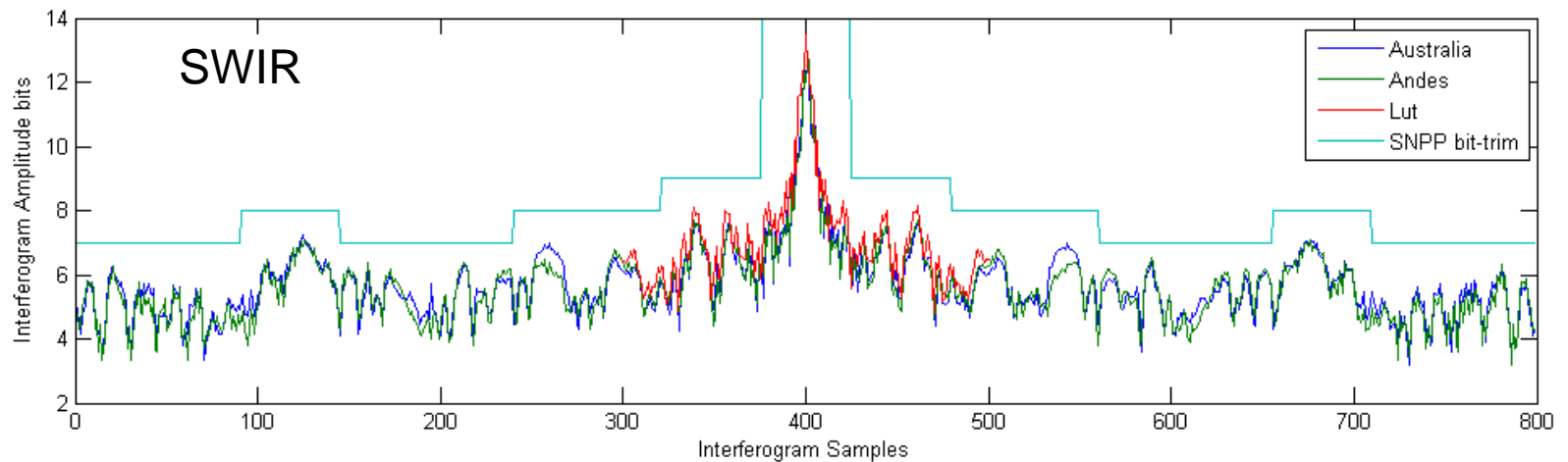
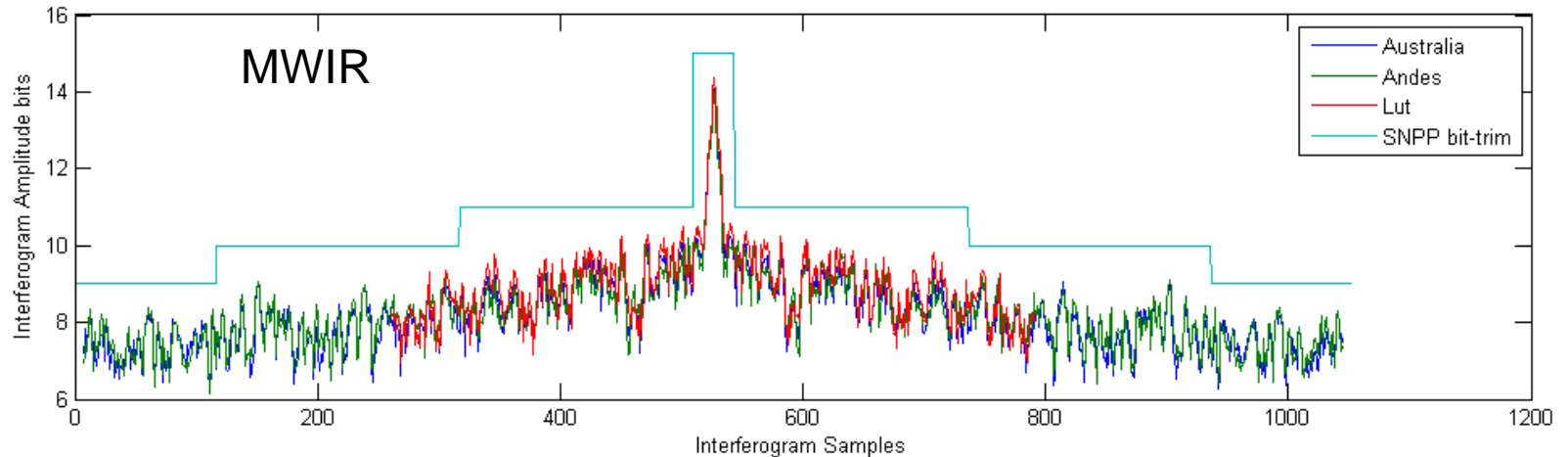
- ▶ Bit-trim is a lossless data compression technique
- ▶ Needs to be optimized for best performance
 - Bit-trim too conservative waste bandwidth
 - Too aggressive corrupt bright scene data
- ▶ J1 can benefit from SNPP data
- ▶ Compare largest interferogram amplitude for each interferogram point of a scene with bit-trim mask
- ▶ Pick SNPP scenes with high dynamic range
 - Australia February 23, 2012 (orbit 01671)
 - Andes Mountains March 12, 2013 (orbit 07113)
 - Lut Desert, Iran July 14, 2012 (orbit 03689)
- ▶ Use same bit-trim mask for J1 as presently used for SNPP

LWIR Bit-Trim Mask



- ▶ Absolute value of maximum interferogram at each interferogram position is plotted with positive part of bit-trim mask
- ▶ SNPP interferograms are always below bit-trim mask

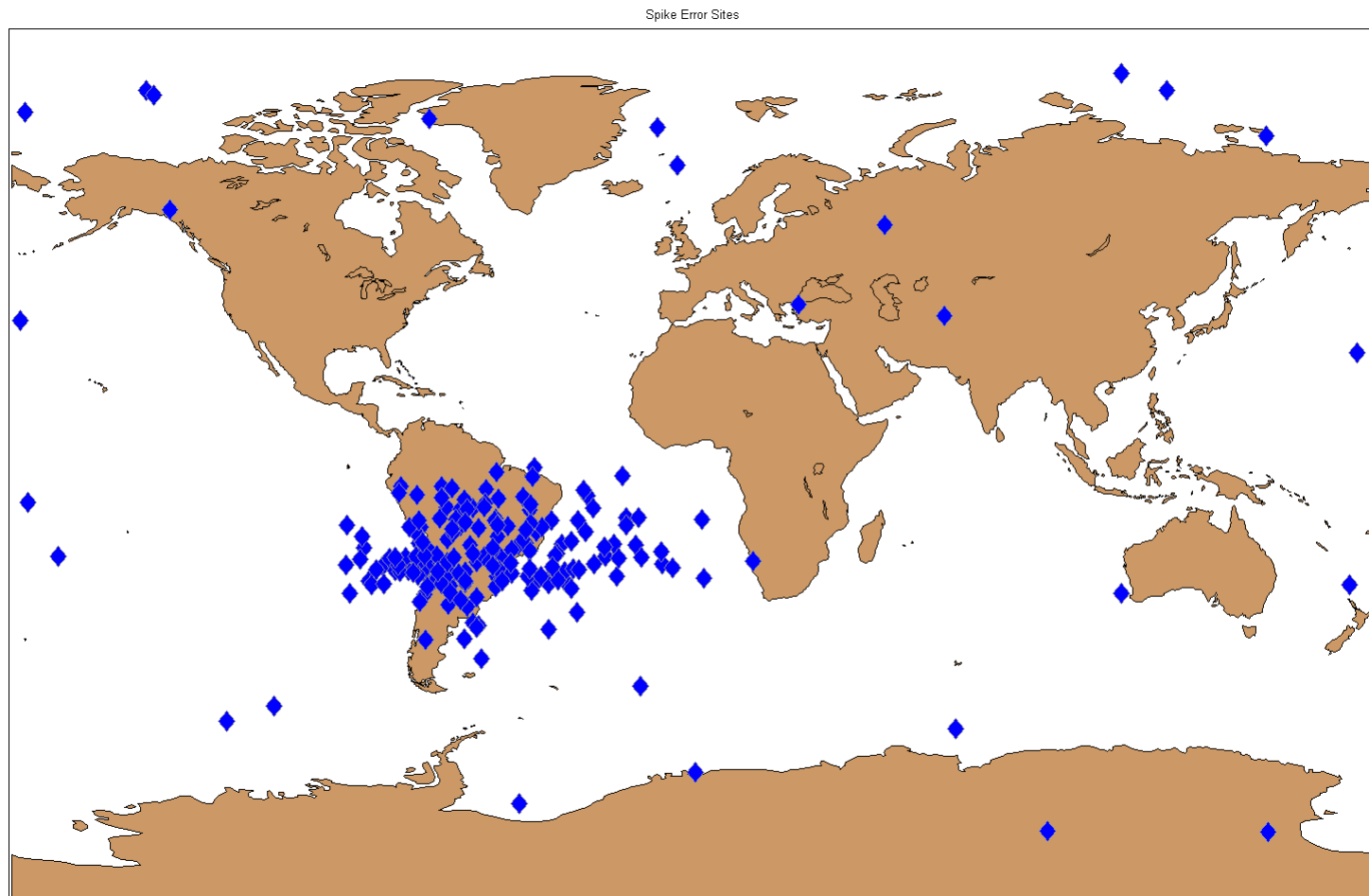
MWIR and SWIR Bit-Trim Masks



Interferogram Spikes

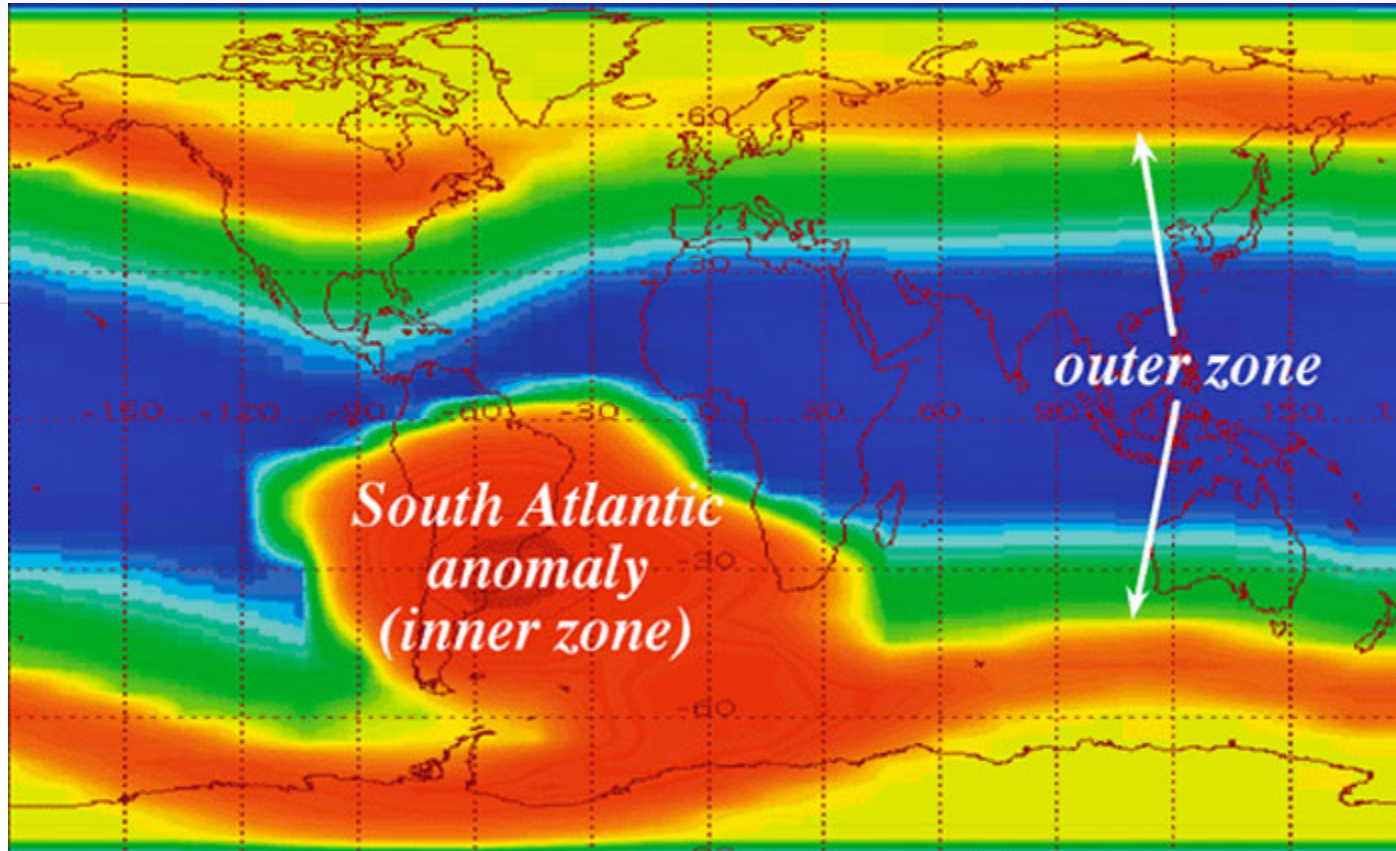
- ▶ Radiation can cause spikes in interferograms
- ▶ Impulse mask designed to zero out interferogram spikes
- ▶ SWIR is most affected (smallest detector current)
- ▶ Impulse mask operates on interferograms before FIR filter
- ▶ Electrical offsets and low frequency signals cause false triggers
- ▶ Impulse mask must be set high to avoid false triggers
- ▶ Small spikes are not presently being detected/corrected
- ▶ Many more small spikes than large spikes
- ▶ A method of detecting spikes is through interferogram asymmetry
- ▶ Small spikes can be detected/corrected on the ground

Geographical Distribution of Interferograms with Spikes



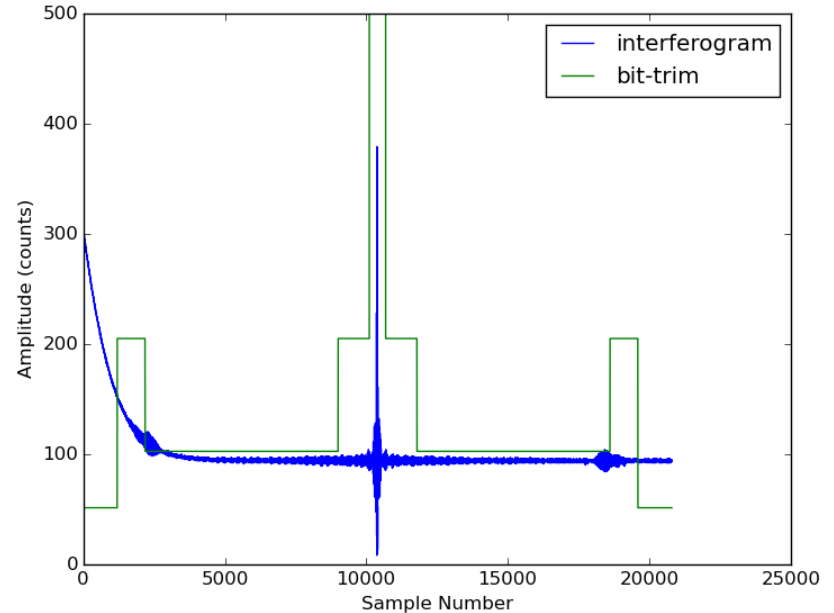
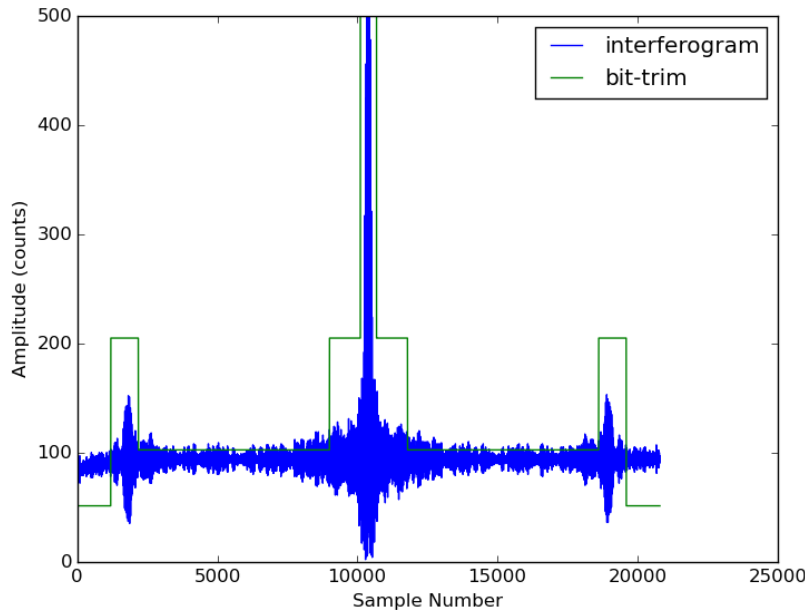
► Medium sized SW spike January to May 2015

Low Earth Orbit Radiation Distribution



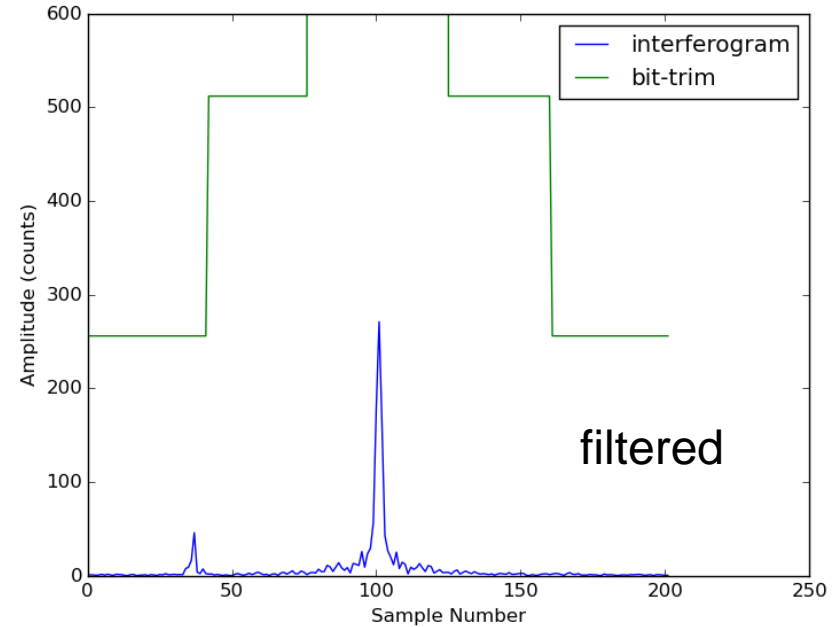
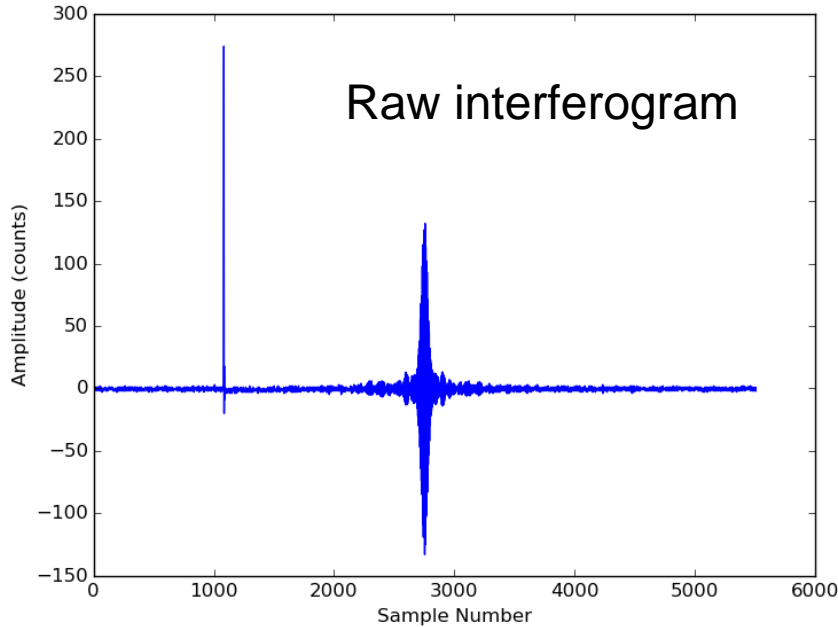
► From NASA/SAMPEX satellite

Can't Use Scaled Bit-Trim Mask for Impulse Mask



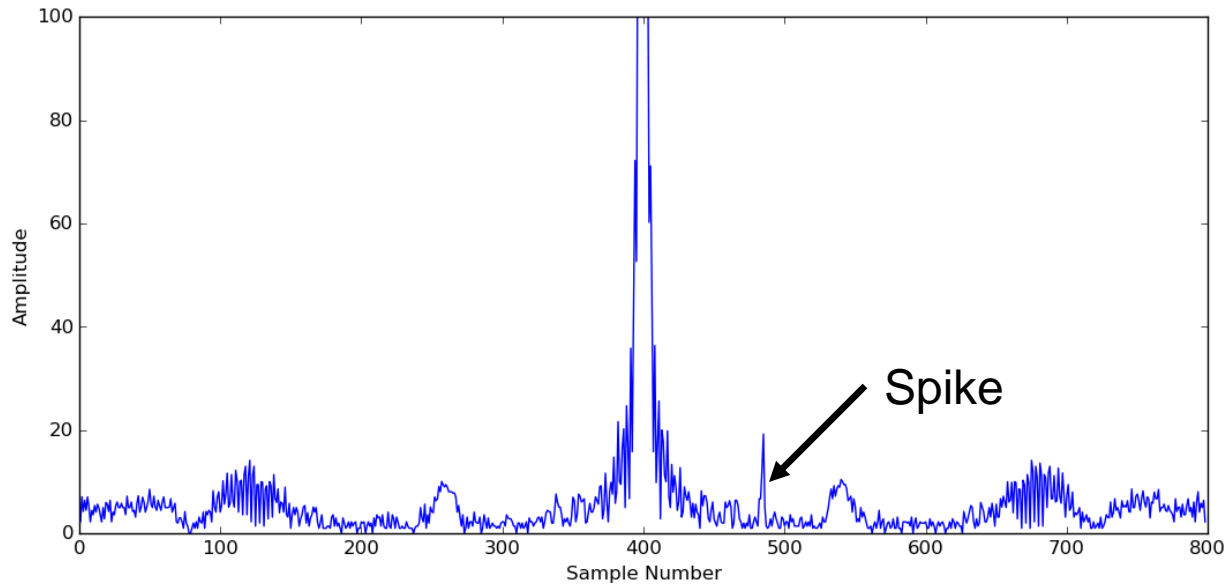
- ▶ Diagnostic mode allows view of raw interferograms
- ▶ Bit-trim mask scaled to raw interferogram levels
- ▶ Electronic offset about 95 counts for LW and MW
- ▶ Beginning of scan transient can be around 200 counts

Example of Spike in SW Interferogram



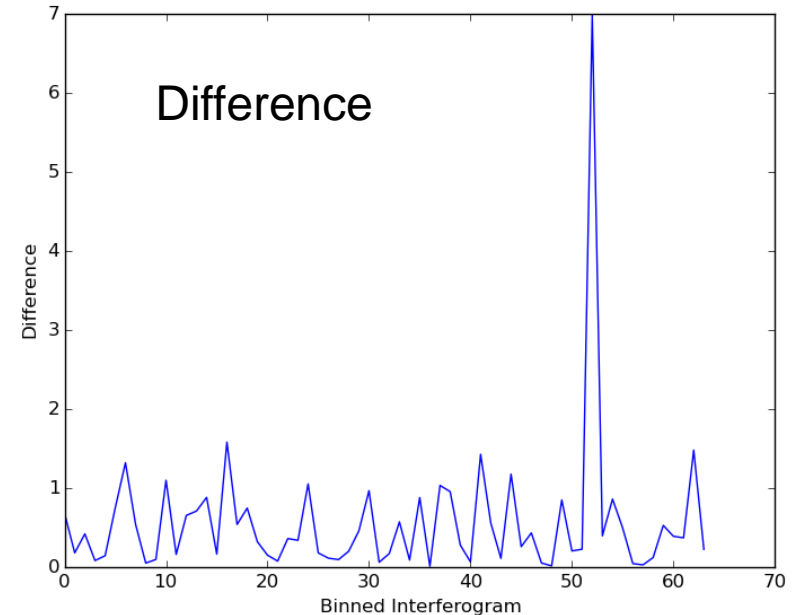
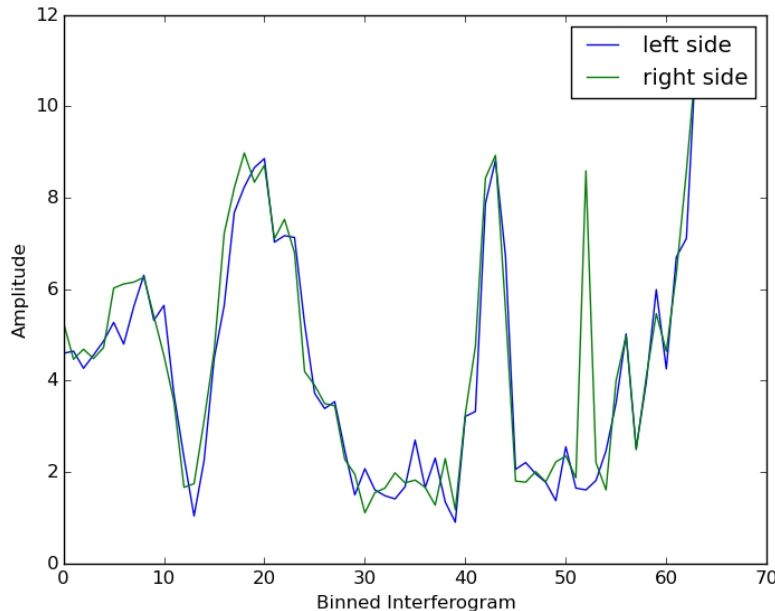
- ▶ Filtered interferogram is absolute value
- ▶ Many SW interferogram have small amplitudes
 - High dynamic range in the SW scenes
- ▶ Xin Jin estimated 123 spikes/day for side (less than 0.07%)

Detecting Interferogram Spikes



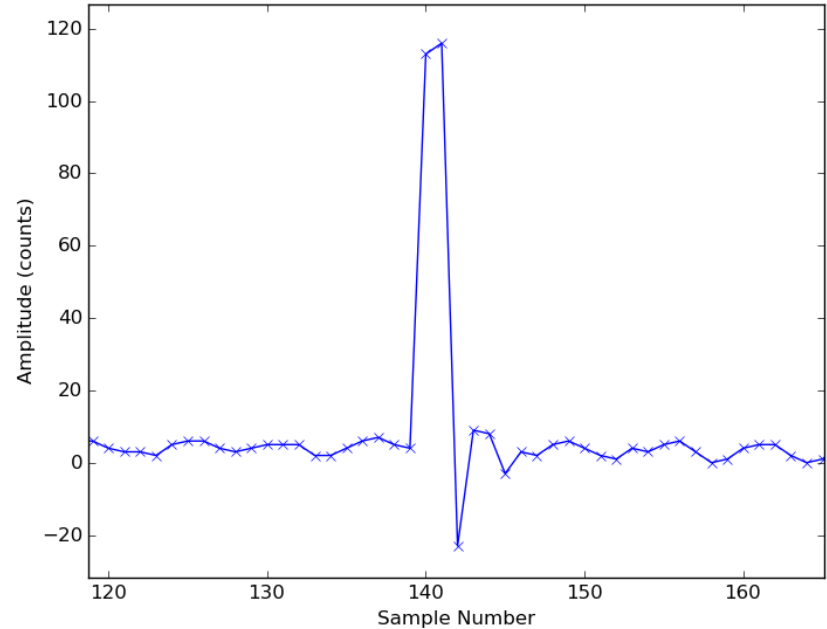
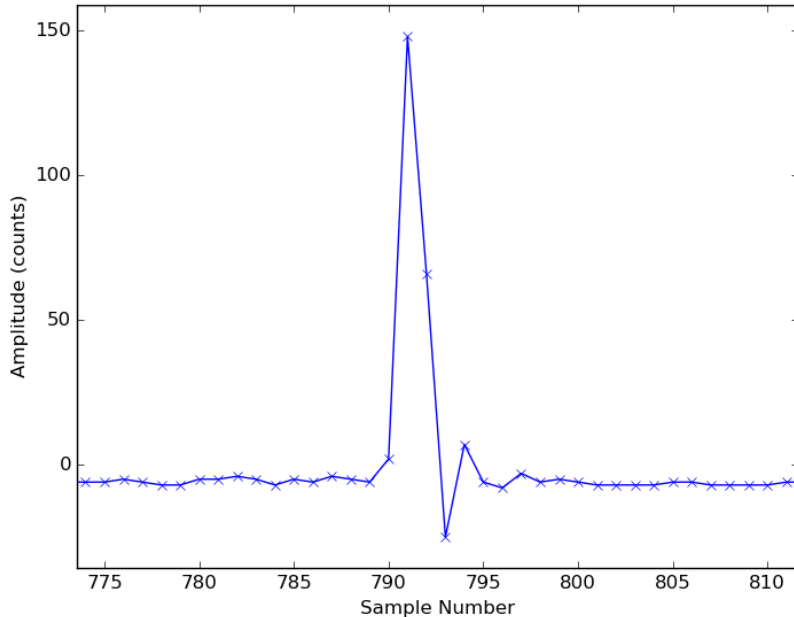
- ▶ A simple amplitude mask isn't very effective to detect spikes
 - Bright scenes can be larger than spikes
- ▶ Interferograms should be symmetric
- ▶ Interferogram phase makes direct left side to right side comparisons difficult
- ▶ Absolute value of interferogram plotted

Binned Interferogram



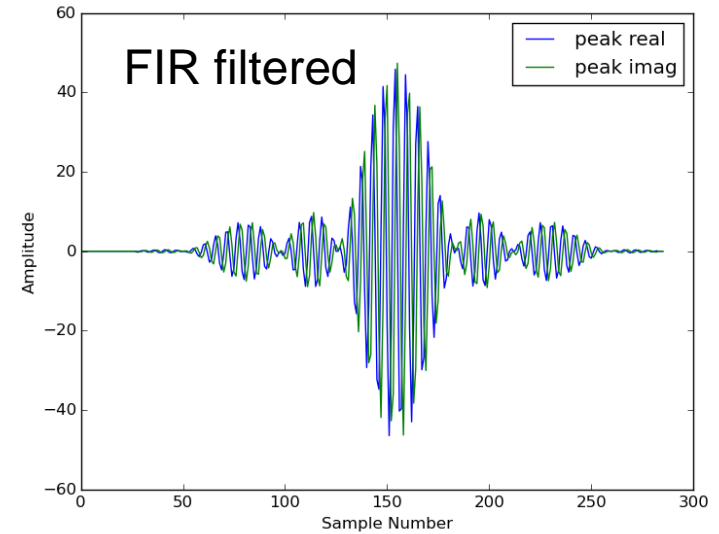
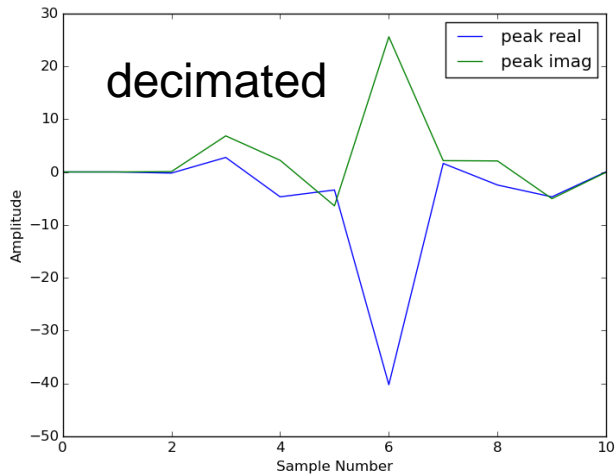
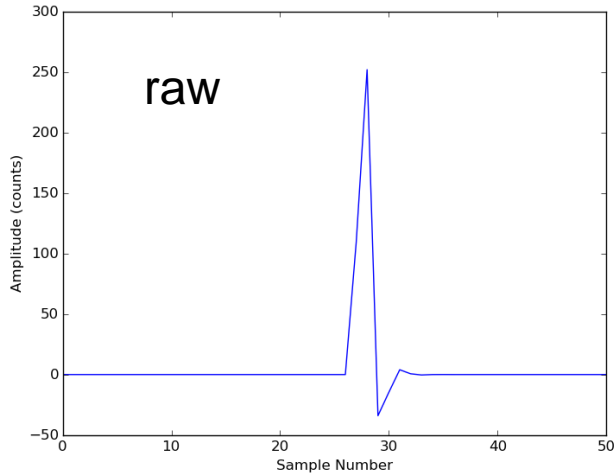
- ▶ Interferograms can be binned to make side to side comparisons
- ▶ Example is for 6 interferogram points/bin and skip ZPD area
- ▶ Right side of interferogram has been flipped
- ▶ Difference clearly show spike

Spikes Are Not Single Sample Events



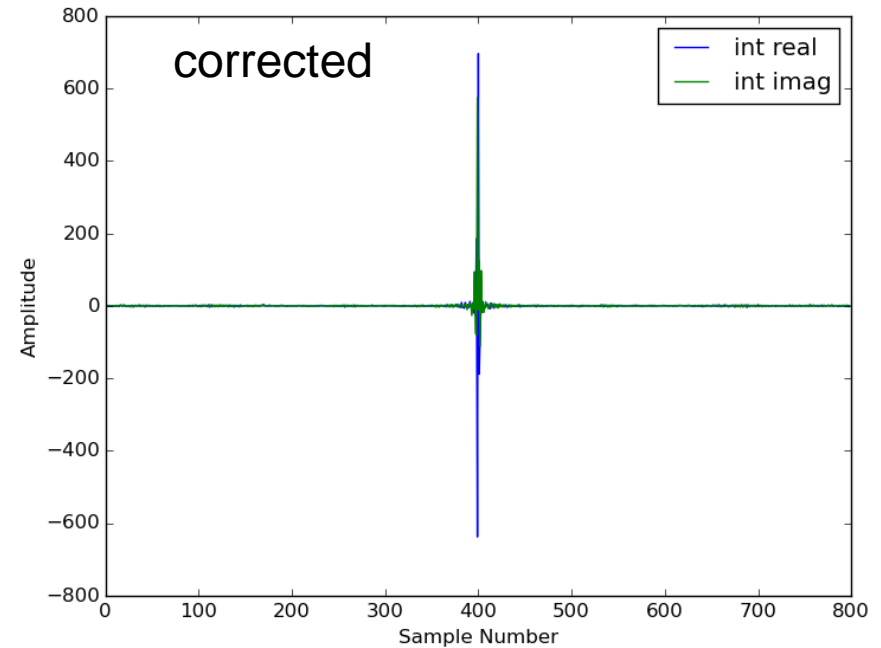
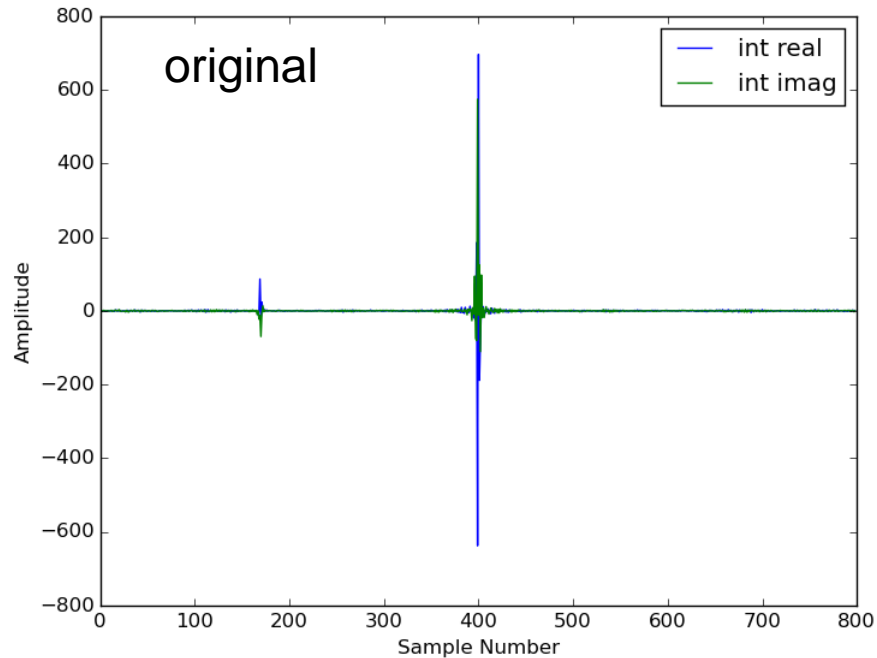
- ▶ Raw diagnostic mode data
- ▶ Data points indicated by “x” connected by straight lines
- ▶ Shape similar to that of a damped oscillator
- ▶ Least-squares fit to spike
- ▶ Subtract modeled spike from interferogram

Affect of Filtering and Decimating on a Spike



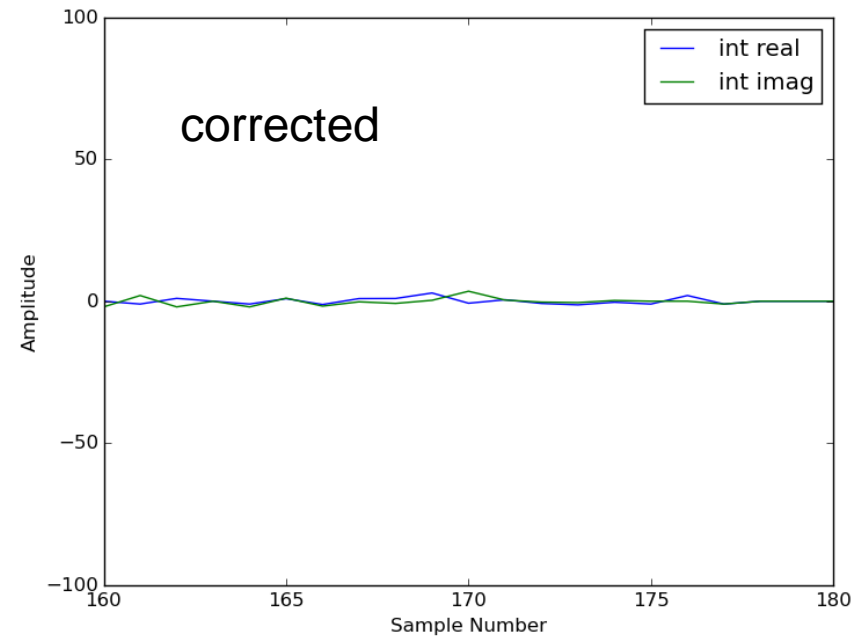
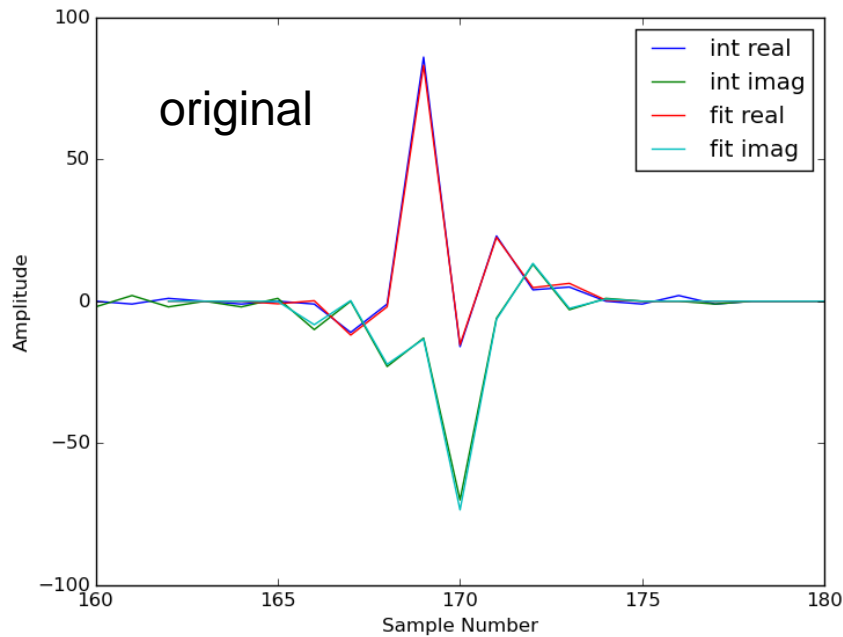
- ▶ Modeled spike
- ▶ SW band
- ▶ Fit uses real and imaginary component

Example of Spike Removed from Interferogram



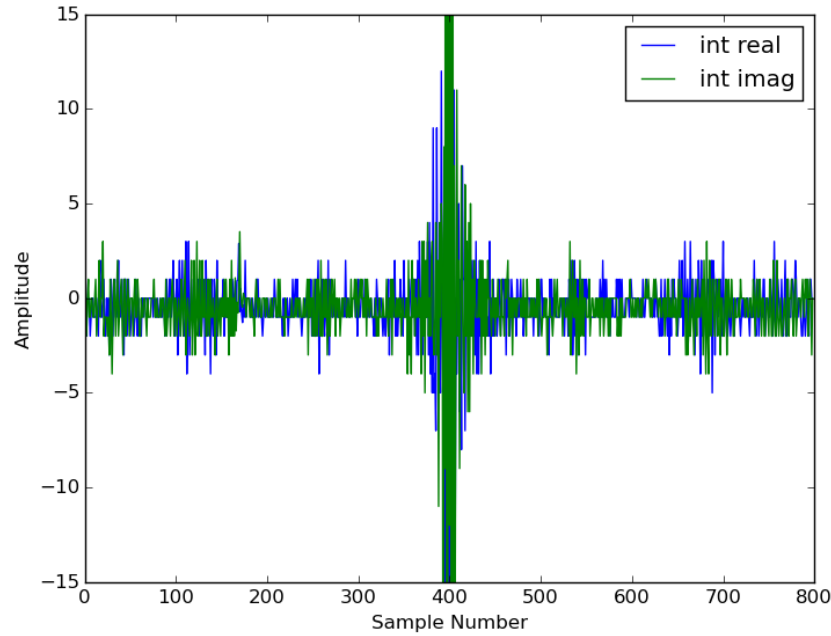
- ▶ Correction through subtracting modeled spike from original interferogram
- ▶ No residual error visible
- ▶ FOR 27, FOV6, 2/18/2015 18:11:11.367

Expanded Vertical Scale



- ▶ Fit to spike is very good
- ▶ Residual error not visible in expanded view of interferogram

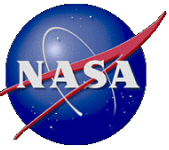
Expanded View of Corrected Interferogram



- ▶ Spike residual error not visible
- ▶ Quantization noise clearly visible

Conclusions

- ▶ CrIS J1 has excellent NEdN performance
- ▶ Evidence for vibration effects in ground testing
 - Not an issue for MN
 - Noticeable for PFL and PFH
- ▶ Some FOVs show consistent differences in side 1 to side 2 NEdN
- ▶ Bit-trim mask optimization for CrIS SNPP can be applied to J1
- ▶ Impulse mask needs to be set high to avoid false triggers
- ▶ Number of interferogram effected by spikes is low with respect to operability requirement of 99%
- ▶ Radiation spikes can be detected and removed through ground processing



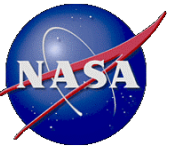
Geolocation Assessment Tool and Correction Model for JPSS CrIS

Likun Wang^{1*}, Bin Zhang¹, Denis Tremblay², Yong Han³, Mark Esplin⁴, Joe Predina⁵, Lawrence Suwinski⁶, Yong Chen¹, and Xin Jin⁷

- 1.* Univ. of Maryland, College Park, MD; Likun.Wang@noaa.gov
2. Science Data Processing Inc., Laurel, MD
3. NOAA/NESDIS/STAR, College Park, MD
4. Space Dynamics Laboratory, Utah State University, Logan, UT
5. Logistikos Engineering LLC, IN
6. Exelis, Fort Wayne, IN
7. ERT Inc., Laurel, MD

SUOMI NPP SDR Science and Validated Product Maturity Review
College Park, MD; December 18-20 2013





Content



1. Introduction

- **Specification, Algorithms, and Issues**

2. Assessment Method

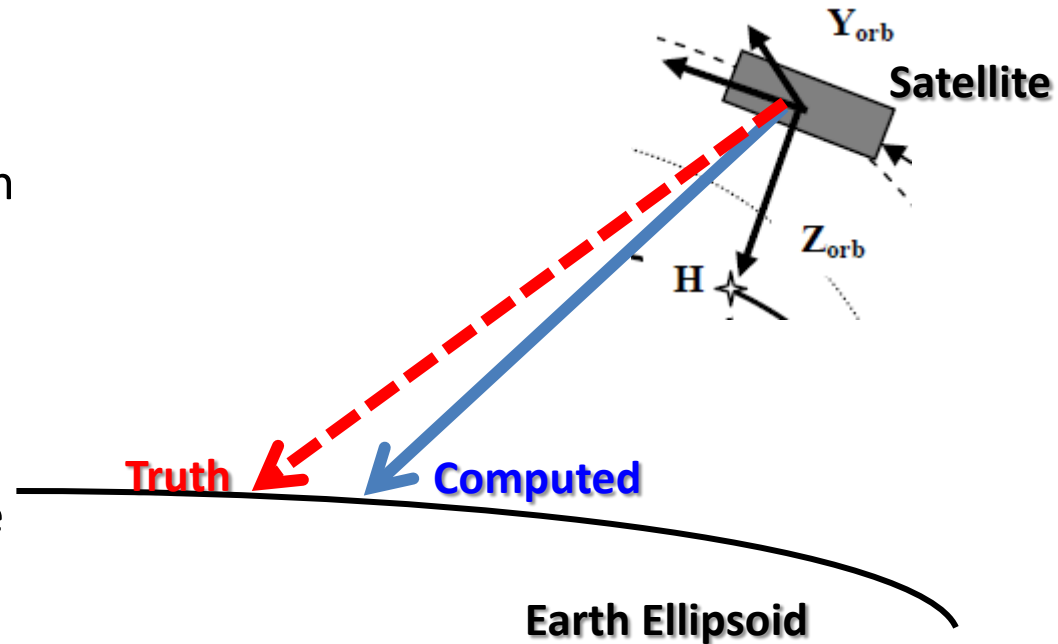
- **Using VIIRS Image Bands as a truth**
- **New Collocation Method (Super Fast !!!)**
- **Full Angles Assessment (All Scan Positions)**
- **The results are based on angles instead of distance.**

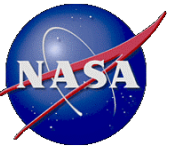
3. Correction Model

- **New Geometric Calibration Parameters based on Assessment Results**

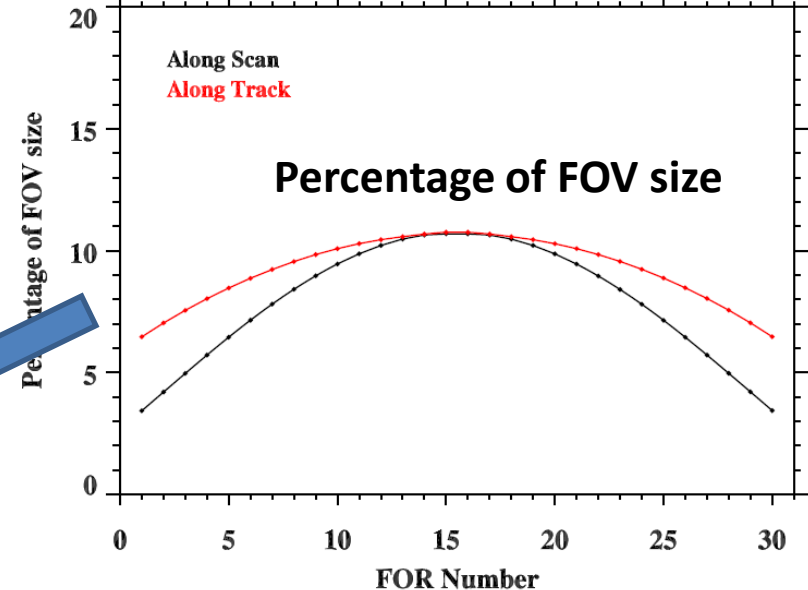
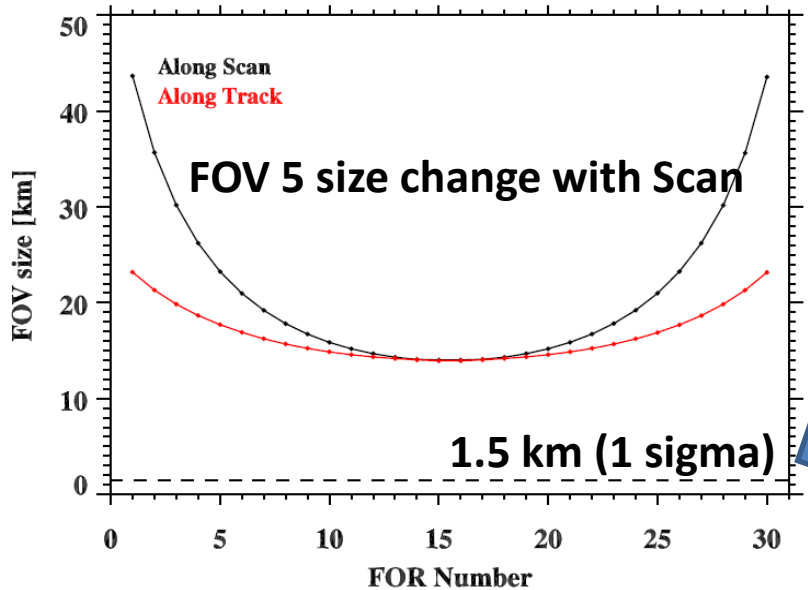
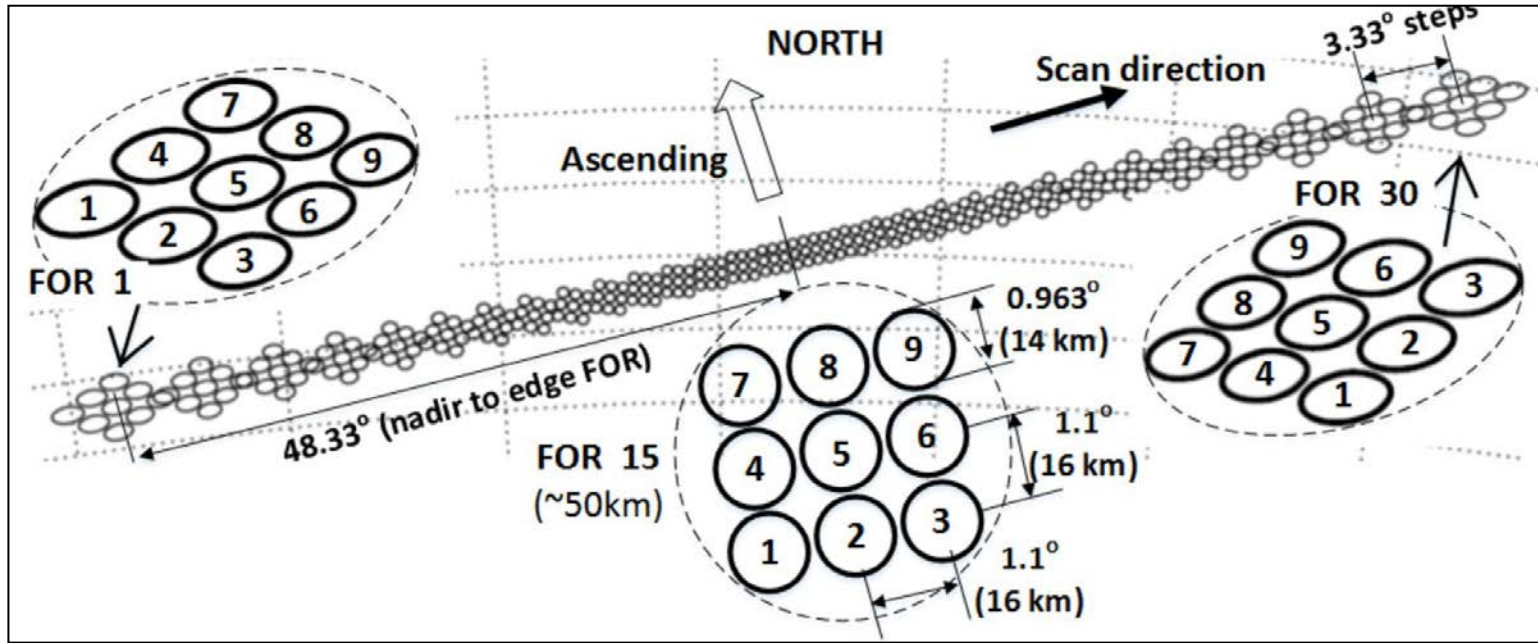
4. Summary and future work

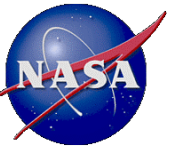
- The goal of the geometric calibration is to map CrIS line-of-sight (LOS) pointing vectors to geodetic longitude and latitude at each field of view (FOV) (9) for each scan position (30).
- The purpose of geolocation assessment is to identify the error characteristics of LOS pointing vector by comparing them with the truth.
- Furthermore, if the systematic errors are found, a new set of co-alignment parameters should be retrieved based on assessment results to improve the geolocation accuracy.





CrIS Scan Patterns and Specification

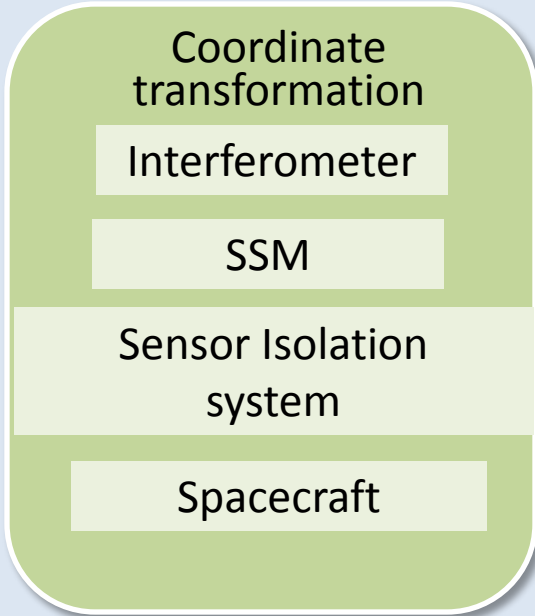




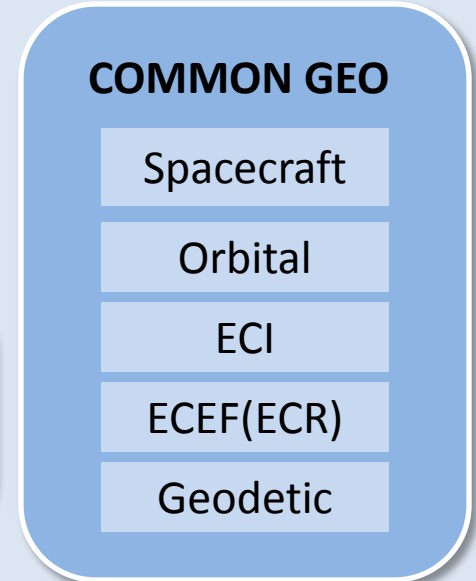
Overview of Satellite Geolocation Components



CrIS (or other instrument)



JPSS or any satellite



Function call to common geo:
ellipIntersect(outPt,inst2SC,exitVec, dlat,lon,satazm,satzen,range)

GEOLOCATION ASSESSMENT

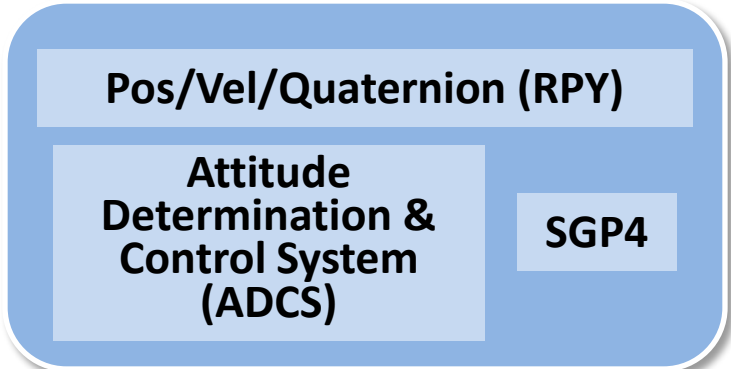
- GCP/Maps/Ground truth
- the other instrument measurements with enough geolocation accuracy
- Comparing the truth and CrIS Geo fields

feedback

Geolocate each FOV



ADCS



CrIS Geometric Calibration Algorithm

Sensor Specific Algorithm

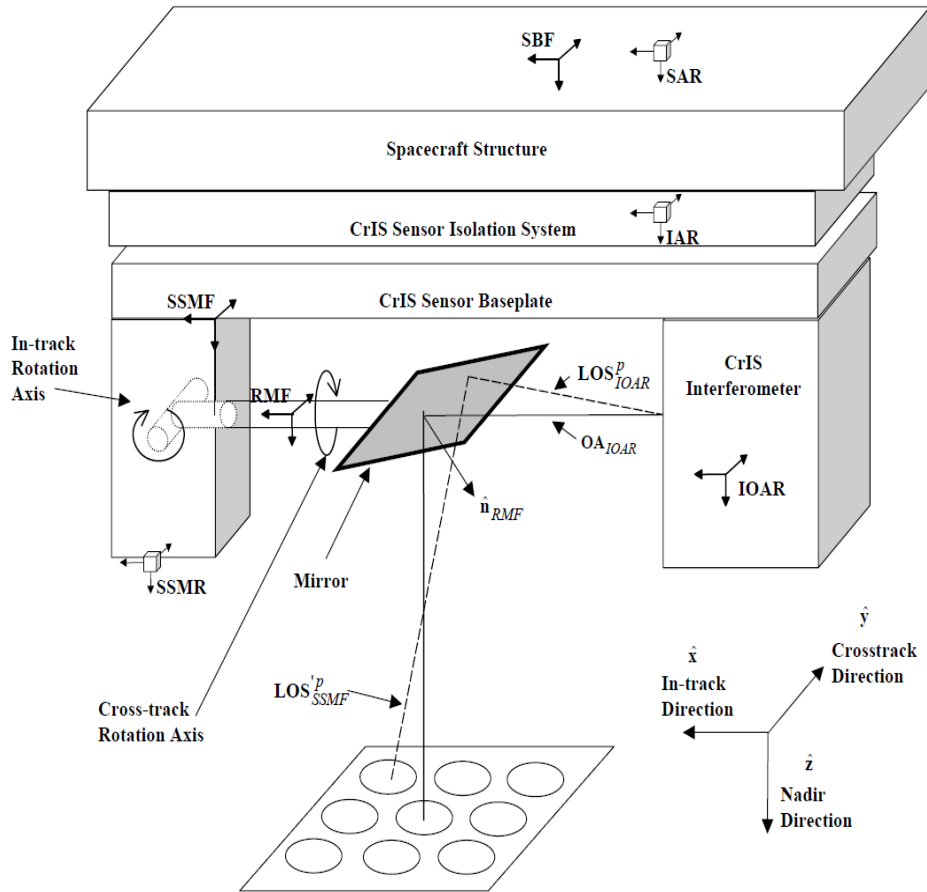
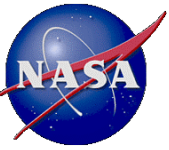


Figure 48: Sensor Algorithm Level Coordinate Systems

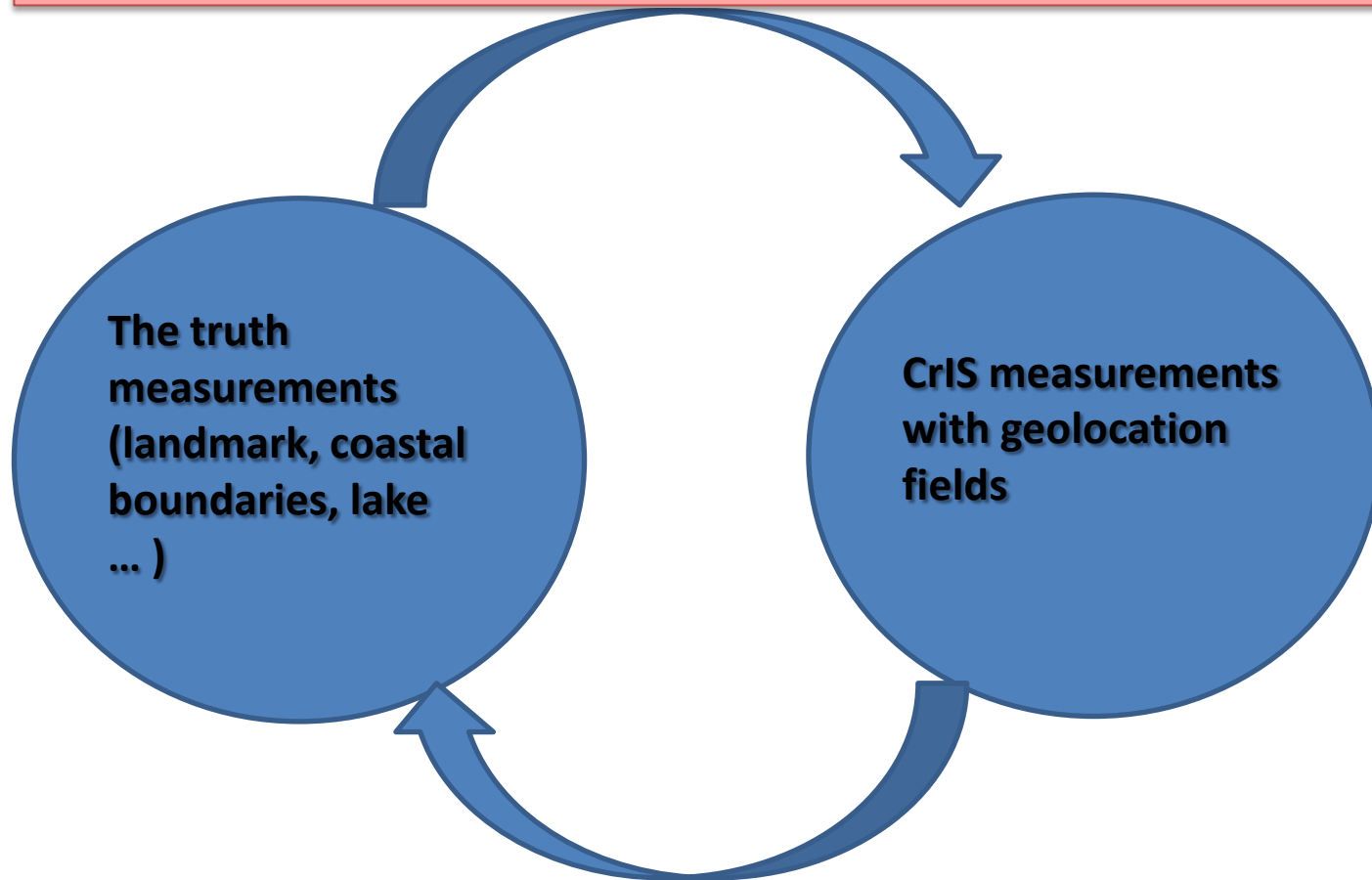
SDR Algorithm Process

- 1) LOS in IOAR coordinate = ILS parameters (3x3)
- 2) Convert from IOAR to SSMF coordinate
- 3) Compute normal to SSM mirror in SSMF (30 Scan Pos)
- 4) Apply SSM mirror rotation to get LOS in SSMF coordinate
- 5) Convert from SSMF to SSMR coordinate
- 6) Convert from SSMR to IAR coordinate
- 7) Convert from IAR to SAR
- 8) SAR coordinate = SBF coordinate



Geolocation Assessment Method

Method 2: 1) Simulating CrIS measurements from the truth measurements and 2) comparing them with actual CrIS measurements



Method 1: 1) Retrieving land features (coast lines) from CrIS measurements; and 2) comparing them with the truth dataset

Method 1 Does Not Work

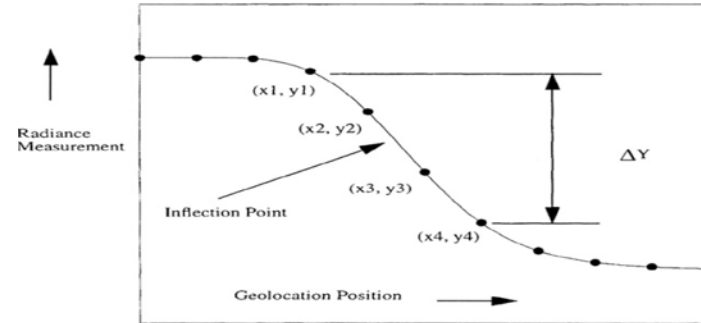
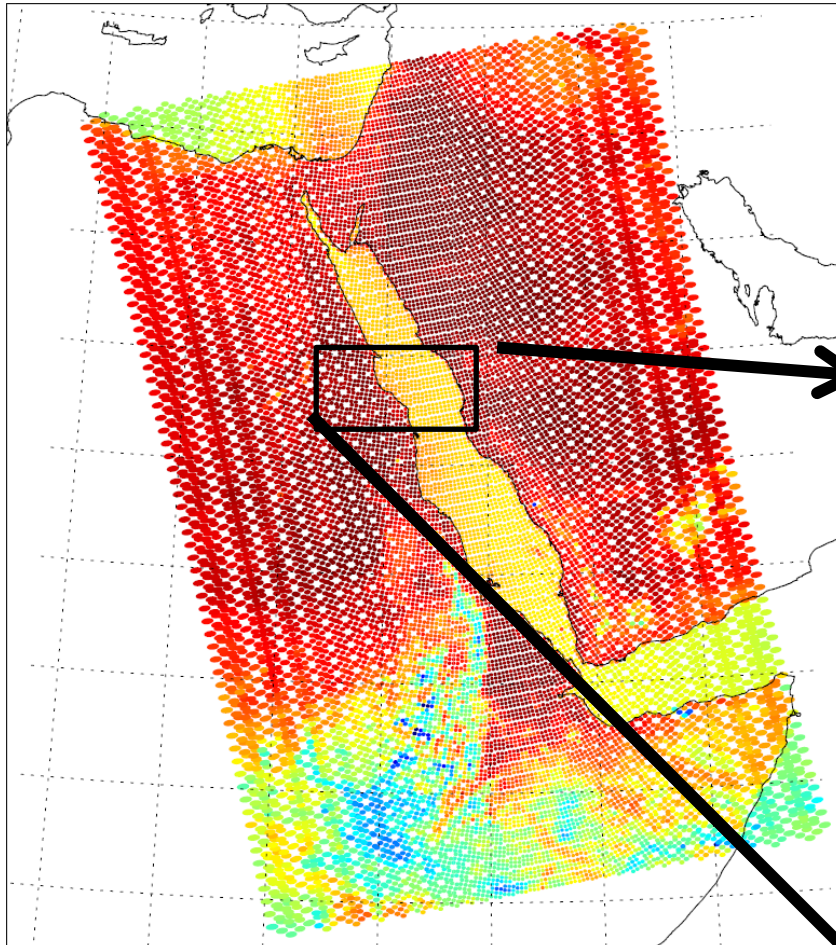
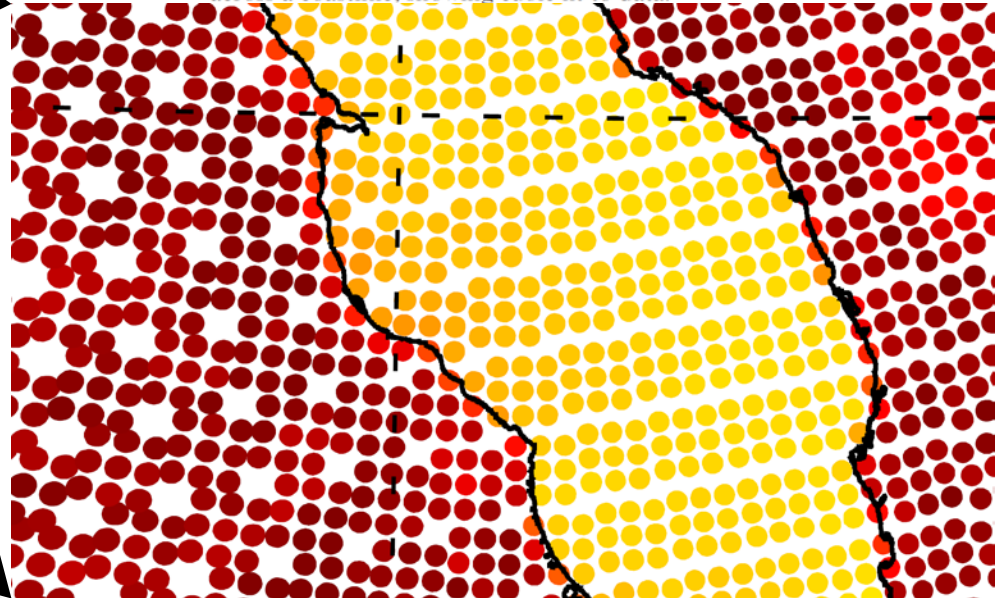


FIG. 5. Schematic of measurement change as radiometer scans across a coastline, showing cubic fit to data.

From Smith 2009

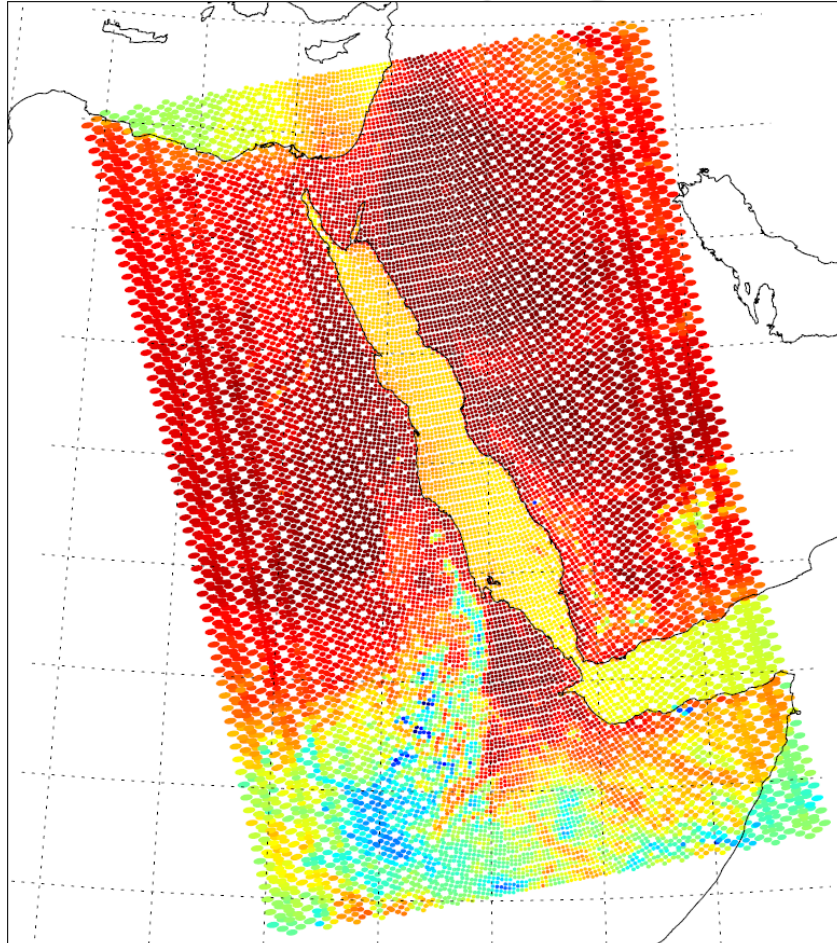


CrIS data with 3-km sub-pixel geolocation Errors

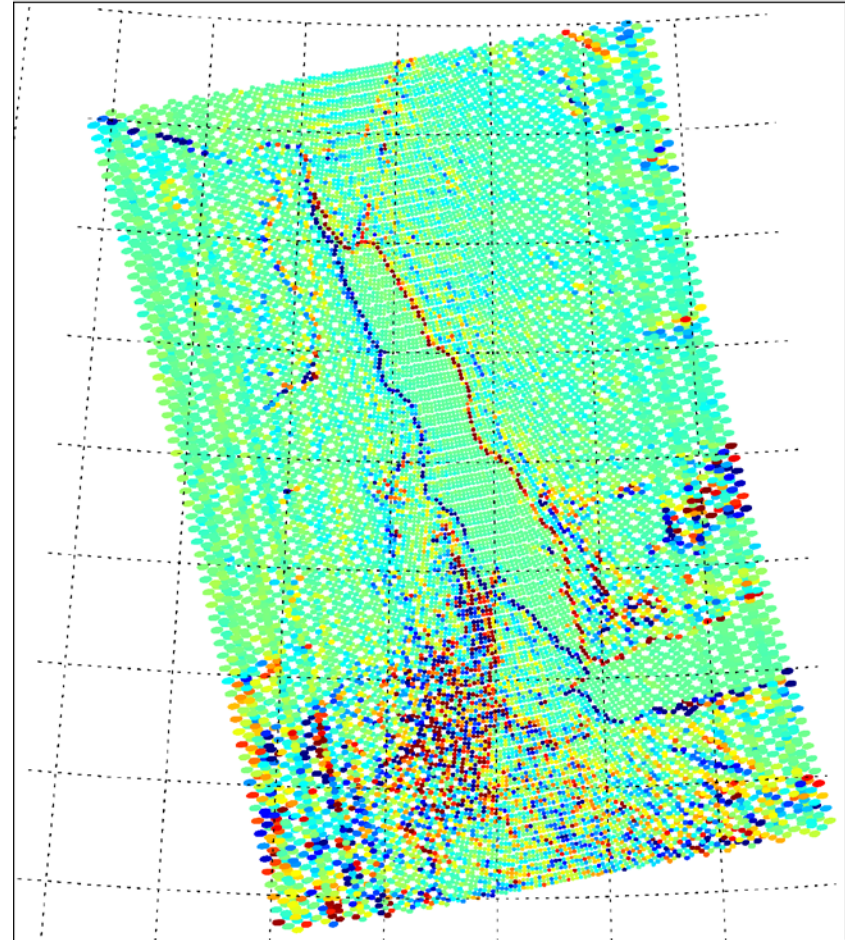
Unlike an imager, it is very hard to assess geolocation sub-pixel accuracy for CrIS using the land feature method because of 1) relatively large footprint size (above 14 km); 2) the gap between footprints; and 3) Uneven spatial distribution of CrIS Footprints

Method 2 Does Work

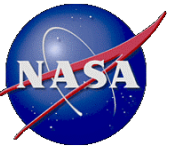
CrIS data with 3-km sub-pixel geolocation Errors



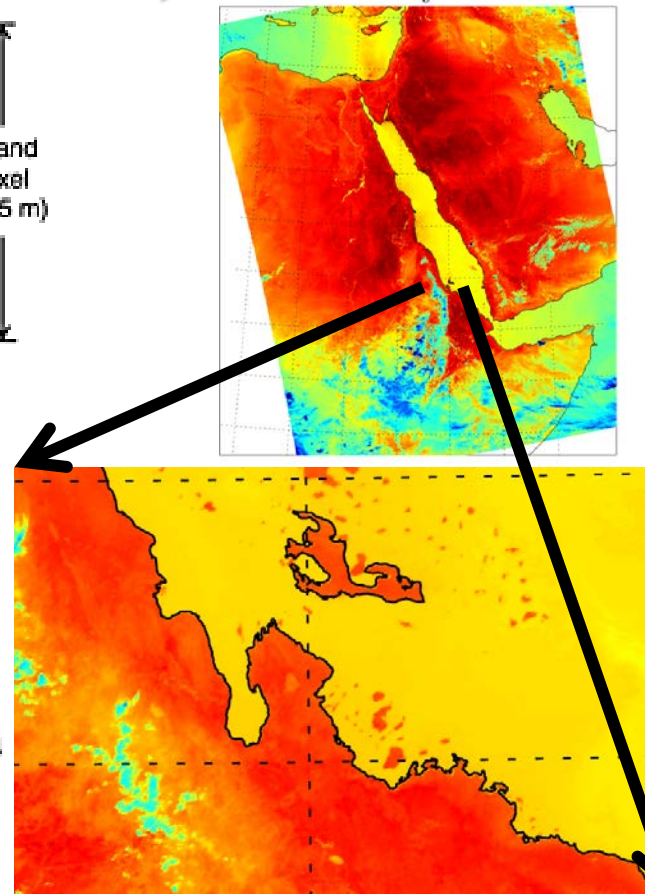
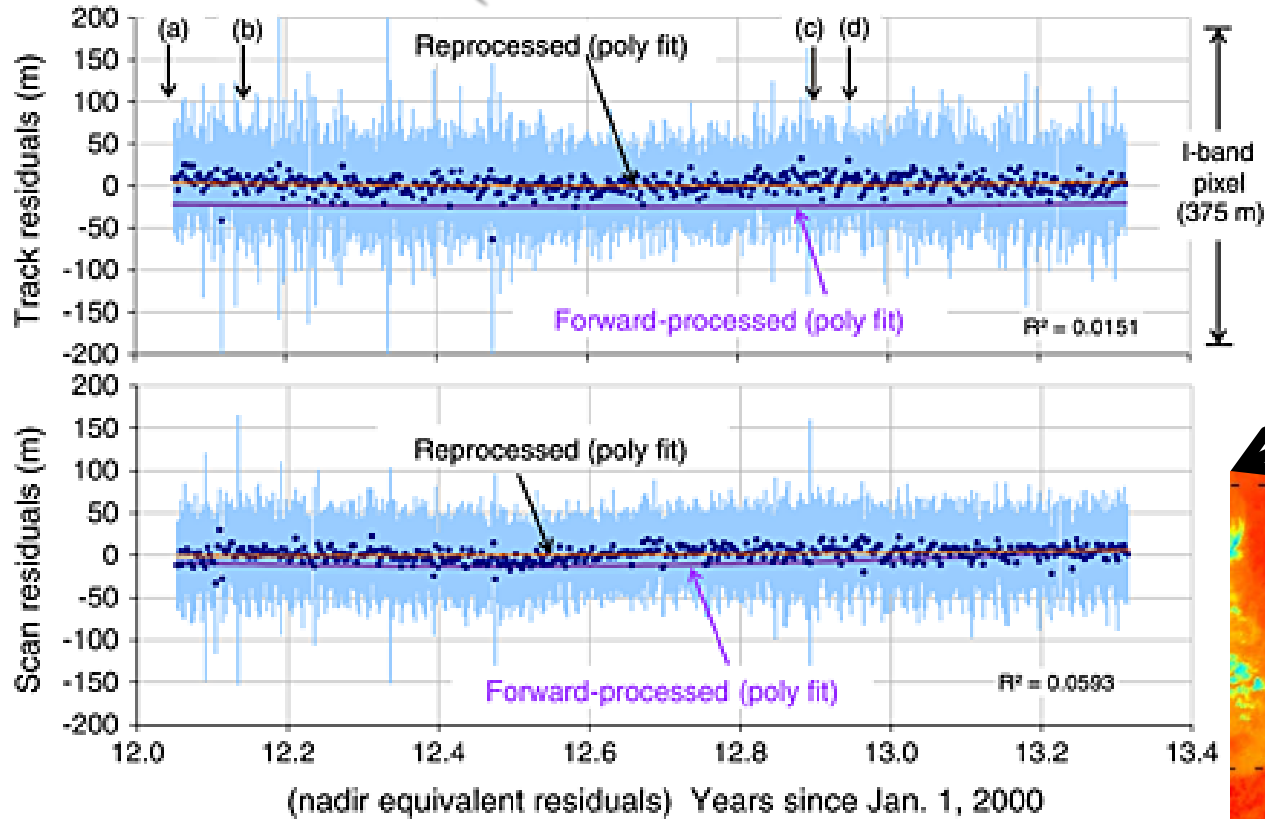
original CrIS-VIIRS Image



Using VIIRS to simulate CrIS and then take the difference between CrIS and VIIRS, the geolocation errors immediately showed up.



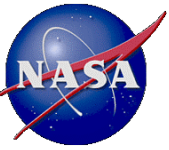
Reference: Using VIIRS Geolocation (I5 band: 375m resolution)



from Wolf et al. 2013

Table 2. VIIRS Geolocation Accuracy

Residuals	First Update	Second Update
	23 February 2012	18 April 2013
Track mean	-24 m, -7%	2 m, 1%
Scan mean	-8 m, -2%	2 m, 1%
Track RMSE	75 m, 20%	70 m, 19%
Scan RMSE	62 m, 17%	60 m, 16%



CrIS Geolocation Assessment for NPP

- what have not been done



JOURNAL OF GEOPHYSICAL RESEARCH: ATMOSPHERES, VOL. 118, 1–15, doi:10.1002/2013JD020376, 2013

Paper published in Suomi NPP Cal/Val Special Issue

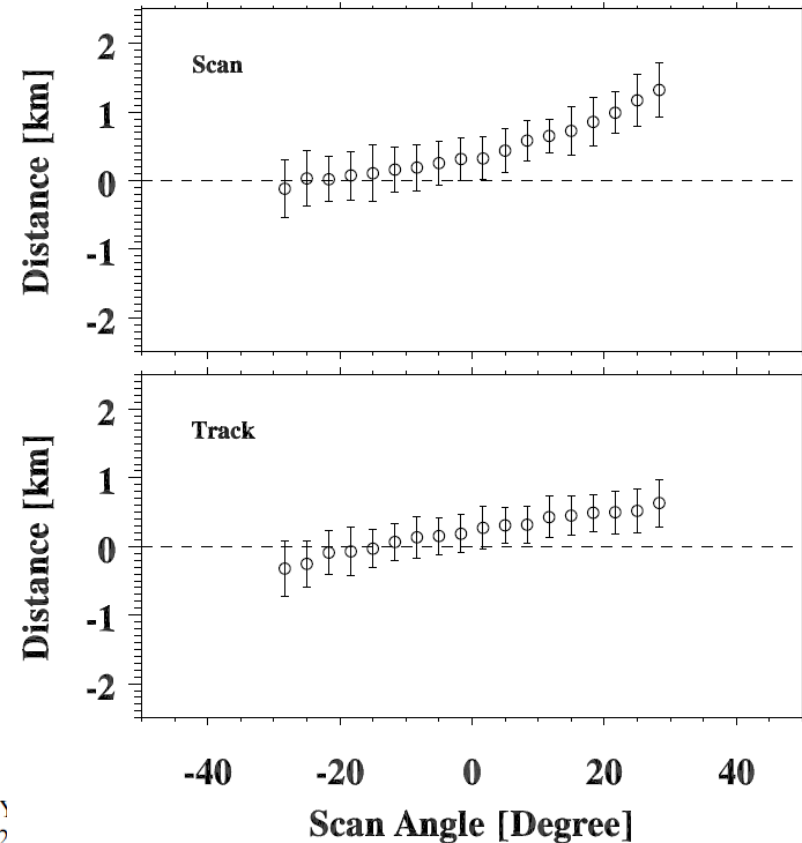
Geolocation assessment for CrIS sensor data records

Likun Wang,¹ Denis A. Tremblay,² Yong Han,³ Mark Esplin,⁴ Denise E. Hagan,⁵ Joe Predina,⁶ Lawrence Suwinski,⁶ Xin Jin,⁷ and Yong Chen¹

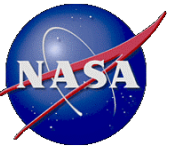
Received 17 June 2013; revised 23 October 2013; accepted 27 October 2013.

[1] As important as spectral and radiometric calibration, the geometric calibration is one of the requisites for the Suomi National Polar-Orbiting Partnership Cross-track Infrared Sounder (CrIS) Sensor Data Records (SDR). In this study, spatially collocated measurements from the Visible Infrared Imaging Radiometer Suite (VIIRS) band I5 are used to evaluate the geolocation performance of the CrIS SDR by taking advantage of high spatial resolution and accurate geolocation of VIIRS measurements. The basic idea is to find the best collocation position between VIIRS and CrIS measurements by shifting VIIRS images in the track and scan directions. The retrieved best collocation position is then used to evaluate the CrIS geolocation performance by assuming the VIIRS geolocation as a reference. Sensitivity tests show that the method can well detect geolocation errors of CrIS within 30° scan angle. When the method was applied to evaluate the geolocation performance of the CrIS SDR, geolocation errors that were caused by software coding errors were successfully identified. After this error was corrected and the engineering packets V35 were released, the geolocation accuracy is 0.347 ± 0.051 km (1σ) in the scan direction and 0.219 ± 0.073 km in the track direction at nadir.

Citation: Wang, L., D. A. Tremblay, Y. Han, M. Esplin, D. E. Hagan, J. Predina, L. Suwinski, X. Jin, and Y. Chen, 2013, Geolocation assessment for CrIS sensor data records, *J. Geophys. Res. Atmos.*, 118, doi:10.1002/2013JD020376



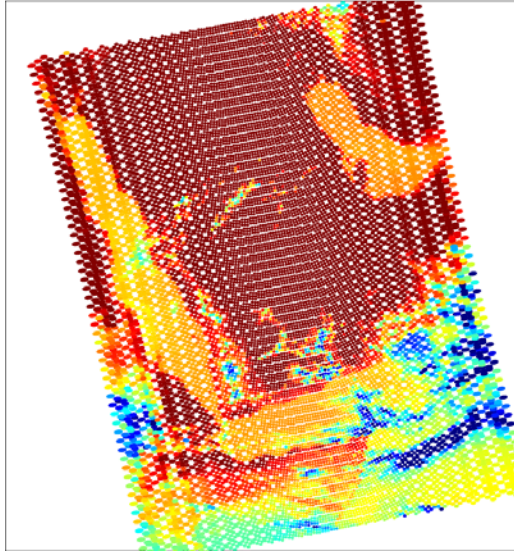
1. Limited to scan angles less than 30 degree, especially at nadir → **full angles' assessment**
2. Assessments are based on distance in in-track and cross-track direction → **based on angles**
3. Correction model → **a new set of co-alignment parameters**



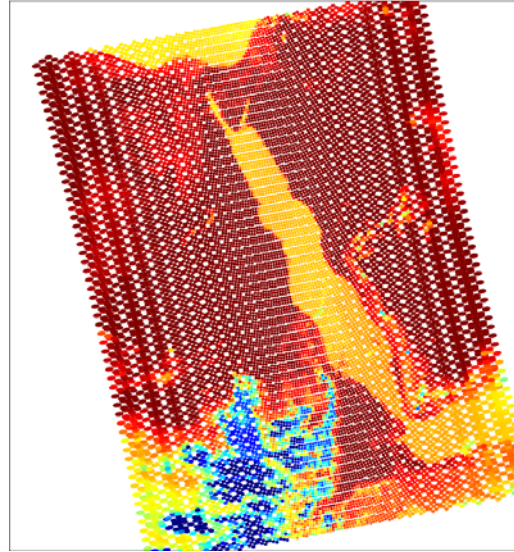
Misalignment between CrIS and VIIRS at the end of scan



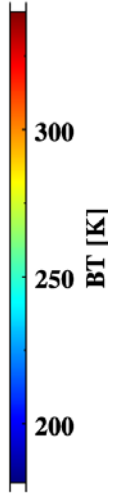
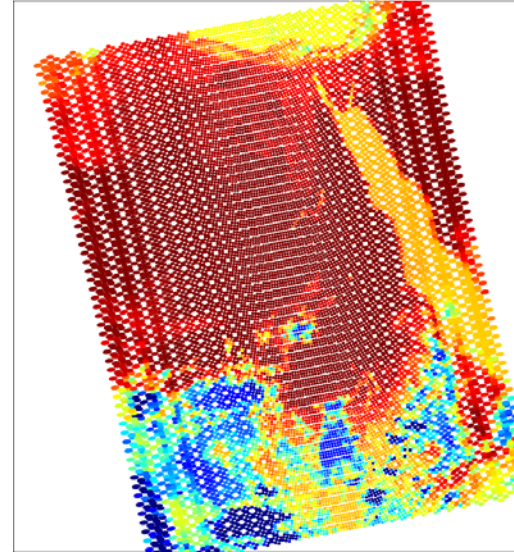
CrIS Image at 900.000cm-1



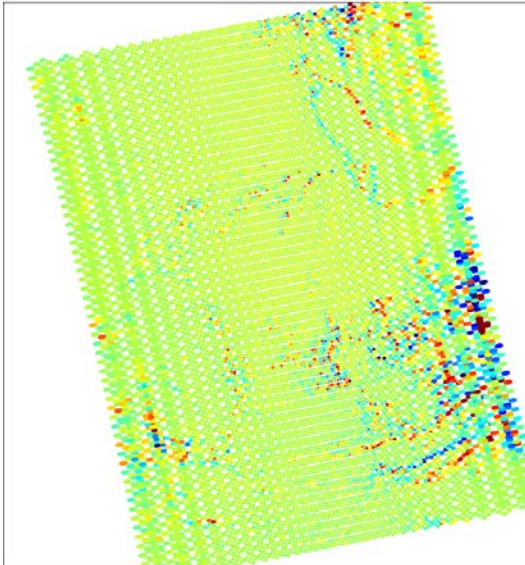
CrIS Image at 900.000cm-1



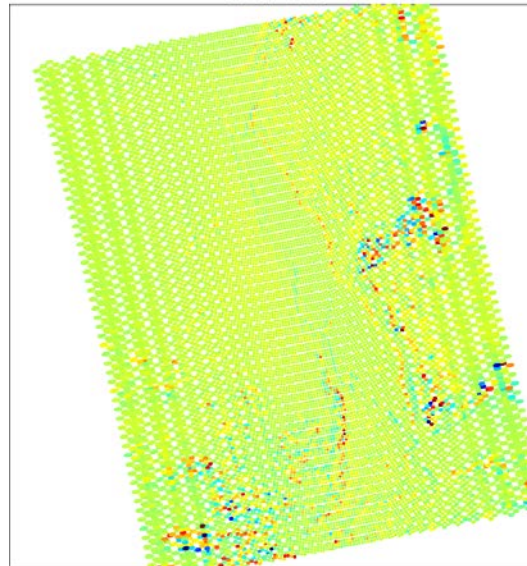
CrIS Image at 900.000cm-1



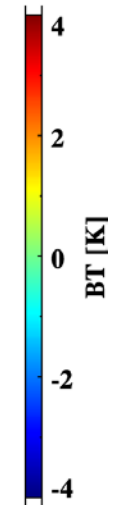
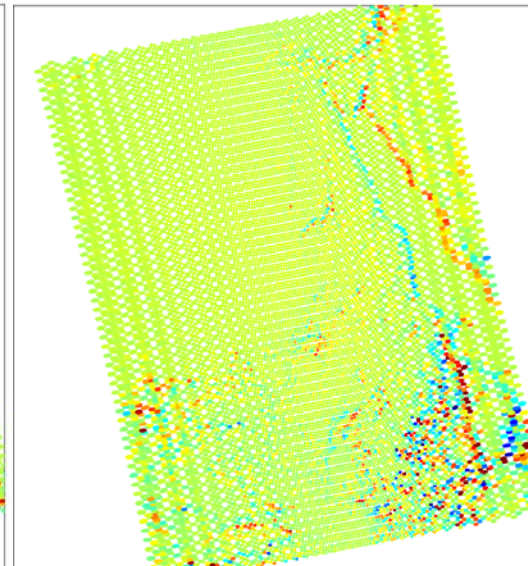
CrIS-VIIRS I5

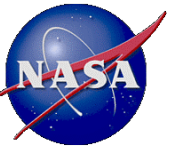


CrIS-VIIRS I5



CrIS-VIIRS I5

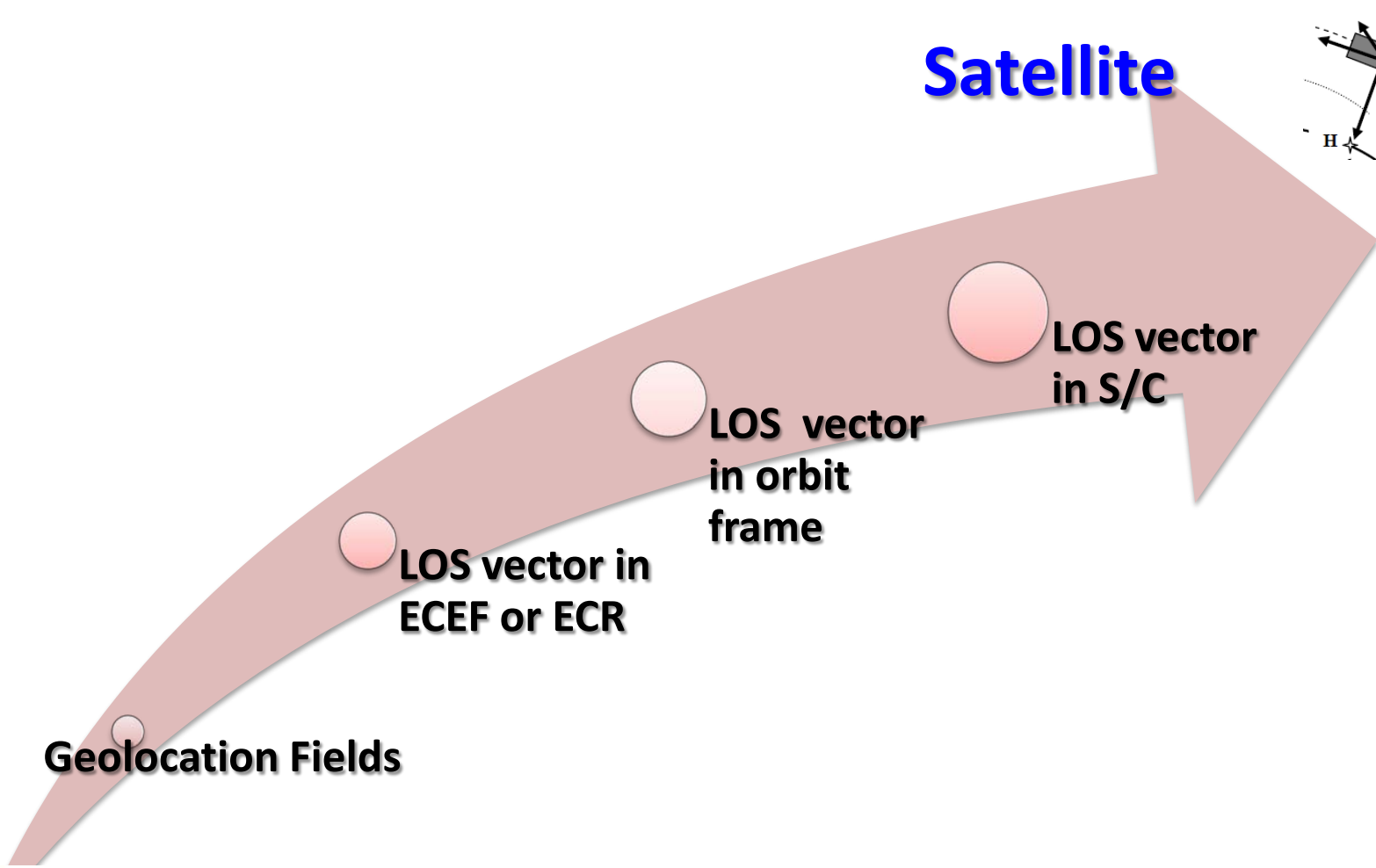
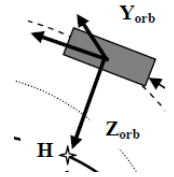




Retrieved the true LOS vector



Satellite



Geolocation Fields

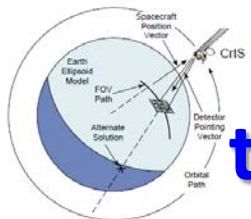
LOS vector in ECEF or ECR

LOS vector in orbit frame

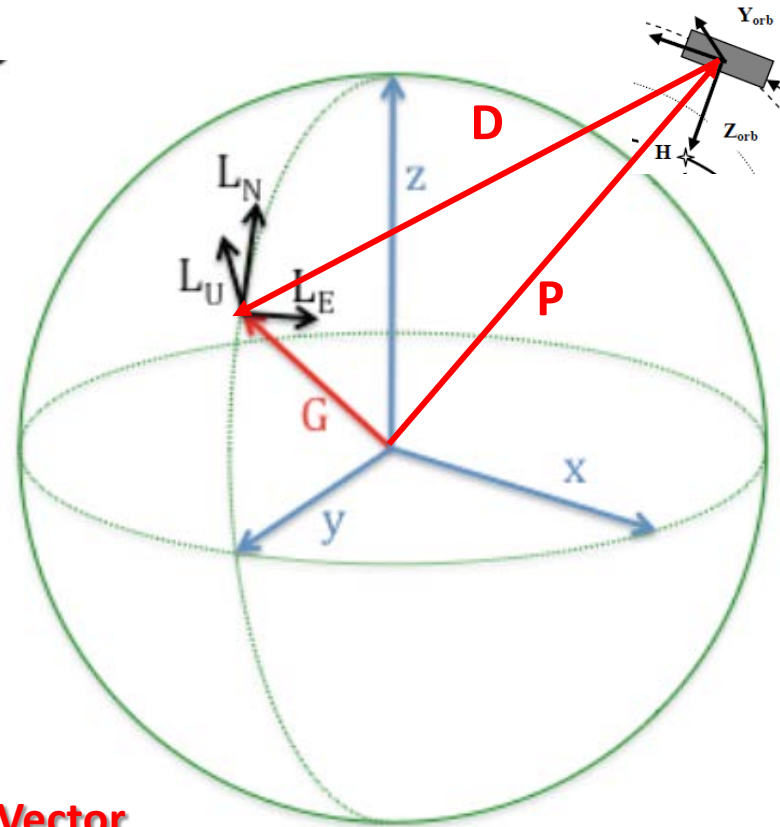
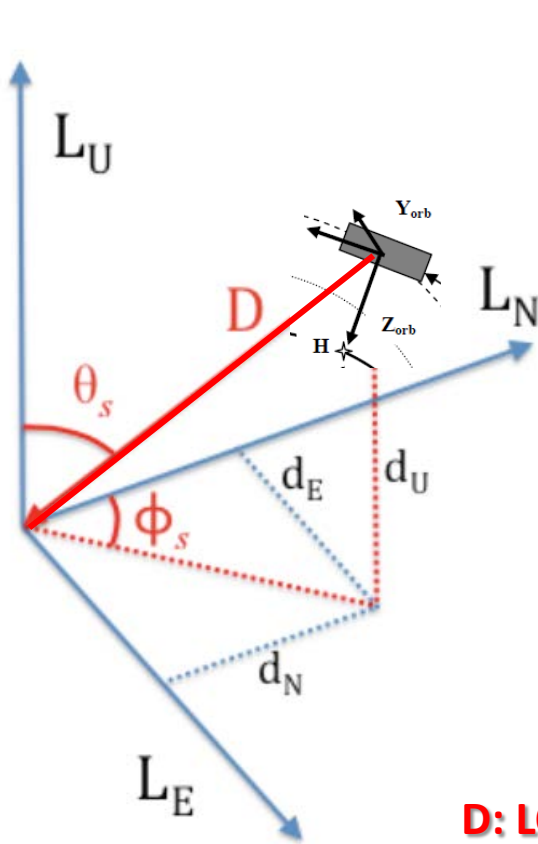
LOS vector in S/C

Assuming that Common Geolocation part is correct

the Earth



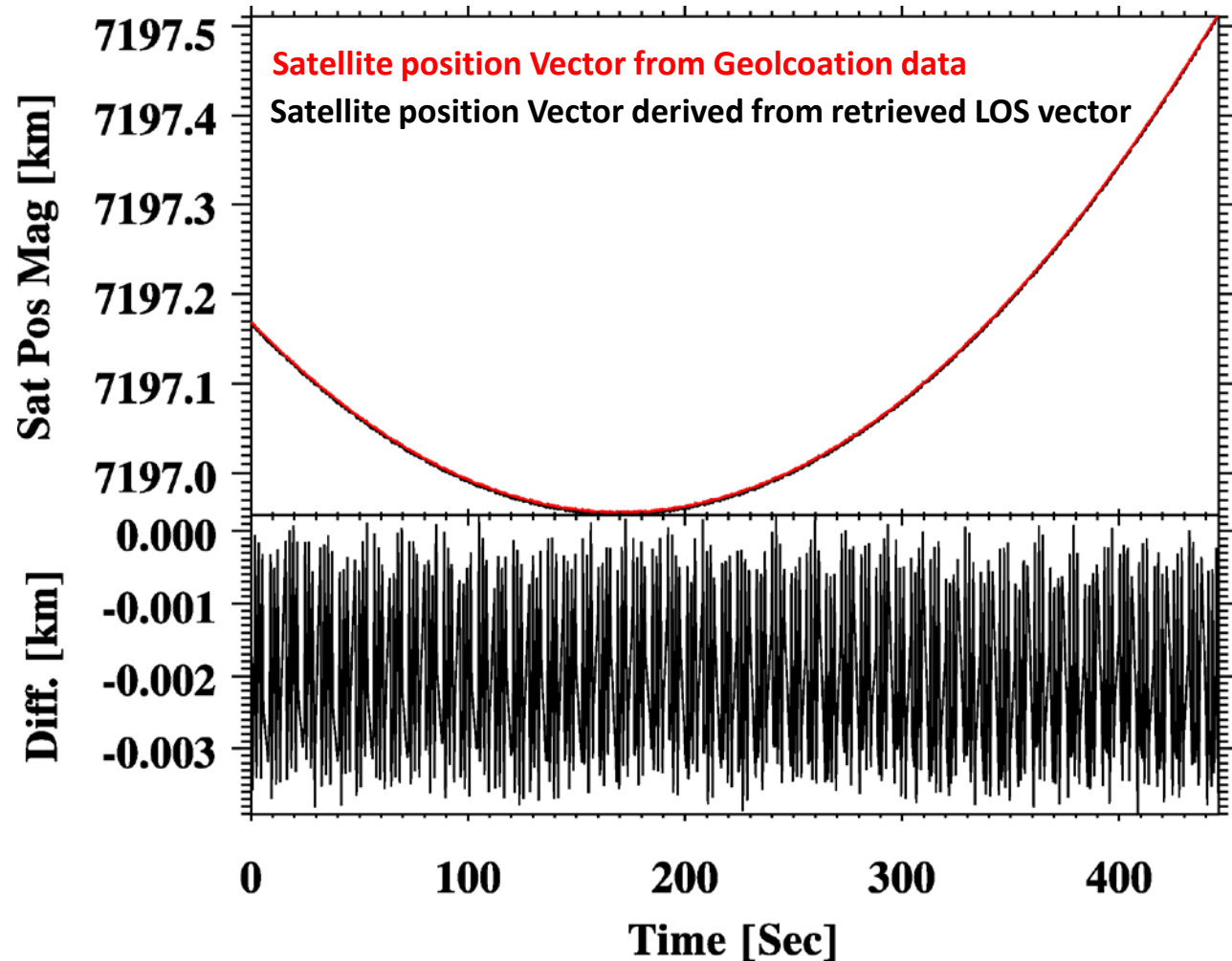
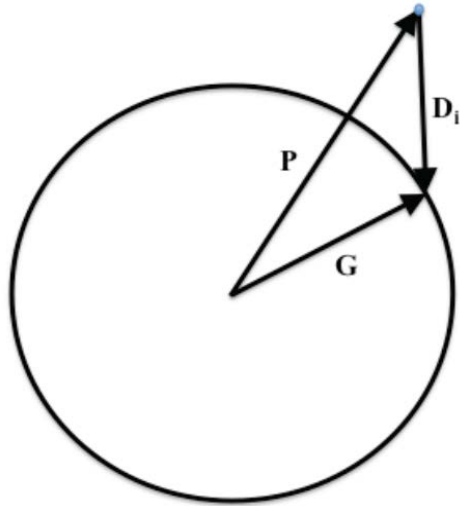
Retrieved CrIS LOS Pointing Vector in ECR or ECEF



D: LOS Pointing Vector
P: Satellite Position Vector
G: FOV position Vector on Earth Ellipsoid

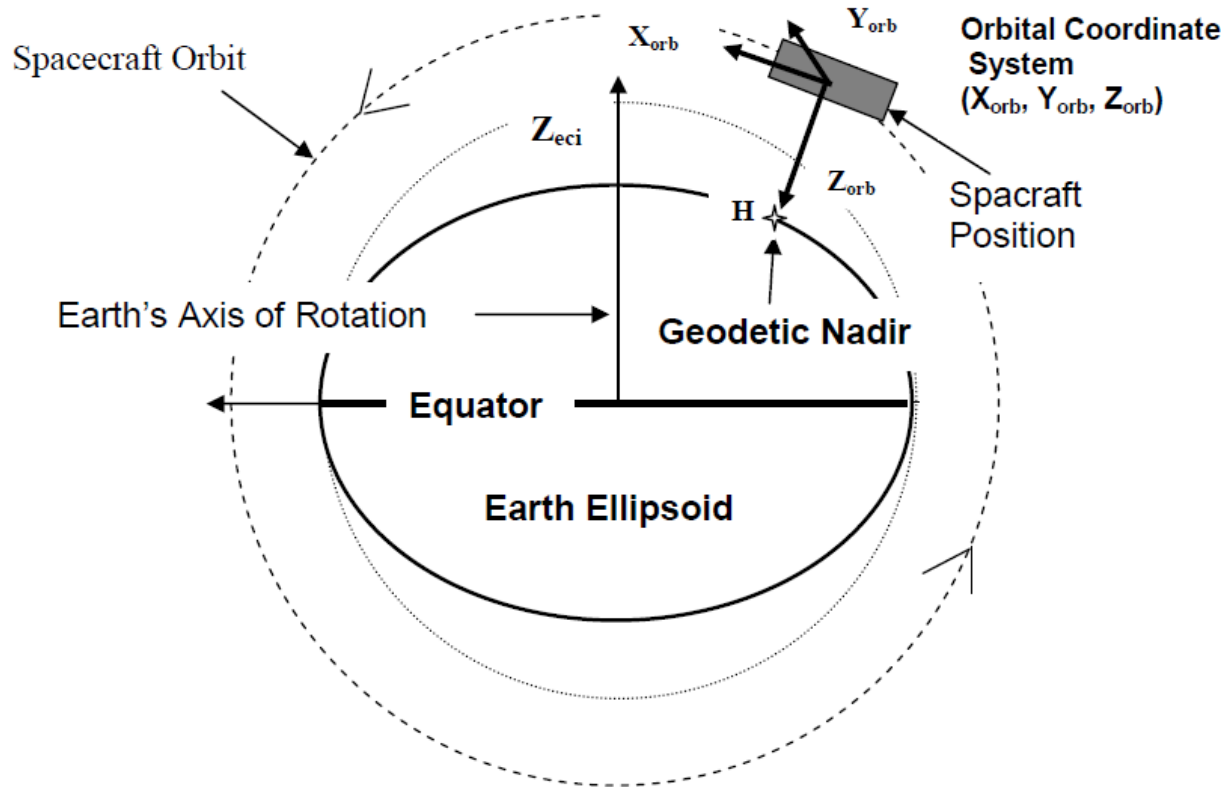
[Zenith, Azimuth, Range] →
 [East, North, Up] in local Cartesian
 (ENU) coordinates

[East, North, Up] + [Lon, Lat] →
 [X, Y, Z] in ECEF



The retrieved LOS vectors **D** can be indirectly validated by comparing two satellite position vector: the ones saved in CrIS geolocation data and the others derived from the retrieved vector **G** and **D** ($P = G - D$).

Build Orbital Coordinate System (OCS) in ECR or ECEF



- P_{sat} and V_{sat} in ECEF are saved in Geolocation dataset
- $P_{sat} \Rightarrow Z$ axis
- Y axis $\Rightarrow \text{crossp}(Z, V_{sat})$
- X axis $\Rightarrow \text{crossp}(Y, Z)$



From ECEF → OCS



Summary [\[edit\]](#)

Triad method From Wikipedia

We consider the linearly independent reference vectors \vec{R}_1 and \vec{R}_2 . Let \vec{r}_1, \vec{r}_2 be the corresponding measured directions of the reference unit vectors as resolved in a body fixed frame of reference. Then they are related by the equations,

$$\vec{R}_i = A\vec{r}_i \quad (1)$$

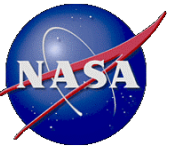
for $i = 1, 2$, where A is a rotation matrix (sometimes also known as a proper [orthogonal matrix](#), i.e., $A^T A = I, \det(A) = +1$). A transforms vectors in the body fixed frame into the frame of the reference vectors. Among other properties, rotational matrices preserve the length of the vector they operate on. Note that the direction cosine matrix A also transforms the cross product vector, written as,

$$\vec{R}_1 \times \vec{R}_2 = A(\vec{r}_1 \times \vec{r}_2) \quad (2)$$

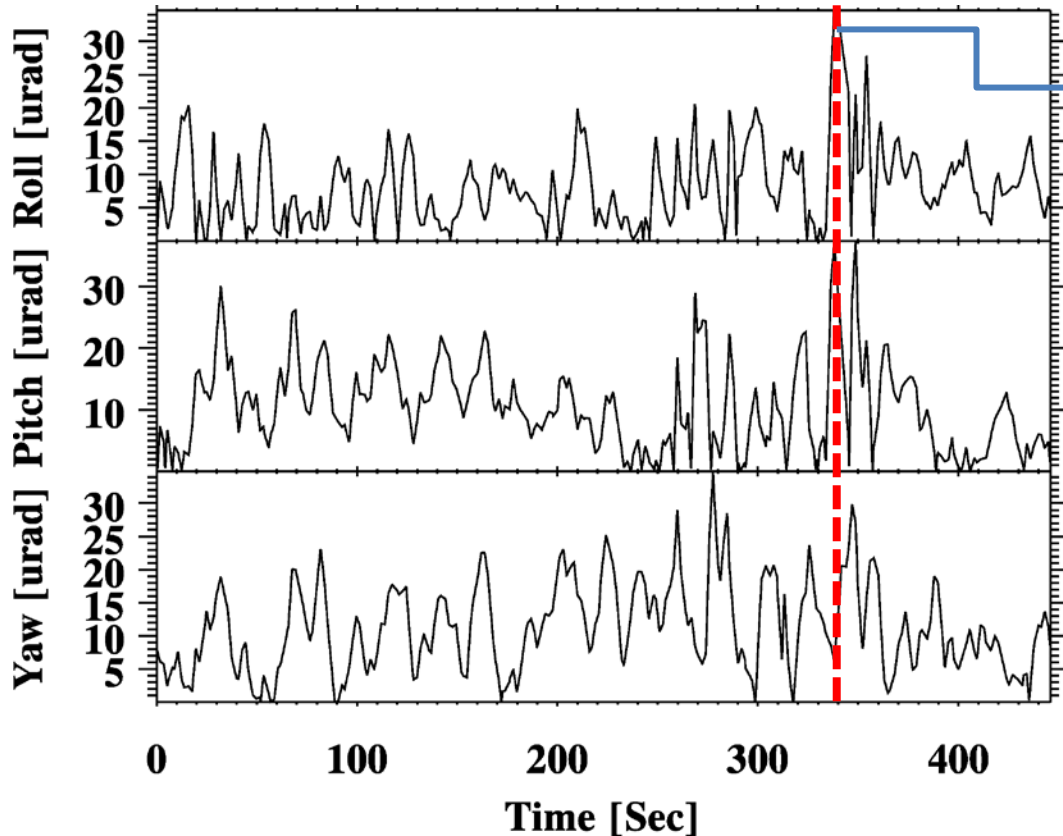
Triad proposes an estimate of the direction cosine matrix A as a solution to the linear system equations given by

$$\begin{bmatrix} \vec{R}_1 \\ \vec{R}_2 \\ (\vec{R}_1 \times \vec{R}_2) \end{bmatrix} = A \begin{bmatrix} \vec{r}_1 \\ \vec{r}_2 \\ (\vec{r}_1 \times \vec{r}_2) \end{bmatrix} \quad (3)$$

**We have Z and X in ECEF, corresponding to [0, 0, 1] and [1, 0, 0] in OCS.
And then we can derive transformation matrix A(ECEF=>OCS)**



From OCS → Spacecraft

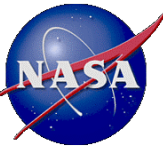


(Roll , Pitch, Yaw) in μrad
 (34.607031 29.572295 12.285854)

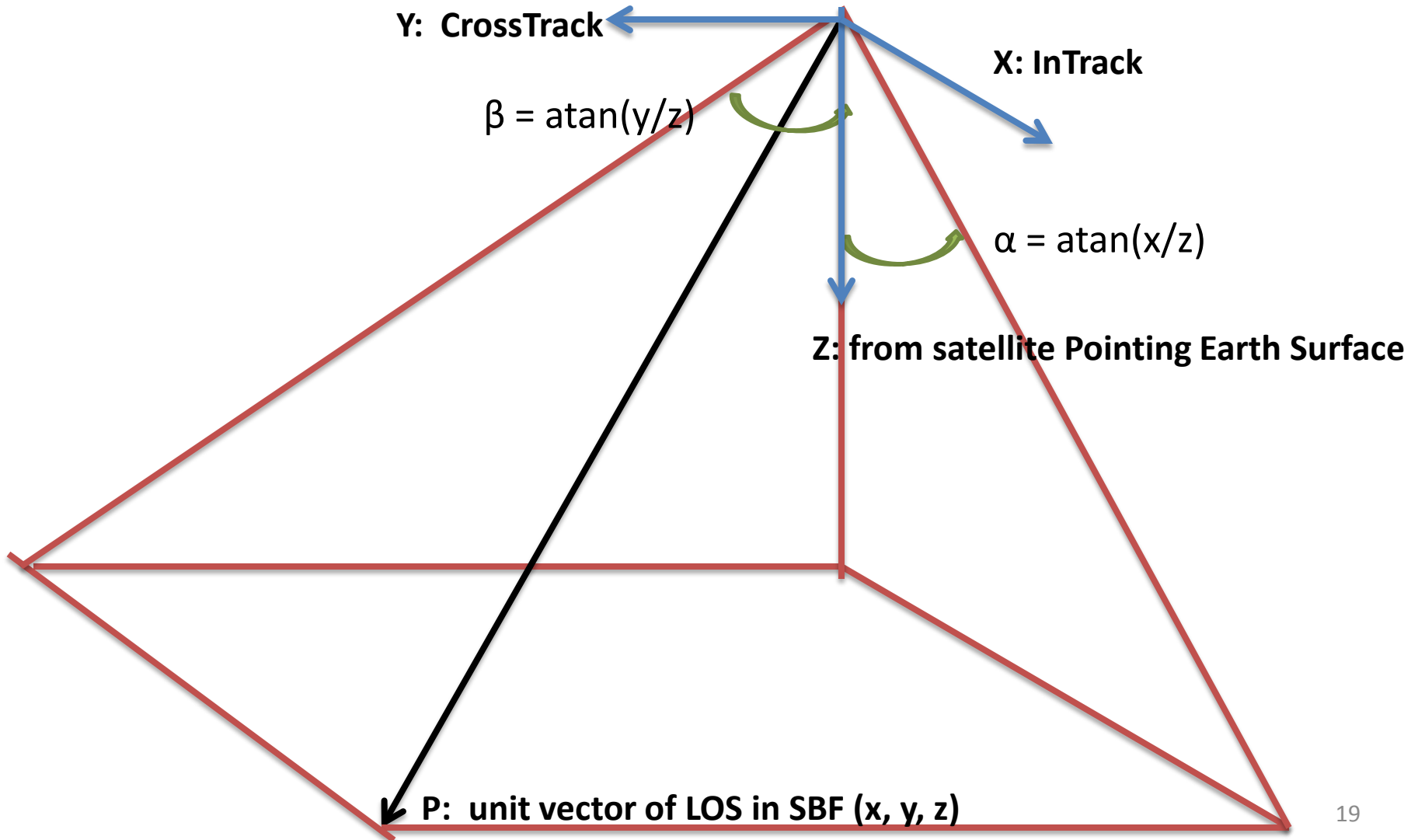
0.9999999995	0.0000122869	-0.0000295723
-0.0000122859	0.9999999993	0.0000346070
0.0000295727	-0.0000346067	0.9999999990

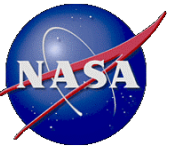
$T_{sc/orb} =$ **The transformation matrix from OCS to Spacecraft coordinates**

$$\begin{bmatrix} \cos \xi_y \cos \xi_p - \sin \xi_y \sin \xi_r \sin \xi_p & \sin \xi_y \cos \xi_p + \cos \xi_y \sin \xi_r \sin \xi_p & -\cos \xi_r \sin \xi_p \\ -\sin \xi_y \cos \xi_r & \cos \xi_y \cos \xi_r & \sin \xi_r \\ \cos \xi_y \sin \xi_p + \sin \xi_y \sin \xi_r \cos \xi_p & \sin \xi_y \sin \xi_p - \cos \xi_y \sin \xi_r \cos \xi_p & \cos \xi_r \cos \xi_p \end{bmatrix}$$

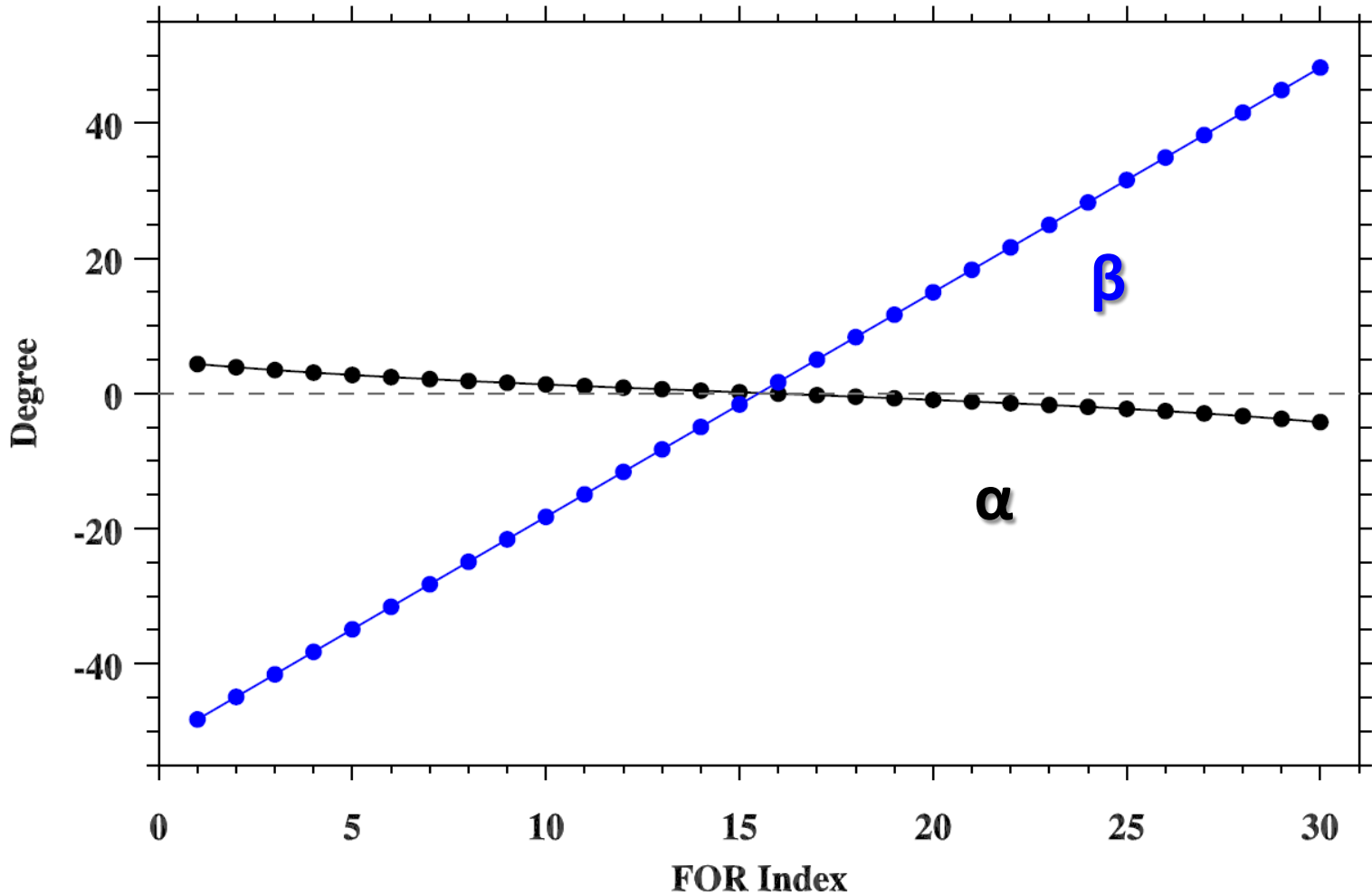


Defining α and β angles of CrIS LOS vector in Spacecraft Coordinate

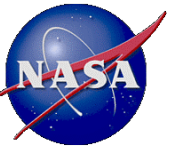




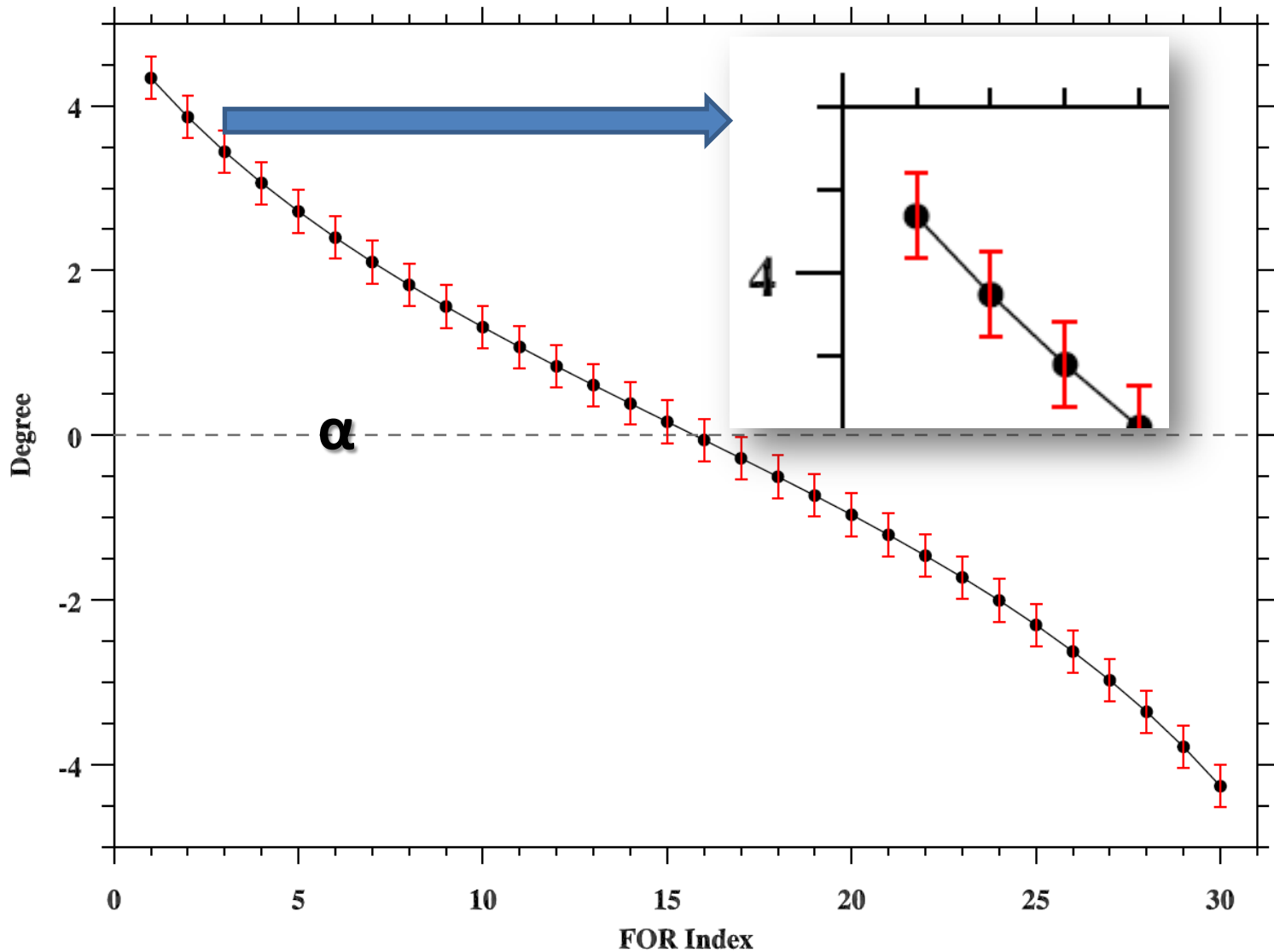
α and β Angles varying with Scan Position (FOV5)



Noted that the yaw patterns of α angles are caused by the Earth Rotation

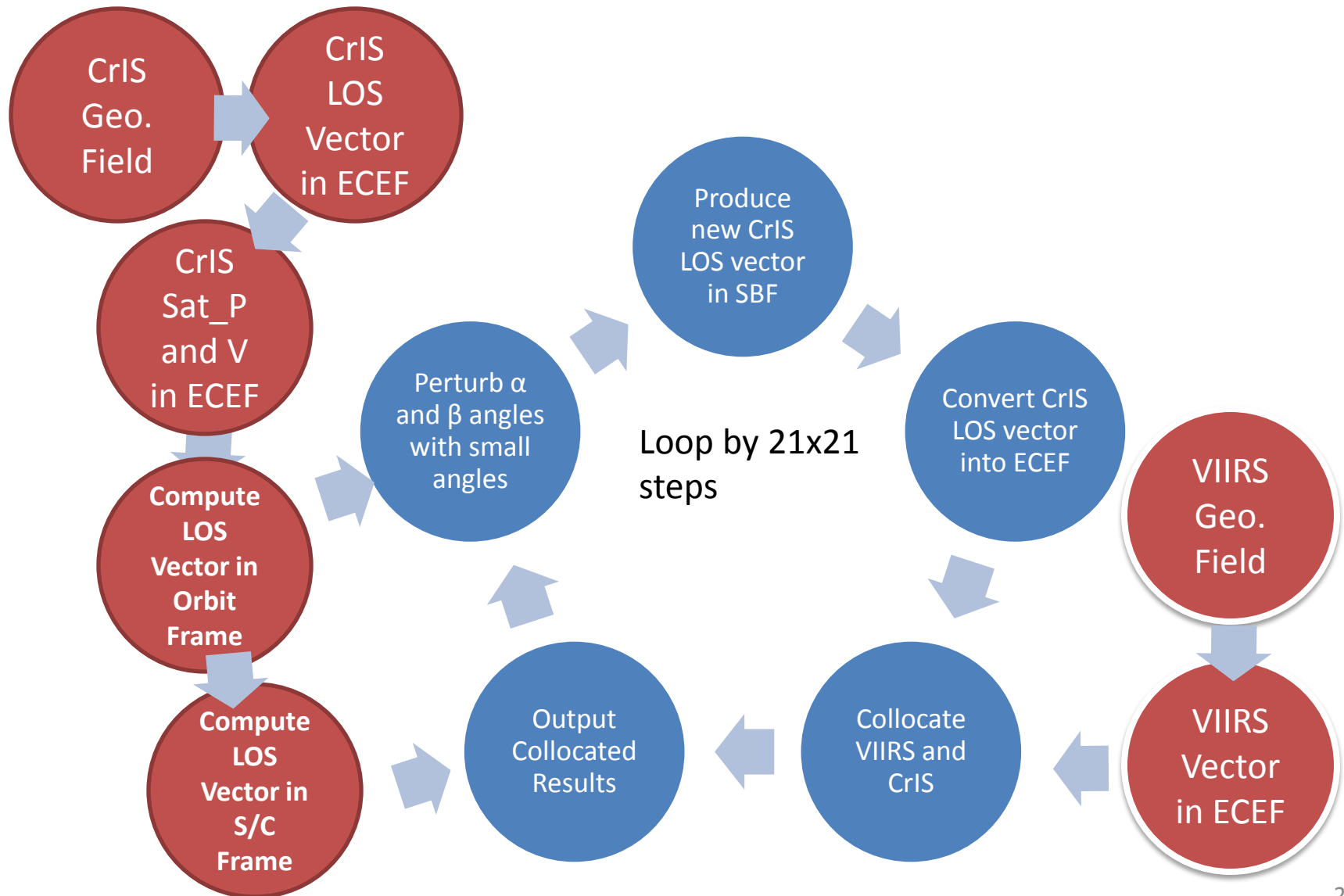


α and β angles are step-by-step perturbed by 21 steps with a angle of $375/833/1000.0$

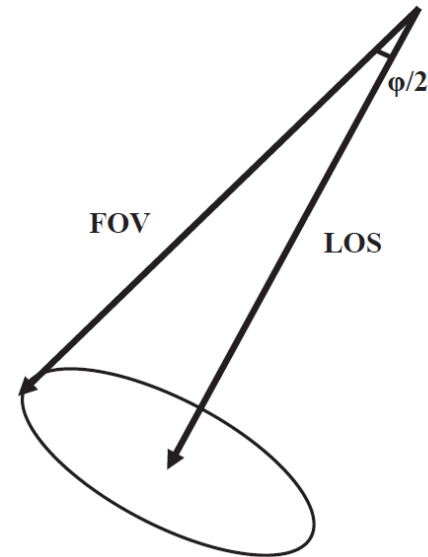
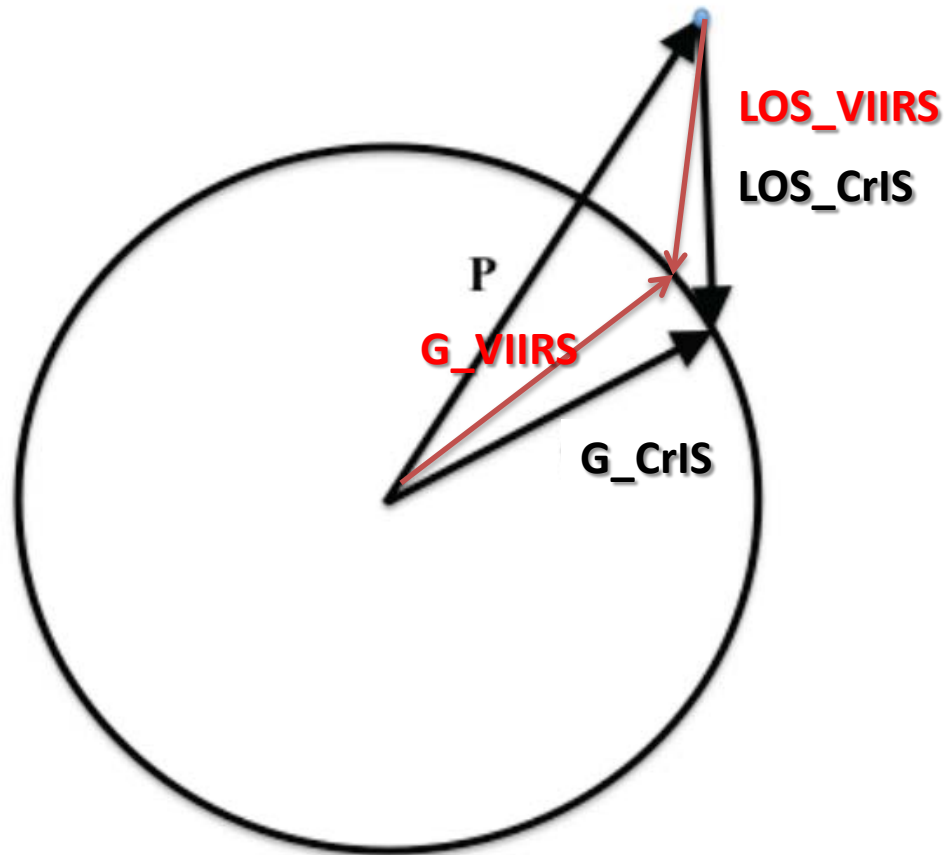




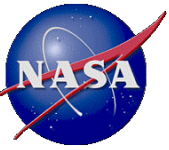
Flowchart for VIIRS-CrIS Geolocation



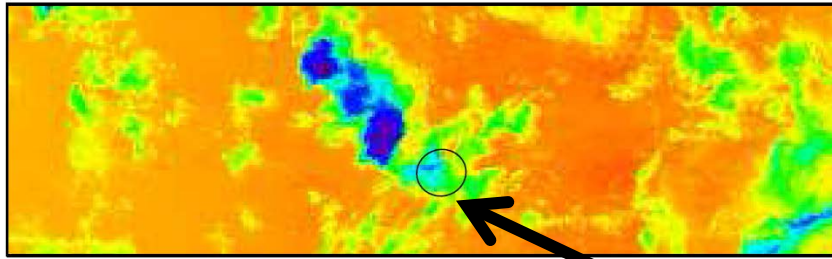
Collocation CrIS with VIIRS



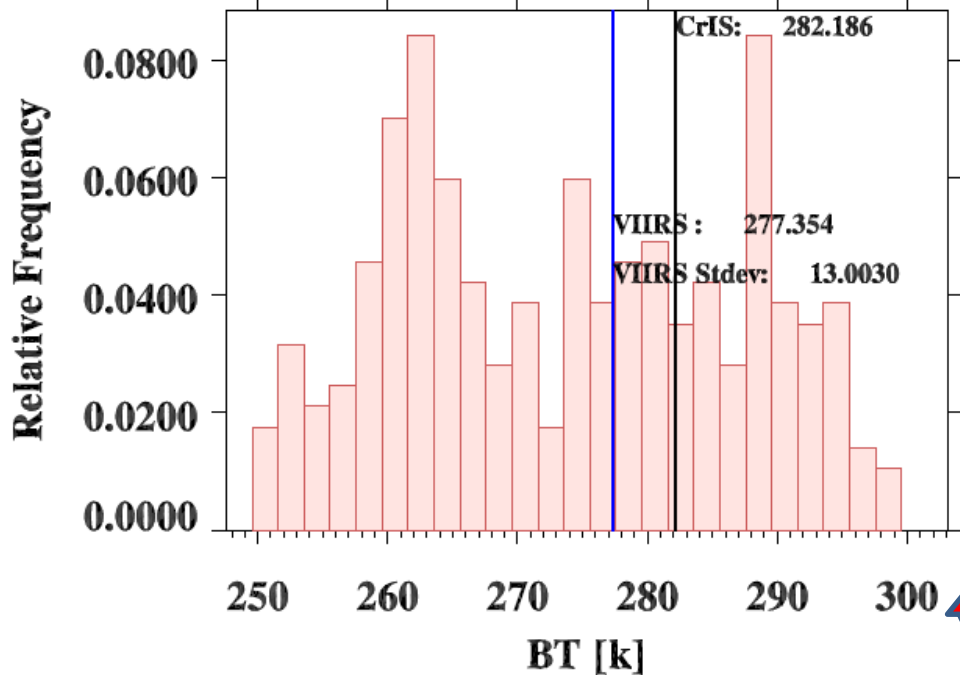
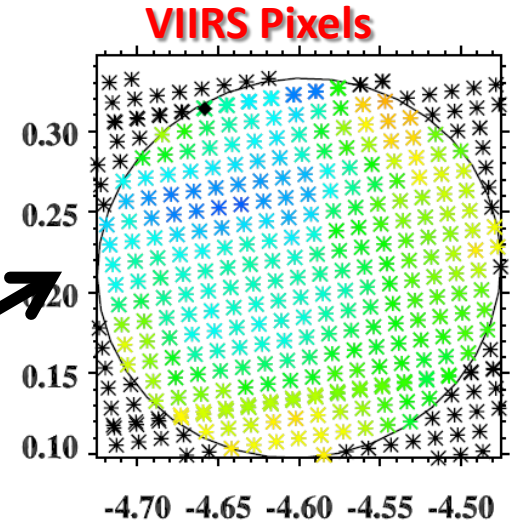
The collocation problem is simplified as, check the angle between two vectors, $[LOS_{VIIRS}, LOS_{CrIS}]$.



Collocating VIIRS with CrIS FOV

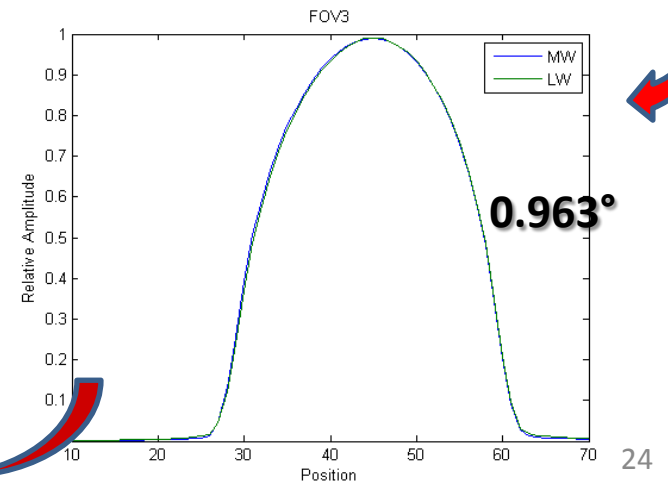


CrIS FOV footprint



Histogram of VIIRS M16 in CrIS FOV

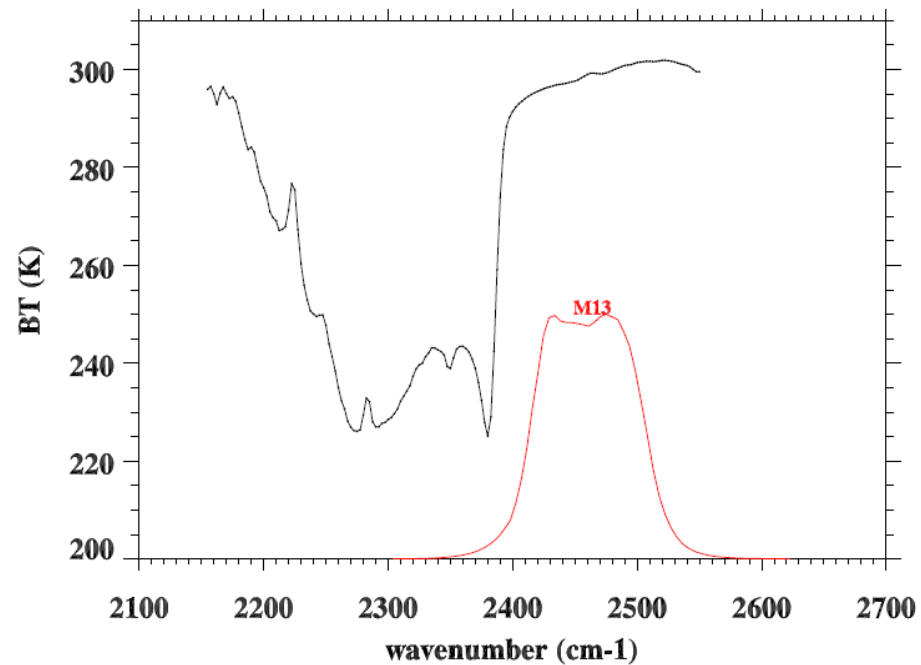
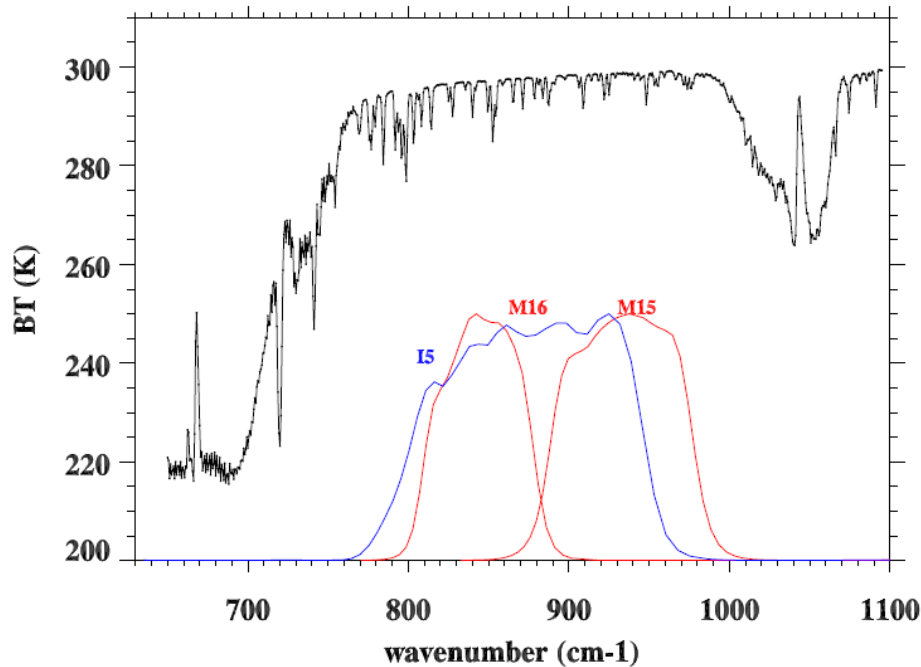
CrIS Spatial Response Function



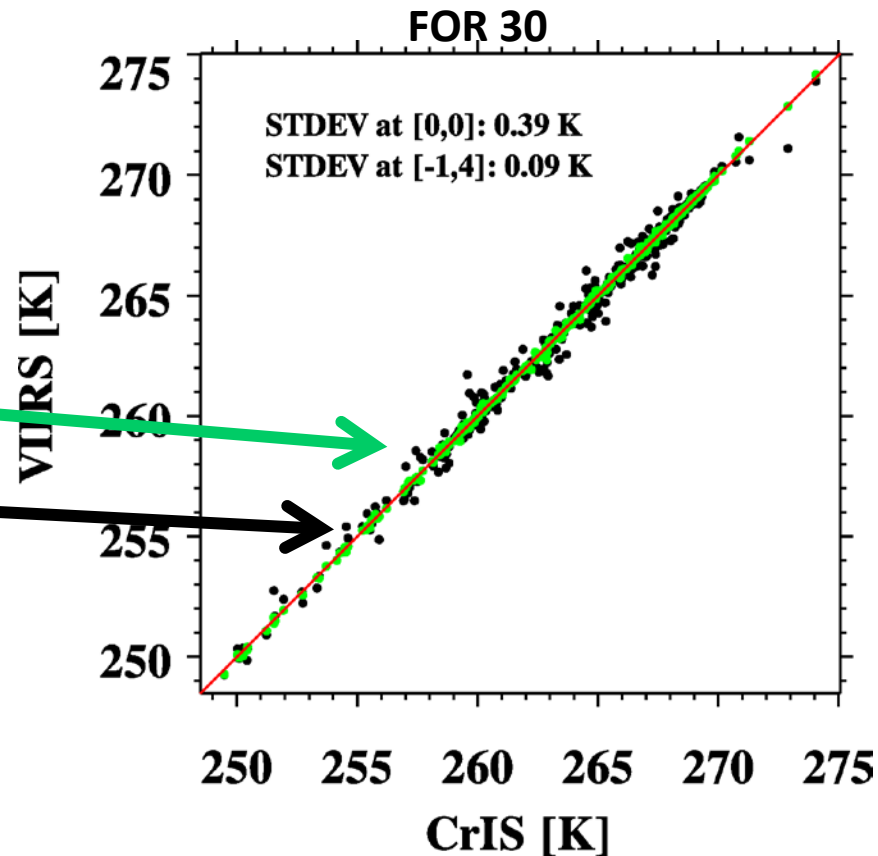
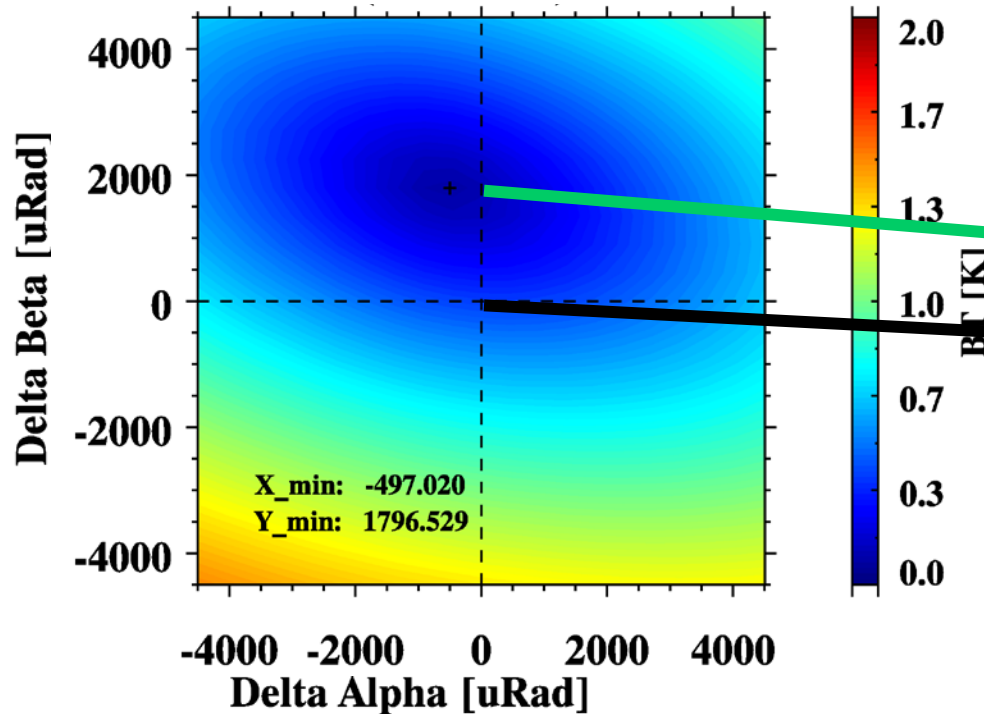
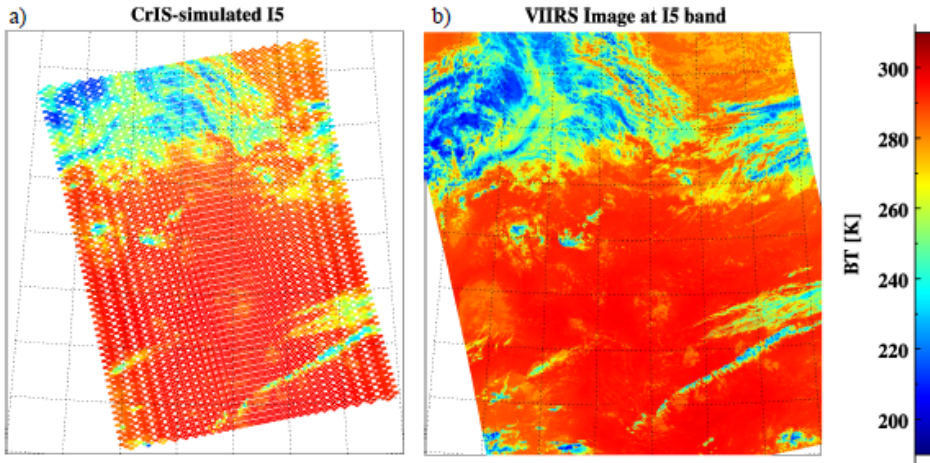
From Mark Esplin

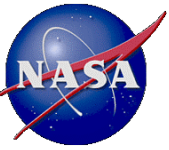
CrIS spectrum is convolved with VIIRS SRFs for I5 band (350m spatial resolution)

$$L_i = \frac{\int_{\nu_1}^{\nu_2} R(\nu) S_i(\nu) d\nu}{\int_{\nu_1}^{\nu_2} S_i(\nu) d\nu}$$

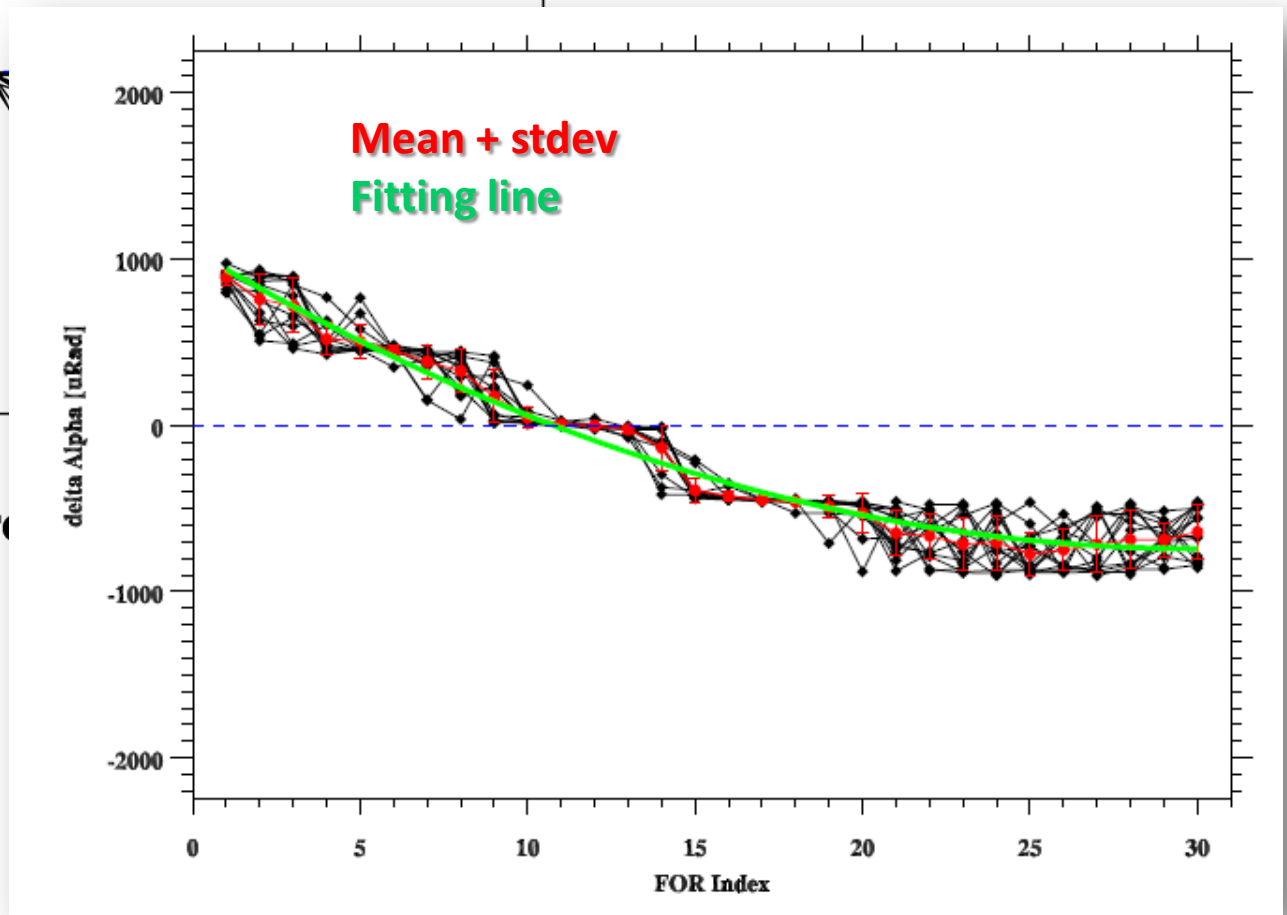
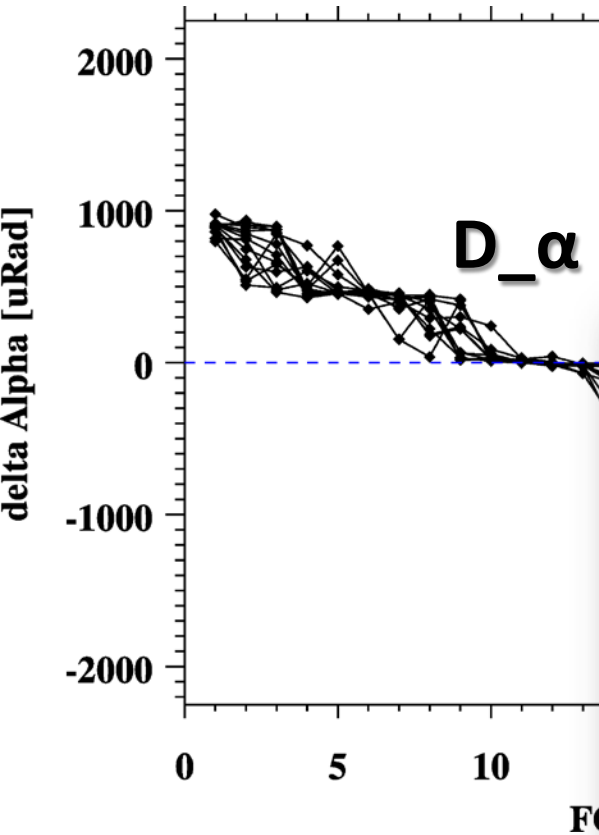


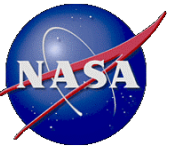
An Example



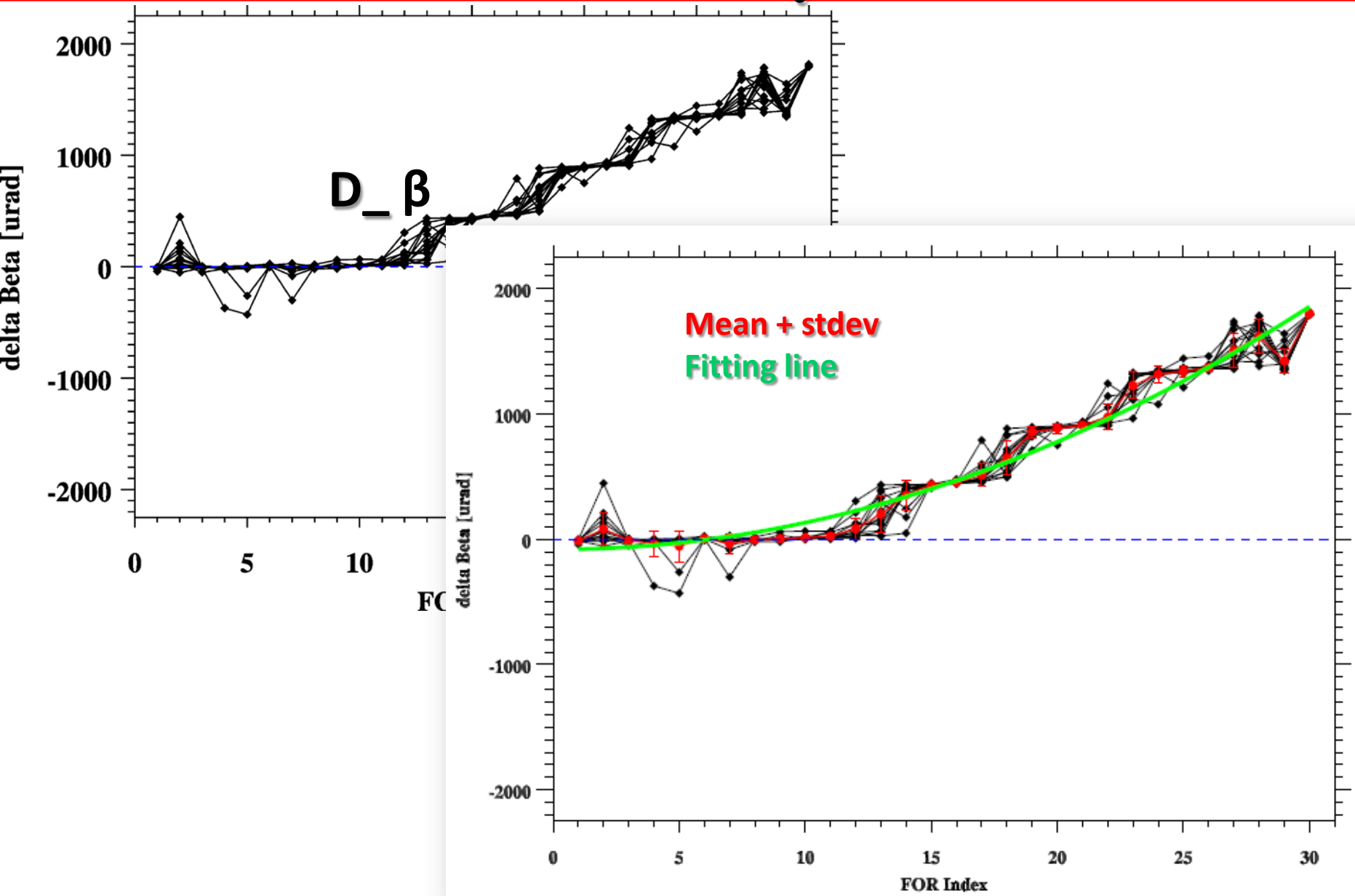


D_α with FOR index based on 15 days' data





D_β with FOR index based on 15 days' data



Retrieval of New Geometric Parameters

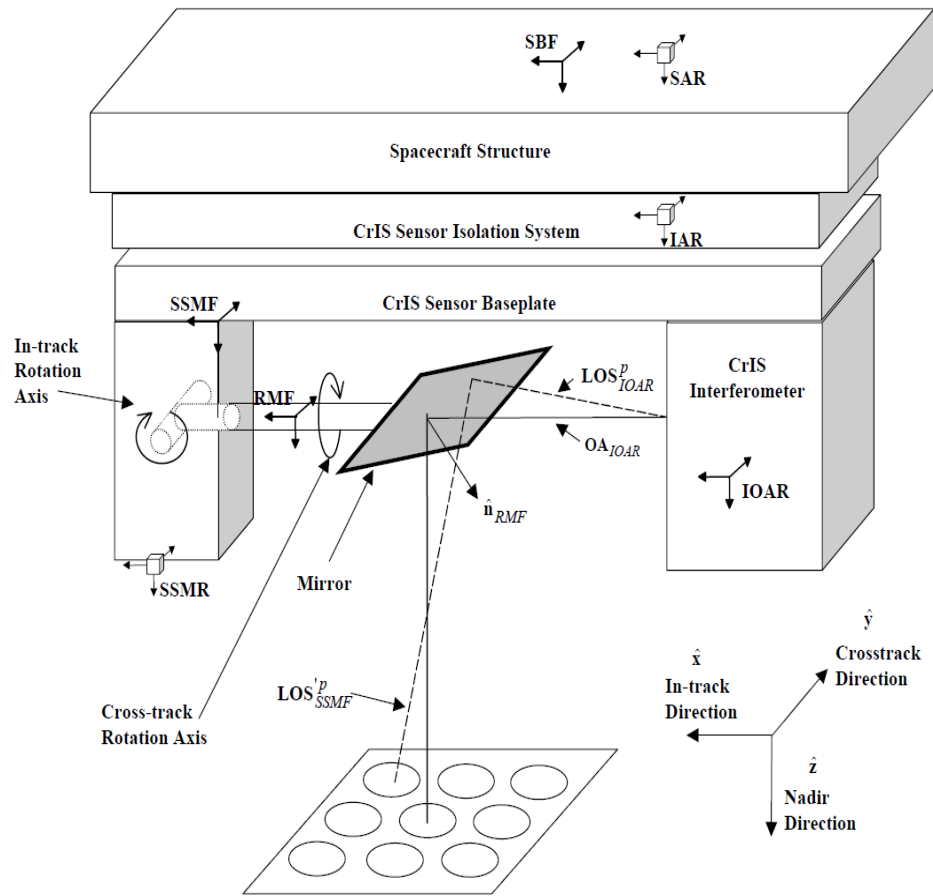


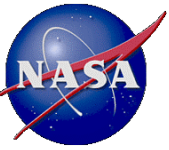
Figure 48: Sensor Algorithm Level Coordinate Systems

Given the assessment results with 60 angles, the best strategy is to retrieve 60 scan mirror rotation angles.

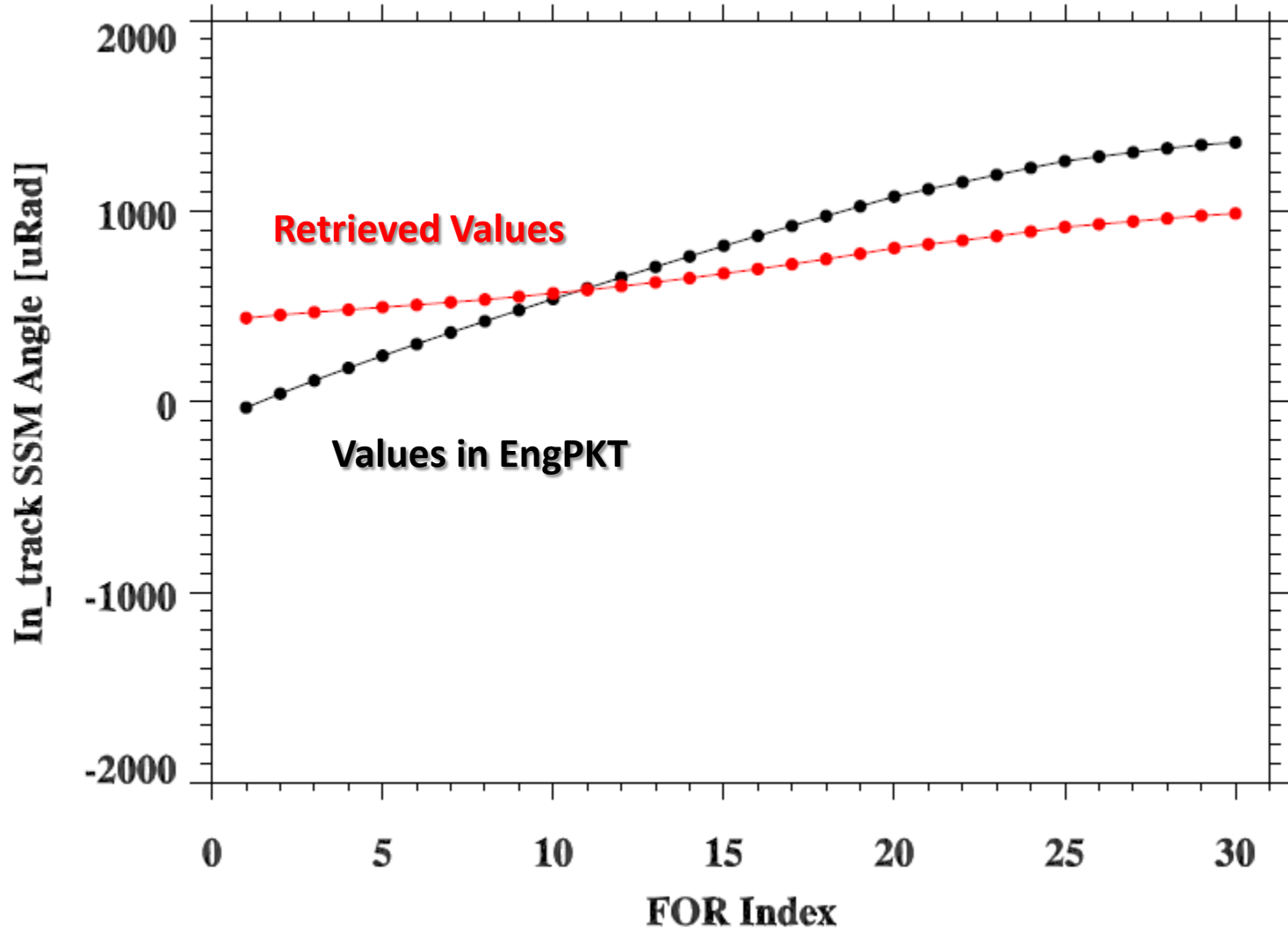
SDR Algorithm Process

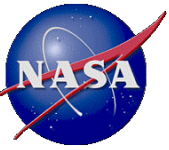
- 1) LOS in IOAR coordinate = ILS parameters (3x3)
- 2) Convert from IOAR to SSMF coordinate **(2 angles)**
- 3) Compute normal to SSM mirror in SSMF (30 Scan Pos) **(60 angles)**
- 4) Apply SSM mirror rotation to get LOS in SSMF coordinate
- 5) Convert from SSMF to SSMR coordinate **(3 angles)**
- 6) Convert from SSMR to IAR coordinate **(3 angles)**
- 7) Convert from IAR to SAR **(3 angles)**
- 8) From SAR=> SBF coordinate **(0 angles)**
- 9) From SBF=> Spacecraft **(3 angles)**

- Retrieved $LOS_{S/C}$ at each scan position on D_α and D_β
- Step-by-step through each matrix to the coordinate SSMF:
 - $LOS_{S/C} \rightarrow LOS_{SBF} \rightarrow LOS_{SAR} \rightarrow LOS_{IAR} \rightarrow LOS_{SMR} \rightarrow LOS_{SSMF}$
- Retrieve the normal vector \mathbf{n}_{SSMF} :
 - $LOS_{SSMF} = LOS'_{SSMF} - 2 * (LOS'_{SSMF} \cdot \mathbf{n}_{SSMF}) \mathbf{n}_{SSMF}$
- The normal vector \mathbf{n}_{SSMF} can be used to retrieve the actual cross-track angle and actual in-track angles of Scan Mirror

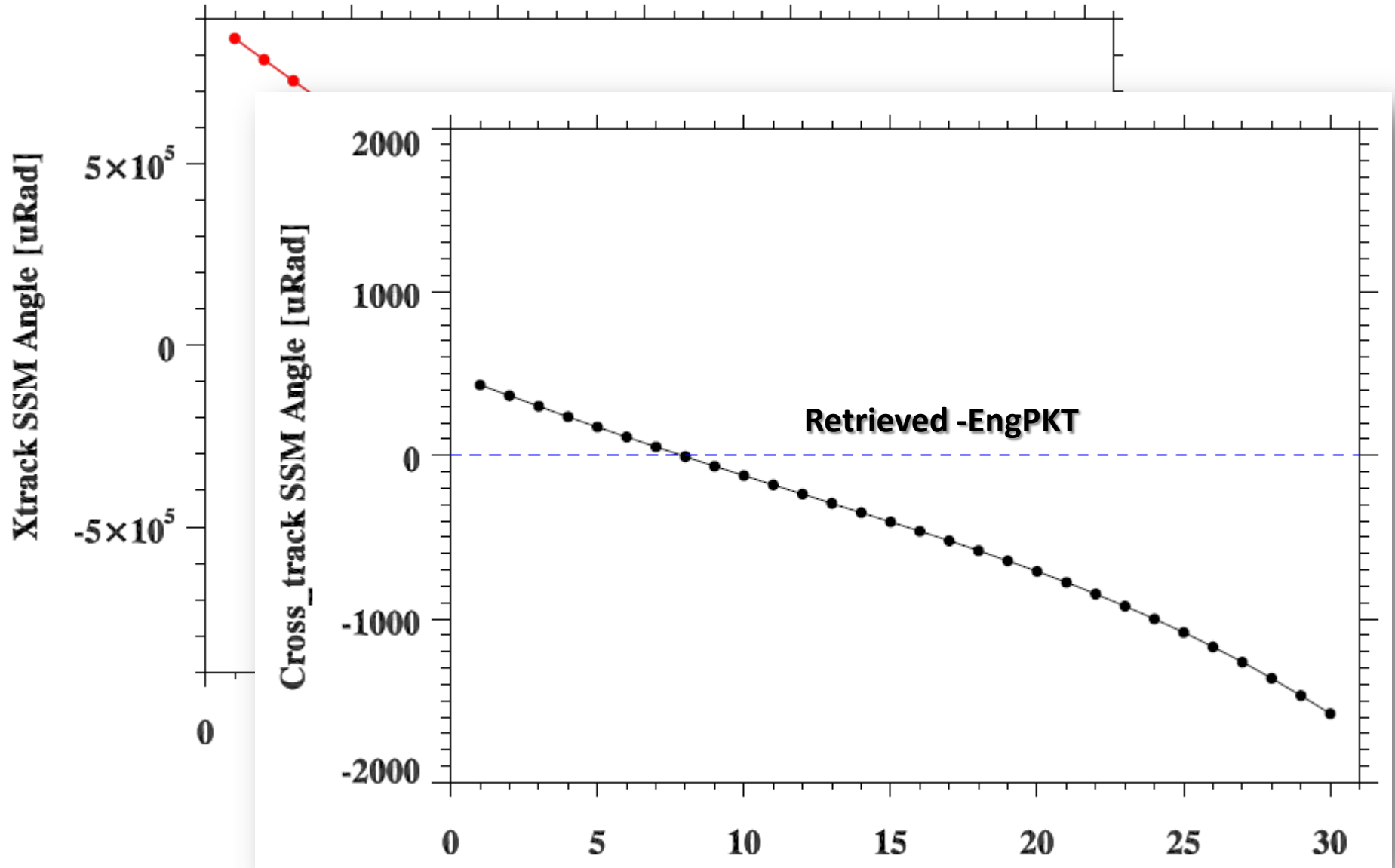


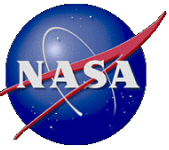
Retrieved SSMF In-track Angles





Retrieved SSMF Cross-track Angles

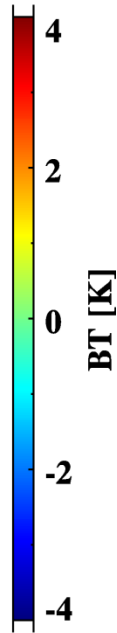
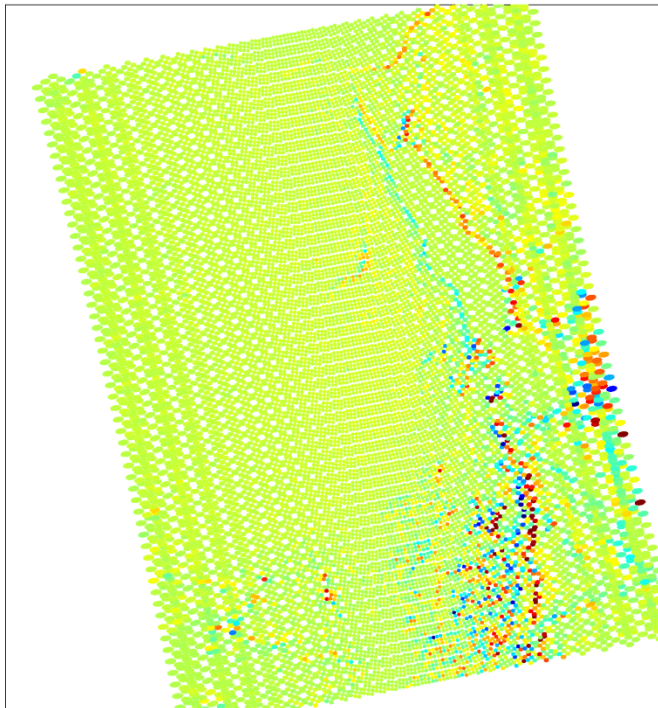




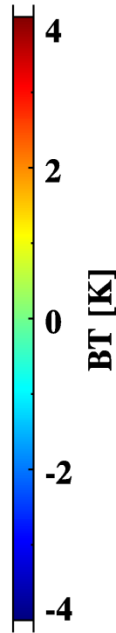
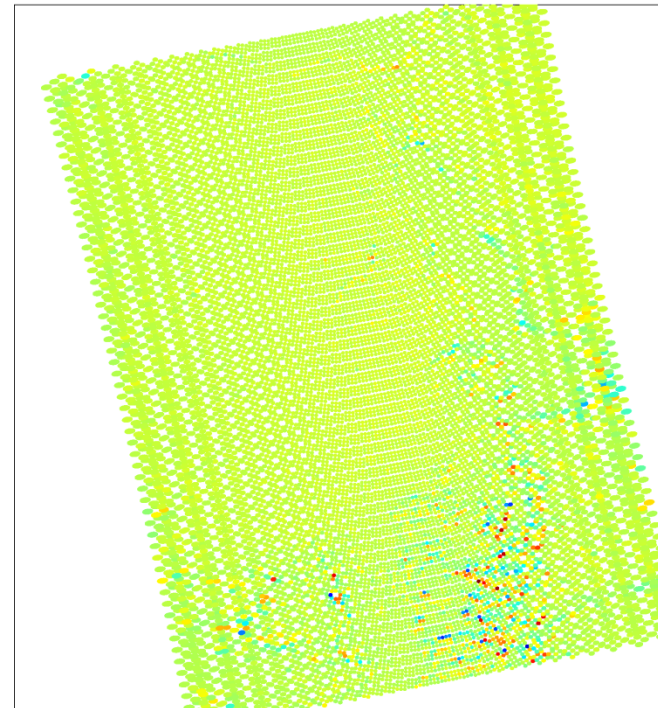
Only correct cross-track direction

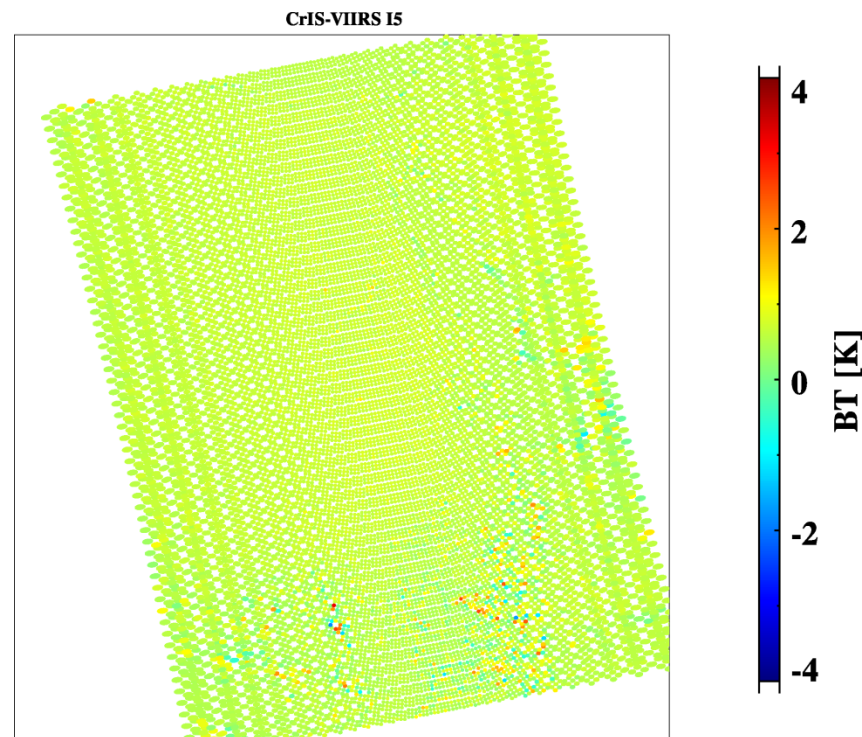
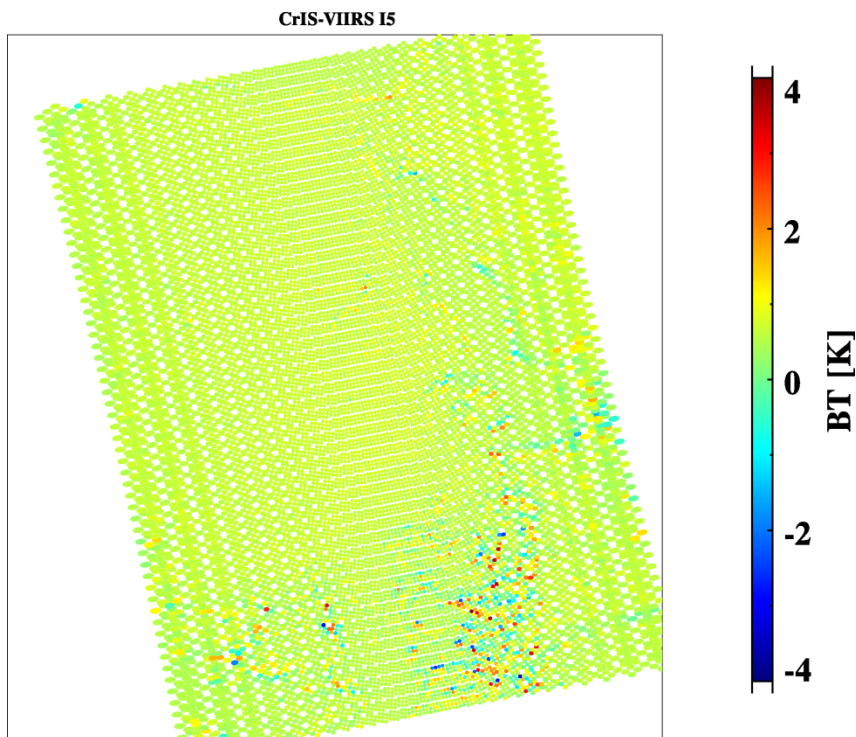


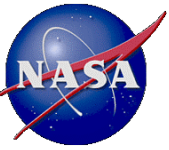
CrIS-VIIRS 15



CrIS-VIIRS 15



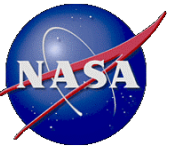


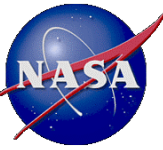


Conclusion and Future Work

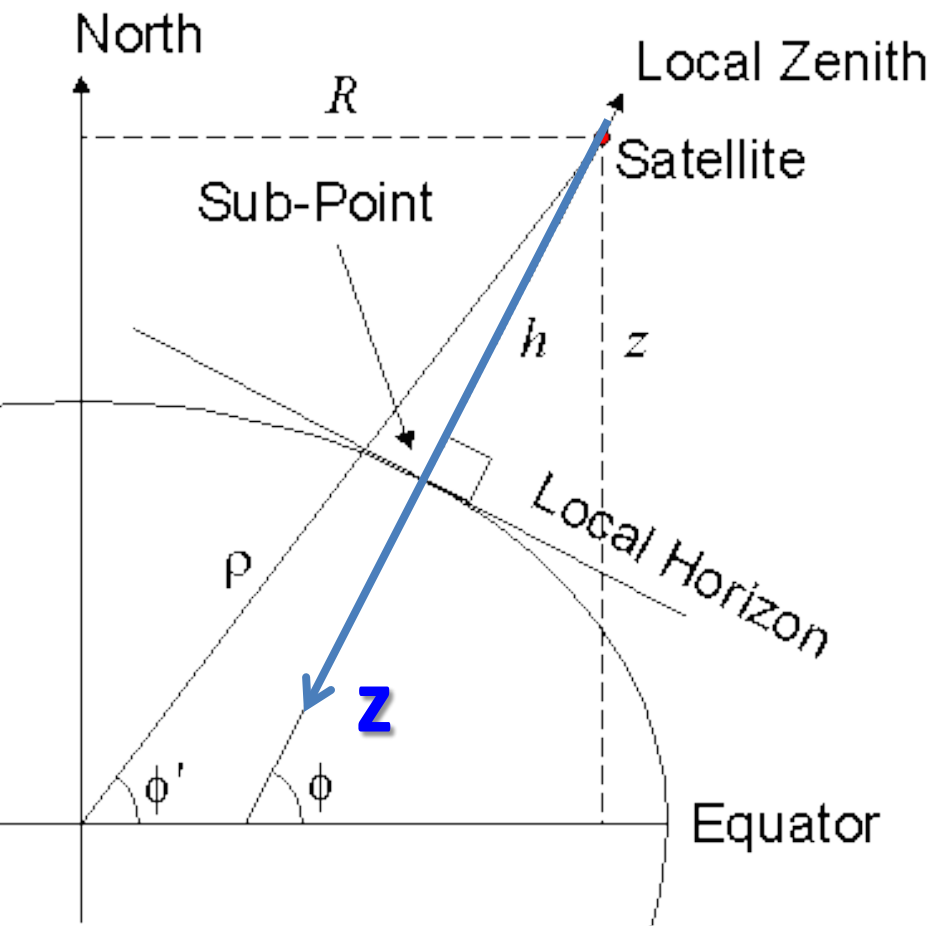


- A new tool is developed to identify the error characteristics of CrIS LOS pointing vector at all scan positions.
- A correction model is developed to retrieve a new set of SSMF scan angles based on assessment results to further improve the geolocation accuracy.
- **Future work**
 - **FOV5 off-axis angle sign change**
 - **Possible angle adjustment**

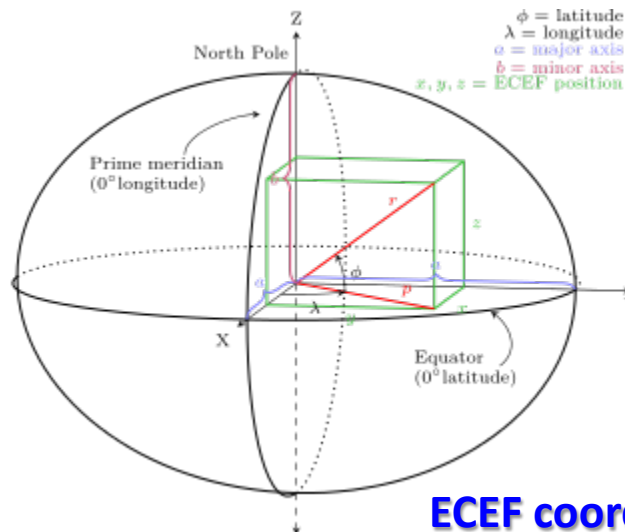




Define Orbital Coordinate System (OCS)



- P_{sat} and V_{sat} in ECEF are saved in SDR
- $p_{sat} \Rightarrow Z$ axis
- Y axis $\Rightarrow \text{crossp}(Z, V_{sat})$
- X axis $\Rightarrow \text{crossp}(Y, Z)$



ECEF coordinates system



STAR JPSS 2015 Annual Science Team Meeting
Session 6c
CrIS Calibration Algorithm Analysis

Daniel L. Mooney

Day 3, August 27 2014



Background

- In late 2014 it became clear we were comparing results based on different low level interpretations of the calibration algorithm in the ATBD
- A list of 11 equations were clearly identified
- We have reduced to five and testing rigorously
- What are we measuring?
 - An extended FOV off-axis interferogram on sensor sampling grid
- What is the product we are delivering?
 - An equivalent on-axis, single ray spectrum corrected for extended FOV apodization and sensor sampling, with responsivity and FIR filter removed by a two point calibration and with non-linearity corrected
 - The details of the process define different algorithms



Five surviving algorithms

	Algorithm	Parameters	Comment
NOAA A1	$N = (SA_u^{-1} \cdot F_{s \rightarrow u} \cdot f_{ATBD}) \cdot \left\{ \frac{S_E - \langle S_{SP} \rangle}{\langle S_{ICT} \rangle - \langle S_{SP} \rangle} \cdot ICT(T, u_{sensor * (1+delta)}) \right\}$	ISA – Sincq, Small N F – Mooney, Small N f – ATBD band_limiting filter ISA = SA ⁻¹	Basline delivered in Jan 1015 ratio before ISA F and ISA reversed calibrated in off-axis grid
CCAST	$N = F_{s \rightarrow u} \cdot ICT(T, u_{sensor}) \cdot f_{raised\ cos} \cdot SA_s^{-1} \cdot f_{raised\ cos} \left\{ \frac{S_E - \langle S_{SP} \rangle}{\langle S_{ICT} \rangle - \langle S_{SP} \rangle} \right\}$	ISA – Sincq, Large N F – double FFT f – raised cos filter	calibration ratio first F & ISA next calibrate on sensor grid
NOAA A2	$N = ICT(T, u_u) \cdot \left\{ \frac{F_{s \rightarrow u} \cdot f_{ATBD} \cdot SA_s^{-1} \cdot f_{ATBD} \cdot \Delta S_1}{F_{s \rightarrow u} \cdot f_{ATBD} \cdot SA_s^{-1} \cdot f_{ATBD} \cdot \Delta S_2} \right\}$	ISA – Sincq, Small N F – Mooney, Small N f – ATBD band_limiting filter	ISA correction and interpolation before calibration ratio small N F and ISA calibrate on user grid
NOAA A3	$N = ICT(T, u_u) \cdot \left\{ \frac{F_{s \rightarrow u} \cdot f_{ATBD} \cdot SA_s^{-1} \cdot f_{ATBD} \cdot \Delta S_1}{F_{s \rightarrow u} \cdot f_{ATBD} \cdot SA_s^{-1} \cdot f_{ATBD} \cdot \Delta S_2} \right\}$	ISA – Sincq, Large N F – Mooney, Large N f – ATBD band_limiting filter	NOAA 2 + large N F and ISA
NOAA A4	$N = ICT(T, u_u) \cdot \frac{F_{s \rightarrow u} \cdot f_{ATBD} \cdot SA_s^{-1} \cdot f_{ATBD} \cdot \left\{ \frac{\Delta S_1}{ \Delta S_2 } \Delta S_2 \right\}}{F_{s \rightarrow u} \cdot f_{ATBD} \cdot SA_s^{-1} \cdot f_{ATBD} \cdot \Delta S_2 }$	Same as NOAA 3 plus rephasing	Remove phase due to ZPD shift before calibration calibrate on user grid

$$\Delta S_1 = FIR^{-1} \cdot (S_E - \langle S_{SP} \rangle)$$

$$\Delta S_2 = FIR^{-1} \cdot (S_{ICT} - \langle S_{SP} \rangle)$$

SA⁻¹ and F are (N x N) maricies, f is a band limiting filter



Formal overview of calibration for all algorithms

- **Formal expression for the FFT of the measured extended FOV interferogram with non-circular FIR before truncation(CrIS processing on spacecraft)**
 - Double integral over angular extent of the Field stop and wavenumber
 - Both the FIR filter and responsivity are inside an integral
 - If H were constant in the pass band it could be easily removed (come back to this later)

$$S_{NCF}[k] = \int_{a1}^{a2} P(a) \cos(a) \int_{u1}^{u2} S_{highres}(u') \rho(u') H(u' \cos(a)) L \text{Sinq}(Lu' \cos(a) - k), N) du' da$$

- **For circular FIR filtering H is already outside the integral(not CrIS)**

$$S_{CF}[k] = H[k] \int_{a1}^{a2} P(a) \cos(a) \int_{u1}^{u2} S_{highres}(u') \rho(u') L \text{Sinq}(Lu' \cos(a) - k), N) du'$$

- **H and responsivity removed by a two-point calibration that implicitly assumes both can be brought out from the interval.**

$$S_{cal}[k] \propto \frac{S_{scene}[k] - S_{space}[k]}{S_{ICT}[k] - S_{space}[k]}$$

- **“Truth” (UW) is defined using single ray on-axis interferograms in user grid(no FOV integration over angle) with a two point calibration**

$$S_{Truth}[k] = \int_{u1}^{u2} S_{highres}(u') \rho(u') L \text{Sinq}(Lu' - k), N) du'$$



Unpeeling the Onion

- **March 12 2014, UW proposed correction for non-circular FIR**
- **April 9 2014, STAR Alternate method to correct non-circular FIR**
- **May 28 2014, UW, working definition of Truth**
- **Dec 17 2014, CCAST compared to NOAA using clear earth scenes**
- **Sept 10 2014, LL & Logistikos, correcting ATBD resampling**
- **Sept 10 2014, LL, Sinc decimation properties**
- **Sept 24 2014, UW, results for non-circular FIR ringing correction**
- **Oct 10, 2014, STAR, Optimized ringing correction using resampling**
- **Jan 14 2015, LL, Exact F computation using analytic approach**
- **Jan 28 2015, Chen & Han, SA correction of gas cell data picks large N periodic Sinc as basis for SA^{-1}**
- **Feb 25 2015, Logistikos, Phase correction before calibration NOAA A4, with half the computation time**
- **March 11 2015, LL, Full simulation side by side comparisons**
- **March 25 2015, STAR, comparison studies rang NOAA 4 highest**
- **April 15 2015, STAR, Fill LBL simulation (ECMWF) compared to clear ocean**
- **April 29 2015, UW, Obs minus calc find NOAA 3 & 4 best match**
- **June 15 2015, LL, Full simulation shows little difference long or short N**



Compare NOAA A4 with CCAST using full up simulation

- **Simulation**
 - Interferograms for scene, ICT, cold space for LBL spectra
 - Full accurate integration of extended FOV
 - Accurate calculation of SA and F transformation matrices
- **Full algorithm based calibration**
- **Effects considered**
 - Computational methods for F and ISA
 - Circular and Non-circular filtering
 - Long and Short Sinq(Lu-k,N)
 - Aliasing
 - band pass filter settings



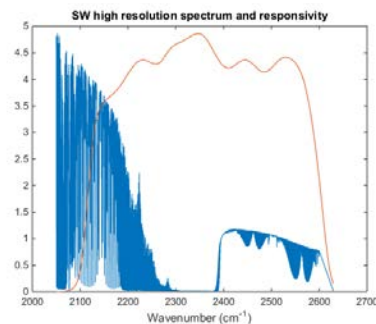
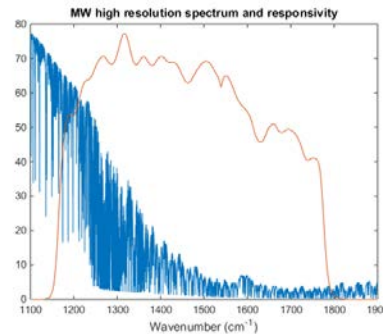
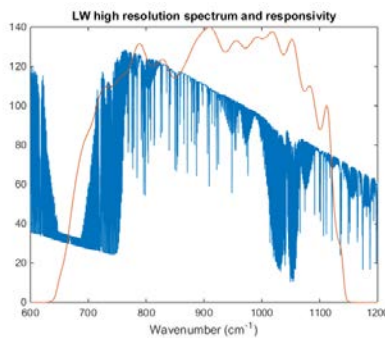
Simulated interferograms

- LBL spectrum & interpolated UW responsivity
- Compute scene, ICT, space for all FOV for each option
- Three types of interferograms: on-axis user, on-axis sensor, extended FOV sensor
- Full double integration over u and field stop for extended FOV

Idealized "Truth"
$$I_u[n] = \sum_{m=1}^M W_m S_{LBL}(u_m) \rho(u_m) e^{i2\pi n \Delta x_0 u_m} \Delta u_{LBL}$$

$$I_s[n] = \sum_{m=1}^M W_m S_{LBL}(u_m) \rho(u_m) e^{i2\pi n \Delta x u_m} \Delta u_{LBL}$$

CrIS Measured
$$I_x[n] = \sum_1^{128} w_q P(a_q) \cos(a_q) \sum_{m=1}^M W_m S_{LBL}(u_m) \rho(u_m) e^{i2\pi n \Delta x u_m \cos(a_q)} \Delta u_{LBL}$$





Improved transformation matrices(2015)

- SA⁻¹ matrix corrects extended FOV spectral distortion

$$SA[k, k'] = \int_{a_{\min}}^{a_{\max}} P(a) \int_{z_1}^{z_2} \text{Sinc}(z - k, N) \text{Sinc}^*(z / \cos(a) - k', N) dz da$$

- F matrix maps from sensor grid (L/N) to user grid (L'/N)

$$F[k, k'] = \int_{z_1}^{z_3} \text{Sinc}(z - k, N) \text{Sinc}^*(zL'/L - k', N) dz$$

- High accuracy methods of computation developed

type	z1	z2	z3	N	error
SA short sinc	uLcos(a)	Z1+Nb	na.	Nb	Exact analytic 1.e-14
SA long sinc	uLcos(a)-Nb	Z1+2Nb	na.	NbNd	GL quadrature 1.e-12
F long sinc	0	NbNd	uL+Nb	Nb	Exact analytic 1.e-14

Band	Decimated interferogram length Nb	Decimation factor Nd	Long interferogram length Nb*Nd
LW	864	24	20736
MW	1050	20	21000
SW	797	26	20722



SA⁻¹ correction is a matrix operation LW example

Short N=864
Decimated by 24

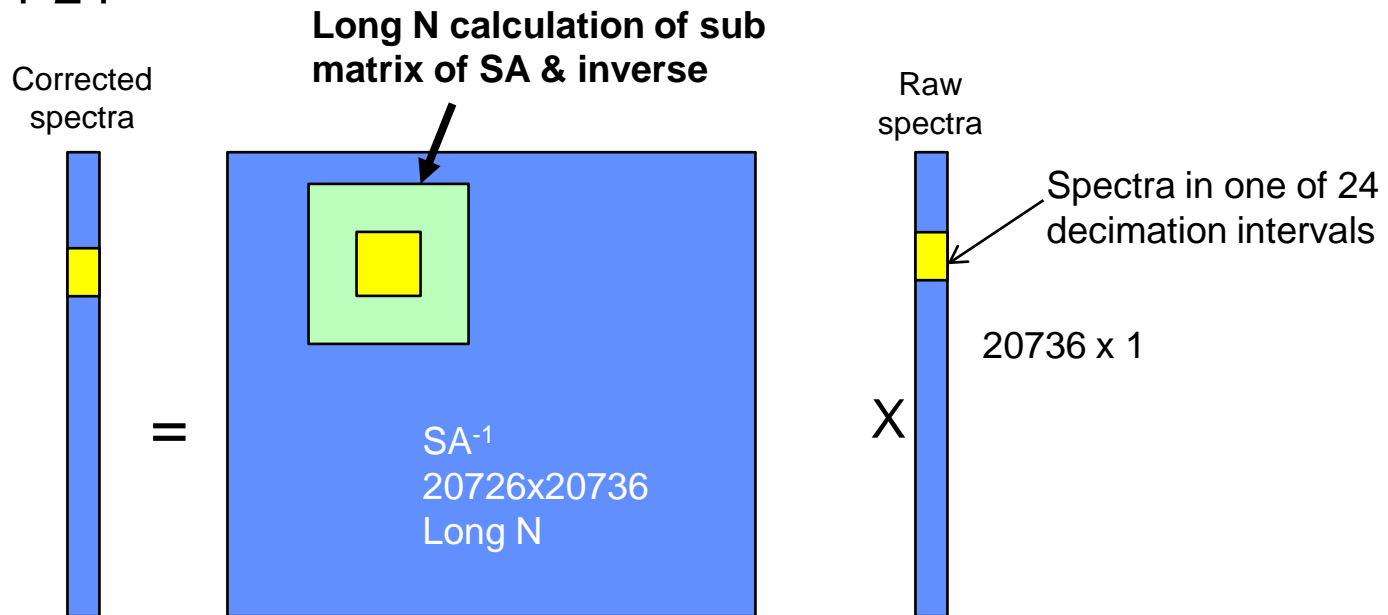
Corrected spectra = SA⁻¹ X Raw spectra

864x863

864 x 1

RINGING EFFECTS AT THE EDGES

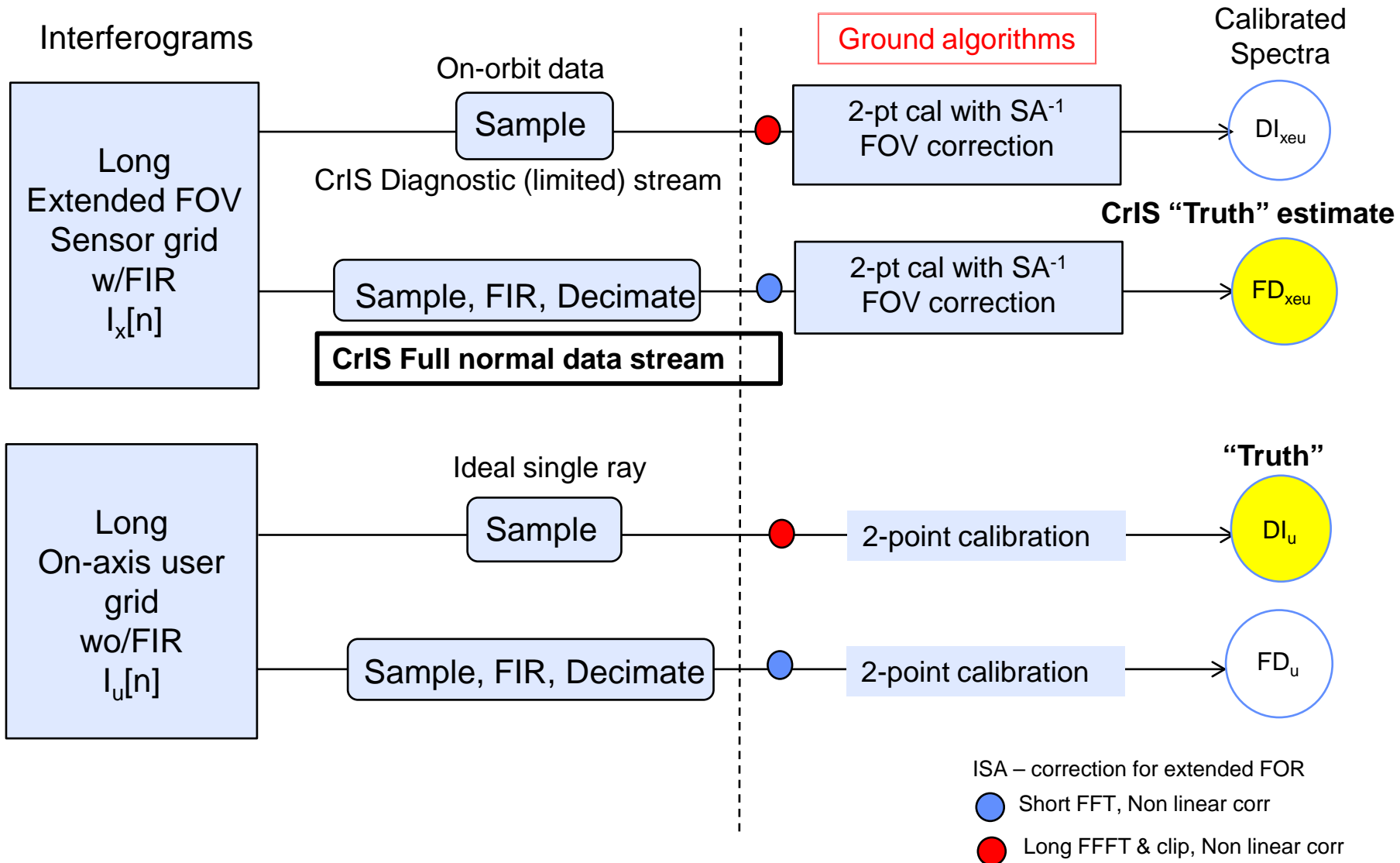
Long N= 864*24



Use bigger matrix to reduce edge effects.
20736²=429,981,696 double integration matrix
elements is prohibitive (72 C_CPS for 36 hours)



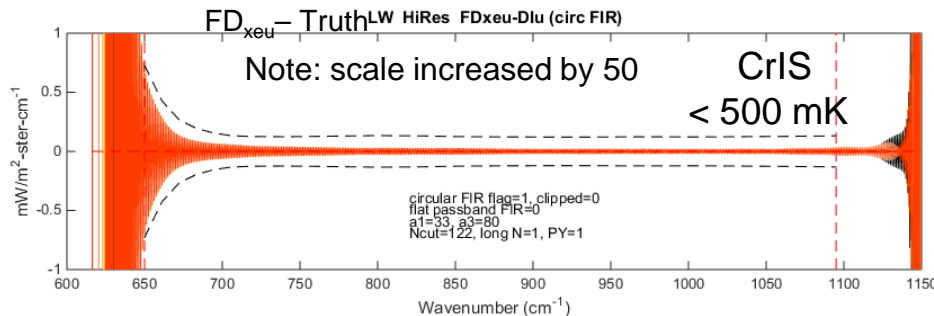
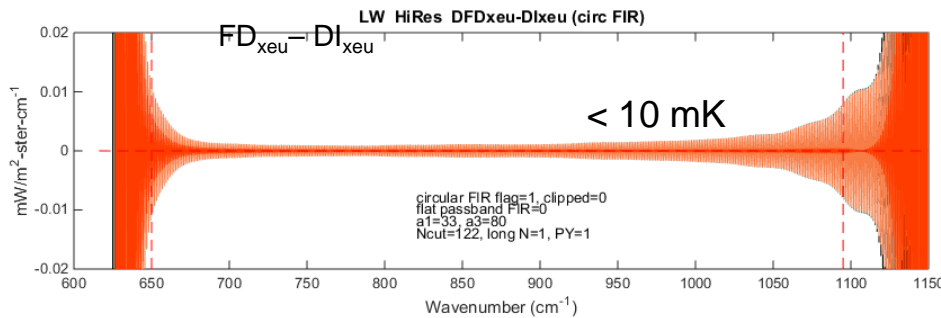
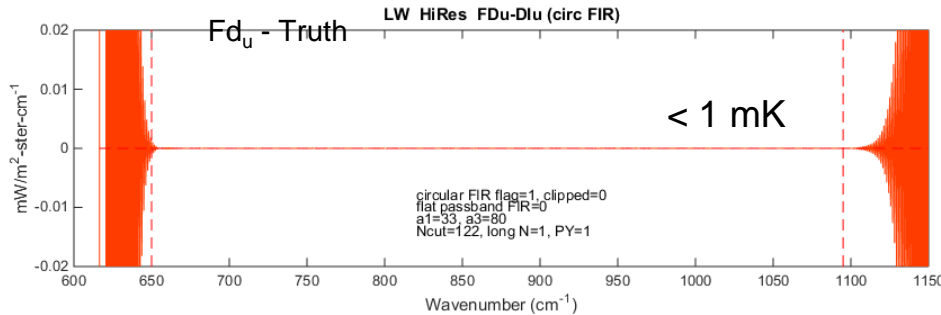
Simulated process to convert extended FOV sensor grid to calibrated on-axis user grid spectra





Even with a circular FIR we have an error

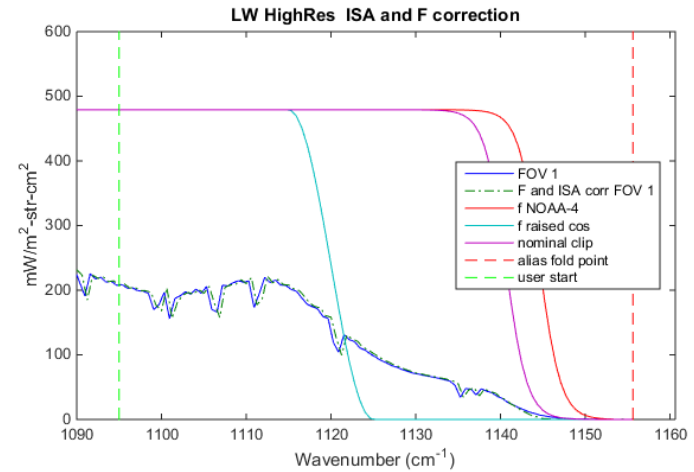
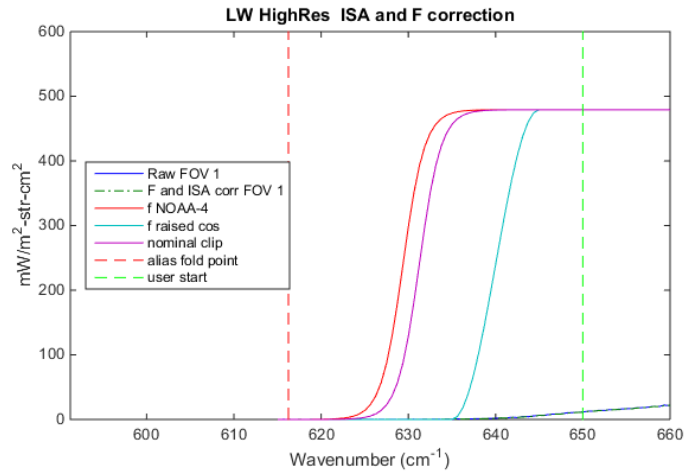
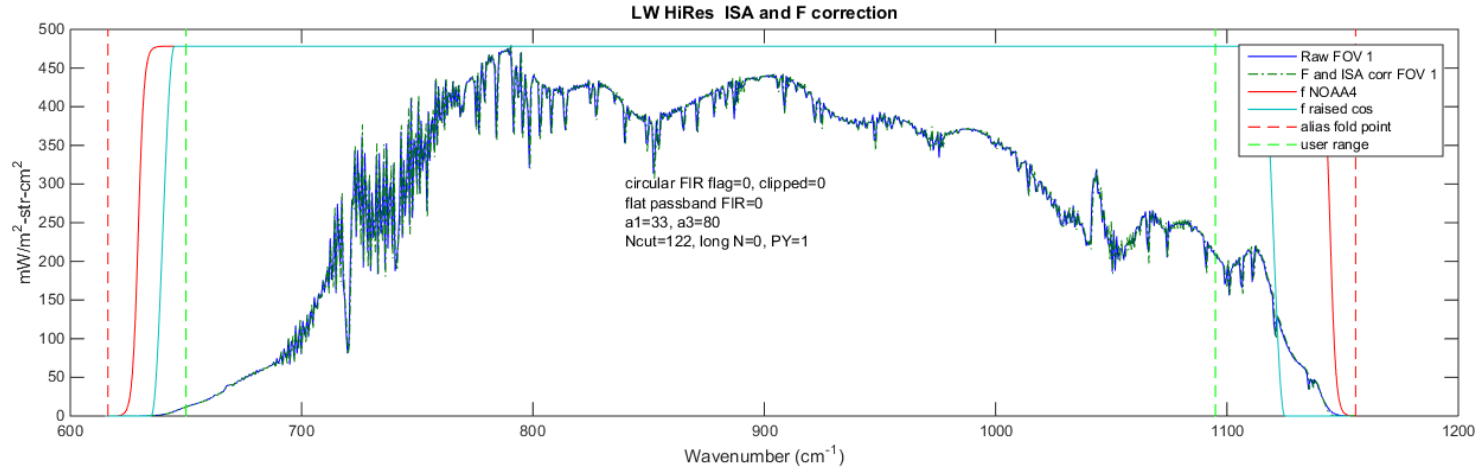
FD- Truth NOAA A4



- FD on-axis: convolution theorem give nearly zero error
- extended FOV FD compared to extended FOV DI
- Bottom: extended FOV FD compared to truth(on-axis D) (THIS IS CrIS)
 - This is the expected ringing due to the full calibration and comparison with truth



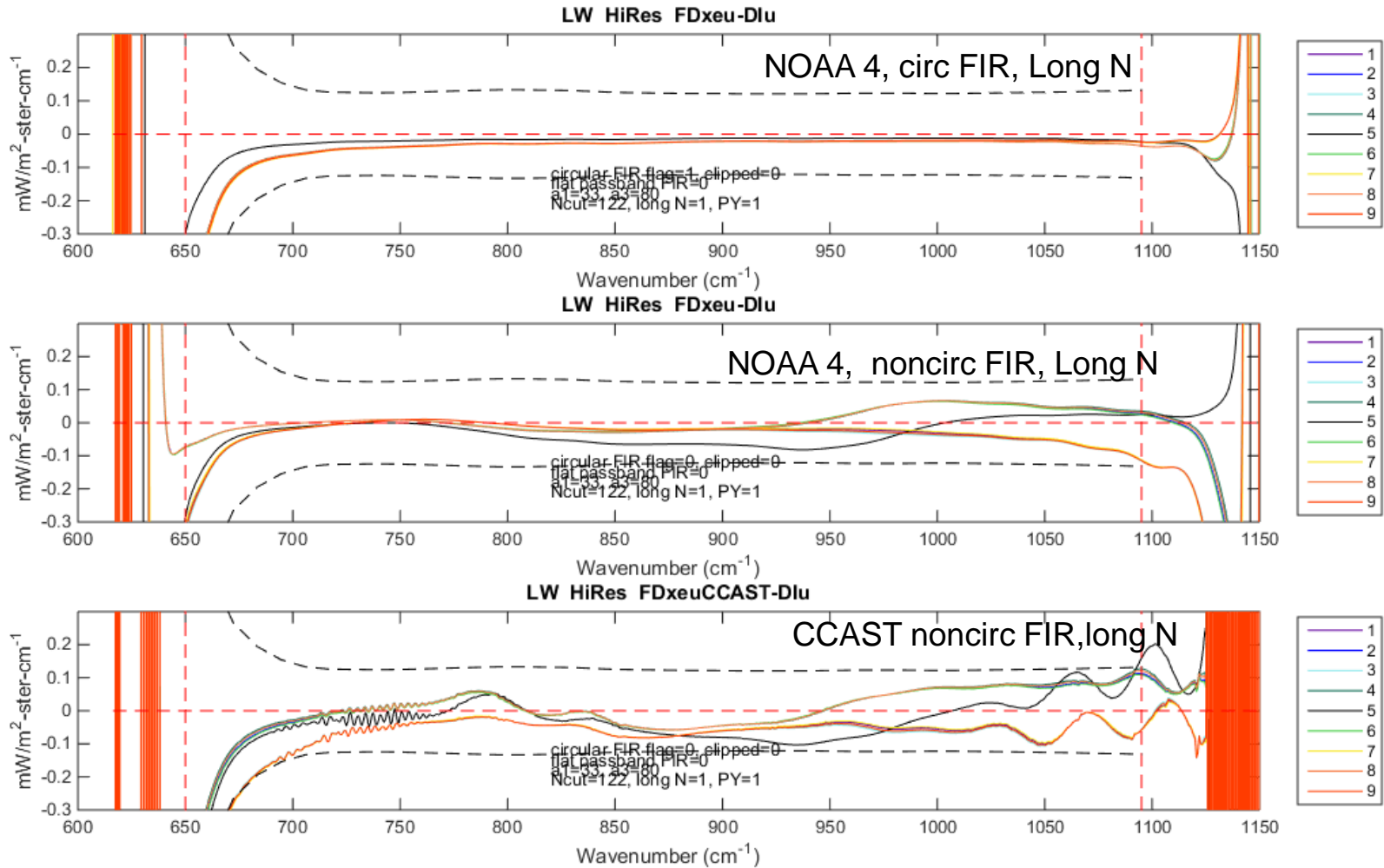
LW raw scene spectra and band limiting filters





LW A4 and CCAST FD – Truth Nyquist ringing envelopes

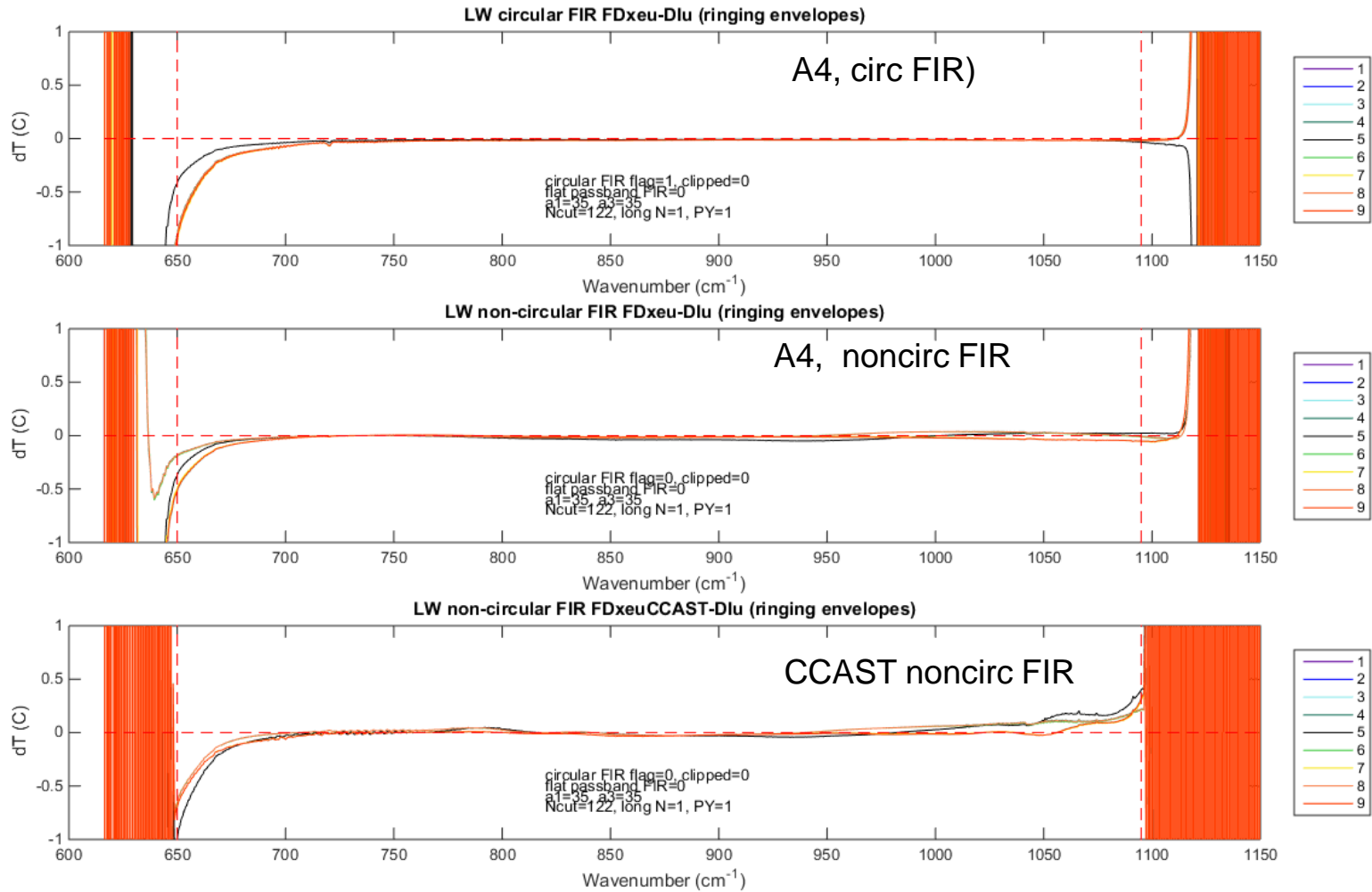
Filtered and decimated off axis spectra (full cal) – long interferogram spectra (full cal)



Dashed line - NEDN

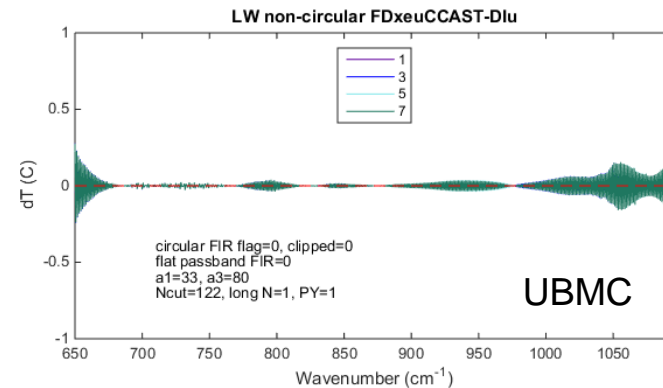
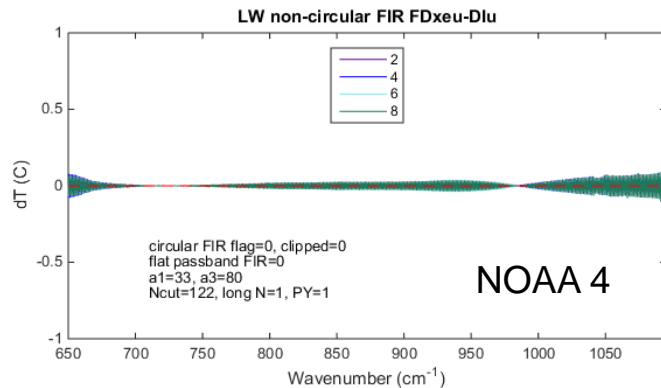
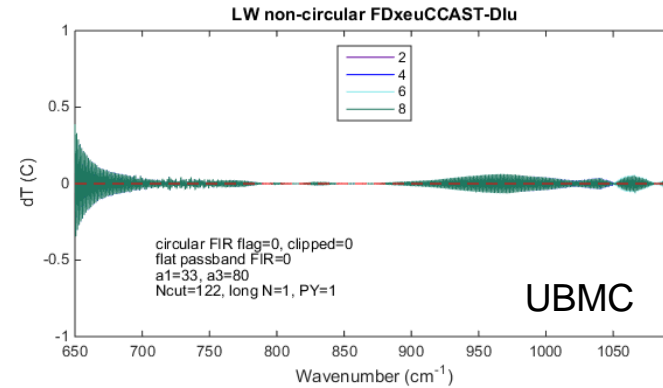
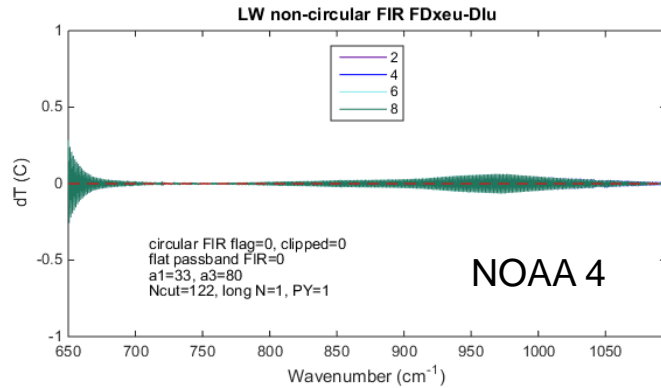


LW color temperature difference for A4 and CCAST relative to TRUTH





LW A4 and UMBC Differences: FOV – FOV5 LL simulation



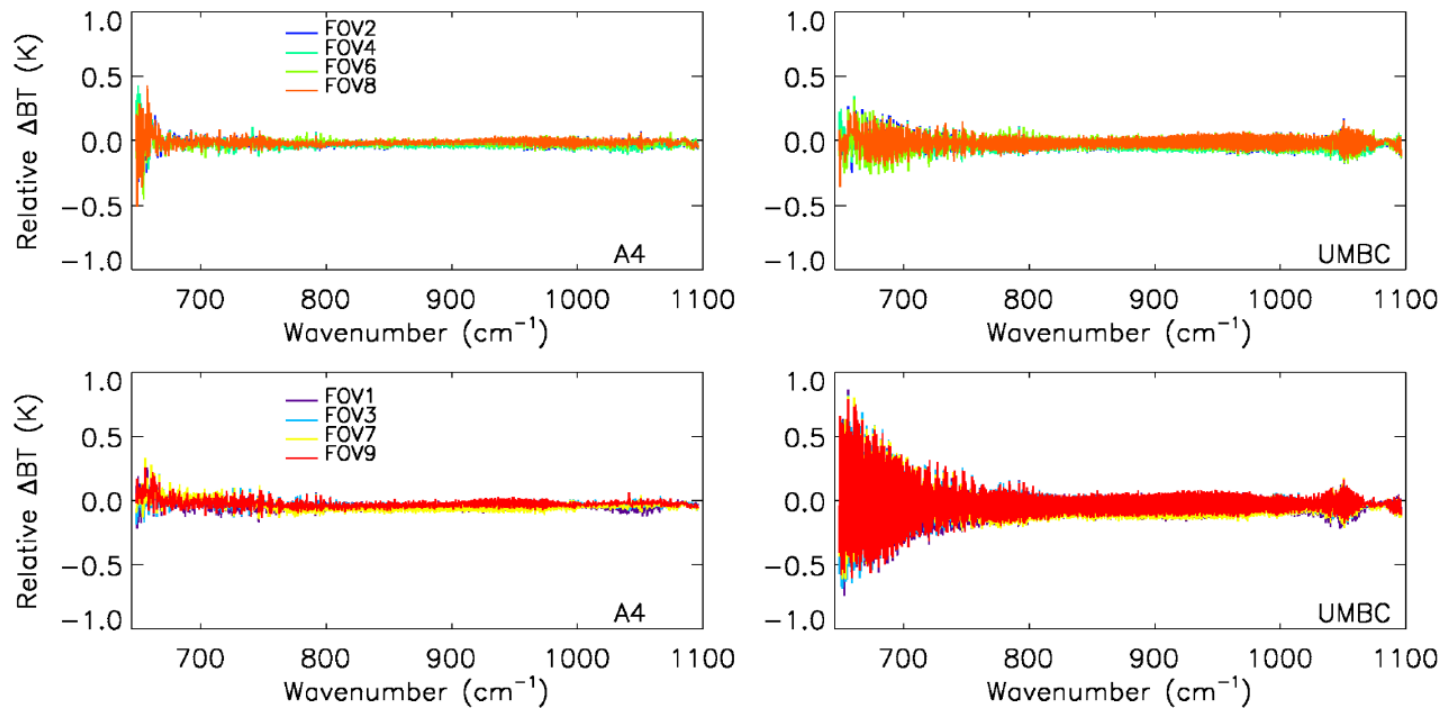


LW A4 and UMBC Differences: FOV -2 – FOV5

STAR Jun10 2015 simulation

A4 and UMBC Differences: FOV-2-FOV

Consistence: $(BT_{obs} - BT_{lbl})_{fov_i} - (BT_{obs} - BT_{lbl})_{fov_5}$



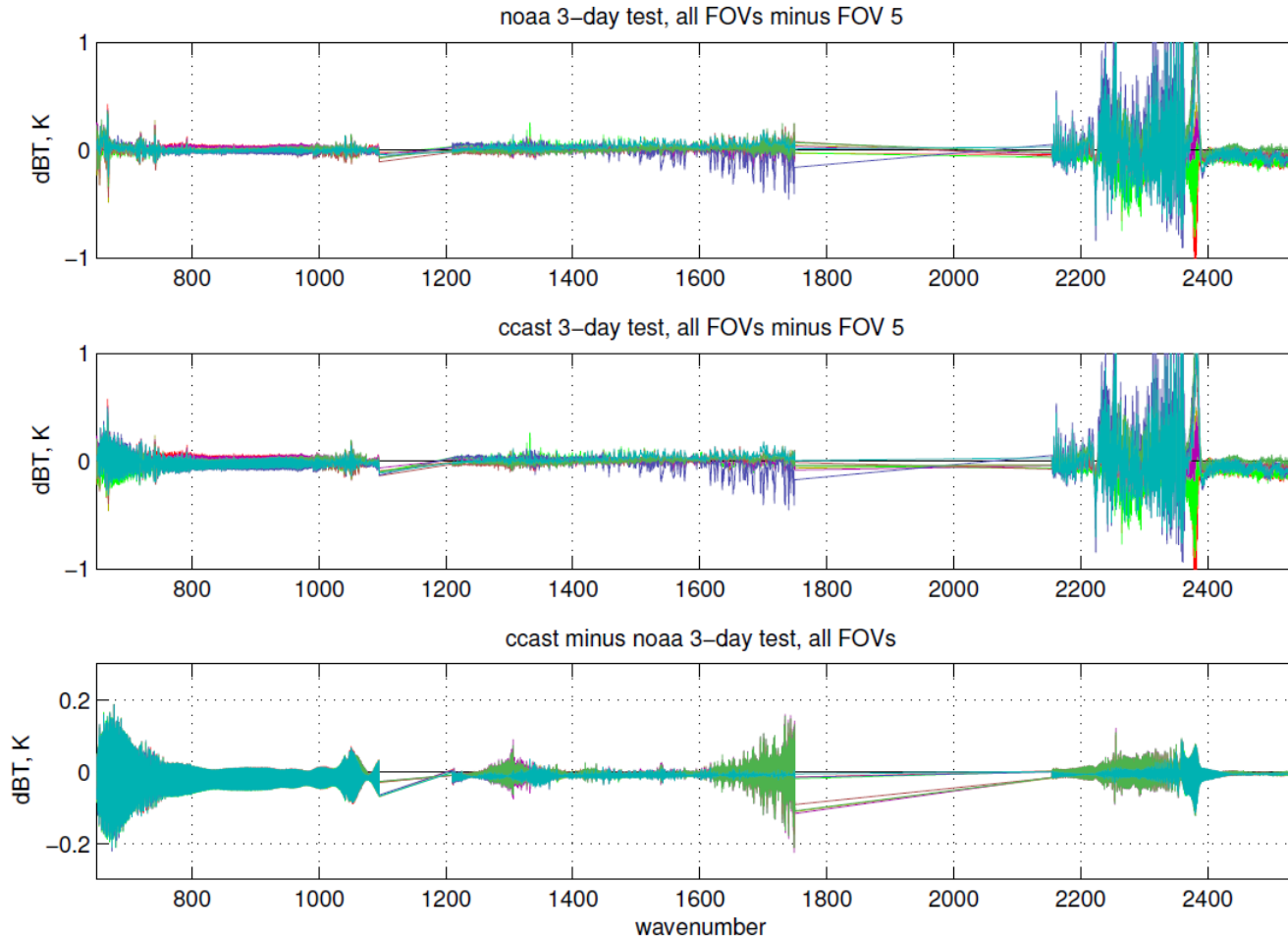
Larger ringing from A-UMBC among corner FOVs

Han & Chen¹ STAR June 10, 2015



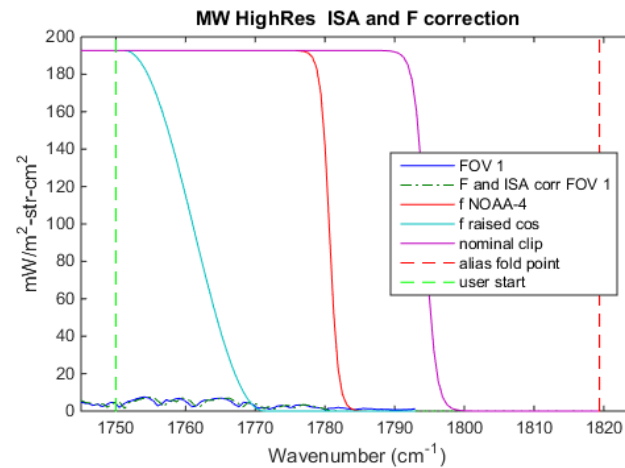
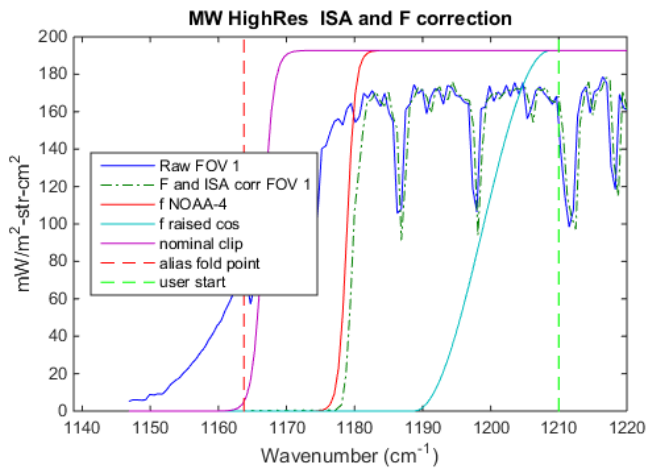
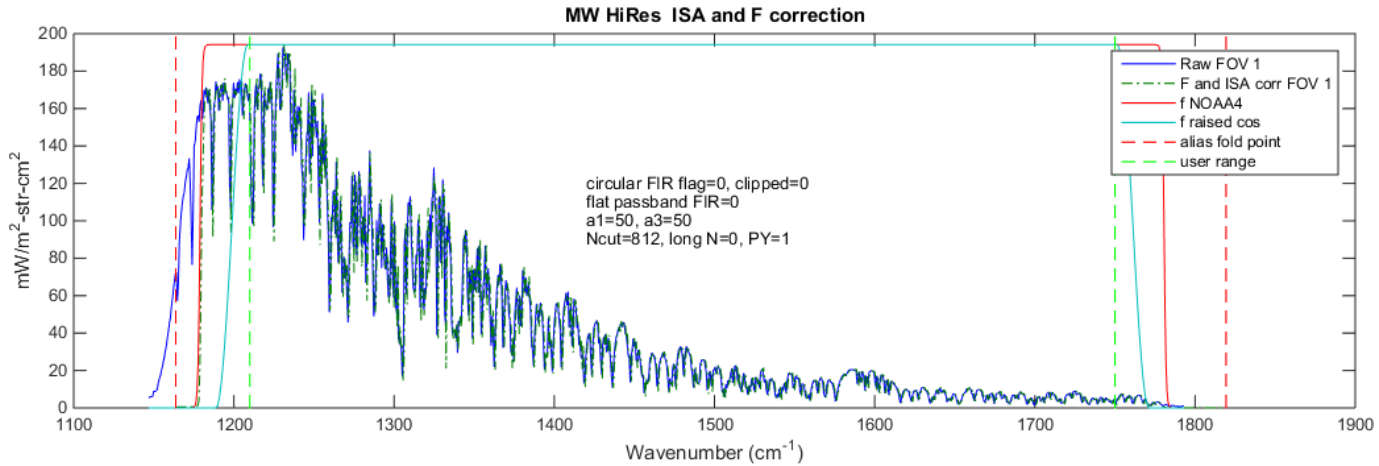
FD – Truth FOVs- FOV5 UMBC ops minus calc Aug 5 2015

relative test overview



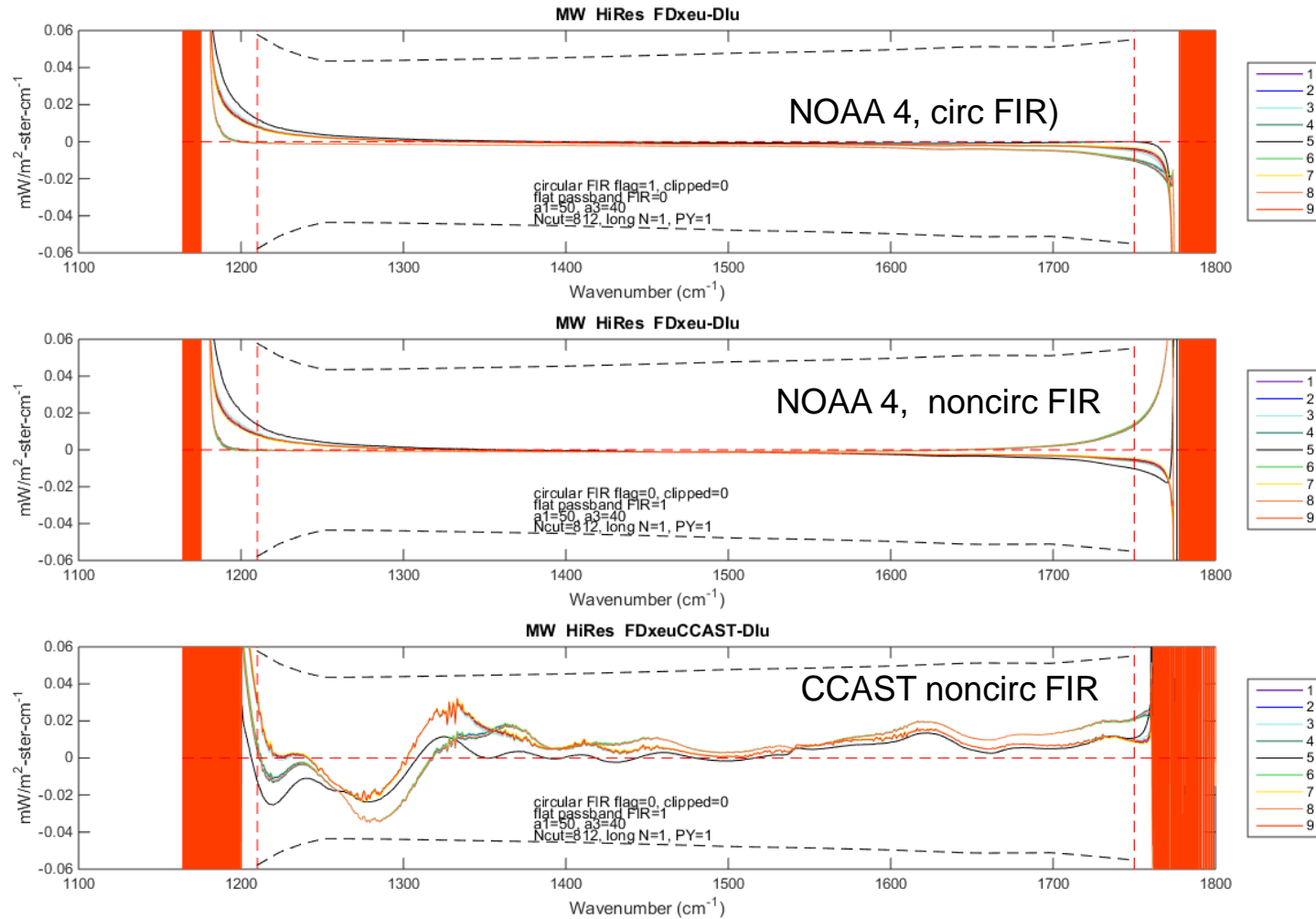


MW raw Scene spectra and band limiting filters





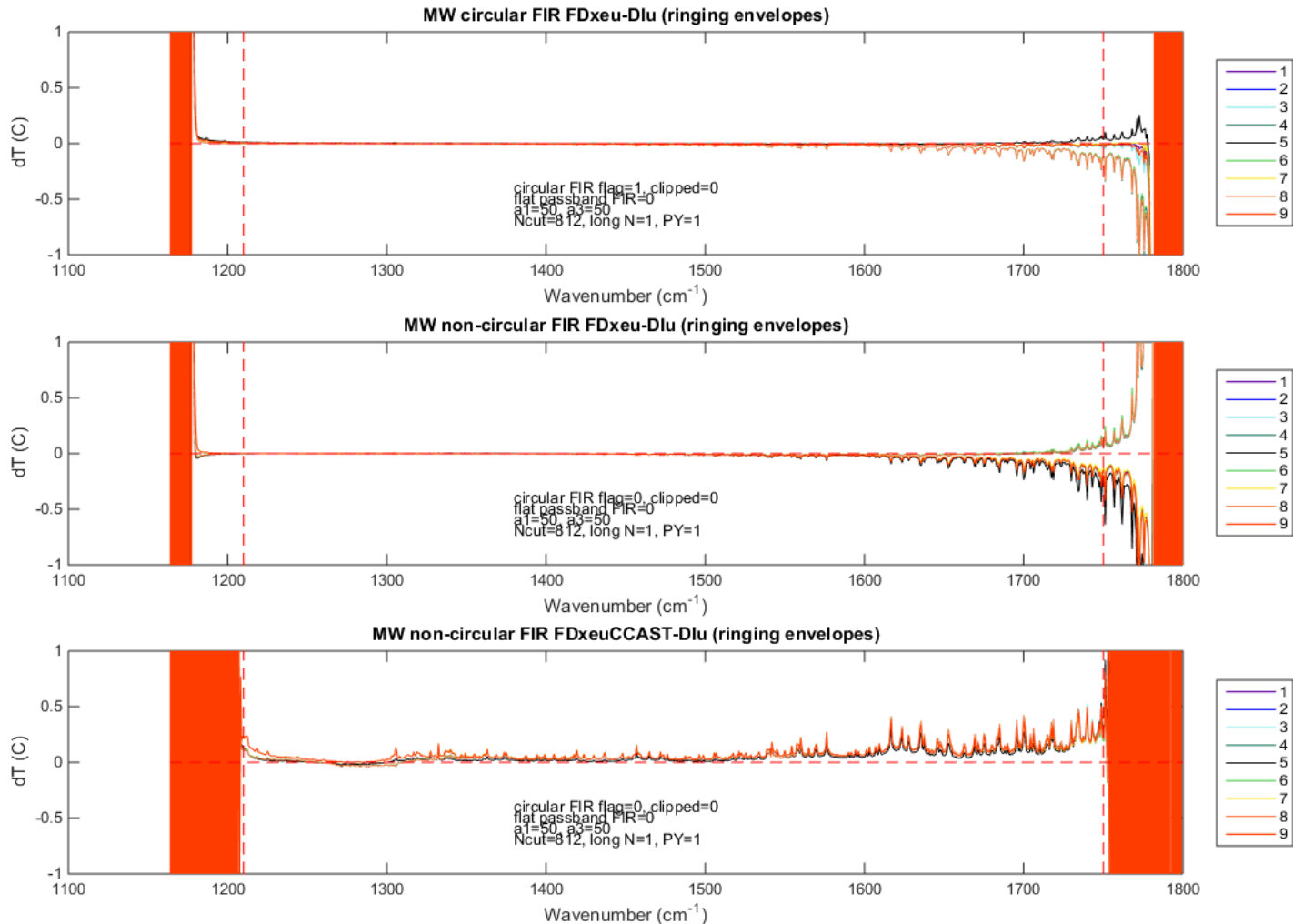
MW FD – Truth NOAA4 and CCAST Nyquist ringing envelopes

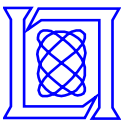


Dashed line - NEDN

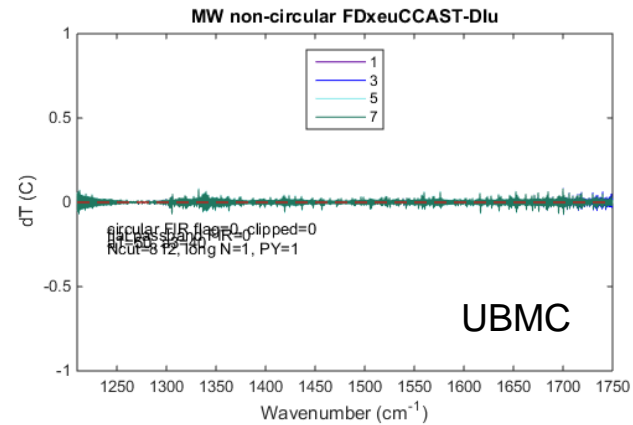
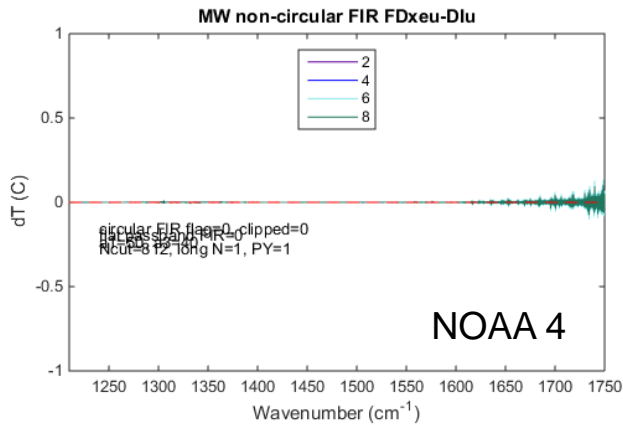
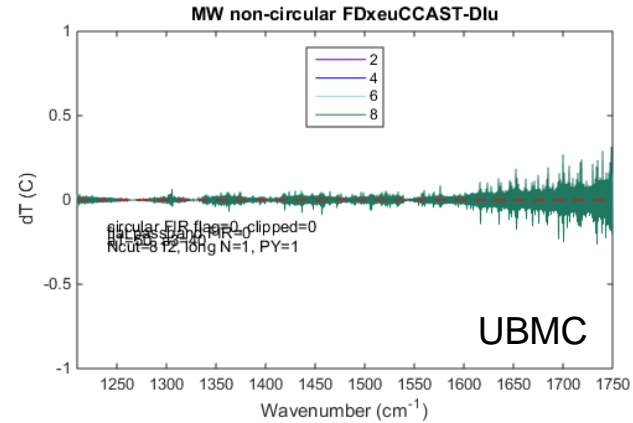
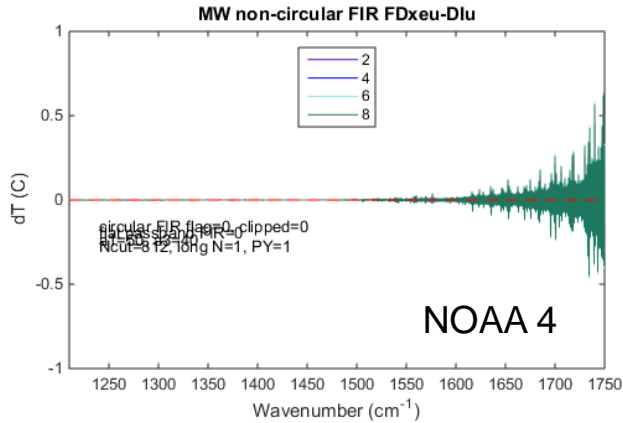


MW Color temperature difference for NOAA4 and CCAST relative to TRUTH





MW A4 and UMBC Differences: FOV -2 – FOV5 LL simulation

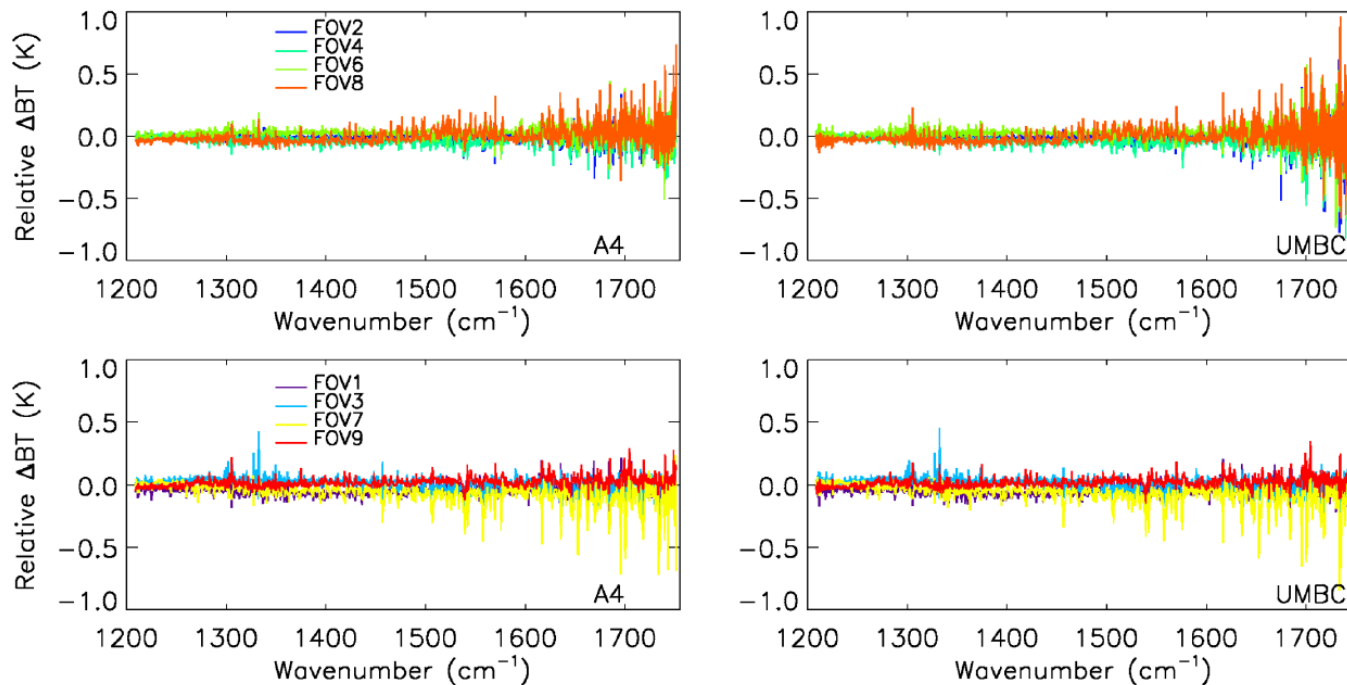




MW A4 and UMBC Differences: FOV -2 – FOV5 STAR Jun10 2015 simulation

A4 and UMBC Differences: FOV-2-FOV

Consistence: $(BT_{obs} - BT_{lbl})_{fov_i} - (BT_{obs} - BT_{lbl})_{fov_5}$

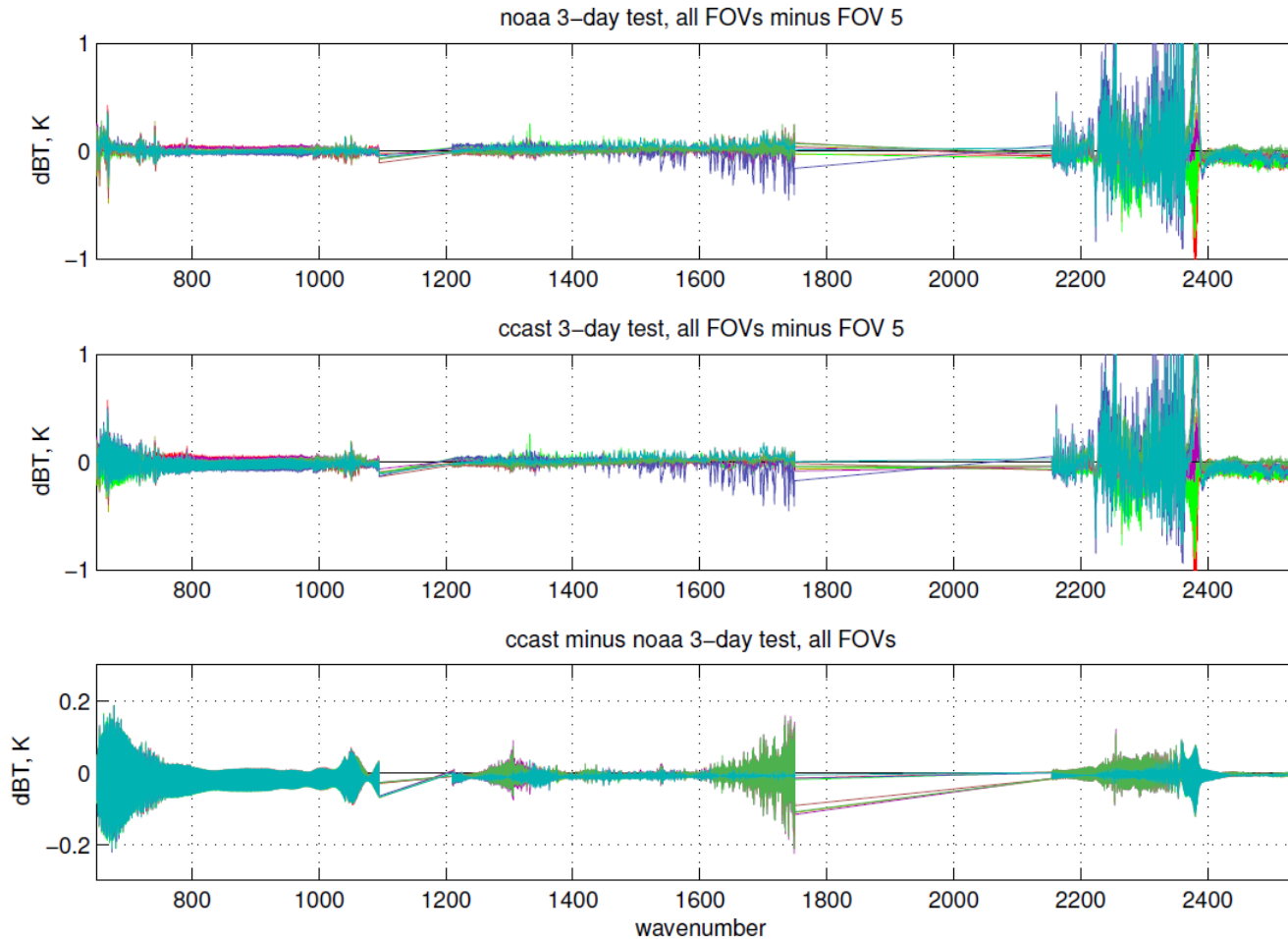


Larger difference from A-UMBC among Side FOVs



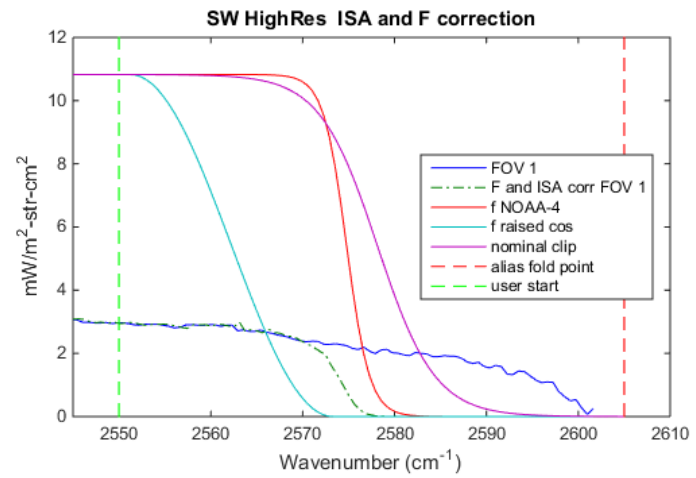
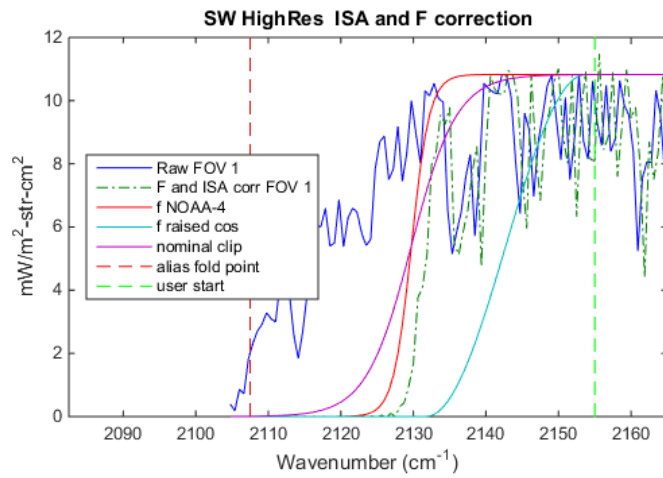
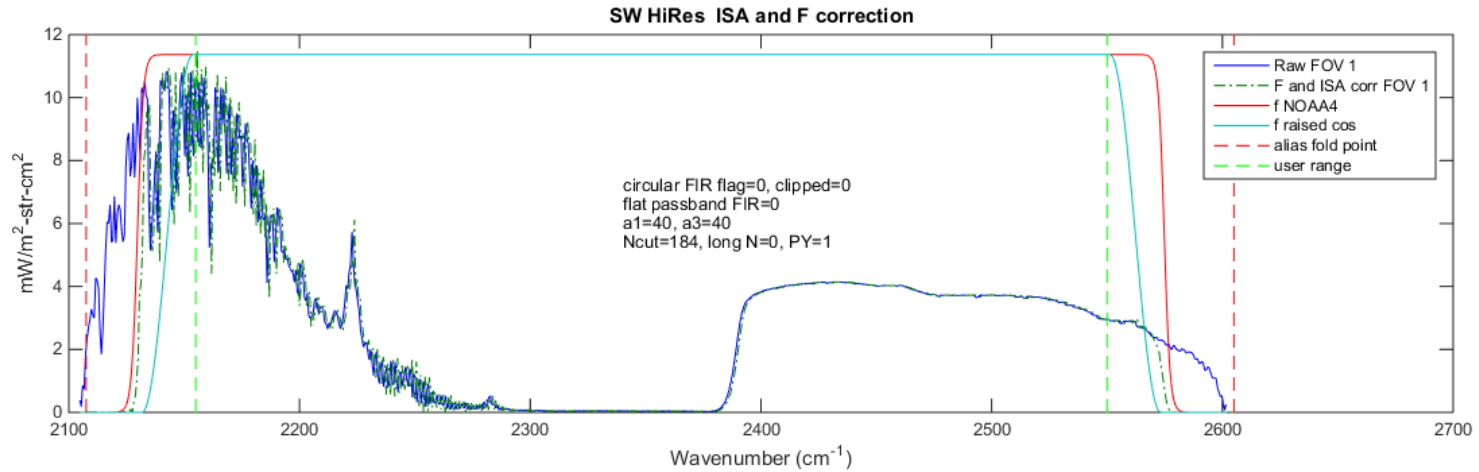
FD – Truth FOVs- FOV5 UMBC ops minus calc Aug 5 2015

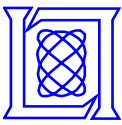
relative test overview



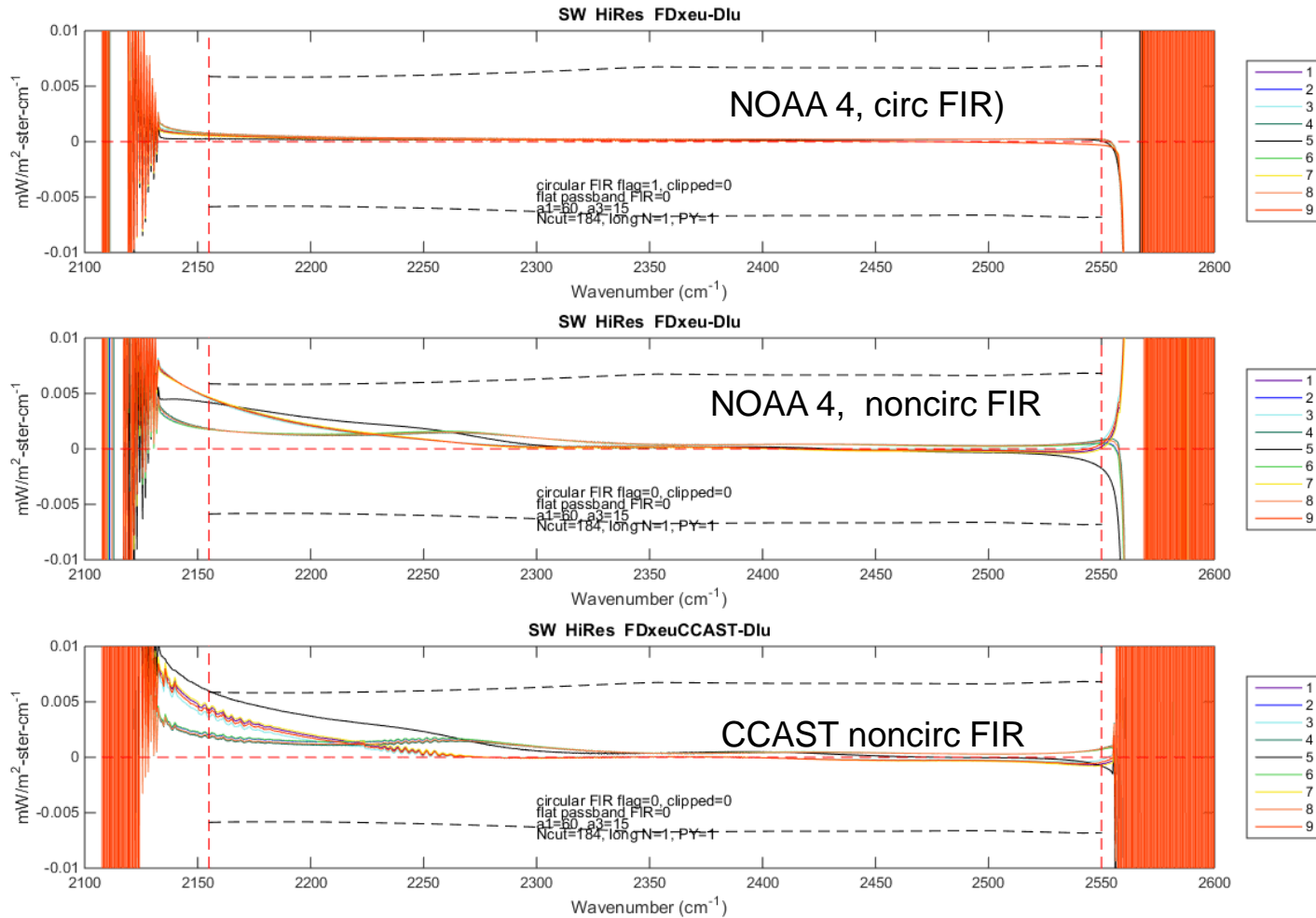


SW band raw spectrum and band limiting filters





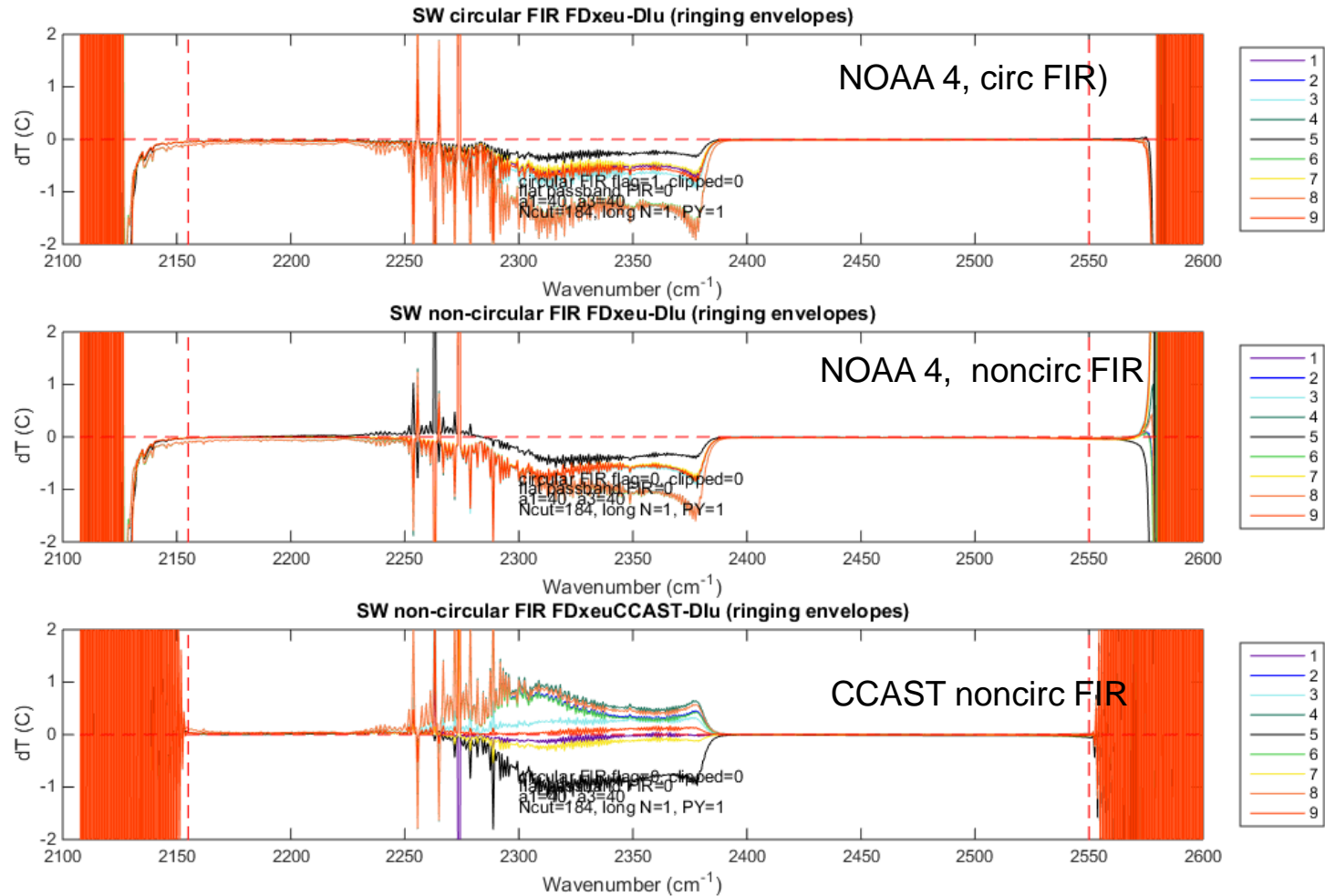
SW non-circ FIR A4 and CCAST Nyquist ringing envelopes



Dashed line - NEDN

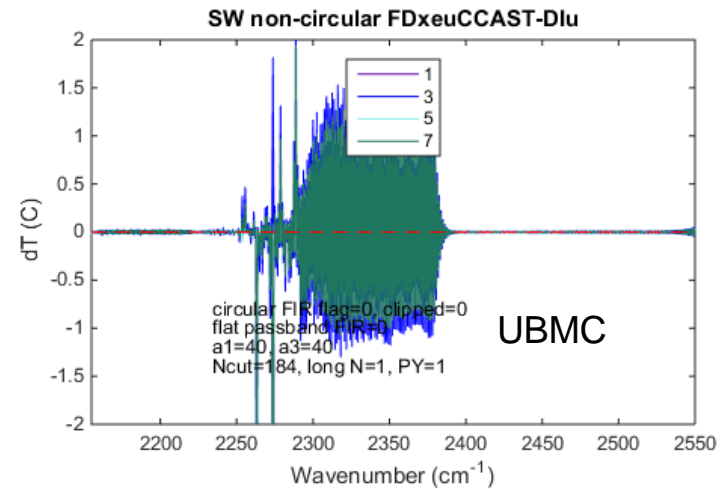
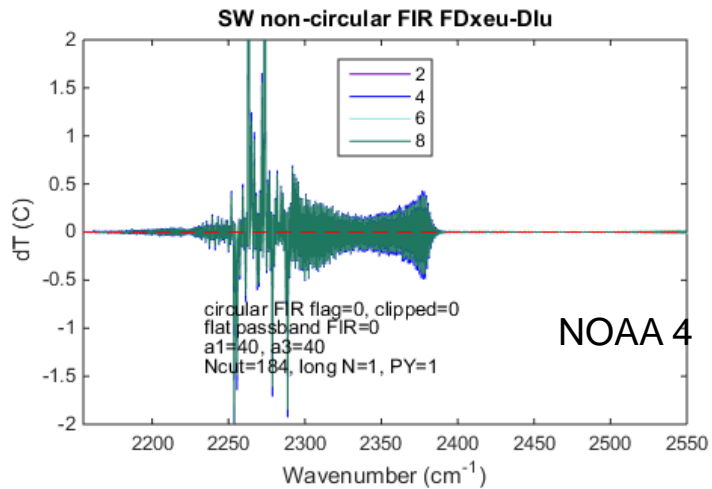
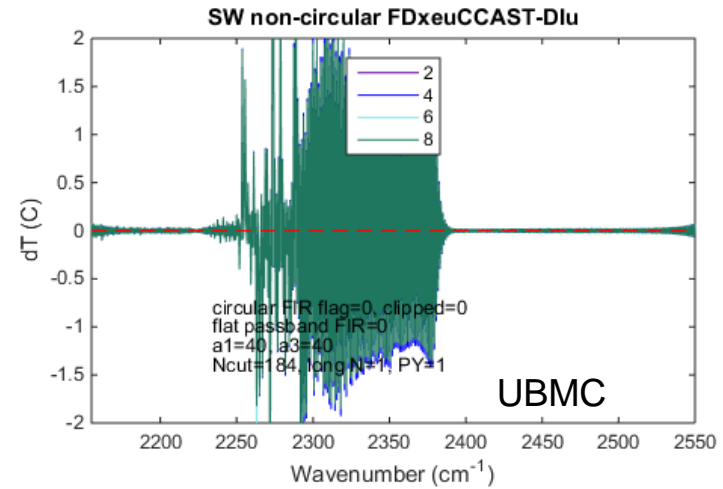
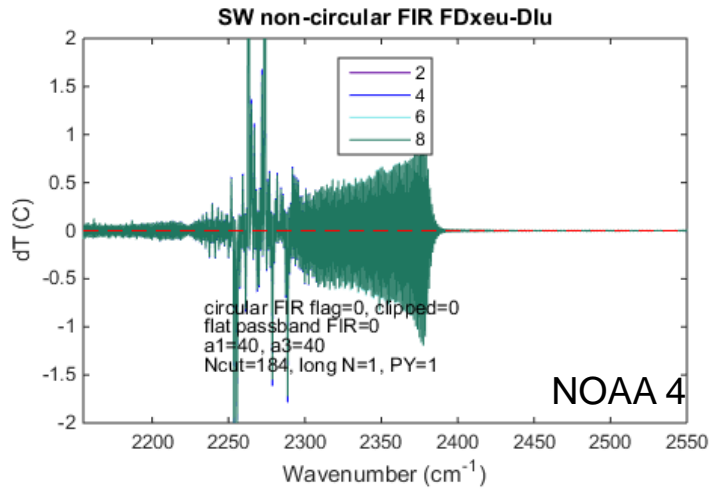


SW Color temperature difference for A4 and CCAST relative to TRUTH





SW A4 and UMBC Differences: FOV -2 - FOV5 LL simulation



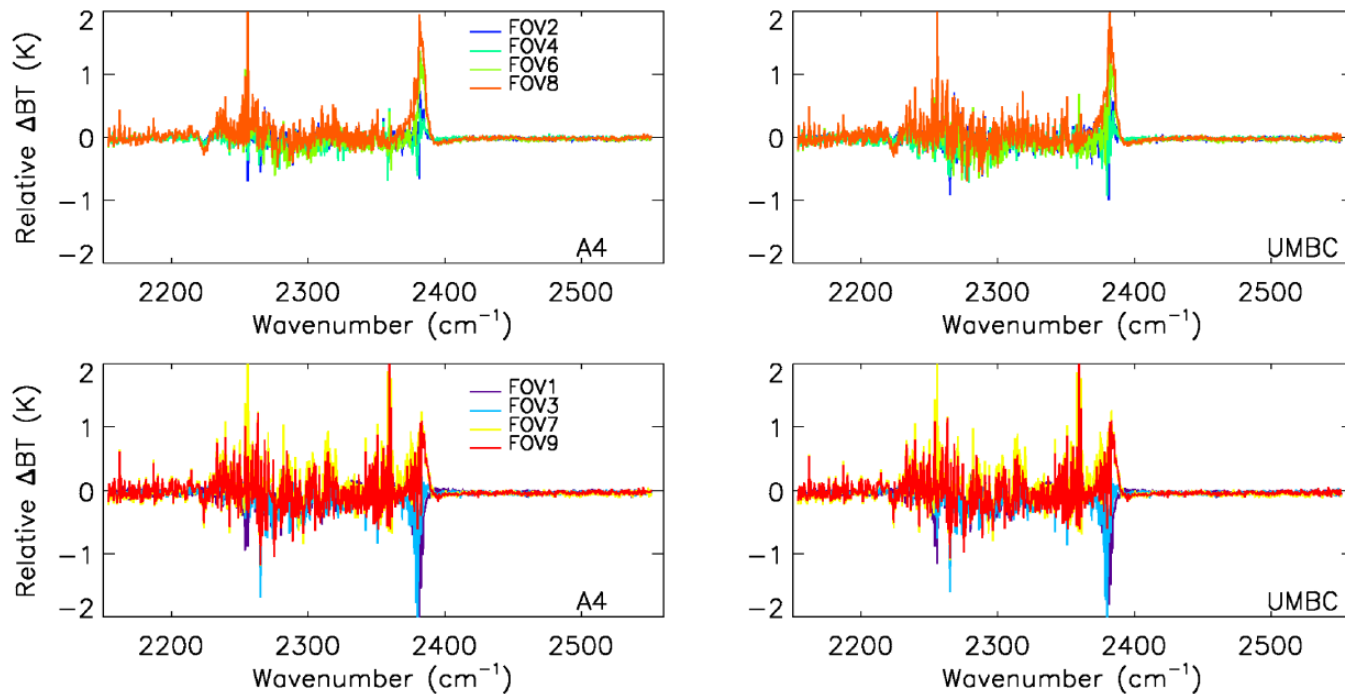


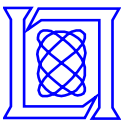
MW A4 and UMBC Differences: FOV -2 – FOV5

STAR Jun10 2015 simulation

A4 and UMBC Differences: FOV-2-FOV

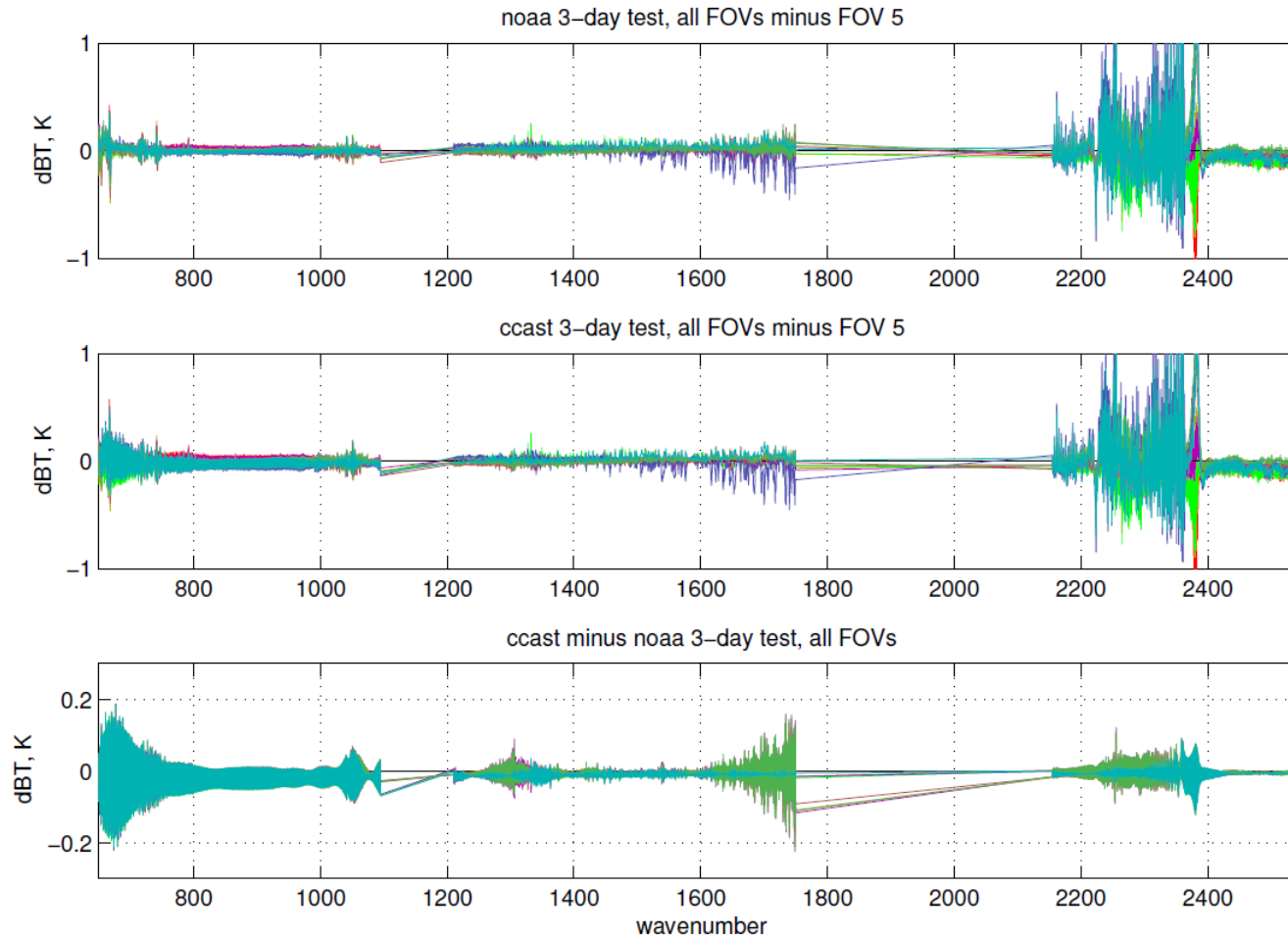
Consistence: $(BT_{obs} - BT_{lbl})_{fov_i} - (BT_{obs} - BT_{lbl})_{fov_5}$





FD – Truth FOVs- FOV5 UMBC ops minus calc Aug 5 2015

relative test overview





Summary

- **Significant improvement in understanding, precision, and speed of the numerical calibration**
- **Focusing on NOAA and CCAST performance optimization**
- **Ongoing work**
 - **Flat passband FIR filters to get closer to circular filter result**
 - **Aliasing of MW and SW spectra**
- **Incorporating optimizations into production code**



HARRIS[®]

J1 CrIS Mission Readiness

J1 CrIS Mission Readiness

**Lawrence Suwinski, Clayton Buttles, Rebecca Malloy
(Frain), Don Ripplinger, Steve Wells**

**Exelis Inc., a wholly-owned subsidiary of Harris Corporation
Space and Intelligence Systems
Fort Wayne, IN**

**STAR JPSS Science Team Annual Meeting
August 24-28, 2015
College Park, MD**

J1 Design Improvements

System Test Summary

Spacecraft Level Testing

J1 Launch Readiness

Summary

J1 Design Improvements



J1 CrIS ICT Performance Greatly Improved From SNPP

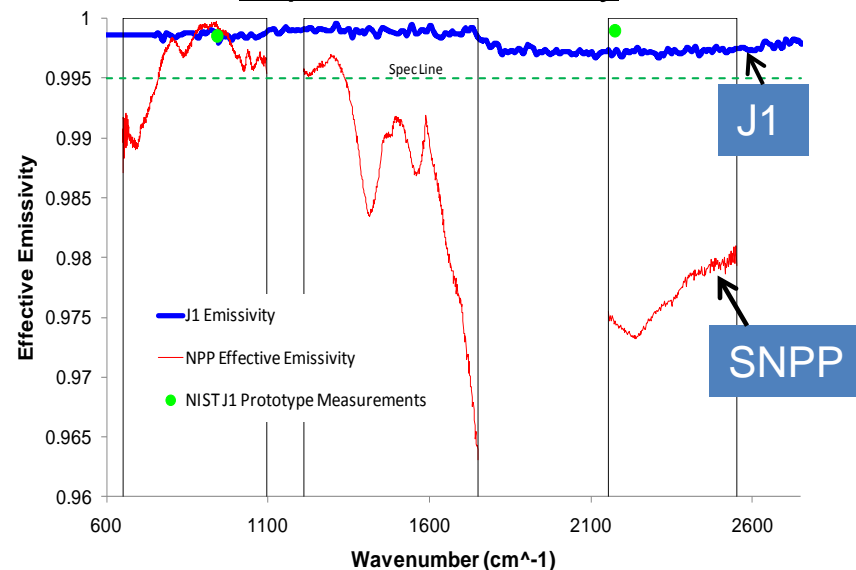


J1 Internal Calibration Target (ICT) redesigned to improve performance

- Specular coating provides increased emissivity and better stray light rejection
- Cavity wedge design helps eliminate views to other optical surfaces within instrument
- Additional PRT provides increased temperature and gradient knowledge
- Results in simplified SDR processing and more accurate calibration performance

Other J1 design improvements include frame and FPGA robustness enhancements

Improved Emissivity



Stray Light Views Eliminated

View From	To	Fractional View to Environment (NPP)	Fractional View to Environment (J1 and up)
ICT Base	ICT Walls	0.000	0.000
ICT Base	ICT Base	0.000	0.000
ICT Base	ICT Baffle	0.175	0.000
ICT Base	Scan Baffle	0.508	0.000
ICT Base	Scan Mirror		
ICT Base	Frame	0.214	0.000
ICT Base	Opto-Mechanical Assembly (OMA)		
ICT Base	Warm Beamsplitter	0.086	0.000
ICT Base	Cold Beamsplitter	0.008	1.000
ICT Base	Space	0.009	0.000

System Test Summary



J1 CrIS Successfully Completed Comprehensive Test Program



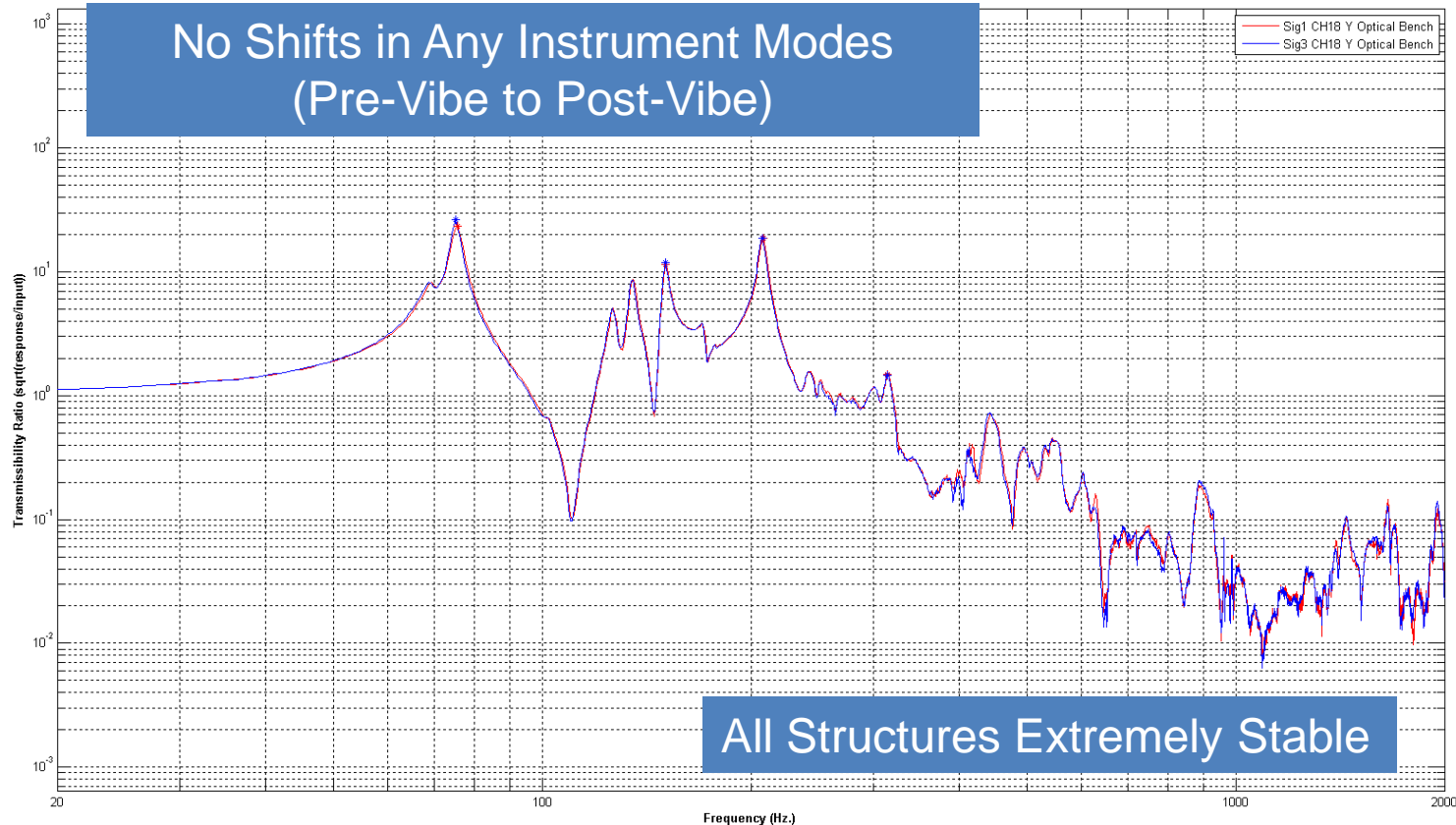
- EMI testing
- Vibration testing
- TVAC testing
 - Noise Equivalent Spectral Radiance (NEdN)
 - Radiometric Performance
 - Radiometric Uncertainty
 - Repeatability
 - Detector Linearity
 - Instrument Line Shape (ILS) / Spectral Accuracy
 - Day in the Life
 - Field of View (FOV) Shape / Coregistration
 - Dynamic Interaction
 - Electrical Performance

- Testing covered large range of frequencies while carefully examining instrument data
 - >5000 Excitation frequencies
 - >2200 Spectral channels monitored
 - All telemetry affecting science data monitored
- Testing was highly successful
 - Nearly all conditions fully compliant
 - Less than 20 minor discrete outages out of >50 million test conditions and/or telemetry points monitored
 - All reviewed by SMEs / user communities and deemed to be acceptable for flight
 - Minor outages at frequencies/levels not seen on spacecraft

Vibration Testing Highlights Exceptional Structural Stability



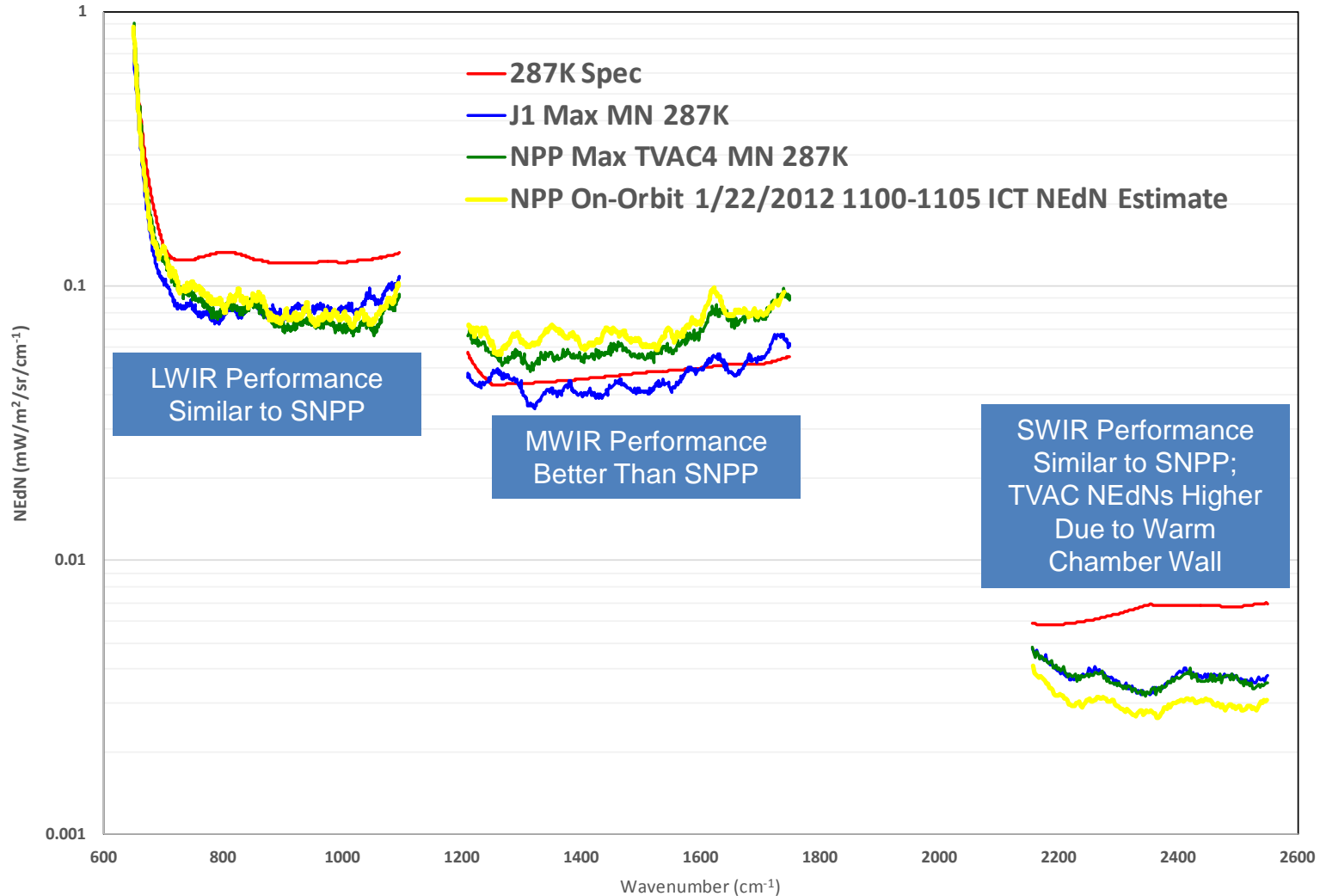
EXELIS



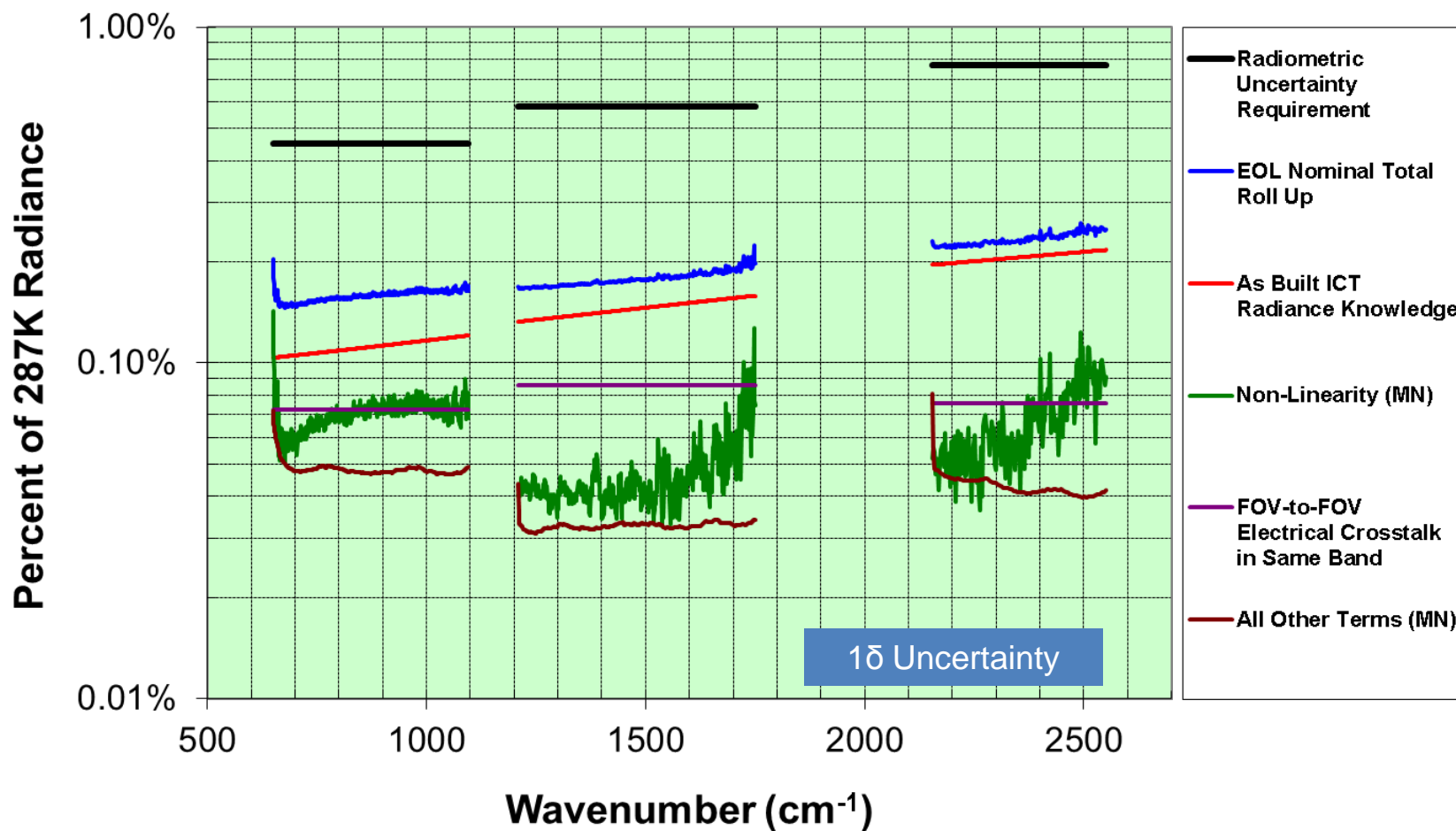
J1 NEdN Performance Equal to or Better Than SNPP



TVAC Mission Nominal NEdN Comparisons



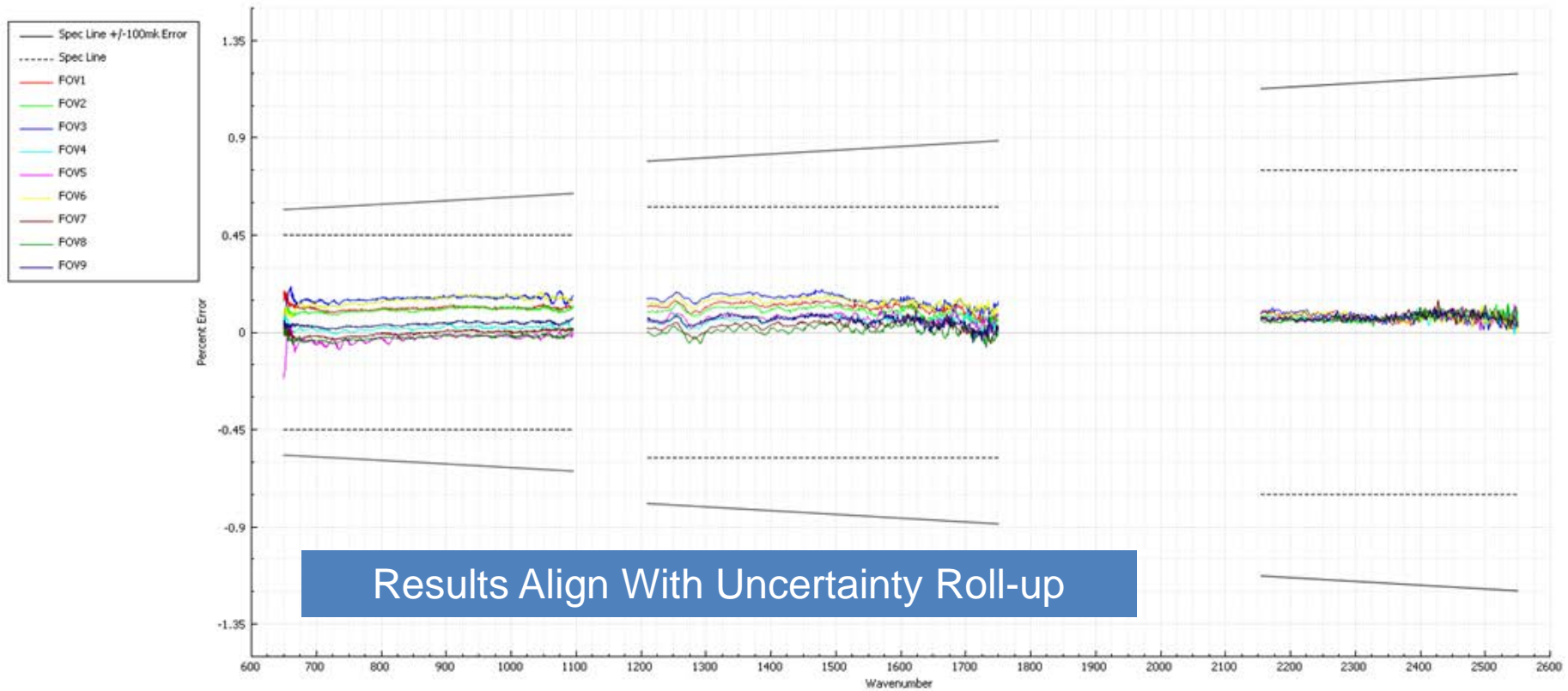
CrIS J1 Radiometric Uncertainty



Uncertainty Roll-up Confirmed With Test Data



Adjusted Radiance Error as % Relative to 287K BB Radiance

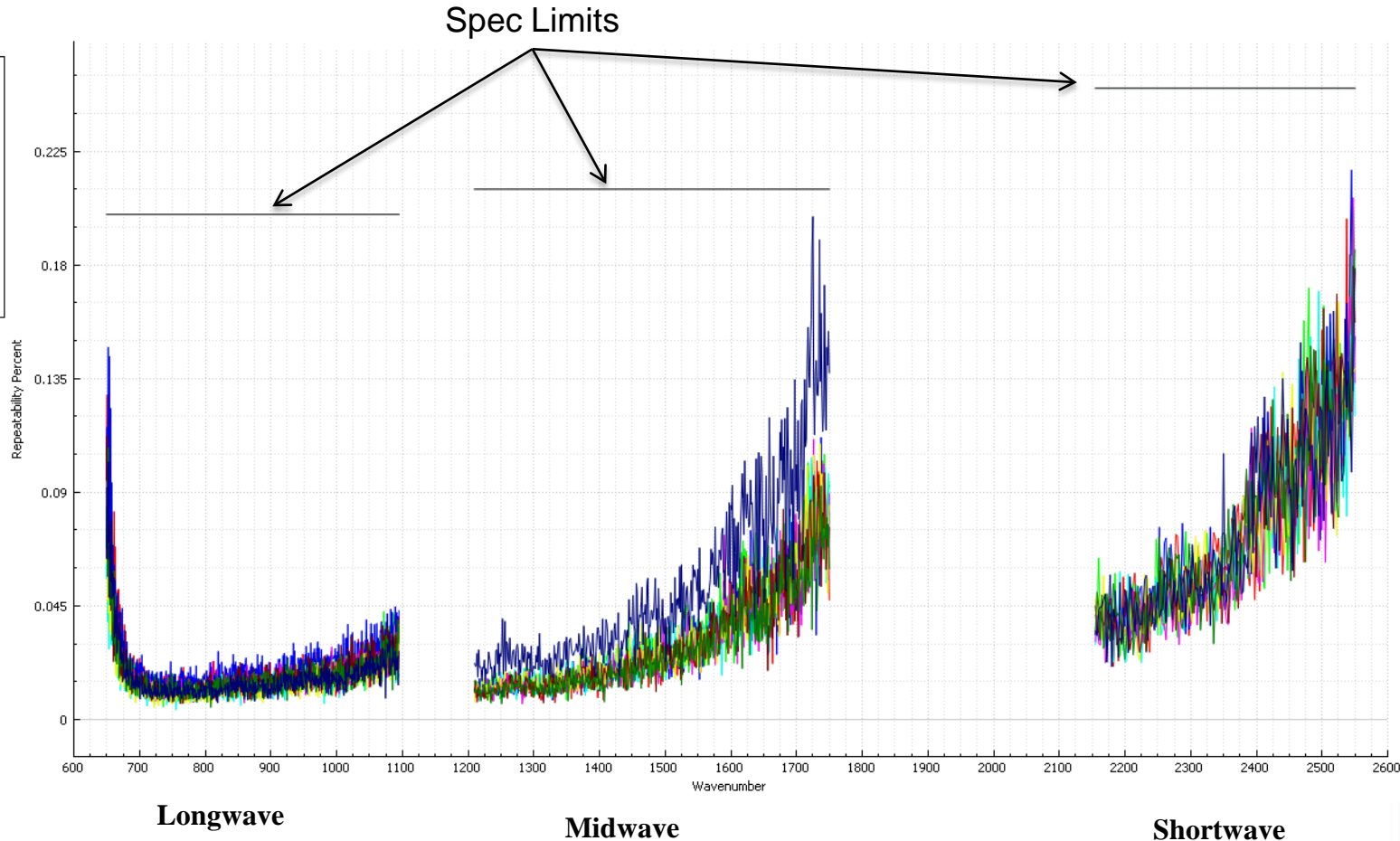


Short Term Repeatability Performance Within Specification



- Spec Line
- FOV1 Real Radiance Repeatability Percent
- FOV2 Real Radiance Repeatability Percent
- FOV3 Real Radiance Repeatability Percent
- FOV4 Real Radiance Repeatability Percent
- FOV5 Real Radiance Repeatability Percent
- FOV6 Real Radiance Repeatability Percent
- FOV7 Real Radiance Repeatability Percent
- FOV8 Real Radiance Repeatability Percent
- FOV9 Real Radiance Repeatability Percent

Repeatability Measured Over 1 Hour

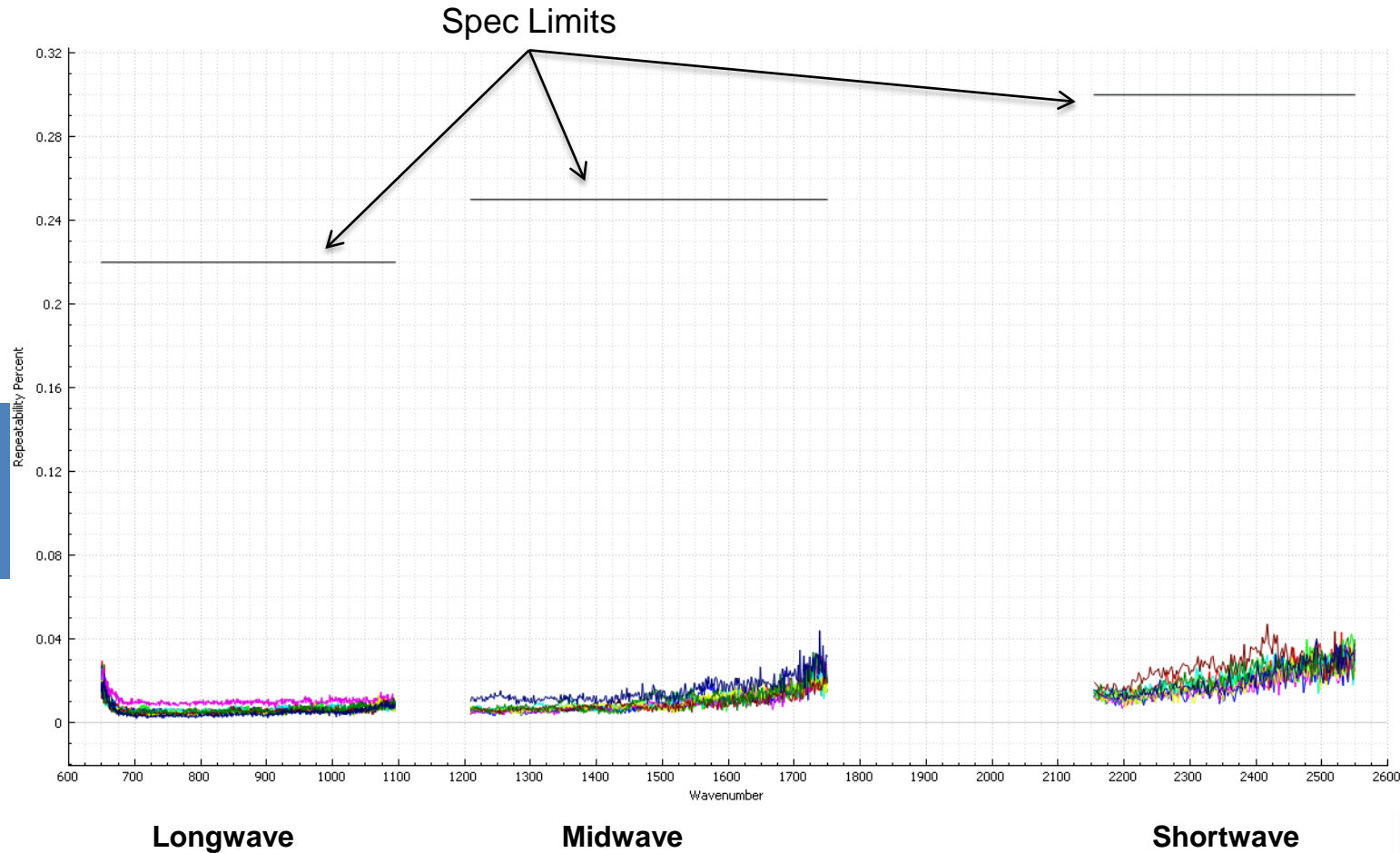


Long Term Repeatability Performance is Outstanding

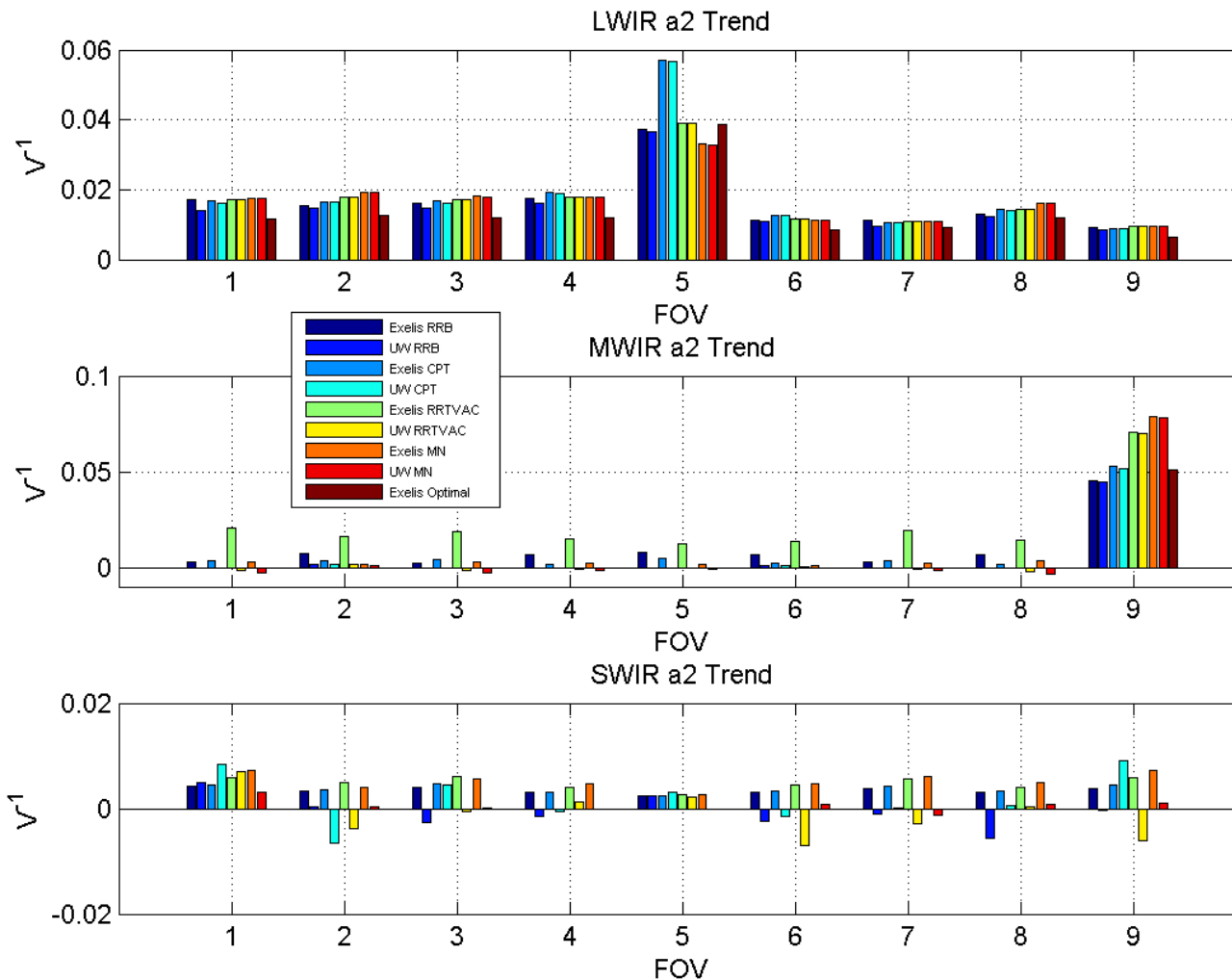


- Spec Line
- FOV1 Real Radiance Repeatability Percent
- FOV2 Real Radiance Repeatability Percent
- FOV3 Real Radiance Repeatability Percent
- FOV4 Real Radiance Repeatability Percent
- FOV5 Real Radiance Repeatability Percent
- FOV6 Real Radiance Repeatability Percent
- FOV7 Real Radiance Repeatability Percent
- FOV8 Real Radiance Repeatability Percent
- FOV9 Real Radiance Repeatability Percent

Repeatability Measured Over >30 Days

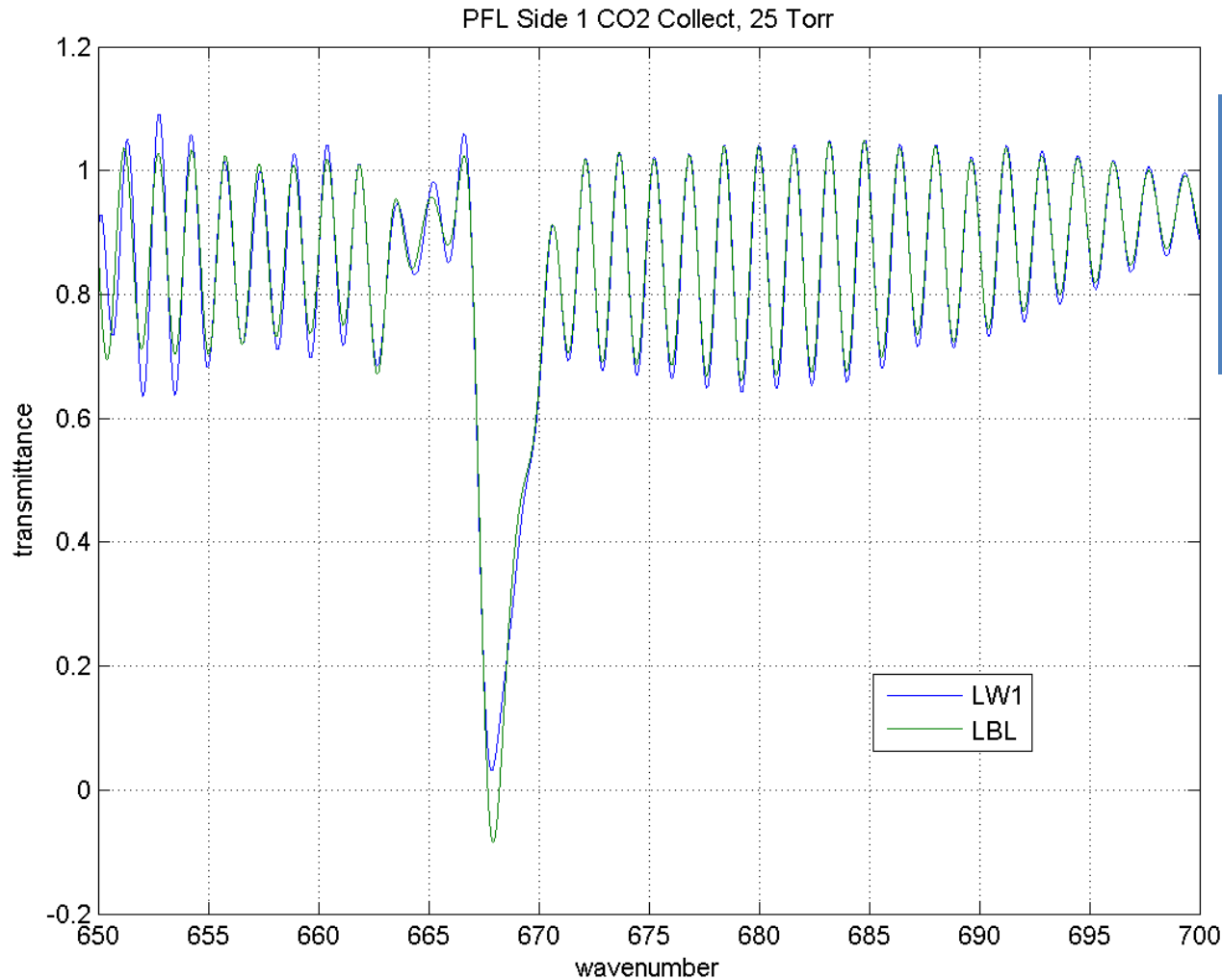


Detector Nonlinearity Levels Stable Over System Test



Harris and UW Values Match Very Closely; Parameters Tuned Further On-Orbit

Spectral Uncertainty Results Show Excellent Agreement With Truth



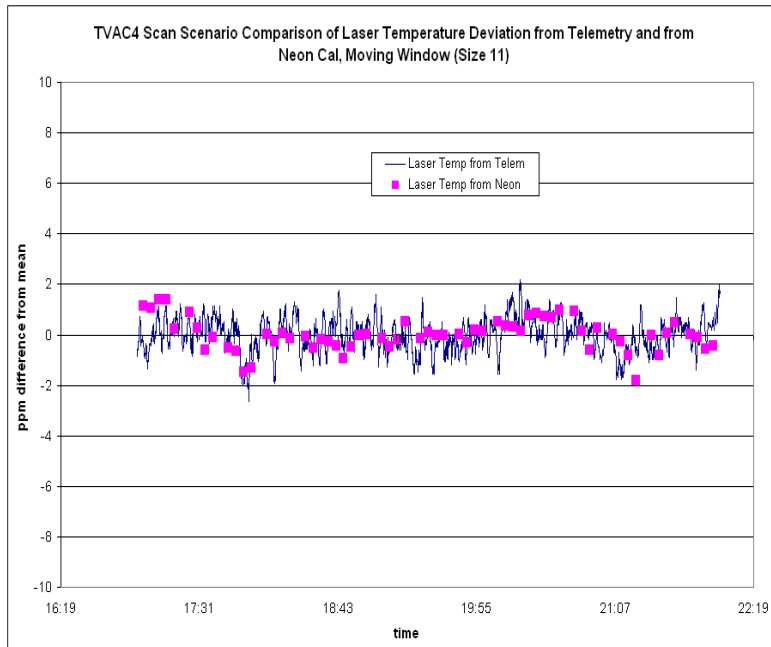
TVAC Spectral Uncertainties Better Than 4.6 ppm at Expected On-Orbit Conditions

On-Orbit Uncertainties Expected to Match or Exceed SNPP 3 ppm Levels

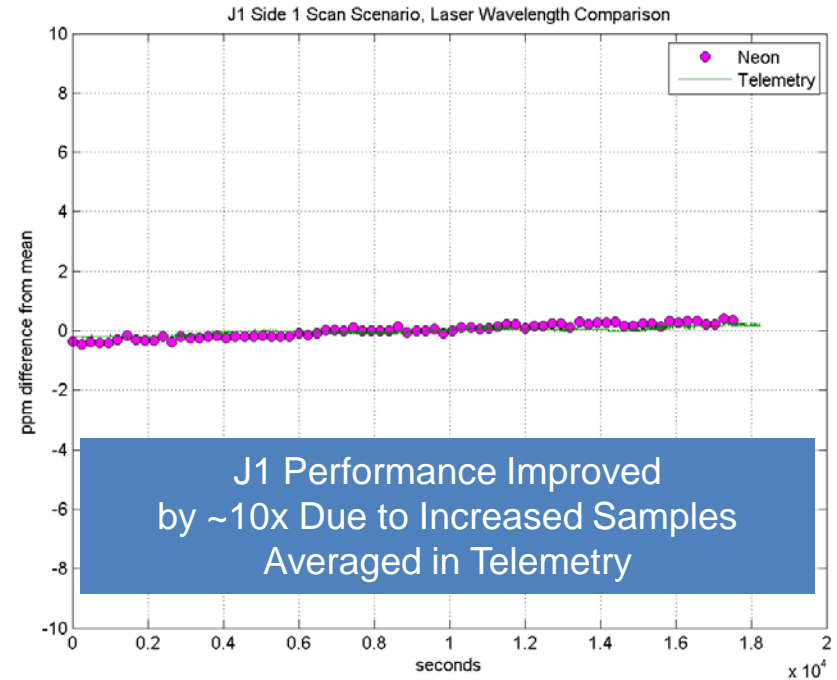
'Day in the Life' Test Demonstrates Improved Spectral Stability from SNPP



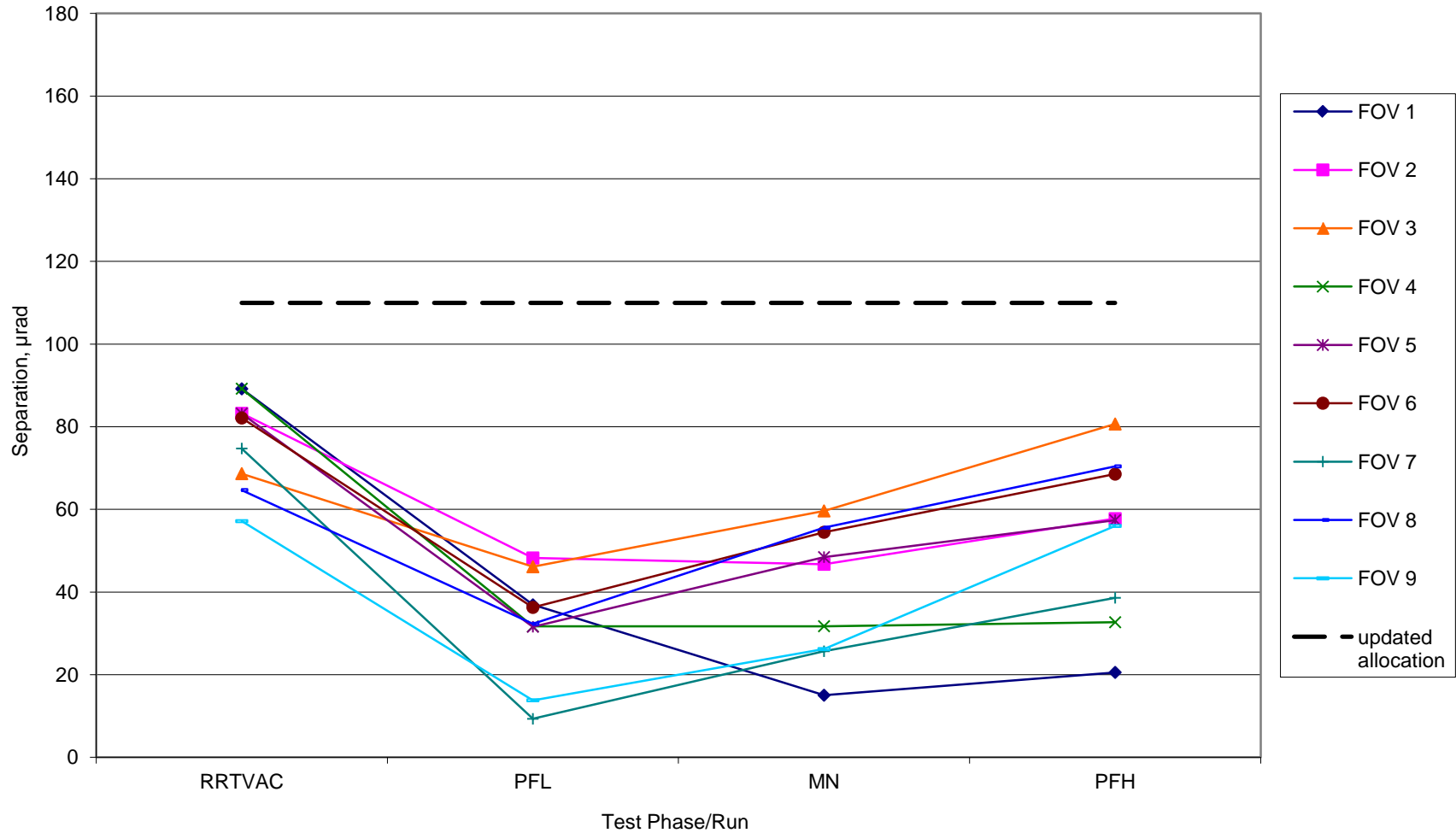
SNPP



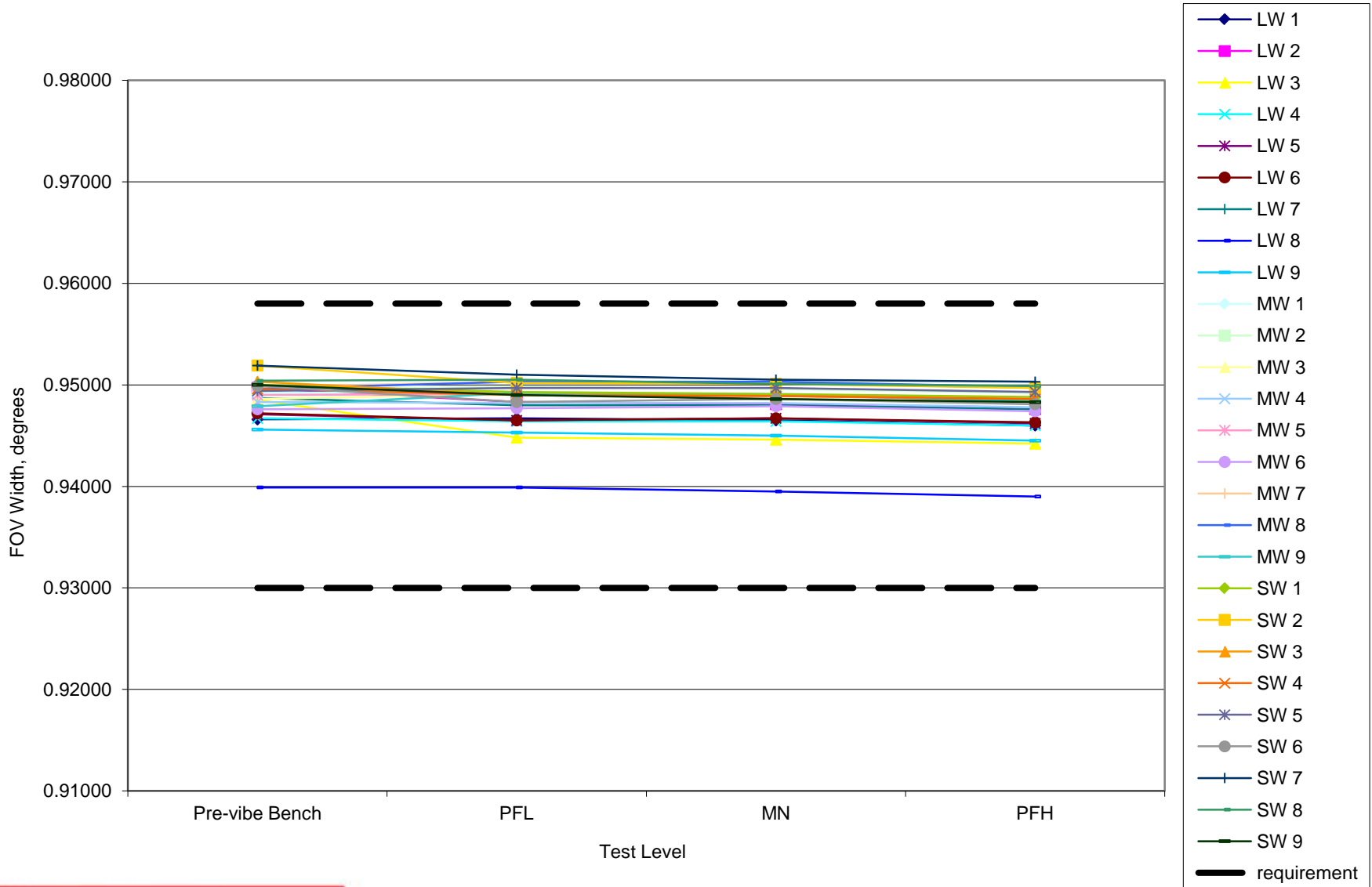
J1



Coregistration Stable Over Thermal Plateaus



FOV Sizes Very Stable and Within Specifications



- Ka band gimbal antenna added to J1 spacecraft
 - Resulted in concern that 6 Hz jitter might impact NEdN
 - Further concerns regarding ICD jitter specification and reaction wheels
- Request made by NASA to characterize NEdN in presence of jitter
 - Jitter introduced to instrument during NEdN collections
 - Vibration Isolation System (VIS) not deployed
 - Transfer function applied analytically to results
- Threshold limits for jitter disturbance levels determined
- Jitter specification updated for J1 and J2 based on test results

TVAC Testing Highly Successful



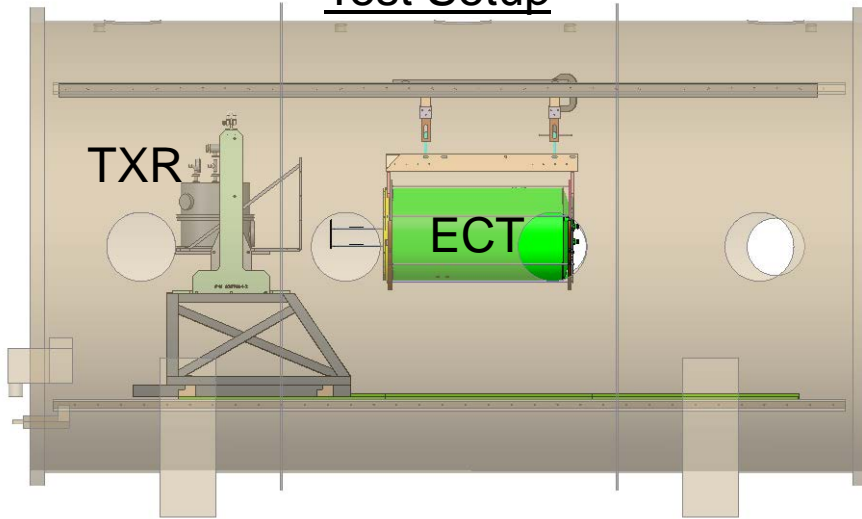
- Electrical Performance tests all meet requirements
- Mapping uncertainty performance met with margin
 - Further optimized on-orbit
- Successful Pre-Ship Review held on 2/10/2015
- J1 CrIS shipped to Ball on 2/12/2015
 - Mechanically integrated to spacecraft on 3/17/2015
 - Fully integrated on 4/14/2015



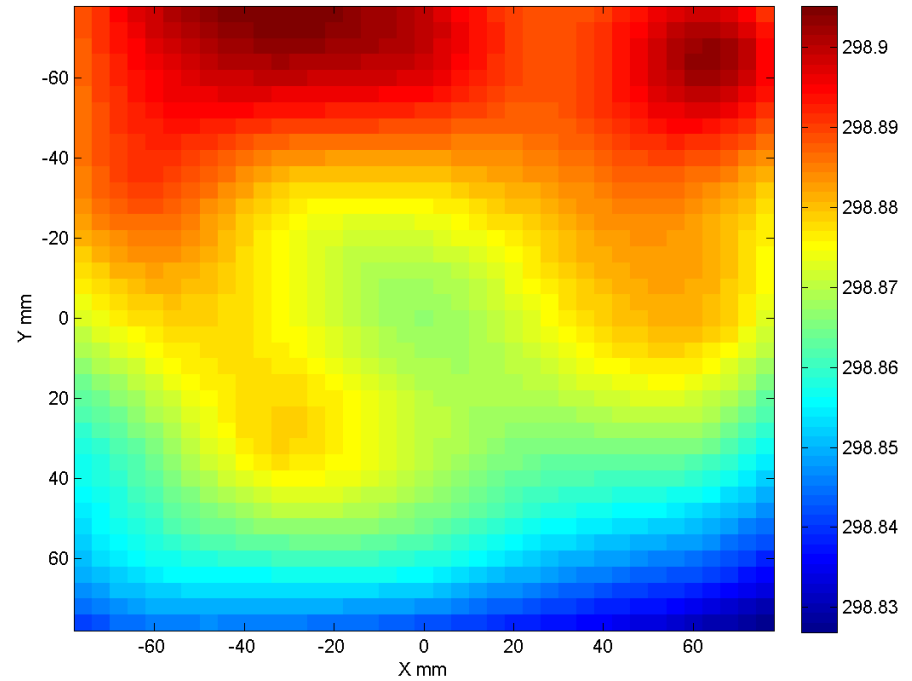
External Calibration Target Performance Verified by NIST Following TVAC



Test Setup



Example Results



Testing Verified ECT Performance as Seen By Sensor During TVAC;
~80 mK Gradient Matches That Seen By CrIS

Parameters Needed for Early Orbit Activation Defined and Ready

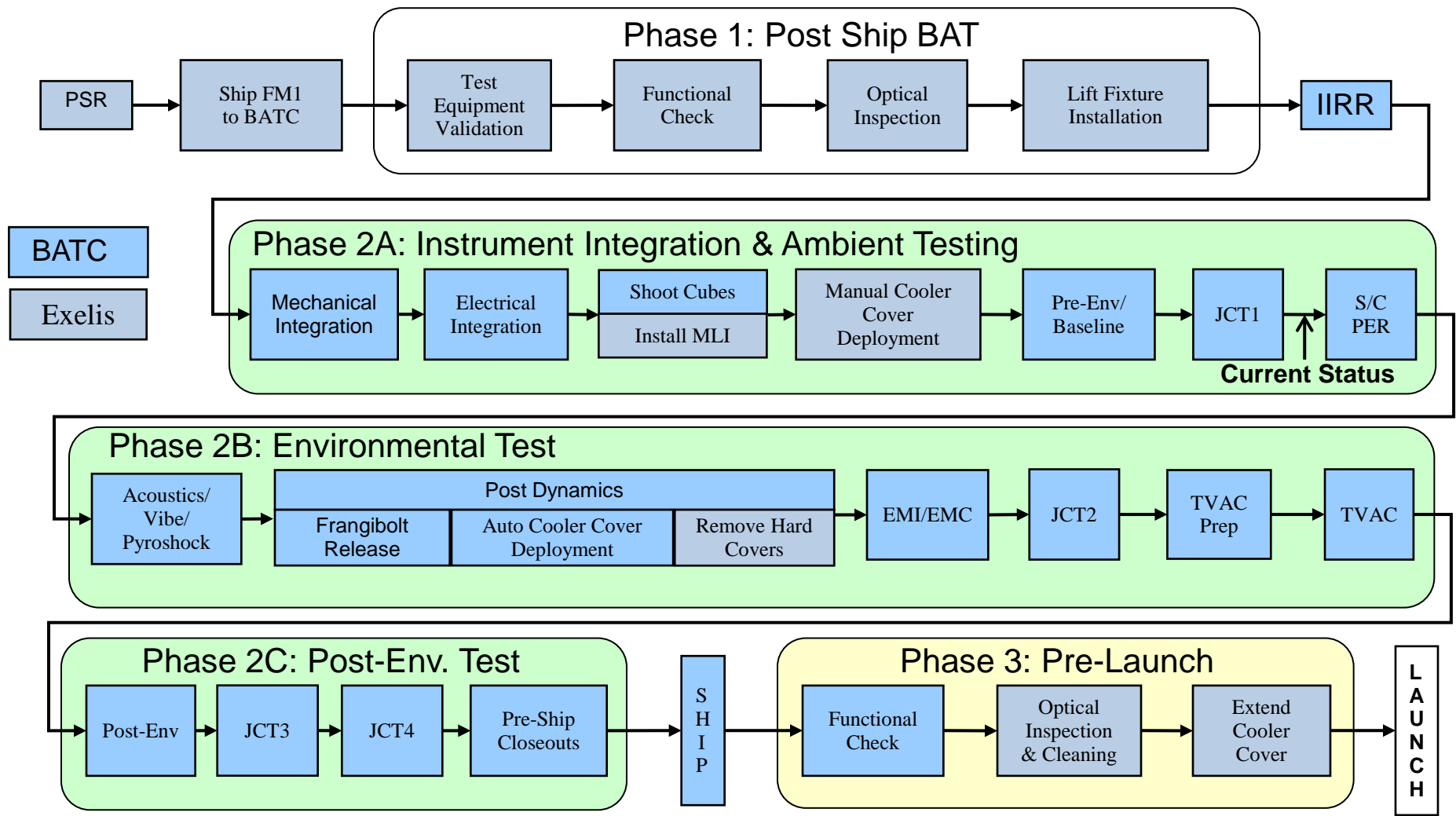


- Bit trim and impulse noise masks ready
 - Same as used during ground testing
 - May change slightly on-orbit if extended interferogram configuration is desired for J1
- ILS parameters calculated
 - Will be further tuned on-orbit
 - Harris, UMBC and UW values agree closely
- Linearity correction parameters determined
 - Will be further tuned on-orbit
 - Harris and UW calculations match well
- Geolocation angles measured and ready
 - Can be further tuned post-launch

Spacecraft level testing



CrIS Proceeding Through Spacecraft Test Flow



Several Spacecraft Level Tests Evaluate Science Performance Data



- Reaction wheel jitter
 - Measured interferometer jitter performance with spacecraft reaction wheels activated
 - All other instruments unpowered
 - Results show there is no expected NEdN impact due to reaction wheels
- Spacecraft to sensor alignment measurements
 - Measure CrIS LOS to spacecraft cube alignment to ensure geolocation accuracy
 - Angles calculated and entered into SDR processing chain
- EMI
 - Measures interferometer and scan mirror performance during EMI injections
 - All telemetry that affects SDR production monitored during tests
- TVAC
 - First NEdN measurement with sensor integrated to spacecraft
 - Ensures CrIS compatibility with other on-board instruments

- Susceptibility measurements of the digital portion of the signal processor CCAs planned for J1
 - J1 design modification allows the signal processors and detectors to be powered independently
- Balance of EMI tests are the same as SNPP
 - EMI testing will be performed at ambient in EMI chamber used for SNPP
 - Detectors will be warm and unpowered, NEdN will not be measured
 - Interferometer and scan mirror performance monitored during EMI injection
 - All telemetry affecting SDR production also monitored
 - EMI self compatibility test will be performed during TVAC
 - Detectors will be cold and powered, NEdN will be monitored
 - Susceptibility measurements will include both servo performance and NEdN

- Same space target and radiant cooler target as used during system TVAC
 - Same targets used for SNPP
- External calibration target (ECT) supplied by Ball
 - Same target used for SNPP
- NEdN can be calculated using scanning or stare mode data collect
 - 2 point calibration (ICT and SCT) while scanning
 - 3 point uses the calibration targets and ECT plate
 - Compared to system level NEdN for self-compatibility evaluation
 - Same process used on SNPP
- Instrument temperatures monitored real-time to ensure sensor safety
 - Same as SNPP

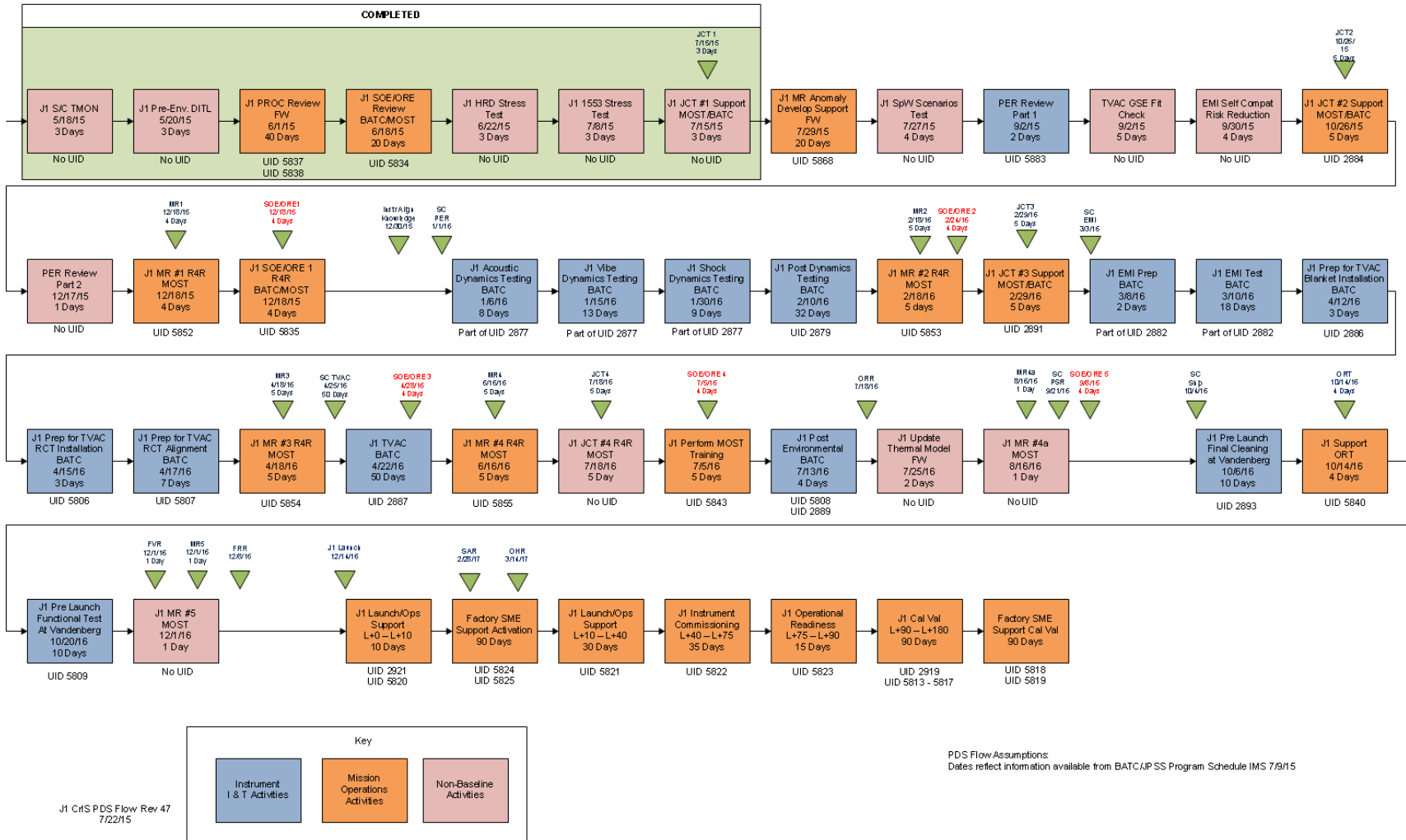
J1 Launch Readiness



Activity Flow Supports Launch Schedule



J1 CrIS PDS Integration & Test and Mission Operations Flow



MOST, Harris and Science Team Roles Clearly Defined



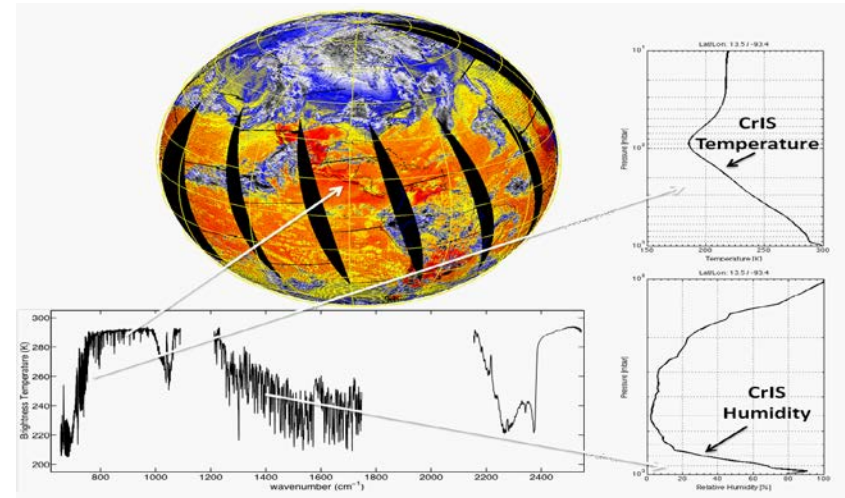
- Mission Operations Support Team (MOST) operates sensor and ensures instrument safety
 - Verifies and performs instrument commanding
 - Monitors sensor alarm limits and responds to anomalous behavior
 - Trends instrument critical telemetry and reviews for anomalies
- Harris supports MOST and Science team
 - Responsible for Early Orbit Activation (EOA) period following launch
 - Includes instrument calibration related activities
 - Supports science team during Intensive Cal Val (ICV)
 - Supports troubleshooting of instrument anomalies as needed
 - Develops/tests commanding as needed to support incremental performance improvements
- Science team ensures optimal calibration of sensor
 - Independent assessment of TVAC data
 - Reviews data and provides input during EOA phase
 - Responsible for ICV and Long Term Monitoring activities

Cal/Val Procedures Ready to Support J1 Mission



Title	Purpose	Status
ROP CRIS-CV-001 - CrIS Bit Trim and Impulse Mask Checks	Checks bit trim and impulse noise masks and modifies as needed	Ready
ROP CRIS-CV-002 - CrIS Noise Equivalent Radiance Difference (NEDN)	Details collection and calculation of NEDN	Ready
ROP CRIS-CV-003 - CrIS IR Channel Programmable Amplifier Gain Check and Adjustment	Checks PGA gain and modifies settings as needed	Ready
ROP CRIS-CV-004 - CrIS Interferometer Optimization	Optimizes metrology laser temperature setpoint and optical ZPD location	Ready
ROP CRIS-CV-005 - CrIS Bias Tilt Offset Calibration	Optimizes interferometer dynamic alignment (DA) mirror bias tilts	Ready
ROP CRIS-CV-006 - CrIS Metrology Laser System Stability Check	Checks metrology laser for stability	Ready
ROP CRIS-CV-007 - CrIS Detector Linearity Check	Checks/trends detector nonlinearity performance	Ready
ROP CRIS-CV-008 - SSM In-Track Mechanism Rotation Compensation	Determines scan mirror null torque offset to optimize geolocation performance	Ready
ROP CRIS-CV-009 - Configure SPs for Truncated Mode or Full Spectral Mode	Configures CrIS to truncated or full resolution mode	Ready

- Initial on-orbit checkouts
- NEdN evaluations
- Comparisons with other instruments
 - SNPP CrIS, VIIRS, IASI, AIRS
- Calibration optimization
 - EOA activities optimize instrument
 - Gain settings
 - Mask checks/tailoring
 - ICV activities optimize calibration
 - Linearity parameters
 - ILS parameters
 - Geolocation parameters
- Goal is high quality validated SDRs



Plot courtesy of University of Wisconsin

- J1 bit trim mask levels same as SNPP
 - Minimizes data rate while avoiding mask clipping
- J1 FIR filter same as updated SNPP filter
 - Mitigates sweep dependence bias observed in early SNPP data
- ROPs updated based on SNPP experience
 - Contingency ROPs developed to support anomaly troubleshooting
 - Several ROPs simplified based on SNPP execution
- Increased diagnostic data collections planned
 - Useful for SNPP troubleshooting
 - Truncated resolution diagnostic data collections for all FOVs
 - Only 3 FOVs collected during SNPP
 - Possible SWIR full resolution diagnostic collect to support impulse mask evaluation

- J1 CrIS completed comprehensive test program
 - Excellent performance during all phases
 - Performance as good or better than SNPP
- Spacecraft testing underway
 - CrIS integrated to J1
 - EMI and TVAC testing upcoming
- Launch readiness activities identified
 - EOA and ICV tasks defined
 - Lessons learned incorporated from SNPP

CrIS Ready to Support Successful J1 Mission